NOVEL THERAPEUTIC APPROACHES FOR THE TREATMENT OF OCULAR DISEASE, VOLUME I

EDITED BY: Kyriaki Thermos, Stephanie C. Joachim, Deniz Hos and Giovanni Casini

frontiers Research Topics

About Frontiers

Frontiers is more than just an open-access publisher of scholarly articles: it is a pioneering approach to the world of academia, radically improving the way scholarly research is managed. The grand vision of Frontiers is a world where all people have an equal opportunity to seek, share and generate knowledge. Frontiers provides immediate and permanent online open access to all its publications, but this alone is not enough to realize our grand goals.

Frontiers Journal Series

The Frontiers Journal Series is a multi-tier and interdisciplinary set of open-access, online journals, promising a paradigm shift from the current review, selection and dissemination processes in academic publishing. All Frontiers journals are driven by researchers for researchers; therefore, they constitute a service to the scholarly community. At the same time, the Frontiers Journal Series operates on a revolutionary invention, the tiered publishing system, initially addressing specific communities of scholars, and gradually climbing up to broader public understanding, thus serving the interests of the lay society, too.

Dedication to Quality

Each Frontiers article is a landmark of the highest quality, thanks to genuinely collaborative interactions between authors and review editors, who include some of the world's best academicians. Research must be certified by peers before entering a stream of knowledge that may eventually reach the public - and shape society; therefore, Frontiers only applies the most rigorous and unbiased reviews.
Frontiers revolutionizes research publishing by freely delivering the most outstanding research, evaluated with no bias from both the academic and social point of view. By applying the most advanced information technologies, Frontiers is catapulting scholarly publishing into a new generation.

What are Frontiers Research Topics?

Frontiers Research Topics are very popular trademarks of the Frontiers Journals Series: they are collections of at least ten articles, all centered on a particular subject. With their unique mix of varied contributions from Original Research to Review Articles, Frontiers Research Topics unify the most influential researchers, the latest key findings and historical advances in a hot research area! Find out more on how to host your own Frontiers Research Topic or contribute to one as an author by contacting the Frontiers Editorial Office: frontiersin.org/about/contact

NOVEL THERAPEUTIC APPROACHES FOR THE TREATMENT OF OCULAR DISEASE, VOLUME I

Topic Editors:
Kyriaki Thermos, University of Crete, Greece
Stephanie C. Joachim, Ruhr University Bochum, Germany
Deniz Hos, University Hospital of Cologne, Germany
Giovanni Casini, University of Pisa, Italy

Table of Contents

Check for
updates

The Potential of Lisosan G as a Possible Treatment for Glaucoma

Rosario Amato[1], Maria Grazia Rossino[1], Maurizio Cammalleri[1,2], Anna Maria Timperio[3], Giuseppina Fanelli[4], Massimo Dal Monte[1,2], Laura Pucci[5]* and Giovanni Casini[1,2]*

[1]Department of Biology, University of Pisa, Pisa, Italy, [2]Interdepartmental Research Center Nutrafood "Nutraceuticals and Food for Health", University of Pisa, Pisa, Italy, [3]Department of Ecological and Biological Sciences, University of Tuscia, Viterbo, Italy, [4]Department of Agriculture and Forest Sciences, University of Tuscia, Viterbo, Italy, [5]National Research Council, Institute of Agricultural Biology and Biotechnology (IBBA), Pisa, Italy

Lisosan G (LG), a fermented powder obtained from whole grains, is a nutritional supplement containing a variety of metabolites with documented antioxidant properties. We have recently demonstrated that orally administered LG protects diabetic rodent retinas from oxidative stress, inflammation, apoptosis, blood-retinal barrier disruption, and functional damage. Here, we investigated whether LG may exert protective effects in a model of glaucoma and measured the amounts of selected LG components that reach the retina after oral LG administration. Six-month-old DBA/2J mice were given an aqueous LG solution in place of drinking water for 2 mo. During the 2 mo of treatment with LG, the intraocular pressure (IOP) was monitored and the retinal ganglion cell (RGC) functional activity was recorded with pattern-electroretinography (PERG). At the end of the 2-mo period, the expression of oxidative stress and inflammatory markers was measured with qPCR, and RGC survival or macroglial activation were assessed with immunofluorescence. Alternatively, LG was administered by gavage and the concentrations of four of the main LG components (nicotinamide, gallic acid, 4-hydroxybenzoic acid, and quercetin) were measured in the retinas in the following 24 h using mass spectrometry. LG treatment in DBA/2J mice did not influence IOP, but it affected RGC function since PERG amplitude was increased and PERG latency was decreased with respect to untreated DBA/2J mice. This improvement of RGC function was concomitant with a significant decrease of both oxidative stress and inflammation marker expression, of RGC loss, and of macroglial activation. All four LG metabolites were found in the retina, although with different proportions with respect to the amount in the dose of administered LG, and with different temporal profiles in the 24 h following administration. These findings are consistent with neuroenhancing and neuroprotective effects of LG in glaucoma that are likely to derive from its powerful antioxidant properties. The co-occurrence of different metabolites in LG may provide an added value to their beneficial effects and indicate LG as a basis for the potential treatment of a variety of retinal pathologies.

Keywords: inflammation, neuroprotection, nutraceuticals, oxidative stress, pattern electroretinogram

INTRODUCTION

Oxidative stress and inflammation can be considered as pathogenetic hallmarks of a variety of retinal diseases, including age related macular degeneration, diabetic retinopathy, retinitis pigmentosa, and glaucoma. Regarding glaucoma, although elevated intraocular pressure (IOP) is commonly considered the main risk factor for this disorder (Gottanka et al., 2005). IOP lowering is not always effective in preventing disease progression, and the form of glaucoma known as normotensive glaucoma develops with the IOP within the normal range, indicating a high degree of complexity in the pathophysiology of this retinal disease (Weinreb et al., 2014). Indeed, a variety of investigations have highlighted the primary role played by oxidative stress and inflammation in the development of glaucoma (Baudouin et al., 2020; Domènech and Marfany, 2020; Garcia-Medina et al., 2020; Mélik Parsadaniantz et al., 2020; Wang et al., 2020), indicating that potential treatments of this sight-threatening disease, characterized by retinal ganglion cell (RGC) degeneration and visual field loss, could be based on the use of antioxidant and/or anti-inflammatory compounds.

Among the various treatment options that may be considered for glaucoma, functional foods and nutraceuticals are particularly attractive. In view of their availability, their ease of use as natural dietary supplements, and the lack of induced collateral side effects (Kalra, 2003; Chauhan et al., 2013), these substances may constitute a strong basis to develop novel drugs for the treatment of this disease (Adornetto et al., 2020) as well as of other retinal pathologies (Rossino and Casini, 2019). The potential of nutraceuticals lies in their powerful antioxidant effects. Indeed, exogenous antioxidants of natural origin may be used to preserve redox homeostasis acting directly as scavengers of free radicals, indirectly by interrupting free radical chain reactions, or both. They may also decrease oxidative stress by inducing the expression of endogenous antioxidant enzymes (Nimse and Pal, 2015; Ahmadinejad et al., 2017). An antioxidant action of nutraceuticals may also reduce inflammation. Indeed, oxidative stress has been recognized as playing a pivotal role in the development of inflammation (Gill et al., 2010; Reuter et al., 2010), which, in glaucoma, would induce macroglial cell activation, characterized by increased glial fibrillary acidic protein (GFAP) expression in Müller cells (Mélik Parsadaniantz et al., 2020), and a marked release of cytokines/chemokines that would damage retinal neurons (Chen et al., 2010).

We have shown recently that Lisosan G (LG), a fermented powder obtained from organic whole grains (*Triticum aestivum*) and registered with the Italian Ministry of Health as a nutritional supplement, protects the retina from oxidative stress and significantly reduces inflammation and the retinal damage associated to diabetic retinopathy (Amato et al., 2018). Its powerful antioxidant properties are likely to be due to a rich variety of compounds, as LG has been shown to contain bioactive substances such as both flavonoid and non-flavonoid polyphenols, alpha-lipoic acid, polyunsaturated fatty acids, and vitamins, among others (La Marca et al., 2013; Lucchesi et al., 2014).

In the present paper, we tested whether LG has the potential to be considered as a valid option for the treatment of glaucoma using the DBA/2J (D2) mouse model, in which the spontaneous increase in IOP starting at 6 mo of age correlates with a glaucomatous age-related RGC loss (Schnichels et al., 2021). To this aim, in D2 mice, the effects of LG were tested on IOP levels, on RGC function and survival, on the expression of oxidative stress and of inflammatory markers, and on macroglial activation. In addition, selected components of LG were assessed in the retina using mass spectrometry.

MATERIALS AND METHODS

Animals

All the procedures were performed in compliance with the ARVO Statement for the Use of Animals in Ophthalmic and Vision Research, the EU Directive (2010/63/EU), and the Italian guidelines for animal care (DL 26/14; Permission number: 349/2018-PR). A total of 34 D2 mice of both sexes (Charles River Laboratories, Calco, Italy) were used in these studies. They were kept in a regulated environment (23 ± 1°C, 50 ± 5% humidity) with a 12 h light/dark cycle (lights on at 8:00 a.m.) with food and water (or a LG solution, *see* below) ad libitum. Non-glaucomatous control mice were not considered since the commonly used C57BL/6J or DBA/2J-Gpnmb+/SjJ show some notable differences in inner retinal neural processing that could have a counterpart in the RGC susceptibility to insults or diseases (Porciatti et al., 2010). Therefore, we focused on differences between LG-treated and untreated DBA/2J mice without introducing a possibly biased, non-glaucomatous control.

Preparation of LG and LG Administration

LG was supplied by Agrisan Company (Larciano, Pistoia, Italy). It is a powder obtained by fermenting and drying whole wheat flour from *Triticum aestivum* grains. The starter cultures typically consist of a mix of lactobacillus and natural yeast strains in a ratio of about 100:1 (Natural Sourdough). Once the product was fermented, it was dried using a vacuum pump at 20–25°C temperature and 2 bar pressure until reaching 12% humidity (48–60 h for 100 kg material).

LG was administered in the form of an aqueous solution of the hydrophilic components of LG. Twelve D2 mice were randomly distributed among control or LG-treated groups ($n = 6$ for each experimental group). The D2 mice used as controls had ad libitum access to food and water, while, for the D2 mice treated with LG (D2+LG), water was replaced with the LG solution. The treatment began at 6 mo of age (baseline), and it was continued for 2 mo (8 mo of age, endpoint). At the end of this period, the mice were sacrificed, and the retinas were dissected and used for molecular and immunohistochemical analyses.

For the analysis of different LG components reaching the retina after LG ingestion, a total of eighteen 6-mo-old D2 mice received an oral administration of LG solution by gavage. The retinas of three mice were dissected and quickly frozen in liquid nitrogen after 0 or 30 min and after 1, 2, 6, or 24 h. The retinas were stored at −80°C until used for mass spectrometry.

The aqueous LG solution had a concentration of 8.3 mg/ml. Preliminary observations showed that the volume of LG solution consumed by these mice was similar to that of drinking water consumed by untreated D2 mice (about 3 ml/mouse/day). Assuming an average mouse body weight of 20 g, this dose corresponded to 1 g LG/Kg/day. This dose was equivalent to that used in previous studies in rats (Longo et al., 2007; Amato et al., 2018) and corresponded to an equivalent dose for humans of 80 mg/Kg (Reagan-Shaw et al., 2008).

The aqueous LG solution administered by gavage had a volume of 1 ml and a concentration of 83 mg LG/ml. Assuming an average mouse body weight of 20 g, this dose corresponded to 4.15 g LG/Kg of body weight (human equivalent dose, 340 mg LG/Kg of body weight).

IOP Measurements and Pattern-electroretinography (PERG)

At baseline and after 1 and 2 mo from the beginning of treatment with LG, mice were dark adapted overnight and anesthetized by intraperitoneal injection of avertin (1.2% tribromoethanol and 2.4% amylene hydrate in distilled water, 0.02 ml/g body weight: Sigma-Aldrich). Anesthetized mice underwent IOP measurement after being positioned on a soft pad. The induction–impact tonometer (Tonolab Colonial Medical Supply, Franconia, NH, United States) was fixed by clamps on an adjustable stand and oriented with the probe aligned with the eye optical axis at a 1–2-mm distance. Five consecutive recordings were averaged to obtain a reliable measure of the IOP. At the end of the IOP assessment, eyes were instilled with saline solution to avoid corneal dryness. Then, the mice were transferred on a custom-made restrainer with unobstructed vision for the assessment of PERG. PERG was recorded from the right eye by means of a silver-silver chloride recording electrode configured to a semicircular loop of about 2 mm radius positioned on the corneal surface. Two stainless-steel needles positioned in the mouse cheek and at the tail root were used as reference and ground electrodes, respectively. The visual stimulus consisted in 98% contrast-reversing bars with 0.05 cycles/deg spatial frequency and 1 Hz temporal frequency delivered at 20 cm distance through a light emitting diode display with a mean luminance of 50 cd/m^2. PERG signals were acquired using a commercially available PERG system (SB700 Advanced; Nikon-Europe, Amsterdam, Netherlands), amplified (10,000-fold) and band-pass filtered (1–30 Hz). Signals deriving from two consecutive recording protocols (PERG-rec1 and PERG-rec2; 300 pattern reversal stimulations each) were superimposed to confirm consistency and averaged to minimize noise. Individual averaged responses (hereinafter referred to as "PERG") were analyzed by retrieving the signal amplitude and the implicit time after detecting the positive peak and the negative trough of the waveform (typically the P1 peak to the N2 trough). Since the recognition of the early negative component of the PERG waveform (N1) is classically ambiguous in D2 mice, we preferred to consider the P1-N2 amplitude as a reliable measure of PERG amplitude together with the time-to-P1 peak as PERG latency, as previously reported

(Saleh et al., 2007). The test-retest reliability, calculated as the individual mean difference between PERG amplitudes of two consecutive recordings (|PERG-rec1 amplitude–PERG-rec2 amplitude|), was performed at the baseline and at the endpoint to estimate the interindividual variability.

Immunofluorescence

Retinas were isolated and immersion fixed for 2 h at 4°C in 4% paraformaldehyde in 0.1 M phosphate buffered saline (PBS), and then stored at 4°C in 25% sucrose in 0.1 M PBS. The immunostaining of RGCs and astrocytes was performed by incubating the retinas with the guinea pig polyclonal antibody directed to RNA-binding protein with multiple splicing (RBPMS, ABN1376, dilution 1:100; Merck, Darmstadt, Germany), a ganglion cell marker (Rodriguez et al., 2014), and the rabbit monoclonal antibody directed to GFAP (ab207165, dilution 1: 400; Abcam, Cambridge, United Kingdom) in PBS containing 5% bovine serum albumin (BSA) and 2% TritonX-100. After overnight incubation, the retinas were rinsed in PBS and incubated with FITC-conjugated anti-guinea pig secondary antibody (F6261; Merck) or AlexaFluor 555-conjugated anti-rabbit secondary antibody (A-32727; Molecular Probes, Eugene, OR, United States) diluted 1:200 in PBS containing 5% BSA and 2% TritonX-100. Finally, the retinas were rinsed in PBS and flat mounted on polarized glass slides with the RGC layer facing up. Images were acquired using an epifluorescence microscope (Ni-E; Nikon-Europe) equipped with a digital camera (DS-Fi1c camera; Nikon-Europe). Image sampling was performed in order to obtain four radial tiles (440 × 330 μm) in central and peripheral retina (center: 500 μm from the optic nerve head; periphery: 500 μm far from the peripheral edge). RGC density was measured in D2 retinas at baseline (D2b), in D2 retinas at the endpoint (D2e), and in D2+LG retinas as the average of the number of RBPMS immunopositive somata per mm^2. The GFAP immunostaining was quantified as the average of the mean gray levels recorded in the sampled areas, after normalization to background, using ImageJ software (U. S. National Institutes of Health, Bethesda, Maryland, United States). The involvement of Müller glia activation was highlighted in virtual z-stack projections (150 μm) following image convolution filtering and 3D reconstruction with ImageJ. Finally, the concurrence between RGC loss and glial activation was analyzed by correlating the values of RBPMS and GFAP immunostainings.

Quantitative Real-Time PCR

Quantitative real-time PCR (qPCR) was used to determine the expression of oxidative stress markers, including nuclear factor erythroid 2–related factor 2 (Nrf2), heme oxygenase-1 (HO-1), superoxide dismutase 2 (SOD-2), and glutamate-cysteine ligase catalytic subunit (GCLC), or of inflammatory markers, including interleukin 1 beta (IL-1β), interleukin 6 (IL-6), tumor necrosis factor alpha (TNF-α), and ionized calcium binding adaptor molecule 1(Iba1). Ribosomal protein L13A mRNA (Rpl13a) was used as an endogenous control. In all the experiments, three independent samples from each experimental group were analyzed. Total RNA was extracted and purified using RNeasy

TABLE 1 | Primer sequences.

Gene	Forward primer (5′-3′)	Reverse Primer (5′-3′)
Nrf2	TCTTGGAGTAAGTCGAGAAGTGT	GTTGAAACTGAGCGAAAAAGGC
HO-1	AAGCCGAGAATGCTGAGTTCA	GCGTGTAGATATGGTACAAGGA
SOD-2	CAGACCTGCCTTACGACTATGG	CTCGGTGGCGTTGAGATTGTT
GCLC	GGGGTGACGAGGTGGAGTA	GTTGGGGTTTGTCCTCTCCC
IL-1β	CCAAGCCTTATCGGAAATGA	TTGTCGTTGCTTGGTTCTCC
IL-6	GCCTTCCCTACTTCACAAGTC	AGTGCATCATCGTTGTTCATAC
TNF-α	GCCTCTTCTCATTCCTGCTTG	CACTTGGTGGTTTGCTACGAC
Iba1	CGAATGCTGGAGAAACTTGG	AGCCCCACCGTGTGACAT
Rpl13a	CACTCTGGAGGAGAAACGGAAGG	GCAGGCATGAGGCAAACAGTC

TABLE 2 | Amounts of the selected compounds in LG and in the administered dose of LG.

Compound	mg/mg LG	mg/administered dose of LG
Gallic acid	0.1928 ± 0.0418	16.0100 ± 3.4700
Hydroxy benzoic acid	0.0163 ± 0.0003	1.3530 ± 0.0289
Quercetin	0.0023 ± 0.0004	0.1897 ± 0.0364
Nicotinamide	0.0018 ± 0.0005	0.1501 ± 0.0432

Mini Kit (Qiagen, Hilden, Germany). Then it was resuspended in RNAse-free water, and quantified by spectrophotometry (BioSpectrometer basic; Eppendorf AG, Hamburg, Germany). Starting from 1 µg of total RNA, first-strand cDNA was generated using a QuantiTect Reverse Transcription Kit (Qiagen). qPCR was performed using SsoAdvanced Universal SYBR Green Supermix on a CFX Connect Real-Time PCR Detection System provided with the software CFX manager (Bio-Rad Laboratories, Hercules, CA, United States). Primer sets were designed to hybridize to unique regions of the appropriate gene sequence according to published mouse cDNA sequences in the GenBank database (**Table 1**). Expression levels were quantified with the ΔΔCt method.

Ultra-high Performance Liquid Chromatography and Mass Spectrometry (UHPLC-MS)

The main components of LG were determined in the LG powder (1 mg sample) using the same procedure as described below for the retinas. The most abundant were gallic acid, 4-hydroxybenzoic acid, quercetin, and nicotinamide (**Table 2**), therefore these metabolites were chosen as the LG components to be determined in the retina. To this aim, LG was administered to the mice by gavage and the retinas were dissected at different time points. The two retinas from each mouse were pooled together and they were resuspended in 0.2 ml of ice cold ultra-pure water (18 MΩ-cm) to lyse the cells. Three independent samples were analyzed for each time point. The tubes were plunged into dry ice or in a circulating bath at −25°C for 0.5 min and then into a water bath at 37°C for 0.5 min. Subsequently, 0.6 ml of −20°C methanol and then 0.4 ml of −20°C chloroform were added to each tube. The tubes were

mixed every 5 min for 30 min, then they were centrifuged at 1000 × g for 1 min at 4°C, before being transferred to −20°C for 2–8 h. After centrifugation at 15,000 × g for 10 min at 4°C, the supernatants were collected and dried. Finally, the dried samples were resuspended in 0.1 ml of water and transferred to glass autosampler vials for LC-MS analysis. The supernatants were injected (20 µl) into a UHPLC system (Ultimate 3000; ThermoFisher Scientific, Waltham, MA, United States) and run in negative ion mode for determination of 4-hydroxy benzoic acid and in positive ion mode for the other. A ReproSil C18 column (2.0 mm × 150 mm, 2.5 µm; Dr Maisch, Ammerbuch-Entringen, Germany) was used for metabolite separation. Chromatographic separations were achieved at a column temperature of 30°C and flow rate of 0.2 ml/min. For positive ion mode (+) MS analyses, a 0–100% linear gradient of solvent A (ddH$_2$O, 0.1% formic acid) to B (acetonitrile, 0.1% formic acid) was employed over 20 min returning to 100% A in 3 min. For negative ion mode chromatographic separations A 0–100% linear gradient of solvent A (double-distilled 18 MΩ-cm water, 10 mm ammonium acetate) to B (100% acetonitrile, 10 mm ammonium acetate) was employed over 20 min, returning to 100% A in 3 min and a -min post-time solvent A hold. The UHPLC system was coupled online with a mass spectrometer Q Exactive (ThermoFisher) scanning in full MS mode (2 µ scans) at 70,000 resolution in the 60–1000 m/z range. Data files were processed by MAVEN. 8.1 (http://genomics-pubs.princeton.edu/mzroll/) upon conversion of raw files into mzXML format through MassMatrix (Yellow Springs, OH, United States). Standard curves were obtained with several calibration points (2–0.00002 mg) of gallic acid, 4-hydroxybenzoic acid, quercetin, and nicotinamide analytical standards (Sigma Aldrich, St Louis, MO, United States).

Statistical Analysis

For the analysis of LG bioactivity, the sample size (*n* = 6) was calculated in order to ensure an effect size on the main output parameter (PERG amplitude) as narrow as 1.5 µV with an α error of 0.05 and 1-β power of 0.08. Data displaying the effect of one categorical variable (treatment) were analyzed using unpaired *t*-test. Data describing the effect of two combined categorical variables (treatment and time) were analyzed with two-way ANOVA with Bonferroni *post-hoc* test for multiple comparisons. The correlation between two dependent variables was tested with the two-tailed Pearson's test for linear regression
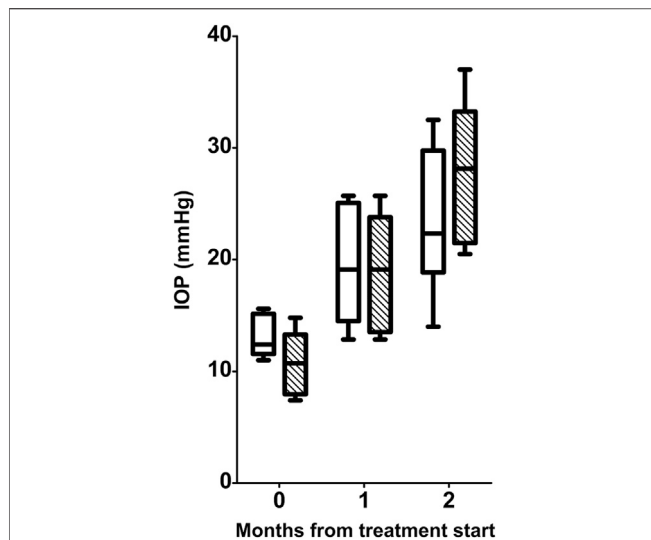
FIGURE 1 | Longitudinal analysis of IOP levels in D2 (white boxes) and D2+LG (dashed boxes). Box plots describe the statistical distribution of data deriving from the average of IOPs measured in individual right and left eyes of $n = 6$ mice. Statistical differences were tested using two-way ANOVA with Bonferroni *post-hoc* test. The effect of time was highly significant ($p < 0.0001$), while the effect of LG at each time was not significant ($p = 0.6782$).

analysis and performing ANCOVA for the comparison between groups identified according to a categorical variable. Data were expressed as mean ± SEM of the respective n values (Prism 8; GraphPad software, San Diego, CA, United States). Differences with $p < 0.05$ were considered significant.

RESULTS

LG Does Not Affect IOP

As shown in **Figure 1**, during the 2-mo period of the experiment, the IOP of D2 mice increased from 13.13 ± 1.85 mmHg to 23.50 ± 6.38 mmHg, while the IOP of D2+LG mice went from 10.78 ± 3.08 mmHg to 27.93 ± 6.50 mmHg (effect of time, $p < 0.0001$). No differences were observed in IOP levels at any time between D2 and D2+LG mice (effect of LG, $p = 0.6782$).

LG Improves the PERG Responses

The test-retest analysis between individual PERG-rec1 and PERG-rec2 displayed an amplitude interindividual variability of 0.58 ± 0.05 μV (95% CI 0.42–0.73) in D2 and 0.59 ± 0.03 μV (95% CI 0.49–0.70) in D2 + LG retinas at the baseline. Similarly, at the endpoint the variability was
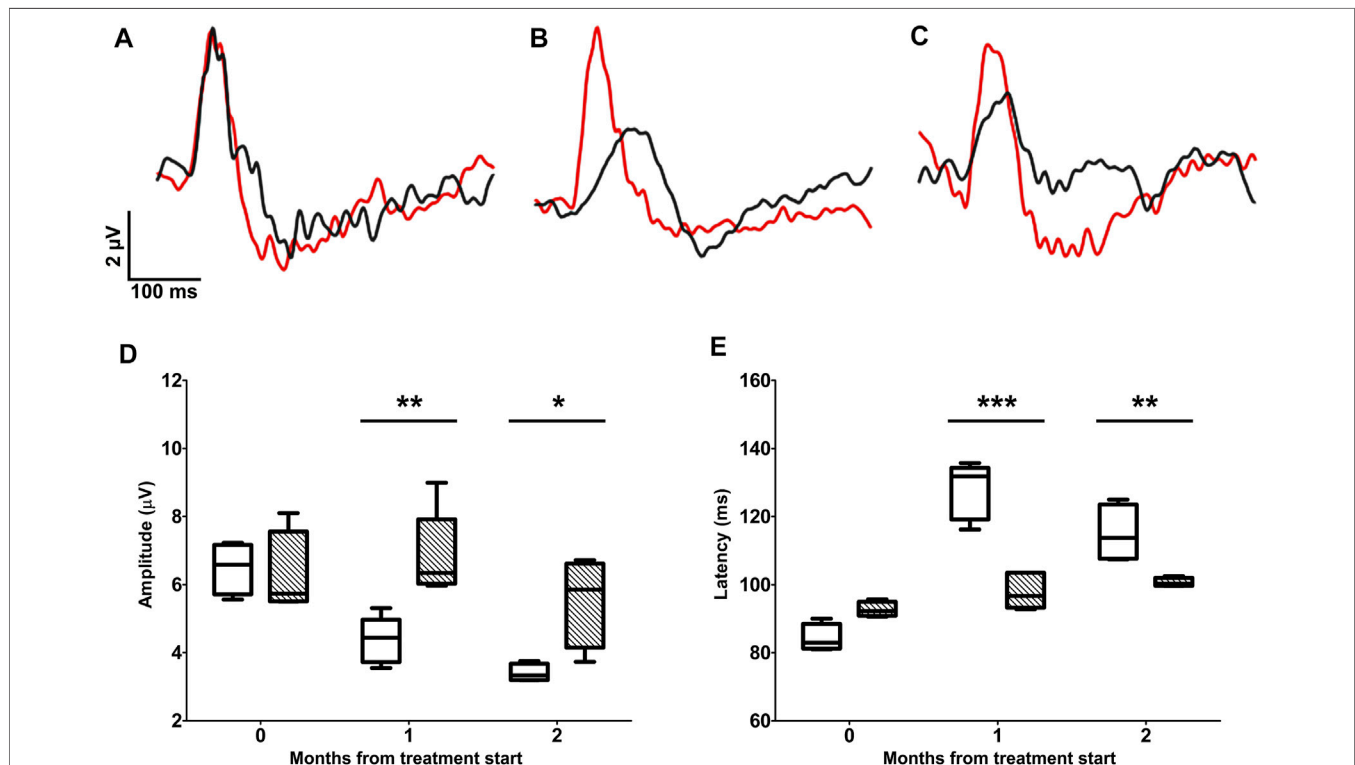
FIGURE 2 | Longitudinal evaluation of RGC activity using PERG. PERG responses were recorded before the beginning of the treatment **(A)** and after 1 **(B)** or 2 **(C)** months of treatment in D2 (black traces) and D2+LG (red traces) mice. PERG responses were analyzed by retrieving the peak-to-trough amplitude and time-to-peak latency, as shown in the inset in **(A)**. The distribution of PERG amplitudes **(D)** and PERG latencies **(E)** in D2 (white boxes) and D2+LG (dashed boxes) deriving from $n = 6$ mice are shown by box plots. Statistical differences were tested using two-way ANOVA with Bonferroni *post-hoc* test. *$p < 0.05$, **$p < 0.01$, ***$p < 0.001$.

FIGURE 3 | Endpoint qPCR analysis for the expression of oxidative stress **(A)** and inflammation-related **(B)** markers in D2 (white box) and D2+LG (dashed boxes) groups after 2 mo of treatment. Box plots describe the statistical distribution of $n = 6$ independent retinas. Differences between groups were tested using two-tailed t-test. $*p < 0.05$, $**p < 0.01$ vs D2.
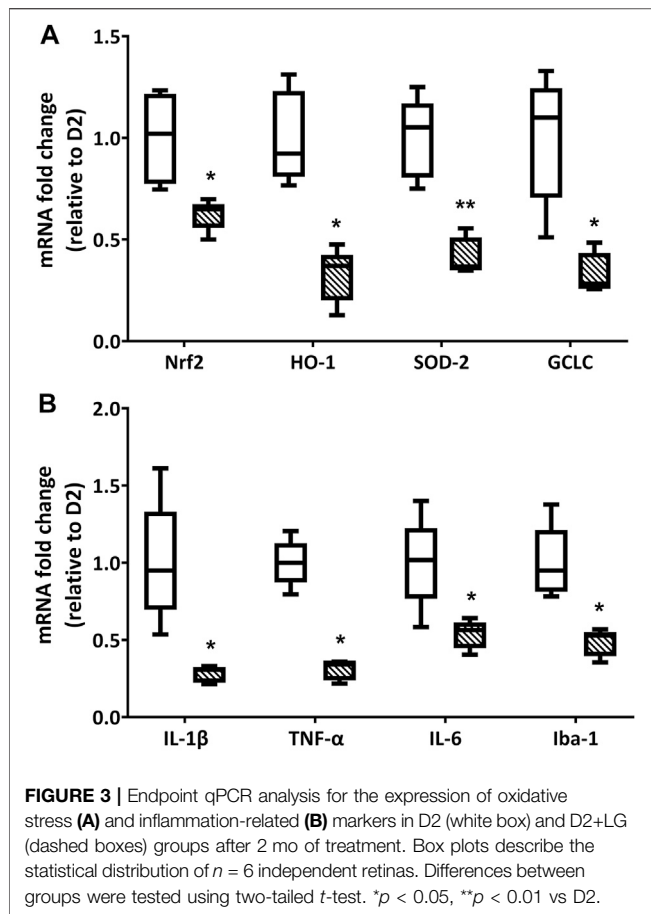
0.56 ± 0.06 μV (95% CI 0.34–0.77) in D2 and 0.57 ± 0.09 μV (95% CI 0.31–0.83) in D2+LG retinas. By comparing the interindividual variability retrieved in both groups between baseline and endpoints, we did not observe any significant effect of either the time ($p = 0.77$) or the treatment ($p = 0.85$). Therefore, since the interindividual variability was constant among experimental groups over time, we considered the averages between PERG-rec1 and PERG-rec2 waveforms in order to minimize the noise contribution in the analysis of RGC activity (**Figures 2A–C**). PERG responses were similar in D2 and D2+LG mice at the baseline (PERG amplitude, $p > 0.99$; PERG latency, $p = 0.1533$). During the follow-up period, D2 mice displayed a time-dependent decline in PERG amplitude resulting in a~ 53% loss at the endpoint compared to baseline. The decrease in PERG amplitude appeared less evident in the D2+LG group than in the D2 group (effect of LG, $p = 0.013$), since the values remained around baseline levels after 1 mo of treatment and were only partially reduced after 2 mo (**Figure 2D**). Thus, LG treatment resulted in a significant maintenance of the endpoint PERG amplitude compared to the D2 group (D2 amplitude: 3.4 ± 0.38 μV; D2+LG amplitude: 5.5 ± 0.66 μV; $p = 0.019$). PERG latency (**Figure 2E**) was increased over the period under investigation in both groups (effect of time, $p <$

0.001). However, PERG latency recorded in D2+LG mice after 1 and 2 mo was lower than in the D2 group (effect of LG, $p < 0.001$), thus resulting partially preserved at the endpoint (D2 latency: 114.99 ± 4.26 ms; D2+LG latency: 100.68 ± 0.64 ms; $p = 0.0067$).

LG Reduces Oxidative Stress and Inflammatory Markers

The treatment with LG produced a significant decrease in the expression of oxidative stress-related genes. Indeed, as shown in **Figure 3A**, the qPCR analysis revealed an expression of Nrf2 mRNA that was slightly above 50% of that measured in D2 retinas, while the expression levels of HO-1, SOD-2, and GCLC mRNAs were all less than 50% of those detected in D2 retinas. Similarly, the mRNAs of inflammatory markers (**Figure 3B**) were also reduced to about 50% (IL-6 and Iba-1) or less (IL-1β and TNF-α) of the values measured in the retinas of D2 mice.

LG Preserves RGC Density

The RGC density was evaluated as the number of RBPMS immunopositive cells/mm^2 sampled in peripheral and central areas of D2b, D2e, and D2+LG retinas (**Figures 4A–F**). The RBPMS immunopositive cell density was influenced by the sampling location, resulting lower in the retinal periphery than in the retinal center ($p = 0.0397$). As shown in **Figure 4G**, in D2 retinas there was a dramatic decrease of immunolabeled RGC density with a loss of about 57% from baseline to endpoint both in central and in peripheral retinal locations. In D2+LG retinas, the decrease of RGC density reached 39% in central retina and 26% in the periphery. The retinas belonging to the D2+LG group displayed a significantly higher RBPMS immunopositive cell density than those of the D2e group (center, $p = 0.0106$; periphery, $p = 0.0114$). Interestingly, there was no statistically significant difference between peripheral RGC density in D2b and in D2+LG retinas.

LG Attenuates Macroglial Activation

Macroglial reactivity was analyzed using GFAP immunolabeling of retinas of the D2 and D2+LG groups. GFAP immunopositive astrocytes in D2 retinas displayed a typical reactive phenotype with slightly hypertrophic and poorly organized branching. In addition, a prominent presence of GFAP immunopositive profiles with a punctate appearance was evident among astrocytic processes (**Figure 5A**). In contrast, astrocytes in D2+LG retinas displayed thinner processes and a more organized arborization, with more sporadic and less evident GFAP immunopositive profiles among astrocytic processes (**Figure 5B**). Interestingly, the z-stack projection of the analyzed areas in the D2 retinas revealed that the GFAP immunopositive puncta corresponded to vertically oriented processes spanning the thickness of the retina and reminding the typical pattern of activated Müller cells (**Figure 5C**). As expected, these processes were less evident in D2+LG retinas (**Figure 5D**). Accordingly, the levels of GFAP
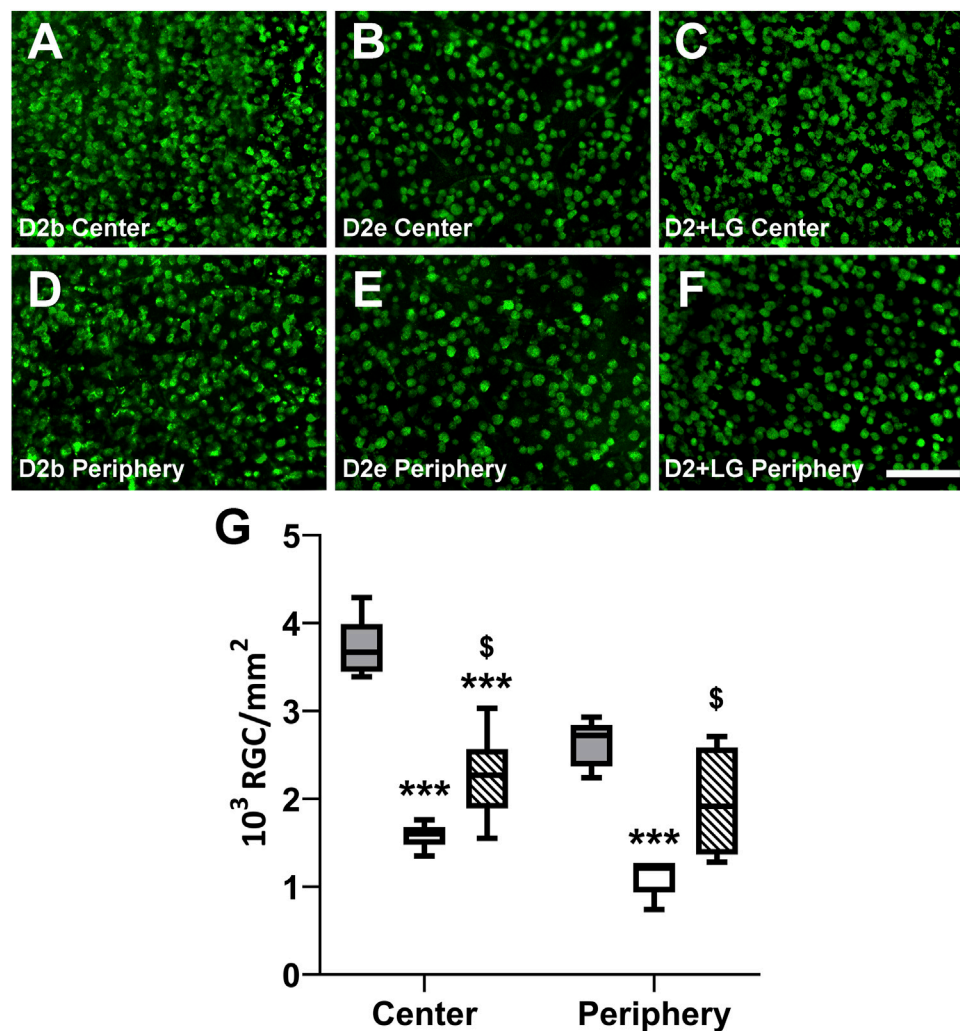
FIGURE 4 | Baseline and endpoint densitometric analysis of RBPMS-immunostained RGCs in whole mount retinas. Immunofluorescence photomicrographs show representative RBPMS immunostaining in central and peripheral areas of D2b, **(A,D)**, D2e **(B,E)** and D2+LG **(C,F)** retinas. Scale bar, 100 μm. **(G)** analysis of RBPMS positive cell density in D2b (gray boxes), D2e (white boxes), and D2+LG (dashed boxes) retinas. Box plots describe the statistical distribution of $n = 4$ independent retinas. Data were analyzed using two-way ANOVA with Bonferroni *post-hoc* test. *$p < 0.05$ vs D2.

immunostaining in the D2+LG retinas were significantly lower than those in D2 retinas both in central and in peripheral retinal regions (**Figure 6A**). In addition, the RBPMS immunopositive cell densities negatively correlated with the GFAP immunofluorescence levels (center, $p = 0.0005$; periphery, $p = 0.05$; **Figure 6B**) and the ratio between the two parameters was increased in D2+LG retinas as compared to D2 retinas ($p < 0.0001$; **Figure 6C**).

Characterization of LG Components and Their Detection in the Retina

The characterization of the main LG components has been provided in previous papers (Longo et al., 2007; La Marca et al., 2013; Lucchesi et al., 2014; Gabriele et al., 2018). Our

findings were in line with these data and indicated a series of metabolites as the main bioactive components of the LG solution used in the present studies. We choose four of them, namely gallic acid, 4-hydroxybenzoic acid, quercetin, and nicotinamide, for tracing their presence in the retina after oral LG administration. Gallic acid was the compound with the highest amount within the LG solution and, consequently, within the dose of LG administered to the mice by gavage (**Table 2**). As shown in **Figures 7A–D**, all four compounds were detected in the retina after LG administration and the variations of their concentrations in the retinal tissue were characterized by specific time courses. In particular, the maximum concentration of nicotinamide was observed after 6 h, while those of the other compounds were reached as soon as 30 min after LG
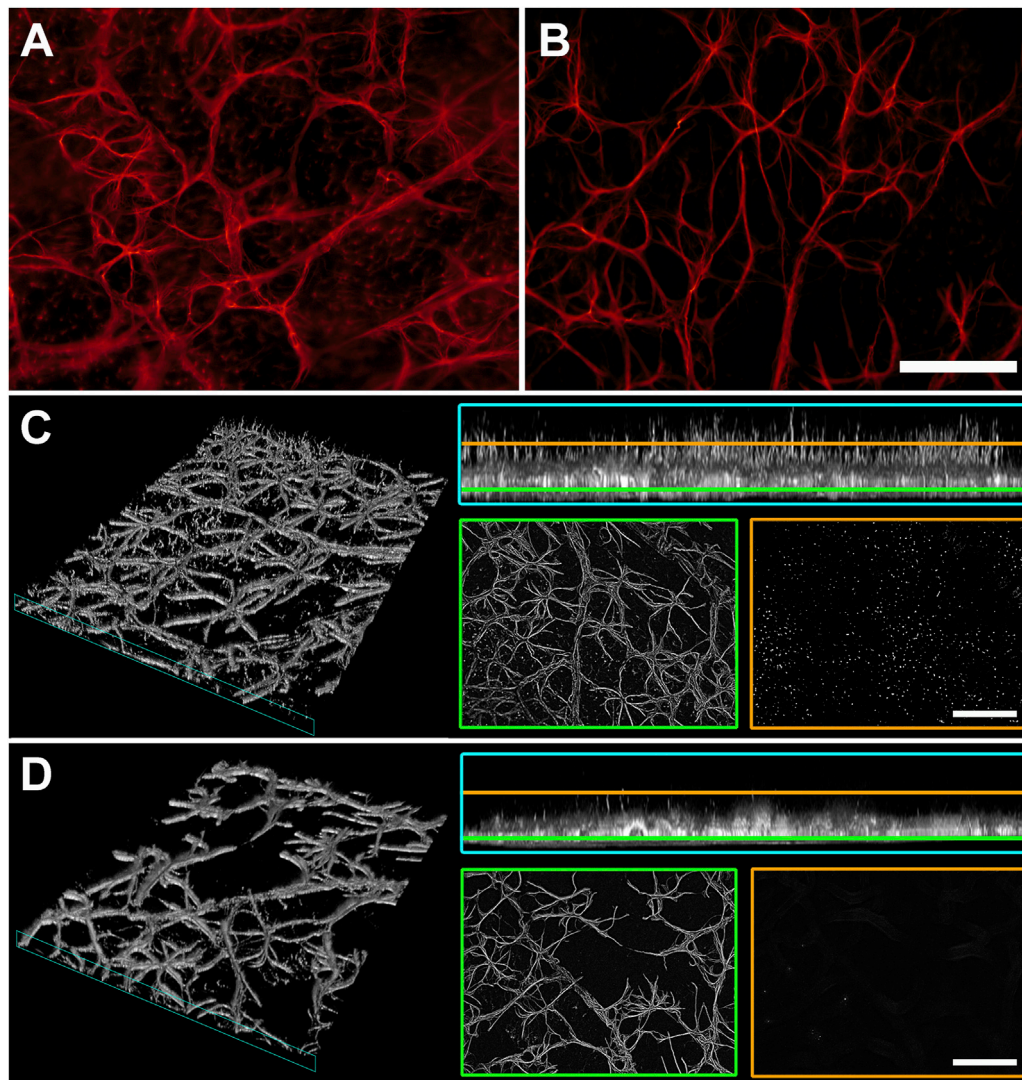
FIGURE 5 | GFAP immunostaining in whole mount retinas of D2 **(A)** and D2+LG **(B)** mice for the evaluation of macroglia activation. **(C,D)** virtual 3D reconstructions of 70 μm z-stacks of D2 and D2+LG retinas, respectively, displaying GFAP-immunopositive processes in the retinal thickness (cyan insets) and surface projections distancing 10 μm (yellow) and 45 μm (green) from the uppermost focal plan. Scale bars, 100 μm.

administration (the actual values are reported in **Table 3**). In addition, levels that were still in the range of its maximum concentration were observed for gallic acid after 24 h from LG administration (the longest time period investigated). At this time, detectable, although low, levels of nicotinamide were also measured. In contrast, quercetin levels decreased quickly within 2 h and even quicker was the decrease of the levels of 4-hydroxybenzoic acid after a large peak recorded at 30 min. Considering the ratio between the amount in the administered LG and the maximum amount recovered in the retina (**Figure 7E**), it turned out that a very high proportion (around 38%) of the 4-hydroxybenzoic acid administered with LG could reach the retina, while only 0.01% of the ingested gallic acid could be recovered. The other values

were, on average, 5.55% for quercetin and 8.76% for nicotinamide.

DISCUSSION

The present research strongly suggests that the administration of a dietary supplement may reduce significantly the pathologic changes associated to glaucoma and ameliorate visual function. Many substances of natural origin have been tested for their protective roles against glaucoma progression, although studies at the clinical level have not confirmed these potential benefits for the human pathology yet (Hernández-Rabaza et al., 2019; Adornetto et al., 2020). Nevertheless, nutritional supplements with antioxidant, anti-

FIGURE 6 | (A) densitometric analysis of GFAP immunostaining in central and peripheral areas of D2 (white box) and D2+LG (dashed boxes). **(B)** correlation of GFAP immunofluorescence levels with the correspondent RGC density per optical filed in central and peripheral retinal areas. **(C)** ratio between GFAP immunostaining and RGC density in central and peripheral retinal areas of D2 (white box) and D2+LG (dashed boxes) mice. Box plots describe the statistical distribution of $n = 4$ independent retinas. Data were analyzed using two-way ANOVA with Bonferroni *post-hoc* test. **$p < 0.01$, ***$p < 0.001$.

inflammatory, and/or neuroprotective features still promise important advancements when their properties are better investigated at the clinical level and their bioavailability is improved. In particular, the maintenance of RGC function, as evaluated with PERG analysis, together with the prevention of RGC loss, indicate a dual effect of neuroenhancement and neuroprotection exerted by LG in glaucoma.

The Potential of LG for the Treatment of Retinal Diseases

In the present work, a specific nutraceutical, LG, was investigated. From the results, we can infer that it provides significant neuroenhancement and neuroprotection against the structural and functional retinal damage induced by glaucoma and that at least some of its components reach the retina after oral administration. We have recently tested the effectiveness of LG in protecting the retina in an experimental model of diabetic retinopathy and we found that it could inhibit oxidative stress, apoptosis, and vascular endothelial growth factor expression. At the same time, it also prevented blood-retinal barrier damage, reduced the levels of inflammatory markers and partially restored visual function (Amato et al., 2018). This wide range of positive effects could be explained with the powerful antioxidant effects of LG, assuming that most, if not all, pathologic changes in the diabetic retina are induced by an initial phase of oxidative stress [see (Rossino and Casini, 2019; Rossino et al., 2019) for discussion]. A similar interpretation may be proposed to explain the protective effects of LG in glaucoma. Indeed, although IOP elevation is known as one of the most recurrent risk factors for glaucoma (Nickells et al., 2012) and is the main target of pharmaceutical treatments (Stein et al., 2021), often it could manifest only at late stages of the disease or may not occur, as in the case of normotensive glaucoma (Weinreb et al., 2014). Similar to diabetic

retinopathy, oxidative stress is likely to represent a major trigger also for glaucoma (Domènech and Marfany, 2020; Garcia-Medina et al., 2020; Harada et al., 2020; Wang et al., 2020), and LG, which does not have any effect on the rise of IOP characteristic of D2 mice, is likely to exert its protective effect thanks to its powerful antioxidant properties.

The antioxidant effects of LG may be due to direct radical scavenging and/or strengthening of antioxidant defenses through the activation of Nrf2 and the expression of antioxidant enzymes (La Marca et al., 2013). Similar to our previous findings in a diabetic retinopathy model (Amato et al., 2018), LG treatment did not result in an increase of HO-1, SOD-2 or GCLC expression, indicating that the antioxidant effect of LG is likely to be due to its radical scavenging properties. This is in line with the observed decrease of Nrf2 mRNA: we may interpret these data assuming that radical scavenging by LG reduces the level of oxidative stress, which, in turn, determines a decrease of Nrf2 expression (and likely a decreased Nrf2 nuclear translocation, as observed in diabetic rat retinas (Amato et al., 2018)), which results in decrease of antioxidant enzyme expression.

As reported in primary rat hepatocytes (La Marca et al., 2013), in human endothelial progenitor cells (Giusti et al., 2017), and in diabetic rat retinas (Amato et al., 2018), a further effect of LG is inhibition of the nuclear translocation of nuclear factor kappa-light-chain-enhancer of activated B cells (NF-kB), an oxidant-sensitive transcription factor that regulates the expression of factors involved in inflammation. Thanks to this interaction with NF-kB and in accordance with the reported relationships between oxidative stress and inflammation (Gill et al., 2010; Lugrin et al., 2014), the reduced oxidative stress is likely to be responsible for the observed decrease of the expression of inflammatory markers and of macroglial activation (Subirada et al., 2018; Domènech and Marfany, 2020). In addition, the finding of a negative correlation, both in central and in peripheral retinal regions, between RGC density and macroglial activation (evaluated with mean GFAP immunofluorescence levels) supports a tight relationship between intensity of the
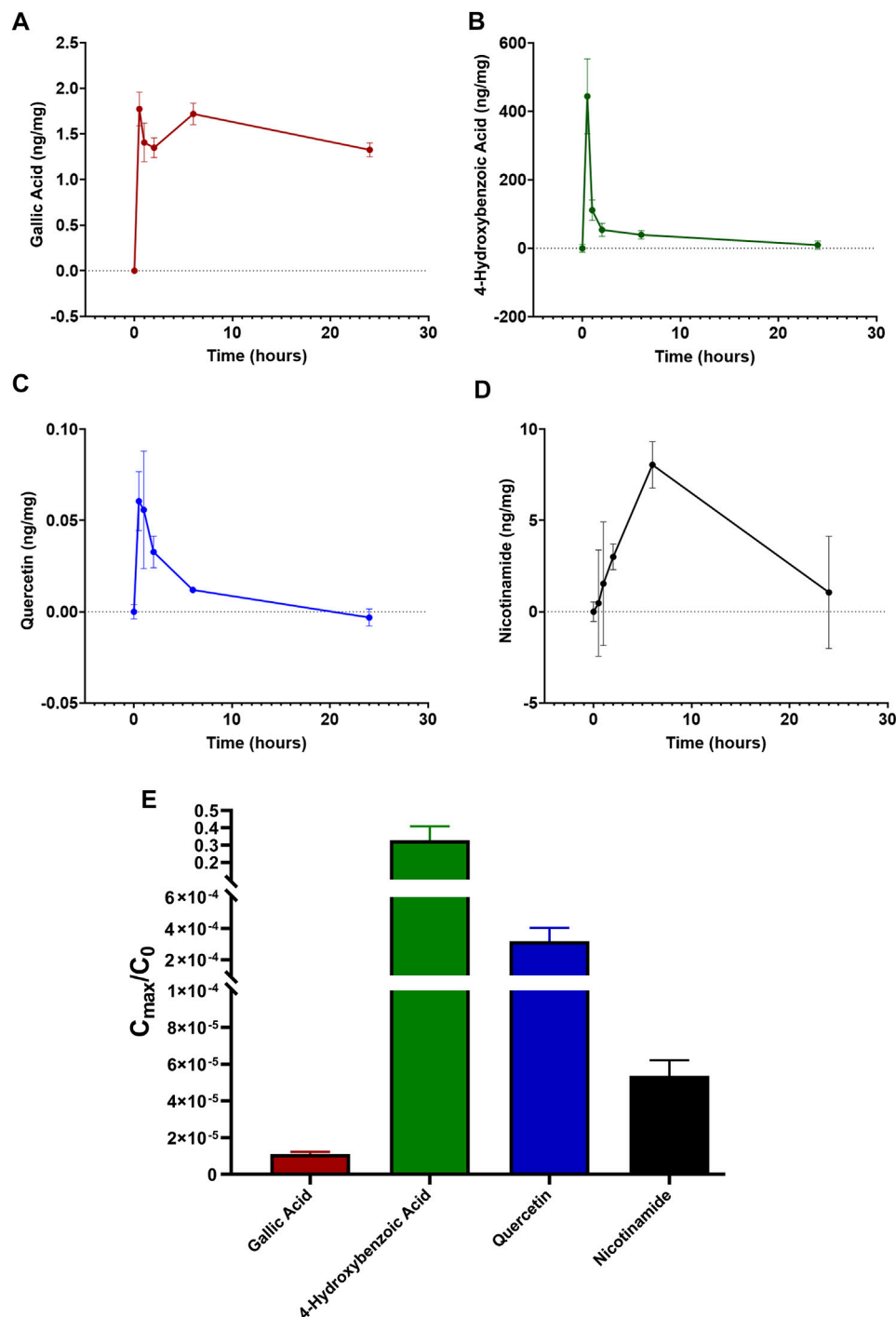
FIGURE 7 | Time-dependent retinal profile of gallic acid **(A)**, 4-hydroxybenzoic acid **(B)**, quercetin **(C)**, and nicotinamide **(D)** amount after administration of 1 mg LG by oral gavage. **(E)** corresponding ratios calculated as the maximal amount of each compound reaching the retina (C_{max}) divided by the initial amount of the same compound administered in 1 mg of LG (C_0). Data are expressed as mean ± SEM of n = 3 independent samples.

inflammatory response and the rate of RGC loss. Therefore, the more favorable conditions in D2+LG retinas compared to those in D2 retinas, with lower levels of both oxidative stress and inflammation, would support RGC survival and maintenance of retinal function. In particular, our results indicate that a large proportion of RGCs is lost

during the 2 mo of the experiments, probably due to the dramatic increase in IOP levels in the same period. The treatment with LG saves a significant portion of these RGCs, and this is particularly relevant in peripheral retina, where LG treatment results in virtually complete rescue of the RGCs. According to these observations, both

TABLE 3 | Pharmacokinetic parameters of the selected compounds in the retina.

Compound	C_{max} (ng/mg*)	T_{max} (h)	AUC_{0-24h} (ng·h/mg*)
Gallic acid	1.770 ± 0.184	0.5	36.150 ± 2.284
Hydroxy benzoic acid	444.250 ± 109.713	0.5	958.500 ± 291.500
Quercetin	0.061 ± 0.016	0.5	0.263 ± 0.049
Nicotinamide	8.040 ± 1.274	6	106.900 ± 52.210

C_{max}, maximum concentration; T_{max}, time of C_{max}; AUC_{0-24h}, area under the concentration versus time curve from 0 to 24 h; *mg of retinal tissue (wet weight).

preclinical and clinical studies have reported RGC loss and PERG defects in glaucomatous retinas, which were protected by antioxidant treatments obtained with nutritional supplements (Parisi et al., 2014; Cammalleri et al., 2020; Himori et al., 2021; Oddone et al., 2021).

Together, these observations strongly indicate LG as a basis for the potential treatment of a variety of retinal pathologies, also considering that the use of LG on human subjects is facilitated by the fact that it has been recognized and registered by the Italian Ministry of Health as a nutritional supplement.

LG Components Reaching the Retina After Oral Administration

The characterization of LG components has been provided in different papers (Longo et al., 2007; La Marca et al., 2013; Lucchesi et al., 2014; Gabriele et al., 2018). In general, a fermentation process induces the production or extraction of bioactive compounds from several natural sources. In particular, in the preparation of LG it determines an increase in both polyphenol content and antioxidant capacity. Indeed, the fermentative process not only decreases anti-nutrients, improves protein digestibility, and reduces allergenicity, but also provides a higher content of bioactive compounds and antioxidant activity (Gabriele and Pucci, 2017). The compounds whose levels are mostly increased in LG after fermentation are gallic acid, linolenic acid, linoleic acid, and lipoic acid (La Marca et al., 2013; Gabriele et al., 2018). Of them, gallic acid is likely to be the most abundant metabolite in the hydrophilic fraction that we used in our experiments, while other highly present components were 4-hydroxybenzoic acid, quercetin, and nicotinamide.

Bioavailability is a pharmacokinetic term referring to the fraction of bioactive compound that reaches the blood circulation without undergoing alterations. In general, ingested natural substances of vegetal origin are subjected to profound alteration of their structure due to digestive processes in the gastrointestinal tract and hepatic metabolism and only a small fraction of them can finally reach the various tissues of the body, therefore investigations to improve this aspect are of fundamental importance [see (Rossino and Casini, 2019) for review]. We have evaluated the fraction of LG metabolites that reach the retina since this is the most valuable information for further studies on LG metabolites to increase their retinal content and improve their efficacy. Interestingly, our data show very different behaviors for some of the metabolites that were analyzed: although the retinal concentration of gallic acid remained

stable for 24 h post administration, the fraction of this metabolite reaching the retina was minimal, while 4-hydroxybenzoic acid could reach the retina in relatively high amounts, but its levels were drastically decreased after only 1 h from ingestion. These differences are likely to depend on the size, chemical structure and lipophilicity of the compound (Del Amo et al., 2017) and constitute important factors to consider in designing drug delivery methods to improve retinal availability.

Protective Actions of LG Components in Glaucoma

As noted above, LG is made of several different components, therefore the possibility exists that the effects of LG reported in this investigation may derive, at least in part, from components that are different from those analyzed here in detail, although they are likely to be present only in low amounts in the hydrophilic LG fraction used in our studies. For instance, fatty acids like linoleic and linolenic acids, as well as α-lipoic acid and vitamins have been identified in LG and they have been postulated to mediate antioxidant effects of LG in primary rat hepatocytes (La Marca et al., 2013). In any case, while considering this, we favor the idea that the effects of LG observed in the present study are due to the components that are present in highest amounts in the hydrophilic fraction, which include gallic acid, quercetin, 4-hydroxybenzoic acid, and nicotinamide.

Gallic acid is a phenolic acid known as a potent antioxidant molecule and a neuroprotectant (Daglia et al., 2014), while 4-hydroxybenzoic acid is one of the phenolic derivatives of benzoic acid, which are known for their antioxidant properties (Beata and Ivan, 2012). It is only slightly soluble in water, which may explain the relatively low amount of this compound, with respect to gallic acid, in the hydrophilic fraction of LG used in our studies. It has been shown that intraocular delivery in glaucomatous rabbit eyes of pilocarpine-loaded biodegradable thermogels functionalized with gallic acid to provide antioxidant capacity results in improved total ocular antioxidant status, enhancement of the retinal antioxidant defense system, and preservation of retinal histology and ERG responses (Lai and Luo, 2015; Chou et al., 2016; 2017). Similarly, a benzoic acid derivative used in a thermogel coloaded with pilocarpine has been reported to enhance antioxidant capacity and neuroprotection in rabbit eyes with glaucoma (Luo et al., 2020).

Quercetin is a flavonol found in vegetables and fruits, and its properties as a potential beneficial treatment for diabetic retinopathy as well as for other ocular diseases have been reviewed recently (Rossino and Casini, 2019; Zhao et al., 2021). Concerning glaucoma, quercetin has been found to reduce excitotoxic damage to RGCs (Zhou et al., 2019) and to improve mitochondrial function, RGC survival, and ERG responses (Gao et al., 2017) in rat models of ocular hypertension.

Nicotinamide is a form of vitamin B3 and a precursor of nicotinamide adenine dinucleotide (NAD⁺) and nicotinamide

adenine dinucleotide phosphate, which are involved in different aspects of cellular metabolism (Amjad et al., 2021). Both clinical and experimental data suggest that NAD$^+$ supplementation may be therapeutic in neurodegenerative retinal diseases such as age-related macular degeneration and glaucoma (Kouassi Nzoughet et al., 2019; Cimaglia et al., 2020; Hui et al., 2020). Supporting these observations, findings in D2 mice reported a significant decrease of retinal NAD$^+$ levels with age, while oral administration of nicotinamide and/or gene therapy for the expression of a NAD$^+$-producing enzyme reduced mitochondrial abnormalities and protected RGCs from degeneration (Williams et al., 2017; Williams et al., 2018). In addition, a recent work also showed that a nicotinamide-rich diet may efficiently rescue RGCs and mitochondria, and preserves flicker-induced PERG adaptation in D2 mice (Chou et al., 2020).

CONCLUSION

The present study confirms and expands the notion that LG may reveal as a powerful therapeutic tool to treat glaucoma, diabetic retinopathy and, very likely, other sight-threatening retinal diseases. The data presented herein indicate that LG contains different metabolites with documented anti-glaucoma properties. Together with other metabolites, their co-occurrence in LG may provide an added value to their beneficial effects in glaucoma and other retinal diseases. A limitation of the present study could be the characterization of the LG components in the retina that needs to be further integrated with a full pharmacokinetic analysis. Concurrently, the challenge is to increase the amount of LG metabolites that may reach the retina after oral administration, a task that we plan to tackle in the near future using nanotechnology approaches.

REFERENCES

Adornetto, A., Rombolà, L., Morrone, L. A., Nucci, C., Corasaniti, M. T., Bagetta, G., et al. (2020). Natural Products: Evidence for Neuroprotection to Be Exploited in Glaucoma. *Nutrients* 12 (10), 3158. doi:10.3390/nu12103158

Ahmadinejad, F., Geir Møller, S., Hashemzadeh-Chaleshtori, M., Bidkhori, G., and Jami, M. S. (2017). Molecular Mechanisms Behind Free Radical Scavengers Function Against Oxidative Stress. *Antioxidants* 6 (3), 51. doi:10.3390/antiox6030051

Amato, R., Rossino, M. G., Cammalleri, M., Locri, F., Pucci, L., Dal Monte, M., et al. (2018). Lisosan G Protects the Retina from Neurovascular Damage in Experimental Diabetic Retinopathy. *Nutrients* 10 (12), 1932. doi:10.3390/nu10121932

Amjad, S., Nisar, S., Bhat, A. A., Shah, A. R., Frenneaux, M. P., Fakhro, K., et al. (2021). Role of NAD+ in Regulating Cellular and Metabolic Signaling Pathways. *Mol. Metab.* 49, 101195. doi:10.1016/j.molmet.2021.101195

Baudouin, C., Kolko, M., Melik-Parsadaniantz, S., and Messmer, E. M. (2020). Inflammation in Glaucoma: From the Back to the Front of the Eye, and Beyond. *Prog. Retin. Eye Res.* 17, 100916. doi:10.1016/j.preteyeres.2020.100916

Beata, V., and Ivan, K. (2012). Antioxidant Properties of Benzoic Acid Derivatives Against Superoxide Radical. *Free Radicals Antioxid.* 2 (4), 62–67. doi:10.5530/ax.2012.4.11

DATA AVAILABILITY STATEMENT

The raw data supporting the conclusions of this article will be made available by the authors, without undue reservation.

ETHICS STATEMENT

The animal study was reviewed and approved by "Organismo preposto al benessere degli animali," University of Pisa, Italy.

AUTHOR CONTRIBUTIONS

RA, LP, and GC designed the study, RA and GC wrote the manuscript, AT and GF performed the mass spectrometry experiments, RA and MR performed the other experiments and analyzed the data. MC, MDM, and LP collaborated to data analysis and preparation of manuscript. MC, MDM, LP, and GC contributed reagents and materials. All authors approved the manuscript.

FUNDING

ACKNOWLEDGMENTS

Cammalleri, M., Dal Monte, M., Amato, R., Bagnoli, P., and Rusciano, D. (2020). A Dietary Combination of Forskolin with Homotaurine, Spearmint and B Vitamins Protects Injured Retinal Ganglion Cells in a Rodent Model of Hypertensive Glaucoma. *Nutrients* 12 (4), 1189. doi:10.3390/nu12041189

Chauhan, B., Kumar, G., Kalam, N., and Ansari, S. H. (2013). Current Concepts and Prospects of Herbal Nutraceutical: A Review. *J. Adv. Pharm. Technol. Res.* 4 (1), 4–8. doi:10.4103/2231-4040.107494

Chen, M., Muckersie, E., Forrester, J. V., and Xu, H. (2010). Immune Activation in Retinal Aging: A Gene Expression Study. *Invest. Ophthalmol. Vis. Sci.* 51 (11), 5888–5896. doi:10.1167/iovs.09-5103

Chou, S.-F., Luo, L.-J., and Lai, J.-Y. (2016). Gallic Acid Grafting Effect on Delivery Performance and Antiglaucoma Efficacy of Antioxidant-Functionalized Intracameral Pilocarpine Carriers. *Acta Biomater.* 38, 116–128. doi:10.1016/j.actbio.2016.04.035

Chou, S. F., Luo, L. J., and Lai, J. Y. (2017). In Vivo Pharmacological Evaluations of Pilocarpine-Loaded Antioxidant-Functionalized Biodegradable Thermogels in Glaucomatous Rabbits. *Sci. Rep.* 7, 42344. doi:10.1038/srep42344

Chou, T. H., Romano, G. L., Amato, R., and Porciatti, V. (2020). Nicotinamide-Rich Diet in DBA/2J Mice Preserves Retinal Ganglion Cell Metabolic Function as Assessed by PERG Adaptation to Flicker. *Nutrients* 12 (7), 1910. doi:10.3390/nu12071910

Cimaglia, G., Votruba, M., Morgan, J. E., André, H., and Williams, P. A. (2020). Potential Therapeutic Benefit of NAD(+) Supplementation for Glaucoma and

Age-Related Macular Degeneration. *Nutrients* 12 (9), 2871. doi:10.3390/nu12092871

Daglia, M., Lorenzo, A., Nabavi, S., Talas, Z., and Nabavi, S. (2014). Polyphenols: Well Beyond the Antioxidant Capacity: Gallic Acid and Related Compounds as Neuroprotective Agents: You Are what You Eat!. *Curr. Pharm. Biotechnol.* 15 (4), 362–372. doi:10.2174/1389201015014082520737

Del Amo, E. M., Rimpelä, A.-K., Heikkinen, E., Kari, O. K., Ramsay, E., Lajunen, T., et al. (2017). Pharmacokinetic Aspects of Retinal Drug Delivery. *Prog. Retin. Eye Res.* 57, 134–185. doi:10.1016/j.preteyeres.2016.12.001

Domènech, B. E., and Marfany, G. (2020). The Relevance of Oxidative Stress in the Pathogenesis and Therapy of Retinal Dystrophies. *Antioxidants* 9 (4), 347. doi:10.3390/antiox9040347

Gabriele, M., Pucci, L., Árvay, J., and Longo, V. (2018). Anti-inflammatory and Antioxidant Effect of Fermented Whole Wheat on TNFα-Stimulated HT-29 and NF-κB Signaling Pathway Activation. *J. Funct. Foods* 45, 392–400. doi:10.1016/j.jff.2018.04.029

Gabriele, M., and Pucci, L. (2017). Diet Bioactive Compounds: Implications for Oxidative Stress and Inflammation in the Vascular System. *Endocr. Metab. Immune Disord. Drug Targets* 17 (4), 264–275. doi:10.2174/1871530317666170921142055

Gao, F. J., Zhang, S. H., Xu, P., Yang, B. Q., Zhang, R., Cheng, Y., et al. (2017). Quercetin Declines Apoptosis, Ameliorates Mitochondrial Function and Improves Retinal Ganglion Cell Survival and Function in In Vivo Model of Glaucoma in Rat and Retinal Ganglion Cell Culture In Vitro. *Front. Mol. Neurosci.* 10, 285. doi:10.3389/fnmol.2017.00285

Garcia-Medina, J. J., Rubio-Velazquez, E., Lopez-Bernal, M. D., Cobo-Martinez, A., Zanon-Moreno, V., Pinazo-Duran, M. D., et al. (2020). Glaucoma and Antioxidants: Review and Update. *Antioxidants* 9 (11), 1031. doi:10.3390/antiox9111031

Gill, R., Tsung, A., and Billiar, T. (2010). Linking Oxidative Stress to Inflammation: Toll-like Receptors. *Free Radic. Biol. Med.* 48 (9), 1121–1132. doi:10.1016/j.freeradbiomed.2010.01.006

Giusti, L., Gabriele, M., Penno, G., Garofolo, M., Longo, V., Del Prato, S., et al. (2017). A Fermented Whole Grain Prevents Lipopolysaccharides-Induced Dysfunction in Human Endothelial Progenitor Cells. *Oxid. Med. Cel Longev.* 2017 (10), 1026268. doi:10.1155/2017/1026268

Gottanka, J., Kuhlmann, A., Scholz, M., Johnson, D. H., and Lu¨tjen-Drecoll, E. (2005). Pathophysiologic Changes in the Optic Nerves of Eyes with Primary Open Angle and Pseudoexfoliation Glaucoma. *Invest. Ophthalmol. Vis. Sci.* 46 (11), 4170–4181. doi:10.1167/iovs.05-0289

Harada, C., Noro, T., Kimura, A., Guo, X., Namekata, K., Nakano, T., et al. (2020). Suppression of Oxidative Stress as Potential Therapeutic Approach for Normal Tension Glaucoma. *Antioxidants* 9 (9), 874. doi:10.3390/antiox9090874

Hernández-Rabaza, V., López-Pedrajas, R., and Almansa, I. (2019). Progesterone, Lipoic Acid, and Sulforaphane as Promising Antioxidants for Retinal Diseases: A Review. *Antioxidants* 8 (3), 53. doi:10.3390/antiox8030053

Himori, N., Inoue Yanagimachi, M., Omodaka, K., Shiga, Y., Tsuda, S., Kunikata, H., et al. (2021). The Effect of Dietary Antioxidant Supplementation in Patients with Glaucoma. *Clin. Ophthalmol.* 15, 2293–2300. doi:10.2147/opth.s314288

Hui, F., Tang, J., Williams, P. A., McGuinness, M. B., Hadoux, X., Casson, R. J., et al. (2020). Improvement in Inner Retinal Function in Glaucoma with Nicotinamide (Vitamin B3) Supplementation: A Crossover Randomized Clinical Trial. *Clin. Exp. Ophthalmol.* 48 (7), 903–914. doi:10.1111/ceo.13818

Kalra, E. K. (2003). Nutraceutical-definition and Introduction. *AAPS PharmSci.* 5 (3), 27. doi:10.1208/ps050325

Kouassi Nzoughet, J., Chao de la Barca, J. M., Guehlouz, K., Leruez, S., Coulbault, L., Allouche, S., et al. (2019). Nicotinamide Deficiency in Primary Open-Angle Glaucoma. *Invest. Ophthalmol. Vis. Sci.* 60 (7), 2509–2514. doi:10.1167/iovs.19-27099

La Marca, M., Beffy, P., Pugliese, A., and Longo, V. (2013). Fermented Wheat Powder Induces the Antioxidant and Detoxifying System in Primary Rat Hepatocytes. *PLoS One* 8 (12), e83538. doi:10.1371/journal.pone.0083538

Lai, J.-Y., and Luo, L.-J. (2015). Antioxidant Gallic Acid-Functionalized Biodegradable In Situ Gelling Copolymers for Cytoprotective Antiglaucoma Drug Delivery Systems. *Biomacromolecules* 16 (9), 2950–2963. doi:10.1021/acs.biomac.5b00854

Longo, V., Chirulli, V., Gervasi, P. G., Nencioni, S., and Pellegrini, M. (2007). Lisosan G, A Powder of Grain, Does Not Interfer with the Drug Metabolizing Enzymes and Has a Protective Role on Carbon Tetrachloride-Induced Hepatotoxicity. *Biotechnol. Lett.* 29 (8), 1155–1159. doi:10.1007/s10529-007-9378-6

Lucchesi, D., Russo, R., Gabriele, M., Longo, V., Del Prato, S., Penno, G., et al. (2014). Grain and Bean Lysates Improve Function of Endothelial Progenitor Cells from Human Peripheral Blood: Involvement of the Endogenous Antioxidant Defenses. *PLoS One* 9 (10), e109298. doi:10.1371/journal.pone.0109298

Lugrin, J., Rosenblatt-Velin, N., Parapanov, R., and Liaudet, L. (2014). The Role of Oxidative Stress During Inflammatory Processes. *Biol. Chem.* 395 (2), 203–230. doi:10.1515/hsz-2013-0241

Luo, L.-J., Nguyen, D. D., and Lai, J.-Y. (2020). Benzoic Acid Derivative-Modified Chitosan-G-poly(N-Isopropylacrylamide): Methoxylation Effects and Pharmacological Treatments of Glaucoma-Related Neurodegeneration. *J. Control. Release* 317, 246–258. doi:10.1016/j.jconrel.2019.11.038

Mélik Parsadaniantz, S., Réaux-le Goazigo, A., Sapienza, A., Habas, C., and Baudouin, C. (2020). Glaucoma: A Degenerative Optic Neuropathy Related to Neuroinflammation?. *Cells* 9 (3), 535. doi:10.3390/cells9030535

Nickells, R. W., Howell, G. R., Soto, I., and John, S. W. M. (2012). Under Pressure: Cellular and Molecular Responses During Glaucoma, A Common Neurodegeneration with Axonopathy. *Annu. Rev. Neurosci.* 35, 153–179. doi:10.1146/annurev.neuro.051508.135728

Nimse, S. B., and Pal, D. (2015). Free Radicals, Natural Antioxidants, and Their Reaction Mechanisms. *RSC Adv.* 5 (35), 27986–28006. doi:10.1039/c4ra13315c

Oddone, F., Rossetti, L., Parravano, M., Sbardella, D., Coletta, M., Ziccardi, L., et al. (2021). Citicoline in Ophthalmological Neurodegenerative Disease: A Comprehensive Review. *Pharmaceuticals* 14 (3), 281. doi:10.3390/ph14030281

Parisi, V., Centofanti, M., Gandolfi, S., Marangoni, D., Rossetti, L., Tanga, L., et al. (2014). Effects of Coenzyme Q10 in Conjunction with Vitamin E on Retinal-Evoked and Cortical-Evoked Responses in Patients with Open-Angle Glaucoma. *J. Glaucoma* 23 (6), 391–404. doi:10.1097/ijg.0b013e318279b836

Porciatti, V., Chou, T. H., and Feuer, W. J. (2010). C57BL/6J, DBA/2J, and DBA/2J.Gpnmb Mice Have Different Visual Signal Processing in the Inner Retina. *Mol. Vis.* 16, 2939–2947.

Reagan-Shaw, S., Nihal, M., and Ahmad, N. (2008). Dose Translation from Animal to Human Studies Revisited. *Faseb J.* 22 (3), 659–661. doi:10.1096/fj.07-9574LSF

Reuter, S., Gupta, S. C., Chaturvedi, M. M., and Aggarwal, B. B. (2010). Oxidative Stress, Inflammation, and Cancer: How Are They Linked?. *Free Radic. Biol. Med.* 49 (11), 1603–1616. doi:10.1016/j.freeradbiomed.2010.09.006

Rodriguez, A. R., de Sevilla Müller, L. P., and Brecha, N. C. (2014). The RNA Binding Protein RBPMS Is a Selective Marker of Ganglion Cells in the Mammalian Retina. *J. Comp. Neurol.* 522 (6), 1411–1443. doi:10.1002/cne.23521

Rossino, M. G., and Casini, G. (2019). Nutraceuticals for the Treatment of Diabetic Retinopathy. *Nutrients* 11 (4), 771. doi:10.3390/nu11040771

Rossino, M. G., Dal Monte, M., and Casini, G. (2019). Relationships Between Neurodegeneration and Vascular Damage in Diabetic Retinopathy. *Front. Neurosci.* 13, 1172. doi:10.3389/fnins.2019.01172

Saleh, M., Nagaraju, M., and Porciatti, V. (2007). Longitudinal Evaluation of Retinal Ganglion Cell Function and IOP in the DBA/2J Mouse Model of Glaucoma. *Invest. Ophthalmol. Vis. Sci.* 48 (10), 4564–4572. doi:10.1167/iovs.07-0483

Schnichels, S., Paquet-Durand, F., Löscher, M., Tsai, T., Hurst, J., Joachim, S. C., et al. (2021). Retina in a Dish: Cell Cultures, Retinal Explants and Animal Models for Common Diseases of the Retina. *Prog. Retin. Eye Res.* 81 (100880), 25. doi:10.1016/j.preteyeres.2020.100880

Stein, J. D., Khawaja, A. P., and Weizer, J. S. (2021). Glaucoma in Adults-Screening, Diagnosis, and Management. *JAMA* 325 (2), 164–174. doi:10.1001/jama.2020.21899

Subirada, P. V., Paz, M. C., Ridano, M. E., Lorenc, V. E., Vaglienti, M. V., Barcelona, P. F., et al. (2018). A Journey into the Retina: Müller Glia

Commanding Survival and Death. *Eur. J. Neurosci.* 47 (12), 1429–1443. doi:10.1111/ejn.13965

Wang, M., Li, J., and Zheng, Y. (2020). The Potential Role of Nuclear Factor Erythroid 2-Related Factor 2 (Nrf2) in Glaucoma: A Review. *Med. Sci. Monit.* 26 (26), e921514. doi:10.12659/MSM.921514

Weinreb, R. N., Aung, T., and Medeiros, F. A. (2014). The Pathophysiology and Treatment of Glaucoma. *JAMA* 311 (18), 1901–1911. doi:10.1001/jama.2014.3192

Williams, P. A., Harder, J. M., Cardozo, B. H., Foxworth, N. E., and John, S. W. M. (2018). Nicotinamide Treatment Robustly Protects from Inherited Mouse Glaucoma. *Commun. Integr. Biol.* 11 (1), e1356956. doi:10.1080/19420889.2017.1356956

Williams, P. A., Harder, J. M., Foxworth, N. E., Cochran, K. E., Philip, V. M., Porciatti, V., et al. (2017). Vitamin B3 modulates Mitochondrial Vulnerability and Prevents Glaucoma in Aged Mice. *Science* 355 (6326), 756–760. doi:10.1126/science.aal0092

Zhao, L., Wang, H., and Du, X. (2021). The Therapeutic Use of Quercetin in Ophthalmology: Recent Applications. *Biomed. Pharmacother.* 137 (111371), 6. doi:10.1016/j.biopha.2021.111371

Zhou, X., Li, G., Yang, B., and Wu, J. (2019). Quercetin Enhances Inhibitory Synaptic Inputs and Reduces Excitatory Synaptic Inputs to OFF- and ON-type Retinal Ganglion Cells in a Chronic Glaucoma Rat Model. *Front. Neurosci.* 13, 672. doi:10.3389/fnins.2019.00672

Check for
updates

Collagen Mimetic Peptides Promote Corneal Epithelial Cell Regeneration

Robert O. Baratta[1], Brian J. Del Buono[1], Eric Schlumpf[1], Brian P. Ceresa[2] and
David J. Calkins[3]*

[1]Stuart Therapeutics, Stuart, FL, United States, [2]Department of Ophthalmology and Visual Sciences, University of Louisville
School of Medicine, Louisville, KY, United States, [3]Department of Ophthalmology and Visual Sciences, Vanderbilt Eye Institute,
Vanderbilt University Medical Center, Nashville, TN, United States

The cornea of the eye is at risk for injury through constant exposure to the extraocular environment. A highly collagenous structure, the cornea contains several different types distributed across multiple layers. The anterior-most layer contains non-keratinized epithelial cells that serve as a barrier to environmental, microbial, and other insults. Renewal and migration of basal epithelial cells from the limbus involve critical interactions between secreted basement membranes, composed primarily of type IV collagen, and underlying Bowman's and stromal layers, which contain primarily type I collagen. This process is challenged in many diseases and conditions that insult the ocular surface and damage underlying collagen. We investigated the capacity of a collagen mimetic peptide (CMP), representing a fraction of a single strand of the damaged triple helix human type I collagen, to promote epithelial healing following an acute corneal wound. *In vitro*, the collagen mimetic peptide promoted the realignment of collagen damaged by enzymic digestion. In an *in vivo* mouse model, topical application of a CMP-containing formulation following a 360° lamellar keratectomy targeting the corneal epithelial layer accelerated wound closure during a 24 h period, compared to vehicle. We found that the CMP increased adherence of the basal epithelium to the underlying substrate and enhanced density of epithelial cells, while reducing variability in the regenerating layer. These results suggest that CMPs may represent a novel therapeutic to heal corneal tissue by repairing underlying collagen in conditions that damage the ocular surface.

Keywords: corneal collagen damage, collagen mimetic peptides, ocular surface disease, collagen molecular activity, collagen reparative, anti-inflammation, regeneration

INTRODUCTION

Collagen plays a well-known role as a biomechanical structural support for the integrity of most tissues and organs. Collagens represent the major component of the extracellular matrix (ECM) and basement membranes, while in all connective tissues, including in the eye, collagens provide the major structural backbone. Disruption of and damage to the collagen in these structures inhibit recovery of tissues that they support.

In addition to providing biomechanical structural support, collagens serve a variety of additional functions. For example, specific cell-surface and intracellular receptors interact with collagens. Signaling by these receptors plays a key role in cellular adhesion, differentiation, growth, and other cellular activities, as well as the survival of cells both *in vivo* and *in vitro* (Vogel, 2001; Gelse et al., 2003). Collagens also are involved in the entrapment, local storage, and delivery of growth factors

and cytokines. Through these receptor interactions and storage and delivery functions, collagen plays a key role in organ development, wound healing, and tissue repair (Hay, 1981; Yamaguchi et al., 1990; Zhu et al., 1999; Schlegel et al., 2004; Chattopadhyay and Raines, 2014; Kumar et al., 2014). Likewise, damage to collagen, particularly to the triple helix domain that is found in all collagen types, including type I collagen, disrupts this "cell interaction" role (San Antonio et al., 2020).

Collagen is a primary component of the cornea of the eye, contributing some 90% of the thickness through its distribution in distinct layers (Meek, 2009). The anterior-most corneal epithelium contains non-keratinized cells that protect against a variety of insults or injuries. The renewal and migration of basal epithelial cells occur at the limbus, which is the border between the transparent cornea and the opaque sclera of the eye (Mobaraki et al., 2019). This process includes secretion of type IV collagen-based basement membrane for adherence to underlying Bowman's and stromal layers, which are primarily type I collagen, and is challenged in conditions that insult the ocular surface (reviewed in Baratta et al., 2021). Thus, the corneal epithelium and its basement membrane rely on the integrity of underlying collagen networks for immediate support and integrity.

The replacement cycle of collagen is quite slow in most tissues, including the cornea (Paik et al., 2018). We have suggested elsewhere that a tissue repair technology that could reestablish collagen fibrillar organization could restore both the biomechanical, structural role of collagen membranes and normal and healthy cell signaling (Baratta et al., 2021). A signature characteristic of collagen is a triple helical structure—a set of three polypeptide chains comprising repeating sequences of glycine-x-y triplets where x and y often (but not always) represent proline and hydroxyproline (Kadler et al., 2007). To this end, collagen mimetic peptides (CMPs) show great promise for their capacity to directly repair damaged triple helical collagen. CMPs are synthesized as fractional single strands of type I collagen and are specifically designed as fragments that intercalate into damaged and/or are partially digested triple helices, thus restoring their role in the structure and signaling (Chattopadhyay et al., 2012; Chattopadhyay et al., 2016; Chattopadhyay and Raines, 2014). For example, fragments of collagens IV, XV, and XVIII promote the growth of blood vessels and tumor cells and influence a variety of other cellular activities (Ortega and Werb, 2002). Synthesized CMPs of collagen type I specifically target areas of collagen disruption associated with skin wounds by reforming the native triple helix through intercalating into disrupted collagen (Chattopadhyay et al., 2012; Chattopadhyay et al., 2016).

Here, we test the capacity of a CMP delivered topically as an eyedrop to encourage rapid epithelial cell regrowth following an acute injury to the mouse cornea. We find that compared to a vehicle, CMP treatment accelerated the reestablishment of the epithelial layer and promoted structural adherence of the basal epithelium to the underlying anterior stroma surface. By reducing variability during regeneration, CMPs may show broad promise as therapeutics for ocular surface disease and injury.

MATERIALS AND METHODS

Collagen Mimetic Peptides

We produced a single-strand, seven-repeat ((Pro-Pro-Gly)$_7$) CMP (manufactured by Bachem, AG, Germany). This CMP does not form triple helices with itself but rather intercalates with high selectivity into damaged endogenous type I collagen as shown in both *in vitro* and *in vivo* experimental models (Chattopadhyay et al., 2012; Chattopadhyay et al., 2016; Chattopadhyay and Raines, 2014). The CMP was dissolved in phosphate buffered saline, which served as a vehicle, at concentrations of 25 and 250 nM. To demonstrate the effect of CMP treatment on collagen alignment, we coated Petri dishes with human type I collagen in sterile double distilled water at 100 µg/ml and incubated at 37°C for 2 h. These dishes were then treated with 100 U/ml collagenase at 37°C for 1.5 h, rinsed with phosphate buffered saline (PBS) to remove excess collagenase, and then exposed to either TNC buffer solution or CMP (100 µM) at 37°C for 12 h and again rinsed. Following Kivanany et al. (2018), we used differential interference contrast optics at ×60 magnification to obtain photomicrographs from multiple samples of each condition ($n = 7$), which were edge-enhanced using MATLAB (MathWorks, Natick, MA). The alignment of collagen strands was determined using MATLAB routines as previously described (Cooper et al., 2018).

Animal Model of Corneal Epithelial Wounding

All animal experiments were in accordance with and approved by the University of Louisville Institutional Animal Care and Use Committee. Adult (8–10 weeks) female C57BL6/J mice from Jackson Laboratory (Bar Harbor, ME, United States) were maintained in 12 h light/dark cycle and allowed water and standard rodent chow ad libitum. Based on the variability measured in the previous use of this model of corneal wound healing, cohort size was set at $n = 7$ (Peterson et al., 2014; Rush et al., 2016). Following precedence in this field, we chose female mice due to their generally slower corneal healing rate (Wang et al., 2012). To investigate the ability of the CMP to promote healing of the ocular surface, we damaged the corneal epithelium using our previously published technique (Peterson et al., 2014; Rush et al., 2016). Mice were anesthetized with an intraperitoneal injection of ketamine (100 mg/kg) and xylazine (8 mg/kg; Butler Schein, Dublin, OH, United States). Under surgical microscopy control, we used a 1.5 mm diameter standard corneal surgical trephine centered on the mouse eye to demarcate a symmetric 360° circular incision in one cornea only of each mouse. This corresponds to a wound exposure covering about 70% of the corneal diameter limbus to the limbus (Henriksson et al., 2009). The wound was created manually using an Algerbrush ® II with a 0.5 mm burr (Alger Company, Inc., Lago Vista, TX, United States) by removing the epithelium and epithelial basement membranes through abrasive contact with the superficial (anterior) stroma. The wound bed was copiously irrigated with a balanced saline solution to remove remnants
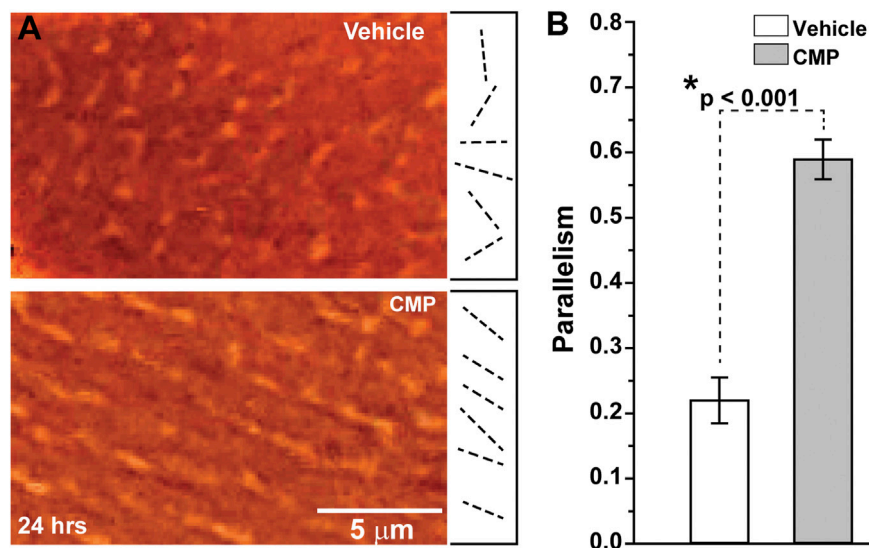
FIGURE 1 | CMP realigns collagen fibers damaged by collagenase *in vitro*. **(A)** Edge-enhanced differential interference contrast images of applied type I collagen damaged by collagenase and treated with a vehicle (top) or CMP (bottom). Example vectors (dashed lines) assigned by algorithm show a higher degree of parallelism in CMP-treated preparations. **(B)** Vectors in preparations treated with CMP have a higher average tendency for parallel alignment compared to a vehicle (*: $p < 0.001$). Data: mean ± SEM; $n = 7$.

of epithelial cells. Immediately after wounding, corneas were visualized using sterile fluorescein sodium ophthalmic strips USP (Fluorets; Chauvin Laboratory, Aubenas, France) dampened with sterile PBS and obtained photomicrographs of all eyes using a stereoscopic zoom microscope (SMZ1000, Nikon, Tokyo, Japan) equipped with a digital sight DS-Fi2 camera (Nikon). After imaging, wounded eyes were treated with a single drop (10 μl) of either PBS or CMP (25 nM or 250 nM). Based on the published work of Peterson et al. (2014) and Rush et al. (2016), the interval between 16 and 24 h offers the greatest difference between untreated wounds and wounds treated with known pro-regenerative factors. Thus, we estimated effect size based on these earlier results and imaged the cornea in anesthetized mice as described above at 16 and 24 h post-injury. The area of each wound was measured using ImageJ software.

Histology and Quantification

Following sacrifice at 24 h, enucleated eyes were placed in 4% paraformaldehyde overnight, washed, and embedded in paraffin for histological sectioning and hematoxylin and eosin (H&E) staining to visualize the regenerated corneal epithelium. From differential interference contrast micrographs, we quantified, using ImageJ, the density of stroma layers per unit area (in arbitrary units), length of junctions of complete adherence between regenerated basal epithelium and the underlying anterior stromal surface, the number of epithelial cell nuclei in the basal layer in random samples of fixed area across the cornea, and epithelial surface variability. The latter was determined by quantifying the number of nuclei in adjacent segments of a fixed area covering the wound zone and determining how the number in each segment deviated from the average for the sample.

Sections (3–4/eye) were chosen randomly through a series containing the central-most 20–30% cornea by a naïve observer. From these, 30–100 micrographs were sampled from regions of interest, depending on the measurement, by a naïve observer. Quantification of outcomes as described was conducted blindly.

Statistical Analysis

All data are presented as mean ± standard error of the mean (SEM). Statistical analyses and graphs were made using Sigma Plot Version 14 (Systat, San Jose, CA). Outlier analysis was performed using Grubbs' test (Graphpad Software, San Diego CA). Parametric statistics were performed (*t*-test, analysis of variance) if data passed normality and equal variance tests; otherwise, we performed non-parametric statistics (Mann–Whitney, ANOVA on Ranks). Statistical significance was defined as $p \leq 0.05$.

RESULTS

Collagen Mimetic Peptides Accelerate Corneal Wound Healing

When damaged by collagenase, collagen that had been coated onto plates demonstrated highly disorientated strands, as shown by differential interference contrast microscopy (**Figure 1A**, top). Treatment with a CMP following collagenase treatment appeared to promote alignment of the collagen strands in parallel orientation (**Figure 1A**, bottom), similar to collagen in endogenous tissues in the absence of injury (Hapach et al., 2015). Parallel alignment is known to promote corneal keratocyte migration *in vitro* (Kivanany et al., 2018). We
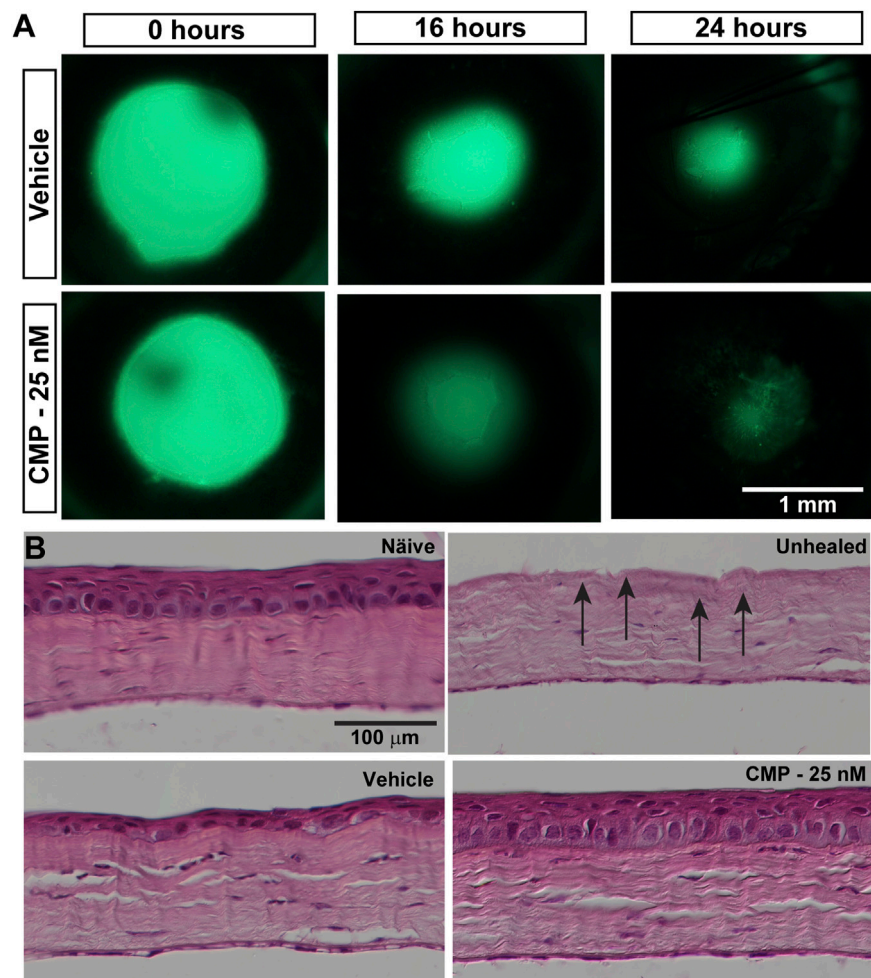
FIGURE 2 | CMP promotes healing of corneal epithelium in mice. **(A)** Representative images showing residual corneal epithelial wounds visualized by fluorescein staining *in vivo* at the time of the initial wound (0 h) and 16 and 24 h later. Treatment with CMP (25 nM shown) appeared to accelerate the regeneration of the epithelium, as seen by smaller wound areas at 16 and 24 h. **(B)** Representative differential interference contrast images of H&E-stained histological sections through naïve and wounded cornea either left unhealed (by immediate sacrifice, arrows) or treated with either a vehicle or CMP and sacrificed 24 h later.

quantified the tendency for parallel alignment following an algorithm that assigns vectors to individual collagen strands in multiple random images sampled from the preparations (Cooper et al., 2018; Kivanany et al., 2018). This algorithm then calculates the overall tendency, in which a value of 1 indicates perfect parallelism and 0 corresponds to random alignment. Treatment of collagenase-damaged collagen with CMP improved alignment three-fold compared to a vehicle ($p < 0.001$; **Figure 1B**).

Given our finding that CMP treatment can rapidly repair collagen fibrils damaged by enzymatic digestion *in vitro* and its demonstrated reparative capacity for cutaneous wounds (Chattopadhyay et al., 2016), we tested its influence on the repair of epithelial cells *in vivo* following an acute injury of the cornea in mice. After wounding, topical fluorescein defined the area of epithelial injury by penetrating the underlying exposed corneal stroma (**Figure 2A**). Initial wound size, determined by measuring this area, did not differ between vehicle- and CMP-treated eyes ($p = 0.38$). Compared to vehicle-

treated eyes, treatment with CMP (25 nM) appeared to accelerate healing early. At both 16 and 24 h following wounding, the area of residual injury appeared smaller for eyes treated with CMP compared to those treated with a vehicle (**Figure 2A**). This was not due to differences in wound depth. In post-mortem histological sections (**Figure 2B**), the density of stroma for both vehicle- and CMP-treated eyes did not differ from either naïve stroma or stroma in eyes obtained immediately following wounding without a healing period ($p = 0.15$). This indicates consistency in the depth of the wound we created to remove the epithelium and its basement membrane.

To determine whether these qualitative trends were significant, we calculated how the ratio of residual wound size changed during the 24 h experimental period. For vehicle-treated eyes, the ratio of the residual wound area at 24 h to initial size (0 h) depended significantly on the ratio of wound size at 16 h to initial ($p = 0.03$; **Figure 3A**). For CMP-treated eyes, the ratio of residual to initial wound area clustered tightly at smaller values
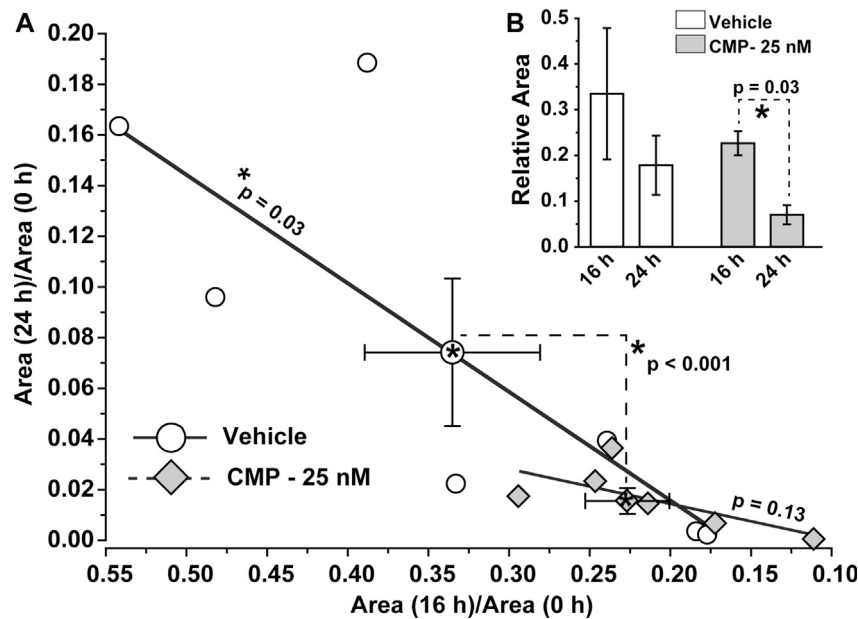
FIGURE 3 | CMP accelerates the rate of epithelium wound closure. **(A)** For vehicle-treated eyes, the ratio of residual wound area at 24 h to initial (0 h) size decreases with a diminishing ratio of the area at 16 h to initial. The slope of the best-fitting regression line differs significantly from 0 (*, $p = 0.03$). For CMP-treated eyes (25 nM), accelerated closure clusters both ratios at smaller values, yielding an insignificant regression ($p = 0.13$). The cluster of ratios for a vehicle vs. CMP cohorts differed significantly (dashed lines, $p < 0.001$), as shown by multivariable analysis of variance to compare the means (mean ± SEM) **(B**, inset). Relative wound size calculated as the ratio of residual wound area at 16 h to initial and at 24 compared to 16 h for vehicle- and CMP-treated eyes (mean ± SEM). Wound area diminished significantly between 24 and 16 h compared to the initial 16 h period for CMP eyes ($p = 0.03$) but not for a vehicle ($p = 0.10$). Importantly, initial wound size for CMP-treated eyes (1.41 ± 0.13 mm) did not differ from vehicle-treated eyes (1.54 ± 0.17 mm, $p = 0.38$; $n = 7$ for each cohort).

for both 16 and 24 h, with no dependence between the two ($p = 0.13$; **Figure 3A**). The difference between a vehicle and CMP clusters was significant ($p < 0.001$), as determined by multivariable analysis of variance with time post-injury and treatment condition as variables. Similarly, the rate of wound closure accelerated for CMP-treated eyes between 16 and 24 h. The ratio of residual size at 24 compared to 16 h was significantly smaller than 16 compared to initial wound size for CMP-treated eyes ($p = 0.03$), but not for the vehicle (**Figure 3B**). These results indicate that treatment with CMP accelerates corneal wound healing over time, beginning with smaller residual wounds by 16 h compared to initial wound size. Interestingly, wound closure for both 16 and 24 h was 15–20% slower for a higher concentration of CMP (250 nM) compared to the 25 nM concentration used in the studies shown in **Figure 2** (data not shown).

Collagen Mimetic Peptides Improve Reorganization of Regenerated Corneal Epithelium

Next, we determined how treatment with CMP influenced corneal healing at the structural level by examining histological sections through the wound region. High magnification images revealed significant histological differences between vehicle- and CMP-treated eyes (**Figure 4**). Vehicle-treated corneas demonstrated intermittent gaps between

the basal epithelium and underlying stromal surface (**Figure 4A**, left), while CMP-treated eyes demonstrated a higher degree of adherence (**Figure 4B**). This was so for both concentrations of CMP tested (**Figures 4A, B**, right). At the proliferative edge of the epithelium, the basal layer in vehicle-treated eyes appeared thinner and less organized than that in the CMP-treated ones (**Figure 4C**).

When quantified, the total length of adherence between the basal epithelium and underlying substrate decreased after wounding by 36% in vehicle-treated eyes compared to naïve corneas prepared and sectioned in the same way (**Figure 4D**). In contrast, treatment with CMP at both concentrations increased adherence to the same levels as naïve ($p \geq 0.37$). Similarly, the number of epithelial cells per unit area in the basal epithelial layer was greater for both CMP concentrations compared to a vehicle ($p \leq 0.04$) and was higher than naïve for 250 nM ($p = 0.008$; **Figure 4E**). Finally, we determined whether CMP influenced variability in the organization of the epithelial layer. We quantified the number of nuclei in adjacent segments of a fixed area for each cornea and measured how the number in each segment deviated from the average for the entire sample. By this measure (**Figure 4F**), vehicle-treated corneas demonstrated three-fold greater variability than naïve ($p < 0.001$). Treatment with 250 nM CMP reduced deviation by 54% compared to a vehicle ($p < 0.001$) but remained higher than naïve ($p = 0.04$). Treatment with 25 nM CMP improved variability but not significantly compared to a vehicle ($p = 0.10$). Thus, CMP
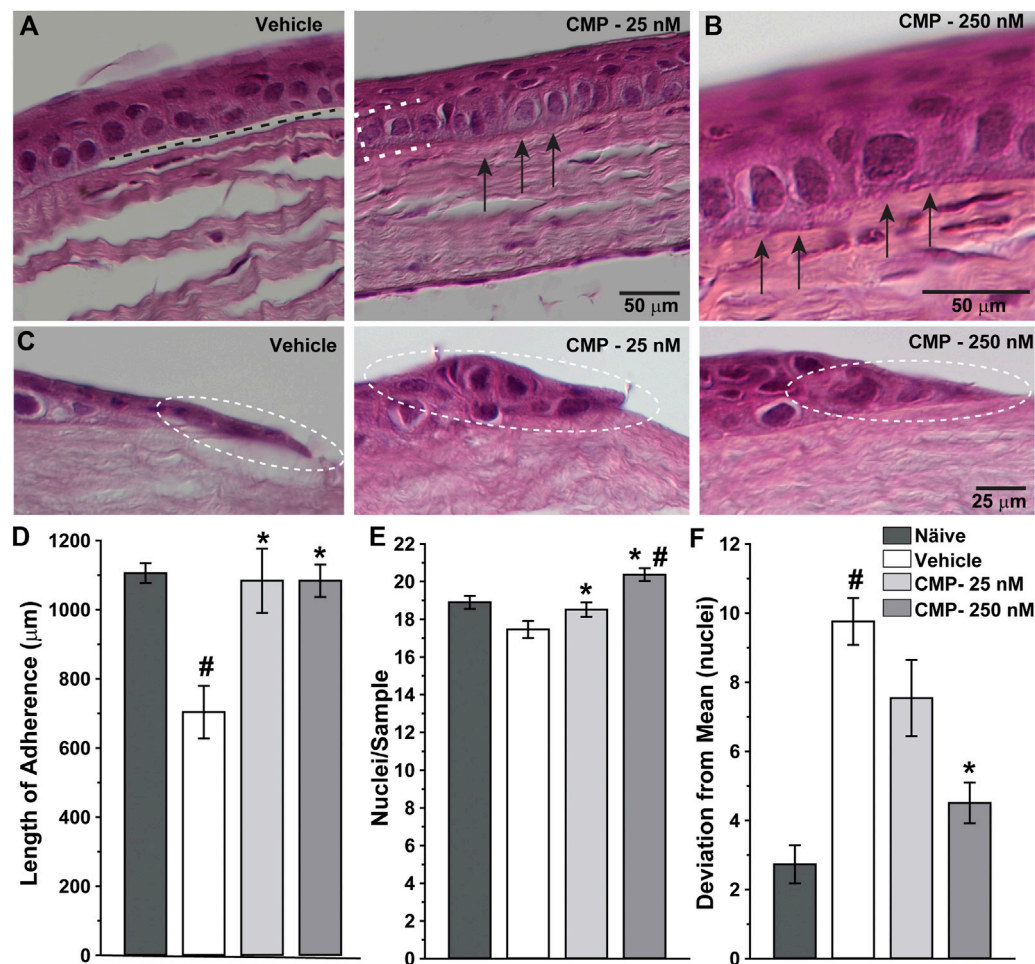
FIGURE 4 | CMP enhances the structure of healing corneal epithelium. Representative differential interference contrast images of histological sections with hematoxylin and eosin staining through regenerated epithelium (**A**, **B**) and the proliferative edge (**C**) 24 h following induced corneal injury. While vehicle-treated eyes demonstrated frequent gaps beneath the epithelium (**A**, left; dashed line), treatment with CMP enhanced adherence of the basal layer (brackets) to the underlying anterior stromal surface (arrows) for both 25 (**A**, right) and 250 nM (**B**, at higher magnification) concentrations of CMP. At the proliferative edge of the wound (**C**), compared to a vehicle, CMP increases the number of new epithelial cells adhering to the corneal stroma (circles). **(D)** Length of contiguous segments of adherence between basal epithelium and underlying stromal layer calculated from random samples of histological sections through cornea 24 h following epithelial removal ($n = 6–11$ each). Compared to naïve eyes, vehicle-treated corneas demonstrated a 36% reduction in the average length of adherent surface (#: $p < 0.001$). Treatment with CMP significantly increased adherence compared to a vehicle (*: $p \leq 0.02$), comparable to adherence in naïve corneas ($p \geq 0.37$). **(E)** The number of epithelial cell nuclei in basal layer quantified in random samples ($n = 29–100$ each). Treatment with CMP increased the number of cells per sample significantly compared to a vehicle (*: $p \leq 0.04$); the number of cells following 250 nM CMP treatment exceeded naïve (#: $p = 0.008$) **(F)**. Deviation in the number of epithelial nuclei in each random sample from (**A**) compared to the mean number for each cohort. The vehicle group was significantly more variable than naïve (#: $p < 0.001$); treatment with 250 nM CMP reduced deviation by 54% compared to a vehicle (*: $p < 0.001$) but remained higher than naïve ($p = 0.04$).

improved regeneration and organization of the basal epithelium with greater adherence of the epithelial cells to the underlying stromal surface.

DISCUSSION

The cornea is a highly collagenous structure susceptible to environmental and other insults and a number of diseases affecting the ocular surface (Eghrari et al., 2015). Our results show that CMPs have the potential as therapeutic agents to address conditions that challenge the cellular integrity of the cornea, albeit an effective treatment must demonstrate long-term benefits to vision without compromising corneal transparency. This CMP by design bypasses normal, intact collagen but anneals to and directly repairs damaged collagen (Chattopadhyay et al., 2012; Chattopadhyay et al., 2016; Chattopadhyay and Raines, 2014). Our results suggest that treatment with CMP improved the regularity of collagen *in vitro*, as shown by increased parallelism of apparent type I collagen strands damaged by collagenase and treated with CMP vs. a vehicle (**Figure 1**). While this is an indirect measure, the pattern is similar to the aligned orientation of individual collagen strands reported in previous *in vitro* studies (Hapach, et al., 2015; Kivanany et al., 2018).

Treatment with CMP also had beneficial effects *in vivo*. Topical application accelerated healing following an acute injury to the mouse eye that removed the corneal epithelium from some 70% of the corneal surface (**Figure 2**). A multivariable analysis of variance indicated a significant difference in the ratio of residual to initial wound size over time post-injury between CMP and a vehicle (**Figure 3A**). Clustering of the ratio at lower values for both 16 and 24 h suggests that CMP treatment induced a faster rate of healing, especially between 16 and 24 h (**Figure 3B**). CMP treatment also significantly enhanced adherence of the basal epithelial cell layer to the underlying substrate and resulted in a greater number of epithelial cells per unit area (**Figure 4**), including the proliferative edge of the epithelium where renewal occurs (Ljubimov and Saghizadeh, 2015; Mobaraki et al., 2019). Collagen peptides derived from fish scales similarly enhance adherence of the corneal epithelium and reduce inflammatory signaling (Subhan et al., 2017). Our CMP also increased the regularity of the epithelium, with less variability in the number of cells between adjacent samples compared to a vehicle (**Figure 4F**).

In total, our results indicate that CMP accelerates healing, presumably through its known action of intercalating into damaged collagen strands Chattopadhyay et al. (2012), presumably where the epithelial basement membrane was removed and stroma disturbed in our wound model. In most species, the collagenous substrate between the basement membrane and stroma corresponds to Bowman's layer, which is underdeveloped in mice (Wilson, 2020). Even so, the specificity of our CMP to intercalate exclusively in damaged collagen strands suggests potential utility in clinical conditions that damage the collagenous complex consisting of the basement membrane, Bowman's layer, and the stroma. In terms of the direct action of CMPs, prior work using similar CMPs demonstrates unequivocally their exclusive intercalation into and healing of fragmented collagen helices; this design underlies their efficacy in other wound models (Chattopadhyay et al., 2012; Chattopadhyay et al., 2016; Chattopadhyay and Raines, 2014). However, this action does not preclude the possibility that by intercalation, they occlude enzymic active sites, thereby reducing further degradation. Single strand forms of CMPs selectively target degraded regions of a collagen triple-helix and strongly hybridize to type I collagen fibrils (Wang et al., 2005; Li and Yu, 2013). An intact and well-organized collagen scaffold is known to be a prerequisite for regrowth of the basal epithelium, the only mitotic cells in the layer (Ljubimov and Saghizadeh, 2015). The basal epithelial cells create a basement membrane enriched in type IV collagen as they migrate from the corneal edge, a process that is challenged in many diseases and conditions (Torricelli et al., 2013). Type IV collagen, like all non-fibrillar collagen types, contains a type I domain which is a site of collagenase damage (Exposito et al., 2010). The CMP could act directly at that site through its propensity for binding to damaged type I collagen (Dones et al., 2019). Both superficial underlying stromal tissue and mid-stroma contain primarily type I collagen (Ihanamäki et al., 2004; Meek, 2009; Wilson, 2020). Thus, alternatively, or in a combined action, the CMP could repair the distressed apical surface of the stroma and, as such, providing an enhanced substrate for cell migration and ultimate restoration of homeostasis. Healthy triple helix collagen is known to be involved in promoting cellular signaling that is a hallmark of normal tissue homeostasis (San Antonio et al., 2020). Thus, CMPs could contribute to the rate and quality of corneal healing through the restoration of ligand binding that is involved in cellular signaling in healthy tissue, perhaps thereby also providing a potential secondary anti-inflammatory effect (Lebbink et al., 2006; An et al., 2016).

Similar CMPs have demonstrated efficacy not only in detecting damaged collagen Takita et al. (2018), Dones et al. (2019) but also in promoting healing of skin wounds (Chattopadhyay et al., 2016). Synthesized collagen peptides that promote tear adherence to the ocular surface also facilitate epithelium stabilization in animal models of dry eye disease (Lee et al., 2017). There are myriad clinical implications of having a therapeutic tool available to directly repair damaged collagen in ocular surface disease, especially those affecting corneal collagen (Baratta et al., 2021). These include dry eye syndrome, keratitis, corneal ulceration, laceration and melting, and recurrent corneal erosion. There are few therapeutic options for these indications, and those that are available are relatively slow acting and lack effectiveness at directly healing the structural backbone of the cornea. CMPs offer an additional potential therapeutic approach for treating a wide variety of ophthalmic indications where collagen damage is present. The potential ability of CMPs to reduce inflammation and scar formation, which can represent abnormal upregulation of collagen repair, also would be an important area for further research.

DATA AVAILABILITY STATEMENT

The original contributions presented in the study are included in the article/Supplementary Material. Further inquiries can be directed to the corresponding author.

ETHICS STATEMENT

The animal study was reviewed and approved by the University of Louisville Institutional Animal Care and Use Committee.

AUTHOR CONTRIBUTIONS

RB, BD, ES, BC, and DC designed research; BC performed research; DC analyzed data; RB and DC wrote the paper.

FUNDING

REFERENCES

An, B., Lin, Y.-S., and Brodsky, B. (2016). Collagen Interactions: Drug Design and Delivery. *Adv. Drug Deliv. Rev.* 97, 69–84. doi:10.1016/j.addr.2015.11.013

Baratta, B. O., Schlumpf, E., Del Buono, B. J., Delorey, S., and Calkins, D. J. (2021). Corneal Collagen as a Potential Therapeutic Target in Dry Eye Disease. *Surv. Ophthalmol.* S0039-6257 (21), 00104–1. in press. doi:10.1016/j.survophthal.2021.04.006

Chattopadhyay, S., and Raines, R. T. (2014). Collagen-based Biomaterials for Wound Healing. *Biopolymers* 101 (8), 821–833. doi:10.1002/bip.22486

Chattopadhyay, S., Murphy, C. J., McAnulty, J. F., and Raines, R. T. (2012). Peptides that Anneal to Natural Collagen *In Vitro* and *Ex Vivo*. *Org. Biomol. Chem.*, 10 (30), 5892–5897. doi:10.1039/c2ob25190f

Chattopadhyay, S, Guthrie, K. M., Teixeira, L., Murphy, C. J., Dubielzig, R. R., McAnulty, J. F., et al. (2016). Anchoring a Cytoactive Factor in a Wound Bed Promotes Healing. *J. Tissue Eng. Regen. Med.* 10 (12), 1012–1020. doi:10.1002/term.1886

Cooper, M. L., Pasini, S., Lambert, W. S., D'Alessandro, K. B., Yao, V., Risner, M. L., et al. (2020). Redistribution of Metabolic Resources Through Astrocyte Networks Mitigates Neurodegenerative Stress. *Proc. Natl. Acad. Sci. USA* 117 (31), 18810–18821. doi:10.1073/pnas.2009425117

Dones, J. M., Tanrikulu, I. C., Chacko, J. V., Schroeder, A. B., Hoang, T. T., Gibson, A. L. F., et al. (2019). Optimization of Interstrand Interactions Enables Burn Detection with a Collagen-Mimetic Peptide. *Org. Biomol. Chem.* 17 (46), 9906–9912. doi:10.1039/c9ob01839e

Eghrari, A. O., Riazuddin, S. A., and Gottsch, J. D. (2015). Overview of the Cornea. *Prog. Mol. Biol. Transl Sci.* 134, 7–23. doi:10.1016/bs.pmbts.2015.04.001

Exposito, J.-Y., Valcourt, U., Cluzel, C., and Lethias, C. (2010). The Fibrillar Collagen Family. *Ijms* 11 (2), 407–426. doi:10.3390/ijms11020407

Gelse, K., Pöschl, E., and Aigner, T. (2003). Collagens-structure, Function, and Biosynthesis. *Adv. Drug Deliv. Rev.* 55 (12), 1531–1546. doi:10.1016/j.addr.2003.08.002

Hapach, L. A., VanderBurgh, J. A., Miller, J. P., and Reinhart-King, C. A. (2015). Manipulation Of*in Vitro*collagen Matrix Architecture for Scaffolds of Improved Physiological Relevance. *Phys. Biol.* 12 (6), 061002. doi:10.1088/1478-3975/12/6/061002

Hay, E. D. (1981). Extracellular Matrix. *J. Cel Biol* 91 (3 Pt 2), 205s–223s. doi:10.1083/jcb.91.3.205s

Henriksson, J. T., McDermott, A. M., and Bergmanson, J. P. (2009). Dimensions and Morphology of the Cornea in Three Strains of Mice. *Invest. Ophthalmol. Vis. Sci.* 50 (8), 3648–3654. doi:10.1167/iovs.08-2941

Ihanamäki, T., Pelliniemi, L. J., and Vuorio, E. (2004). Collagens and Collagen-Related Matrix Components in the Human and Mouse Eye. *Prog. Retin. Eye Res.* 23 (4), 403–434. doi:10.1016/j.preteyeres.2004.04.002

Kadler, K. E., Baldock, C., Bella, J., and Boot-Handford, R. P. (2007). Collagens at a Glance. *J. Cel Sci* 120 (Pt 12), 1955–1958. doi:10.1242/jcs.03453

Kivanany, P., Grose, K., Yonet-Tanyeri, N., Manohar, S., Sunkara, Y., Lam, K., et al. (2018). An *In Vitro* Model for Assessing Corneal Keratocyte Spreading and Migration on Aligned Fibrillar Collagen. *Jfb* 9 (4), 54. doi:10.3390/jfb9040054

Kumar, V. A., Taylor, N. L., Jalan, A. A., Hwang, L. K., Wang, B. K., and Hartgerink, J. D. (2014). A Nanostructured Synthetic Collagen Mimic for Hemostasis. *Biomacromolecules* 15 (4), 1484–1490. doi:10.1021/bm500091e

Lebbink, R. J., de Ruiter, T., Adelmeijer, J., Brenkman, A. B., van Helvoort, J. M., Koch, M., et al. (2006). Collagens Are Functional, High Affinity Ligands for the Inhibitory Immune Receptor LAIR-1. *J. Exp. Med.* 203 (6), 1419–1425. doi:10.1084/jem.20052554

Lee, H., Kim, C. E., Ahn, B.-N., and Yang, J. (2017). Anti-Inflammatory Effect of Hydroxyproline-GQDGLAGPK in Desiccation Stress-Induced Experimental Dry Eye Mouse. *Sci. Rep.* 7 (1), 7413. doi:10.1038/s41598-017-07965-4

Li, Y., and Yu, S. M. (2013). Targeting and Mimicking Collagens via Triple Helical Peptide Assembly. *Curr. Opin. Chem. Biol.* 17 (6), 968–975. doi:10.1016/j.cbpa.2013.10.018

Ljubimov, A. V., and Saghizadeh, M. (2015). Progress in Corneal Wound Healing. *Prog. Retin. Eye Res.* 49, 17–45. doi:10.1016/j.preteyeres.2015.07.002

Meek, K. M. (2009). Corneal Collagen-Its Role in Maintaining Corneal Shape and Transparency. *Biophys. Rev.* 1 (2), 83–93. doi:10.1007/s12551-009-0011-x

Mobaraki, M., Abbasi, R., Omidian Vandchali, S., Ghaffari, M., Moztarzadeh, F., and Mozafari, M. (2019). Corneal Repair and Regeneration: Current Concepts and Future Directions. *Front. Bioeng. Biotechnol.* 7, 135. doi:10.3389/fbioe.2019.00135

Ortega, N., and Werb, Z. (2002). New Functional Roles for Non-collagenous Domains of Basement Membrane Collagens. *J. Cel Sci* 115 (Pt 22), 4201–4214. doi:10.1242/jcs.00106

Paik, D. C., Trokel, S. L., and Suh, L. H. (2018). Just What Do We Know About Corneal Collagen Turnover?. *Cornea* 37 (11), e49–e50. doi:10.1097/ICO.0000000000001685

Peterson, J. L., Phelps, E. D., Doll, M. A., Schaal, S., and Ceresa, B. P. (2014). The Role of Endogenous Epidermal Growth Factor Receptor Ligands in Mediating Corneal Epithelial Homeostasis. *Invest. Ophthalmol. Vis. Sci.* 55, 2870–2880. doi:10.1167/iovs.13-12943

Rush, J. S., Bingaman, D. P., Chaney, P. G., Wax, M. B., and Ceresa, B. P. (2016). Administration of Menadione, Vitamin K3, Ameliorates Off-Target Effects on Corneal Epithelial Wound Healing Due to Receptor Tyrosine Kinase Inhibition. *Invest. Ophthalmol. Vis. Sci.* 57 (14), 5864–5871. doi:10.1167/iovs.16-19952

San Antonio, J. D., Jacenko, O., Fertala, A., and Orgel, J. P. R. O. (2020). Collagen Structure-Function Mapping Informs Applications for Regenerative Medicine. *Bioengineering* 8 (1), 3. doi:10.3390/bioengineering8010003

Schlegel, K. A., Donath, K., Rupprecht, S., Falk, S., Zimmermann, R., Felszeghy, E., et al. (2004). De Novo bone Formation Using Bovine Collagen and Platelet-Rich Plasma. *Biomaterials* 25 (23), 5387–5393. doi:10.1016/j.biomaterials.2003.12.043

Subhan, F., Kang, H. Y., Lim, Y., Ikram, M., Baek, S. Y., Jin, S., et al. (2017). Fish Scale Collagen Peptides Protect against CoCl2/TNF-Alpha-Induced Cytotoxicity and Inflammation via Inhibition of ROS, MAPK, and NF-kappaB Pathways in HaCaT Cells. *Oxid Med. Cel Longev* 2017, 9703609. doi:10.1155/2017/9703609

Takita, K. K., Fujii, K. K., Kadonosono, T., Masuda, R., and Koide, T. (2018). Cyclic Peptides for Efficient Detection of Collagen. *Chembiochem* 19 (15), 1613–1617. doi:10.1002/cbic.201800166

Torricelli, A. A. M., Singh, V., Santhiago, M. R., and Wilson, S. E. (2013). The Corneal Epithelial Basement Membrane: Structure, Function, and Disease. *Invest. Ophthalmol. Vis. Sci.* 54 (9), 6390–6400. doi:10.1167/iovs.13-12547

Vogel, W. F. (2001). Collagen-receptor Signaling in Health and Disease. *Eur. J. Dermatol.* 11 (6), 506–514.

Wang, A. Y., Mo, X., Chen, C. S., and Yu, S. M. (2005). Facile Modification of Collagen Directed by Collagen Mimetic Peptides. *J. Am. Chem. Soc.* 127, 4130–4131. doi:10.1021/ja043191s

Wang, S. B., Hu, K. M., Seamon, K. J., Mani, V., Chen, Y., and Gronert, K. (2012). Estrogen Negatively Regulates Epithelial Wound Healing and Protective Lipid Mediator Circuits in the Cornea. *FASEB j.* 26 (4), 1506–1516. doi:10.1096/fj.11-198036

Wilson, S. E. (2020). Bowman's Layer in the Cornea- Structure and Function and Regeneration. *Exp. Eye Res.*, 195, 108033. doi:10.1016/j.exer.2020.108033

Yamaguchi, Y., Mann, D. M., and Ruoslahti, E. (1990). Negative Regulation of Transforming Growth Factor-β by the Proteoglycan Decorin. *Nature* 346, 281–284. doi:10.1038/346281a0

Zhu, Y., Oganesian, A., Keene, D. R., and Sandell, L. J. (1999). Type IIA Procollagen Containing the Cysteine-Rich Amino Propeptide Is Deposited in the Extracellular Matrix of Prechondrogenic Tissue and Binds to TGF-β1 and BMP-2. *J. Cel Biol* 144 (5), 1069–1080. doi:10.1083/jcb.144.5.1069

Check for updates

Restoring the Extracellular Matrix: A Neuroprotective Role for Collagen Mimetic Peptides in Experimental Glaucoma

Nolan R. McGrady[1], Silvia Pasini[1], Robert O. Baratta[2], Brian J. Del Buono[2], Eric Schlumpf[2] and David J. Calkins[1]*

[1]Department of Ophthalmology and Visual Sciences, Vanderbilt Eye Institute, Vanderbilt University Medical Center, Nashville, TN, United States, [2]Stuart Therapeutics, Inc., Stuart, FL, United States

Optic neuropathies are a major cause of visual disabilities worldwide, causing irreversible vision loss through the degeneration of retinal ganglion cell (RGC) axons, which comprise the optic nerve. Chief among these is glaucoma, in which sensitivity to intraocular pressure (IOP) leads to RGC axon dysfunction followed by outright degeneration of the optic projection. Current treatments focus entirely on lowering IOP through topical hypotensive drugs, surgery to facilitate aqueous fluid outflow, or both. Despite this investment in time and resources, many patients continue to lose vision, underscoring the need for new therapeutics that target neurodegeneration directly. One element of progression in glaucoma involves matrix metalloproteinase (MMP) remodeling of the collagen-rich extracellular milieu of RGC axons as they exit the retina through the optic nerve head. Thus, we investigated the ability of collagen mimetic peptides (CMPs) representing various single strand fractions of triple helix human type I collagen to protect RGC axons in an inducible model of glaucoma. First, using dorsal root ganglia maintained *in vitro* on human type I collagen, we found that multiple CMPs significantly promote neurite outgrowth (+35%) compared to vehicle following MMP-induced fragmentation of the $\alpha 1(I)$ and $\alpha 2(I)$ chains. We then applied CMP to adult mouse eyes *in vivo* following microbead occlusion to elevate IOP and determined its influence on anterograde axon transport to the superior colliculus, the primary RGC projection target in rodents. In glaucoma models, sensitivity to IOP causes early degradation in axon function, including anterograde transport from retina to central brain targets. We found that CMP treatment rescued anterograde transport following a 3-week +50% elevation in IOP. These results suggest that CMPs generally may represent a novel therapeutic to supplement existing treatments or as a neuroprotective option for patients who do not respond to IOP-lowering regimens.

Keywords: ocular collagen, collagen mimetic peptides, glaucoma, optic neuropathy, collagen reparative, extracellular matrix, neuroprotection

INTRODUCTION

Optic neuropathies are a major cause of vision loss and disability worldwide. These are collectively characterized as conditions that involve the specific degeneration of retinal ganglion cell (RGC) axons, approximately 1.5 million of which comprise the optic nerve and retinal projection to the visual brain. Glaucoma is the most common chronic optic neuropathy. Progression evolves from sensitivity to intraocular pressure (IOP), the hallmark feature of glaucoma, with age exacerbating risk. Approximately 112 million will be afflicted worldwide by 2040 (Tham et al., 2014), with annual direct costs for IOP-lowering treatments in the United States alone approaching $6 billion (Rein, 2013). Despite this investment, an estimated 40–50% of patients will still progress to irreversible vision loss due to continuing degeneration (Leske et al., 2003; Susanna et al., 2015). Since the optic projection is part of the central nervous system (CNS), it does not regenerate intrinsically (Calkins et al., 2017; Wareham et al., 2020). Thus, there is substantial need for new therapeutics that prevent or treat vision loss by directly promoting survival of RGCs and their axons independent of the etiological roots of degeneration.

Stress from sensitivity to IOP in glaucoma is conveyed at the optic nerve head, where RGC axons pass unmyelinated in exiting the retina to form the myelinated optic nerve proper. From there, RGC degeneration proceeds in both directions. A distal degenerative program includes early decline of anterograde axon transport to central brain targets, followed by disassembly of the myelinated axon in the optic nerve (Crish et al., 2010; Crish and Calkins, 2015). Correspondingly, the proximal degenerative program reduces the RGC dendritic arbor, which loses complexity as excitatory synapses are eliminated in a complement-dependent process (Williams et al., 2016; Risner et al., 2018). Importantly, RGC bodies and the unmyelinated axon segment in the retina persist until much later in progression (see Calkins, 2012), enabling both to adapt early in progression to extend axon signaling as long as possible (Calkins, 2021). This persistence lies at the root of hope for regenerative therapies to restore the distal axon projection and visual signaling to the brain (Calkins et al., 2017).

The optic nerve head is an important site of pathological changes in glaucoma for other reasons as well. In the adult CNS, the extracellular matrix (ECM) plays a critical role as a biologically active scaffold for maintaining biophysical and biomechanical stability and structure and as a mediator for the diffusion and availability of signaling molecules, such as those mediating interactions between axons and astrocytes (Barros et al., 2011). Collagen is highly abundant, and the matrix of the retina and optic nerve contain regions of highly concentrated collagen types I, III, IV, V, and VI (Morrison et al., 1988; Huang et al., 2013). This holds true for the optic nerve head as well, where collagen concentrates densely as part of the extra-axonal milieu (Sawaguchi et al., 1999). There, astrocyte glia cells form a dense lateral plexus that secretes collagen as a key element of the ECM to support RGC axon function (Hernandez, 2000). In glaucoma, disruptions in this collagen are part of remodeling of the matrix, which includes both

protease-mediated breakdown and generation or deposition of new matrix (Chintala, 2006; Wallace et al., 2014; Schneider and Fuchshofer, 2016). Similar protease-mediated collagen degradation and remodeling occurs in glaucomatous retina (Gupta et al., 2017; Hernandez et al., 1990), and elevated IOP is associated with increased levels of collagens I, IV and VI in retina and optic nerve head (Hernandez, 2000; Guo et al., 2005; Schneider and Fuchshofer, 2016). In the CNS, as the ECM and its collagen continue to remodel and neural tissue is lost, formation of a glial scar, necessary to maintain nerve tract volume, presents a physical and biochemical barrier to axon repair in disease and injury (Bradbury and Carter, 2011; Soleman et al., 2013).

Thus, in CNS disease and injury, biochemical degradation and remodeling of the ECM is viewed as a critical factor in neurodegeneration (Maguire, 2018). Therapies that rebuild or leverage the matrix hold great therapeutic potential to promote neural repair and regeneration (Ren et al., 2015; Song and Dityatev, 2018). A signature characteristic of collagen is a triple helical structure, in which individual collagen triple helices are knowns as tropocollagen (TC). This structure includes a set of three polypeptide chains comprising repeating sequences of glycine-x-y triplets, where x and y often (but not always) represent proline and hydroxyproline (Kadler et al., 2007). Collagen mimetic peptides (CMPs) show great promise for their capacity to directly repair damaged triple helical collagen. This is especially so for therapies utilizing type I collagen, which is known for its very low antigenicity, robust bioavailability, and capacity to be modified for therapeutic platforms (Hapach et al., 2015). Mimetics of type I show promise in remodeling endogenous collagen damaged in tissues ranging from cartilage to peripheral nerve (Fallas et al., 2010). Fractional single strand CMPs of type I collagen are specifically designed to intercalate into fragmented and partially digested triple helices, thus restoring reforming the native triple helix and is role in maintaining structure and signaling (Chattopadhyay et al., 2012, 2016; Chattopadhyay and Raines, 2014). Recently we demonstrated that a mimetic of type I collagen was efficacious in promoting repair and structural integrity of the corneal epithelium following an acute injury (Baratta RO. et al., 2021). Similarly, fragments of collagens IV, XV and XVIII promote the growth of blood vessels and tumor cells and influence a variety of other cellular activities (Ortega and Werb, 2002).

Given the therapeutic potential of repairing damaged collagen in the ECM and the importance of an intact ECM to CNS structure and function, we tested the capacity of CMPs to promote neurite outgrowth in culture under conditions of collagen fragmentation. We found that multiple CMPs demonstrate reparative capacity *in vitro*, enhancing both length and coverage of outgrowth from dorsal root ganglia explants. To test their therapeutic capacity *in vivo*, we found that ocular delivery of a CMP prevented functional deficits in the RGC projection to the brain following induced elevations of IOP in the most prevalent model of experimental glaucoma, microbead occlusion (Calkins et al., 2018; Calkins, 2021). Thus, CMPs may have broad therapeutic potential to protect neurons in disease or injury under duress from fragmented

FIGURE 1 | Digestion of collagen I by matrix metalloproteinase 1 (MMP-1). **(A)** SDS-PAGE electrophoresis gel shows dual bands representing reaction products for intact α1(I) and α2(I) chains of human type 1 atelocollagen (brackets). Cleavage with activated MMP-1 (60 nM) reduces both α1(I) and α2(I) while increasing their ¾ (TC^A) and ¼ (TC^B) fragments, respectively. **(B)** Level of combined full length of α1(I) and α2(I) chains reduce by 85% following MMP-1 cleavage relative to intact collagen (*, $p < 0.001$; n = 9 for each condition).

collagen in the extra-axonal milieu as is commonly seen in disease or injury.

MATERIALS AND METHODS

Collagen Digestion Protein Assay

Following Galazka et al. (1996), we activated 60 nM metalloproteinase 1 (MMP-1, Biolegend, San Diego, CA) with 2 mM 4-aminophenylmercuric acetate (APMA, Sigma, St. Louis, MO) at 37°C in TCN buffer (25 mM Tris-HCl, 10 mM CaCl2, 150 mM NaCl, pH 7.5) for 30 min as an expediency, before adding human type 1 atelocollagen (3.375 mg, 0.2 mg/ml, Advance BioMatrix, Carlsbad, CA), which is a soluble form of tropocollagen with little or no immunogenicity (Hanai et al., 2012). This mixture was incubated at 37°C for an additional 6 h (h). We measured collagen digestion with SDS-PAGE using 4–20% polyacrylamide gels (Bio-Rad Laboratories, Hercules, CA) under reducing conditions; longer incubation periods did not increase levels of digested collagen. We stained the gels with EZ-Run Protein gel staining solution for 60 min followed by multiple washes with double distilled water (DDW) and imaged the results using the Bio-Rad ChemiDoc MP imaging system under ultraviolet (UV) light (n = 9 samples per condition).

Dorsal Root Ganglia Cultures

Twelve-well culture plates were coated overnight at 37°C either with MMP-1-digested collagen as prepared above or with intact human type 1 atelocollagen, both diluted with DDW to a concentration of 100 mg/ml, followed by multiple washings with DDW to remove unbound substrate. We produced four distinct single-strand, 7-repeat, 21-residue collagen mimetic peptides (CMPs) analogous to CMPs that have been reported

to intercalate with high affinity and selectivity into damaged type I collagen *in vitro* and *in vivo* (Chattopadhyay et al., 2012, 2016; Chattopadhyay and Raines, 2014). These were manufactured in limited quantity by Bachem, AG (Germany), with the following sequences: CMP 05A (Pro-Hyp-Gly)$_7$, CMP 09C (Pro-trans-Flp-Gly)$_6$-Pro-Cys-Gly, CMP 10A (Hyp-Pro-Gly)$_7$-P, and CMP 13A (cis-Flp-Hyp-Gly)$_7$, where proline (Pro), hydroxyproline (Hyp), glycine (Gly), 4-fluoro-proline (Flp), and the undecapeptide tachykinin neuropeptide substance P (P) are abbreviated as indicated.

After washing with DDW, plates were coated either with CMP (100 μl; 100 μM) or vehicle (DDW) and incubated at 37°C for 5 h. The coating solutions were removed, and the plates washed with DDW. We aseptically dissected and cultured dorsal root ganglia (DRG) from E19 Sprague-Dawley rats (Charles River, Wilmington, MA) onto the pre-coated plates in AN$_2$ medium (n = 16–18 explants per condition). This contained Minimum Essential Media (MEM) with 10% calf bovine serum (Thermo Scientific, Waltham, MA), as well as 50 μg/ml ascorbic acid, 1.4 mM L-glutamine, and 5 ng/ml nerve growth factor (Thermo Scientific, Waltham, MA). We added 0.6% glucose and 10^{-5} M fluoro-2′-deoxyuridine (Sigma-Aldrich, St. Louis, MO) and incubated in a 5% CO$_2$ humidified incubator at 37°C. After 48 h, we prepared complete montages of each DRG explant in culture. These were collected from multi-focus stacks of high-magnification (100x) photomicrographs using phase-contrast optics and a motorized stage with autofocus set to optimize edge detection of individual neurites. Using Fiji ImageJ software (https://imagej.net/ImageJ), we measured from these montages the area of the field extending from the edge and surrounding the explant with neurite coverage and the longest neurite extending from the edge of each explant. We chose DRG explants for these initial studies since previous work has shown that intact collagen is an important substrate for DRG growth, which is quite robust in culture (Sango et al., 1993; Hari et al., 2004).

Animal Studies

Recently we found that ocular delivery of a CMP was efficacious in promoting repair of corneal collagen *in vivo* without noticeable side effects to the eye (Baratta RO. et al., 2021). Here we used this same CMP (CMP 03A, (Pro-Pro-Gly)$_7$) also manufactured by Bachem, AG (Germany) for use in our glaucoma model; an additional batch was produced for other purposes with attachment of the Tide Fluor™ 2 (AAT Bioquest, Sunnyvale, CA, United States) moiety as a fluorescent reporter. The Vanderbilt University Institutional Animal Care and Use Committee approved all experimental procedures. Following our previous publications (Sappington et al., 2010; Chen et al., 2011; Weitlauf et al., 2014; Calkins et al., 2018; Cooper et al., 2020), we used microbead occlusion to elevate intraocular pressure (IOP) unilaterally in 6 to 8-week-old C57BL/6 mice (n = 5 per cohort; Charles River Laboratory, Wilmington, MA). Briefly, for 1–2 days prior to elevation, we obtained baseline IOP measurements bilaterally in anesthetized (2.5% isoflurane) mice using TonoPen XL (Medtronic Solan, Minneapolis MN United States), which were averaged (day 0). Following these
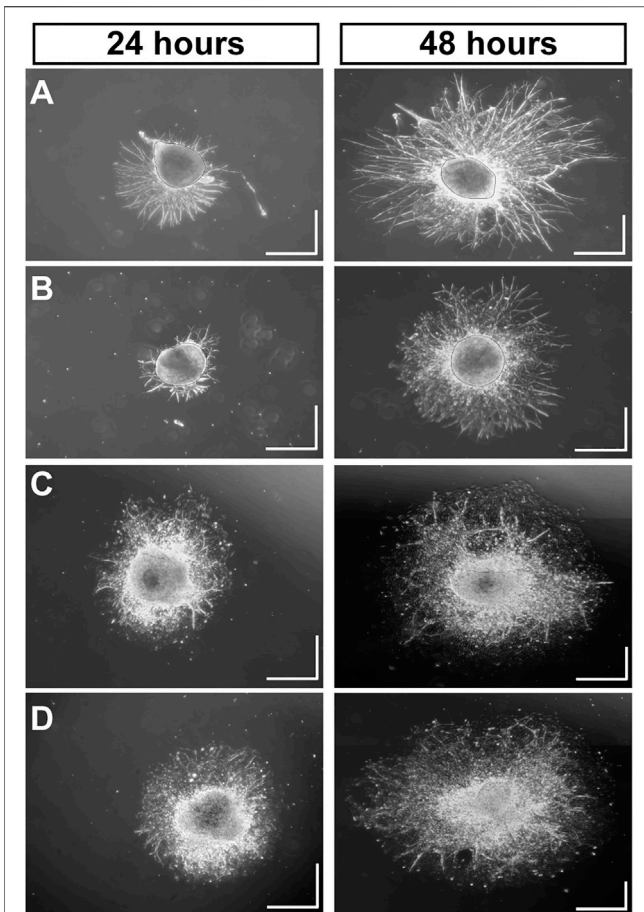
FIGURE 2 | Mimetic Peptides are Neurotrophic. Dorsal root ganglia (DRG) explants 24 and 48 h after plating on intact collagen **(A)** vs. partially digested collagen treated with vehicle **(B)**. Treatment with CMP 10A **(C)** and CMP 09C **(D)**, both at a concentration of 100 μM, increases DRG neurite outgrowth and the area of the field around the explant with neurite coverage compared to vehicle. Scale = 0.5 mm in each direction.

measurements, we elevated IOP unilaterally by injecting 1.5 μl of 15 μm polystyrene microbeads (Invitrogen, Carlsbad CA United States) into the anterior chamber; the fellow eye received an equal volume of sterile saline to serve as an internal control. We measured IOP weekly for the duration of the experiment. Both eyes received vehicle (phosphate buffered saline or PBS) or CMP (in PBS) *via* a single intravitreal injection (1.5 μl) at day 10 post-microbead injection; topical application (10 μl) gave indistinguishable results in pilot studies. During handling, mice were maintained on a 12 h light-dark cycle with standard rodent chow available *ad libitum*.

Two days prior to sacrifice, we anesthetized mice with 2.5% isoflurane and injected 1.5 μl of 1 mg/ml solution of cholera toxin subunit B (CTB) conjugated to Alexa-555 (Molecular Probes, Eugene, OR) into the vitreous body of both eyes following our established protocol for mice (Ward et al., 2014; Calkins et al., 2018; Risner et al., 2021). The mice were perfused transcardially with PBS followed by 4% paraformaldehyde and the brains dissected, and

cryoprotected in 30% sucrose. We prepared coronal midbrain sections (50 μm) using a freezing sliding microtome and photographed alternating sections of the superior colliculus using a Nikon Ti Eclipse microscope (Nikon Instruments Inc, Melville, NY). We quantified the intensity of CTB signal (intact transport) using a custom ImagePro macro (Media Cybernetics, Bethesda, MD) as previously described in several of our publications (Weitlauf et al., 2014; Lambert et al., 2019; Cooper et al., 2020; Risner et al., 2021). All animal experiments were approved by the Vanderbilt University Medical Center Institutional Animal Care and Use Committee. We did not observe overt signs of ocular inflammation, irritation, or other pathology associated with intraocular injections or treatment. consistent with our previous studies utilizing multiple injections (e.g., Cooper et al., 2020; Risner et al., 2021).

Statistical Analysis

All data are presented as mean ± standard error of the mean (SEM). Statistical analyses and graphs were made using Sigma Plot Version 14 (Systat, San Jose, CA). Outlier analysis was performed using Grubbs' test (Graphpad Software, San Diego CA). Parametric statistics were performed (*t*-test, analysis of variance) if data passed normality and equal variance tests; otherwise, we performed non-parametric statistics (Mann-Whitney, ANOVA on Ranks, Welch's test). Statistical significance was defined as $p \leq 0.05$.

RESULTS

Collagen Mimetic Peptides Enhance Neuronal Outgrowth In Vitro

SDS-PAGE electrophoresis demonstrated dual bands characteristic of type I collagen corresponding to intact α1(I) and α2(I) chains (**Figure 1A**). These denatured to their ¾ length (TC^A) and ¼ length (TC^B) fragments, respectively, following digestion with MMP-1, corresponding to cleavage roughly ¾ length away from the N terminus (Chung et al., 2004). We found that MMP-1 cleavage reduced the level of combined full length of α1(I) and α2(I) chains by 85% following relative to intact chains (*p* < 0.001; **Figure 1B**).

Using MMP-1 to cleave type I collagen as shown (**Figure 1**), we tested how degradation influences growth of neurites from DRG explants and whether CMP treatment counters the effect. After 24 h, montages of collapsed z-stacks of phase contrast micrographs of explants on intact collagen showed modest neurite outgrowth, which increased substantially by 48 h (**Figure 2A**). Plating on damaged collagen reduced the extent of outgrowth (**Figure 2B**), while explants plated on damaged collagen treated with two distinct CMPs (each at 100 μM) demonstrated improved outgrowth (**Figures 2C,D**). To measure neurite outgrowth accurately, we visualized explants live using multi-focal high-magnification phase contrast microscopy to optimize identification and
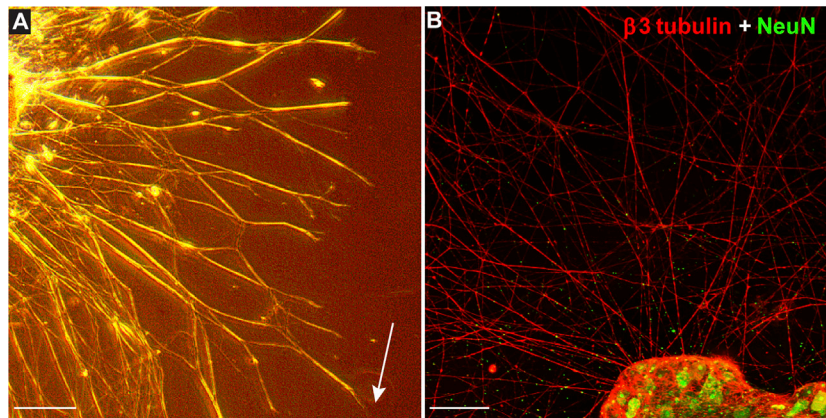
FIGURE 3 | Measuring Explant Outgrowth. **(A)** DRG explant 48 h after plating on intact collagen visualized live through multi-focal high-magnification phase contrast microscopy to optimize identification and measurement of longest neurite (arrow). Confocal micrograph of similar explant **(B)** shows neurites immune-labeled for β3-tubulin (red) extending from DRG neurons labeled against NeuN (green). Scale = 250 **(A)** or 100 **(B)** μm.
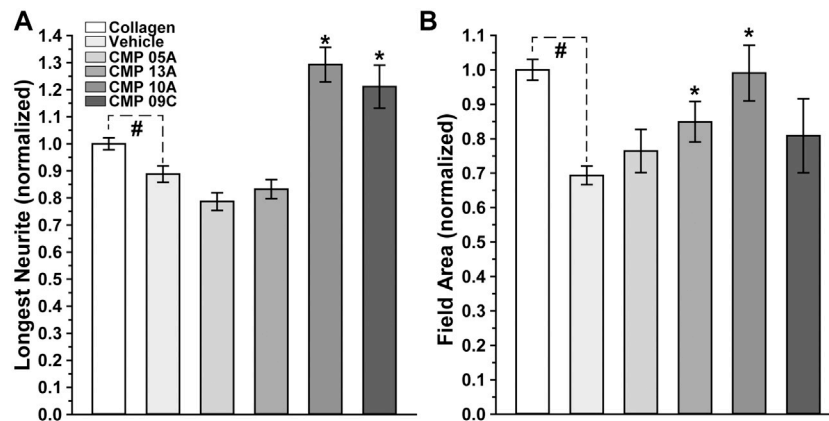
FIGURE 4 | Neurite Outgrowth Following CMP Treatment. Longest neurite outgrowth **(A)** and explant field area **(B)** at 48 h normalized to their values for intact collagen (n = 178). Explants plated on digested collagen and treated with vehicle only (n = 139) demonstrate significantly diminished neurite length ($p = 0.014$) and field area ($p < 0.001$) compared to intact collagen (#). Treatment with CMPs 10A (n-17) and 09C (n = 16) extended the longest neurites, significantly beyond even intact collagen (*, $p \leq 0.036$), while CMPs 13A (n = 17) and 10A increased field area compared to vehicle (*, $p \leq 0.03$).

measurement (**Figure 3A**). This method was preferred to post hoc measurement of neurites visualized post-fixation using antibodies against β3 tubulin (**Figure 3B**).

We quantified these trends by measuring both the longest neurite extending from each explant and the area of the field extending from and surrounding the explant with neurite coverage, both normalized to their values measured under conditions of intact collagen. Compared to intact collagen, the longest neurites of vehicle-treated explants plated on MMP-digested collagen were 15% shorter ($p = 0.014$; **Figure 4A**). In contrast, two CMPs of the four tested in this condition induced neurite outgrowth that was 29% (CMP 10A) and 21% (CMP 09C) greater than even intact collagen ($p \leq 0.036$). Similarly, vehicle-treated explants demonstrated 30% smaller field areas compared to explants on intact collagen ($p < 0.001$; **Figure 4B**). Again, two CMPs significantly improved outgrowth compared

to vehicle ($p \leq 0.03$), one of which (CMP 10A) also induced greater neurite outgrowth.

Collagen Mimetic Peptide Improves Axon Transport in Experimental Glaucoma

Our experiments with DRG explants demonstrate the reparative capacity of CMPs to promote neurite outgrowth under conditions of collagen degradation, at least *in vitro*. Recently we found that a similarly structured CMP promoted repair of corneal collagen and protection of epithelial cells *in vivo* (Baratta RO. et al., 2021). Here we used this same CMP (CMP 03A) to test whether it demonstrates a protective effect for neurons *in vivo*. To do so, we stressed the retinal ganglion cell (RGC) projection to the visual brain by elevating intraocular pressure (IOP) using microbead occlusion in mice (Sappington et al., 2010; Chen et al., 2011;
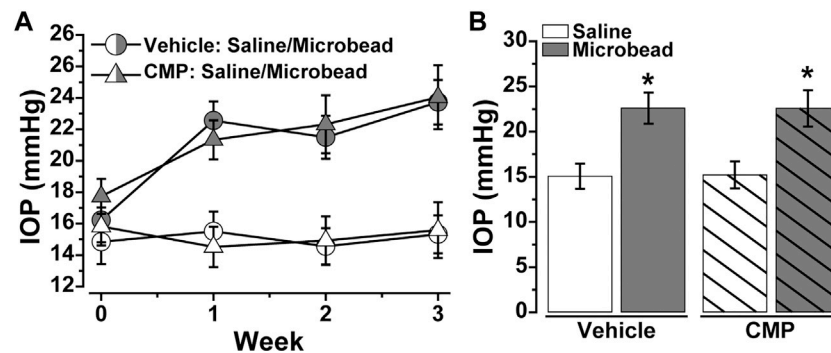
FIGURE 5 | Ocular Delivery of a Mimetic Peptide Does Not Influence IOP. **(A)** Mean intraocular pressure (IOP) in mice treated with vehicle (O) vs. CMP 03A (Δ) prior to (day 0) and following (days ≥1) a single unilateral injection of polystyrene microbeads or equivalent volume of saline; CMP or vehicle delivery *via* intravitreal injection occurred on day 10 post-microbead. **(B)** Microbead injection significantly elevated IOP for both vehicle (22.59 ± 1.72 vs. 15.06 ± 1.40 mmHg, *p* < 0.001) and CMP (22.57 ± 2.01 vs. 15.21 ± 1.49 mm Hg, *p* < 0.001). IOP did not differ between cohorts for either the saline- or microbead-injected eye (*p* ≥ 0.70). Statistics: Student's t-test (D). Data = mean ± SEM.
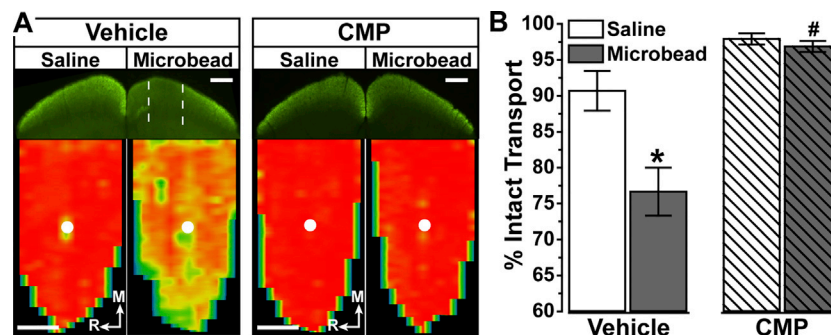
FIGURE 6 | Collagen Mimetic Peptides May Preserve Anterograde Axon Transport. **(A)**. Single sections through superior colliculus **(top)** showing regions of intact CTB transport (green) for mice receiving either vehicle (n = 5) and CMP 03A (n = 4). Colliculus serving projection from the saline-injected control eye had fully intact transport, while microbead-induced IOP elevation in the fellow eye created regions of degraded transport (dotted lines) in vehicle-treated mice. Retinotopic maps **(bottom)** reconstructed from serial sections through colliculus with optic disc indicated (white circles). Levels of intact CTB signal ranges from 0% (blue) to 50% (green) to 100% (red). Medial (M) and rostral (R) orientations are indicated. Scale = 500 µm. **(B)**. For vehicle-treated mice, intact transport significantly declined with microbead-induced elevations in IOP compared to the colliculus from saline eye (*, *p* = 0.01). Compared to vehicle, CMP-treated microbead eyes demonstrated significant enhancement of transport to the colliculus (#, *p* = 0.015). There was no difference in transport between vehicle and CMP mice for saline controls (*p* = 0.44), and transport in drug treated mice showed no difference between microbead and saline eyes (*p* = 0.16). Data = mean ± SEM.

Calkins et al., 2018). Prior to the procedure (day 0), baseline IOP for each eye did not differ between cohorts slated for vehicle vs. CMP treatment (*p* = 0.52; **Figure 5A**). Unilateral microbead injection induced a significant 40–50% elevation in IOP for both vehicle and CMP cohorts compared to the contralateral saline-injected eye that persisted through the 3-weeks experimental period (*p* < 0.001; **Figure 5B**). Ocular pressure did not differ between cohorts for either eye during this period (*p* ≥ 0.70).

Degradation of active anterograde axonal transport from retina to central brain targets is an early indicator of RGC degeneration in experimental glaucoma, both for chronic and acute models (Calkins et al., 2017; Cooper et al., 2020; Calkins, 2021). In mice with microbead-induced IOP elevations, transport deficits to the superior colliculus occur within 2–3 weeks, well before and as an antecedent to actual axonal degeneration in the optic nerve (Ward et al., 2014; Risner et al., 2018; Cooper et al.,

2020). This is an important observation since the colliculus represents the primary target for RGCs in the rodent visual system. Furthermore, experimental interventions that slow or abate transport degradation also prevent subsequent stages of degeneration (Lambert et al., 2011, 2017, 2020; Dapper et al., 2013; Bernardo-Colón et al., 2018). With this in mind, we measured whether treatment with CMP could reduce the progression of anterograde transport degradation with IOP elevation.

In vehicle-treated mice, 3 weeks of IOP elevation reduced RGC axonal transport from the retina to the colliculus, which is evident in the retinotopic spatial representation of intact CTB transport (**Figure 6A**). Intravitreal delivery of CMP appeared to protect against this degradation, as the retinotopic map of intact transport remained unchanged with elevated IOP compared to the control eye. When quantified, transport from vehicle-treated

eyes with elevated IOP diminished by 15–20% ($p = 0.01$, **Figure 6B**), consistent with recent results (Risner et al., 2018; Cooper et al., 2020). In contrast, transport from CMP-treated eyes did not change with elevated IOP and was significantly protected compared to vehicle ($p = 0.015$).

DISCUSSION

Our fundamental finding is that certain mimetics of endogenous type I collagen have reparative or even protective properties for neurons under stress. In all tissues, collagen represents an important component of the ECM, and damage to collagen slows recovery from injury or disease (Sandhu et al., 2012). Under conditions of collagen challenged by MMP digestion (**Figure 1**), multiple CMPs promoted neurite outgrowth from dorsal root ganglia (DRG) explants, both in terms of longest neurite and area outside the explant represented by neurite coverage (**Figures 2–4**). These results are consistent with early studies showing that intact collagen is an important substrate for DRG growth (Sango et al., 1993; Hari et al., 2004), while delivery of ECM protein promotes neurite outgrowth following peripheral nerve injury (Deister et al., 2007). These results are even more impressive when we consider that DRG neurons in culture can release MMPs (Kawasaki et al., 2008), creating an additional challenge to CMP treatment.

Since DRG are a component of the peripheral nervous system (Berta et al., 2017), we also tested the *in vivo* efficacy of CMP treatment in protecting axonal function of retinal ganglion cells (RGCs), which form the optic projection of the central nervous system (CNS). With stress from elevated IOP, RGC axons undergo an early period of functional degradation prior to frank degeneration, marked by deficits in anterograde transport to central brain targets (Crish et al., 2010; Calkins, 2012; Crish and Calkins, 2015; Wareham et al., 2020). We showed that intraocular delivery of CMP during a period of elevated IOP ameliorated deficits in the retinotopic representation of active transport in the superior colliculus (**Figures 5**, **6**), the primary target for RGC axons in rodents. Elevated IOP is an important risk factor for RGC degeneration and vision loss in glaucoma (Susanna et al., 2015), and slowing or stopping transport deficits in experimental models of glaucoma slows subsequent degenerative stages that occur in longer periods of microbead glaucoma, including axon degeneration followed by RGC body elimination (Lambert et al., 2011, 2017, 2020; Dapper et al., 2013). Interestingly, this same CMP (CMP 03A) promoted repair of the corneal epithelial layer following acute injury (Baratta RO. et al., 2021), thus motivating our use of it here.

In the adult CNS, ECM plays a critical role as a biologically active scaffold for maintaining biophysical stability and structure. Collagens, especially types I and IV, contribute to the matrix of the retina, optic nerve, and optic nerve head (Morrison et al., 1988; Sawaguchi et al., 1999; Huang et al., 2013). As in other tissues, collagen in these proximal structures of the optic projection is vulnerable to degradation and reorganization as matrix remodeling progresses in injury or disease. For example, following transection of monkey optic nerve, collagen type IV accumulates (Morrison et al., 1990), and levels of matrix metalloproteinases MMP3 and MMP9 increase along with tissue inhibitors of MMPs TIMP1 and TIMP2 (Agapova et al., 2003). Changes in the balance between MMP and TIMP levels are indicative of ongoing attempts at self-repair or remodeling, often with broad ramifications for axonal survival in disease or regeneration following acute trauma (Ahmed et al., 2005). In glaucoma, chronic sensitivity to IOP likely involves interplay between matrix degradation and synthesis of new matrix (Morrison et al., 1990; Wallace et al., 2014). Since similar changes in collagen content occur in optic nerve head and peripapillary sclera in glaucoma (Quigley et al., 1991), CMP treatment could ostensibly act in multiple ocular locations. Modulating MMP activity either pharmacologically or genetically reduces the chances for glial scarring and enhances the potential for RGC axon regeneration to preserve vision (Gaublomme et al., 2014; Tran et al., 2019).

We have argued earlier that a tissue repair technology that reestablishes collagen fibrillar organization could restore both biomechanical and structural functions of collagen membranes and normal and healthy cell signaling (Baratta R. O. et al., 2021), and ECM is increasingly viewed as an avenue for therapeutics (Ren et al., 2015). The results we describe here for DRG cultures and in our experimental glaucoma model support the idea that CMP treatment could accelerate repair or protect against further axonal injury through the established action of CMPs intercalating into damaged collagen strands (Chattopadhyay et al., 2012). This approach could represent a shift in how we address RGC axon degeneration. Experimental neuronal-based therapeutics for glaucoma or optic nerve trauma have relied nearly exclusively on targeting factors intrinsic to pro-apoptotic pathways, including oxidative, metabolic, inflammatory, and transcriptional stressors (Calkins, 2021). Because these pathways often involve redundant arms or are dependent on a delicate balance with other intracellular pathways, neuronal-based therapies have failed to reach the clinical ophthalmological market to any appreciable extent. Emerging preclinical approaches to retinal, optic nerve, and other CNS degeneration increasingly leverage delivery scaffolds comprising matrix-like or collagenous hydrogel (Xiong et al., 2009; Ren et al., 2015). Our approach differs fundamentally from these because it attempts not to use collagen to deliver a drug, but to directly repair endogenous collagen in the RGC axonal ECM to slow progression. The small number of CMPs tested here demonstrate modest reparative properties; we are examining whether other CMPs will show similar properties as we continue our studies with more extensive experimentation that incorporates additional outcome measures. A corollary is that this therapeutic approach could also reduce secondary inflammation that accelerates RGC degeneration in optic neuropathy that often arises with collagen degradation (Baratta R. O. et al., 2021). A simple intravitreal injection of CMP that could affect widespread repair of ECM and promote RGC survival could offer an alternative for millions suffering from optic neuropathies, both chronic and acute.

DATA AVAILABILITY STATEMENT

The raw data supporting the conclusions of this article will be made available by the authors, without undue reservation.

ETHICS STATEMENT

The animal study was reviewed and approved by the Vanderbilt University Institutional Animal Care and Use Committee.

AUTHOR CONTRIBUTIONS

RB, BDB, ES and DC designed research; NM and SP performed research and analyzed the data; RB and DC wrote the paper.

FUNDING

REFERENCES

Agapova, O. A., Kaufman, P. L., Lucarelli, M. J., Gabelt, B. T., and Hernandez, M. R. (2003). Differential Expression of Matrix Metalloproteinases in Monkey Eyes with Experimental Glaucoma or Optic Nerve Transection. *Brain Res.* 967 (1-2), 132–143. doi:10.1016/s0006-8993(02)04234-8

Ahmed, Z., Dent, R. G., Leadbeater, W. E., Smith, C., Berry, M., and Logan, A. (2005). Matrix Metalloproteases: Degradation of the Inhibitory Environment of the Transected Optic Nerve and the Scar by Regenerating Axons. *Mol. Cel Neurosci* 28 (1), 64–78. doi:10.1016/j.mcn.2004.08.013

Baratta, R. O., Schlumpf, E., Del Buono, B. J., DeLorey, S., and Calkins, D. J. (2021a). Corneal Collagen as a Potential Therapeutic Target in Dry Eye Disease. *Surv. Ophthalmol.* 2021, S0039-S6257(21)00104-111. doi:10.1016/j.survophthal.2021.04.006

Baratta, R. O., Del Buono, B. J., Schlumpf, E., Ceresa, B. P., and Calkins, D. J. (2021b). Collagen Mimetic Peptides Promote Corneal Epithelial Cell Regeneration. *Front. Pharmacol.* 12, 705623. doi:10.3389/fphar.2021.705623

Barros, C. S., Franco, S. J., and Müller, U. (2011). Extracellular Matrix: Functions in the Nervous System. *Cold Spring Harb Perspect. Biol.* 3 (1), a005108. doi:10.1101/cshperspect.a005108

Bernardo-Colón, A., Vest, V., Clark, A., Cooper, M. L., Calkins, D. J., Harrison, F. E., et al. (2018). Antioxidants Prevent Inflammation and Preserve the Optic Projection and Visual Function in Experimental Neurotrauma. *Cell Death Dis* 9 (11), 1097. doi:10.1038/s41419-018-1061-4

Berta, T., Qadri, Y., Tan, P. H., and Ji, R. R. (2017). Targeting Dorsal Root Ganglia and Primary Sensory Neurons for the Treatment of Chronic Pain. *Expert Opin. Ther. Targets* 21 (7), 695–703. doi:10.1080/14728222.2017.1328057

Bradbury, E. J., and Carter, L. M. (2011). Manipulating the Glial Scar: Chondroitinase ABC as a Therapy for Spinal Cord Injury. *Brain Res. Bull.* 84 (4-5), 306–316. doi:10.1016/j.brainresbull.2010.06.015

Calkins, D. J. (2021). Adaptive Responses to Neurodegenerative Stress in Glaucoma. *Prog. Retin. Eye Res.* 84, 100953. doi:10.1016/j.preteyeres.2021.100953

Calkins, D. J. (2012). Critical Pathogenic Events Underlying Progression of Neurodegeneration in Glaucoma. *Prog. Retin. Eye Res.* 31 (6), 702–719. doi:10.1016/j.preteyeres.2012.07.001

Calkins, D. J., Lambert, W. S., Formichella, C. R., McLaughlin, W. M., and Sappington, R. M. (2018). The Microbead Occlusion Model of Ocular Hypertension in Mice. *Methods Mol. Biol.* 1695, 23–39. doi:10.1007/978-1-4939-7407-8_3

Calkins, D. J., Pekny, M., Cooper, M. L., and Benowitz, L. (2017). The challenge of Regenerative Therapies for the Optic Nerve in Glaucoma. *Exp. Eye Res.* 157, 28–33. doi:10.1016/j.exer.2017.01.007

Chattopadhyay, S., Guthrie, K. M., Teixeira, L., Murphy, C. J., Dubielzig, R. R., McAnulty, J. F., et al. (2016). Anchoring a Cytoactive Factor in a Wound Bed Promotes Healing. *J. Tissue Eng. Regen. Med.* 10 (12), 1012–1020. doi:10.1002/term.1886

Chattopadhyay, S., Murphy, C. J., McAnulty, J. F., and Raines, R. T. (2012). Peptides that Anneal to Natural Collagen *In Vitro* and *Ex Vivo*. *Org. Biomol. Chem.* 10 (30), 5892–5897. doi:10.1039/c2ob25190f

Chattopadhyay, S., and Raines, R. T. (2014). Review Collagen-Based Biomaterials for Wound Healing. *Biopolymers* 101 (8), 821–833. doi:10.1002/bip.22486

Chen, H., Wei, X., Cho, K. S., Chen, G., Sappington, R., Calkins, D. J., et al. (2011). Optic Neuropathy Due to Microbead-Induced Elevated Intraocular Pressure in the Mouse. *Invest. Ophthalmol. Vis. Sci.* 52 (1), 36–44. doi:10.1167/iovs.09-5115

Chintala, S. K. (2006). The Emerging Role of Proteases in Retinal Ganglion Cell Death. *Exp. Eye Res.* 82 (1), 5–12. doi:10.1016/j.exer.2005.07.013

Chung, L., Dinakarpandian, D., Yoshida, N., Lauer-Fields, J. L., Fields, G. B., Visse, R., et al. (2004). Collagenase Unwinds Triple-Helical Collagen Prior to Peptide Bond Hydrolysis. *EMBO J.* 23 (15), 3020–3030. doi:10.1038/sj.emboj.7600318

Cooper, M. L., Pasini, S., Lambert, W. S., D'Alessandro, K. B., Yao, V., Risner, M. L., et al. (2020). Redistribution of Metabolic Resources through Astrocyte Networks Mitigates Neurodegenerative Stress. *Proc. Natl. Acad. Sci. U S A.* 117 (31), 18810–18821. doi:10.1073/pnas.2009425117

Crish, S. D., and Calkins, D. J. (2015). Central Visual Pathways in Glaucoma: Evidence for Distal Mechanisms of Neuronal Self-Repair. *J. Neuroophthalmol* 35 Suppl 1 (Suppl. 1), S29–S37. doi:10.1097/WNO.0000000000000291

Crish, S. D., Sappington, R. M., Inman, D. M., Horner, P. J., and Calkins, D. J. (2010). Distal Axonopathy with Structural Persistence in Glaucomatous Neurodegeneration. *Proc. Natl. Acad. Sci. U S A.* 107 (11), 5196–5201. doi:10.1073/pnas.0913141107

Dapper, J. D., Crish, S. D., Pang, I. H., and Calkins, D. J. (2013). Proximal Inhibition of P38 MAPK Stress Signaling Prevents Distal Axonopathy. *Neurobiol. Dis.* 59, 26–37. doi:10.1016/j.nbd.2013.07.001

Deister, C., Aljabari, S., and Schmidt, C. E. (2007). Effects of Collagen 1, Fibronectin, Laminin and Hyaluronic Acid Concentration in Multi-Component Gels on Neurite Extension. *J. Biomater. Sci. Polym. Ed.* 18 (8), 983–997. doi:10.1163/156856207781494377

Fallas, J. A., O'Leary, L. E., and Hartgerink, J. D. (2010). Synthetic Collagen Mimics: Self-Assembly of Homotrimers, Heterotrimers and Higher Order Structures. *Chem. Soc. Rev.* 39 (9), 3510–3527. doi:10.1039/b919455j

Galazka, G., Windsor, L. J., Birkedal-Hansen, H., and Engler, J. A. (1996). APMA (4-aminophenylmercuric Acetate) Activation of Stromelysin-1 Involves Protein Interactions in Addition to Those with Cysteine-75 in the Propeptide. *Biochemistry* 35 (34), 11221–11227. doi:10.1021/bi960618e

Gaublomme, D., Buyens, T., De Groef, L., Stakenborg, M., Janssens, E., Ingvarsen, S., et al. (2014). Matrix Metalloproteinase 2 and Membrane Type 1 Matrix Metalloproteinase Co-regulate Axonal Outgrowth of Mouse Retinal Ganglion Cells. *J. Neurochem.* 129 (6), 966–979. doi:10.1111/jnc.12703

Guo, L., Moss, S. E., Alexander, R. A., Ali, R. R., Fitzke, F. W., and Cordeiro, M. F. (2005). Retinal Ganglion Cell Apoptosis in Glaucoma Is Related to Intraocular Pressure and IOP-Induced Effects on Extracellular Matrix. *Invest. Ophthalmol. Vis. Sci.* 46 (1), 175–182. doi:10.1167/iovs.04-0832

Gupta, V., Mirzaei, M., Gupta, V. B., Chitranshi, N., Dheer, Y., Vander Wall, R., et al. (2017). Glaucoma Is Associated with Plasmin Proteolytic Activation Mediated through Oxidative Inactivation of Neuroserpin. *Sci. Rep.* 7 (1), 8412. doi:10.1038/s41598-017-08688-2

Hanai, K., Kojima, T., Ota, M., Onodera, J., and Sawada, N. (2012). Effects of Atelocollagen Formulation Containing Oligonucleotide on Endothelial Permeability. *J. Drug Deliv.* 2012, 245835. doi:10.1155/2012/245835

Hapach, L. A., VanderBurgh, J. A., Miller, J. P., and Reinhart-King, C. A. (2015). Manipulation of *In Vitro* Collagen Matrix Architecture for Scaffolds of Improved Physiological Relevance. *Phys. Biol.* 12 (6), 061002. doi:10.1088/1478-3975/12/6/061002

Hari, A., Djohar, B., Skutella, T., and Montazeri, S. (2004). Neurotrophins and Extracellular Matrix Molecules Modulate Sensory Axon Outgrowth. *Int. J. Dev. Neurosci.* 22 (2), 113–117. doi:10.1016/j.ijdevneu.2003.12.002

Hernandez, M. R., Andrzejewska, W. M., and Neufeld, A. H. (1990). Changes in the Extracellular Matrix of the Human Optic Nerve Head in Primary Open-Angle Glaucoma. *Am. J. Ophthalmol.* 109 (2), 180–188. doi:10.1016/s0002-9394(14)75984-7

Hernandez, M. R. (2000). The Optic Nerve Head in Glaucoma: Role of Astrocytes in Tissue Remodeling. *Prog. Retin. Eye Res.* 19 (3), 297–321. doi:10.1016/s1350-9462(99)00017-8

Huang, W., Fan, Q., Wang, W., Zhou, M., Laties, A. M., and Zhang, X. (2013). Collagen: a Potential Factor Involved in the Pathogenesis of Glaucoma. *Med. Sci. Monit. Basic Res.* 19, 237–240. doi:10.12659/MSMBR.889061

Kadler, K. E., Baldock, C., Bella, J., and Boot-Handford, R. P. (2007). Collagens at a Glance. *J. Cel Sci* 120 (Pt 12), 1955–1958. doi:10.1242/jcs.03453

Kawasaki, Y., Xu, Z. Z., Wang, X., Park, J. Y., Zhuang, Z. Y., Tan, P. H., et al. (2008). Distinct Roles of Matrix Metalloproteases in the Early- and Late-phase Development of Neuropathic Pain. *Nat. Med.* 14 (3), 331–336. doi:10.1038/nm1723

Lambert, W. S., Carlson, B. J., Formichella, C. R., Sappington, R. M., Ahlem, C., and Calkins, D. J. (2017). Oral Delivery of a Synthetic Sterol Reduces Axonopathy and Inflammation in a Rodent Model of Glaucoma. *Front. Neurosci.* 11, 45. doi:10.3389/fnins.2017.00045

Lambert, W. S., Carlson, B. J., Ghose, P., Vest, V. D., Yao, V., and Calkins, D. J. (2019). Towards a Microbead Occlusion Model of Glaucoma for a Non-human Primate. *Sci. Rep.* 9 (1), 11572. doi:10.1038/s41598-019-48054-y

Lambert, W. S., Pasini, S., Collyer, J. W., Formichella, C. R., Ghose, P., Carlson, B. J., et al. (2020). Of Mice and Monkeys: Neuroprotective Efficacy of the P38 Inhibitor BIRB 796 Depends on Model Duration in Experimental Glaucoma. *Sci. Rep.* 10 (1), 8535. doi:10.1038/s41598-020-65374-6

Lambert, W. S., Ruiz, L., Crish, S. D., Wheeler, L. A., and Calkins, D. J. (2011). Brimonidine Prevents Axonal and Somatic Degeneration of Retinal Ganglion Cell Neurons. *Mol. Neurodegener* 6 (1), 4. doi:10.1186/1750-1326-6-4

Leske, M. C., Heijl, A., Hussein, M., Bengtsson, B., Hyman, L., and Komaroff, E. (2003). Factors for Glaucoma Progression and the Effect of TreatmentFactors for Glaucoma Progression and the Effect of Treatment: the Early Manifest Glaucoma Trial. *Arch. Ophthalmol.* 121, 48–56. doi:10.1001/archopht.121.1.48

Maguire, G. (2018). Neurodegenerative Diseases Are a Function of Matrix Breakdown: How to Rebuild Extracellular Matrix and Intracellular Matrix. *Neural Regen. Res.* 13 (7), 1185–1186. doi:10.4103/1673-5374.235026

Morrison, J. C., Dorman-Pease, M. E., Dunkelberger, G. R., and Quigley, H. A. (1990). Optic Nerve Head Extracellular Matrix in Primary Optic Atrophy and Experimental Glaucoma. *Arch. Ophthalmol.* 108 (7), 1020–1024. doi:10.1001/archopht.1990.01070090122053

Morrison, J. C., Jerdan, J. A., L'Hernault, N. L., and Quigley, H. A. (1988). The Extracellular Matrix Composition of the Monkey Optic Nerve Head. *Invest. Ophthalmol. Vis. Sci.* 29 (7), 1141–1150.

Ortega, N., and Werb, Z. (2002). New Functional Roles for Non-collagenous Domains of Basement Membrane Collagens. *J. Cel Sci* 115 (Pt 22), 4201–4214. doi:10.1242/jcs.00106

Quigley, H. A., Dorman-Pease, M. E., and Brown, A. E. (1991). Quantitative Study of Collagen and Elastin of the Optic Nerve Head and Sclera in Human and Experimental Monkey Glaucoma. *Curr. Eye Res.* 10 (9), 877–888. doi:10.3109/02713689109013884

Rein, D. B. (2013). Vision Problems Are a Leading Source of Modifiable Health Expenditures. *Invest. Ophthalmol. Vis. Sci.* 54, ORSF18–22. doi:10.1167/iovs.13-12818

Ren, T., van der Merwe, Y., and Steketee, M. B. (2015). Developing Extracellular Matrix Technology to Treat Retinal or Optic Nerve Injury(1,2,3). *eNeuro* 2 (5), ENEURO.0077-15.2015. doi:10.1523/ENEURO.0077-15.2015

Risner, M. L., Pasini, S., Cooper, M. L., Lambert, W. S., and Calkins, D. J. (2018). Axogenic Mechanism Enhances Retinal Ganglion Cell Excitability during Early Progression in Glaucoma. *Proc. Natl. Acad. Sci. U S A.* 115 (10), E2393–E2402. doi:10.1073/pnas.1714888115

Risner, M. L., Pasini, S., McGrady, N. R., D'Alessandro, K. B., Yao, V., Cooper, M. L., et al. (2021). Neuroprotection by WldS Depends on Retinal Ganglion Cell Type and Age in Glaucoma. *Mol. Neurodegener* 16 (1), 36. doi:10.1186/s13024-021-00459-y

Sandhu, S., Gupta, S., Bansal, H., and Singla, K. (2012). Collagen in Health and Disease. *J. Orofacial Res.* 2 (3), 153–159. doi:10.5005/jp-journals-10026-1032

Sango, K., Horie, H., Inoue, S., Takamura, Y., and Takenaka, T. (1993). Age-related Changes of DRG Neuronal Attachment to Extracellular Matrix Proteins *In Vitro*. *Neuroreport* 4 (6), 663–666. doi:10.1097/00001756-199306000-00015

Sappington, R. M., Carlson, B. J., Crish, S. D., and Calkins, D. J. (2010). The Microbead Occlusion Model: a Paradigm for Induced Ocular Hypertension in Rats and Mice. *Invest. Ophthalmol. Vis. Sci.* 51 (1), 207–216. doi:10.1167/iovs.09-3947

Sawaguchi, S., Yue, B. Y., Fukuchi, T., Abe, H., Suda, K., Kaiya, T., et al. (1999). Collagen Fibrillar Network in the Optic Nerve Head of normal Monkey Eyes and Monkey Eyes with Laser-Induced Glaucoma-Aa Scanning Electron Microscopic Study. *Curr. Eye Res.* 18 (2), 143–149. doi:10.1076/ceyr.18.2.143.5385

Schneider, M., and Fuchshofer, R. (2016). The Role of Astrocytes in Optic Nerve Head Fibrosis in Glaucoma. *Exp. Eye Res.* 142, 49–55. doi:10.1016/j.exer.2015.08.014

Soleman, S., Filippov, M. A., Dityatev, A., and Fawcett, J. W. (2013). Targeting the Neural Extracellular Matrix in Neurological Disorders. *Neuroscience* 253, 194–213. doi:10.1016/j.neuroscience.2013.08.050

Song, I., and Dityatev, A. (2018). Crosstalk between Glia, Extracellular Matrix and Neurons. *Brain Res. Bull.* 136, 101–108. doi:10.1016/j.brainresbull.2017.03.003

Susanna, R., De Moraes, C. G., Cioffi, G. A., and Ritch, R. (2015). Why Do People (Still) Go Blind from Glaucoma? *Trans. Vis. Sci. Tech.* 4 (21), 1. doi:10.1167/tvst.4.2.1

Tham, Y. C., Li, X., Wong, T. Y., Quigley, H. A., Aung, T., and Cheng, C. Y. (2014). Global Prevalence of Glaucoma and Projections of Glaucoma burden through 2040: a Systematic Review and Meta-Analysis. *Ophthalmology* 121 (11), 2081–2090. doi:10.1016/j.ophtha.2014.05.013

Tran, N. M., Shekhar, K., Whitney, I. E., Jacobi, A., Benhar, I., Hong, G., et al. (2019). Single-Cell Profiles of Retinal Ganglion Cells Differing in Resilience to Injury Reveal Neuroprotective Genes. *Neuron* 104 (6), 1039–e12. doi:10.1016/j.neuron.2019.11.006

Wallace, D. M., Murphy-Ullrich, J. E., Downs, J. C., and O'Brien, C. J. (2014). The Role of Matricellular Proteins in Glaucoma. *Matrix Biol.* 37, 174–182. doi:10.1016/j.matbio.2014.03.007

Ward, N. J., Ho, K. W., Lambert, W. S., Weitlauf, C., and Calkins, D. J. (2014). Absence of Transient Receptor Potential Vanilloid-1 Accelerates Stress-Induced Axonopathy in the Optic Projection. *J. Neurosci.* 34 (9), 3161–3170. doi:10.1523/JNEUROSCI.4089-13.2014

Wareham, L. K., Risner, M. L., and Calkins, D. J. (2020). Protect, Repair, and Regenerate: towards Restoring Vision in Glaucoma. *Curr. Ophthalmol. Rep.* 8 (4), 301–310. doi:10.1007/s40135-020-00259-5

Weitlauf, C., Ward, N. J., Lambert, W. S., Sidorova, T. N., Ho, K. W., Sappington, R. M., Calkins, D. J., et al. (2014). Short-term Increases in Transient Receptor Potential Vanilloid-1 Mediate Stress-Induced Enhancement of Neuronal Excitation. *J. Neurosci.* 34 (46), 15369–15381. doi:10.1523/JNEUROSCI.3424-14.2014

Williams, P. A., Tribble, J. R., Pepper, K. W., Cross, S. D., Morgan, B. P., Morgan, J. E., et al. (2016). Inhibition of the Classical Pathway of the Complement cascade Prevents Early Dendritic and Synaptic Degeneration in Glaucoma. *Mol. Neurodegener* 11, 26. doi:10.1186/s13024-016-0091-6

Xiong, Y., Mahmood, A., and Chopp, M. (2009). Emerging Treatments for Traumatic Brain Injury. *Expert Opin. Emerg. Drugs* 14 (1), 67–84. doi:10.1517/14728210902769601

Publisher's Note: All claims expressed in this article are solely those of the authors and do not necessarily represent those of their affiliated organizations, or those of the publisher, the editors and the reviewers. Any product that may be evaluated in this article, or claim that may be made by its manufacturer, is not guaranteed or endorsed by the publisher.

Differential Mechanisms of Action and Efficacy of Vitamin E Components in Antioxidant Cytoprotection of Human Retinal Pigment Epithelium

R. Scott Duncan[1], Daniel T. Hurtado[2], Conner W. Hall[1] and Peter Koulen[1,2]*

[1]Vision Research Center, Department of Ophthalmology, School of Medicine, University of Missouri—Kansas City, Kansas City, MO, United States, [2]Department of Biomedical Sciences, School of Medicine, University of Missouri—Kansas City, Kansas City, MO, United States

The purpose of this study was to determine if different vitamin E components exhibit similar efficacy and mechanism of action in protecting Retinal pigment epithelium (RPE) cells from oxidative damage. We hypothesized that α-tocopherol (αT) is unique among vitamin E components in its cytoprotective mechanism of action against oxidative stress in RPE cells and that it requires protein synthesis for optimal antioxidant effect. We used cell viability assays, fluorescent chemical labeling of DNA and actin and immuno-labeling of the antioxidant proteins Nrf2 and Sod2 and of the tight junction protein, ZO-1, and confocal microscopy to determine the effects of αT and γT against oxidative stress in immortalized human RPE cells (hTERT-RPE). Using the four main vitamin E components, αT, γT, δ-tocopherol (δT) and α-tocotrienol (αTr), we ascertained that they exhibit similar, but not identical, antioxidant activity as αT when used at equimolar concentrations. In addition, we determined that the exposure time of RPE cells to α-tocopherol is critical for its ability to protect against oxidative damage. Lastly, we determined that αT, but not γT, partially requires the synthesis of new proteins within a 24-h period and prior to exposure to tBHP for optimal cytoprotection. We conclude that, unlike γT and δT, αT appears to be unique in its requirement for transport and/or signaling for it to be an effective antioxidant. As a result, more focus should be paid to which vitamin E components are used for antioxidant interventions.

Keywords: retina, antioxidant, retinal pigment epithelium (RPE), age related macular degeneration (AMD), vitamin E, tocopherol, oxidative stress

---

Abbreviations: ANOVA, analysis of variance; αT, γT, δT, alpha tocopherol, gamma tocopherol and delta tocopherol, respectively; αTr, alpha tocotrienol; AMD, age-related macular degeneration; CHX, cycloheximide; DNA, deoxyribonucleic acid; DAPI, 4′,6-diamidino-2-phenylindole; hTERT, human telomerase reverse transcriptase; Nrf2, nuclear factor erythroid 2-related factor 2; RPE, retinal pigment epithelium; Sod2, superoxide dismutase 2; tBHP, tert-butyl hydroperoxide; VC, vehicle control; ZO-1, zona occludens.

INTRODUCTION

Non-exudative or dry Age-Related Macular Degeneration (AMD), the most common form of AMD, is the leading cause of blindness in people over the age of 65 (Wong et al., 2014; Fleckenstein et al., 2021; Thomas et al., 2021). Dry AMD exhibits some genetic predisposition, but it is a multifactorial disease likely also requiring more than one therapeutic approach for treatment. Dry AMD pathophysiology includes Drusen deposition, oxidative stress, inflammation, geographic atrophy and, ultimately, vascular dysfunction (Hageman et al., 2001; Romero-Vazquez et al., 2021; Tisi et al., 2021; Toma et al., 2021). As a result, compounds that alter Drusen formation, reduce oxidative stress and inflammation, have the potential to prevent cellular loss and control of vascular changes can be potential therapeutic targets (Cabral de Guimaraes et al., 2021; Romero-Vazquez et al., 2021; Toma et al., 2021).

Oxidative stress is a major contributor to retinal pigment epithelium (RPE) dysfunction and cell death in dry AMD (Kunchithapautham et al., 2014; Marazita et al., 2016; Romero-Vazquez et al., 2021; Tisi et al., 2021; Toma et al., 2021). Common sources of oxidative stress in the retina include intrinsic factors such as mutations in complement factor genes, mitochondrial dysfunction and aging as well as extrinsic factors including excessive exposure to sunlight (blue light) and cigarette smoke (Hageman et al., 2001; Tomany et al., 2004; Edwards et al., 2005; Hageman et al., 2005; Khan et al., 2006; Seddon et al., 2006; Chakravarthy et al., 2007; Fletcher et al., 2008; He and Tombran-Tink, 2010; Kunchithapautham et al., 2014; Rohrer et al., 2016; Borras et al., 2019). Vitamin E has been studied as a potential therapy for diseases consisting of oxidative damage (Matsura, 2019; Cabral de Guimaraes et al., 2021). Vitamin E, and its constituent vitamers, exert at least some of their protective effects against oxidative stress through their direct free radical neutralizing effects, or as antioxidants. This is supported by extensive research over several decades (Sen et al., 2006; Traber and Atkinson, 2007; Zingg, 2019). More recently, however, it has become increasingly clear that tocopherols and tocotrienols can serve as signaling molecules to activate kinases and transcription factors alter gene expression (Chiricosta et al., 2019; Ghani et al., 2019; Gugliandolo et al., 2019; Mehrabi et al., 2019; Zingg, 2019; Hidalgo et al., 2020; Moore et al., 2020; Ding et al., 2021; Ungurianu et al., 2021; Willems et al., 2021).

The Age-Related Eye disease Study 1 (AREDS 1) clinical trial determined whether the oral delivery of nutritional supplements vitamin A, vitamin C, vitamin E, zinc and copper could improve outcomes in patients with wet and dry forms of AMD (Age-Related Eye Disease Study Research Group, 2001; Sackett and Schenning, 2002; SanGiovanni et al., 2008; Pemp et al., 2010; Chew et al., 2013). These supplements appeared to slightly reduce the risk for progression to wet AMD in some patients, but they had no effect on dry AMD. A follow-up study, AREDS 2, added omega-3 fatty acids and the carotenoids, lutein and zeaxanthin, but these additional compounds had no additional beneficial effect of patient outcomes compared to AREDS 1 (Age-Related Eye Disease Study 2 Research Group, 2013; Agrón et al., 2021).

Overall, the studies suggested that vitamin, zinc and carotenoid supplementation alone is not effective in combating AMD.

There were limitations to the study design that did not adequately address whether vitamin E can exhibit therapeutic potential. One of the major problems with the AREDS studies was that the route of administration was oral, meaning that the supplements were subjected to first-pass metabolism leading likely to insufficient amounts reaching the affected tissues, namely the RPE (Hensley et al., 2004; Azzi, 2018; Uchida et al., 2018). First-pass metabolism in the liver changes the composition of vitamin E vitamers from predominately γ-tocopherol (γT) and other forms to primarily α-tocopherol (αT) (Azzi, 2018; Uchida et al., 2018). No clinical trial to date has tested whether alternative routes of vitamin E administration can improve clinical outcomes in dry AMD patients. Lastly, studying multiple test compounds or drugs at the same time in a mixture, or cocktail, resulting in complex pharmacokinetics and/or pharmacodynamics remains extremely challenging. With regard to vitamin E, it is reasonable to test individual tocopherols or tocotrienols or well-defined combinations thereof.

Vitamin E concentrations in blood serum has been determined in previous studies, but the concentrations in the retina obtained from normal dietary intake is not precisely known (Müller and Pallauf, 2003; Arigony et al., 2013; Azzi, 2018; Jamro et al., 2019; Zingg, 2019). Studies using animals such as rodents, canine and bovine sources indicate that the serum concentration of supplemented tocopherols, particularly αT, is in the low micromolar range (Müller and Pallauf, 2003; Jamro et al., 2019). As alluded to earlier, clinical studies utilizing vitamin E are difficult to interpret as γT and δT and tocotrienols are metabolized rapidly leaving only elevated levels of At (Hosomi et al., 2019).

The central nervous system, including the retina, has a high oxygen demand and, therefore, has an elevated rate of respiration leading to increased generation of reactive oxygen species from mitochondria (Liu et al., 2006; Rohrer et al., 2016). Furthermore, blue light can cause free radical formation in photoreceptor outer segments possibly leading to oxidative stress (Dalvi et al., 2019; Zhang et al., 2019). Vitamin E can reduce of polyunsaturated fatty acid auto-oxidation in the membranes of photoreceptor outer segments (Robison et al., 1982).

This study, to our knowledge, is the first of its kind in determining the comparative kinetics and cytoprotective efficacy between αT and γT against oxidative damage, the effects of these tocopherols on the expression and subcellular localization of antioxidant and structural proteins, and the requirement for protein synthesis for these observed effects in RPE cells.

Here, we determined whether specific components of vitamin E exhibit unique cytoprotective properties in immortalized human RPE cells (hTERT-RPE cells). We used supra-physiological concentrations (>25 µM) of γT, δT and αTr to ascertain whether they elicit similar cytoprotective effects as αT (Azzi, 2018). In addition, we determined whether short-term (4-h) versus longer-term (24-h) exposure to tocopherols results in a similar degree of cytoprotection against oxidative stress and cell death.

As cell signaling events often lead to changes in gene expression, and subsequent protein expression, we also determined whether αT and γT affect the expression of the antioxidant proteins, nuclear factor erythroid 2-related factor 2 (Nrf2) and superoxide dismutase 2 (Sod2) and the structural proteins, actin and zona occludens (ZO-1). In addition, we determined whether exposure of hTERT-RPE cells to tocopherols requires the synthesis of new proteins within a 24-h period and prior to exposure to tBHP for cytoprotection. If synthesis of new proteins by tocopherol-mediated cellular signaling is required for some or all their cytoprotective effects, this will provide clearer evidence of the importance of the signaling function of tocopherols, in addition to their direct antioxidant function, and shed light on new potential therapeutic targets.

MATERIALS AND METHODS

Cell Culture and Treatments

Human telomerase reverse transcriptase-overexpressing RPE (hTERT-RPE) cells were provided by American Type Culture Collection (ATCC, # CRL-4000) and were maintained according to ATCC instructions. In brief, cells were grown in DMEM:F12 (1:1) + 10% FBS +10 μg/ml gentamicin to >50% density before splitting for growth or to full confluence for use in experiments. Tocopherols were obtained from Sigma-Aldrich (Millipore-Sigma, Burlington, MA, United States). Tocopherols were diluted in cell culture-grade DMSO to a working stock solution concentration of 100 mM and diluted in cell culture media to a final concentration of 100 μM. Tocopherol exposure times were either 4 h or 24 h prior to treatment with oxidant. Tert-butyl hydroperoxide (tBHP) (70% dilution, Acros Organics, Antwerp, Belgium), the oxidant used in this study, was diluted in ultrapure water (>18 Ω ohm·ml^{-1}) to a final working concentration of 100 mM. The tBHP was diluted in culture media to a final concentration of between 100–500 μM for oxidative stress of cells. Cycloheximide (CHX) (Millipore Sigma, Burlington, MA, United States), used to inhibit protein synthesis, was diluted in PBS to a stock solution of 10 mM. CHX was diluted in media at a final concentration of 1 μM (IC50~0.53 μM) and applied to cell 1 h prior to addition of tocopherols. A vehicle control (VC) was used as a control for each chemical or compound treatment. Experiments were carried out in triplicate.

Calcein-AM Assay and Cell Staining

The calcein-AM assay was used to measure cellular esterase activity, a surrogate of cell viability. Calcein-AM dye (Invitrogen/Thermo Fisher Scientific, Waltham, MA, United States) was suspended in cell culture-grade DMSO to a final stock concentration of 2 mM and diluted in media to final concentration of 2–5 μM. The assay was carried out in detail as described elsewhere (Duncan et al., 2007). In brief, cellular loading of calcein-AM was carried out in Dulbecco's PBS (Millipore Sigma) for 20 min. Plates were read at 485 nm/535 nm (excitation/emission) in a Flex Station three multi-mode plate reader (Molecular Devices). Detector sensitivity in plate reader assays was determined automatically by the instrument. Changes in calcein fluorescence in all experimental groups were compared to fluorescence values for the control groups.

An alternative measure of calcein fluorescence was conducted by observing calcein-AM dye-loaded cells from each condition under a fluorescence microscope. The camera exposure time settings were kept constant throughout image acquisition so that relative fluorescence intensities of cells and cellular morphology could be calculated from images. This approach was included to address high levels of calcein fluorescence in attached damaged cells that may give false positive readings in a plate reader assay.

For cell staining of fixed cells, nuclei were labeled with dilute 4′,6-diamidine-2′-phenylindole dihydrochloride (DAPI) stain (Millipore Sigma) and fluorescent dye 594 nm-labeled phalloidin (phalloidin-594; Abnova, Taipei City, Taiwan). Phalloidin labels only filamentous actin; non-filamentous, or globular, actin was not labeled. For DAPI and phalloidin labeling, cells were rinsed with DPBS and fixed for 20 min in 4% paraformaldehyde (PFA). After rinsing, PBS containing 0.5 μg/ml DAPI and 1:1,000 dilution of phalloidin-594 was added to cells followed by incubation for 2 h. Cells were then rinsed three times with PBS and mounted onto glass slides with Aqua Polymount medium (Polysciences, Warrington, PA, United States).

Immunocytochemistry

Immunocytochemistry on treated cells was carried out as described elsewhere (Duncan et al., 2007). In brief, treated cells were rinsed with PBS, fixed with 4% paraformaldehyde for 20 min and then rinsed three times each for 5 min. After blocking, antibodies were applied to fixed cells overnight at 4°C. Antibodies used were mouse anti-Nrf2 (Abcam #ab89443) at 1:200, mouse anti-ZO-1 (Invitrogen #33-9100) at 1:200 and mouse anti-Sod2 (Invitrogen #A21990) at 1:250. Alexafluor™488- or Alexafluor™594-conjugated goat anti-rabbit or mouse IgG secondary antibodies (Invitrogen) were used for fluorescent labeling of cells. Coverslips were mounted using Aqua Polymount medium (Polysciences).

Microscopy

Microscope images were acquired using a Leica TCS SP5-X white light laser scanning confocal microscope (Leica Microsystems, Mannheim, Germany) with fully motorized stage and CTR 6500 controller. DAPI and phalloidin labeling was detected using a diode laser (405 nm) with a detection range of 410–470 nm and tunable white light laser set at 590 nm excitation with a detection range of 600–650 nm. All images were acquired using 40X or 63X oil objectives and images were saved as Leica LIF files for later analysis.

Image Analysis

Images were analyzed using Image-J FIJI software (open source, NIH, Bethesda, MD, United States). Images were converted to maximum intensity projection images in eight- or 16-bit TIFF format. Images were thresholded to remove background fluorescence leaving signal specific for the protein of interest. Mean and maximum grey level (intensity), area, % area and integrated density were calculated. Where necessary, histogram analyses were carried out to determine the counts at each pixel intensity. A cell counter tool in FIJI was used to manually count cell nuclei. To measure nuclear Nrf2 levels, colocalization analysis was conducted using the FIJI coloc2 tool.
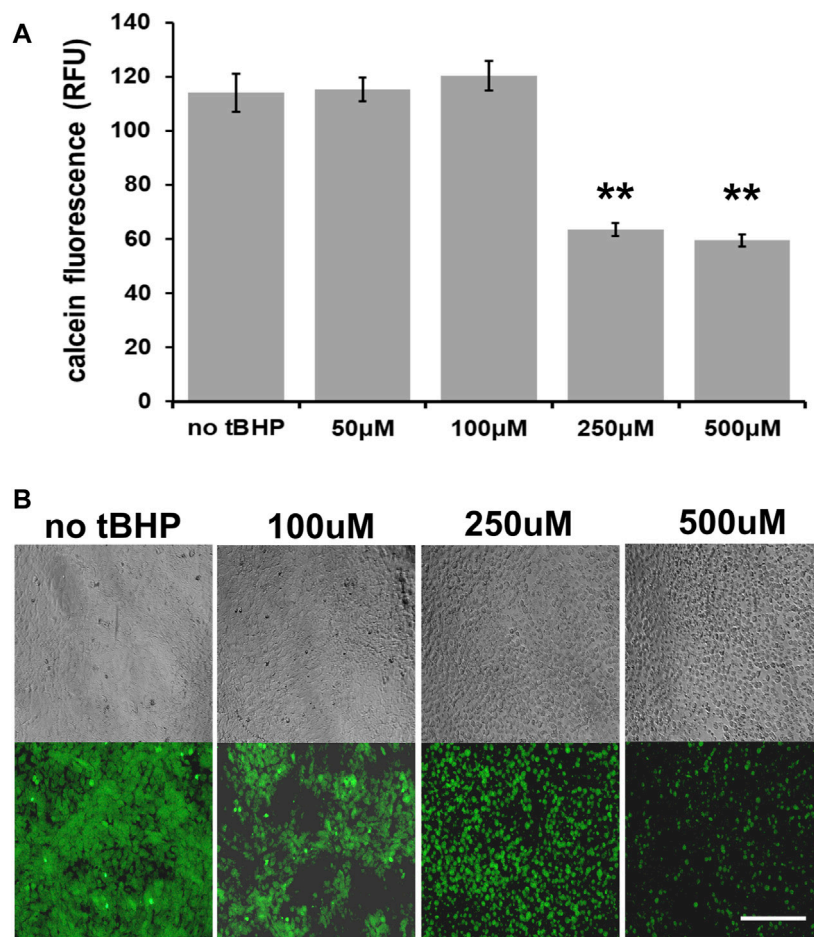
FIGURE 1 | Sensitivity of hTERT-RPE cells to tert-butyl hydroperoxide (tBHP). **(A)** Calcein assay results of hTERT-RPE) cells exposed to different concentrations of tBHP (50, 100, 250, and 500 μM) for 24 h to establish a kill curve. Exposure of cells to 250 and 500 μM tBHP led to 44 and 47% reduction in calcein fluorescence, respectively. Calcein-AM assay data are an average of eight samples. One-way analysis of variance (ANOVA) analysis was performed to determine differences between groups. **p = ≤ 0.01 versus VC-tBHP. **(B)** Microscopic images of calcein-stained tBHP-exposed hTERT-RPE cells visually showing the tBHP concentration response. Top panel row—representative phase contrast images; bottom panel row—representative calcein fluorescence (488 nm/530 nm excitation/emission) images. Scale bar is 100 μm.

Statistics

Statistical difference between more than two groups, which includes all of the data herein, was carried out using a one-way ANOVA with a post hoc Bonferroni correction using GraphPad Prism software (GraphPad, San Diego, CA, United States).

RESULTS

Sensitivity of hTERT-RPE Cells to tBHP-Mediated Oxidative Stress Damage

We first determined the optimal tBHP concentration to use for cytoprotection experiments. At confluence (100% cell density), 100 μM tBHP exhibits no noticeable loss of cell viability (as determined by a calcein fluorescence plate reader assay) while 250 and 500 μM decreases viability by 44 and 47%, respectively (**Figure 1A**). As a result, we used a high tBHP concentration of 500 μM in this study to determine cytoprotection provided by

vitamin E components. Although high concentrations of tBHP (250–500 μM) reduced cellular esterase activity measured by calcein fluorescence, microscopic observation of calcein-AM loaded cells revealed that few cells became detached within 24 h after tBHP exposure and instead exhibited loss of cellular morphology, a common sign of cell death (**Figure 1B**) This microscopy approach allows a qualitative in addition to quantitative assessment of cell health unlike plate reader assays which offer only quantitative data.

Cytoprotective Effects of the Main Vitamin E Components Against Oxidative Damage in hTERT-RPE Cells

To determine if vitamin E components protect hTERT-RPE against severe (lethal) oxidative damage elicited by 500 μM tBHP and help maintain cell viability, we exposed hTERT-RPE cells to vitamin E components (αT, γT, δT and αTr—100 μM of
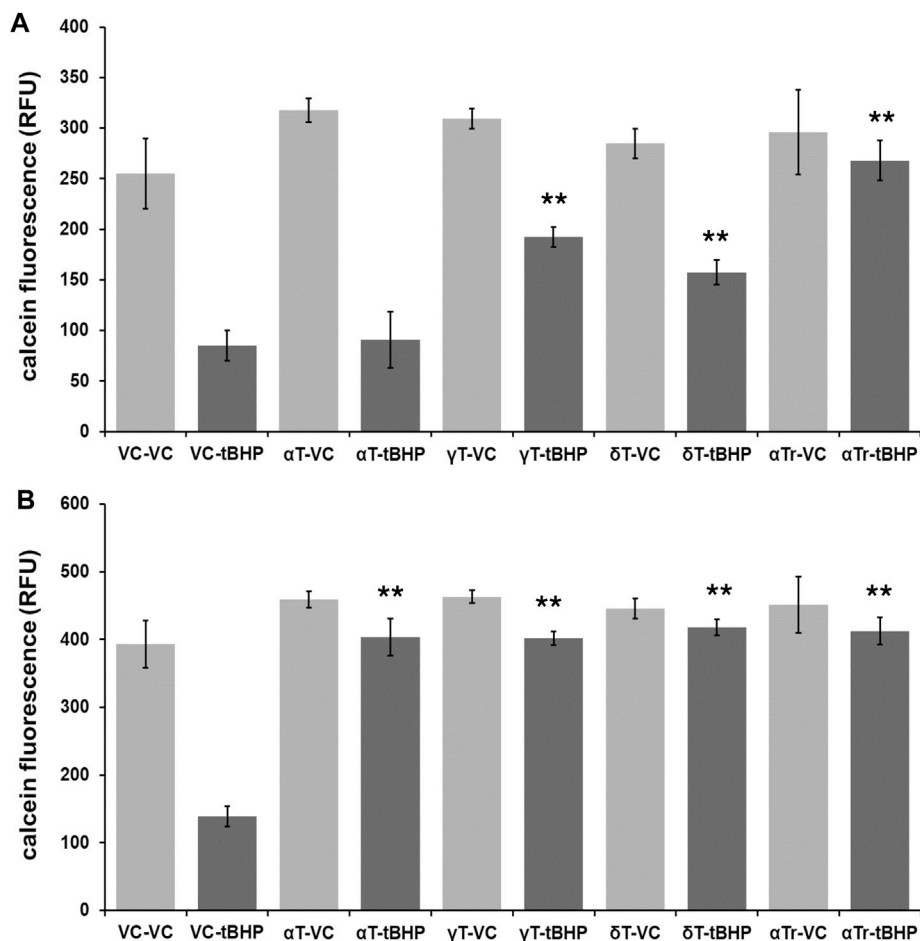
FIGURE 2 | Viability of RPE cells exposed to tocopherols and αTr for either four or 24 h followed by exposure to tBHP (500 μM) for 24 h measured using the calcein-acetomethoxy ester (AM) assay. **(A)** Calcein-AM assay results of hTERT-REP cells exposed to 4-h of vitamin E components or vehicle control (VC) followed by 24-h tBHP exposure. Light gray bars are conditions with no tBHP while dark gray bars are conditions with 500 μM tBHP. The 4-h αT exposure offered no protection of hTERT-RPE cells against tBHP. **(B)** Calcein-AM assay results of hTERT-REP cells exposed to vitamin E components (or VC) for 24-h followed by 24-h tBHP exposure. Light gray bars are conditions with no tBHP while dark gray bars are conditions with 500 μM tBHP. At 24 h, all vitamin E components protected (≥85% protection) hTERT-RPE cells against tBHP. One-way ANOVA analysis with post hoc Bonferroni correction was performed to determine differences between groups. **p = ≤ 0.01 versus vehicle control (VC)-tBHP. Calcein assay data from each data set are from an average of four samples. Data for 4-h tocopherol and 24-h tocopherol groups were compared using a one-way ANOVA with Tukey's post hoc test to determine whether tocopherol protection was time-dependent.

each) for either four or 24 h, washed cells and then exposed cells to tBHP (500 μM) for an additional 24 h. After the 24-h tBHP insult, we carried out a calcein assay to measure cell viability. None of the tocopherols (α-, γ-, and δ) nor αTr exhibited any measurable toxicity at 100 μM (**Figure 2**).

The shorter 4-h tocopherol exposure time resulted in a differential degree of protection with γT and δT and αTr offering some protection (60, 50, and 90%, respectively) (**Figure 2A**). The 4-h αT exposure offered no protection against tBHP (**Figure 2A**). The longer 24-h tocopherol exposure time resulted 90% protection with all vitamers tested (**Figure 2B**). This suggests that the protective effect of αT against oxidative stress is time-dependent, whereas the other vitamers are not.

After 24-h exposure to tBHP, cells remained largely attached to plate wells making the calcein assay limited in determining the

percentage of non-viable cells. As a result, we use microscopic methods to measure loss of cellular morphology and nuclear shrinkage (pyknotic nuclei) as surrogate markers of apoptotic cell death.

Effects of Tocopherols and α-Tocotrienol on Actin Dynamics

The actin cytoskeleton is critical for the maintenance of cell morphology, development and motility. Since cellular morphology is significantly affected by cell death, including apoptosis (Laster and Mackenzie, 1996; Levee et al., 1996), we labeled filamentous actin with fluorescently labeled phalloidin, which binds with high affinity to filamentous but not globular actin. This labeling allowed us to easily visualize changes in cell morphology that accompany cell death.
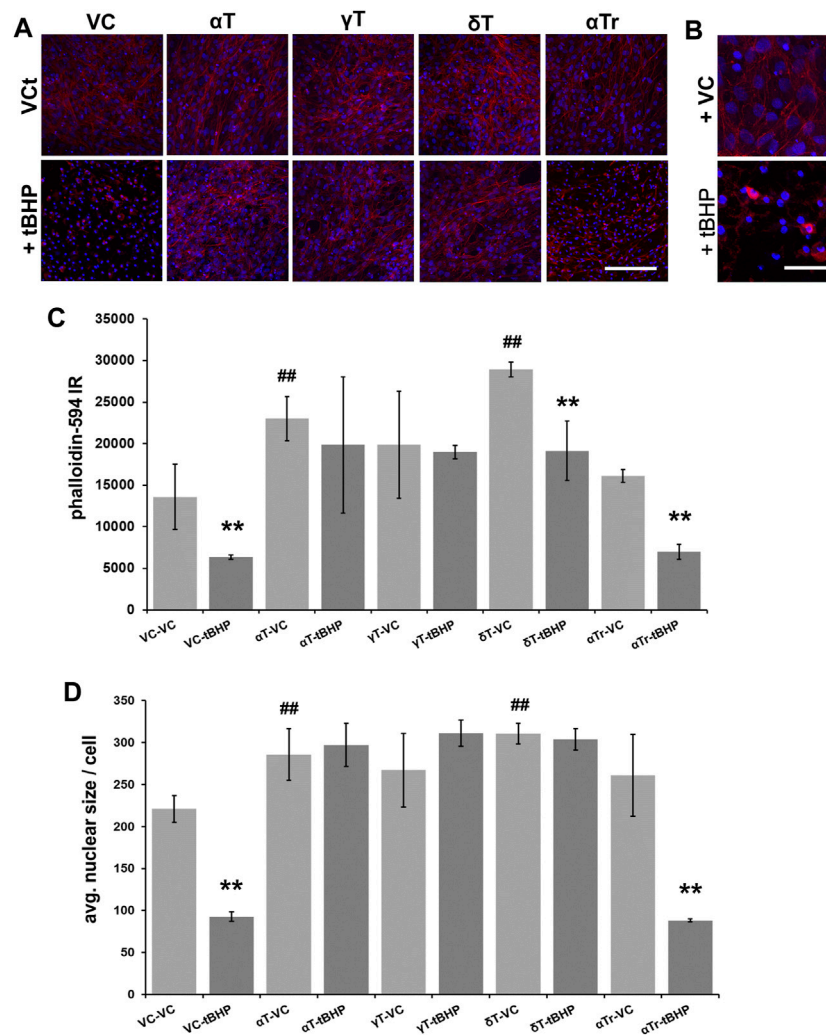
FIGURE 3 | Effect of 24-h αT, γT and δT and αTr exposure on RPE actin dynamics after subsequent tBHP-induced oxidative stress. RPE cells were exposed to a vehicle control (VC) αT, γT or δT or αTr for 24 h prior to tBHP. **(A)** tBHP reduced phalloidin fluorescence (red) and nuclear area (DAPI, blue fluorescence). A reduction in filamentous actin (phalloidin (red) fluorescence) is suggestive of actin destabilization observed in cell death resembling apoptosis. Nuclear size (blue) is reduced during cell death, particularly during apoptosis. Images were acquired at 40X magnification; scale bar is 100 μm. **(B)** A close up image of tBHP-mediated reduction in filamentous actin labeling by phalloidin and reduction in nucleus size caused by tBHP exposure. Scale bar is 25 μm. **(C)** Graphical data showing that exposure of cells to αT and γT, and to a lesser extent δT, prevented this effect in hTERT-RPE cells. αTr, however, could not prevent the reduction of phalloidin staining and nuclear size. **(D)** Exposure of cells to αT and δT led to an increase in nuclear size. Exposure of cells to tBHP led to a reduction in nucleus size indicative of pyknosis. The exposure of cells to αT, γT and δT prevented the tBHP-mediated reduction in nuclear size, while exposure of cells to αTr did not. **p ≤ 0.01 with tBHP versus the same condition without tBHP; ##p ≤ 0.01 with tocopherol versus without tocopherol. Microfluorimetric analyses are from an average of three images. One-way ANOVA analysis with post hoc Bonferroni correction was performed to determine differences between groups.

Pre-exposure of cells to αT and δT (100 μM of each) for 24 h increased phalloidin labeling of filamentous actin, suggesting that actin was stabilized by these tocopherols (**Figure 3A**). Gamma-tocopherol appeared to increase phalloidin-594 fluorescence, but it failed to reach statistical significance (**Figures 3A,C**). Pre-exposure of cells to γT and δT prevented tBHP-mediated actin destabilization, whereas αTr did not. Pre-exposure to αTr resulted in a decrease in phalloidin labeling in cells to the degree observed in controls,

suggesting that αTr may preserve some measures of cell viability (cellular esterase activity (**Figure 1**), but not maintenance of the actin cytoskeleton. (**Figure 3**). These results also suggest that there are differences in the vitamers tested in their ability to protect RPE from oxidative damage.

To determine if αT, γT, δT and αTr prevent tBHP-mediated formation of pyknotic nuclei, we measured DAPI-stained nuclei to measure the average nuclear size (**Figures 3A,D**).
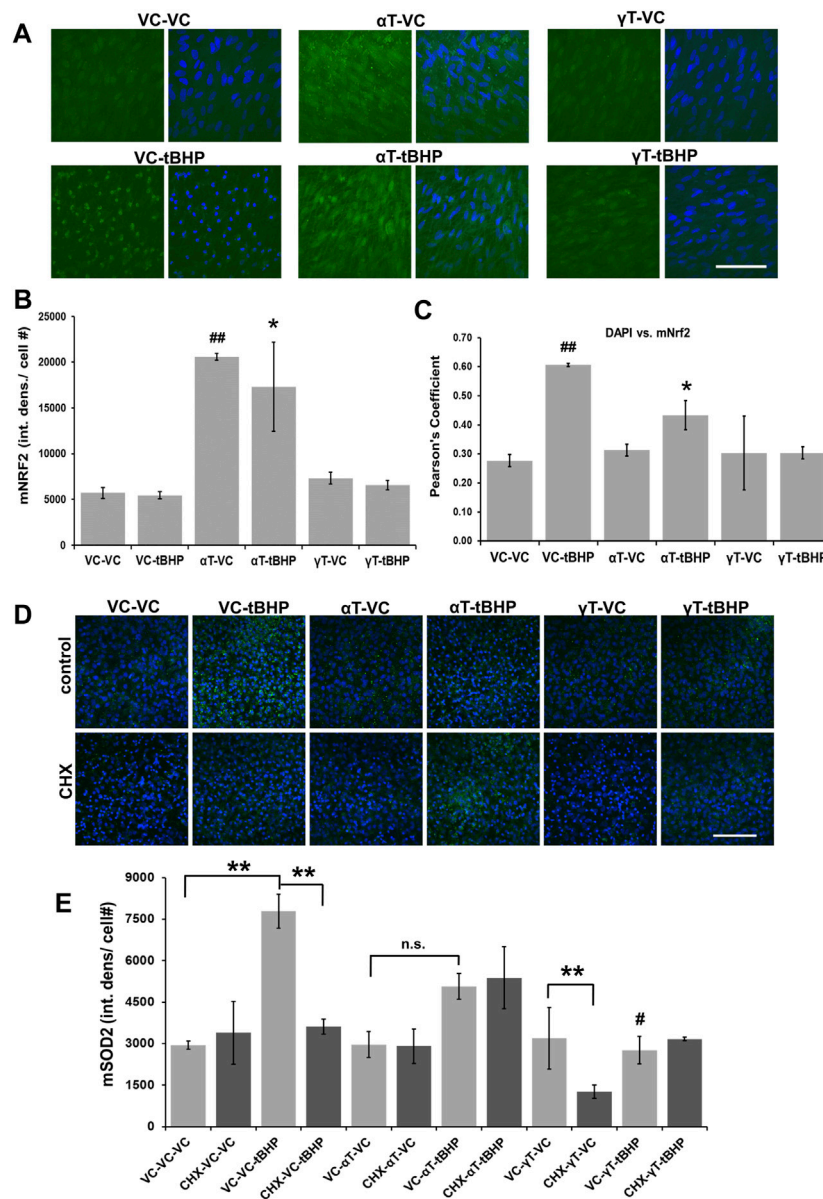
FIGURE 4 | Effect of αT, γT and Sublethal Oxidative Stress on Antioxidant Nrf2 and Sod2 Protein Expression. **(A)** The image panel shows Nrf2 IR (green) and the nucleus (blue) in the presence or absence of αT or γT with or without tBHP. Images are 63x magnification and the scale bar is 50 μm. **(B)** Quantitative graphical data calculated from images revealed that αT induced Nrf2 expression (Nrf2 IR) by 3.8-fold. Furthermore, oxidative stress by tBHP had no effect on αT-mediated increase in Nrf2 IR. **(C)** Colocalization analysis between Nrf2 IR and DAPI fluorescence reveals that tBHP, but not αT nor γT, leads to Nrf2-DAPI colocalization ($r^2 = 0.60$). The presence of prevented this tBHP-mediated nuclear translocation of nrf2 and resulting Nrf2-DAPI colocalization. Microfluorimetric analyses are from an average of three images. *$p = \leq 0.05$ versus VC-tBHP, *##$p = \leq 0.01$ versus VC-VC as determined by one-way ANOVA analysis with Bonferroni post hoc test. **(D)** The image panel shows SOD2 IR (green) and the nucleus (blue) in the presence or absence of CHX as well as αT or γT with or without tBHP. Images are 40x magnification and the scale bar is 100 μm. **(E)** Quantitative data calculated from images revealed that exposure of cells to either αT or γT had no effect of SOD2 IR, while exposure to sublethal (100 μM) tBHP led to a 2.6-fold increase in SOD2 IR. Exposure of cells to αT does not significantly reduce tBHP-mediated induction of Sod2. Exposure of cells to γT led to a 64% reduction in tBHP-mediated induction of SOD2. Exposure of cells to CHX had no effect on Sod2 IR, but CHX with γT led to a 60% decrease in Sod2 IR. CHX reversed tBHP-mediated induction of Sod2. CHX had no effect on αT's nor γT's ability to reduce the induction of Sod2 mediated by tBHP. **$p = \leq 0.01$; n.s.—not significant; #$p = \leq 0.01$ versus VC-αT-tBHP as determined by one-way ANOVA analysis with Bonferroni post hoc test.

None of the vitamin E components alone affected nuclear size or number. Exposure to tBHP led to a 40% decrease in nuclear size indicative of the nuclear shrinkage (pyknosis) observed in later stages of cell death resembling that of apoptosis (**Figures 3A,B**). All three tocopherols (αT, γT and δT), but not αTr, prevented tBHP-mediated nuclear shrinkage (pyknosis).

Effects of αT and γT and Sublethal Oxidative Stress on Nrf2 and SOD2 Immunoreactivity

After establishing sublethal versus lethal concentrations of tBHP for hTERT-RPE cells, we determined what effect αT and γT and/or sublethal tBHP exposures had on the expression of nuclear factor erythroid 2-related factor 2 (Nrf2) and superoxide dismutase 2 (SOD2). We decided to focus on αT and γT because 1) much more is known about αT than any other form of tocopherol, and it is generally considered the prototypical tocopherol and 2) γT is also relatively well studied and it is the most abundant tocopherol from food sources. Furthermore, a few studies have compared the activity of αT and γT thereby determining that there are differences in their activity.

Nrf2 is a redox sensitive transcription factor that regulates the expression of genes involved in the cellular antioxidant response while Sod2 is a mitochondrial antioxidant enzyme that is critical for maintaining redox balance in cells (Murakami et al., 1998; Venugopal and Jaiswal, 1998; Itoh et al., 1999; Melov et al., 1999). These proteins were chosen as they should be useful markers for the cellular response against oxidative stress.

Exposure of cells to αT, but not γT, led to a 4-fold increase in Nrf2 IR while exposure to tBHP had no effect on the amplitude of Nrf2 IR (**Figures 4A,B**). Exposure of cells to αT followed by tBHP led to a 3.5-fold increase in Nrf2 IR while exposure to γT followed by tBHP had no effect on Nrf2 IR similar to that of tBHP or γT exposures alone (**Figures 4A,B**).

To determine what effect αT, γT and/or tBHP had on NRf2 nuclear translocation, we measured the colocalization between DAPI DNA stain in the nucleus and Nrf2 IR (**Figure 4C**). Although exposure to tBHP had no effect on the amplitude of Nrf2 IR, tBHP exposure did increase the amount of Nrf2 IR in the nucleus as determined by an increase in DAPI-Nrf2 colocalization and Pearson's correlation test ($r^2 = 0.61$ (VC-tBHP) vs. 0.28 (VC-NT)) (**Figure 4C**). This suggests that a 24-h period of oxidative stress leads to the nuclear translocation of Nrf2, but not an increase in its expression levels. Alpha-tocopherol exposure itself for 24 h led to the upregulation of Nrf2 expression but not Nrf2 nuclear translocation. αT, but not γT, reduced the tBHP-mediated nuclear translocation of Nrf2 by 27% further highlighting a differential effect between αT and γT on Nrf2 activity.

Exposure of cells to either αT or γT had no effect of SOD2 IR, suggesting that they, themselves, cannot induce SOD2 gene expression (**Figures 4D,E**). Exposure of cells to sublethal (100 μM) tBHP for 24 h led to a 2.6-fold increase in SOD2 IR, which was expected as others have shown that the Sod2 gene is induced by oxidative stress (Murakami et al., 1998; Melov et al., 1999). Exposure of cells to αT does not significantly reduce tBHP-mediated induction of Sod2, but it shows a trend toward a decrease ($p = 0.22$) (**Figure 4E**). Exposure of cells to γT led to a 64% reduction in tBHP-mediated induction of SOD2. Together, this suggests that γT is superior to αT in reducing the oxidative stress elicited by the level of tBHP needed for Sod2 gene induction.

To determine if synthesis of new proteins is required for tocopherol-mediated cytoprotection, we pre-treated hTERT-RPE cells with the protein synthesis inhibitor, cycloheximide, 1 h prior to tocopherol exposure and 24 h prior to tBHP exposure.

Exposure of cells to CHX, with or without αT, also had no effect on Sod2 IR, CHX together with γT led to a 60% decrease in Sod2 IR (**Figure 4E**). CHX completely reversed the tBHP-mediated induction of Sod2, suggesting that protein synthesis is required for tBHP induction of Sod2 (**Figure 4E**). CHX had no effect on αT's nor γT's ability to reduce the induction of Sod2 mediated by tBHP (**Figure 4E**), indicating that the mechanism by which these tocopherols reduce tbHP-mediated Sod2 is not dependent upon protein synthesis.

Effects of αT and γT on ZO-1 Under Conditions of Oxidative Stress

RPE barrier function (retinal-blood barrier) is compromised in AMD which prompted us to detect and measure the actin-interacting tight junction protein, ZO-1, as a measure of possible barrier integrity (Penfold et al., 1990). ZO-1 is a protein critical for tight junction formation and reports from others (Pu et al., 2005; Yang et al., 2015), and bioinformatics analysis, suggests that the ZO-1 gene may be regulated by oxidative stress.

We determined whether αT and γT and/or sublethal tBHP exposures had on the expression of zona occludens 1 (ZO-1) a critical component of tight junctions in endothelial and epithelial cells, such as RPE (Pu et al., 2005; Yang et al., 2015). ZO-1 directly interacts with multiple proteins in tight junctions and with the actin cytoskeleton (Nybom and Magnusson, 1996; Itoh et al., 1997).

Exposure of cells to either αT or γT had no effect of ZO-1 IR (**Figures 5A,B**). Exposure of cells to sublethal (100 μM) tBHP for 24 h led to a 63% increase in ZO-1 IR, particularly in the nucleus (**Figure 5C**). Nuclear localization of ZO-1 has been reported elsewhere and has been shown to play a role in multiple cellular functions (Zhong et al., 2012; Guo et al., 2017; Lesage et al., 2017). Similarly, exposure of cells to αT does not significantly reduce tBHP-mediated induction of ZO-1, but it shows a trend toward a decrease (**Figure 5C**). Exposure of cells to γT led to a 50% reduction in tBHP-mediated induction of ZO-1 (**Figure 5C**). This suggests that, unlike αT, γT prevents the effects of tBHP on ZO-1 expression (**Figure 5C**), thus is more potent than αT in maintaining RPE function.

Exposure of cells to CHX, with or without αT or γT, also had no effect on ZO-1 IR. Addition of the protein synthesis inhibitor, CHX, does not significantly reduce tBHP-mediated induction of ZO-1, but it shows a trend toward a decrease (**Figure 5C**). This suggests that protein synthesis may be a factor in the induction of ZO-1 expression elicited by oxidative stress (tBHP). CHX and αT prior to tBHP exposure, however, had no effect on ZO-1 IR, while CHX completely reversed the ability of γT to reduce tBHP-mediated increase in ZO-1 IR (**Figure 5C**). This suggests that, unlike αT, γT prevents the effects of tBHP on ZO-1 expression and these effects require protein synthesis (**Figure 5C**).
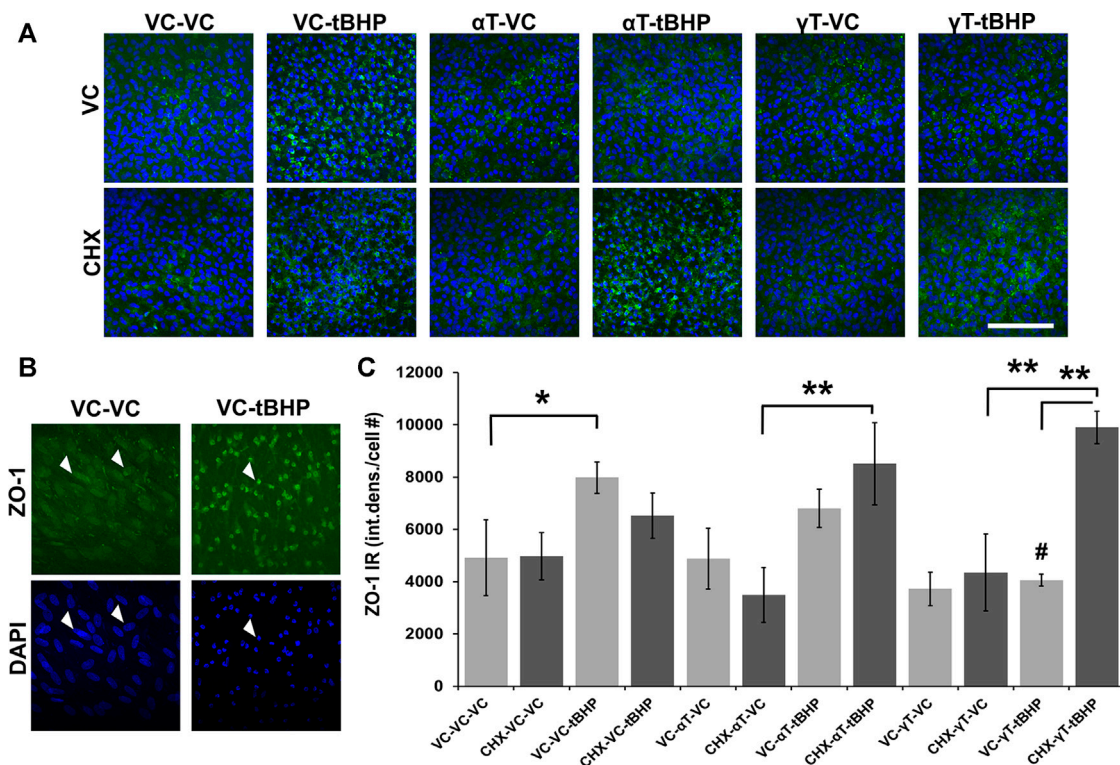
FIGURE 5 | Effect of αT, γT, Oxidative Stress and Protein Synthesis on ZO-1 Expression. **(A)** The image panel shows ZO-1 IR (green) and the nucleus (blue) in the presence or absence of αT or γT, with or without tBHP and with or without CHX. Images are 63x magnification and the scale bar is 50 μm. **(B)** Optically magnified images demonstrating condensed ZO-1 IR (white arrows) and nuclear shrinkage (white arrows) observed under conditions of oxidative stress. **(C)** Quantitative graphical data calculated from images revealed that tBHP alone, but neither αT nor γT alone, induced ZO-1 expression (ZO-1 IR, green) by 2.6-fold. The presence of αT reduced the effect of tBHP on ZO-1 induction, but it failed to reach statistical significance. The presence of γT, however, completely prevented tBHP's effect on ZO-1 induction. Furthermore, inhibition of protein synthesis with CHX did not significantly affect tBHP-mediated ZO-1 induction nor αT-tBHP's effect on ZO-1 IR. CHX, however, completely prevented γT's reversal of tBHP-mediated ZO-1 induction. Microfluorimetric analyses are from an average of three images. *$p = \leq 0.05$, **$p = \leq 0.01$ with tBHP versus the same condition without tBHP as determined by one-way ANOVA analysis with Bonferroni post hoc test.

Effects of αT and γT on Nuclear Shrinkage Under Conditions of Severe Oxidative Stress

Quantitation of pyknotic nuclei, nuclei that appear to be half or less the size of normal nuclei, were counted and expressed as a percentage of the total (**Figures 6A,B**). Exposure of cells to tBHP led to a 37% increase in nuclear pyknosis compared to controls (**Figure 6B**). Exposure of cells to αT or γT had no effect on baseline nuclear pyknosis. Exposure of cells to αT or γT decrease tBHP-mediated nuclear pyknosis by 55 and 89%, respectively (**Figure 6B**).

Pretreatment of cells with CHX, itself, lead to a 4.3-fold increase in nuclear pyknosis compared to control not treated with CHX (13% overall increase) (**Figure 6B**). CHX treatment prior to tBHP, led to a 10% decrease in nuclear pyknosis compared to tBHP alone (5% decrease overall), suggesting that protein synthesis is required, in part, for nuclear pyknosis. Pretreatment of cells with CHX prior to αT led to an 18-fold increase the nuclear pyknosis compared to cells exposed to αT alone (19% overall increase in nuclear pyknosis (**Figure 6B**). Exposure of cells to CHX prior to αT and tBHP led to a 1.7-fold

increase in nuclear pyknosis (13% overall increase) compared to αT and tBHP without CHX pre-exposure, suggesting that some protein synthesis is required for αT to reduce tBHP-mediated nuclear shrinkage.

Pretreatment of cells with CHX prior to γT led to an 11-fold increase the nuclear pyknosis compared to cells exposed to γT alone (31% overall increase in nuclear pyknosis) (**Figures 6A,B**). Exposure of cells to CHX prior to γT and tBHP led to a 2-fold increase in nuclear pyknosis (5% overall increase) compared to γT and tBHP without CHX pre-exposure, suggesting that some protein synthesis is required for γT to reduce tBHP-mediated cell death (**Figure 6**).

DISCUSSION

Here, we determined that specific vitamin E components exhibit unique cytoprotective properties in immortalized human RPE cells. We used supraphysiological concentrations of γT, δT and αTr to ascertain whether they exhibit similar cytoprotective activity as αT. In addition, we determined whether short-term versus longer-term exposure to tocopherols leads to similar
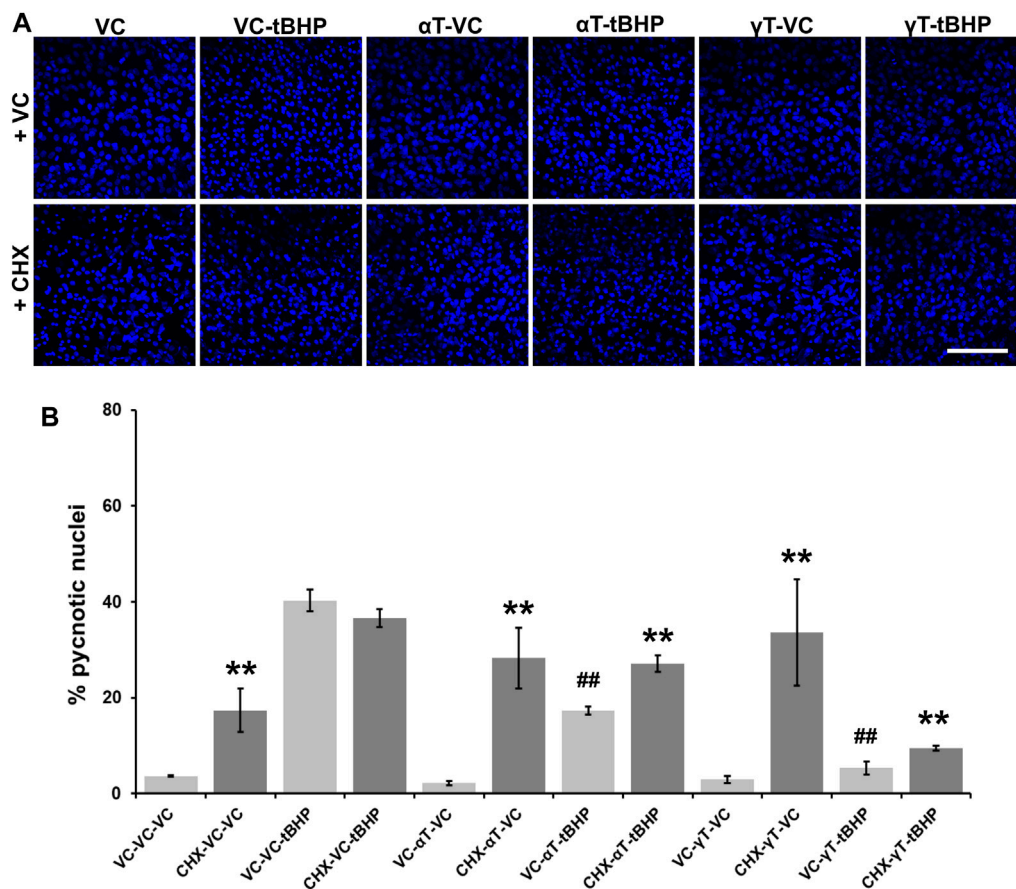
FIGURE 6 | Effect of CHX and long-term (24-h) tocopherol exposure of hTERT-RPE cells on tBHP-mediated cytotoxicity. hTERT-RPE cells were exposed to CHX for 1 h followed by αT or γT for 24 h prior to tBHP. **(A)** Image panels showing DAPI labeling of nuclei (blue) in cells exposed to CHX, αT or γT and tBHP. Top row represents conditions without CHX while the bottom row represents conditions with CHX. Nucleus area (blue fluorescence) is reduced during cell death by a process resembling apoptosis. Images acquired at 40x magnification; scale bar is 100 µm. **(B)** Measurement of pyknotic nuclei, nuclei that are half the size of average normal nuclei and not merely reduced in size, was carried out on CHX-, tocopherol- and tBHP-exposed cells. Exposure of cells to CHX (dark bars) alone increases the percentage of pyknotic nuclei in the cell population from 4% in control cells (light bars) to 17%. Exposure of cells to tBHP led to an increase in the percentage of pyknotic nuclei from 4 to 40%. Exposure of cells to either tocopherol alone had no effect on the percentage of pyknotic nuclei, but exposure to CHX and tocopherols led to an increase in the percentage of pyknotic nuclei from 2 to 28% for αT and 3–34% for γT. The presence of αT prior to tBHP insult reduced the percentage of pyknotic nuclei by 57% compared to cells treated with tBHP alone. Inhibition of protein synthesis by CHX partially reversed this αT protection by 47%. The presence of γT prior to tBHP insult reduced the percentage of pyknotic nuclei by 87% compared to cells treated with tBHP alone. Inhibition of protein synthesis by CHX partially reversed this γT protection by 44%. Microfluorimetric analyses are from an average of three images. **$p \leq 0.01$ with CHX versus the same condition without CHX, ##$p \leq 0.01$ with tBHP versus the same condition without tBHP as determined by one-way ANOVA analysis with Bonferroni post hoc test.

degree of cytoprotection against oxidative stress and cell death. Both γT, δT and αTr require less time than αT to protect cells against tBHP, suggesting that αT acts through a different mechanism of action than direct antioxidant activity to exert its full protective effects. We focused primarily on αT and γT because there are more published studies on these two tocopherols than other vitamin E components and they are metabolized differently (Azzi, 2018; Uchida et al., 2018). Our results suggest that αT and γT exhibit different kinetics and/or potencies for antioxidant activity, different effects on Nrf2 expression and different effects on actin stability, Sod2 and ZO-1 expression mediated by oxidative stress. As a result of our data, the selection of specific tocopherol vitamers as therapeutic antioxidants may need to be considered,

particularly γT, due to its different pharmacokinetic and pharmacodynamic properties than αT.

To our knowledge, this study is the first measuring the comparative kinetics and cytoprotective efficacy between αT and γT against oxidative damage, the expression and subcellular localization of antioxidant and structural proteins, and the requirement for protein synthesis for these effects in RPE cells.

Many plant-based vitamin E sources contain predominantly γT and lesser concentrations of other tocopherols (Jiang et al., 2001; Szewczyk et al., 2021). Since North American diets contain more γT than other tocopherols, higher levels of γT tocopherol are ingested, but it is more rapidly eliminated from the body (in bile). αT, on the other

hand, persists at higher plasma concentrations due to much greater retention in the body. There are conflicting reports about which tocopherol form exhibits the most potent antioxidant activity (Kamal-Eldin and Appelqvist, 1996). Based on literature, the upper physiologic concentration of vitamin E in mammals is in the low micromolar range (<25 μM) (Arigony et al., 2013; Jamro et al., 2019). Based on this we chose to use 100uM tocopherols and tocotrienols, as this concentration is up to 10 times higher than concentrations achieved through a normal diet but could still be achieved using dietary supplementation.

We selected a short (4-h) tocopherol exposure time based on the assumption that it would not allow for as much cellular uptake through tocopherol transport proteins as the 24-h exposure period. Therefore, the shorter 4-h tocopherol exposure period was a better approach for determining the direct antioxidant effect while the 24-h period was a better approach for looking at cellular uptake and subsequent cell signaling, in addition to direct antioxidant properties.

Our rationale for selecting the measurement of actin, nuclei, Nrf2, Sod2 and ZO-1 is based on numerous studies where the detection and measurement of these proteins serve to assess the functional integrity (actin and ZO-1) and cellular response to oxidative stress (Nrf2 and Sod2) and viability (actin and nuclear staining) of epithelial cells (Penfold et al., 1990; Murakami et al., 1998; Venugopal and Jaiswal, 1998; Itoh et al., 1999; Melov et al., 1999; Pu et al., 2005; Yang et al., 2015).

To assess cell death in RPE in response to tBHP, we labeled actin filaments with fluorescently tagged phalloidin. Phalloidin is a cell permeable phallotoxin from the death cap mushroom that binds with high affinity to filamentous actin, but not depolymerized or monomeric actin (Cooper, 1987). During apoptotic cell death, some components of the cytoskeleton, including actin, have been shown to become destabilized or relocate to the periphery of the cell (Reed, 1995). As a result, hTERT-RPE cells exposed to tBHP exhibit reduced filamentous actin and phalloidin labeling. DAPI labels DNA in cells and during apoptotic cell death, nuclear condensation occurs. During this process, DNA migrates to the periphery of the nucleus near the nuclear envelope as part of a process called pyknosis (Reed, 1995). hTERT-RPE cells exposed to tBHP resulted in pyknotic nuclei. Since we did not measure caspase activation or other direct apoptotic markers, we could not prove that cell death was carried out by an apoptotic process. In this study, however, we were more interested in observing and measuring cellular morphology than a specific apoptotic process.

Since Nrf2 is a major regulator of the cellular antioxidant response, we decided to measure the effect of tBHP and tocopherols on its expression. We predicted that tBHP, and not tocopherols themselves, would increase Nrf2 expression. Much to our surprise, however, tBHP had no effect on Nrf2 expression but αT, not γT, did. The only effect of tBHP we were able to observe was the relative increase in nuclear Nrf2 IR compared to other treatments. Our results indicate that αT itself can upregulate Nrf2 expression, thereby potentially priming the RPE cells for a more effective antioxidant response. Interestingly, αT, but not γT, was able to reduce

tBHP-mediated Nrf2 nuclear translocation suggesting that αT ang γT exhibit differential effects on Nrf2 activity.

Sod2 is an important antioxidant enzyme located in mitochondria, a common source of free radical formation (Murakami et al., 1998; Melov et al., 1999). We determine whether tBHP induces Sod2 expression because it has been shown in multiple studies to become induced in response to oxidative stress (Murakami et al., 1998; Melov et al., 1999). We also determined whether tocopherols could affect Sod2 expression. As expected, tBHP increased Sod2 IR, but neither αT nor γT had an effect on Sod2 IR. In fact, γT, and to a lesser extent, αT, decreased Sod2 IR elicited by tBHP. Since inhibiting protein synthesis with CHX didn't change the inhibitory effect of αT or γT on tBHP-mediate-Sod2 expression, we conclude that these effects of αT and γT may not require the synthesis of new protein.

We determined whether tBHP, αT or γT or a combination of tocopherols and tBHP had an effect on the expression of the tight junction and actin-binding protein, ZO-1. We reasoned that a reduction or redistribution of ZO-1 may have significant negative ramifications for RPE tissue integrity and barrier function while an increase in ZO-1 IR would represent improvement in RPE function. Both tBHP and αT, alone, led to an increase in ZO-1 IR and the combination of both led to an additive increase in ZO-1. ZO-1 IR in these cells was predominantly nuclear and not located at the plasma membrane where one would expect to see it. Several reports have identified nuclear localization of ZO-1 which corroborate our findings. For example, in lung and breast tumor cells, ZO-1 has been observed in cytonuclear compartments and is involved in NFκB signaling (Lesage et al., 2017). The HIV Tat proteins has been shown to alter the expression pattern of ZO-1 in murine brain endothelial cells (Pu et al., 2005) and to cause nuclear localization of ZO-1 in human brain vascular endothelial cells (Zhong et al., 2012). The observation that ZO-1 is expressed on the cell surface and in the cytoplasmic and nuclear regions is interesting, but the ramifications for these different expression patterns are not clear.

The upregulation of ZO-1 by αT, tBHP and both αT and tBHP suggest that, 1) αT may help protect barrier function by creating more cellular ZO-1 protein, 2) cells may respond to oxidative stress by upregulating ZO-1 to help maintain proper barrier and, 3) the presence of both produce an additive effect. The fact that γT does not have the same effect on ZO-1 expression indicates that the two tocopherols exhibit different activities or interact with different cellular processes.

Cycloheximide inhibits protein synthesis by preventing the translocation of transfer RNA in the ribosomal active site. To determine if protein synthesis is required for tocopherol's protective effects, we exposed cells to CHX 1 h before the addition of tocopherols so that the inhibition of protein synthesis would occur before, or in the early stages of, tocopherol-mediated signal transduction. The presence of CHX should not have any effect on tocopherols direct antioxidant activities. CHX can be toxic to some cells at concentrations needed to block protein synthesis, so we removed the CHX within 1 h, when the tocopherols were added, to allow cells to recover from its toxic effects prior to exposing cells to tBHP. CHX and tBHP toxicity are not additive; this suggests that, as expected, the mechanism of action of CHX and tBHP are mutually exclusive.

Future studies need to be carried out to determine whether αT, γT and δT can affect RPE function, particularly the secretion of neurotrophic and protective factors, uptake of shed photoreceptor outer segments and barrier function as determined by transepithelial resistance. In addition, several questions regarding the *in vitro* and *in vivo* kinetics and potency of different tocopherol and tocotrienols must be answered. It is also reasonable to assume that specific tocopherol-tocotrienol combination formulations, together with localized delivery methods, in lieu of systemic administration, may provide great therapeutic potential in diseases where oxidative stress is a major contributor.

DATA AVAILABILITY STATEMENT

The original contributions presented in the study are included in the article/Supplementary Material, further inquiries can be directed to the corresponding author.

AUTHOR CONTRIBUTIONS

PK conceived and designed the experiments. RSD, DTH, and CWH performed the experiments. All authors analyzed the data. RSD and PK wrote the paper. All authors edited and reviewed the paper.

FUNDING

ACKNOWLEDGMENTS

REFERENCES

Age-Related Eye Disease Study 2 Research Group (2013). Lutein + Zeaxanthin and omega-3 Fatty Acids for Age-Related Macular Degeneration: The Age-Related Eye Disease Study 2 (AREDS2) Randomized Clinical Trial. *JAMA* 309 (19), 2005–2015. doi:10.1001/jama.2013.4997

Age-Related Eye Disease Study Research Group (2001). A Randomized, Placebo-Controlled, Clinical Trial of High-Dose Supplementation with Vitamins C and E, Beta Carotene, and Zinc for Age-Related Macular Degeneration and Vision Loss: AREDS Report No. 8. *Arch. Ophthalmol.* 119 (10), 1417–1436. doi:10.1001/archopht.119.10.1417

Agrón, E., Mares, J., Clemons, T. E., Swaroop, A., Chew, E. Y., Keenan, T. D. L., et al. (2021). Dietary Nutrient Intake and Progression to Late Age-Related Macular Degeneration in the Age-Related Eye Disease Studies 1 and 2. *Ophthalmology* 128 (3), 425–442. doi:10.1016/j.ophtha.2020.08.018

Arigony, A. L., de Oliveira, I. M., Machado, M., Bordin, D. L., Bergter, L., Prá, D., et al. (2013). The Influence of Micronutrients in Cell Culture: A Reflection on Viability and Genomic Stability. *Biomed. Res. Int.* 2013, 597282. doi:10.1155/2013/597282

Azzi, A. (2018). Many Tocopherols, One Vitamin E. *Mol. Aspects Med.* 61, 92–103. doi:10.1016/j.mam.2017.06.004

Borras, C., Canonica, J., Jorieux, S., Abache, T., El Sanharawi, M., Klein, C., et al. (2019). CFH Exerts Anti-Oxidant Effects on Retinal Pigment Epithelial Cells Independently from Protecting Against Membrane Attack Complex. *Sci. Rep.* 9 (1), 13873. doi:10.1038/s41598-019-50420-9

Cabral de Guimaraes, T. A., Daich Varela, M., Georgiou, M., and Michaelides, M. (2021). Treatments for Dry Age-Related Macular Degeneration: Therapeutic Avenues, Clinical Trials and Future Directions. *Br. J. Ophthalmol.* bjophthalmol-2020-318452. Online ahead of print. doi:10.1136/bjophthalmol-2020-318452

Chakravarthy, U., Augood, C., Bentham, G. C., de Jong, P. T., Rahu, M., Seland, J., et al. (2007). Cigarette Smoking and Age-Related Macular Degeneration in the EUREYE Study. *Ophthalmology* 114 (6), 1157–1163. doi:10.1016/j.ophtha.2006.09.022

Chew, E. Y., Clemons, T. E., Agrón, E., Sperduto, R. D., Sangiovanni, J. P., Kurinij, N., et al. (2013). Long-Term Effects of Vitamins C and E, β-Carotene, and Zinc on Age-Related Macular DegenerationLong-Term Effects of Vitamins C and E, Beta-Carotene, and Zinc on Age-Related Macular Degeneration: AREDS Report No. 35. *Ophthalmology* 120 (8), 1604–1611. doi:10.1016/j.ophtha.2013.01.021

Chiricosta, L., Gugliandolo, A., Tardiolo, G., Bramanti, P., and Mazzon, E. (2019). Transcriptomic Analysis of MAPK Signaling in NSC-34 Motor Neurons Treated with Vitamin E. *Nutrients* 11 (5), 1081. doi:10.3390/nu11051081

Cooper, J. A. (1987). Effects of Cytochalasin and Phalloidin on Actin. *J. Cel Biol* 105 (4), 1473–1478. doi:10.1083/jcb.105.4.1473

Dalvi, S., Galloway, C. A., Winschel, L., Hashim, A., Soto, C., Tang, C., et al. (2019). Environmental Stress Impairs Photoreceptor Outer Segment (POS) Phagocytosis and Degradation and Induces Autofluorescent Material Accumulation in hiPSC-RPE Cells. *Cell Death Discov* 5, 96–16. doi:10.1038/s41420-019-0171-9

Ding, Y., Fan, J., Fan, Z., and Zhang, K. (2021). γ-Tocotrienol Reverses Multidrug Resistance of Breast Cancer Cells through the Regulation of the γ-Tocotrienol-NF-κB-P-gp axis. *J. Steroid Biochem. Mol. Biol.* 209, 105835. doi:10.1016/j.jsbmb.2021.105835

Duncan, R. S., Hwang, S. Y., and Koulen, P. (2007). Differential Inositol 1,4,5-Trisphosphate Receptor Signaling in a Neuronal Cell Line. *Int. J. Biochem. Cel Biol* 39 (10), 1852–1862. doi:10.1016/j.biocel.2007.05.003

Edwards, A. O., Ritter, R., 3rd, Abel, K. J., Manning, A., Panhuysen, C., and Farrer, L. (2005). Complement Factor H Polymorphism and Age-Related Macular Degeneration. *Science* 308 (5720), 421–424. doi:10.1126/science.1110189

Fleckenstein, M., Keenan, T. D. L., Guymer, R. H., Chakravarthy, U., Schmitz-Valckenberg, S., Klaver, C. C., et al. (2021). Age-Related Macular Degeneration. *Nat. Rev. Dis. Primers* 7 (1), 31. doi:10.1038/s41572-021-00265-2

Fletcher, A. E., Bentham, G. C., Agnew, M., Young, I. S., Augood, C., Chakravarthy, U., et al. (2008). Sunlight Exposure, Antioxidants, and Age-Related Macular Degeneration. *Arch. Ophthalmol.* 126 (10), 1396–1403. doi:10.1001/archopht.126.10.1396

Ghani, S. M. A., Goon, J. A., Azman, N. H. E. N., Zakaria, S. N. A., Hamid, Z., and Ngah, W. Z. W. (2019). Comparing the Effects of Vitamin E Tocotrienol-Rich Fraction Supplementation and α-Tocopherol Supplementation on Gene Expression in Healthy Older Adults. *Clinics (Sao Paulo)* 74, e688. doi:10.6061/clinics/2019/e688

Gugliandolo, A., Chiricosta, L., Silvestro, S., Bramanti, P., and Mazzon, E. (2019). α-Tocopherol Modulates Non-Amyloidogenic Pathway and Autophagy in an *In Vitro* Model of Alzheimer's Disease: A Transcriptional Study. *Brain Sci.* 9 (8), 196. doi:10.3390/brainsci9080196

Guo, J., Cai, H., Zheng, J., Liu, X., Liu, Y., Ma, J., et al. (2017). Long Non-Coding RNA NEAT1 Regulates Permeability of the Blood-Tumor Barrier via miR-181d-5p-Mediated Expression Changes in ZO-1, Occludin, and Claudin-5. *Biochim. Biophys. Acta Mol. Basis Dis.* 1863 (9), 2240–2254. doi:10.1016/j.bbadis.2017.02.005

Hageman, G. S., Anderson, D. H., Johnson, L. V., Hancox, L. S., Taiber, A. J., Hardisty, L. I., et al. (2005). A Common Haplotype in the Complement Regulatory Gene Factor H (HF1/CFH) Predisposes Individuals to Age-Related Macular Degeneration. *Proc. Natl. Acad. Sci. U S A.* 102 (20), 7227–7232. doi:10.1073/pnas.0501536102

Hageman, G. S., Luthert, P. J., Victor Chong, N. H., Johnson, L. V., Anderson, D. H., and Mullins, R. F. (2001). An Integrated Hypothesis that Considers Drusen as Biomarkers of Immune-Mediated Processes at the RPE-Bruch's Membrane Interface in Aging and Age-Related Macular Degeneration. *Prog. Retin. Eye Res.* 20 (6), 705–732. doi:10.1016/s1350-9462(01)00010-6

He, Y., and Tombran-Tink, J. (2010). Mitochondrial Decay and Impairment of Antioxidant Defenses in Aging RPE Cells. *Adv. Exp. Med. Biol.* 664, 165–183. doi:10.1007/978-1-4419-1399-9_20

Hensley, K., Benaksas, E. J., Bolli, R., Comp, P., Grammas, P., Hamdheydari, L., et al. (2004). New Perspectives on Vitamin E: Gamma-Tocopherol and Carboxyethylhydroxychroman Metabolites in Biology and Medicine. *Free Radic. Biol. Med.* 36 (1), 1–15. doi:10.1016/j.freeradbiomed.2003.10.009

Hidalgo, M., Rodríguez, V., Kreindl, C., and Porras, O. (2020). Biological Redox Impact of Tocopherol Isomers Is Mediated by Fast Cytosolic Calcium Increases in Living Caco-2 Cells. *Antioxidants (Basel)* 9 (2), 155. doi:10.3390/antiox9020155

Hosomi, A., Arita, M., Sato, Y., Kiyose, C., Ueda, T., Igarashi, O., et al. (2019). Affinity for Alpha-Tocopherol Transfer Protein as a Determinant of the Biological Activities of Vitamin E Analogs. *FEBS Lett.* 409, 105–108. doi:10.1016/s0014-5793(97)00499-7

Itoh, K., Ishii, T., Wakabayashi, N., and Yamamoto, M. (1999). Regulatory Mechanisms of Cellular Response to Oxidative Stress. *Free Radic. Res.* 31 (4), 319–324. doi:10.1080/10715769900300881

Itoh, M., Nagafuchi, A., Moroi, S., and Tsukita, S. (1997). Involvement of ZO-1 in Cadherin-Based Cell Adhesion through its Direct Binding to Alpha Catenin and Actin Filaments. *J. Cel Biol* 138 (1), 181–192. doi:10.1083/jcb.138.1.181

Jamro, E. L., Bloom, M. S., Browne, R. W., Kim, K., Greenwood, E. A., and Fujimoto, V. Y. (2019). Preconception Serum Lipids and Lipophilic Micronutrient Levels Are Associated with Live Birth Rates after IVF. *Reprod. Biomed. Online* 39 (4), 665–673. doi:10.1016/j.rbmo.2019.06.004

Jiang, Q., Christen, S., Shigenaga, M. K., and Ames, B. N. (2001). Gamma-Tocopherol, the Major Form of Vitamin E in the US Diet, Deserves More Attention. *Am. J. Clin. Nutr.* 74 (6), 714–722. doi:10.1093/ajcn/74.6.714

Kamal-Eldin, A., and Appelqvist, L. A. (1996). The Chemistry and Antioxidant Properties of Tocopherols and Tocotrienols. *Lipids* 31 (7), 671–701. doi:10.1007/BF02522884

Khan, J. C., Thurlby, D. A., Shahid, H., Clayton, D. G., Yates, J. R., Bradley, M., et al. (2006). Smoking and Age Related Macular Degeneration: The Number of Pack Years of Cigarette Smoking Is a Major Determinant of Risk for Both Geographic Atrophy and Choroidal Neovascularisation. *Br. J. Ophthalmol.* 90 (1), 75–80. doi:10.1136/bjo.2005.073643

Kunchithapautham, K., Atkinson, C., and Rohrer, B. (2014). Smoke Exposure Causes Endoplasmic Reticulum Stress and Lipid Accumulation in Retinal Pigment Epithelium through Oxidative Stress and Complement Activation. *J. Biol. Chem.* 289 (21), 14534–14546. doi:10.1074/jbc.M114.564674

Laster, S. M., and Mackenzie, J. M., Jr (1996). Bleb Formation and F-Actin Distribution during Mitosis and Tumor Necrosis Factor-Induced Apoptosis. *Microsc. Res. Tech.* 34 (3), 272–280. doi:10.1002/(SICI)1097-0029(19960615)34::3<272:AID-JEMT10>3.0.CO;2-J

Lesage, J., Suarez-Carmona, M., Neyrinck-Leglantier, D., Grelet, S., Blacher, S., Hunziker, W., et al. (2017). Zonula Occludens-1/nf-Kb/cxcl8: A New Regulatory axis for Tumor Angiogenesis. *FASEB J.* 31 (4), 1678–1688. doi:10.1096/fj.201600890R

Levee, M. G., Dabrowska, M. I., Lelli, J. L., Jr, and Hinshaw, D. B. (1996). Actin Polymerization and Depolymerization during Apoptosis in HL-60 Cells. *Am. J. Physiol.* 271 (6 Pt 1), C1981–C1992. doi:10.1152/ajpcell.1996.271.6.C1981

Liu, D., Chan, S. L., de Souza-Pinto, N. C., Slevin, J. R., Wersto, R. P., Zhan, M., et al. (2006). Mitochondrial UCP4 Mediates an Adaptive Shift in Energy Metabolism and Increases the Resistance of Neurons to Metabolic and Oxidative Stress. *Neuromolecular Med.* 8 (3), 389–414. doi:10.1385/NMM:8:3:389

Marazita, M. C., Dugour, A., Marquioni-Ramella, M. D., Figueroa, J. M., and Suburo, A. M. (2016). Oxidative Stress-Induced Premature Senescence Dysregulates VEGF and CFH Expression in Retinal Pigment Epithelial Cells: Implications for Age-Related Macular Degeneration. *Redox Biol.* 7, 78–87. doi:10.1016/j.redox.2015.11.011

Matsura, T. (2019). Protective Effect of Tocotrienol on *In Vitro* and *In Vivo* Models of Parkinson's Disease. *J. Nutr. Sci. Vitaminol (Tokyo)* 65 (Supplment), S51–S53. doi:10.3177/jnsv.65.S51

Mehrabi, S., Nasirinezhad, F., Barati, M., Abutaleb, N., Barati, S., Dereshky, B. T., et al. (2019). The Effect of Alpha-Tocopherol on Morphine Tolerance-Induced Expression of C-Fos Proto-Oncogene from a Biotechnological Perspective. *Recent Pat Biotechnol.* 13 (2), 137–148. doi:10.2174/1872208312666181120105333

Melov, S., Coskun, P., Patel, M., Tuinstra, R., Cottrell, B., Jun, A. S., et al. (1999). Mitochondrial Disease in Superoxide Dismutase 2 Mutant Mice. *Proc. Natl. Acad. Sci. U S A.* 96 (3), 846–851. doi:10.1073/pnas.96.3.846

Moore, C., Palau, V. E., Mahboob, R., Lightner, J., Stone, W., and Krishnan, K. (2020). Upregulation of pERK and C-JUN by γ-Tocotrienol and Not α-tocopherol Are Essential to the Differential Effect on Apoptosis in Prostate Cancer Cells. *BMC Cancer* 20 (1), 428. doi:10.1186/s12885-020-06947-6

Müller, A. S., and Pallauf, J. (2003). Effect of Increasing Selenite Concentrations, Vitamin E Supplementation and Different Fetal Calf Serum Content on GPx1 Activity in Primary Cultured Rabbit Hepatocytes. *J. Trace Elem. Med. Biol.* 17 (3), 183–192. doi:10.1016/S0946-672X(03)80024-X

Murakami, K., Kondo, T., Kawase, M., Li, Y., Sato, S., Chen, S. F., et al. (1998). Mitochondrial Susceptibility to Oxidative Stress Exacerbates Cerebral Infarction that Follows Permanent Focal Cerebral Ischemia in Mutant Mice with Manganese Superoxide Dismutase Deficiency. *J. Neurosci.* 18 (1), 205–213. doi:10.1523/JNEUROSCI.18-01-00205.1998

Nybom, P., and Magnusson, K. E. (1996). Modulation of the Junctional Integrity by Low or High Concentrations of Cytochalasin B and Dihydrocytochalasin B Is Associated with Distinct Changes in F-Actin and ZO-1. *Biosci. Rep.* 16 (4), 313–326. doi:10.1007/BF01855015

Pemp, B., Polska, E., Karl, K., Lasta, M., Minichmayr, A., Garhofer, G., et al. (2010). Effects of Antioxidants (AREDS Medication) on Ocular Blood Flow and Endothelial Function in an Endotoxin-Induced Model of Oxidative Stress in Humans. *Invest. Ophthalmol. Vis. Sci.* 51 (1), 2–6. doi:10.1167/iovs.09-3888

Penfold, P. L., Provis, J. M., Furby, J. H., Gatenby, P. A., and Billson, F. A. (1990). Autoantibodies to Retinal Astrocytes Associated with Age-Related Macular Degeneration. *Graefes Arch. Clin. Exp. Ophthalmol.* 228 (3), 270–274. doi:10.1007/BF00920033

Pu, H., Tian, J., Andras, I. E., Hayashi, K., Flora, G., Hennig, B., et al. (2005). HIV-1 Tat Protein-Induced Alterations of ZO-1 Expression Are Mediated by Redox-Regulated ERK 1/2 Activation. *J. Cereb. Blood Flow Metab.* 25 (10), 1325–1335. doi:10.1038/sj.jcbfm.9600125

Reed, J. C. (1995). Regulation of Apoptosis by Bcl-2 Family Proteins and its Role in Cancer and Chemoresistance. *Curr. Opin. Oncol.* 7 (6), 541–546. doi:10.1097/00001622-199511000-00012

Robison, W. G., Kuwabara, T., and Bieri, J. G. (1982). The Roles of Vitamin E and Unsaturated Fatty Acids in the Visual Process. *Retina* 2 (4), 263–281. doi:10.1097/00006982-198202040-00012

Rohrer, B., Bandyopadhyay, M., and Beeson, C. (2016). Reduced Metabolic Capacity in Aged Primary Retinal Pigment Epithelium (RPE) Is Correlated with Increased Susceptibility to Oxidative Stress. *Adv. Exp. Med. Biol.* 854, 793–798. doi:10.1007/978-3-319-17121-0_106

Romero-Vazquez, S., Llorens, V., Soler-Boronat, A., Figueras-Roca, M., Adan, A., and Molins, B. (2021). Interlink between Inflammation and Oxidative Stress in Age-Related Macular Degeneration: Role of Complement Factor H. *Biomedicines* 309 (7), 763. doi:10.3390/biomedicines9070763

Sackett, C. S., and Schenning, S. (2002). The Age-Related Eye Disease Study: the Results of the Clinical Trial. *Insight* 27 (1), 5–7.

SanGiovanni, J. P., Chew, E. Y., Agrón, E., Clemons, T. E., Ferris, F. L., 3rd, Gensler, G., et al. (2008). The Relationship of Dietary ω-3 Long-Chain Polyunsaturated Fatty Acid Intake with Incident Age-Related Macular DegenerationThe Relationship of Dietary Omega-3 Long-Chain Polyunsaturated Fatty Acid Intake with Incident Age-Related Macular Degeneration: AREDS Report No. 23. *Arch. Ophthalmol.* 126 (9), 1274–1279. doi:10.1001/archopht.126.9.1274

Seddon, J. M., George, S., and Rosner, B. (2006). Cigarette Smoking, Fish Consumption, omega-3 Fatty Acid Intake, and Associations with Age-Related Macular Degeneration: the US Twin Study of Age-Related Macular Degeneration. *Arch. Ophthalmol.* 124 (7), 995–1001. doi:10.1001/archopht.124.7.995

Sen, C. K., Khanna, S., and Roy, S. (2006). Tocotrienols: Vitamin E Beyond Tocopherols. *Life Sci.* 78 (18), 2088–2098. doi:10.1016/j.lfs.2005.12.001

Szewczyk, K., Chojnacka, A., and Górnicka, M. (2021). Tocopherols and Tocotrienols-Bioactive Dietary Compounds; what Is Certain, what Is Doubt? *Int. J. Mol. Sci.* 22 (12), 6222. doi:10.3390/ijms22126222

Thomas, C. J., Mirza, R. G., and Gill, M. K. (2021). Age-Related Macular Degeneration. *Med. Clin. North. Am.* 105 (3), 473–491. doi:10.1016/j.mcna.2021.01.003

Tisi, A., Feligioni, M., Passacantando, M., Ciancaglini, M., and Maccarone, R. (2021). The Impact of Oxidative Stress on Blood-Retinal Barrier Physiology in Age-Related Macular Degeneration. *Cells* 10 (1), 64. doi:10.3390/cells10010064

Toma, C., De Cillà, S., Palumbo, A., Garhwal, D. P., and Grossini, E. (2021). Oxidative and Nitrosative Stress in Age-Related Macular Degeneration: A Review of Their Role in Different Stages of Disease. *Antioxidants (Basel)* 10 (5), 653. doi:10.3390/antiox10050653

Tomany, S. C., Cruickshanks, K. J., Klein, R., Klein, B. E., and Knudtson, M. D. (2004). Sunlight and the 10-Year Incidence of Age-Related Maculopathy: the Beaver Dam Eye Study. *Arch. Ophthalmol.* 122 (5), 750–757. doi:10.1001/archopht.122.5.750

Traber, M. G., and Atkinson, J. (2007). Vitamin E, Antioxidant and Nothing More. *Free Radic. Biol. Med.* 43 (1), 4–15. doi:10.1016/j.freeradbiomed.2007.03.024

Uchida, T., Nomura, S., Oda, H., and Ikeda, S. (2018). γ-Tocopherol Is Metabolized Faster Than α-Tocopherol in Young Japanese Women. *J. Nutr. Sci. Vitaminol (Tokyo)* 64 (6), 399–403. doi:10.3177/jnsv.64.399

Ungurianu, A., Zanfirescu, A., Niţulescu, G., and Margină, D. (2021). Vitamin E Beyond its Antioxidant Label. *Antioxidants (Basel)* 10 (5), 634. doi:10.3390/antiox10050634

Venugopal, R., and Jaiswal, A. K. (1998). Nrf2 and Nrf1 in Association with Jun Proteins Regulate Antioxidant Response Element-Mediated Expression and Coordinated Induction of Genes Encoding Detoxifying Enzymes. *Oncogene* 17 (24), 3145–3156. doi:10.1038/sj.onc.1202237

Willems, S., Gellrich, L., Chaikuad, A., Kluge, S., Werz, O., Heering, J., et al. (2021). Endogenous Vitamin E Metabolites Mediate Allosteric PPARγ Activation with Unprecedented Co-Regulatory Interactions. *Cel Chem. Biol.* 28 (10), 1489–1500. doi:10.1016/j.chembiol.2021.04.019

Wong, W. L., Su, X., Li, X., Cheung, C. M., Klein, R., Cheng, C. Y., et al. (2014). Global Prevalence of Age-Related Macular Degeneration and Disease burden Projection for 2020 and 2040: A Systematic Review and Meta-Analysis. *Lancet Glob. Health* 2 (2), e106–16. doi:10.1016/S2214-109X(13)70145-1

Yang, J. G., Zhou, C. J., Li, X. Y., Sun, P. R., Li, S. P., and Ren, B. C. (2015). Alteration of UCP2 and ZO-1 Expression in Trabecular Meshwork of Neovascular Glaucoma Patients. *J. Glaucoma* 24 (4), 291–296. doi:10.1097/IJG.0b013e31829d9b91

Zhang, W., Ma, Y., Zhang, Y., Yang, J., He, G., and Chen, S. (2019). Photo-Oxidative Blue-Light Stimulation in Retinal Pigment Epithelium Cells Promotes Exosome Secretion and Increases the Activity of the NLRP3 Inflammasome. *Curr. Eye Res.* 44 (1), 67–75. doi:10.1080/02713683.2018.1518458

Zhong, Y., Zhang, B., Eum, S. Y., and Toborek, M. (2012). HIV-1 Tat Triggers Nuclear Localization of ZO-1 via Rho Signaling and cAMP Response Element-Binding Protein Activation. *J. Neurosci.* 32 (1), 143–150. doi:10.1523/JNEUROSCI.4266-11.2012

Zingg, J. M. (2019). Vitamin E: Regulatory Role on Signal Transduction. *IUBMB Life* 71 (4), 456–478. doi:10.1002/iub.1986

Conflict of Interest: The authors declare that the research was conducted in the absence of any commercial or financial relationships that could be construed as a potential conflict of interest.

Publisher's Note: All claims expressed in this article are solely those of the authors and do not necessarily represent those of their affiliated organizations, or those of the publisher, the editors and the reviewers. Any product that may be evaluated in this article, or claim that may be made by its manufacturer, is not guaranteed or endorsed by the publisher.

Relevance of Peptide Homeostasis in Metabolic Retinal Degenerative Disorders: Curative Potential in Genetically Modified Mice

Etelka Pöstyéni[1†], Alma Ganczer[1,2†], Andrea Kovács-Valasek[1] and Robert Gabriel[1,2]*

[1]Department of Experimental Zoology and Neurobiology, University of Pécs, Pécs, Hungary, [2]János Szentágothai Research Centre, University of Pécs, Pécs, Hungary

The mammalian retina contains approximately 30 neuropeptides that are synthetized by different neuronal cell populations, glia, and the pigmented epithelium. The presence of these neuropeptides leaves a mark on normal retinal molecular processes and physiology, and they are also crucial in fighting various pathologies (e.g., diabetic retinopathy, ischemia, age-related pathologies, glaucoma) because of their protective abilities. Retinal pathologies of different origin (metabolic, genetic) are extensively investigated by genetically manipulated *in vivo* mouse models that help us gain a better understanding of the molecular background of these pathomechanisms. These models offer opportunities to manipulate gene expression in different cell types to help reveal their roles in the preservation of retinal health or identify malfunction during diseases. In order to assess the current status of transgenic technologies available, we have conducted a literature survey focused on retinal disorders of metabolic origin, zooming in on the role of retinal neuropeptides in diabetic retinopathy and ischemia. First, we identified those neuropeptides that are most relevant to retinal pathologies in humans and the two clinically most relevant models, mice and rats. Then we continued our analysis with metabolic disorders, examining neuropeptide-related pathways leading to systemic or cellular damage and rescue. Last but not least, we reviewed the available literature on genetically modified mouse strains to understand how the manipulation of a single element of any given pathway (e.g., signal molecules, receptors, intracellular signaling pathways) could lead either to the worsening of disease conditions or, more frequently, to substantial improvements in retinal health. Most attention was given to studies which reported successful intervention against specific disorders. For these experiments, a detailed evaluation will be given and the possible role of converging intracellular pathways will be discussed. Using these converging intracellular pathways, curative effects of peptides could potentially be utilized in fighting metabolic retinal disorders.

Keywords: diabetic retinopathy, ischemia, neuropeptides, apoptosis, oxidative stress, inflammation

1 INTRODUCTION

Neuropeptides (NPs) are essential for maintaining a healthy nervous system and are present in many forms and sizes. They act as neurotransmitters, neuromodulators, immunomodulators and play a non-negligible role in endocrine regulation (Burbach, 2011). NPs are produced by neuronal and non-neuronal cells alike and are also expressed in abundance by various cell types of the retina (Bagnoli et al., 2003).

The mammalian retina is a multi-layered, light-sensitive organ of neural origins and contains five major classes of neurons, namely the photoreceptors (PR), horizontal cells (HC), bipolar cells (BC), amacrine cells (AC) and retinal ganglion cells (RGC) which all play a role in the generation of the visual signal. Homeostasis in the retina is also complemented by support from glial cells (most importantly the Müller glia—MC, microglia and astrocytes) and epithelial cells, which form the retinal pigment epithelium (RPE). MCs and the RPE simultaneously contribute significantly to NP production and they are known to express multiple types of NPs while retinal neurons (mainly ACs) tend to always express a singular type (for a summary, see **Table 1** but please note that peptides are represented in alphabetic order and not in order of relevance). Besides the glial and epithelial support, healthy vascularization is also crucial for maintaining normal retinal function. The

TABLE 1 | Peptides and proteins markedly relevant for retinal health in the mouse, rat and human retinas.

Row	Peptides	Abbreviation	Source	Receptors	Receptor expression	Main function
				Peptides and other factors markedly relevant for retinal health in the mouse, rat and human retinas[a]		
1	Angiotensin II	Ang II	PR[3], (GC)[3], MC[3] (Senanayake et al., 2007) + extraretinal	AT1R (vasoconstrictor), AT2R (vasodilatator)	AT1R: RPE[1,3], PR[1,3], ON BC[2], AC[1,2,3], GC[1,3], MC[2,3], astrocyte[2] AT2R: RPE[1,3], AC[1,2], GC[1,2,3], MC[3] (Choudhary et al., 2017; Verma et al., 2019)	Regulation of blood pressure
2	Angiotensin (1-7)	Ang (1-7)	MC[3] (Senanayake et al., 2007)	MasR	PR[1], GC[1], MC[1] (Prasad et al., 2014)	Counteracts Ang II
3	Erythropoietin	EPO	RPE[3], neuroretina[3], + extraretinal (Hernández and Simó, 2012; Luo et al., 2015) + extraretinal	EPOR	GC[1,3] (Shah et al., 2009)	Hormone, cytokine, red blood cell production
4	Glucagon-like Peptide-1	GLP-1	Extraretinal	GLP-1R	MC[2], INL[2], GCL[2,3] (Zhang et al., 2009; Zhang et al., 2011; Hebsgaard et al., 2018)	Glucose dependent insulin secretion, inhibits glucagon secretion
5	Neuropeptide Y	NPY	AC[1,2,3], dAC[1,2,3] (Sinclair and Nirenberg, 2001; Christiansen et al., 2018a)	Y1, Y2, Y4, Y5	RPE[2,3], PR[2], BC[2], HC[2], AC[2], GC[2], MC[2,3], microglia[2] (Santos-Carvalho et al., 2015)	Retina development, neuromodulator
6	Pituitary adenylate cyclase-activating polypeptide	PACAP	HC[2], AC[2], (GC)[2] (Izumi et al., 2000)	PAC1R, VPAC1R, VPAC2R	PAC1R: AC[2], GC[2] (Dénes et al., 2014)	Neuromodulator
7	Somatostatin	SST	RPE[3], AC[1,2], dAC[1,2], neuroretina[3] (Cristiani et al., 2002; Dubovy et al., 2017)	sst1-5	sst$_{2A}$: rodBC[1,2], HC[1,2], AC[1,2] sst$_4$: GC[1] (Cristiani et al., 2002)	Hormone, neurotransmitter, neuromodulator
8	Substance P	SP	BC[1], AC[1,2,3], dAC[3], GC[3] (Cuenca et al., 1995; Casini et al., 2000; Catalani et al., 2004)	NK1, (NK3)	NK1: ON BC[1], AC[1,2], dAC[2], GC[2] NK3: OFF BC[1,2], AC[2] (Casini et al., 2000; Catalani et al., 2004)	Neurotransmitter, neuromodulator

Row	Other factors	Abbreviation	Source		Receptor expression	Main function
9	Brain-derived neurotrophic factor	BDNF	AC[1,2], (GC)[1,2], MC[3] (Bennett et al., 1999; Oku et al., 2002; Vecino et al., 2002; Avwenagha et al., 2006)	TrkB	PR[3], AC[1,2], GC[1,2] (Cellerino and Kohler, 1997; Vecino et al., 1998; Vecino et al., 2002)	Neuron growth, differentation and survival, synaptogenesis
10	Pigment epitethlium derived factor	PEDF	RPE (Rebustini et al., 2021)	PEDF-R	RPE, PR (Rebustini et al., 2021)	Neurothrophic, anti-angiogenic, anti-tumorigenic
11	Vascular endothelial growth factor	VEGF	RPE[2], PR[3], HC[3], BC[3], AC[3], (GC)[3], MC[3] (Sall et al., 2004; Saint-Geniez et al., 2008)	VEGFR1, VEGFR2, VEGFR3	VRGF2R: RPE[2,3], PR, MC (Famiglietti et al., 2003; Saint-Geniez et al., 2008)	Angiogenesis

A variety of neuropeptides and other proteins are expressed in the mammalian retina, along with their receptors, and these molecules play a diverse role in maintaining normal retinal function. Amacrine cells ACs, müller cells and the cells of the pigment epithelium contribute the most significantly to intraretinal neuropeptide production. Ganglion cells are represented in brackets as the peptides and proteins released from their axons exert their effects outside of the retina. Abbreviations: AC, amacrine cell; BC, bipolar cell; dAC, displaced amacrine cell; GC, ganglion cell; GCL, ganglion cell layer; HC, horizontal cell; INL, inner nuclear layer; IPL, inner plexiform layer; MC, Müller cell; PR, photoreceptor; RPE, retinal pigment epithelium.
[a]Peptides and proteins contained in this table are listed in alphabetical order and not in any order of importance or other relevance: [1]mouse, [2]rat, [3]human.

neurovascular unit, which encompasses all neuronal, glial and vascular elements that exist in close interdependence, is an especially vulnerable target for pathologies affecting retinal integrity (Nian et al., 2021). Retinal diseases are the leading cause of blindness worldwide and can be divided into two major categories based on their origin: genetic or metabolic. Both of these pose a substantial threat to retinal health and vision.

In the last few decades, the advancement of technology has opened the way for a new era in scientific research. The development of genetically modified (GM) animal models, in particular, has led to a wealth of knowledge concerning the genetic background and the genotype-phenotype connection of disease pathogenesis at molecular level. Mice, for example, have proven to be especially useful models in this regard. These transgenic models also allow researchers to test novel and innovative therapeutic approaches, bringing us once again closer to fully understanding disease etiology. One notable field of research where transgenic animal models have proven to be truly effective is the mimicking of typical human retinal pathologies with genetic origin; the MGI (Mouse Genome Informatics) database currently contains 27 different transgenic models which can be used as a model for multiple retinal diseases (e.g., retinitis pigmentosa, age-related macular degeneration, retinoblastoma, Stargardt disease, cone-rod dystrophy) (for an extensive summary, see **Supplementary Table S1**). The development of animal models of hereditary retinal diseases is based, first and foremost, on the identification of disease causing genes, which can then later be removed or (re)introduced to the genome of the model animal. Results from such experiments have already been extremely useful in answering fundamental questions regarding both disease pathophysiology and normal gene function (Flannery, 1999; Haruyama et al., 2009; Maeda and Maeda, 2018).

Diseases of metabolic origin (e.g., diabetic retinopathy, damage caused by ischemia or complications related to aging), however, have proven to be more challenging to replicate with transgenic models as their genetic background is significantly more complex and their pathophysiology is affected by a combination of (often unmapped) genetic and environmental factors (Ramkumar et al., 2010; Fletcher et al., 2011).

In the last 50 years, the mouse retina has been the subject of extensive research. Genetically modified mouse strains have served on the forefront of transgenic research (Jaenisch and Mintz, 1974) and have been frequently utilized ever since (Navabpour et al., 2020). In general, the mouse can be considered a well-known and acknowledged model of the mammalian retina, along with the rat (Ellenbroek and Youn, 2016). Rats, while not typically applied as transgenic models, have played a crucial role in physiological and biomedical research (Smith et al., 2019), yielding numerous non-GM models mimicking human pathologies (Szpirer, 2020). Because of that, we chose to build the current review first and foremost on the research carried out in mice, supported by data obtained from rat models and, whenever possible, complemented by information regarding the workings of the human retina.

The aim of the present study, therefore, has been to provide a summary on the current status of genetic mouse models utilized in the research of retinal NPs, with particular attention paid to the utilization of said models in studying major retinal diseases of metabolic origin. To achieve this, we will i) discuss the current understanding of NPs expressed in the mammalian retina, ii) the roles they play in enhancing or alleviating disease pathophysiology in major retinal diseases of metabolic origin (namely diabetic retinopathy, ischemia), and iii) highlight intracellular pathways where transgenic modifications connected to NP expression can offer us further insight to combat retinal degeneration. More specifically, we highlight how neuropeptide-related research embedded into different knockout and transgenic mouse models can help us answer a plethora of previously unanswered questions about complex manifestations of metabolic retinal diseases and their new promising therapeutic opportunities.

2 NEUROPEPTIDES MOST RELEVANT FOR RETINAL HEALTH

In the present day, NPs are generally defined as biologically active substances that are produced by neurons in order to modulate nervous system functions. While the precise term "neuropeptide" has only been coined by David de Wied in 1971 (de Wied, 2000; Burbach, 2011), signal molecules of this kind have been the focus of extensive study since the early days of endocrinology, as many of them had first been discovered as part of the hormonal regulatory system (Burbach, 2011). The diversity in origin (neuronal or non-neuronal) and function (neurotransmitter, neuromodulator or an agent of endocrine, paracrine or autocrine regulation) has provided a substantial material for research. Beside the classical molecules produced by nerve cells, putative NPs (produced by glial cells, for example) also play an important role in maintaining a healthy and functioning nervous system (Burbach, 2011). NPs are (both in the classical and putative sense) also expressed in the retina (Bagnoli et al., 2003) by both neurons, glia and cells of the RPE (**Table 1**). A variety of NPs have been demonstrated to play an important and diverse role in maintaining healthy retinal function and therefore could already be used to prevent tissue and cell damage when tissue integrity is compromised as a result of pathological processes (Otani et al., 2000; Junk et al., 2002; Zhang et al., 2011). While there are many questions still waiting to be answered, our current knowledge regarding NPs far exceeds the boundaries of this article. As such, this paper focuses specifically on peptides with substantial influence on retinal health. For a short summary of the selected peptides discussed in detail, please refer to **Table 1**.

2.1 The Retinal Renin-Angiotensin System

The renin-angiotensin system (RAS) plays an essential role in regulating blood pressure and keeping fluid volume and electrolyte composition under control. Currently, the existence of a local RAS in the retina seems well supported (see row 3 of **Table 1**), considering that its individual components (hormonal and enzymatic alike) appear to be all expressed in retinal tissue (Choudhary et al., 2016).

The active form of angiotensin, angiotensin II (Ang II), is generated by the cleavage of angiotensinogen into angiotensin I in the presence of renin, which in turn is cleaved by the angiotensin converting enzyme (ACE) to form Ang II. The release of Ang II is generally known to induce vasoconstriction, thirst and the release of aldosterone (Culman et al., 1995) and has also been demonstrated to possess pro-inflammatory effects (Ruiz-Ortega et al., 2001; Chen et al., 2006; Ruiz-Ortega et al., 2006; Wilkinson-Berka et al., 2019), which are all conveyed through the angiotensin II type 1 receptor (AT1R; Forrester et al., 2018). AT1 receptors are G-protein coupled receptors that ultimately trigger the release of Ca^{2+} from the endoplasmic reticulum which results in the activation of protein kinase C (PKC) and additional kinase enzyme activation in the extracellular signal-regulated kinase (ERK1/2) pathway (Simões et al., 2020). In contrast, the type 2 receptor (AT2R) is generally understood to act against AT1R, as it is known to elicit vasodilation through the generation of nitric oxide (NO) and contribute to cell survival (Reinecke et al., 2003; Carey, 2017; Verma et al., 2019). The signaling pathways connected to AT2R, however, are not yet fully understood (Sadybekov and Katritch, 2020). It is believed that AT2R activation does not follow the traditional G-protein coupled receptor mechanisms and affects downstream mediators instead of directly altering cyclic adenosine monophosphate (cAMP) or Ca^{2+} levels. It has been proposed that receptor activation causes ERK1/2 dephosphorylation (Porrello et al., 2009), counteracting the effects of AT1R. Connections between AT2R activation and an increase in NO and cyclic guanosine monophosphate (cGMP) production have also been observed (Porrello et al., 2009). The AT1R is expressed by a large variety of retinal cells (RPE, PR, AC, GC, MC and certain ON BC) in the human, rat and mouse retinas (Senanayake et al., 2007; Choudhary et al., 2016), while AT2R expression is less widespread and not expressed by PR and BC in mice (Verma et al., 2019) (for comparison, see row 1 of **Table 1**).

Besides Ang II, other derivatives of Ang I also exist: angiotensin-(1-7) or Ang (1-7) is a peptide generated by angiotensin converting enzyme 2 (ACE2), which also plays an important role in counteracting the effects of Ang II and therefore has been studied for its protective properties (Santos et al., 2018). The effects of Ang (1-7) (including anti-inflammatory and antiproliferative effects, antioxidant properties and vasodilation through NO release) are conveyed through the Mas receptor, forming the ACE2/Ang (1-7)/Mas protective axis (Fletcher et al., 2010; Peiró et al., 2013; Prasad et al., 2014). The Mas receptor so far has been connected to adenylate cyclase-related signal pathways (through Gαi2), with receptor activation having negative impact on cAMP levels and ERK1/2 phosphorylation (Burghi et al., 2017). Ang (1-7) and its receptor are also expressed in the retina (see row 2 of **Table 1**) (Senanayake et al., 2007; Verma et al., 2012; Prasad et al., 2014). Ang (1-7) is present in the MCs of the human retina (Senanayake et al., 2007) and the mouse retina contains the Mas receptor on PRs, GCs and MCs (Prasad et al., 2014).

2.2 Erythropoietin

Erythropoietin (EPO) is a glycoprotein hormone primarily produced by the kidneys under hypoxia and its main function is the stimulation of erythropoiesis. However, EPO production has been demonstrated in various tissues beside the kidneys, including the retina, where the hormone is suspected to play an important role during retinal development (Reid and Lois, 2017). The EPO receptor (EPOR) is expressed in both nuclear layers in addition to its expression in the GCL and the RPE of the human retina, and human and mouse GCs are both known to express EPOR (Hernández and Simó, 2012; Luo et al., 2015; Shah et al., 2009; see row 3 of **Table 1**). Ligand binding of the EPO receptor is known to trigger dimerization, although the pathways associated with the erythropoietic and neuroprotective functions of EPO seem to differ to some degree (Sollinger et al., 2017). In the first step of the signaling pathway, the dimerization of the EPOR activates the janus kinase 2 (JAK2) enzyme, which is also present in neurons (Digicaylioglu and Lipton, 2001). The neuroprotective capabilities of EPO appear to be conveyed through nuclear factor kappa B (NF-κB), mitogen-activated protein kinase (MAPK), signal transducer and activator of transcription 5 (STAT5) and phosphoinositide 3-kinase (PI3K) activation (Ma et al., 2016; Sollinger et al., 2017). The neuroprotective properties of this hormone are likely conveyed through anti-apoptotic, anti-inflammatory, antioxidative pathways and through its effects on angiogenesis. The duality between its erythropoietic and non-erythropoietic (or tissue protective) effects likely stems from EPO having two different receptor types (McVicar et al., 2011).

2.3 Glucagon-Like Peptide-1

Glucagon-like peptide-1 (GLP-1) is first and foremost recognized as an incretin hormone that regulates glucose-dependent insulin secretion. GLP-1, at the same time, can be detected in the mammalian retina (expression confirmed in the rat retina by Zhang et al., 2009; and in the human retina by Hebsgaard et al., 2018). GLP-1 has been found to convey a wide array of neuroprotective effects in retinal diseases (see **Section 5** for more information). While the GLP-1R is undoubtedly present in retinal tissue (Zhang et al., 2009; Zhang et al., 2011; Hebsgaard et al., 2018; see row 4 of **Table 1**), locating and identifying specific GLP-1R expressing cell types have proven quite challenging as the specificity of the antibodies used to label GLP-1R have been called into question (Hebsgaard et al., 2018). So far, GLP-1R has been localized to the inner retina, mainly to the GCL and to MCs in the rat retina (Zhang et al., 2011) and the GCL in humans (Hebsgaard et al., 2018). GLP-1R agonists, including exenatide, liraglutide, lixisenatide, semaglutide and others, are already routinely used in the treatment of diabetic retinopathy (Pang et al., 2018). The GLP-1 receptor is, to our current understanding, a G-protein coupled receptor that acts through the regulation of adenylate cyclase activity and protein kinase A (PKA), activating the PI3K and mammalian target of rapamycin (mTOR) pathways (Carlessi et al., 2017).

2.4 Neuropeptide Y

Neuropeptide Y (or NPY for short) is one of the most well-known on the list of neuroprotective peptides. It has been first isolated by Tatemoto in 1981 from porcine nervous tissue (Tatemoto and Mutt, 1981) and later from the human retina (Straznicky et al.,

1992). It belongs to the NPY family of peptides with a series of different NPY receptor subtypes sorted into three different subfamilies (Larhammar et al., 2001). Out of the different subtypes, Y1 and Y2 appear to be the most common in the retina with Y4 and Y5 present in certain non-neuronal cell types (Santos-Carvalho et al., 2014; reviewed in detail by Santos-Carvalho et al., 2015) (see row 5 of **Table 1**). NPY receptors are thought to act mostly through the inhibition of adenylate cyclase and the cAMP pathway (Martins et al., 2015), although the Y2 and Y4 receptors have been shown to couple to Gq in rabbit smooth muscle cells (Misra et al., 2004). NPY, in general, exerts its effect through the reduction of Ca^{2+} influx and moderates changes in intracellular Ca^{2+} levels (D'Angelo and Brecha, 2004; Alvaro et al., 2009). In the mouse retina, NPY is expressed by both ACs and displaced ACs (dAC), which is very similar to the labelling experienced in rats (Sinclair and Nirenberg, 2001). In the human retina, NPY is also expressed by ACs and dACs (Christiansen et al., 2018a).

2.5 Pituitary Adenylyl Cyclase-Activating Polypeptide

Pituitary adenylyl cyclase-activating polypeptide (PACAP) has first been isolated from the hypothalamus in 1989 (Miyata et al., 1989) and come in two forms based on amino acid length, namely PACAP-38 and PACAP-27, with PACAP-38 (referred to simply as PACAP going forward) being the target of extensive research for its neuroprotective capabilities (reviewed by Gábriel et al., 2019). PACAP belongs to the same family as vasoactive intestinal polypeptide (VIP), together with glucagon and secretin. There are three different receptors conveying the effects of PACAP, named PAC1-R (highest affinity), VPAC1-R and VPAC2-R. The signal pathways activated by PACAP receptors are well mapped and PAC1-R and VPAC-1R are known to act both through the activation of adenylate cyclase/PKA/MAPK axis and the phospholipase/inositol trisphosphate/protein kinase C (PLC/IP3/PKC) axis, while VPAC-2R has only been connected to adenylate cyclase activation (Gábriel et al., 2019). In the rat retina, PACAP is expressed by ACs, GCs and HCs while the PAC1-R has been localized to ACs, GCs and the MCs (Izumi et al., 2000; Dénes et al., 2014; see row 6 of **Table 1**). PACAP is also able to interfere with the stress response through the stimulation of corticotropin releasing hormone secretion (Agarwal et al., 2005). A glucocorticoid analogue, namely dexamethasone, proved its long-term and safe effect in diabetic macular edema treatment. PACAP can impact the hypothalamo-pituitary axis and could counterbalance the effects of corticotropin releasing hormone activity, thus influencing damage caused by diabetic conditions (Bucolo et al., 2018).

VIP is expressed by ACs in the retina (Pérez de Sevilla Müller et al., 2019). Originally, VIP has been described as a vasodilatator but possesses a variety of other functions that it exerts through the VPAC1-R and VPAC2-R (Atlasz et al., 2010; reviewed by Cervia et al., 2019). However, the effectiveness of VIP retinoprotective functions seem to fall short compared to PACAP (Szabadfi et al., 2012a).

2.6 Somatostatin

Somatostatin (SST), also called somatotropin release inhibiting factor, is yet another peptide hormone that has been proven to possess neuroprotective properties. SST is expressed in the retina in both of its known active forms (SST-14 and SST-28). SST is produced mainly by the RPE and GABA-ergic ACs (Cristiani et al., 2002; Hernández et al., 2014; Postyeni et al., 2021) and its receptors are present on the PRs, HCs, ACs and RGCs (Cervia et al., 2008a; see row 7 of **Table 1**). The five G-protein coupled SST receptor types (sst1-5) are all present in the human retina according to the work published by Pérez-Ibave et al. (2019). Li and colleagues suggest that sst5 exerts its effect through the NO/cGMP/protein kinase G pathways and the suppression of T-type Ca^{2+} channels (Li et al., 2019), while sst4 was proposed to modulate L-type Ca^{2+} channels instead (Farrell et al., 2014). Sst2 also acts through the production of cGMP (Mastrodimou et al., 2006) and Thermos and colleagues proposed that sst1 likely acts as an autoreceptor (Thermos et al., 2006).

SST receptor mRNA levels have been specifically measured in the mouse retina, suggesting the abundant expression of sst2 and sst4, accompanied by the less prominent expression of sst1 and very low mRNA levels for sst3 and sst5 overall (Cristiani et al., 2002). Immunoreactivity for sst2A was observed in rodBC, HC and AC, including tyrosine hydroxylase immunoreactive, GABA-erg and glycinerg ACs. SST labeling has been demonstrated in ACs and dACs in the mouse retina but not in GCs, similar to rats (Cristiani et al., 2002).

2.7 Substance P

Another important peptide with significant neuroprotective effects is substance P (SP), a member of the tachykinin peptide family. As a neurotransmitter, SP is known to have excitatory effects on both amacrine and retinal ganglion cells (Zalutsky and Miller, 1990). As a neuromodulator, SP stimulates dopamine release (Casini et al., 2004). Out of the three tachykinin receptor types (neurokinin 1, 2 and 3 receptors, abbreviated as NK1, NK2 and NK3, respectively), only NK1 and NK3 are present in the retina. NK1 receptors (with the highest affinity for SP) are found on ON BCs and a diverse population of ACs while NK3 appears to be reserved for ON BCs (Oyamada et al., 1999; Kim et al., 2005; see row 8 of **Table 1**). Interestingly, there seems to be considerable difference between NK1 expression patterns among different mammalian retina models both during development and in adult animals (Catalani et al., 2006). Neurokinin receptors all belong to the group of G-protein coupled receptors and they are responsible for the activation of PLC and adenylate cyclase, and carry the potential to bind all three neurokinin ligands with different affinity: in addition to SP being the preferential ligand of the NK1 receptor, neurokinin A and B are the preferential ligands of the NK2 and NK3 receptors, respectively. MAPKs, ERK1/2 and mTOR and NF-κB are all involved in SP-related signaling through the NK1 (Mashaghi et al., 2016).

In the mouse retina, SP expression has been localized to ACs (Haverkamp and Wässle, 2000). NK1 receptors are expressed by ON bipolar cells (Catalani et al., 2004), although the same labelling isn't present in rats (Casini et al., 1997; Casini et al., 2000). However, the NK1 expression patterns in ACs appear similar in both species and they are present in a diverse group of

ACs, including co-localization with GABA, tyrosine hydroxylase and SP (Casini et al., 2000; Catalani et al., 2004). In humans, SP immunoreactivity was also detected in dACs and GCs (Cuenca et al., 1995).

2.8 Additional Factors

In addition to NPs, a variety of other molecules contribute to the development and maintenance of a healthy retina. Similar to the peptides listed above, the mammalian retina expresses a number of growth factors, hormones and other neurotrophic proteinaceous substances. The brain-derived neurotrophic factor (BDNF) is present in the retina and contributes to both retinal development and health. BDNF is produced by a variety of neurons (PRs, RGCs, ACs) and glia (MCs) alike (Bennett et al., 1999; Oku et al., 2002; Vecino et al., 2002; Avwenagha et al., 2006) and it exerts its effects through a tyrosine kinase receptor, tropomyosin receptor kinase B (TrkB) (reviewed by Fudalej et al., 2021). TrkB has the highest affinity for BDNF as its ligand among growth factors and affects MAPK activity and the PI3K and the PLC gamma pathways (reviewed by Huang and Reichardt, 2003). In the retina, the TrkB receptor is expressed by PR, AC and RGCs (Cellerino and Kohler, 1997; Vecino et al., 1998; Vecino et al., 2002; see row 9 of **Table 1**). Pigment epithelium derived factor (PEDF) is produced by the cells of the RPE, with its receptor (PEDF-R) simultaneously present on cells of the RPE and PRs (see row 10 in **Table 1**). As a consequence, PEDF exerts its protective effects mainly on PRs. Our current knowledge on PEDF action has been reviewed by Rebustini et al. (2021). So far, several potential targets have been reported for the pathways involved in PEDF signaling, including MAPK activation, JAK/STAT, PI3K and additional pathways (Pagan-Mercado and Becerra, 2019). Vascular endothelial growth factors (VEGF-A, B, C and D) are molecules with proangiogenic effects. VEGF can be produced by multiple cells of the retina, including MCs, astrocytes, RGCs and the epithelial cells of the retinal vasculature and the RPE (Saint-Geniez et al., 2008; see row 11 in **Table 1**). While VEGF seems to convey a certain amount of neuroprotection on PRs (Suzuki et al., 2011) and RGCs (Froger et al., 2020), it is also responsible for facilitating pathological neovascularization in the retina. VEGFs exert their effects through tyrosine-kinase type receptors (VEGF-R). VEGF-R1, VEGF-R2 and VEGF-R3 are all expressed in the retina, although VEGF-R2 and R3 expression appears to be upregulated in pathological conditions (Witmer et al., 2002). It is important to note that all VEGF receptors all possess tyrosine kinase activity. VEGF-R2 is considered to be the most important mediator of VEGF-related angiogenesis. After autophosphorylation, the MAPK pathway is activated through PLC gamma (Takahashi et al., 2001). Receptor activation also affects the PI3K pathway, among others (Kowanetz and Ferrara, 2006).

3 GENETICALLY MODIFIED EXPERIMENTAL MODELS IN THE STUDY OF RETINAL HEALTH

In the last few decades, mouse models played a prominent role in furthering our understanding of the cause and effect of retinal diseases as they share several similar biochemical, physiological

and anatomical features with the human retina. Now that the methodology for genetic manipulation is already well-established, it has become an immensely powerful tool that provides detailed step-by-step analysis of disease progression and pathophysiology. At the moment, the MouseMine database contains more than 230 different mouse models connected to different retinal diseases. In fact, the very targets of these investigations could be the individual retinal cell types and retinal synaptic connections. For that, the manipulation of different mouse models is ideally based on a construct with suitable cell-specific promoters, where the transgene is expressed under strict control or after specific induction (e.g., tissue-specific drug-induction). As an option, we can create knockout (KO) models (conditional or conventional), where the inactivation of the target gene helps us understand the biological function of the now missing gene product. As another option, random exogenous transgene integrations, gene knock-in or target gene overexpression are also useful approaches for studying the actual changes of different biological traits. In the perspective of complex metabolic retinal pathologies, the use of these methods cannot only be based on the well-known genetic background of diseases but, with these technologies, it is certainly achievable to describe or modify the specific pathways and mediators involved. Genetically modified mouse lines offer new insight in understanding the altered behavior of different retinal cell types and the changing expression of signal molecules in the manifestation of retinal impairments. The protective effect of NPs could also be made traceable in different disease models at multiple molecular levels. Although there are many studies about the promising effect of NPs and the usefulness of the transgenic approaches in retinal diseases, their combination in the research process remains limited. In the present work, we try to collect available knowledge on the different genetic models in metabolic retinal diseases (DR, ischemia) listing advantages and supplementing with promising therapeutic effects of different NPs.

3.1 Genetic Models in the Research of Neuropeptide Function in the Retina

The past decades have seen an increase in the use of genetically modified animal models in retinal research, which improved our knowledge of the cell-specific developmental, degenerative and rescue processes. They have been widely used in investigations of PR development (Fong et al., 2005) and degeneration (Geiger et al., 1994; Joseph and Li, 1996; Kanan et al., 2010; Tolmachova et al., 2010; Lipinski et al., 2011; Wu et al., 2012; Roman et al., 2018; Zhong et al., 2020); BC (He et al., 2019; Yang et al., 2019), MC (Peant et al., 2007) and GC degeneration (Husain et al., 2014; Wang L. et al., 2020) and also in rescue processes (McNally et al., 1999; Dong et al., 2007; Liu et al., 2012; Garcia-Caballero et al., 2018; Wang et al., 2019). However, the detailed discussion of genetic disorders leading to retinal degeneration are beyond the scope of the present review. At the same time, alterations in NP expression could also be achievable through these genetic models in the retina, offering additional information on normal retinal physiology, as well as the therapeutic role of NPs in pathologies. Indeed, changes in peptide homeostasis elicited by genetic means

TABLE 2 | Effect of neuropeptides on retinas affected by diabetic retinopathy and ischemia.

		Effect of neuropeptides on retinas affected by diabetic retinopathy and ischemia							
Row	Peptide	Effect on retinal pathophysiology[a]						Effect on disease progression	
1		Apoptosis or cell death	Oxidative stress	Autophagy	Immune response and inflammation	BRB breakdown	Neovasularization (VEGF expression)	Diabetic retinopathy	Ischemia
2	AngII		Pro (Wilkinson-Berka et al., 2013)		Pro (Wilkinson-Berka et al., 2019)		Pro (Otani et al., 2000)	Progression (Choudhary et al., 2016)	Progression (Fukuda et al., 2010)
3	Ang (1-7)	Anti (Verma et al., 2012)[b]	Anti (Verma et al., 2012)[b]		Anti (Verma et al., 2012)[b]			Likely protective (Verma, 2012)[b]	
4	EPO	Anti (Luo et al., 2015; Reid and Lois, 2017)	Anti (Luo et al., 2015)		Anti (Reid and Lois, 2017; Xie et al., 2021)	Anti (Xu et al., 2014)	Conflicting results (Reid and Lois, 2017) anti (Bretz et al., 2020)[b]	Conflicting results	Protective (Junk et al., 2002; Mowat et al., 2012)
5	GLP-1	Anti (Zhang et al., 2011; Fan et al., 2014a; Hernández et al., 2016)	Anti (Ramos et al., 2020[b]; Zhou et al., 2021)	Inhibits (Cai et al., 2017)	Anti (Gonçalves et al., 2016; Chung et al., 2020)	Anti (Fan et al., 2014b; Gonçalves et al., 2016)	Anti (Fan et al., 2014b)	Conflicting results (Marso et al., 2016; Simó and Hernández, 2017; Bain et al., 2019; Saw et al., 2019; Dauner and Farley, 2021)	Protective (Gonçalves et al., 2016)
6	NPY				Anti (Ferreira et al., 2010)		Conflicting results, anti in DR (Ou et al., 2020)	Likely protective (Ou et al., 2020)	Conflicting results (Christiansen et al., 2018)
7	PACAP	Anti (Atlasz et al., 2010; Szabadfi et al., 2014; Szabadfi et al., 2016)			Anti (Werling et al., 2016; D'Amico et al., 2017)	Anti (Maugeri et al., 2019)	Anti in DR (D'Amico et al., 2017; Maugeri et al., 2017) no effect in ischemia (Schmid et al., 2012)[b]	Protective (Szabadfi et al., 2016; Gábriel et al., 2019; Maugeri et al., 2019)	Protective (Atlasz et al., 2010; Danyadi et al., 2014; Werling et al., 2014; Vaczy et al., 2016; Werling et al., 2016; Werling et al., 2017)
8	SST/ OCT	Anti (Dal Monte et al., 2012[b]; Wang et al., 2015; Amato et al., 2016)	Anti (Wang et al., 2015)	Inhibits (Amato et al., 2018)	(Hernandez et al., 2020)[b]		Anti (Cervia et al., 2012[b]; Amato et al., 2020)	Protective (Amato et al., 2018)	Protective (Mastrodimou et al., 2005; Wang et al., 2017)
9	SP	Anti (Yang et al., 2013)	Anti (D'Alessandro et al., 2014)		Anti (Baek et al., 2020)		No effect (Schmid et al., 2012)[b]	Protective (Yang et al., 2013)	Protective (Sakamoto et al., 2017)

Diabetic retinopathy and ischemia can both exert their deleterious effects through multiple pathways, including oxidative stress, inflammation, apoptosis and uncontrolled neovascularization that eventually culminate in the disruption and the destruction of the neurovascular unit. Neuropeptides have been shown to exert protective or destructive capabilities under these pathological conditions.
[a]For this review, we only considered results obtained from models of DR or ischemia.
[b]Results obtained from genetically modified animal models.

clearly causes alterations in retinal microanatomy or physiology. For example, overexpression of PAC1R caused a decline in GABAergic AC production (Lang et al., 2010), while overexpression of BDNF modified RGC dendritic branching (Liu et al., 2007). Deletion of the PAC1 receptor has caused a deficit in RGC numbers (Van et al., 2021), and BDNF+/− mice also showed lower cell numbers in the ganglion cell layer and a decline in the inner retinal function observable in the form of decreased amplitude of positive scotopic threshold responses (Gupta et al., 2014). Research carried out in NP gene KO models has demonstrated the prominent role of PACAP in retinal age-related changes (Kovacs-Valasek et al., 2017). A

BDNF KO model has been used to emphasize the role of BDNF in RGC development (Cellerino et al., 2003). The physiological function and distribution of VIP in retinal cells has also been investigated by transgenic technology (Park et al., 2015; Pérez de Sevilla Müller et al., 2019), as well as the role of orexins in retinal function via influencing dopaminergic cells (Qiao et al., 2017). Interaction between peptides can also be turned into a powerful tool; in the BDNF KO model, the BDNF-mediated VIP expression has been studied in ACs (Ladewig et al., 2004). Repeated intravitreal injections of PACAP caused elevated somatostatin containing cell numbers in SST transgenic mice in the aging retina (Postyeni et al., 2021). To reveal the specific effect of neuropeptides exerted in retinal pathologies, the design of new models was mandated, which has also helped recognize the complex biological importance of NPs.

4 METABOLIC RETINAL DISEASES: PATHOLOGY AND NEUROPEPTIDES

Normal retinal function is essential for maintaining visual perception, meaning that any disease or injury that threatens retinal integrity is a cause for substantial concern. Diseases of metabolic origin pose an especially serious problem for people worldwide (Rodríguez et al., 2021; Simó et al., 2021) and the need to find treatment for these conditions is greater than ever. NPs have also been utilized in the fight for maintaining retinal integrity—with varying efficiency (see **Table 2**).

While the neural elements of the retina are especially sensitive to insult and injury, it is important to remember that functioning glial cells, a steady supply of blood and a healthy blood-retina-barrier (BRB) are all necessary for this organ to function. In many cases, the main reason for the loss or impairment of vision lies in the degradation of the neurovascular unit (the functional connective of neuron, glia and the blood vessels) and the loss of integrity in the blood-retina-barrier, which leads to the perturbation of the retinal microenvironment (Simó et al., 2021). Diseases of metabolic origin tend to attack on multiple fronts, making it even harder to combat their effects; the so-called deleterious effects often manifest themselves through the production of reactive oxygen species (ROS), taking substantial resources from the body to combat oxidative stress (Kowluru and Chan, 2007). Inflammation (and the activation of the immune system) is also a common factor in disease pathology (Whitcup et al., 2013). Eventually, the accumulated damage leads to either necrosis or apoptosis. Any damage to the neurovascular unit will threaten retinal integrity as a whole, so pathological processes affecting retinal vasculature or the BRB are extremely dangerous (Erickson et al., 2007; Nian et al., 2021). Because of the high metabolic demand, the retina has extensive capabilities for neovascularization that can quickly spiral out of control when growth factor (mainly VEGF) expression runs unchecked, which provides yet another vulnerability for diseases to exploit (Campochiaro, 2013). Over the course of time and in small, manageable quantities, many of these aspects also contribute to the natural process of aging or senescence (see Figure 10 in Kovács-Valasek et al., 2021).

4.1 Diabetic Retinopathy

Diabetic retinopathy (DR) results from the extensive damage caused to the retinal vasculature and tissue by diabetes mellitus (DM). Because of the high prevalence of DM in modern society, DR has been identified as a major health concern and one of the leading causes of blindness worldwide (Simó-Servat et al., 2019). In patients with diabetes, the increased glucose influx causes an overproduction of advanced glycation end-products (Milne and Brownstein, 2013) and ROS (Sasaki et al., 2010; Kang and Yang, 2020). In the early (or non-proliferative) stage, the pericytes are the first to fall (Romeo et al., 2002), only to be followed by the epithelial cells soon after, leading to a dangerous increase in BRB permeability (Beltramo and Porta, 2013). The degeneration and death of the neuronal elements, however, starts separately and not as a direct result of the damage to the retinal vasculature (Wang and Lo, 2018). In the meantime, glial activity is altered and the micro and macroglia of the retina participate in the development of the immune response (Altmann and Schmidt, 2018). In the late or proliferative stage, the release of growth factors (VEGF) causes uncontrolled neovascularization (Tomita et al., 2021). One of the pathways involved in VEGF-related signaling in pericytes seems to be connected to prostaglandine-endoperoxidase synthase activity, which likely exerts feed forward regulation on VEGF secretion, further aggravating the damage (Giurdanella et al., 2015). As a consequence, DR is characterized by the appearance of microaneurysms and hemorrhages in the retina, the apoptosis of pericytes and endothelial cells, and neovascularization.

Regarding the possible role of neuropeptides, studies on one hand confirmed increased expression for the components of the ACE/AngII/AT1R axis in the diabetic retina (reviewed by Fletcher et al., 2010; further supported by research carried out in mice and rats by Verma et al., 2012). To assess the potential of angiotensin receptor (ATR) blockers in the treatment of DR, a clinical trial using candesartan has been carried out (DIRECT Prevent and Protect trials, Chaturvedi et al., 2008; Sjølie et al., 2008). While the ATR blockade through candesartan could only elicit DR prevention in type 1 and disease regression in type 2 diabetes (most effective in the early stages of DR), the development of microaneurysms was hindered in both diabetes type 1 and 2 (Sjølie et al., 2011). In the Renin-Angiotensin System Study, both ATR blocking effects (losartan) and ACE inhibition (enalapril) were studied in type 1 diabetes. The progression of DR was reduced in both cases (Mauer et al., 2009; Harindhanavudhi et al., 2011). While DIRECT and RASS presented conflicting results in certain areas (Harindhanavudhi et al., 2011), the conclusion seems to be that the ACE/AngII/AT1R axis does play a small but non-negligible role in the development of DR. An enhanced expression of ACE2/Ang (1-7) was shown to be beneficial in alleviating the effects of DR in animal models (Verma et al., 2012). While the therapeutic potential of Ang (1-7) seems promising considering its protective effects (anti-apoptotic, anti-oxidative, anti-inflammatory; see **Table 2**), its short half-life makes it hard to utilize (Verma et al., 2020).

Similarly, patients affected by DR express EPO and its receptors in higher quantities compared to healthy human donors (Hernández et al., 2006; Shah et al., 2009). The

usability of EPO as a therapeutic agent also proposes some controversies; single nucleotide polymorphisms in the EPO gene have been examined, yielding different results on whether different alleles present increased, decreased or caused no susceptibility to DR (reviewed by Reid and Lois, 2017). It is still up to debate whether the high vitreal concentration of EPO is an agent of disease pathology or a compensatory mechanism activated to combat the deleterious influence of DR. On the other hand, the expression of the majority of neuroprotective peptides appear to be downregulated in diabetic retina, including GLP-1 (reviewed by Pang et al., 2018), NPY (studied in human and mice cell cultures and rat retinal explant cultures by Ou et al., 2020), PACAP (research carried out in rats by Giunta et al., 2012), SST (studied in human diabetic retinas by Carrasco et al., 2007). Verma and colleagues have shown in mouse and rat models that during the early stages of diabetes, the vasoprotective components of the retinal RAS are expressed at higher levels but fail to compensate for the progression of the disease and are eventually downregulated (Verma et al., 2012). SP levels were also found to decrease under diabetic conditions and the restoration of endogenous SP helped prevent apoptosis in streptozotocin-induced (STZ) model of diabetes in rats (Yang et al., 2013). This alludes to the possibility that the damage caused by DR might, at least in part, stem from the underproduction of neuropeptides in the retina.

4.1.1 Effect of Neuropeptides on Disease Progression

In this section we examine the role of neuropeptides on oxidative stress, the immune response and vascular alterations caused in the diabetic retina. Recently conducted research provides evidence that GLP-1 possesses anti-oxidant capabilities against oxidative stress in the diabetic retina and it is capable of affecting DNA repair and neurogenesis to a certain level in mice (Ramos et al., 2020). With regards to GLP-1RA, exanatide-4 (E4) and other analogs were able to reduce apoptotic damage and ameliorate the decrease in cell numbers in diabetic rat retinas (Zhang et al., 2011; Fan et al., 2014a). Liraglutide, in addition, was also able to alleviate apoptotic damage to some degree in the human and mouse retina (Hernández et al., 2016). According to Zhou and colleagues, the beneficial effects of liraglutide also manifest in the mitigation of mitochondrial damage, supposedly through the PTEN-induced kinase/Parkin pathway (research carried out in rats by Zhou et al., 2021). Studies validated the protective effects of EPO against cell loss among pericytes and neurons of the retina (Wang et al., 2011; research carried out in rats by Zhang et al., 2009). PACAP, one of the most versatile agents, upregulates anti-apoptotic and downregulates pro-apoptotic pathways in DM and seems to have an autoregulating effect on PAC1R expression in rats (Szabadfi et al., 2014; Szabadfi et al., 2016). PACAP also exerts protection over the neuronal elements in the GCL and dopaminergic ACs of the rat retina (Atlasz et al., 2010; Szabadfi et al., 2012b).

While experimental work on the protective effects of SST provided favorable results, because of the BRB, however, SST or SST analogs delivered through the bloodstream could not be used for a therapeutic approach. On one hand, topical administration

of SST was successful in conveying neuroprotective effects in rats (Hernández et al., 2013). On the other hand, octreotide (OCT), probably the most commonly used SST analog, offers promising prospects in the treatment of DR. Since treatment through intravitreal injections carries certain risks, OCT has also been utilized in the research of intraocular nanoparticle delivery (Amato et al., 2018; Amato et al., 2020). OCT has been demonstrated to reduce apoptosis as well in mouse retinal explants (Amato et al., 2016) and SP injections were capable of restoring and increasing retinal nerve fibre layer thickness in diabetic rats while suppressing apoptosis (Baek et al., 2020).

Immune response seems to be crucial in symptom development. So far, a reduction in ACE2 has been demonstrated to reduce the inflammatory response in cell cultures of the RPE (Fu et al., 2017). In addition, studies connected EPO to reduced inflammatory cytokine production in cell cultures and rats (Lei et al., 2011; McVicar et al., 2011). Some of its effects are likely mediated through the inhibition of microglia activation through the Src/Akt/cofilin pathway according to research carried out in rats (Xie et al., 2021). EPO might also be able to protect rat MCs through the BDNF/TrkB pathway during hyperglycemia (Wang and Xia, 2015). In the case of lixisenatide, the known anti-inflammatory effects of GLP-1RA have also been validated in the mouse retina (Chung et al., 2020). Controversy also arose regarding the effects of GLP-1RA when semaglutide was connected to a higher prevalence of DR in patients receiving treatment (SUSTAIN-6 trial, Marso et al., 2016; Simó and Hernández, 2017). Additional studies have resulted in diverging results between GLP-1RAs and DR prevalence (Dauner and Farley, 2021), with an ongoing discourse on whether the increased prevalence can be explained by the sudden drop of glucose levels at the initiation of treatment (Bain et al., 2019). So far, multiple reviews encompassing the GLP-1RA effect on DR have been published (Pang et al., 2018; Saw et al., 2019). Furthermore, according to our current knowledge, NPY has the capability to suppress the production of NO and the pro-inflammatory cytokine interleukin 1 beta (IL-1β) in microglia through the Y1 receptor (research carried out in cultured cells by Ferreira et al., 2010). Similarly, PACAP has also demonstrated capacity for decreasing IL-1β expression in rats (D'Amico et al., 2017). Additionally, PACAP has been able to downregulate hypoxia-inducible factor expression in diabetic rats (D'Amico et al., 2015). The beneficial effects of SP against the deleterious effects of DR seem to be the consequence of immunosuppression as well (Baek et al., 2020).

Partially due to the increased immune response, BRB breakdown is initiated and as a consequence, vascular permeability is increased in DR. Additionally, this process is also connected to increased VEGF expression. Among the peptides, Ang II has been capable of increasing VEGF expression (Otani et al., 2000) and the migration of bovine pericytes (Nadal et al., 1999) when signaling through the AT1R. Regarding EPO, a number of studies have showed an inhibitory effect of externally administered EPO on VEGF expression in rats (Wang et al., 2011; Mitsuhashi et al., 2013) and it has also been helpful in preventing BRB breakdown in a

comparative study (Xu et al., 2014). E4 also acts toward maintaining BRB integrity, downregulates VEGF expression in rats (Fan et al., 2014b) and mitigates the harmful effects of advanced glycation end in RPE cells (Dorecka et al., 2013). These effects are at least partially conveyed through sirtuin pathways as E4 treatment has caused an increase in sirtuin (SIRT1 and SIRT3) expression in rats (Zeng et al., 2016). In the meantime, Al Sabaani has demonstrated that E4 likely exerts its protective effects on RPE cells under hyperglycemia through the suppression of P66Shc and the inhibition of c-Jun N-terminal kinase and PKC beta activity (Al Sabaani, 2021). NPY has been demonstrated to counteract VEGF functions and protect vascular integrity through the inhibition of the MAPK pathway (Ou et al., 2020). PACAP is partially able to elicit protective effects against DR in the RPE through the activation of the epidermal growth factor receptor (Maugeri et al., 2019). PACAP has also been found to inhibit hyperglycemia-induced endothelial cell proliferation in cell cultures (Castorina et al., 2010), and VEGF expression in rats and cell cultures (D'Amico et al., 2017; Maugeri et al., 2017). Last but not least, OCT has been demonstrated to reduce VEGF expression in an *ex vivo* mouse model of DR (Amato et al., 2016). In the early stages of DR, the protective effects of OCT seem to be in part conveyed through the moderation of autophagy (Amato et al., 2018). Similarly, GLP-1 can also inhibit autophagy (Cai et al., 2017).

4.1.2 Animal Models in Diabetic Retinopathy

The current treatment of DR is based on different approaches (vid. anti-VEGF injections, laser treatments, surgery) and recently, several studies have demonstrated the potential curative potential of different neuropeptides in DR (see above). Hidden in the background of the functional and structural changes of the retina, there is a strong connection between vascular impairments (vasoregression, BRB breakdown, altered hemodynamics) and retinal neurodegeneration (neuron apoptosis, glial dysfunction) (Simó et al., 2014; Rossino et al., 2019), the two main characteristic features of the pathophysiology of DR. Several studies have described that neurodegeneration in the retina already occurs before the vascular changes take place, which makes research aimed at new, promising neuroprotective factors markedly important (Abcouwer and Gardner, 2014; Simó et al., 2014; Simó and Hernández, 2015). Perhaps this is why it has been suggested that gene therapies could target neuroprotection and vasculopathy (Wang J. H. et al., 2020).

Both induced diabetes (e.g., streptozotocin or high-sugar diet induced) and different strain-specific models (e.g., *db/db*, *Ins2*^{Akita}, *Pdgrfr*^{redeye}) with well characterized mutations in one well known gene (e.g., leptin receptor gene, insulin gene, platelet derived growth factor gene), or transgenic models offer excellent research opportunities. In previous works, different neuropeptides have shown promising curative effects in all of the above-mentioned consequences of DR in the retina (Wilkinson-Berka et al., 2019). Genetic models have made it possible to target the molecular processes of these retinal alterations or explore promising therapeutic pathways from different angles; they can highlight new causative events

and/or prospective mediators in processes of inflammation (Bogdanov et al., 2017; Sigurdardottir et al., 2019; Zapadka et al., 2020; Chen et al., 2021; Crespo-Garcia et al., 2021), vascular alterations (Kern et al., 2010; Zhou et al., 2017; Zhu et al., 2018; Lindstrom et al., 2019; Sigurdardottir et al., 2019; Ivanova et al., 2020; Tecilazich et al., 2020), oxidative stress (Kowluru et al., 2006; Bogdanov et al., 2017; Dierschke et al., 2019; Shao et al., 2019; Sigurdardottir et al., 2019; Chen et al., 2021), VEGF production (Lin et al., 2011; Fu et al., 2015; Yin et al., 2021) and the formation of advanced glycation end products (or their receptor) and neuronal/glial cell degeneration (Kezic et al., 2013; Yang et al., 2015; Chen et al., 2021). The contribution of pro-angiogenic VEGF isoforms to the pathomechanism of DR has also been explored using Ins2^{Akita} mice (Bucolo et al., 2021).

4.1.3 Neuropeptides in Genetically Modified Models of Diabetic Retinopathy

BDNF has been found to be a promising agent against DR; intravitreal injections of BDNF rescued dopaminergic ACs in induced diabetes (Seki et al., 2004; Wan et al., 2010). Interestingly, both BDNF production and TrkB receptor expression have been observed to decrease in the diabetic retina (Seki et al., 2004; Ola et al., 2013), similar to the decrease in protective NPs in DR. In VEGF2 receptor KO mice, a reduction occurred in retinal BDNF production, leading to MC loss (Fu et al., 2015). Additionally, the knockdown of TrkB has been shown to cause the downregulation of survival mediators (e.g., protein kinase B, extracellular signal-regulated kinases; Le et al., 2021). In a different set of experiments, increased expression of ACE2/Ang-(1-7) in endothelial nitric oxide synthase$^{-/-}$ (*eNOS*$^{-/-}$) mice with STZ-induced diabetes protected against complications of DR (e.g., infiltrating inflammatory cells, vascular leakage, oxidative damage; Verma et al., 2012). Underproduction of SST during diabetes has also been described (Carrasco et al., 2007), and treatment with SST prevented inflammation, glial activation, and neurodegenerative and functional alterations in *db/db* mice retinas (Hernández et al., 2020). In *db/db* mice, the topical administration of GLP-1 has reduced oxidative stress and promoted the repair of DNA damage (Ramos et al., 2020). Furthermore, treatment with the GLP-1RA liraglutide has prevented the upregulation of proapoptotic/ proinflammatory signals (Hernández et al., 2016). In light of the above section, it should be noted that the application of true transgenic methods in the research of NP effect on DR is still infrequent, although the methodology is available and has already proven its usefulness.

4.2 Ischemia

Ischemia refers to a condition where restricted blood supply leads to tissue and cell damage. Ischemic damage results both from decreased oxygen levels and a shortage in nutrients necessary for cell survival, in addition to the accumulation of toxic metabolites (Osborne et al., 2004). To make things worse, restoring normal blood flow after ischemia results in even more damage, referred to as the ischemia reperfusion injury (IRI) which results from the combined deleterious effects of oxidative stress and inflammation. Glutamate excitotoxicity is a long-term effect of

ischemia and recognized as a major contributor to ischemic retinal cell death; simultaneously, hypoxia-triggered pathological neovascularization also poses a serious concern (Osborne et al., 2004). Currently utilized treatments specifically aimed to minimize ischemic damage include laser photocoagulation, corticosteroid treatment as a form of immune response suppression, vitreoretinal surgery and intraocular injections of VEGF antibodies (O'Leary et al., 2019).

4.2.1 Effect of Neuropeptides on Disease Progression

Considering how ischemia can be used as a model for various pathological processes, the possible protective role of NPs have also been researched in multiple animal models. Just like in DR, certain peptides appear to have quantifiable effects in various aspects of neuroprotection, including anti-oxidant and anti-inflammatory capabilities and the potential to ameliorate the disrupting effects of IRI. For example, OCT has been demonstrated to exert protective effects in the mouse retina against oxidative stress, which at least partially stem from mitigating oxidative damage through decreasing NF-κB p-p65 and intercellular adhesion molecule 1 (ICAM-1) levels (Wang et al., 2015). SP treatment in ischemic retinas was also demonstrated to upregulate antioxidant levels (D'Alessandro et al., 2014). Furthermore, OCT is also known to prevent apoptosis following ischemia (Wang et al., 2015). Additionally, E4, a GLP-1RA of high importance, has been able to exert anti-inflammatory effects in the ischemic rat retina (Gonçalves et al., 2016). E4 also appears to protect against BRB breakdown (Gonçalves et al., 2016) and it has been shown capability to regulate capillary diameter through vasodilation. While some experimental work supports the NO-mediated dilatator effect of E4 through the PI3K/eNOS/NO-cGMP pathway (research conducted in rats by Zhai et al., 2020), other studies do not (study conducted on human patients by Smits et al., 2015).

As ischemia is also known to affect the retinal vasculature, candesartan, one of the important ARBs, has been studied for its potential effect of mitigating ischemic damage through their effect on angiogenesis. Interestingly, conflicting results have been published, with a number of studies reporting pro-angiogenic effects and a supporting effect on VEGF expression, while other groups found these substances to maintain preventive effects against pathological neovascularization (reviewed by Willis et al., 2011; research conducted in mice by Shanab et al., 2015). The work published by Shanab and colleagues seems to resolve the controversy as they found that candesartan promotes reparative angiogenesis but not pathological neovascularization, and the reason for that is that it inhibits inducible nitric oxide synthase expression (Shanab et al., 2015). However, ARBs have proven to be unable to completely negate ischemic damage according to experimental work carried out in rats (Fukuda et al., 2010). Aliskiren, a direct renin inhibitor, was also tested for its effect on ischemia and was found to be more effective in mitigating IRI in the rat retina through the suppression of retinal RAS (Tenkumo et al., 2014).

Furthermore, Christiansen and colleagues tested the effects of intravitreal NPY treatment in a porcine model of acute retinal ischemia and found that it only enhanced ischemic damage (Christiansen et al., 2018b). These observations are markedly important as they contradict earlier results where NPY treatment has been found to convey neuroprotective effects or at least significant change in retinal health could not be observed following treatment (results from cell cultures by Alvaro et al., 2008; earlier experimental work reviewed by Santos-Carvalho et al., 2014; and a study conducted on rat retinas by Martins et al., 2015). Christiansen and colleagues argue that the damaging effect could have been masked in the *ex vivo* models used in earlier studies as NPY has been demonstrated to cause vasoconstriction in the retinal arteries (Prieto et al., 1995; Christiansen et al., 2018b). Regardless, NPY was shown to play no role in pathological retinal neovascularization in the OIR mouse model (Schmid et al., 2012). In the same model, Schmid and colleagues also found that SP was not involved in the pathogenesis of retinal neovascularization despite having angiogenic properties in other tissues (Schmid et al., 2012).

Contrary to the results regarding the lack of NPY and SP participation, another peptide, PACAP has been found helpful in rescuing cells following hypoperfusion, in addition to conveying protective effects in the retina against excitotoxicity (PACAP retinoprotective effects reviewed by Atlasz et al., 2010). Its protective effects under ischemic conditions are further supported by additional and follow-up studies (research carried out in rats by Danyadi et al., 2014; Werling et al., 2014; Vaczy et al., 2016; Werling et al., 2016; Werling et al., 2017). In bilateral common carotied artery occlusion induced ischemia, PACAP was also shown to mitigate damage through the ERK1/2 and Akt pathways, a decrease in inflammatory cytokine production and by acting against MC activation (Werling et al., 2016). Another NP with considerable protective abilities seems to be SST. Although SST itself remains hard to utilize for experimental purposes in ischemia with the BRB intact (study carried out in rats by Mastrodimou et al., 2005), SSTAs and cortistatin were able to induce protective effects under chemically induced ischemia. Wang and colleagues have also explored the protective effects of endogenous SST release triggered by capsaicin in mice (Wang et al., 2017). Capsaicin induced NP release has been reported to protect against NMDA-induced neuronal cell death in the rat retina (Sakamoto et al., 2014), possibly by signaling through NK1 receptors (Sakamoto et al., 2017). This suggests capsaicin activated SP release, similar to the mechanism described for SST by Wang et al. (2017). The possible role of capsaicin as a potent activator of NP release may deserve further attention. Last but not least, it is worth mentioning that ARA290 (an EPO mimetic also referred to as cibenitide) has been reported to possess beneficial effects that could be utilized in the treatment of ischemic retinopathy in cell cultures (O'Leary et al., 2019). We know that ischemia results in increased levels of EPO-R expression in rats (Junk et al., 2002) and elevated concentrations of EPO in the vitreous fluid in mice (Mowat et al., 2012). EPO has been shown to have protective effects against retinal ischemic damage (Junk et al., 2002; Mowat et al., 2012) but the mechanism of its protective actions are not fully understood.
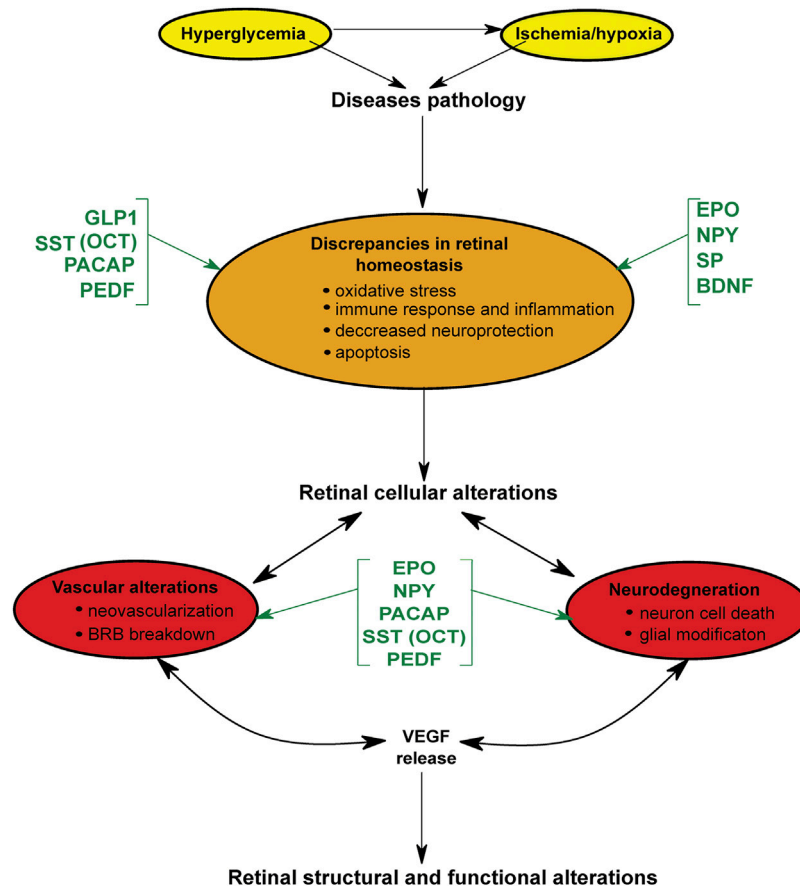
FIGURE 1 | Schematic representation of the curative role and point of action of different neuropeptides and other factors in retinal diseases. Yellow: the initial emergency situation at the onset of disease. Orange: early alterations/damages occurring at cellular level. Red: irreversible damage that leads to pathological structural and functional alterations in the retina. Abbreviations: GLP-1, glucagon-like peptide-1; SST, somatostatin; OCT, octreotide; PACAP, pituitary adenylate cyclase-activating polypeptide; PEDF, Pigment epithelium-derived factor; EPO, erythropoietin; NPY, neuropeptide Y; SP, substance P; BDNF, brain-derived neurotrophic factor; VEGF, Vascular endothelial growth factor.

4.2.2 Animal Models in Ischemia

Animal models of induced and spontaneously occurring ischemia are currently in use to describe pathological changes specific to these conditions, and for testing new therapeutic strategies in the retina. These models are built on cerebral artery occlusion (CAO), chronic carotid ligation, the photocoagulation of retinal vessels, endothelin administration, increased intraocular pressure (IOP) and central retinal artery occlusion (Minhas et al., 2012). These models demonstrate how different pathways and mediators of the molecular cascade contribute to the manifestation of ischemia, with the main participants of the pathophysiology originating from the disturbance of the nutrient and oxygen supply. Different genetic approaches used here target vascular alterations (Murinello et al., 2019; Bats et al., 2020; Gutsaeva et al., 2020; Villacampa et al., 2020), oxidative stress mediators (Chan et al., 2012; Schultz et al., 2016), neuronal cell death (Cervia

et al., 2008b; Zhu et al., 2013; Luo et al., 2021) and inflammation (Portillo et al., 2008; Dvoriantchikova et al., 2014).

4.2.3 Neuropeptides in Genetically Modified Models of Ischemia

The protective role of different neuropeptides has also been investigated in various pathomechanisms and curative treatments. In the OIR mouse model, PEDF has been observed to prevent β-catenin phosphorylation and the activation of several inflammatory and angiogenic factors. Furthermore, PEDF overexpression has also been shown to attenuate VEGF and β-catenin expression (Park et al., 2011). Moreover, EPO signaling has reduced angiogenesis and vascularization following OIR in mice (Bretz et al., 2020). The expression of NPY and substance P has been observed to decrease in the OIR mouse and they do not appear to play any role in neovascularization, which was further validated in the *NPY KO* mice, where it was found that NPY does, in fact, not take part in

vascularization (Schmid et al., 2012). In the *sst1 KO* model, SST and its receptor have played a protective role against hypoxia induced retinal injury by keeping neovascularization under control (Cervia et al., 2012). Moreover, OCT has attenuated electroretinogram alterations and apoptotic signals during hypoxia in the retina of *sst1 KO* mice (Dal Monte et al., 2012). After bilateral carotid artery occlusion, increased damage has been described in PACAP deficient mice compared to wild type mice (Szabadfi et al., 2012c). It is worth noting that at this point in time, there seems to be no true transgenic model available for research aimed at ischemia and IRI.

5 CONCLUSION

As part of the central nervous system, the retina is especially vulnerable to pathologies leading to neuronal cell loss and tissue damage. Diseases affecting the structural integrity of the retina are known to cause irreparable damage, leading to the slow degradation of visual acuity and in certain cases, eventual blindness. Over the years, various NPs have been shown to exert a certain degree of neuroprotective capacity in diabetic and ischemic retinas (**Table 2**), leading to a discovery and development of new therapeutic agents. These molecules are not only able to mitigate severe and irreversible damage (cell death and uncontrolled neovascularization) but also counteract early manifestations of pathological disturbances, including oxidative stress and inflammation (**Figure 1**). Considering the role NPs play in alleviating (or reinforcing) disease pathophysiology, we can summarize the conclusion of the current paper in four concise points.

5.1 Neuropeptide Homeostasis Needs to Be Maintained for a Healthy Retina

While the normal function of NPs is often multifaceted (e.g., SST) or elusive and hard to grasp (e.g., PACAP), it is undeniable that an upset in NP production can lead to serious consequences for retinal health (**Table 2**; **Figure 1**). The fact that NP effects are often only measurable when a) the substance is fed into the system in excessive amounts or b) normal retinal function is disturbed suggests that these molecules are designed to work on a small scale doing the "housekeeping" and maintaining everyday retinal homeostasis. Considering how protective peptide levels are significantly decreased in retinas affected by DR (see **Section 4.1.1**) and how multiple NPs have been more or less effective in mitigating pathological damage, it is safe to assume that these molecules are not just complementary but essential for retinal function. It is worth noting, however, that the cellular localization of NPs and their receptors is yet to be fully mapped in all relevant species.

5.2 Different Neuropeptides Might Require Different Methods of Application

Another important issue has been the selection of the proper delivery system for experiments aiming to better understand the effects of NPs: any systemic delivery is hindered as long as the BRB is intact. One of the successful solutions to circumvent molecule size

constraints has been the use of OCT instead of SST. Regardless, the widespread expression of NPs and NPRs across the body warrants extra care in the selective use of NPs for their retinoprotective ability and topical administration is generally preferred in practice. Eye drops can potentially be utilized as a non-invasive option but this method also suffers from the presence of barriers (Werling et al., 2017). However, eye drops have already been successfully implemented as a method of delivery, including the usage of PACAP against glaucoma (Szabo et al., 2021) and SST against DR (Hernández et al., 2013). While intraocular injections offer a direct solution to the problem of permeability, their invasive nature makes them dangerous as the adverse effects of repeated injections (inflammation, retinal detachment) can have severe consequences on retinal health. To circumvent the necessity for repeated injections, nanoparticle mediated delivery has been tested with promising results for OCT application (Amato et al., 2018). In addition, a number of other methods are being considered, including biodegradable implants (Mandal et al., 2018). It is important to note that NPs used for experimental or therapeutic purposes might also need to be stabilized against degradation and enzymatic breakdown (Mandal et al., 2018; Kovacs et al., 2021), meaning that choosing the method of delivery is crucial for any curative research.

5.3 Not All Neuropeptides Possess the Same Therapeutic Potential

All NPs contribute to retinal health, just not in the same manner and not to the same degree. While most NPs appear to possess neuroprotective capabilities in addition to a variety of other functions (see **Table 1** and **Figure 1**), some of these substances are more effective in combating pathological changes than others. GLP-1 and its analogs, for example, convey a much more widespread effect compared to the other major NPs. Similar to GLP-1 and other GLP-1 receptor agonists, the SST analog octreotide has also proven to be a versatile tool in mitigating damage to the retina under pathological conditions, just like PACAP (**Table 2**). At this point in time, it is probably safe to state that any latent therapeutic potential for all known NPs have been adequately researched. However, even the most effective candidates have proven to be insufficient in combating DR and ischemia on their own. To our surprise, there has been little interest so far in combination treatments utilizing two or more NPs, even though the therapeutic potential of already existing drugs and neuroprotective substances could potentially be increased with the right combination. We strongly believe that it is time for NP research to take the next step and move on from trying to find one ideal substance and focus on exploring the potential in neuroprotective synergies.

5.4 Transgenic Models Are Still Underrepresented in the Research of Neuropeptides

Another conclusion of this study is that transgenic models are still not being exploited to their full potential in the research

of NP effect on retinal health. Combined with the fact that no NP alone has been able to convey full protection against the deleterious effects of DR or ischemia, targeted genetic modification and controlled simultaneous NP overexpression could offer new prospects in scientific research. One option would be the generation of conditional knock-ins connected to NP production, in which different well-known pathological mediators (e.g., VEGF) could act as the driving factor behind the transcription process of NP genes. Considering their widespread protective effects, OCT or PACAP seem to be the most ideal candidates for this job. The second, somewhat different approach could be the application of different enhancer sequences to the transgenic NP construct. At the same time, it is important to mention that NPs with retinoprotective capacity are not only expressed in the retina and ensuring cell and tissue specificity in any construct (e.g., tissue specificity of the promoter) ought to be a major concern.

AUTHOR CONTRIBUTIONS

FUNDING

SUPPLEMENTARY MATERIAL

The Supplementary Material for this article can be found online at: https://www.frontiersin.org/articles/10.3389/fphar.2021.808315/full#supplementary-material

REFERENCES

Abcouwer, S. F., and Gardner, T. W. (2014). Diabetic Retinopathy: Loss of Neuroretinal Adaptation to the Diabetic Metabolic Environment. *Ann. N. Y Acad. Sci.* 1311, 174–190. doi:10.1111/nyas.12412

Agarwal, A., Halvorson, L. M., and Legradi, G. (2005). Pituitary Adenylate Cyclase-Activating Polypeptide (PACAP) Mimics Neuroendocrine and Behavioral Manifestations of Stress: Evidence for PKA-Mediated Expression of the Corticotropin-Releasing Hormone (CRH) Gene. *Brain Res. Mol. Brain Res.* 138 (1), 45–57. doi:10.1016/j.molbrainres.2005.03.016

Al Sabaani, N. (2021). Exendin-4 Inhibits High Glucose-Induced Oxidative Stress in Retinal Pigment Epithelial Cells by Modulating the Expression and Activation of p66Shc. *Cutan. Ocul. Toxicol.* 40 (3), 175–186. doi:10.1080/15569527.2020.1844727

Altmann, C., and Schmidt, M. H. H. (2018). The Role of Microglia in Diabetic Retinopathy: Inflammation, Microvasculature Defects and Neurodegeneration. *Int. J. Mol. Sci.* 19 (1), 110. doi:10.3390/ijms19010110

Alvaro, A. R., Martins, J., Costa, A. C., Fernandes, E., Carvalho, F., Ambrósio, A. F., et al. (2008). Neuropeptide Y Protects Retinal Neural Cells against Cell Death Induced by Ecstasy. *Neuroscience* 152 (1), 97–105. doi:10.1016/j.neuroscience.2007.12.027

Alvaro, A. R., Rosmaninho-Salgado, J., Ambrósio, A. F., and Cavadas, C. (2009). Neuropeptide Y Inhibits [Ca2+]i Changes in Rat Retinal Neurons through NPY Y1, Y4, and Y5 Receptors. *J. Neurochem.* 109 (5), 1508–1515. doi:10.1111/j.1471-4159.2009.06079.x

Amato, R., Biagioni, M., Cammalleri, M., Dal Monte, M., and Casini, G. (2016). VEGF as a Survival Factor in *Ex Vivo* Models of Early Diabetic Retinopathy. *Invest. Ophthalmol. Vis. Sci.* 57 (7), 3066–3076. doi:10.1167/iovs.16-19285

Amato, R., Catalani, E., Dal Monte, M., Cammalleri, M., Di Renzo, I., Perrotta, C., et al. (2018). Autophagy-mediated Neuroprotection Induced by Octreotide in an *Ex Vivo* Model of Early Diabetic Retinopathy. *Pharmacol. Res.* 128, 167–178. doi:10.1016/j.phrs.2017.09.022

Amato, R., Giannaccini, M., Dal Monte, M., Cammalleri, M., Pini, A., Raffa, V., et al. (2020). Association of the Somatostatin Analog Octreotide with Magnetic Nanoparticles for Intraocular Delivery: a Possible Approach for the Treatment of Diabetic Retinopathy. *Front. Bioeng. Biotechnol.* 8, 144. doi:10.3389/fbioe.2020.00144

Atlasz, T., Szabadfi, K., Kiss, P., Racz, B., Gallyas, F., Tamas, A., et al. (2010). Pituitary Adenylate Cyclase Activating Polypeptide in the Retina: Focus on the Retinoprotective Effects. *Ann. N. Y Acad. Sci.* 1200, 128–139. doi:10.1111/j.1749-6632.2010.05512.x

Avwenagha, O., Bird, M. M., Lieberman, A. R., Yan, Q., and Campbell, G. (2006). Patterns of Expression of Brain-Derived Neurotrophic Factor and Tyrosine Kinase B mRNAs and Distribution and Ultrastructural Localization of Their Proteins in the Visual Pathway of the Adult Rat. *Neuroscience* 140 (3), 913–928. doi:10.1016/j.neuroscience.2006.02.056

Baek, S. M., Kim, K., Kim, S., Son, Y., Hong, H. S., and Yu, S. Y. (2020). SP Prevents T2DM Complications by Immunomodulation. *Sci. Rep.* 10 (1), 16753. doi:10.1038/s41598-020-73994-1

Bagnoli, P., Dal Monte, M., and Casini, G. (2003). Expression of Neuropeptides and Their Receptors in the Developing Retina of Mammals. *Histol. Histopathol.* 18 (4), 1219–1242. doi:10.14670/HH-18.1219

Bain, S. C., Klufas, M. A., Ho, A., and Matthews, D. R. (2019). Worsening of Diabetic Retinopathy with Rapid Improvement in Systemic Glucose Control: A Review. *Diabetes Obes. Metab.* 21 (3), 454–466. doi:10.1111/dom.13538

Bats, M. L., Bougaran, P., Peghaire, C., Gueniot, F., Abelanet, A., Chan, H., et al. (2020). Therapies Targeting Frizzled-7/β-Catenin Pathway Prevent the Development of Pathological Angiogenesis in an Ischemic Retinopathy Model. *FASEB J.* 34 (1), 1288–1303. doi:10.1096/fj.201901886R

Beltramo, E., and Porta, M. (2013). Pericyte Loss in Diabetic Retinopathy: Mechanisms and Consequences. *Curr. Med. Chem.* 20 (26), 3218–3225. doi:10.2174/09298673113209990022

Bennett, J. L., Zeiler, S. R., and Jones, K. R. (1999). Patterned Expression of BDNF and NT-3 in the Retina and Anterior Segment of the Developing Mammalian Eye. *Invest. Ophthalmol. Vis. Sci.* 40 (12), 2996–3005.

Bogdanov, P., Solà-Adell, C., Hernández, C., García-Ramírez, M., Sampedro, J., Simó-Servat, O., et al. (2017). Calcium Dobesilate Prevents the Oxidative Stress and Inflammation Induced by Diabetes in the Retina of Db/db Mice. *J. Diabetes Complications* 31 (10), 1481–1490. doi:10.1016/j.jdiacomp.2017.07.009

Bretz, C. A., Ramshekar, A., Kunz, E., Wang, H., and Hartnett, M. E. (2020). Signaling through the Erythropoietin Receptor Affects Angiogenesis in Retinovascular Disease. *Invest. Ophthalmol. Vis. Sci.* 61 (10), 23. doi:10.1167/iovs.61.10.23

Bucolo, C., Gozzo, L., Longo, L., Mansueto, S., Vitale, D. C., and Drago, F. (2018). Long-term Efficacy and Safety Profile of Multiple Injections of Intravitreal Dexamethasone Implant to Manage Diabetic Macular Edema: A Systematic Review of Real-World Studies. *J. Pharmacol. Sci.* 138 (4), 219–232. doi:10.1016/j.jphs.2018.11.001

Bucolo, C., Barbieri, A., Viganò, I., Marchesi, N., Bandello, F., Drago, F., et al. (2021). Short-and Long-Term Expression of Vegf: A Temporal Regulation of a Key Factor in Diabetic Retinopathy. *Front. Pharmacol.* 12, 707909. doi:10.3389/fphar.2021.707909

Burbach, J. P. (2011). What Are Neuropeptides? *Methods Mol. Biol.* 789, 1–36. doi:10.1007/978-1-61779-310-3_1

Burghi, V., Fernández, N. C., Gándola, Y. B., Piazza, V. G., Quiroga, D. T., Guilhen Mario, É., et al. (2017). Validation of Commercial Mas Receptor Antibodies for

Utilization in Western Blotting, Immunofluorescence and Immunohistochemistry Studies. *PloS one* 12 (8), e0183278. doi:10.1371/journal.pone.0183278

Cai, X., Li, J., Wang, M., She, M., Tang, Y., Li, J., et al. (2017). GLP-1 Treatment Improves Diabetic Retinopathy by Alleviating Autophagy through GLP-1R-ERK1/2-HDAC6 Signaling Pathway. *Int. J. Med. Sci.* 14 (12), 1203–1212. doi:10.7150/ijms.20962

Campochiaro, P. A. (2013). Ocular Neovascularization. *J. Mol. Med. (Berl)* 91 (3), 311–321. doi:10.1007/s00109-013-0993-5

Carey, R. M. (2017). Update on Angiotensin AT2 Receptors. *Curr. Opin. Nephrol. Hypertens.* 26 (2), 91–96. doi:10.1097/MNH.0000000000000304

Carlessi, R., Chen, Y., Rowlands, J., Cruzat, V. F., Keane, K. N., Egan, L., et al. (2017). GLP-1 Receptor Signalling Promotes β-cell Glucose Metabolism via mTOR-dependent HIF-1α Activation. *Sci. Rep.* 7 (1), 2661. doi:10.1038/s41598-017-02838-2

Carrasco, E., Hernández, C., Miralles, A., Huguet, P., Farrés, J., and Simó, R. (2007). Lower Somatostatin Expression Is an Early Event in Diabetic Retinopathy and Is Associated with Retinal Neurodegeneration. *Diabetes Care* 30 (11), 2902–2908. doi:10.2337/dc07-0332

Casini, G., Rickman, D. W., Sternini, C., and Brecha, N. C. (1997). Neurokinin 1 Receptor Expression in the Rat Retina. *J. Comp. Neurol.* 389 (3), 496–507. doi:10.1002/(sici)1096-9861(19971222)389:3<496::aid-cne10>3.0.co;2-k

Casini, G., Brecha, N. C., Bosco, L., and Rickman, D. W. (2000). Developmental Expression of Neurokinin-1 and Neurokinin-3 Receptors in the Rat Retina. *J. Comp. Neurol.* 421 (2), 275–287. doi:10.1002/(sici)1096-9861(20000529)421:2<275::aid-cne11>3.0.co;2-q

Casini, G., Dal Monte, M., Fornai, F., Bosco, L., Willems, D., Yang, Q., et al. (2004). Neurokinin 1 Receptor Expression and Substance P Physiological Actions Are Developmentally Regulated in the Rabbit Retina. *Neuroscience* 124 (1), 147–160. doi:10.1016/j.neuroscience.2003.10.049

Castorina, A., Giunta, S., Mazzone, V., Cardile, V., and D'Agata, V. (2010). Effects of PACAP and VIP on Hyperglycemia-Induced Proliferation in Murine Microvascular Endothelial Cells. *Peptides* 31 (12), 2276–2283. doi:10.1016/j.peptides.2010.08.013

Catalani, E., Gangitano, C., Bosco, L., and Casini, G. (2004). Expression of the Neurokinin 1 Receptor in the Mouse Retina. *Neuroscience* 128 (3), 519–530. doi:10.1016/j.neuroscience.2004.07.004

Catalani, E., Dal Monte, M., Gangitano, C., Lucattelli, M., Fineschi, S., Bosco, L., et al. (2006). Expression of Substance P, Neurokinin 1 Receptors (NK1) and Neurokinin 3 Receptors in the Developing Mouse Retina and in the Retina of NK1 Knockout Mice. *Neuroscience* 138 (2), 487–499. doi:10.1016/j.neuroscience.2005.11.020

Cellerino, A., and Kohler, K. (1997). Brain-derived Neurotrophic Factor/neurotrophin-4 Receptor TrkB Is Localized on Ganglion Cells and Dopaminergic Amacrine Cells in the Vertebrate Retina. *J. Comp. Neurol.* 386 (1), 149–160. doi:10.1002/(sici)1096-9861(19970915)386:1<149::aid-cne13>3.0.co;2-f

Cellerino, A., Arango-González, B., Pinzón-Duarte, G., and Kohler, K. (2003). Brain-derived Neurotrophic Factor Regulates Expression of Vasoactive Intestinal Polypeptide in Retinal Amacrine Cells. *J. Comp. Neurol.* 467 (1), 97–104. doi:10.1002/cne.10908

Cervia, D., Casini, G., and Bagnoli, P. (2008a). Physiology and Pathology of Somatostatin in the Mammalian Retina: a Current View. *Mol. Cel Endocrinol.* 286 (1-2), 112–122. doi:10.1016/j.mce.2007.12.009

Cervia, D., Martini, D., Ristori, C., Catalani, E., Timperio, A. M., Bagnoli, P., et al. (2008b). Modulation of the Neuronal Response to Ischaemia by Somatostatin Analogues in Wild-type and Knock-Out Mouse Retinas. *J. Neurochem.* 106 (5), 2224–2235. doi:10.1111/j.1471-4159.2008.05556.x

Cervia, D., Catalani, E., Dal Monte, M., and Casini, G. (2012). Vascular Endothelial Growth Factor in the Ischemic Retina and its Regulation by Somatostatin. *J. Neurochem.* 120 (5), 818–829. doi:10.1111/j.1471-4159.2011.07622.x

Cervia, D., Catalani, E., and Casini, G. (2019). Neuroprotective Peptides in Retinal Disease. *J. Clin. Med.* 8 (8), 1146. doi:10.3390/jcm8081146

Chan, A. S., Saraswathy, S., Rehak, M., Ueki, M., and Rao, N. A. (2012). Neuroglobin protection in Retinal Ischemia. *Invest. Ophthalmol. Vis. Sci.* 53 (2), 704–711. doi:10.1167/iovs.11-7408

Chaturvedi, N., Porta, M., Klein, R., Orchard, T., Fuller, J., Parving, H. H., et al. (2008). Effect of Candesartan on Prevention (DIRECT-Prevent 1) and Progression (DIRECT-Protect 1) of Retinopathy in Type 1 Diabetes: Randomised, Placebo-Controlled Trials. *Lancet* 372 (9647), 1394–1402. doi:10.1016/S0140-6736(08)61412-9

Chen, P., Scicli, G. M., Guo, M., Fenstermacher, J. D., Dahl, D., Edwards, P. A., et al. (2006). Role of Angiotensin II in Retinal Leukostasis in the Diabetic Rat. *Exp. Eye Res.* 83 (5), 1041–1051. doi:10.1016/j.exer.2006.05.009

Chen, J., Shao, Y., Sasore, T., Moiseyev, G., Zhou, K., Ma, X., et al. (2021). Interphotoreceptor Retinol-Binding Protein Ameliorates Diabetes-Induced Retinal Dysfunction and Neurodegeneration through Rhodopsin. *Diabetes* 70 (3), 788–799. doi:10.2337/db20-0609

Choudhary, R., Kapoor, M. S., Singh, A., and Bodakhe, S. H. (2016). Therapeutic Targets of Renin-Angiotensin System in Ocular Disorders. *J. Curr. Ophthalmol.* 29 (1), 7–16. doi:10.1016/j.joco.2016.09.009

Christiansen, A. T., Kiilgaard, J. F., Klemp, K., Woldbye, D. P. D., and Hannibal, J. (2018a). Localization, Distribution, and Connectivity of Neuropeptide Y in the Human and Porcine Retinas-A Comparative Study. *J. Comp. Neurol.* 526 (12), 1877–1895. doi:10.1002/cne.24455

Christiansen, A. T., Sørensen, N. B., Haanes, K. A., Blixt, F. W., la Cour, M., Warfvinge, K., et al. (2018b). Neuropeptide Y Treatment Induces Retinal Vasoconstriction and Causes Functional and Histological Retinal Damage in a Porcine Ischaemia Model. *Acta Ophthalmol.* 96 (8), 812–820. doi:10.1111/aos.13806

Chung, Y. W., Lee, J. H., Lee, J. Y., Ju, H. H., Lee, Y. J., Jee, D. H., et al. (2020). The Anti-inflammatory Effects of Glucagon-like Peptide Receptor Agonist Lixisenatide on the Retinal Nuclear and Nerve Fiber Layers in an Animal Model of Early Type 2 Diabetes. *Am. J. Pathol.* 190 (5), 1080–1094. doi:10.1016/j.ajpath.2020.01.011

Crespo-Garcia, S., Reichhart, N., Kociok, N., Skosyrski, S., and Joussen, A. M. (2021). Anti-Inflammatory Role of Netrin-4 in Diabetic Retinopathy. *Int. J. Mol. Sci.* 22 (9), 4481. doi:10.3390/ijms22094481

Cristiani, R., Petrucci, C., Dal Monte, M., and Bagnoli, P. (2002). Somatostatin (SRIF) and SRIF Receptors in the Mouse Retina. *Brain Res.* 936 (1-2), 1–14. doi:10.1016/s0006-8993(02)02450-2

Cuenca, N., De Juan, J., and Kolb, H. (1995). Substance P-Immunoreactive Neurons in the Human Retina. *J. Comp. Neurol.* 356 (4), 491–504. doi:10.1002/cne.903560402

Culman, J., Höhle, S., Qadri, F., Edling, O., Blume, A., Lebrun, C., et al. (1995). Angiotensin as Neuromodulator/neurotransmitter in central Control of Body Fluid and Electrolyte Homeostasis. *Clin. Exp. Hypertens.* 17 (1-2), 281–293. doi:10.3109/10641969509087071

Dal Monte, M., Latina, V., Cupisti, E., and Bagnoli, P. (2012). Protective Role of Somatostatin Receptor 2 against Retinal Degeneration in Response to Hypoxia. *Naunyn Schmiedebergs Arch. Pharmacol.* 385 (5), 481–494. doi:10.1007/s00210-012-0735-1

D'Alessandro, A., Cervia, D., Catalani, E., Gevi, F., Zolla, L., and Casini, G. (2014). Protective Effects of the Neuropeptides PACAP, Substance P and the Somatostatin Analogue Octreotide in Retinal Ischemia: a Metabolomic Analysis. *Mol. Biosyst.* 10 (6), 1290–1304. doi:10.1039/c3mb70362b

D'Amico, A. G., Maugeri, G., Reitano, R., Bucolo, C., Saccone, S., Drago, F., et al. (2015). PACAP Modulates Expression of Hypoxia-Inducible Factors in Streptozotocin-Induced Diabetic Rat Retina. *J. Mol. Neurosci.* 57 (4), 501–509. doi:10.1007/s12031-015-0621-7

D'Amico, A. G., Maugeri, G., Rasà, D. M., Bucolo, C., Saccone, S., Federico, C., et al. (2017). Modulation of IL-1β and VEGF Expression in Rat Diabetic Retinopathy after PACAP Administration. *Peptides* 97, 64–69. doi:10.1016/j.peptides.2017.09.014

D'Angelo, I., and Brecha, N. C. (2004). Y2 Receptor Expression and Inhibition of Voltage-Dependent Ca2+ Influx into Rod Bipolar Cell Terminals. *Neuroscience* 125 (4), 1039–1049. doi:10.1016/j.neuroscience.2003.10.041

Danyadi, B., Szabadfi, K., Reglodi, D., Mihalik, A., Danyadi, T., Kovacs, Z., et al. (2014). PACAP Application Improves Functional Outcome of Chronic Retinal Ischemic Injury in Rats-Evidence from Electroretinographic Measurements. *J. Mol. Neurosci.* 54 (3), 293–299. doi:10.1007/s12031-014-0296-5

Dauner, D. G., and Farley, J. F. (2021). Comparing the Use of Individual and Composite Terms to Evaluate Adverse Drug Event Disproportionality: a Focus on Glucagon-like Peptide-1 Receptor Agonists and Diabetic Retinopathy. *Expert Opin. Drug Saf.* 20 (4), 475–480. doi:10.1080/14740338.2021.1887136

Dénes, V., Czotter, N., Lakk, M., Berta, G., and Gábriel, R. (2014). PAC1-Expressing Structures of Neural Retina Alter Their PAC1 Isoform Splicing

during Postnatal Development. *Cel. Tissue Res.* 355 (2), 279–288. doi:10.1007/s00441-013-1761-0

de Wied, D. (2000). Peptide Hormones and Neuropeptides: Birds of a Feather. *Trends Neurosci.* 23 (3), 113–114. doi:10.1016/s0166-2236(99)01511-8

Dierschke, S. K., Miller, W. P., Favate, J. S., Shah, P., Imamura Kawasawa, Y., Salzberg, A. C., et al. (2019). O-GlcNAcylation Alters the Selection of mRNAs for Translation and Promotes 4E-BP1-dependent Mitochondrial Dysfunction in the Retina. *J. Biol. Chem.* 294 (14), 5508–5520. doi:10.1074/jbc.RA119.007494

Digicaylioglu, M., and Lipton, S. A. (2001). Erythropoietin-mediated Neuroprotection Involves Cross-Talk between Jak2 and NF-kappaB Signalling Cascades. *Nature* 412 (6847), 641–647. doi:10.1038/35088074

Dong, A., Shen, J., Krause, M., Hackett, S. F., and Campochiaro, P. A. (2007). Increased Expression of Glial Cell Line-Derived Neurotrophic Factor Protects against Oxidative Damage-Induced Retinal Degeneration. *J. Neurochem.* 103 (3), 1041–1052. doi:10.1111/j.1471-4159.2007.04839.x

Dorecka, M., Siemianowicz, K., Francuz, T., Garczorz, W., Chyra, A., Klych, A., et al. (2013). Exendin-4 and GLP-1 Decreases Induced Expression of ICAM-1, VCAM-1 and RAGE in Human Retinal Pigment Epithelial Cells. *Pharmacol. Rep.* 65 (4), 884–890. doi:10.1016/s1734-1140(13)71069-7

Dubovy, S. R., Fernandez, M. P., Echegaray, J. J., Block, N. L., Unoki, N., Perez, R., et al. (2017). Expression of Hypothalamic Neurohormones and Their Receptors in the Human Eye. *Oncotarget* 8 (40), 66796–66814. doi:10.18632/oncotarget.18358

Dvoriantchikova, G., Santos, A. R., Saeed, A. M., Dvoriantchikova, X., and Ivanov, D. (2014). Putative Role of Protein Kinase C in Neurotoxic Inflammation Mediated by Extracellular Heat Shock Protein 70 after Ischemia-Reperfusion. *J. Neuroinflamm.* 11, 81. doi:10.1186/1742-2094-11-81

Ellenbroek, B., and Youn, J. (2016). Rodent Models in Neuroscience Research: Is it a Rat Race? *Dis. Model. Mech.* 9 (10), 1079–1087. doi:10.1242/dmm.026120

Erickson, K. K., Sundstrom, J. M., and Antonetti, D. A. (2007). Vascular Permeability in Ocular Disease and the Role of Tight Junctions. *Angiogenesis* 10 (2), 103–117. doi:10.1007/s10456-007-9067-z

Famiglietti, E. V., Stopa, E. G., McGookin, E. D., Song, P., LeBlanc, V., and Streeten, B. W. (2003). Immunocytochemical Localization of Vascular Endothelial Growth Factor in Neurons and Glial Cells of Human Retina. *Brain Res.* 969 (1-2), 195–204. doi:10.1016/s0006-8993(02)03766-6

Fan, Y., Liu, K., Wang, Q., Ruan, Y., Zhang, Y., and Ye, W. (2014a). Exendin-4 Protects Retinal Cells from Early Diabetes in Goto-Kakizaki Rats by Increasing the Bcl-2/Bax and Bcl-xL/Bax Ratios and Reducing Reactive Gliosis. *Mol. Vis.* 20, 1557–1568.

Fan, Y., Liu, K., Wang, Q., Ruan, Y., Ye, W., and Zhang, Y. (2014b). Exendin-4 Alleviates Retinal Vascular Leakage by Protecting the Blood-Retinal Barrier and Reducing Retinal Vascular Permeability in Diabetic Goto-Kakizaki Rats. *Exp. Eye Res.* 127, 104–116. doi:10.1016/j.exer.2014.05.004

Farrell, S. R., Rankin, D. R., Brecha, N. C., and Barnes, S. (2014). Somatostatin Receptor Subtype 4 Modulates L-type Calcium Channels via Gβγ and PKC Signaling in Rat Retinal Ganglion Cells. *Channels (Austin)* 8 (6), 519–527. doi:10.4161/19336950.2014.967623

Ferreira, R., Xapelli, S., Santos, T., Silva, A. P., Cristóvão, A., Cortes, L., et al. (2010). Neuropeptide Y Modulation of Interleukin-1{beta} (IL-1{beta})-induced Nitric Oxide Production in Microglia. *J. Biol. Chem.* 285 (53), 41921–41934. doi:10.1074/jbc.M110.164020

Flannery, J. G. (1999). Transgenic Animal Models for the Study of Inherited Retinal Dystrophies. *ILAR J.* 40 (2), 51–58. doi:10.1093/ilar.40.2.51

Fletcher, E. L., Phipps, J. A., Ward, M. M., Vessey, K. A., and Wilkinson-Berka, J. L. (2010). The Renin-Angiotensin System in Retinal Health and Disease: Its Influence on Neurons, Glia and the Vasculature. *Prog. Retin. Eye Res.* 29 (4), 284–311. doi:10.1016/j.preteyeres.2010.03.003

Fletcher, E. L., Jobling, A. I., Vessey, K. A., Luu, C., Guymer, R. H., and Baird, P. N. (2011). Animal Models of Retinal Disease. *Prog. Mol. Biol. Transl Sci.* 100, 211–286. doi:10.1016/B978-0-12-384878-9.00006-6

Fong, S. L., Criswell, M. H., Belecky-Adams, T., Fong, W. B., McClintick, J. N., Kao, W. W., et al. (2005). Characterization of a Transgenic Mouse Line Lacking Photoreceptor Development within the Ventral Retina. *Exp. Eye Res.* 81 (4), 376–388. doi:10.1016/j.exer.2005.06.007

Forrester, S. J., Booz, G. W., Sigmund, C. D., Coffman, T. M., Kawai, T., Rizzo, V., et al. (2018). Angiotensin II Signal Transduction: An Update on Mechanisms of Physiology and Pathophysiology. *Physiol. Rev.* 98 (3), 1627–1738. doi:10.1152/physrev.00038.2017

Froger, N., Matonti, F., Roubeix, C., Forster, V., Ivkovic, I., Brunel, N., et al. (2020). VEGF Is an Autocrine/paracrine Neuroprotective Factor for Injured Retinal Ganglion Neurons. *Sci. Rep.* 10 (1), 12409. doi:10.1038/s41598-020-68488-z

Fu, S., Dong, S., Zhu, M., Sherry, D. M., Wang, C., You, Z., et al. (2015). Müller Glia Are a Major Cellular Source of Survival Signals for Retinal Neurons in Diabetes. *Diabetes* 64 (10), 3554–3563. doi:10.2337/db15-0180

Fu, X., Lin, R., Qiu, Y., Yu, P., and Lei, B. (2017). Overexpression of Angiotensin-Converting Enzyme 2 Ameliorates Amyloid β-Induced Inflammatory Response in Human Primary Retinal Pigment Epithelium. *Invest. Ophthalmol. Vis. Sci.* 58 (7), 3018–3028. doi:10.1167/iovs.17-21546

Fudalej, E., Justyniarska, M., Kasarełło, K., Dziedziak, J., Szaflik, J. P., and Cudnoch-Jędrzejewska, A. (2021). Neuroprotective Factors of the Retina and Their Role in Promoting Survival of Retinal Ganglion Cells: A Review. *Ophthalmic Res.* 64 (3), 345–355. doi:10.1159/000514441

Fukuda, K., Hirooka, K., Mizote, M., Nakamura, T., Itano, T., and Shiraga, F. (2010). Neuroprotection against Retinal Ischemia-Reperfusion Injury by Blocking the Angiotensin II Type 1 Receptor. *Invest. Ophthalmol. Vis. Sci.* 51 (7), 3629–3638. doi:10.1167/iovs.09-4107

Gábriel, R., Pöstyéni, E., and Dénes, V. (2019). Neuroprotective Potential of Pituitary Adenylate Cyclase Activating Polypeptide in Retinal Degenerations of Metabolic Origin. *Front. Neurosci.* 13, 1031. doi:10.3389/fnins.2019.01031

García-Caballero, C., Lieppman, B., Arranz-Romera, A., Molina-Martínez, I. T., Bravo-Osuna, I., Young, M., et al. (2018). Photoreceptor Preservation Induced by Intravitreal Controlled Delivery of GDNF and GDNF/melatonin in Rhodopsin Knockout Mice. *Mol. Vis.* 24, 733–745.

Geiger, K., Howes, E., Gallina, M., Huang, X. J., Travis, G. H., and Sarvetnick, N. (1994). Transgenic Mice Expressing IFN-Gamma in the Retina Develop Inflammation of the Eye and Photoreceptor Loss. *Invest. Ophthalmol. Vis. Sci.* 35 (6), 2667–2681.

Giunta, S., Castorina, A., Bucolo, C., Magro, G., Drago, F., and D'Agata, V. (2012). Early Changes in Pituitary Adenylate Cyclase-Activating Peptide, Vasoactive Intestinal Peptide and Related Receptors Expression in Retina of Streptozotocin-Induced Diabetic Rats. *Peptides* 37 (1), 32–39. doi:10.1016/j.peptides.2012.06.004

Giurdanella, G., Anfuso, C. D., Olivieri, M., Lupo, G., Caporarello, N., Eandi, C. M., et al. (2015). Aflibercept, Bevacizumab and Ranibizumab Prevent Glucose-Induced Damage in Human Retinal Pericytes *In Vitro*, through a PLA2/COX-2/VEGF-A Pathway. *Biochem. Pharmacol.* 96 (3), 278–287. doi:10.1016/j.bcp.2015.05.017

Gonçalves, A., Lin, C. M., Muthusamy, A., Fontes-Ribeiro, C., Ambrósio, A. F., Abcouwer, S. F., et al. (2016). Protective Effect of a GLP-1 Analog on Ischemia-Reperfusion Induced Blood-Retinal Barrier Breakdown and Inflammation. *Invest. Ophthalmol. Vis. Sci.* 57 (6), 2584–2592. doi:10.1167/iovs.15-19006

Gupta, V., You, Y., Li, J., Gupta, V., Golzan, M., Klistorner, A., et al. (2014). BDNF Impairment Is Associated with Age-Related Changes in the Inner Retina and Exacerbates Experimental Glaucoma. *Biochim. Biophys. Acta* 1842 (9), 1567–1578. doi:10.1016/j.bbadis.2014.05.026

Gutsaeva, D. R., Shalaby, L., Powell, F. L., Thounaojam, M. C., Abouhish, H., Wetzstein, S. A., et al. (2020). Inactivation of Endothelial ADAM17 Reduces Retinal Ischemia-Reperfusion Induced Neuronal and Vascular Damage. *Int. J. Mol. Sci.* 21 (15), 5379. doi:10.3390/ijms21155379

Harindhanavudhi, T., Mauer, M., Klein, R., Zinman, B., Sinaiko, A., and Caramori, M. L. (2011). Renin Angiotensin System Study (RASS) groupBenefits of Renin-Angiotensin Blockade on Retinopathy in Type 1 Diabetes Vary with Glycemic Control. *Dia Care* 34 (8), 1838–1842. doi:10.2337/dc11-0476

Haruyama, N., Cho, A., and Kulkarni, A. B. (2009). Overview: Engineering Transgenic Constructs and Mice. *Curr. Protoc. Cel. Biol.* Chapter 19, Unit 19. 10. doi:10.1002/0471143030.cb1910s42

Haverkamp, S., and Wässle, H. (2000). Immunocytochemical Analysis of the Mouse Retina. *J. Comp. Neurol.* 424 (1), 1–23. doi:10.1002/1096-9861(20000814)424:1<1::aid-cne1>3.0.co;2-v

He, F., Nichols, R. M., Kailasam, L., Wensel, T. G., and Agosto, M. A. (2019). Critical Role for Phosphatidylinositol-3 Kinase Vps34/PIK3C3 in ON-Bipolar Cells. *Invest. Ophthalmol. Vis. Sci.* 60 (8), 2861–2874. doi:10.1167/iovs.19-26586

Hebsgaard, J. B., Pyke, C., Yildirim, E., Knudsen, L. B., Heegaard, S., and Kvist, P. H. (2018). Glucagon-like Peptide-1 Receptor Expression in the Human Eye. *Diabetes Obes. Metab.* 20 (9), 2304–2308. doi:10.1111/dom.13339

Hernández, C., and Simó, R. (2012). Erythropoietin Produced by the Retina: its Role in Physiology and Diabetic Retinopathy. *Endocrine* 41 (2), 220–226. doi:10.1007/s12020-011-9579-6

Hernández, C., Fonollosa, A., García-Ramírez, M., Higuera, M., Catalán, R., Miralles, A., et al. (2006). Erythropoietin Is Expressed in the Human Retina and it Is Highly Elevated in the Vitreous Fluid of Patients with Diabetic Macular Edema. *Diabetes care* 29 (9), 2028–2033. doi:10.2337/dc06-0556

Hernández, C., García-Ramírez, M., Corraliza, L., Fernández-Carneado, J., Farrera-Sinfreu, J., Ponsati, B., et al. (2013). Topical Administration of Somatostatin Prevents Retinal Neurodegeneration in Experimental Diabetes. *Diabetes* 62 (7), 2569–2578. doi:10.2337/db12-0926

Hernández, C., Simó-Servat, O., and Simó, R. (2014). Somatostatin and Diabetic Retinopathy: Current Concepts and New Therapeutic Perspectives. *Endocrine* 46 (2), 209–214. doi:10.1007/s12020-014-0232-z

Hernández, C., Bogdanov, P., Corraliza, L., García-Ramírez, M., Solà-Adell, C., Arranz, J. A., et al. (2016). Topical Administration of GLP-1 Receptor Agonists Prevents Retinal Neurodegeneration in Experimental Diabetes. *Diabetes* 65 (1), 172–187. doi:10.2337/db15-0443

Hernández, C., Arroba, A. I., Bogdanov, P., Ramos, H., Simó-Servat, O., Simó, R., et al. (2020). Effect of Topical Administration of Somatostatin on Retinal Inflammation and Neurodegeneration in an Experimental Model of Diabetes. *J. Clin. Med.* 9 (8), 2579. doi:10.3390/jcm9082579

Huang, E. J., and Reichardt, L. F. (2003). Trk Receptors: Roles in Neuronal Signal Transduction. *Annu. Rev. Biochem.* 72, 609–642. doi:10.1146/annurev.biochem.72.121801.161629

Husain, S., Abdul, Y., Webster, C., Chatterjee, S., Kesarwani, P., and Mehrotra, S. (2014). Interferon-gamma (IFN-γ)-Mediated Retinal Ganglion Cell Death in Human Tyrosinase T Cell Receptor Transgenic Mouse. *PLoS One* 9 (2), e89392. doi:10.1371/journal.pone.0089392

Ivanova, E., Bianchimano, P., Corona, C., Eleftheriou, C. G., and Sagdullaev, B. T. (2020). Optogenetic Stimulation of Cholinergic Amacrine Cells Improves Capillary Blood Flow in Diabetic Retinopathy. *Invest. Ophthalmol. Vis. Sci.* 61 (10), 44. doi:10.1167/iovs.61.10.44

Izumi, S., Seki, T., Shioda, S., Zhou, C. J., Arimura, A., and Koide, R. (2000). Ultrastructural Localization of PACAP Immunoreactivity in the Rat Retina. *Ann. N. Y Acad. Sci.* 921, 317–320. doi:10.1111/j.1749-6632.2000.tb06985.x

Jaenisch, R., and Mintz, B. (1974). Simian Virus 40 DNA Sequences in DNA of Healthy Adult Mice Derived from Preimplantation Blastocysts Injected with Viral DNA. *Proc. Natl. Acad. Sci. U S A.* 71 (4), 1250–1254. doi:10.1073/pnas.71.4.1250

Joseph, R. M., and Li, T. (1996). Overexpression of Bcl-2 or Bcl-XL Transgenes and Photoreceptor Degeneration. *Invest. Ophthalmol. Vis. Sci.* 37 (12), 2434–2446.

Junk, A. K., Mammis, A., Savitz, S. I., Singh, M., Roth, S., Malhotra, S., et al. (2002). Erythropoietin Administration Protects Retinal Neurons from Acute Ischemia-Reperfusion Injury. *Proc. Natl. Acad. Sci. U S A.* 99 (16), 10659–10664. doi:10.1073/pnas.152321399

Kanan, Y., Centola, M., Bart, F., and Al-Ubaidi, M. R. (2010). Analysis of Genes Differentially Expressed during Retinal Degeneration in Three Mouse Models. *Adv. Exp. Med. Biol.* 664, 3–13. doi:10.1007/978-1-4419-1399-9_1

Kang, Q., and Yang, C. (2020). Oxidative Stress and Diabetic Retinopathy: Molecular Mechanisms, Pathogenetic Role and Therapeutic Implications. *Redox Biol.* 37, 101799. doi:10.1016/j.redox.2020.101799

Kern, T. S., Du, Y., Miller, C. M., Hatala, D. A., and Levin, L. A. (2010). Overexpression of Bcl-2 in Vascular Endothelium Inhibits the Microvascular Lesions of Diabetic Retinopathy. *Am. J. Pathol.* 176 (5), 2550–2558. doi:10.2353/ajpath.2010.091062

Kezic, J. M., Chen, X., Rakoczy, E. P., and McMenamin, P. G. (2013). The Effects of Age and Cx3cr1 Deficiency on Retinal Microglia in the Ins2(Akita) Diabetic Mouse. *Invest. Ophthalmol. Vis. Sci.* 54 (1), 854–863. doi:10.1167/iovs.12-10876

Kim, I. B., Park, M. R., Kang, T. H., Kim, H. J., Lee, E. J., Ahn, M. D., et al. (2005). Synaptic Connections of Cone Bipolar Cells that Express the Neurokinin 1 Receptor in the Rabbit Retina. *Cel. Tissue Res.* 321 (1), 1–8. doi:10.1007/s00441-005-1122-8

Kovács-Valasek, A., Pöstyéni, E., Dénes, V., Mester, A., Sétáló, G., Jr, and Gábriel, R. (2021). Age-Related Alterations of Proteins in Albino Wistar Rat Retina. *Cel. Tissues Organs* 210 (2), 135–150. doi:10.1159/000515447

Kovacs, A. K., Atlasz, T., Werling, D., Szabo, E., Reglodi, D., and Toth, G. K. (2021). Stability Test of PACAP in Eye Drops. *J. Mol. Neurosci.* 71 (8), 1567–1574. doi:10.1007/s12031-020-01532-9

Kovács-Valasek, A., Szabadfi, K., Dénes, V., Szalontai, B., Tamás, A., Kiss, P., et al. (2017). Accelerated Retinal Aging in PACAP Knock-Out Mice. *Neuroscience* 348, 1–10. doi:10.1016/j.neuroscience.2017.02.003

Kowanetz, M., and Ferrara, N. (2006). Vascular Endothelial Growth Factor Signaling Pathways: Therapeutic Perspective. *Clin. Cancer Res.* 12 (17), 5018–5022. doi:10.1158/1078-0432.CCR-06-1520

Kowluru, R. A., and Chan, P. S. (2007). Oxidative Stress and Diabetic Retinopathy. *Exp. Diabetes Res.* 2007, 43603. doi:10.1155/2007/43603

Kowluru, R. A., Kowluru, V., Xiong, Y., and Ho, Y. S. (2006). Overexpression of Mitochondrial Superoxide Dismutase in Mice Protects the Retina from Diabetes-Induced Oxidative Stress. *Free Radic. Biol. Med.* 41 (8), 1191–1196. doi:10.1016/j.freeradbiomed.2006.01.012

Ladewig, T., Fellner, S., Zrenner, E., Kohler, K., and Guenther, E. (2004). BDNF Regulates NMDA Receptor Activity in Developing Retinal Ganglion Cells. *Neuroreport* 15 (16), 2495–2499. doi:10.1097/00001756-200411150-00013

Lang, B., Zhao, L., Cai, L., McKie, L., Forrester, J. V., McCaig, C. D., et al. (2010). GABAergic Amacrine Cells and Visual Function Are Reduced in PAC1 Transgenic Mice. *Neuropharmacology* 58 (1), 215–225. doi:10.1016/j.neuropharm.2009.07.003

Larhammar, D., Wraith, A., Berglund, M. M., Holmberg, S. K., and Lundell, I. (2001). Origins of the many NPY-Family Receptors in Mammals. *Peptides* 22 (3), 295–307. doi:10.1016/s0196-9781(01)00331-x

Le, Y.-Z., Xu, B., Chucair-Elliott, A. J., Zhang, H., and Zhu, M. (2021). VEGF Mediates Retinal Müller Cell Viability and Neuroprotection through BDNF in Diabetes. *Biomolecules* 11 (5), 712. doi:10.3390/biom11050712

Lei, X., Zhang, J., Shen, J., Hu, L. M., Wu, Y., Mou, L., et al. (2011). EPO Attenuates Inflammatory Cytokines by Muller Cells in Diabetic Retinopathy. *Front. Biosci. (Elite Ed.)* 3, 201–211. doi:10.2741/e234

Li, Q., Zhang, Y., Wu, N., Yin, N., Sun, X. H., and Wang, Z. (2019). Activation of Somatostatin Receptor 5 Suppresses T-type Ca^{2+} Channels through NO/cGMP/PKG Signaling Pathway in Rat Retinal Ganglion Cells. *Neurosci. Lett.* 708, 134337. doi:10.1016/j.neulet.2019.134337

Lin, M., Chen, Y., Jin, J., Hu, Y., Zhou, K. K., Zhu, M., et al. (2011). Ischaemia-induced Retinal Neovascularisation and Diabetic Retinopathy in Mice with Conditional Knockout of Hypoxia-Inducible Factor-1 in Retinal Müller Cells. *Diabetologia* 54 (6), 1554–1566. doi:10.1007/s00125-011-2081-0

Lindstrom, S. I., Sigurdardottir, S., Zapadka, T. E., Tang, J., Liu, H., Taylor, B. E., et al. (2019). Diabetes Induces IL-17A-Act1-FADD-dependent Retinal Endothelial Cell Death and Capillary Degeneration. *J. Diabetes Complications* 33 (9), 668–674. doi:10.1016/j.jdiacomp.2019.05.016

Lipinski, D. M., Yusuf, M., Barnard, A. R., Damant, C., Charbel Issa, P., Singh, M. S., et al. (2011). Characterization of a Dominant Cone Degeneration in a green Fluorescent Protein-Reporter Mouse with Disruption of Loci Associated with Human Dominant Retinal Dystrophy. *Invest. Ophthalmol. Vis. Sci.* 52 (9), 6617–6623. doi:10.1167/iovs.11-7932

Liu, X., Grishanin, R. N., Tolwani, R. J., Rentería, R. C., Xu, B., Reichardt, L. F., et al. (2007). Brain-derived Neurotrophic Factor and TrkB Modulate Visual Experience-Dependent Refinement of Neuronal Pathways in Retina. *J. Neurosci.* 27 (27), 7256–7267. doi:10.1523/JNEUROSCI.0779-07.2007

Liu, Q., Collin, R. W., Cremers, F. P., den Hollander, A. I., van den Born, L. I., and Pierce, E. A. (2012). Expression of Wild-type Rp1 Protein in Rp1 Knock-In Mice Rescues the Retinal Degeneration Phenotype. *PLoS One* 7 (8), e43251. doi:10.1371/journal.pone.0043251

Luo, W., Hu, L., and Wang, F. (2015). The Protective Effect of Erythropoietin on the Retina. *Ophthalmic Res.* 53 (2), 74–81. doi:10.1159/000369885

Luo, J., Wang, S., Zhou, Z., and Zhao, Y. (2021). Ad- and AAV8-Mediated ABCA1 Gene Therapy in a Murine Model with Retinal Ischemia/reperfusion Injuries. *Mol. Ther. Methods Clin. Dev.* 20, 551–558. doi:10.1016/j.omtm.2021.01.012

Ma, C., Cheng, F., Wang, X., Zhai, C., Yue, W., Lian, Y., et al. (2016). Erythropoietin Pathway: A Potential Target for the Treatment of Depression. *Int. J. Mol. Sci.* 17 (5), 677. doi:10.3390/ijms17050677

Maeda, A., and Maeda, T. (2018). Modeling Retinal Diseases Using Genetic Approaches in Mice. *Methods Mol. Biol.* 1753, 41–59. doi:10.1007/978-1-4939-7720-8_3

Mandal, A., Pal, D., Agrahari, V., Trinh, H. M., Joseph, M., and Mitra, A. K. (2018). Ocular Delivery of Proteins and Peptides: Challenges and Novel Formulation Approaches. *Adv. Drug Deliv. Rev.* 126, 67–95. doi:10.1016/j.addr.2018.01.008

Marso, S. P., Bain, S. C., Consoli, A., Eliaschewitz, F. G., Jódar, E., Leiter, L. A., et al. (2016). Semaglutide and Cardiovascular Outcomes in Patients with Type 2 Diabetes. *N. Engl. J. Med.* 375 (19), 1834–1844. doi:10.1056/NEJMoa1607141

Martins, J., Elvas, F., Brudzewsky, D., Martins, T., Kolomiets, B., Tralhão, P., et al. (2015). Activation of Neuropeptide Y Receptors Modulates Retinal Ganglion Cell Physiology and Exerts Neuroprotective Actions *In Vitro*. *ASN Neuro* 7 (4), 1759091415598292. doi:10.1177/1759091415598292

Mashaghi, A., Marmalidou, A., Tehrani, M., Grace, P. M., Pothoulakis, C., and Dana, R. (2016). Neuropeptide Substance P and the Immune Response. *Cel. Mol. Life Sci.* 73 (22), 4249–4264. doi:10.1007/s00018-016-2293-z

Mastrodimou, N., Lambrou, G. N., and Thermos, K. (2005). Effect of Somatostatin Analogues on Chemically Induced Ischaemia in the Rat Retina. *Naunyn Schmiedebergs Arch. Pharmacol.* 371 (1), 44–53. doi:10.1007/s00210-004-1011-9

Mastrodimou, N., Kiagiadaki, F., Hodjarova, M., Karagianni, E., and Thermos, K. (2006). Somatostatin Receptors (Sst2) Regulate cGMP Production in Rat Retina. *Regul. Pept.* 133 (1-3), 41–46. doi:10.1016/j.regpep.2005.09.034

Mauer, M., Zinman, B., Gardiner, R., Suissa, S., Sinaiko, A., Strand, T., et al. (2009). Renal and Retinal Effects of Enalapril and Losartan in Type 1 Diabetes. *N. Engl. J. Med.* 361 (1), 40–51. doi:10.1056/NEJMoa0808400

Maugeri, G., D'Amico, A. G., Saccone, S., Federico, C., Cavallaro, S., and D'Agata, V. (2017). PACAP and VIP Inhibit HIF-1α-Mediated VEGF Expression in a Model of Diabetic Macular Edema. *J. Cel. Physiol.* 232 (5), 1209–1215. doi:10.1002/jcp.25616

Maugeri, G., D'Amico, A. G., Bucolo, C., and D'Agata, V. (2019). Protective Effect of PACAP-38 on Retinal Pigmented Epithelium in an *In Vitro* and *In Vivo* Model of Diabetic Retinopathy through EGFR-dependent Mechanism. *Peptides* 119, 170108. doi:10.101610.1016/j.peptides.2019.170108

McNally, N., Kenna, P., Humphries, M. M., Hobson, A. H., Khan, N. W., Bush, R. A., et al. (1999). Structural and Functional rescue of Murine Rod Photoreceptors by Human Rhodopsin Transgene. *Hum. Mol. Genet.* 8 (7), 1309–1312. doi:10.1093/hmg/8.7.1309

McVicar, C. M., Hamilton, R., Colhoun, L. M., Gardiner, T. A., Brines, M., Cerami, A., et al. (2011). Intervention with an Erythropoietin-Derived Peptide Protects against Neuroglial and Vascular Degeneration during Diabetic Retinopathy. *Diabetes* 60 (11), 2995–3005. doi:10.2337/db11-0026

Milne, R., and Brownstein, S. (2013). Advanced Glycation End Products and Diabetic Retinopathy. *Amino acids* 44 (6), 1397–1407. doi:10.1007/s00726-011-1071-3

Minhas, G., Morishita, R., and Anand, A. (2012). Preclinical Models to Investigate Retinal Ischemia: Advances and Drawbacks. *Front. Neurol.* 3, 75. doi:10.3389/fneur.2012.00075

Misra, S., Murthy, K. S., Zhou, H., and Grider, J. R. (2004). Coexpression of Y1, Y2, and Y4 Receptors in Smooth Muscle Coupled to Distinct Signaling Pathways. *J. Pharmacol. Exp. Ther.* 311 (3), 1154–1162. doi:10.1124/jpet.104.071415

Mitsuhashi, J., Morikawa, S., Shimizu, K., Ezaki, T., Yasuda, Y., and Hori, S. (2013). Intravitreal Injection of Erythropoietin Protects against Retinal Vascular Regression at the Early Stage of Diabetic Retinopathy in Streptozotocin-Induced Diabetic Rats. *Exp. Eye Res.* 106, 64–73. doi:10.1016/j.exer.2012.11.001

Miyata, A., Arimura, A., Dahl, R. R., Minamino, N., Uehara, A., Jiang, L., et al. (1989). Isolation of a Novel 38 Residue-Hypothalamic Polypeptide Which Stimulates Adenylate Cyclase in Pituitary Cells. *Biochem. Biophys. Res. Commun.* 164 (1), 567–574. doi:10.1016/0006-291x(89)91757-9

Mowat, F. M., Gonzalez, F., Luhmann, U. F., Lange, C. A., Duran, Y., Smith, A. J., et al. (2012). Endogenous Erythropoietin Protects Neuroretinal Function in Ischemic Retinopathy. *Am. J. Pathol.* 180 (4), 1726–1739. doi:10.1016/j.ajpath.2011.12.033

Murinello, S., Usui, Y., Sakimoto, S., Kitano, M., Aguilar, E., Friedlander, H. M., et al. (2019). miR-30a-5p Inhibition Promotes Interaction of Fas[+] Endothelial Cells and FasL[+] Microglia to Decrease Pathological Neovascularization and Promote Physiological Angiogenesis. *Glia* 67 (2), 332–344. doi:10.1002/glia.23543

Nadal, J. A., Scicli, G. M., Carbini, L. A., Nussbaum, J. J., and Scicli, A. G. (1999). Angiotensin II and Retinal Pericytes Migration. *Biochem. Biophys. Res. Commun.* 266 (2), 382–385. doi:10.1006/bbrc.1999.1834

Navabpour, S., Kwapis, J. L., and Jarome, T. J. (2020). A Neuroscientist's Guide to Transgenic Mice and Other Genetic Tools. *Neurosci. Biobehav Rev.* 108, 732–748. doi:10.1016/j.neubiorev.2019.12.013

Nian, S., Lo, A. C. Y., Mi, Y., Ren, K., and Yang, D. (2021). Neurovascular Unit in Diabetic Retinopathy: Pathophysiological Roles and Potential Therapeutical Targets. *Eye Vis.* 8 (1), 15. doi:10.1186/s40662-021-00239-1

Oku, H., Ikeda, T., Honma, Y., Sotozono, C., Nishida, K., Nakamura, Y., et al. (2002). Gene Expression of Neurotrophins and Their High-Affinity Trk Receptors in Cultured Human Müller Cells. *Ophthalmic Res.* 34 (1), 38–42. doi:10.1159/000048323

Ola, M. S., Nawaz, M. I., El-Asrar, A. A., Abouammoh, M., and Alhomida, A. S. (2013). Reduced Levels of Brain Derived Neurotrophic Factor (BDNF) in the Serum of Diabetic Retinopathy Patients and in the Retina of Diabetic Rats. *Cell Mol Neurobiol* 33 (3), 359–367. doi:10.1007/s10571-012-9901-8

O'Leary, O. E., Canning, P., Reid, E., Bertelli, P. M., McKeown, S., Brines, M., et al. (2019). The Vasoreparative Potential of Endothelial colony-forming Cells in the Ischemic Retina Is Enhanced by Cibinetide, a Non-hematopoietic Erythropoietin Mimetic. *Exp. Eye Res.* 182, 144–155. doi:10.1016/j.exer.2019.03.001

Osborne, N. N., Casson, R. J., Wood, J. P., Chidlow, G., Graham, M., and Melena, J. (2004). Retinal Ischemia: Mechanisms of Damage and Potential Therapeutic Strategies. *Prog. Retin. Eye Res.* 23 (1), 91–147. doi:10.1016/j.preteyeres.2003.12.001

Otani, A., Takagi, H., Oh, H., Suzuma, K., Matsumura, M., Ikeda, E., et al. (2000). Angiotensin II-Stimulated Vascular Endothelial Growth Factor Expression in Bovine Retinal Pericytes. *Invest. Ophthalmol. Vis. Sci.* 41 (5), 1192–1199.

Ou, K., Copland, D. A., Theodoropoulou, S., Mertsch, S., Li, Y., Liu, J., et al. (2020). Treatment of Diabetic Retinopathy through Neuropeptide Y-Mediated Enhancement of Neurovascular Microenvironment. *J. Cel Mol Med* 24 (7), 3958–3970. doi:10.1111/jcmm.15016

Oyamada, H., Takatsuji, K., Senba, E., Mantyh, P. W., and Tohyama, M. (1999). Postnatal Development of NK1, NK2, and NK3 Neurokinin Receptors Expression in the Rat Retina. *Brain Res. Dev. Brain Res.* 117 (1), 59–70. doi:10.1016/s0165-3806(99)00099-1

Pagan-Mercado, G., and Becerra, S. P. (2019). Signaling Mechanisms Involved in PEDF-Mediated Retinoprotection. *Adv. Exp. Med. Biol.* 1185, 445–449. doi:10.1007/978-3-030-27378-1_73

Pang, B., Zhou, H., and Kuang, H. (2018). The Potential Benefits of Glucagon-like Peptide-1 Receptor Agonists for Diabetic Retinopathy. *Peptides* 100, 123–126. doi:10.1016/j.peptides.2017.08.003

Park, K., Lee, K., Zhang, B., Zhou, T., He, X., Gao, G., et al. (2011). Identification of a Novel Inhibitor of the Canonical Wnt Pathway. *Mol. Cel Biol* 31 (14), 3038–3051. doi:10.1128/MCB.01211-10

Park, S. J., Borghuis, B. G., Rahmani, P., Zeng, Q., Kim, I. J., and Demb, J. B. (2015). Function and Circuitry of VIP+ Interneurons in the Mouse Retina. *J. Neurosci.* 35 (30), 10685–10700. doi:10.1523/JNEUROSCI.0222-15.2015

Pérez-Ibave, D. C., Garza-Rodríguez, M. L., Pérez-Maya, A. A., Rodríguez-Sánchez, I. P., Luna-Muñoz, M., Martínez-Moreno, C. G., et al. (2019). Expression of Growth Hormone and Growth Hormone Receptor Genes in Human Eye Tissues. *Exp. Eye Res.* 181, 61–71. doi:10.1016/j.exer.2019.01.011

Péant, C., Dosso, A., Eder-Colli, L., and Chiodini, F. (2007). Functional Study in NSE-Hu-Bcl-2 Transgenic Mice: a Model for Retinal Diseases Starting in Müller Cells. *Doc Ophthalmol.* 115 (3), 203–209. doi:10.1007/s10633-007-9077-6

Peiró, C., Vallejo, S., Gembardt, F., Palacios, E., Novella, S., Azcutia, V., et al. (2013). Complete Blockade of the Vasorelaxant Effects of Angiotensin-(1-7) and Bradykinin in Murine Microvessels by Antagonists of the Receptor Mas. *J. Physiol.* 591 (9), 2275–2285. doi:10.1113/jphysiol.2013.251413

Pérez de Sevilla Müller, L., Solomon, A., Sheets, K., Hapukino, H., Rodriguez, A. R., and Brecha, N. C. (2019). Multiple Cell Types Form the VIP Amacrine Cell Population. *J. Comp. Neurol.* 527 (1), 133–158. doi:10.1002/cne.24234

Porrello, E. R., Delbridge, L. M., and Thomas, W. G. (2009). The Angiotensin II Type 2 (AT2) Receptor: an Enigmatic Seven Transmembrane Receptor. *Front. Biosci. (Landmark Ed.)* 14, 958–972. doi:10.2741/3289

Portillo, J. A., Van Grol, J., Zheng, L., Okenka, G., Gentil, K., Garland, A., et al. (2008). CD40 Mediates Retinal Inflammation and Neurovascular Degeneration. *J. Immunol.* 181 (12), 8719–8726. doi:10.4049/jimmunol.181.12.8719

Pöstyéni, E., Kovács-Valasek, A., Dénes, V., Mester, A., Sétáló, G., and Gábriel, R. (2021). PACAP for Retinal Health: Model for Cellular Aging and Rescue. *Ijms* 22 (1), 444. doi:10.3390/ijms22010444

Prasad, T., Verma, A., and Li, Q. (2014). Expression and Cellular Localization of the Mas Receptor in the Adult and Developing Mouse Retina. *Mol. Vis.* 20, 1443–1455.

Prieto, D., Simonsen, U., and Nyborg, N. C. (1995). Regional Involvement of an Endothelium-Derived Contractile Factor in the Vasoactive Actions of Neuropeptide Y in Bovine Isolated Retinal Arteries. *Br. J. Pharmacol.* 116 (6), 2729–2737. doi:10.1111/j.1476-5381.1995.tb17234.x

Qiao, S. N., Zhou, W., Liu, L. L., Zhang, D. Q., and Zhong, Y. M. (2017). Orexin-A Suppresses Signal Transmission to Dopaminergic Amacrine Cells from Outer and Inner Retinal Photoreceptors. *Invest. Ophthalmol. Vis. Sci.* 58 (11), 4712–4721. doi:10.1167/iovs.17-21835

Ramkumar, H. L., Zhang, J., and Chan, C. C. (2010). Retinal Ultrastructure of Murine Models of Dry Age-Related Macular Degeneration (AMD). *Prog. Retin. Eye Res.* 29 (3), 169–190. doi:10.1016/j.preteyeres.2010.02.002

Ramos, H., Bogdanov, P., Sampedro, J., Huerta, J., Simó, R., and Hernández, C. (2020). Beneficial Effects of Glucagon-like Peptide-1 (GLP-1) in Diabetes-Induced Retinal Abnormalities: Involvement of Oxidative Stress. *Antioxidants (Basel)* 9 (9), 846. doi:10.3390/antiox9090846

Rebustini, I. T., Bernardo-Colón, A., Nalvarte, A. I., and Becerra, S. P. (2021). Delivery Systems of Retinoprotective Proteins in the Retina. *Int. J. Mol. Sci.* 22 (10), 5344. doi:10.3390/ijms22105344

Reid, G., and Lois, N. (2017). Erythropoietin in Diabetic Retinopathy. *Vis. Res* 139, 237–242. doi:10.1016/j.visres.2017.05.010

Reinecke, K., Lucius, R., Reinecke, A., Rickert, U., Herdegen, T., and Unger, T. (2003). Angiotensin II Accelerates Functional Recovery in the Rat Sciatic Nerve *In Vivo*: Role of the AT2 Receptor and the Transcription Factor NF-kappaB. *FASEB J.* 17 (14), 2094–2096. doi:10.1096/fj.02-1193fje

Rodríguez, M. L., Millán, I., and Ortega, Á. L. (2021). Cellular Targets in Diabetic Retinopathy Therapy. *Wjd* 12 (9), 1442–1462. doi:10.4239/wjd.v12.i9.1442

Roman, D., Zhong, H., Yaklichkin, S., Chen, R., and Mardon, G. (2018). Conditional Loss of Kcnj13 in the Retinal Pigment Epithelium Causes Photoreceptor Degeneration. *Exp. Eye Res.* 176, 219–226. doi:10.1016/j.exer.2018.07.014

Romeo, G., Liu, W. H., Asnaghi, V., Kern, T. S., and Lorenzi, M. (2002). Activation of Nuclear Factor-kappaB Induced by Diabetes and High Glucose Regulates a Proapoptotic Program in Retinal Pericytes. *Diabetes* 51 (7), 2241–2248. doi:10.2337/diabetes.51.7.2241

Rossino, M. G., Dal Monte, M., and Casini, G. (2019). Relationships between Neurodegeneration and Vascular Damage in Diabetic Retinopathy. *Front. Neurosci.* 13, 1172. doi:10.3389/fnins.2019.01172

Ruiz-Ortega, M., Lorenzo, O., Suzuki, Y., Rupérez, M., and Egido, J. (2001). Proinflammatory Actions of Angiotensins. *Curr. Opin. Nephrol. Hypertens.* 10 (3), 321–329. doi:10.1097/00041552-200105000-00005

Ruiz-Ortega, M., Rupérez, M., Esteban, V., Rodríguez-Vita, J., Sánchez-López, E., Carvajal, G., et al. (2006). Angiotensin II: a Key Factor in the Inflammatory and Fibrotic Response in Kidney Diseases. *Nephrol. Dial. Transpl.* 21 (1), 16–20. doi:10.1093/ndt/gfi265

Sadybekov, A., and Katritch, V. (2020). Breaking the Enigma Code of Angiotensin II Type 2 Receptor Signaling. *Structure* 28 (4), 390–392. doi:10.1016/j.str.2020.03.004

Saint-Geniez, M., Maharaj, A. S., Walshe, T. E., Tucker, B. A., Sekiyama, E., Kurihara, T., et al. (2008). Endogenous VEGF Is Required for Visual Function: Evidence for a Survival Role on Müller Cells and Photoreceptors. *PloS one* 3 (11), e3554. doi:10.1371/journal.pone.0003554

Sakamoto, K., Kuroki, T., Okuno, Y., Sekiya, H., Watanabe, A., Sagawa, T., et al. (2014). Activation of the TRPV1 Channel Attenuates N-Methyl-D-Aspartic Acid-Induced Neuronal Injury in the Rat Retina. *Eur. J. Pharmacol.* 733, 13–22. doi:10.1016/j.ejphar.2014.03.035

Sakamoto, K., Kuroki, T., Sagawa, T., Ito, H., Mori, A., Nakahara, T., et al. (2017). Opioid Receptor Activation Is Involved in Neuroprotection Induced by TRPV1 Channel Activation against Excitotoxicity in the Rat Retina. *Eur. J. Pharmacol.* 812, 57–63. doi:10.1016/j.ejphar.2017.07.002

Sall, J. W., Klisovic, D. D., O'Dorisio, M. S., and Katz, S. E. (2004). Somatostatin Inhibits IGF-1 Mediated Induction of VEGF in Human Retinal Pigment Epithelial Cells. *Exp. Eye Res.* 79 (4), 465–476. doi:10.1016/j.exer.2004.06.007

Santos, R. A. S., Sampaio, W. O., Alzamora, A. C., Motta-Santos, D., Alenina, N., Bader, M., et al. (2018). The ACE2/Angiotensin-(1-7)/MAS Axis of the Renin-Angiotensin System: Focus on Angiotensin-(1-7). *Physiol. Rev.* 98 (1), 505–553. doi:10.1152/physrev.00023.2016

Santos-Carvalho, A., Álvaro, A. R., Martins, J., Ambrósio, A. F., and Cavadas, C. (2014). Emerging Novel Roles of Neuropeptide Y in the Retina: from Neuromodulation to Neuroprotection. *Prog. Neurobiol.* 112, 70–79. doi:10.1016/j.pneurobio.2013.10.002

Santos-Carvalho, A., Ambrósio, A. F., and Cavadas, C. (2015). Neuropeptide Y System in the Retina: From Localization to Function. *Prog. Retin. Eye Res.* 47, 19–37. doi:10.1016/j.preteyeres.2015.03.001

Sasaki, M., Ozawa, Y., Kurihara, T., Kubota, S., Yuki, K., Noda, K., et al. (2010). Neurodegenerative Influence of Oxidative Stress in the Retina of a Murine Model of Diabetes. *Diabetologia* 53 (5), 971–979. doi:10.1007/s00125-009-1655-6

Saw, M., Wong, V. W., Ho, I. V., and Liew, G. (2019). New Anti-hyperglycaemic Agents for Type 2 Diabetes and Their Effects on Diabetic Retinopathy. *Eye (Lond)* 33 (12), 1842–1851. doi:10.1038/s41433-019-0494-z

Schmid, E., Nogalo, M., Bechrakis, N. E., Fischer-Colbrie, R., Tasan, R., Sperk, G., et al. (2012). Secretoneurin, Substance P and Neuropeptide Y in the Oxygen-Induced Retinopathy in C57Bl/6N Mice. *Peptides* 37 (2), 252–257. doi:10.1016/j.peptides.2012.07.024

Schultz, R., Witte, O. W., and Schmeer, C. (2016). Increased Frataxin Levels Protect Retinal Ganglion Cells after Acute Ischemia/Reperfusion in the Mouse Retina *In Vivo*. *Invest. Ophthalmol. Vis. Sci.* 57 (10), 4115–4124. doi:10.1167/iovs.16-19260

Seki, M., Tanaka, T., Nawa, H., Usui, T., Fukuchi, T., Ikeda, K., et al. (2004). Involvement of Brain-Derived Neurotrophic Factor in Early Retinal Neuropathy of Streptozotocin-Induced Diabetes in Rats: Therapeutic Potential of Brain-Derived Neurotrophic Factor for Dopaminergic Amacrine Cells. *Diabetes* 53 (9), 2412–2419. doi:10.2337/diabetes.53.9.2412

Senanayake, Pd., Drazba, J., Shadrach, K., Milsted, A., Rungger-Brandle, E., Nishiyama, K., et al. (2007). Angiotensin II and its Receptor Subtypes in the Human Retina. *Invest. Ophthalmol. Vis. Sci.* 48 (7), 3301–3311. doi:10.1167/iovs.06-1024

Shah, S. S., Tsang, S. H., and Mahajan, V. B. (2009). Erythropoietin Receptor Expression in the Human Diabetic Retina. *BMC Res. Notes* 2, 234. doi:10.1186/1756-0500-2-234

Shanab, A. Y., Elshaer, S. L., El-Azab, M. F., Soliman, S., Sabbineni, H., Matragoon, S., et al. (2015). Candesartan Stimulates Reparative Angiogenesis in Ischemic Retinopathy Model: Role of Hemeoxygenase-1 (HO-1). *Angiogenesis* 18 (2), 137–150. doi:10.1007/s10456-014-9451-4

Shao, Y., Chen, J., Dong, L. J., He, X., Cheng, R., Zhou, K., et al. (2019). A Protective Effect of PPARα in Endothelial Progenitor Cells through Regulating Metabolism. *Diabetes* 68 (11), 2131–2142. doi:10.2337/db18-1278

Sigurdardottir, S., Zapadka, T. E., Lindstrom, S. I., Liu, H., Taylor, B. E., Lee, C. A., et al. (2019). Diabetes-mediated IL-17A Enhances Retinal Inflammation, Oxidative Stress, and Vascular Permeability. *Cell Immunol* 341, 103921. doi:10.1016/j.cellimm.2019.04.009

Simó, R., and Hernández, C. (2015). Novel Approaches for Treating Diabetic Retinopathy Based on Recent Pathogenic Evidence. *Prog. Retin. Eye Res.* 48, 160–180. doi:10.1016/j.preteyeres.2015.04.003

Simó, R., and Hernández, C. (2017). GLP-1R as a Target for the Treatment of Diabetic Retinopathy: Friend or Foe? *Diabetes* 66 (6), 1453–1460. doi:10.2337/db16-1364

Simões, S. C., Balico-Silva, A. L., Parreiras-E-Silva, L. T., Bitencourt, A. L. B., Bouvier, M., and Costa-Neto, C. M. (2020). Signal Transduction Profiling of Angiotensin II Type 1 Receptor with Mutations Associated to Atrial Fibrillation in Humans. *Front. Pharmacol.* 11, 600132. doi:10.3389/fphar.2020.600132

Simó, R., and Hernández, C.European Consortium for the Early Treatment of Diabetic Retinopathy (EUROCONDOR) (2014). Neurodegeneration in the

Diabetic Eye: New Insights and Therapeutic Perspectives. *Trends Endocrinol. Metab.* 25 (1), 23–33. doi:10.1016/j.tem.2013.09.005

Simó, R., Simó-Servat, O., Bogdanov, P., and Hernández, C. (2021). Neurovascular Unit: A New Target for Treating Early Stages of Diabetic Retinopathy. *Pharmaceutics* 13 (8), 1320. doi:10.3390/pharmaceutics13081320

Simó-Servat, O., Hernández, C., and Simó, R. (2019). Diabetic Retinopathy in the Context of Patients with Diabetes. *Ophthalmic Res.* 62 (4), 211–217. doi:10.1159/000499541

Sinclair, J. R., and Nirenberg, S. (2001). Characterization of Neuropeptide Y-Expressing Cells in the Mouse Retina Using Immunohistochemical and Transgenic Techniques. *J. Comp. Neurol.* 432 (3), 296–306. doi:10.1002/cne.1104

Sjølie, A. K., Klein, R., Porta, M., Orchard, T., Fuller, J., Parving, H. H., et al. (2008). Effect of Candesartan on Progression and Regression of Retinopathy in Type 2 Diabetes (DIRECT-Protect 2): a Randomised Placebo-Controlled Trial. *Lancet* 372 (9647), 1385–1393. doi:10.1016/S0140-6736(08)61411-7

Sjølie, A. K., Klein, R., Porta, M., Orchard, T., Fuller, J., Parving, H. H., et al. (2011). Retinal Microaneurysm Count Predicts Progression and Regression of Diabetic Retinopathy. Post-hoc Results from the DIRECT Programme. *Diabet Med.* 28 (3), 345–351. doi:10.1111/j.1464-5491.2010.03210.x

Smith, J. R., Bolton, E. R., and Dwinell, M. R. (2019). The Rat: A Model Used in Biomedical Research. *Methods Mol. Biol.* 2018, 1–41. doi:10.1007/978-1-4939-9581-3_1

Smits, M. M., Muskiet, M. H., Tonneijck, L., Kramer, M. H., Diamant, M., van Raalte, D. H., et al. (2015). GLP-1 Receptor Agonist Exenatide Increases Capillary Perfusion Independent of Nitric Oxide in Healthy Overweight Men. *Arterioscler Thromb. Vasc. Biol.* 35 (6), 1538–1543. doi:10.1161/ATVBAHA.115.305447

Sollinger, C., Lillis, J., Malik, J., Getman, M., Proschel, C., and Steiner, L. (2017). Erythropoietin Signaling Regulates Key Epigenetic and Transcription Networks in Fetal Neural Progenitor Cells. *Sci. Rep.* 7 (1), 14381. doi:10.1038/s41598-017-14366-0

Straznicky, C., Vickers, J. C., Gábriel, R., and Costa, M. (1992). A Neurofilament Protein Antibody Selectively Labels a Large Ganglion Cell Type in the Human Retina. *Brain Res.* 582 (1), 123–128. doi:10.1016/0006-8993(92)90325-4

Suzuki, M., Ozawa, Y., Kubota, S., Hirasawa, M., Miyake, S., Noda, K., et al. (2011). Neuroprotective Response after Photodynamic Therapy: Role of Vascular Endothelial Growth Factor. *J. Neuroinflammation* 8, 176. doi:10.1186/1742-2094-8-176

Szabadfi, K., Danyadi, B., Kiss, P., Tamas, A., Fabian, E., Gabriel, R., et al. (2012a). Protective Effects of Vasoactive Intestinal Peptide (VIP) in Ischemic Retinal Degeneration. *J. Mol. Neurosci.* 48 (3), 501–507. doi:10.1007/s12031-012-9774-9

Szabadfi, K., Atlasz, T., Kiss, P., Reglodi, D., Szabo, A., Kovacs, K., et al. (2012b). Protective Effects of the Neuropeptide PACAP in Diabetic Retinopathy. *Cel Tissue Res* 348 (1), 37–46. doi:10.1007/s00441-012-1349-0

Szabadfi, K., Atlasz, T., Kiss, P., Danyadi, B., Tamas, A., Helyes, Z., et al. (2012c). Mice Deficient in Pituitary Adenylate Cyclase Activating Polypeptide (PACAP) Are More Susceptible to Retinal Ischemic Injury *In Vivo*. *Neurotox Res.* 21 (1), 41–48. doi:10.1007/s12640-011-9254-y

Szabadfi, K., Szabo, A., Kiss, P., Reglodi, D., Setalo, G., Jr, Kovacs, G., et al. (2014). PACAP Promotes Neuron Survival in Early Experimental Diabetic Retinopathy. *Neurochem. Int.* 64, 84–91. doi:10.1016/j.neuint.2013.11.005

Szabadfi, K., Reglodi, D., Szabo, A., Szalontai, B., Valasek, A., Setalo, G., Jr, et al. (2016). Pituitary Adenylate Cyclase Activating Polypeptide, A Potential Therapeutic Agent for Diabetic Retinopathy in Rats: Focus on the Vertical Information Processing Pathway. *Neurotox Res.* 29 (3), 432–446. doi:10.1007/s12640-015-9593-1

Szabo, E., Patko, E., Vaczy, A., Molitor, D., Csutak, A., Toth, G., et al. (2021). Retinoprotective Effects of PACAP Eye Drops in Microbead-Induced Glaucoma Model in Rats. *Int. J. Mol. Sci.* 22 (16), 8825. doi:10.3390/ijms22168825

Szpirer, C. (2020). Rat Models of Human Diseases and Related Phenotypes: a Systematic Inventory of the Causative Genes. *J. Biomed. Sci.* 27 (1), 84. doi:10.1186/s12929-020-00673-8

Takahashi, T., Yamaguchi, S., Chida, K., and Shibuya, M. (2001). A Single Autophosphorylation Site on KDR/Flk-1 Is Essential for VEGF-A-dependent Activation of PLC-Gamma and DNA Synthesis in Vascular Endothelial Cells. *EMBO J.* 20 (11), 2768–2778. doi:10.1093/emboj/20.11.2768

Tatemoto, K., and Mutt, V. (1981). Isolation and Characterization of the Intestinal Peptide Porcine PHI (PHI-27), a New Member of the Glucagon-Ssecretin Family. *Proc. Natl. Acad. Sci. U S A.* 78 (11), 6603–6607. doi:10.1073/pnas.78.11.6603

Tecilazich, F., Phan, T. A., Simeoni, F., Scotti, G. M., Dagher, Z., and Lorenzi, M. (2020). Patrolling Monocytes Are Recruited and Activated by Diabetes to Protect Retinal Microvessels. *Diabetes* 69 (12), 2709–2719. doi:10.2337/db19-1043

Tenkumo, K., Hirooka, K., Sherajee, S. J., Nakamura, T., Itano, T., Nitta, E., et al. (2014). Effect of the Renin Inhibitor Aliskiren against Retinal Ischemia-Reperfusion Injury. *Exp. Eye Res.* 122, 110–118. doi:10.1016/j.exer.2014.03.011

Thermos, K., Bagnoli, P., Epelbaum, J., and Hoyer, D. (2006). The Somatostatin Sst1 Receptor: an Autoreceptor for Somatostatin in Brain and Retina? *Pharmacol. Ther.* 110 (3), 455–464. doi:10.1016/j.pharmthera.2005.09.003

Tolmachova, T., Wavre-Shapton, S. T., Barnard, A. R., MacLaren, R. E., Futter, C. E., and Seabra, M. C. (2010). Retinal Pigment Epithelium Defects Accelerate Photoreceptor Degeneration in Cell Type-specific Knockout Mouse Models of Choroideremia. *Invest. Ophthalmol. Vis. Sci.* 51 (10), 4913–4920. doi:10.1167/iovs.09-4892

Tomita, Y., Lee, D., Tsubota, K., Negishi, K., and Kurihara, T. (2021). Updates on the Current Treatments for Diabetic Retinopathy and Possibility of Future Oral Therapy. *J. Clin. Med.* 10 (20), 4666. doi:10.3390/jcm10204666

Vaczy, A., Reglodi, D., Somoskeoy, T., Kovacs, K., Lokos, E., Szabo, E., et al. (2016). The Protective Role of PAC1-Receptor Agonist Maxadilan in BCCAO-Induced Retinal Degeneration. *J. Mol. Neurosci.* 60 (2), 186–194. doi:10.1007/s12031-016-0818-4

Van, C., Condro, M. C., Ko, H. H., Hoang, A. Q., Zhu, R., Lov, K., et al. (2021). Targeted Deletion of PAC1 Receptors in Retinal Neurons Enhances Neuron Loss and Axonopathy in a Model of Multiple Sclerosis and Optic Neuritis. *Neurobiol. Dis.* 160, 105524. doi:10.1016/j.nbd.2021.105524

Vecino, E., Caminos, E., Ugarte, M., Martín-Zanca, D., and Osborne, N. N. (1998). Immunohistochemical Distribution of Neurotrophins and Their Receptors in the Rat Retina and the Effects of Ischemia and Reperfusion. *Gen. Pharmacol.* 30 (3), 305–314. doi:10.1016/s0306-3623(97)00361-3

Vecino, E., García-Crespo, D., García-Grespo, D., García, M., Martinez-Millán, L., Sharma, S. C., et al. (2002). Rat Retinal Ganglion Cells Co-express Brain Derived Neurotrophic Factor (BDNF) and its Receptor TrkB. *Vis. Res* 42 (2), 151–157. doi:10.1016/s0042-6989(01)00251-6

Verma, A., Shan, Z., Lei, B., Yuan, L., Liu, X., Nakagawa, T., et al. (2012). ACE2 and Ang-(1-7) Confer protection against Development of Diabetic Retinopathy. *Mol. Ther.* 20 (1), 28–36. doi:10.1038/mt.2011.155

Verma, A., Zhu, P., de Kloet, A., Krause, E., Sumners, C., and Li, Q. (2019). Angiotensin Receptor Expression Revealed by Reporter Mice and Beneficial Effects of AT2R Agonist in Retinal Cells. *Exp. Eye Res.* 187, 107770. doi:10.1016/j.exer.2019.107770

Verma, A., Zhu, P., Xu, K., Du, T., Liao, S., Liang, Z., et al. (2020). Angiotensin-(1-7) Expressed from Lactobacillus Bacteria Protect Diabetic Retina in Mice. *Transl Vis. Sci. Technol.* 9 (13), 20. doi:10.1167/tvst.9.13.20

Villacampa, P., Liyanage, S. E., Klaska, I. P., Cristante, E., Menger, K. E., Sampson, R. D., et al. (2020). Stabilization of Myeloid-Derived HIFs Promotes Vascular Regeneration in Retinal Ischemia. *Angiogenesis* 23 (2), 83–90. doi:10.1007/s10456-019-09681-1

Wan, C., Liu, N. N., Liu, L. M., Cai, N., and Chen, L. (2010). Effect of Adenovirus-Mediated Brain Derived Neurotrophic Factor in Early Retinal Neuropathy of Diabetes in Rats. *Int. J. Ophthalmol.* 3 (2), 145–148. doi:10.3980/j.issn.2222-3959.2010.02.12

Wang, W., and Lo, A. C. Y. (2018). Diabetic Retinopathy: Pathophysiology and Treatments. *Int. J. Mol. Sci.* 19 (6), 1816. doi:10.3390/ijms19061816

Wang, P., and Xia, F. (2015). EPO Protects Müller Cell under High Glucose State through BDNF/TrkB Pathway. *Int. J. Clin. Exp. Pathol.* 8 (7), 8083–8090.

Wang, Z. Y., Zhao, K. K., and Zhao, P. Q. (2011). Erythropoietin Therapy for Early Diabetic Retinopathy through its Protective Effects on Retinal Pericytes. *Med. Hypotheses* 76 (2), 266–268. doi:10.1016/j.mehy.2010.10.017

Wang, J., Sun, Z., Shen, J., Wu, D., Liu, F., Yang, R., et al. (2015). Octreotide Protects the Mouse Retina against Ischemic Reperfusion Injury through Regulation of Antioxidation and Activation of NF-κB. *Oxid. Med. Cel. Longev.* 2015, 970156. doi:10.1155/2015/970156

Wang, J., Tian, W., Wang, S., Wei, W., Wu, D., Wang, H., et al. (2017). Anti-inflammatory and Retinal Protective Effects of Capsaicin on Ischaemia-Induced Injuries through the Release of Endogenous Somatostatin. *Clin. Exp. Pharmacol. Physiol.* 44 (7), 803–814. doi:10.1111/1440-1681.12769

Wang, J., Zhao, J., Cui, X., Mysona, B. A., Navneet, S., Saul, A., et al. (2019). The Molecular Chaperone Sigma 1 Receptor Mediates rescue of Retinal Cone Photoreceptor Cells via Modulation of NRF2. *Free Radic. Biol. Med.* 134, 604–616. doi:10.1016/j.freeradbiomed.2019.02.001

Wang, J. H., Roberts, G. E., and Liu, G. S. (2020). Updates on Gene Therapy for Diabetic Retinopathy. *Curr. Diab Rep.* 20 (7), 22. doi:10.1007/s11892-020-01308-w

Wang, L., Klingeborn, M., Travis, A. M., Hao, Y., Arshavsky, V. Y., and Gospe, S. M., 3rd (2020). Progressive Optic Atrophy in a Retinal Ganglion Cell-specific Mouse Model of Complex I Deficiency. *Sci. Rep.* 10 (1), 16326. doi:10.1038/s41598-020-73353-0

Werling, D., Reglodi, D., Kiss, P., Toth, G., Szabadfi, K., Tamas, A., et al. (2014). Investigation of PACAP Fragments and Related Peptides in Chronic Retinal Hypoperfusion. *J. Ophthalmol.* 2014, 563812. doi:10.1155/2014/563812

Werling, D., Reglodi, D., Banks, W. A., Salameh, T. S., Kovacs, K., Kvarik, T., et al. (2016). Ocular Delivery of PACAP1-27 Protects the Retina from Ischemic Damage in Rodents. *Invest. Ophthalmol. Vis. Sci.* 57 (15), 6683–6691. doi:10.1167/iovs.16-20630

Werling, D., Banks, W. A., Salameh, T. S., Kvarik, T., Kovacs, L. A., Vaczy, A., et al. (2017). Passage through the Ocular Barriers and Beneficial Effects in Retinal Ischemia of Topical Application of PACAP1-38 in Rodents. *Int. J. Mol. Sci.* 18 (3), 675. doi:10.3390/ijms18030675

Whitcup, S. M., Nussenblatt, R. B., Lightman, S. L., and Hollander, D. A. (2013). Inflammation in Retinal Disease. *Int. J. Inflam* 2013, 724648. doi:10.1155/2013/724648

Wilkinson-Berka, J. L., Rana, I., Armani, R., and Agrotis, A. (2013). Reactive Oxygen Species, Nox and Angiotensin II in Angiogenesis: Implications for Retinopathy. *Clin. Sci. (Lond)* 124 (10), 597–615. doi:10.1042/CS20120212

Wilkinson-Berka, J. L., Suphapimol, V., Jerome, J. R., Deliyanti, D., and Allingham, M. J. (2019). Angiotensin II and Aldosterone in Retinal Vasculopathy and Inflammation. *Exp. Eye Res.* 187, 107766. doi:10.1016/j.exer.2019.107766

Willis, L. M., El-Remessy, A. B., Somanath, P. R., Deremer, D. L., and Fagan, S. C. (2011). Angiotensin Receptor Blockers and Angiogenesis: Clinical and Experimental Evidence. *Clin. Sci. (Lond)* 120 (8), 307–319. doi:10.1042/cs20100389

Witmer, A. N., Blaauwgeers, H. G., Weich, H. A., Alitalo, K., Vrensen, G. F., and Schlingemann, R. O. (2002). Altered Expression Patterns of VEGF Receptors in Human Diabetic Retina and in Experimental VEGF-Induced Retinopathy in Monkey. *Invest. Ophthalmol. Vis. Sci.* 43 (3), 849–857.

Wu, G. S., Jiang, M., Liu, Y. H., Nagaoka, Y., and Rao, N. A. (2012). Phenotype of Transgenic Mice Overexpressed with Inducible Nitric Oxide Synthase in the Retina. *PLoS One* 7 (8), e43089. doi:10.1371/journal.pone.0043089

Xie, H., Zhang, C., Liu, D., Yang, Q., Tang, L., Wang, T., et al. (2021). Erythropoietin Protects the Inner Blood-Retinal Barrier by Inhibiting Microglia Phagocytosis via Src/Akt/cofilin Signalling in Experimental Diabetic Retinopathy. *Diabetologia* 64 (1), 211–225. doi:10.1007/s00125-020-05299-x

Xu, H., Zhang, L., Gu, L., Lu, L., Gao, G., Li, W., et al. (2014). Subretinal Delivery of AAV2-Mediated Human Erythropoietin Gene Is Protective and Safe in Experimental Diabetic Retinopathy. *Invest. Ophthalmol. Vis. Sci.* 55 (3), 1519–1530. doi:10.1167/iovs.13-13155

Yang, J. H., Guo, Z., Zhang, T., Meng, X. X., and Xie, L. S. (2013). Restoration of Endogenous Substance P Is Associated with Inhibition of Apoptosis of Retinal Cells in Diabetic Rats. *Regul. Pept.* 187, 12–16. doi:10.1016/j.regpep.2013.09.001

Yang, S., He, H., Ma, Q. S., Zhang, Y., Zhu, Y., Wan, X., et al. (2015). Experimental Study of the Protective Effects of SYVN1 against Diabetic Retinopathy. *Sci. Rep.* 5, 14036. doi:10.1038/srep14036

Yang, Y., Liu, W., Sun, K., Jiang, L., and Zhu, X. (2019). Tmem30a Deficiency Leads to Retinal Rod Bipolar Cell Degeneration. *J. Neurochem.* 148 (3), 400–412. doi:10.1111/jnc.14643

Yin, Z., Tan, R., Yuan, T., Chen, S., Quan, Y., Hao, Q., et al. (2021). Berberine Prevents Diabetic Retinopathy through Inhibiting HIF-1α/VEGF/NF-κ B Pathway in Db/db Mice. *Pharmazie* 76 (4), 165–171. doi:10.1691/ph.2021.01012

Zalutsky, R. A., and Miller, R. F. (1990). The Physiology of Substance P in the Rabbit Retina. *J. Neurosci.* 10 (2), 394–402. doi:10.1523/JNEUROSCI.10-02-00394.1990

Zapadka, T. E., Lindstrom, S. I., Taylor, B. E., Lee, C. A., Tang, J., Taylor, Z. R. R., et al. (2020). RORγt Inhibitor-SR1001 Halts Retinal Inflammation, Capillary Degeneration, and the Progression of Diabetic Retinopathy. *Int. J. Mol. Sci.* 21 (10), 3547. doi:10.3390/ijms21103547

Zeng, Y., Yang, K., Wang, F., Zhou, L., Hu, Y., Tang, M., et al. (2016). The Glucagon like Peptide 1 Analogue, Exendin-4, Attenuates Oxidative Stress-Induced Retinal Cell Death in Early Diabetic Rats through Promoting Sirt1 and Sirt3 Expression. *Exp. Eye Res.* 151, 203–211. doi:10.1016/j.exer.2016.05.002

Zhai, R., Xu, H., Hu, F., Wu, J., Kong, X., and Sun, X. (2020). Exendin-4, a GLP-1 Receptor Agonist Regulates Retinal Capillary Tone and Restores Microvascular Patency after Ischaemia-Reperfusion Injury. *Br. J. Pharmacol.* 177 (15), 3389–3402. doi:10.1111/bph.15059

Zhang, Y., Wang, Q., Zhang, J., Lei, X., Xu, G. T., and Ye, W. (2009). Protection of Exendin-4 Analogue in Early Experimental Diabetic Retinopathy. *Graefes Arch. Clin. Exp. Ophthalmol.* 247 (5), 699–706. doi:10.1007/s00417-008-1004-3

Zhang, Y., Zhang, J., Wang, Q., Lei, X., Chu, Q., Xu, G. T., et al. (2011). Intravitreal Injection of Exendin-4 Analogue Protects Retinal Cells in Early Diabetic Rats. *Invest. Ophthalmol. Vis. Sci.* 52 (1), 278–285. doi:10.1167/iovs.09-4727

Zhong, Y., Mohan, K., Liu, J., Al-Attar, A., Lin, P., Flight, R. M., et al. (2020). Loss of CLN3, the Gene Mutated in Juvenile Neuronal Ceroid Lipofuscinosis, Leads to Metabolic Impairment and Autophagy Induction in Retinal Pigment Epithelium. *Biochim. Biophys. Acta Mol. Basis Dis.* 1866 (10), 165883. doi:10.1016/j.bbadis.2020.165883

Zhou, Q., Frost, R. J. A., Anderson, C., Zhao, F., Ma, J., Yu, B., et al. (2017). let-7 Contributes to Diabetic Retinopathy but Represses Pathological Ocular Angiogenesis. *Mol. Cel Biol* 37 (16), e00001–17. doi:10.1128/MCB.00001-17

Zhou, H. R., Ma, X. F., Lin, W. J., Hao, M., Yu, X. Y., Li, H. X., et al. (2020). Neuroprotective Role of GLP-1 Analog for Retinal Ganglion Cells via PINK1/Parkin-Mediated Mitophagy in Diabetic Retinopathy. *Front. Pharmacol.* 11, 589114. doi:10.3389/fphar.2020.589114

Zhu, Y., Zhang, L., Sasaki, Y., Milbrandt, J., and Gidday, J. M. (2013). Protection of Mouse Retinal Ganglion Cell Axons and Soma from Glaucomatous and Ischemic Injury by Cytoplasmic Overexpression of Nmnat1. *Invest. Ophthalmol. Vis. Sci.* 54 (1), 25–36. doi:10.1167/iovs.12-10861

Zhu, L., Xu, J., Liu, Y., Gong, T., Liu, J., Huang, Q., et al. (2018). Prion Protein Is Essential for Diabetic Retinopathy-Associated Neovascularization. *Angiogenesis* 21 (4), 767–775. doi:10.1007/s10456-018-9619-4

GLOSSARY

AC amacrine cell

ACE angiotensin converting enzyme

ACE2 angiotensin converting enzyme 2

Ang II angiotensin II

ARB angiotensin receptor blocker

ATR angiotensin receptor

AT1R angiotensin II type 1 receptor

AT2R angiotensin II type 2 receptor

BC bipolar cell

BDNF brain-derived neurotrophic factor

BRB blood-retina-barrier

cAMP cyclic adenosine monophosphate

CAO cerebral artery occlusion

cGMP cyclic guaninosine monophosphate

dAC displaced amacrine cell

DM diabetes mellitus

DR diabetic retinopathy

E4 exendin-4

eNOS endothelial nitric oxid synthase

EPO erythropoietin

ERK1/2 extracellular signal-regulated kinase

GLP-1 glucagon-like peptide-1

GLP-1R glucagon-like peptide-1 receptor

GLP-1RA glucagon-like peptide-1 receptor agonist

GM genetically modified

HC horizontal cell

ICAM intercellular adhesion molecule

IL-1β interleukin 1 beta

IOP intraocular pressure

IP3 inositol trisphosphate

IRI ischemia reperfusion injury

JAK janus kinase

KO knockout

MAPK mitogen activated protein kinase

mTOR target of rapamycin

NF-κB nuclear factor kappa B

NK neurokinin

NO nitric oxide

NP neuropeptide

NPY neuropeptide Y

OCT octreotide

PACAP pituitary adenylyl cyclase-activating polypeptide

PE pigment epithelium

PEDF pigment epithelium derived factor

PI3K phosphoinositide 3-kinase

PKA protein kinase A

PKC protein kinase C

PLC phospholipase C

PR photoreceptor

RAS renin-angiotensin system

RGC retinal ganglion cell

ROS reactive oxygen species

RPE retinal pigment epithelium

SIRT sirtuin

SP substance P

SST somatostatin

STAT signal transducer and activator of transcription

STZ streptozotocin

TrkB tropomyosin receptor kinase B

VEGF vascular endothelial growth factor

VIP vasoactive intestinal polypeptide

Synthesis, Characterization, and *in vivo* Evaluation of a Novel Potent Autotaxin-Inhibitor

Daniel Hunziker[1†], Sabrina Reinehr[2†], Marina Palmhof[2], Natalie Wagner[2], Thomas Biniasch[2], Gesa Stute[2], Patrizio Mattei[1], Petra Schmitz[1], Patrick DiGiorgio[1], Jérôme Hert[1], Markus G. Rudolph[1], Joerg Benz[1], Martine Stihle[1], Bernard Gsell[1], Stephan Müller[1], Rodolfo Gasser[1,3], Nina Schonhoven[2], Christoph Ullmer[4†]* and Stephanie C. Joachim[2†]*

[1]F. Hoffmann-La Roche Ltd., Pharma Research and Early Development, Therapeutic Modalities, Small Molecule Research, Roche Innovation Center Basel, Basel, Switzerland, [2]Experimental Eye Research Institute, University Eye Hospital, Ruhr-University Bochum, Bochum, Germany, [3]F. Hoffmann-La Roche Ltd., Pharma Research and Early Development, Pharmaceutical Sciences, Roche Innovation Center Basel, Basel, Switzerland, [4]F. Hoffmann-La Roche Ltd., Pharma Research and Early Development, Ophthalmology Discovery, Roche Innovation Center Basel, Basel, Switzerland

The autotaxin-lysophosphatidic acid (ATX-LPA) signaling pathway plays a role in a variety of autoimmune diseases, such as rheumatoid arthritis or neurodegeneration. A link to the pathogenesis of glaucoma is suggested by an overactive ATX-LPA axis in aqueous humor samples of glaucoma patients. Analysis of such samples suggests that the ATX-LPA axis contributes to the fibrogenic activity and resistance to aqueous humor outflow through the trabecular meshwork. In order to inhibit or modulate this pathway, we developed a new series of ATX-inhibitors containing novel bicyclic and spirocyclic structural motifs. A potent lead compound (IC_{50} against ATX: 6 nM) with good *in vivo* PK, favorable *in vitro* property, and safety profile was generated. This compound leads to lowered LPA levels *in vivo* after oral administration. Hence, it was suitable for chronic oral treatment in two rodent models of glaucoma, the experimental autoimmune glaucoma (EAG) and the ischemia/reperfusion models. In the EAG model, rats were immunized with an optic nerve antigen homogenate, while controls received sodium chloride. Retinal ischemia/reperfusion (I/R) was induced by elevating the intraocular pressure (IOP) in one eye to 140 mmHg for 60 min, followed by reperfusion, while the other untreated eye served as control. Retinae and optic nerves were evaluated 28 days after EAG or 7 and 14 days after I/R induction. Oral treatment with the optimized ATX-inhibitor lead to reduced retinal ganglion cell (RGC) loss in both glaucoma models. In the optic nerve, the protective effect of ATX inhibition was less effective compared to the retina and only a trend to a weakened neurofilament distortion was detectable. Taken together, these results provide evidence that the dysregulation of the ATX-LPA axis in the aqueous humor of glaucoma patients, in addition to the postulated outflow impairment, might also contribute to RGC loss. The observation that ATX-inhibitor treatment in both glaucoma models did not result in significant IOP increases or decreases after oral treatment indicates that protection from RGC loss due to inhibition of the ATX-LPA axis is independent of an IOP lowering effect.

Keywords: autoimmune glaucoma model, ischemia, glaucoma, autotaxin (ATX), lysophosphatidic acid, optic nerve, retina, retinal ganglion ceils

1 INTRODUCTION

Autotaxin (ATX) or ectonucleotide pyrophosphatase/phosphodiesterase 2 (ENPP2) is an extracellular zinc-dependent enzyme that converts lysophosphatidyl choline (LPC) into the bioactive phospholipid lysophosphatidic acid (LPA) and choline. LPA acts as a bioactive growth factor-like phospholipid consisting of a glycerol backbone, a phosphate group and a fatty acid chain that can vary in length and degree of saturation. LPA mediates most of its biological effects through six G-protein-coupled receptors (GPCRs) known as LPAR1-6, thus stimulating a variety of biological functions including proliferation, migration, invasion, and survival of many cell types. ATX has attracted substantial interest over the last decade as a potential therapeutic target since the ATX-LPA axis was shown to play a key role in a variety

of physiological and pathological conditions including fibrotic diseases, arthritis, glaucoma, and a number of other disorders (Matralis et al., 2019). The first and only ATX-inhibitor to enter clinical trials, Ziritaxestat (GLPG-1690), for idiopathic pulmonary fibrosis has advanced to clinical phase 3 (Maher et al., 2018). The ISABELA phase 3 trial, however, was discontinued recently as the benefit-risk profile no longer supported continuing these studies.

PF-8380 (1) was one of the early ATX-inhibitor tool compounds published by Pfizer, which showed inhibition of LPA generation *in vivo* (Gierse et al., 2010). In order to obtain a new set of proprietary ATX-inhibitors, we initially used 1 as a template for structure-based inhibitor optimization with subsequent removal of liabilities identified for 1. Basically, 1 can be divided into three parts, which can to some extent be optimized individually (**Figure 1A**) while keeping the fit of the
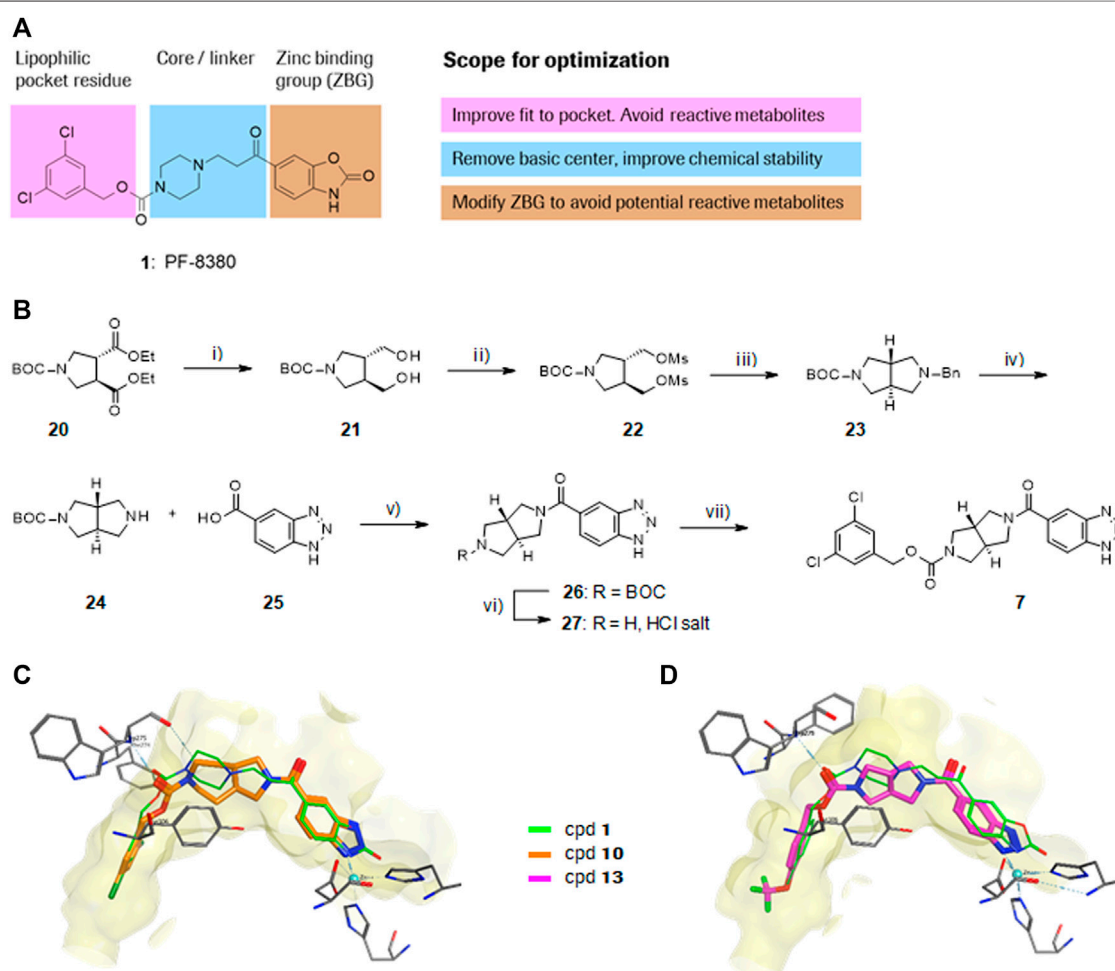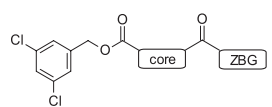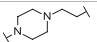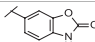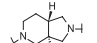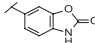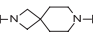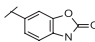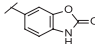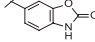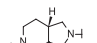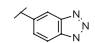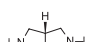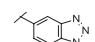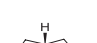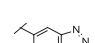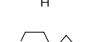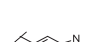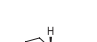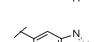
FIGURE 1 | Structure, synthesis and co-crystal structures of ATX-inhibitors. **(A)** Structure of PF-8380 (1) with an outline of the general approach for modification and optimization. **(B)** Synthesis of ATX-inhibitor 7. i) 4M LiBH$_4$, THF, RT, 91–95% crude; ii) MsCl, NEt$_3$, DCM, -10°C, 94% crude; iii) BnNH$_2$, K$_2$CO$_3$, CH$_3$CN, 95°C, 24 h, 53%; iv) H$_2$, Pd/C, 1 bar, MeOH, 96%; v) HATU, NMM, DMF, RT, 16 h, 83%; vi) HCl/^{i}PrOH (~5–6M), RT, 87%; vii) (3,5-dichlorophenyl)methanol, CDI, NEt$_3$, CH$_3$CN, reflux, 87%. **(C)** X-ray crystal structures of human ATX in complex with 1 and 10 (overlay). Both inhibitors interact with the zinc ion in the active site (light blue) and stretch into a lipophilic pocket which corresponds to the fatty acid binding site of LPC (left). Besides the fit to the lipophilic pocket, other key interactions for 10 are the binding of the benzotriazole to the active site zinc ion and an H-bond of the carbamate oxygen to the backbone NH of Trp275. **(D)** X-ray crystal structures of 1 and 13 (overlay), with an essentially identical pattern of contacts with the enzyme.

TABLE 1 | Initial screening of central cores and zinc binding groups.

Cmpd	Core	ZBG	hATX IC$_{50}$ [nM]	LogD (pH 7.4)	Solubility [µg/mL], pH 6.5	Mic CL h/m/r [µL/m/mg prot]	GSH adducts
1			3	2.7	<1	65/78/84	pos
2			3	3.7	<1	39/74/nd	pos
3			220	3.6	<1	92/81/nd	nd
4			17	3.6	<1	54/149/nd	pos
5			65	3.3	19	64/288/335	pos
6			4	3.5	9	23/65/nd	pos
7			4	3.1	9	16/17/10	pos
8			265	3.1	34	23/68/nd	pos
9			67	3.6	3	30/63/29	pos
10			1	3.5[a]	7	252/727/nd	nd

[a]Calculated value; nd = not determined.Initial screening of central cores and zinc binding groups (ZBG).

molecule to the active site of ATX preserved. One important liability for **1** was substantial formation of reactive metabolites as observed by glutathione (GSH) addition to both the benzoxazol-2-one zinc-binding group (ZBG) and to the dichlorophenyl moiety. In addition, the 1,4-arrangement of a carbonyl group and charged nitrogen of the piperazine core could potentially result in some chemical instability. Besides this, metabolic stability of **1** was found to be limited and solubility was determined to be very low (**Table 1**). With this approach, we pursued a similar path as described by others for another set of ATX-inhibitors (Kuttruff et al., 2017).

Initial expression analysis of ATX revealed highest expression in adipocytes and retina (Giganti et al., 2008). Cellular resolution of ATX expression in the eye, analyzed by *in situ* hybridization, is restricted to epithelial cells of the ciliary body and retinal pigment epithelial cells (Narita et al., 1994). Both are secretory epithelial cells that have anatomically tight junctions and are localized on stroma, which are rich in capillaries with fenestrated endothelium and might be the main producer of abundant ATX found in human vitreous fluid (Abu El-Asrar et al., 2013) and aqueous humor (Iyer et al., 2012). The link to the pathogenesis of primary open-angle glaucoma (POAG) is suggested by elevated levels of ATX, LPA, and LPC in North American (in both Caucasians and African Americans) and Japanese POAG patients that correlated with elevation of intraocular pressure (IOP) (Honjo et al., 2018; Ho et al., 2020). Also, lysophosphatidic lipase D activity was elevated in the aqueous humor of POAG patients relative to age matched control (cataract) subjects (Iyer et al., 2012). A recent study suggests that aqueous ATX levels can distinguish glaucoma subtypes and serve as a promising biomarker for open-angle glaucoma subtypes (Igarashi et al., 2021).

Trabecular meshwork has been proposed as the relevant target tissue where ATX was induced during mechanical stress in isolated human cells (Iyer et al., 2012). The resulting LPA regulates plasticity and fibrogenic activity in the Schlemm's canal (Pattabiraman et al., 2014). The product of ATX, LPA, has in turn been demonstrated to impair aqueous humor outflow facility in the porcine enucleated eye (Mettu et al., 2004) and increase IOP of rabbit eyes after intracameral instillation (Nakamura et al., 2021). Inhibition of lysophosphatidic lipase D activity by topical and intracameral delivery of a chemical ATX-inhibitor significantly decreases IOP in rabbits, suggesting that ATX is a potential therapeutic target for lowering IOP in glaucoma patients (Iyer et al., 2012).

The role of ATX in POAG patients seems to go beyond IOP control. ATX expression was increased by more than 10-fold in astrocytes isolated from the optic nerve head of glaucoma patients (Hernandez et al., 2002). It was already shown that stearoyl-LPA or hypoxia reduced the viability of retinal ganglion cells (RGCs) and a LPA1R antagonist was neuroprotective and led to RGC survival in a mouse model of oxygen-induced retinopathy (Yang et al., 2009). As glaucomatous optic neuropathy involves specific degeneration of the RGCs, an overactive ATX-LPA axis in glaucoma might also contribute to neuropathy. We sought to elaborate protective effects by ATX inhibition using lead compound **13** (ATX-i) in two glaucoma models of RGC degeneration, an ischemia/reperfusion (I/R) model and an experimental autoimmune glaucoma (EAG) model.

In the EAG model, neuroprotective mechanisms can be analyzed independently from an elevated IOP. Here, an immunization with antigens, such as the optic nerve antigen homogenate (ONA) leads to a degeneration of RGCs and optic nerve axons after 28 days (Laspas et al., 2011; Noristani et al., 2016). In previous studies, an increase in microglia numbers as well as an activation of the complement system were noted prior to cell death (Noristani et al., 2016; Reinehr et al., 2016). Furthermore, antibody deposits were detected in glaucomatous retinas (Joachim et al., 2012a), which might contribute to retinal and optic nerve degeneration in the EAG model.

Retinal I/R is a common rodent model to induce retinal damage. In the majority of studies, it is achieved through an IOP increase above the systolic level for a defined time period (Adachi et al., 1996; Joachim et al., 2012b). In the I/R model, our group and others described degeneration of RGCs, a thinning of the inner retinal layers, and consequently observed impaired retinal function by decreased a-wave and b-wave electroretinogram (ERG) amplitudes in the ischemic eyes (Schmid et al., 2014; Wu et al., 2020). In a recent study, we noted that ischemic processes have a strong destructive effect on RGCs. Less RGCs could be detected on protein level already 2 h after I/R and on mRNA level at 12 h (Palmhof et al., 2019). In addition, 2 h after I/R induction, microglia/macrophages are already in an active state (Wagner et al., 2020).

The goal of this project was to investigate if an orally bioavailable ATX-inhibitor protects from damage of the retina in two different preclinical glaucoma models. For this purpose, a novel ATX-inhibitor (**13**) from a new chemical series amenable for chronic oral delivery was tested in the EAG as well as in an I/R model. We investigated if retinal function and structure could be protected through the ATX-inhibitor in both models.

2 MATERIALS AND METHODS

2.1 Synthesis of ATX-Inhibitors

A representative synthesis for an inhibitor with a new bicyclic central core is given in this section for compound **7**. Detailed syntheses and analytical data for the other compounds **2–6** and **8–15** described in this paper are provided in the **Supplementary**

Material Section 1.1, S1.1–S1.13. Synthesis of compound **7** was done according to **Figure 1B**:

(*3R,4R*)-tert-Butyl 3,4-bis(hydroxymethyl)pyrrolidine-1-carboxylate (**21**).

Lithium borohydride (3.60 g, 165 mmol) was added at −5°C in several portions to a solution of (*3R,4R*)-1-tert-butyl 3,4-diethyl pyrrolidine-1,3,4-tricarboxylate (20.9 g, 66.1 mmol) in tetrahydrofuran (350 ml). After 2 h, the ice bath was removed, then after 18 h, the reaction was stopped by dropwise addition of methanol (150 ml), while keeping the reaction temperature at 25°C under ice cooling. After 2 h, the hydrogen release had stopped and the mixture was evaporated (Rodríguez Sarmiento et al., 2003). The residue was partitioned between ethyl acetate and 50% aq. ammonium chloride solution. The organic layer was washed with brine, dried over magnesium sulfate, filtered, and evaporated to afford the title compound **21** (14.3 g, 94%) as a colorless oil, MS: 254.5 [M + Na]$^+$. ^{1}H NMR (CDCl$_3$, 300 MHz) δ 3.68 (br s, 2H), 3.4–3.6 (m, 4H), 3.29 (br s, 2H), 2.93 (br t, 2H, J = 9.5 Hz), 2.13 (br s, 2H), 1.39 (s, 9H). (*3R,4R*)-tert-Butyl 3,4-bis((methylsulfonyloxy)methyl)pyrrolidine-1-carboxylate (**22**).

A solution of methanesulfonyl chloride (21.1 g, 185 mmol) in dichloromethane (30 ml) was added dropwise at 0°C to a solution of (*3R,4R*)-tert-butyl 3,4-bis(hydroxymethyl)pyrrolidine-1-carboxylate (**21**; 14.23 g, 61.5 mmol) and *N,N*-diisopropylethylamine (47.7 g, 369 mmol) in dichloromethane (300 ml), then after 90 min, the reaction mixture was washed with water. The organic layer was washed with 50% aq. sodium hydrogencarbonate solution, water and brine, dried over magnesium sulfate, and evaporated to afford the title compound **22** (22.4 g, 94%) as a dark red oil, MS: 332.4 [M–isobutene + H]$^+$.

^{1}H NMR (CDCl$_3$, 300 MHz) δ 4.26 (br d, 4H, J = 4.8 Hz), 3.6–3.7 (m, 2H), 3.25 (br dd, 2H, J = 7.0, 11.2 Hz), 3.06 (s, 6H), 2.53 (br s, 2H), 1.46 (m, 9H).

(*3aS,6aS*)-tert-Butyl 5-benzylhexahydropyrrolo [3,4-c]pyrrole-2(*1H*)-carboxylate (**23**).

To a clear orange solution of (*3R,4R*)-tert-butyl 3,4-bis((methylsulfonyloxy)methyl)-pyrrolidine-1-carboxylate (**22**; 13.42 g, 34.6 mmol) in acetonitrile (200 ml) were added potassium carbonate (23.9 g, 173 mmol) and phenylmethanamine (11.1 g, 104 mmol). The suspension was heated to 95°C for 24 h, then after cooling, the reaction mixture was partitioned between ethyl acetate 10% and aq. citric acid solution. The aqueous layer was basified to pH 7 with sodium hydrogen carbonate solution and extracted 4 times with ethyl acetate. The combined ethyl acetate layers were dried over magnesium sulfate, filtered, and evaporated to afford the title compound **23** (5.52 g, 53%) as light yellow solid, MS: 303.6 [M + H]$^+$.

^{1}H NMR (CDCl$_3$, 300 MHz) δ 7.2–7.3 (m, 5H), 3.8–3.9 (m, 2H), 3.4–3.7 (m, 2H), 2.8–3.0 (m, 4H), 2.59 (dt, 2H, J = 3.5, 9.6 Hz), 2.1–2.3 (m, 2H), 1.45 (s, 9H).

(*3aS,6aS*)-tert-Butyl hexahydropyrrolo [3,4-c]pyrrole-2(*1H*)-carboxylate (**24**).

To a solution of (*3aS,6aS*)-tert-butyl 5-benzylhexahydropyrrolo [3,4-c]pyrrole-2(*1H*)-carboxylate (**23**; 2.22 g, 7.34 mmol) in methanol (20 ml) was added palladium (10% on carbon,

220 mg, 7.34 mmol) and the reaction mixture was stirred under a hydrogen atmosphere (1 bar) at room temperature for 24 h, then insoluble material was removed by filtration through diatomaceous earth. The filtrate was concentrated to produce the title compound **24** (1.60 g, 100%). White waxy solid, MS: 213.5 (M + H)$^+$.

^{1}H NMR (CDCl$_3$, 300 MHz) δ 3.5–3.7 (m, 2H), 2.9–3.1 (m, 4H), 2.63 (dt, 2H, J = 4.0, 9.9 Hz), 2.0–2.3 (m, 2H), 1.87 (br s, 1H), 1.46 (s, 9H).

(3aS,6aS)-tert-Butyl 5-(1H-benzo [d][1,2,3]triazole-5-carbonyl) hexahydropyrrolo [3,4-c]pyrrole-2(1H)-carboxylate (**26**).

O-(7-azabenzotriazol-1-yl)-N,N,N′,N′-tetramethyluronium hexafluoro-phosphate (HATU, 915 mg, 2.41 mmol) was added at 0°C to a solution of (3aS,6aS)-tert-butyl hexahydropyrrolo [3,4-c] pyrrole-2(1H)-carboxylate (**24**; 511 mg, 2.41 mmol), N-methylmorpholine (730 mg, 7.22 mmol) and 1H-benzo [d] [1,2,3]triazole-5-carboxylic acid (**25**, 393 mg, 2.41 mmol) in N,N-dimethylformamide (13 ml). The reaction mixture was allowed to reach room temperature over 16 h and was then partitioned between ethyl acetate and sat aq. sodium hydrogen carbonate solution. The organic layer was washed with water and brine dried over magnesium sulfate filtered and evaporated. Chromatography (silica gel; gradient dichloromethane to dichloromethane/methanol/25% aq. Ammonia solution 90:10: 0.25) afforded the title compound **26** (718 mg, 83%) as a light yellow foam, MS: 358.5 [M + H]$^+$.

^{1}H NMR (CDCl$_3$, 300 MHz) δ 14.43 (br s, 1H), 8.03 (br s, 1H), 7.82 (br d, 1H, J = 6.9 Hz), 7.59 (br d, 1H, J = 9.1 Hz), 3.9–4.1 (m, 1H), 3.5–3.8 (m, 3H), 3.3–3.5 (m, 2H), 3.0–3.2 (m, 2H), 2.2–2.5 (m, 2H), 1.49 (s, 9H).

(1H-Benzo [d][1,2,3]triazol-5-yl) ((3aR,6aR)-hexahydropyrrolo [3,4-c]pyrrol-2(1H)-yl)methanone hydrochloride (**27**).

To a light yellow solution of (3aS,6aS)-tert-butyl 5-(1H-benzo [d][1,2,3]triazole-5-carbonyl)hexahydropyrrolo [3,4-c]pyrrole-2(1H)-carboxylate (**26**, 733 mg, 2.05 mmol) in 2-propanol (8 ml) was added hydrochloric acid solution (5–6 M in 2-propanol, 9 ml, 45 mmol) at room temperature and then the reaction mixture was evaporated. The residue was triturated with ethyl acetate and the precipitate was collected by filtration to afford the title compound **27** (523 mg, 87%). Light yellow solid, MS: 256.5 [M–H]$^-$.

^{1}H NMR ((CD$_3$)$_2$SO, 300 MHz) δ 9.68 (br s, 2H), 8.11 (s, 1H), 7.95 (br d, 1H, J = 8.5 Hz), 7.59 (d, 1H, J = 8.5 Hz), 3.77 (dd, 1H, J = 6.5, 10.9 Hz), 3.3–3.6 (m, 5H), 2.8–3.0 (m, 3H), 2.2–2.4 (m, 2H).

(3aS,6aS)-5-(1H-Benzotriazole-5-carbonyl)-hexahydro-pyrrolo [3,4-c]pyrrole-2-carboxylic acid 3,5-dichloro-benzyl ester (**7**).

To a solution of (3,5-dichlorophenyl)methanol (21.4 mg, 121 μmol) in acetonitrile (5 ml) was added N,N′-carbonyldiimidazole (20.6 mg, 127 μmol) at room temperature, then after 3 h, triethylamine (61.3 mg, 606 μmol) and (1H-benzo [d][1,2,3]triazol-5-yl) ((3aR,6aR)-hexahydropyrrolo [3,4-c] pyrrol-2(1H)-yl)methanone hydrochloride (**27**; 40 mg, 121 μmol) were added and the reaction mixture was heated at reflux. After 16 h, the reaction mixture was partitioned between ethyl acetate and sat. aq. ammonium chloride solution, the organic layer was washed with sat. aq. sodium hydrogen carbonate solution and brine, dried over magnesium sulfate,

filtered, and evaporated. Chromatography (silica gel; gradient dichloromethane to dichloromethane/methanol/25% aq. ammonia solution 90:10:0.25) produced the title compound **7** (38 mg, 68%) as a light-yellow foam. ^{1}H NMR (CDCl$_3$, 300 MHz) δ 14.60 (br s, 1H), 8.00 (br s, 1H), 7.80 (br s, 1H), 7.58 (br d, 1H, J = 8.7 Hz), 7.2–7.4 (m, 3H), 5.09 (d, 2H, J = 3.0 Hz), 4.0–4.1 (m, 1H), 3.8–3.9 (m, 1H), 3.6–3.8 (m, 2H), 3.3–3.5 (m, 2H), 3.1–3.3 (m, 2H), 2.2–2.5 (m, 2H). LC-HRMS (m/z) [M + H]$^+$ calcd for [C$_{21}$H$_{19}$Cl$_2$N$_5$O$_3$+H]$^+$: 460.0938, found: 460.0943, UV purity (230–300 nm): 99%.

2.2 In vitro Studies

2.2.1 Autotaxin Inhibition Assay

Inhibition of human ATX was determined using the fluorogenic Amplex-Red in vitro assay, which was adapted from Ferry et al. (Ferry et al., 2008). DMSO-containing compound solutions were transferred to a 384-well assay plate (Greiner #781096, Monroe, NC, United States) and 6.6 nM in-house generated ATX enzyme in assay buffer (50 mM Tris-HCl, 120 mM NaCl, 20 mM CaCl$_2$, 5 mM KCl, 0.01% Triton-X100, pH 8.0) was added. After a 10-min incubation at room temperature, choline oxidase (7.3 U/ml; Sigma-Aldrich #C5896-1KU, St. Louis, MO, United States) and horseradish peroxidase (14.7 U/ml; F. Hoffmann-La Roche Ltd. #11378783, 1MU/4.311 g lyophilizate, Basel, Switzerland) were added and mixed. Thereafter, 110 μM LPC 18:1 (Avanti Polar Lipids #845875SP, Alabaster, AL, United States) and 183.3 μM Amplex Red (Chemodex #A-022, St. Gallen, Switzerland) were added. Plates were sealed and incubated for 5 min. The final assay concentrations were ATX 3 nM, choline oxidase 2 U/ml, horseradish peroxidase 4 U/ml, LPC 18:1 30 μM, Amplex Red 50 μM, and DMSO 2%. Background values were measured within 15 min and activity values after 90 min of incubation (Perkin Elmer Envision; Ex 535 nm/Em 587 nm; Perkin Elmer AG, Schwerzenbach, Switzerland).

2.2.2 HT-Solubility Assay

This assay was performed on a TECAN station starting from 10 mM DMSO stock solutions of the test compounds. Two aliquots of the test compound were dried and dissolved in phosphate buffer at pH 6.5. Sonication supports optimal re-solubilization. The solutions were then filtered and diluted (3 different dilution levels for each compound) followed by quantification of the dissolved material with Rapid-Fire MS. Quantification was performed for each test compound with a 6-point calibration curve prepared with the same DMSO starting solution.

2.2.3 Glutathione Addition Screening

All sample handling was performed based on a 96-well plate format using an automated pipetting system. The test compounds, positive controls (diclofenac, troglitazone, nefazodone, 4-[[1-(4-fluorophenyl)-2-methyl-1H-imidazol-4-yl]ethynyl]-2-methylpyridine) and solvent control (DMSO) were incubated with human liver microsomes supplemented with NADPH and reduced GSH. Stable GSH conjugates whose production can be assumed to be the result of chemically reactive metabolites were detected using a quadrupole

time of flight mass spectrometer run in untargeted full scan accurate mass MSE mode (Waters Xevo G1 QTOFMSE; Waters GmbH, Eschborn, Germany). This generic GSH adduct detection method and the assay workflow are taking advantage of the specific fragmentation behavior of the peptide moiety upon collision induced dissociation of GSH adducts and so are largely independent of the conjugate ("X") itself.

2.2.4 Artificial Membrane Permeability Assay

The assay was performed in an automated fashion on 96-well microplates. The permeation of drugs was measured using a "sandwich" construction: A filter-plate was coated with phospholipids (membrane) and placed into a donor compartment containing a compound/buffer solution. Finally, the top of filter-plate was filled with buffer solution (acceptor). Donor concentration was measured at t-start (reference) and compared with the donor and acceptor concentration after a certain time (t-end) to calculate the extent of passage of the compound through the membrane. The main readout of the assay was the permeability value Pe expressed in $10^{-6} * $ cm/s. Secondary readouts determined were the amount of compound in the donor and acceptor compartments as well as the retention in the membrane. Depending on the permeation rate and the membrane retention the compounds were classified as low (Pe < 0.2 and membrane < 20%) or medium and high (Pe ≥ 0.2 or Pe < 0.2 and membrane ≥ 20%). Each sample was measured in triplicate and a standard deviation was determined for the permeation constant Pe.

2.2.5 Lipophilicity

The experiment started with the accurate coating of the hydrophobic layer (0.45 μm PVDF membranes), which was fixed on the bottom of each DIFI©-tube (Weidmann Medical Technology AG, Rapperswil, Switzerland). The coated membranes were then connected to a 96-well plate which has been prefilled with exactly 150 μl of the selected aqueous buffer solution (25 mM phosphate buffer, pH 7.4). The buffer solution contains already the compound of interest with a maximum starting concentration of 85 μM. To expand the measurement range down to logD = −0.5 and up to logD = +4, it is necessary to carry out the procedure at two different octanol/water ratios: One with an excess of octanol for hydrophilic compounds (logD < 1) and one with a low volume of octanol for the lipophilic compounds (logD > 1). Therefore, parts of the DIFI©-tubes were filled with 15 μl 1-octanol and another part with 1 μl 1-octanol. The resulting sandwich guarantees that the membrane was completely dipped in the buffer solution. The plate was then sealed and shaken for 12 h at room temperature (23°C). During this time, the substance is distributed between the layer, the octanol, and the buffer solution. After having reached a distribution equilibrium, the DIFI©-tubes were easily disassembled from the top of the 96-well plate, so that the remaining sample concentration in the aqueous phase could be analyzed by LC/MS.

2.2.6 In vitro Microsomal Stability Assay

Incubations of a test compound at a concentration of 1 μM with microsomes (0.5 mg/ml) from the appropriate species (human,

mouse, or rat) plus cofactor NADPH were performed in 96-well plates at 37°C on a TECAN automated liquid handling system (Tecan Group Ltd., Männedorf, Switzerland). After pre-incubation of the test compound with the microsomes for 10 min, the enzymatic reaction was started by the addition of cofactors. Aliquots of the incubations are removed at 1, 3, 6, 9, 15, 25, 35, and 45 min and are then quenched with 1:3 (v/v) acetonitrile containing internal standards. Samples were then cooled and centrifuged before analysis of the supernatant by LC-MS/MS. Logarithmic Peak area ratios (test compound peak area/internal standard peak area) were plotted against incubation time and a linear fit made to the data with emphasis upon the initial rate of compound disappearance. The slope of the fit was then used to calculate the intrinsic clearance: Clint (μL/min/mg protein) = −slope (min-1) * 1,000/[protein concentration (mg/ml)].

2.3 In vivo Studies

2.3.1 Animals

All procedures concerning animals adhered to the ARVO statement for the use of animals in ophthalmic and vision research. Experiments performed at F. Hoffmann-La Roche (Basel) complied with the Swiss Federal and Cantonal laws on animal research and AAALAC regulations and received prior approval by the Cantonal Veterinary Office. The animal care committee of North Rhine-Westphalia (Germany) approved all in vivo experiments of the EAG and I/R studies. For the EAG model, male Lewis rats (Charles River, Sulzfeld, Germany), 6 weeks of age, were used. The I/R model was performed on 7- to 8-weeks old Brown-Norway rats (Charles River). All animals were kept under environmentally controlled conditions with free access to chow and water. Detailed observations and health checks, including eye exams, were performed regularly.

2.3.2 Single Dose PK and Exposure Analysis From in vivo Studies

Exposures in animals treated with ATX-inhibitors were determined from K_2EDTA treated plasma by LC-MS/MS at different time points. 25 μL of plasma was used for a single concentration determination. Concentration/time profiles were analyzed with MS Excel (Microsoft Corporation, Redmond, WA, United States).

For PK experiments for **7**, **13**, **14**, and **15**, respectively, animals were treated either iv or po and exposures were determined at different time points after compound administration. Suitable formulations for **13** were, for example, NMP:Tris buffer pH 8.5 (30%/70%) for iv administration with a nominal drug concentration of 1 mg/ml (dose 2 mg/kg) and a suspension in NMP:gelatine/NaCl (10%/90%) for po administration with a nominal drug concentration of 2.5 mg/ml (dose 10 mg/kg). PK parameters in **Table 2** were estimated from the concentration time profiles using Phoenix WinNonlin software (Certara, Princeton, NJ, United States).

2.3.3 Plasma LPA Profiles in Rat for Compound 13

Male Wistar rats (n = 5/group) were dosed orally by gavage with vehicle or 3, 10, and 30 mg/kg of compound **13**, respectively. Plasma samples were collected in triplicates at 0, 1, 3, 6, and 24 h and were added to heparinated tubes and kept at 0°C until further processing. Sampling and immediate processing at 0°C is crucial

TABLE 2 | Pharmacokinetic data in rats. **(A)** Intravenous bolus administration for compound **7**, **13**, **14**, and **15**. **(B)** Oral administration for compound **7**, **13**, **14**, **15** by gavage and food admix for compound **13**. Abbreviations: AUC: area under the curve; CLp: plasma clearance; n: number of animals; FA: food admix; Oral F: oral bioavailability; T1/2: half-life; Tmax: time to maximal concentration; Vdss, volume of distribution.

A

Compound	Dose (mg/kg)	N	CLp (ml/min/kg)	Vdss (L/kg)	T1/2 (h)	AUC(0-inf) (hr*ng/mL)
14	3	2	47	0.9	1.3	1,070
13	2	3	1.6	0.3	2.6	21,000
7	3	2	23	1.3	0.8	2,140
15	3	2	156	1.7	0.35	321

B

Compound	Dose (mg/kg)	N	Cmax (ng/ml)	Tmax (h)	AUC(0-inf) (hrs*ng/mL)	T1/2 (h)	Oral F (%)
14	30	3	130	0.5	660	3.8	6
13	10	2	17,690	0.75	130,000	4.6	80
13 (FA)	20	3	2,980	17	260,000	13	80
7	20	2	2,500	0.25	7,900	1.6	54
15	30	3	18	0.25	30	1.9	1.1

Bold values in this table are referring to the compound identifiers, which are kept in bold throughout the manuscript.

for the measurements of basal levels, since at higher temperatures, LPA is produced rapidly according to the ATX activity in the sample. One aliquot was used to determine basal levels of LPAs 16:0, 18:0, 18:1, and 20:4 as well as exposure of **13** by LC-MS/MS. A detailed method for LPA analysis is described in the **Supplementary Material Section 1.3**. The other 2 aliquots were used to determine ATX activity by incubation of the sample at 37°C for 4 h, followed again by analysis of LPA levels in the same way as for the basal LPA levels. LPA profiles were analyzed using MS Excel (Microsoft Corporation).

2.3.4 Oral Treatment with Compound 13

Diets containing compound **13** were manufactured by ssniff Spezialdiäten GmbH (Soest, Germany). Calculations of the daily doses were based on average food intake of rats used in the studies. The regular chow diet for the 60 mg/kg dose was calculated as 8.5 kg and mixed with a solution of **13** in ethanol (4.8%, w/w). The amount of **13** used was 1.0 g per kg of food. After mixing, ethanol was removed in vacuo until dryness. For the preparation of the 20 mg/kg dose, the same procedure was used by applying 0.333 g of **13** per kg of food.

The oral treatment with the ATX-inhibitor **13** (ATX-i; 20 mg/kg; Roche) started 7 days prior to immunization and 3 days prior I/R induction and continued throughout the study. The regular chow diet for the treatment groups was replaced with the same chow diet containing the treatment substance.

2.3.5 Animal Models (EAG, I/R)

For the EAG model, preparation and immunization of the optic nerve antigen (ONA = bovine optic nerve homogenate) was carried out as previously described (Laspas et al., 2011; Joachim et al., 2013). Rats received an intraperitoneal injection with 8 mg/ml ONA. The antigen was mixed with incomplete Freund's adjuvant (500 μl) plus 3 μg pertussis toxin (both Sigma Aldrich, St. Louis, MO, United States). The animals of the control group were injected with NaCl in Freund's adjuvant and pertussis toxin. Rats were sacrificed 28 days after immunization.

An established I/R model was used (Schmid et al., 2014; Renner et al., 2017). Therefore, rats were anesthetized with a ketamine/xylazine/vetranquil cocktail (0.65/0.65/0.2 ml). One eye per animal was dilated with 5% tropicamide (Pharma Stulln, Stulln, Germany) and anesthetized topically with conjuncain (Bausch and Lomb, Berlin, Germany). Additionally, a pain medication injection of metamizole (Novalgin; Zentiva, Frankfurt am Main, Germany) was administered subcutaneously. IOP was raised to 140 mmHg for 60 min by elevating a saline reservoir connected to a needle, which was placed into the anterior chamber of the eye. Retinal ischemia was confirmed by observing whitening of the retina via an ophthalmoscope (Mini 300; Heine Optotechnik, Herrsching, Germany). Reperfusion was later reassured by observing the returning blood flow. The contralateral eye was used as a control. Analyses were performed 7 and 14 days after ischemia induction.

2.3.6 IgG Measurement in Aqueous Humor and Serum (EAG)

Aqueous humor and serum were collected at the end of the EAG study. IgG levels were measured in serum and aqueous humor samples from the EAG study (both: 6-7 samples/group) using a sandwich enzyme-linked immunosorbent assay (ELISA) kit (eBioscience, Frankfurt, Germany) according to the manufacturer's instructions. In brief, samples of aqueous humor from both groups were prediluted 1,000- or 2,000-fold in assay buffer, serum samples were diluted 100,000- or 200,000-fold in assay buffer. 75 μl of assay buffer were inserted into each sample well. 25 μl of the prediluted sample were added to the appropriate wells. All samples were incubated, and the absorbance was read at 405 nm using a microplate reader (AESKU.Reader with Gen5 ELISA Software, AESKU.DIAGNOSTICS, Wendelsheim, Germany) (Reinehr et al., 2018; Tsai et al., 2018).

2.3.7 Intraocular Pressure Measurements (EAG)

The IOP was measured in both eyes of each animal in the EAG study with a rebound tonometer (Tonolab; iCare, Oy, Finland) 1 week before as well as 1, 2, and 3 weeks after

TABLE 3 | Primary and secondary antibodies used for immunohistology and Western Blot analysis of the retina or optic nerve.

Immunohistology antibodies

Primary antibodies / **Secondary antibodies**

Antibody	Company	Catalog number	Tissue	Dilution	Antibody	Catalog number	Company	Dilution
Anti-Brn-3a	Santa Cruz	sc-31984	Retina	1:100	Donkey anti-goat Alexa Fluor 488	705-545-147	Dianova	1:500
Anti-Brn-3a	Santa Cruz	sc-8429	Retina	1:100	Donkey anti-mouse Alexa Fluor 555	ab150106	Abcam	1:500
Anti-cleaved caspase 3	Sigma-Aldrich	C8487	Retina	1:100	Donkey anti-rabbit Alexa 555	A31572	Invitrogen	1:500
Anti-ED1	Millipore	MAB1435	Retina	1:400	Goat anti-mouse Alexa Fluor 488	A21424	Invitrogen	1:500
			Optic nerve	1:200	Goat anti-mouse Alexa Fluor 555	A11029	Invitrogen	1:500
Anti-GFAP	Millipore	AB5541	Retina	1:400	Donkey anti-chicken Cy3	AP194C	Millipore	1:500
			Optic nerve	1:500				
Anti-GLT1	Life Technology	AB1783	Retina	1:500	Donkey anti-guinea pig Alexa Fluor 488	706–545-148	Jackson ImmunoResearch	1:500
Anti-Iba1	Wako	019-19741	Retina	1:400	Donkey anti-rabbit Alexa Fluor 555	A31572	Invitrogen	1:500
			Optic nerve		Goat anti-rabbit Alexa Flour 488	A11008	Invitrogen	1:500
Anti-SMI-32	Covance	SMI-32P	Optic nerve	1:6,000	Goat anti-mouse Alexa Fluor 488	A-11029	Invitrogen	1:400

Western Blot antibodies

Primary antibodies / **Secondary antibodies**

Antibody	Company	Catalog number	Tissue	Dilution	Antibody	Catalog number	Company	Dilution
Anti-β-actin	Sigma-Aldrich	A2228	Retina	1:5,000	Donkey anti-mouse DL800	926-32212	LI-COR	1:20,000
Anti-β-actin	Cell Signaling	4970S	Retina	1:1,000	Donkey anti-rabbit DL800	SA5-10044	Thermo Fisher	1:20,000
Anti-β-III-tubulin	R&D Systems	MAB1195	Retina	1:15,000	Donkey anti-mouse Alexa Fluor 680	A10038	Invitrogen	1:5,000
Anti-GFAP	Millipore	AB5541	Retina	1:3,000	Donkey anti-chicken IR680RD	925-68075	LI-COR	1:20,000
Anti-Iba1	SySy	234,003	Retina	1:1,000	Donkey anti-rabbit Alexa Fluor 680	A10043	Invitrogen	1:5,000

immunization (n = 5–6 animals/group). The tonometer was held horizontally in front of the animal's eye (Pease et al., 2006). 10 measurements per eye were recorded. From these values, the mean value was calculated (Reinehr et al., 2019a).

2.3.8 Electroretinogram Measurements (I/R)

ERG measurements were performed on all eyes 7 and 14 days after I/R induction as previously described (Schmid et al., 2014; Palmhof et al., 2018). Before performing the ERG under dim red light, rats were dark adapted overnight. The readings were done using a full-field flash electroretinograph (HMs ERG system, OcuScience, Henderson, NV, United States). After anesthesia with a ketamine/xylazine cocktail (100/4 mg/kg) eyes were dilated and topically anesthetized. Reference electrodes were placed subcutaneously below the right and left ear and a ground electrode was placed in the base of the tail. Silver thread recording electrodes were placed in the center of the cornea. Scotopic flash ERGs were recorded at 0.1, 0.3,

1, 3, 10, and 25 cd*s/m^2 for each eye (7 days: 5-6 eyes/group; 14 days: 6-7 eyes/group). Signals obtained from the corneal surface were then amplified, digitized, and averaged using ERG View 4.380R software (OcuScience).

2.3.9 Histology of Retina and Optic Nerve (EAG, I/R)

After explantation, eyes and optic nerves were fixed in 4% paraformaldehyde for 60 min (eyes) or 120 min (optic nerves) and then treated with 30% sucrose overnight. Afterwards, the retinas and optic nerves were embedded in NEG-50 Tissue-Tek medium (Thermo Fisher, Waltham, MA, United States). Cryo-cross sections of the eyes (10 μm) or longitudinal sections of the optic nerves (4 μm) were cut on a microtome (Thermo Fisher), mounted on Histobond Superfrost$^+$ slides (Thermo Fisher) and fixed in ice cold acetone for 10 min.

Retinal cross-sections from the I/R studies were stained with hematoxylin and eosin (H&E) to visualize retinal layers and

changes in the thickness of the layers using standard protocols (7 days: 5-6 retinas/group; 14 days: 6-7 retinas/group). The thickness of the ganglion cell layer (GCL) was analyzed with the measuring tool of the ZEN2012 image analysis software (Zeiss, Oberkochen, Germany). Therefore, they were measured three times and the value was averaged (Palmhof et al., 2019).

Longitudinal optic nerve sections (EAG: 5-6 nerves/group, I/R 14 days: 6-7 nerves/group) were stained with H&E and luxol fast blue (LFB). Of each staining, three areas per optic nerve section were documented with a microscope equipped with a CCD camera (Axio Imager M1; Zeiss) as previously described (Palmhof et al., 2019). One photo was taken of the proximal part, one of the middle and one of the distal part, right in front of the chiasma.

Cell infiltration in optic nerve sections stained with H&E was evaluated by using a scoring system ranging from 0 to 4 by a masked observer: 0 = no infiltration; 1 = mild cellular infiltration of the optic nerve or optic nerve sheath; 2 = moderate infiltration; 3 = severe infiltration; and 4 = massive infiltration of the optic nerve parenchyma and nodule infiltration (Shindler et al., 2006; Horstmann et al., 2016; Renner et al., 2017). The average score for each optic nerve was used for statistical analysis.

The grade of demyelination was monitored in optic nerve sections stained with LFB. Therefore, staining was scored from 0 to 2 and categorized as follows: 0 = no demyelination; 0.5 = mild demyelination; 1 = moderate demyelination; 1.5 = advanced demyelination; and 2 = severe demyelination up to dissolution of the tissue. The average score for each optic nerve was used for later statistical evaluation (Liu et al., 2014; Horstmann et al., 2016; Wilmes et al., 2018).

2.3.10 Immunohistology of Retina and Optic Nerve (EAG, I/R)

In order to identify certain cell types, specific antibodies were used for immunofluorescence staining in retinas and optic nerves (Casola et al., 2016; Renner et al., 2017; Palmhof et al., 2019). First, the sections were rinsed in phosphate buffered saline solution (PBS). Subsequently, they were blocked and permeabilized with a mixture of serum, 0.1% TritonX-100 and PBS. The primary antibodies (**Table 3**) were incubated at room temperature overnight followed by incubation with fluorescence labeled secondary antibodies for 1 h (**Table 3**). In addition, the cell nuclei were stained with DAPI (Serva Electrophoresis, Heidelberg, Germany) for 5 min. Finally, the sections were mounted in Shandon mount media (Thermo Fisher).

Six retinal or optic nerve sections were used for each staining. In the EAG study, 5-6 retinas/group as well as 5-6 nerves/group were included in the evaluation. Regarding the I/R studies, in the I/R 7 days study 5-6 retinas/group were included, while the I/R 14 days study consisted of 6-7 retinas/group and 5-6 nerves/group. All sections were examined with a fluorescence microscope (Axio Imager M1). Photographs were taken in two central and two peripheral areas of the retina. In the optic nerve, three photographs were captured (proximal, middle, central). In general, the same camera setting, including exposure time, was applied on all images obtained for one staining protocol. Then, these photographs were masked and cut with a predefined window (Corel PaintShop Pro, Ottawa, ONT, Canada). For each retinal or optic nerve field, the number of Brn-3a$^+$,

cleaved caspase 3$^+$, Iba1$^+$, and ED1$^+$ labeled cell bodies were counted using ImageJ Software (NIH; Bethesda, MD, United States). In regard to ED1$^+$ cells, only the one colocalized with Iba1$^+$ ones were included in the analysis.

Measurement and analysis of GFAP labeled areas in the retina was performed using ImageJ software with established protocols (Palmhof et al., 2019). Briefly, images were transformed into grayscale (32-bit). To minimize interferences with background labeling, a rolling ball radius of 50 pixels for EAG and I/R was subtracted. Then, for each picture a suitable lower threshold was determined. The ideal threshold can be obtained when the greyscale picture corresponds with the original one. After all lower thresholds from each picture were obtained, the mean value was calculated, and this number was then used for the final analysis. The percentage of the labeled area was then measured between these defined thresholds (EAG: lower threshold: 8.87; upper threshold: 85.00; I/R: lower threshold: 9.82; upper threshold: 165.00).

The optic nerve neurofilament (SMI-32) evaluation was based on a scoring system: 0 = intact structure; 1 = shortened axons, neurofilament swellings, building of retraction bulb; and 2 = loss of structural integrity, fissures, many retraction bulbs (Schlamp et al., 2006; Wang et al., 2011; Reinehr et al., 2018).
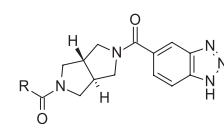
The GFAP signal in the optic nerve was also evaluated based on a scoring system: 0 = parallel arranged GFAP structure, less ramifications; 1 = strong and mostly organized gliosis, beginning of destruction; and 2 = loss of structure, strong, and disorganized ramification.
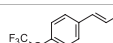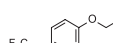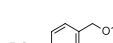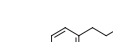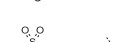
2.3.11 Western Blot Analysis of Retinal Tissue (I/R)

In order to quantify the protein level in I/R retina samples at 7 and 14 days, Western Blot analysis were performed (Casola et al., 2016). First, retinas (7 days: 5 retinas/group; 14 days: 5-6 retinas/group) were lysed in RIPA buffer (Cell Signaling Technology, Frankfurt, Germany) plus protease inhibitor (Sigma-Aldrich). Then, the protein concentration for each sample was determined using a BCA-kit. 10 μg protein was pipetted into each SDS-gel lane (NuPAGE, Invitrogen, Carlsbad, CA, United States) for electrophoresis (50 min, 200 V). Afterwards, the proteins were transferred onto a nitrocellulose membrane and blotted for 60 min at 200 V (Wet Blotter; X Cell sure Lock, Invitrogen). The same primary antibodies as used for immunohistology (**Table 3**) were applied to detect the protein expressions of ganglion cell and glia markers. Fluorescence labeled secondary antibodies were applied and detected using an Odyssey Infrared Imaging System (LI-COR Biosciences, Lincoln, NE, United States). Band intensities were compared between groups.

2.3.12 Statistical Analysis (EAG, I/R)

Data are presented as mean ± SD, unless noted otherwise. Regarding the *in vivo* data, groups were compared by ANOVA, followed by Tukey post-hoc test (Statistica; V 13; Dell, Tulsa, OK, United States). *p*-values below 0.05 were considered to be statistically significant. ONA/I/R vs. control and ONA + ATX-i/I/R + ATX-i vs. control: *$p < 0.05$, **$p < 0.01$, ***$p < 0.001$. ONA + ATX-i/I/R + ATX-i vs ONA/I/R: #$p < 0.05$, ##$p < 0.01$, ###$p < 0.001$.

TABLE 4 | Data of ATX-inhibitors with benzotriazole ZBG and *trans*-octahydropyrrolopyrrole core. A clearance value of 10 μL/m/mg prot indicates a low microsomal clearance, which is essentially below the detection limit of the assay.

Cmpd	R	hATX IC$_{50}$ [nM]	LogD (pH 7.4)	Solubility [μg/mL], pH 6.5	Permeability Pe [10^{-6} * cm/s]	Mic CL h/m/r [μL/m/mg prot]	GSH adducts
11		1	2.3	<1	*Na*	10/10/*na*	Neg
12		137	3.2	8	1.8	10/*na*/10	Neg
13		6	3.2	28	4.5	10/10/10	Neg
14		6	2.5	46	2.7	10/27/40	Neg
15		8	2.0	190	0.4	10/10/*na*	Neg

Na = not available.

3 RESULTS

3.1 Design, Synthesis, and Characterization of ATX-Inhibitors

3.1.1 Synthetic Approach

A representative synthesis of an ATX-inhibitor with a new central core is shown in **Figure 1B** for compound **7**. Similar approaches were used for the other compounds (**Supplementary Material Section 1.1, S1.1–S1.13** for procedures and analytical data). Synthesis of compound **7** started from enantiomerically pure di-carboxylic acid ester **20** (Rodríguez Sarmiento et al., 2003). Diester **20** was reduced to di-methanol **21** with LiBH$_4$ in THF, followed by mesylation in the presence of methanesulfonyl chloride and NEt$_3$ to afford **22** in high yield over two steps. Treatment of **22** with phenylmethanamine and potassium carbonate in CH$_3$CN at 95°C for 24 h gave the BOC-protected bicyclic intermediate **23**. De-benzylation of **23** was achieved by catalytic hydrogenation with palladium on charcoal in MeOH at RT to afford the desired bicyclic building block **24**. This material was coupled with commercially available *1H*-benzotriazole-5-carboxylic acid (**25**) in the presence of HATU and NMM in DMF at RT in high yield (83%) to provide **26** which was subsequently de-protected with HCl in ^{i}PrOH (~5 M) at RT, affording HCl salt **27**. Then, [3,5-dichlorophenyl]methanol was treated with CDI in CH$_3$CN at RT followed by addition of **27** and Net$_3$. This mixture was heated to reflux for 16 h to provide the desired compound **7** in 68% yield and an excellent purity of 99% after purification.

3.1.2 Modification of the Core and the ZBG

Our initial goal was the replacement of the piperidine core of **1** with different bicyclic and spirocyclic cores, resulting in removal of the basic nitrogen and the potentially labile β-aminocarbonyl

structure. Initially, both the ZBG and the lipophilic pocket substituent were kept constant to allow direct comparison of the new inhibitors with **1**. Besides activity, lipophilicity (LogD), solubility and *in vitro* metabolic stability against human, rat, and mouse microsomes (**Table 1**: column CL h/m/r), an additional key parameter that was investigated was the formation of reactive intermediates after metabolic activation followed by trapping and adduct formation with glutathione (**Table 1**: column GSH adducts). It was found that for example introduction of a trans octahydro-pyrrolo-pyridine core was possible without loss of activity (compound **2**), however, lipophilicity increased significantly, solubility remained low and formation of GSH adducts was still observed. Similar observations were made when spirocyclic building blocks were introduced as central cores. Compound **4** retained good activity, while the different orientation of the core in **3** led to significant loss of activity. In both cases, LogD increased, and solubility remained low without a significant gain in metabolic stability *in vitro* against microsomes. Introduction of a *cis*-octahydropyrrolopyrrole core (compound **5**) led to loss of activity, while a slight increase in solubility was observable. With all new derivatives **3**, **4**, and **5** GSH adducts were still observed. It became clear from these early data that additional changes to both the ZBG and the lipophilic pocket binder (represented by the dichlorobenzyl moiety in **1–5**) were required.

The next step was modification of the ZBG, which was done in a similar way as described by others (Kuttruff et al., 2017). For this change, the benzotriazole ZBG was found to be particularly interesting. Hence, this ZBG was combined with several of the most promising cores and results are shown in **Table 1** with compounds **6–10**. Introduction of this ZBG resulted in a minimally reduced or equal lipophilicity, and a minor trend towards better solubility. The best potency was achieved with
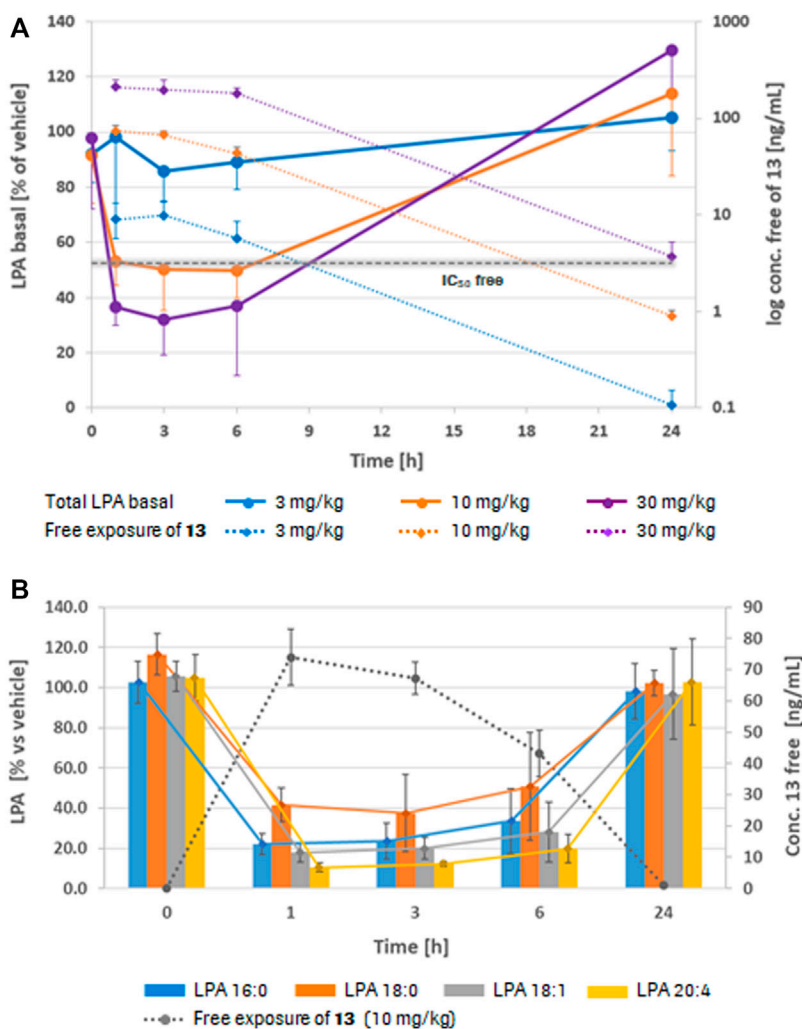
FIGURE 2 | Plasma LPA profiles in rat (PK/PD). **(A)** Dose and free exposure dependent lowering of total basal plasma LPA *in vivo* in rat at 1, 3, 6, and 24 h after dosing with **13**, normalized to the vehicle control. For all doses (3, 10, and 30 mg/kg po), 5 animals/group were used. **(B)** Inhibition of the formation of 4 different LPA species in rat plasma after a single oral dose of **13** (10 mg/kg, n = 5) at the same time points, normalized to the vehicle control (LPA formation was measured after incubation of the plasma samples at 37°C for 2 h). Values are mean ± SD.

the *cis*-decahydropyrroloazepine core (compound **10**), however, this core resulted in a markedly reduced metabolic stability. In contrast, the most balanced potency and property profile was observed with the *trans*-octahydropyrrolopyrrole, which also showed the most promising metabolic stability. However, since all compounds **6**–**9** retained the GSH flag, it became clear that additional changes to the dichlorobenzyl portion of the molecule were necessary.

3.1.3 Modification of the Lipophilic Pocket Residue
Several lipophilic pocket residues were investigated, and a set of representative compounds is shown in **Table 4**. Cinnamic acid derivatives such as **11** showed a high potency, a reduced lipophilicity and improved metabolic stability, but solubility turned out to be very low. Interestingly, a shift of the oxygen such as in compound **12** resulted in a significant loss of activity.

Attempts to introduce some more polar functional groups were partially successful: Methylsulfone **16** retained a decent potency with the expected reduction of LogD, markedly improved solubility and better metabolic stability, but these improvements were accompanied by a significant loss in permeability. Compounds **13** and **14** showed the most balanced overall profile with decent potency and acceptable LogD, solubility, permeability and *in vitro* metabolic stability against microsomes. For compound **15**, most parameters were also promising, but the permeability was considerably lower. Notably, all examples in **Table 4** did not show a potential for reactive metabolites and no GSH adducts could be observed any more. This was in line with the understanding that in **1** both the ZBG and the dichlorobenzyl moiety were prone to metabolic activation, which is supported by the GSH data given in **Table 1**.
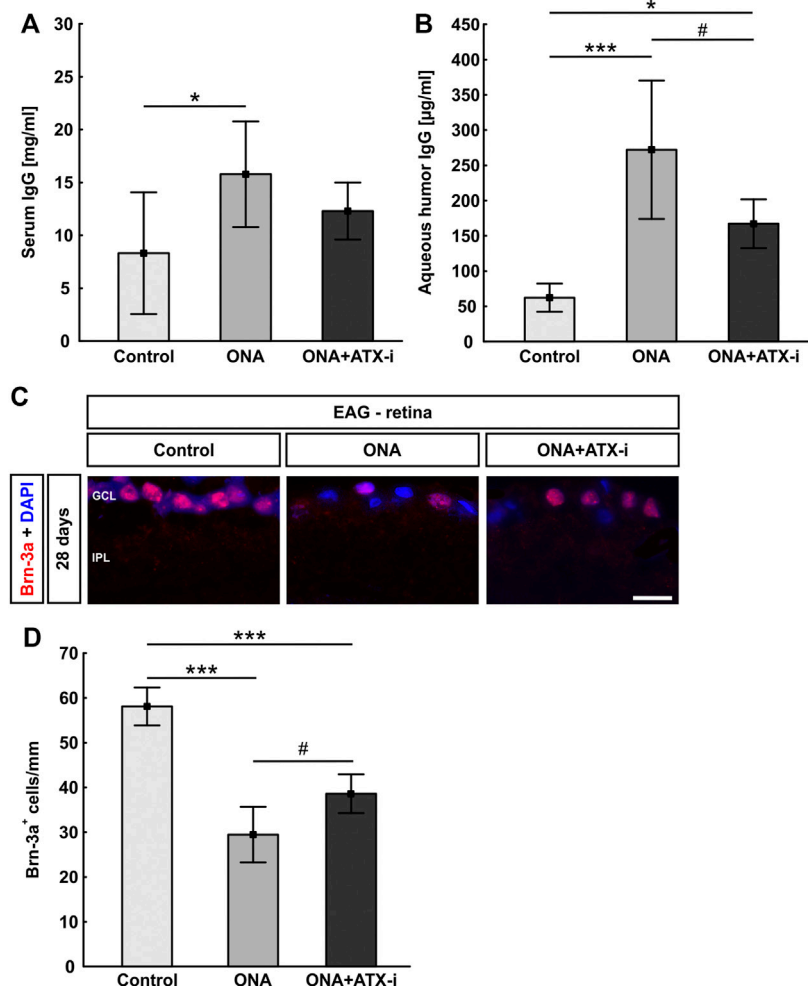
FIGURE 3 | Inhibited immune response and RGC loss in EAG. **(A)** Serum IgG levels were only increased in the ONA group, but not in ONA + ATX-i animals compared to controls. **(B)** IgG levels in the aqueous humor were significantly enhanced in ONA and ONA + ATX-i animals. However, in the ONA + ATX-i group, a lower IgG concentration was observable when compared to ONA samples. **(C)** RGCs were labelled with an antibody against Brn-3a (red), while cell nuclei were counterstained with DAPI (blue). **(D)** Significantly fewer RGCs were noted in ONA and ONA + ATX-i retinas compared to controls. Nevertheless, significantly more Brn-3a^{+} RGCs were detected in ONA + ATX-i animals compared to ONA ones. Values are mean ± SD. 6–7 samples/group. Abbreviations: GCL = ganglion cell layer; IPL = inner plexiform layer. Scale bar: 20 μm *$p < 0.05$; ***$p < 0.001$; #$p < 0.05$.

3.1.4 X-Ray Co-crystal Structures of Compounds 1, 10, and 13

In order to confirm the binding mode of the novel ATX-inhibitors with different cores and modified ZBGs, selected compounds were soaked into apo-crystals of rat ATX and their structures were determined by X-ray crystallography. Procedures and data for all X-ray structures are provided in the **Supplementary Material Section 1.2** and **Supplementary Table S1**. The structures for **10** (**Figure 1C**) and **13** (**Figure 1D**) showed an identical binding mode as the one determined for the seed compound **1**, with an interaction of the ZBG with the active site zinc ion and a good fit to the lipophilic pocket. In all cases, the oxygen of the carbonyl group of the carbamate forms a hydrogen bond to the backbone NH of Trp 275. These structural data also indicated that introduction of several bicyclic cores was possible as long as the exit vectors would still allow the ZBG

to interact with the zinc ion and ensure proper fit to the lipophilic pocket in a low energy conformation. In case of **10**, a cis fusion between the 5-membered and the 7-membered rings of the core is tolerated, whereas in the case of **13** a trans fusion of the two 5-membered pyrrolidine rings was preferred over a cis fusion as suggested by compound **8**, which was considerably less potent (**Table 1**).

3.2 Evaluation of *in vivo* PK and LPA Modulating Properties

A set of representative compounds with the most promising *in vitro* data was investigated with regard to pharmacokinetic properties *in vivo* in rat at a single dose (compounds **7**, **13**, **14**, and **15**; **Tables 2A,B**). The main goal of the PK analysis was to investigate, if *in vitro* microsomal stability would translate into
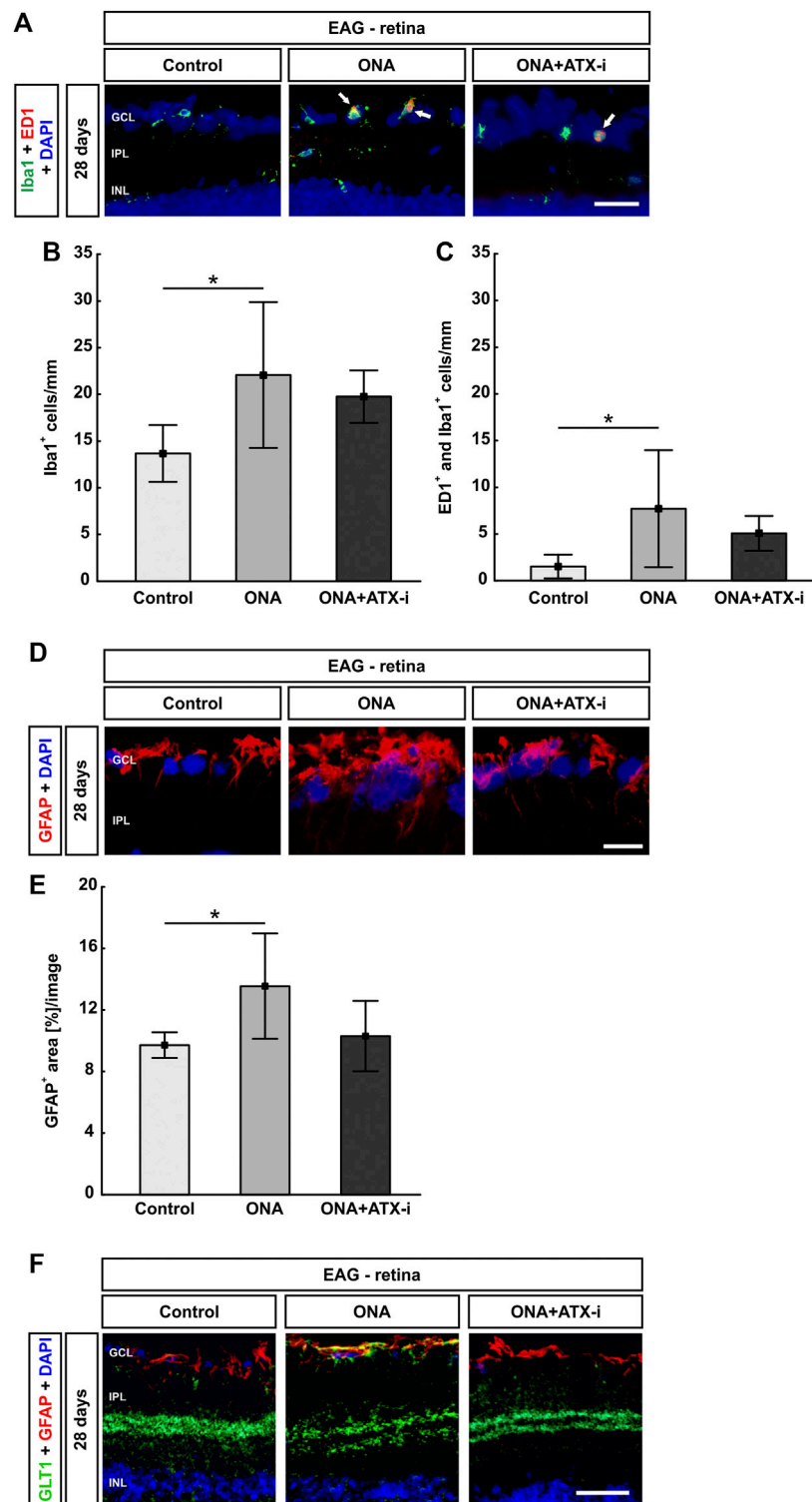
FIGURE 4 | Less glial response in EAG retina. **(A)** The total number of microglia was stained with an antibody against Iba1 (green) and activated microglia were additionally marked with ED1 (red, arrows). DAPI counterstained cell nuclei (blue). **(B)** Iba1$^+$ cell numbers were significantly increased in ONA retinas, but not in ONA + ATX-i animals, compared to controls. **(C)** Furthermore, significantly more activated microglia were only detected in the ONA group. No alterations could be observed in ONA + ATX-i retinas compared to controls. **(D)** Retinal cross-sections were stained with an antibody against GFAP (red; astrocytes). DAPI (blue) labelled cell nuclei. **(E)** The GFAP$^+$ area was significantly increased in ONA retinas, but not in ONA + ATX-i animals compared to controls. **(F)** Retinal cross-sections were co-labelled with antibodies against GFAP (red) and GLT1 (green), while DAPI counterstained cell nuclei (blue). In control as well as in ONA + ATX-i retinas, GLT1 was predominantly observed in the inner plexiform layer. In contrast, enhanced staining patterns in the nerve fiber and GCL, in co-localization with GFAP, could be noted in the ONA group. Values are mean ± SD. 5-6 retinas/group. Abbreviations: GCL = ganglion cell layer; IPL = inner plexiform layer; INL = inner nuclear layer. Scale bars: 20 μm *$p < 0.05$.

sufficient exposure *in vivo*. As the number of animals for the individual PK experiments was kept low, a statistical comparison between the individual compounds was not attempted. While for examples **7**, **14**, and **15** insufficient *in vivo* exposures were reached at the indicated doses, compound **13** showed sufficient oral bioavailability and low plasma clearance *in vivo* as well as a suitable half-life to allow for bid or food admix dosing. Hence, these data indicated that **13** was a suitable candidate for further PK/PD assessment *in vivo*.

Compound **13** was then used in an acute PK/PD experiment in rats at 3 doses (3, 10, and 30 mg/kg po, qd; n = 5/group) and plasma levels of 4 different LPA species (LPA 16:0, 18:0, 18:1, and 20:4) were determined by LC/MS. For **13**, a dose dependent plasma exposure resulted in a dose dependent lowering of total plasma LPA (as the sum of the 4 LPA species). Basal levels of LPA 16:0, 18:0, and 18:1 were quite low (approx. 10, 4, and 8 nM, respectively) and relatively close to the detection limit of the LC/MS method (approx. 2 nM), whereas LPA 20:4 had a higher basal concentration of about 84 nM. Therefore, modulation of total basal LPA was largely driven by modulation of LPA 20:4 (**Figure 2A**). An IC_{50} of approx. 3.2 ng/ml (free plasma concentration) was determined for the lowering of total basal LPA.

To better observe the modulation of the individual LPA species, a second set of plasma samples was incubated at 37°C for 2 h prior to LC/MS analysis. Due to continued ATX activity in the incubated plasma, LPA levels (LPA 16:0: 1,600 nM; 18:0: 800 nM; 18:1: 900 nM; and 20:4: 6,500 nM, respectively) turned out substantially higher through conversion of plasma LPC to LPA. Any differences in LPA levels observed after treatment with **13** can therefore be considered as a result of inhibition of plasma ATX. **Figure 2B** shows modulation of the four different LPA species after plasma incubation, indicating that after a single dose of **13** of 10 mg/kg, formation of all four LPA species were significantly inhibited for 6 h and more. However, no inhibition of LPA formation was visible 24 h post-dose. This is in line with the plasma exposures of **13** at the different time points (dotted line). Data for all LPA species resulting from plasma incubations indicated a lower IC_{50} of about 0.7 ng/ml (free concentration) for **13** in blood. Compound **13** was then further investigated in a food admix PK at a dose of ~20 mg/kg per day, based on average body weight and normal food consumption which suggested that this dose should result in efficient LPA modulation *in vivo* based on the AUC. Results of this study are summarized in **Table 2B**.

3.3 *In vivo* Studies
3.3.1 Effects of ATX-Inhibitor Treatment in the EAG Model
No Alterations in Intraocular Pressure
The IOP was measured 1 week before as well as 1, 2, and 3 weeks after the immunization in all groups. One week before immunization, the IOP was unaltered in ONA animals (10.34 ± 0.67 mmHg) compared to controls (10.36 ± 1.03 mmHg; p = 0.999). Also, no alterations were observed in ONA + ATX-i treated animals (10.91 ± 0.50 mmHg; p = 0.521).

At 1 week, IOP remained unchanged in the ONA group (10.44 ± 0.62 mmHg) in comparison to controls (11.26 ± 0.54 mmHg; p = 0.058). No changes were detected in the ONA + ATX-i group compared to controls (10.54 ± 0.40 mmHg; p = 0.142). At 2 weeks, the IOP remained unaltered in ONA (10.74 ± 0.55 mmHg; p = 0.119) as well as in ONA + ATX-i groups (10.85 ± 0.42 mmHg; p = 0.276) compared to controls (11.36 ± 0.52 mmHg). No changes in the IOP were observed in ONA (10.77 ± 0.77 mmHg; p = 0.205) and ONA-ATX-i animals (10.69 ± 0.60 mmHg; p = 0.197) in comparison to controls (11.47 ± 0.62 mmHg) 3 weeks after immunization (**Supplementary Figure S1**).

Altered IgG Levels After ATX-i Treatment
After ONA immunization, serum IgG levels were significantly increased compared to controls (ONA: 15.78 ± 5.00 mg/ml; control: 8.31 ± 5.76 mg/ml; p = 0.024). After ATX-i treatment, no significant differences were observed in ONA + ATX-i animals (12.30 ± 2.70 mg/ml) in comparison to the control group (p = 0.339; **Figure 3A**). In the aqueous humor, IgG levels were also significantly enhanced in the ONA (272.24 ± 98.17 μg/ml; p < 0.001) as well as in the ONA + ATX-i group (167.26 ± 34.50 μg/ml; p = 0.025) compared to controls (62.31 ± 19.91 μg/ml). However, ONA + ATX-i animals displayed a significantly lower IgG concentration in the aqueous humor compared to the ONA group (p = 0.025; **Figure 3B**).

Mild Protection of Retinal Ganglion Cells and Less Glial Cell Response
Brn-3a⁺ RGC numbers were significantly decreased in ONA animals (29.47 ± 6.20 cells/mm) compared to controls (58.11 ± 4.22 cells/mm; p < 0.001). Furthermore, significantly fewer Brn-3a⁺ cells were detected in ONA + ATX-i retinas in comparison to the control group (38.59 ± 4.33 cells/mm; p < 0.001). However, a higher number of Brn-3a⁺ RGCs was noted in ONA + ATX-i animals when compared to the ONA group (p = 0.032; **Figures 3C,D**), suggesting a mild protective effect on RGCs through ATX-i treatment.

Iba1⁺ microglia cell counts were significantly increased in ONA animals (22.06 ± 7.81 cells/mm) compared to controls (13.67 ± 3.04 cells/mm; p = 0.037). No changes were noted in the ONA + ATX-i retinas when compared to controls (19.76 ± 2.82 cells/mm; p = 0.192; **Figures 4A,B**). Significantly more ED1⁺ and Iba1⁺ microglia were observed in the ONA group (7.70 ± 6.27 cells/mm; p = 0.042), but not in the ONA + ATX-i group (5.08 ± 1.86 cells/mm), compared to controls (1.52 ± 1.28 cells/mm; p = 0.354; **Figures 4A,C**).

The area analysis of GFAP revealed a larger area in ONA retinas (13.55 ± 3.42 area [%]/section) in comparison to controls (9.72 ± 0.84 area [%]/section; p = 0.041). No changes could be noted in the ONA + ATX-i group (10.30 ± 2.29 area [%]/section; p = 0.924; **Figures 4D,E**).

Additionally, GFAP was co-labeled with an antibody against GLT1, a marker for protoplasmic astrocytes (Velmeshev et al., 2019). In control as well as in ONA + ATX-i retinas, GLT1 was predominantly observed in the inner plexiform layer. In contrast, enhanced staining patterns in the nerve fiber and GCL in co-
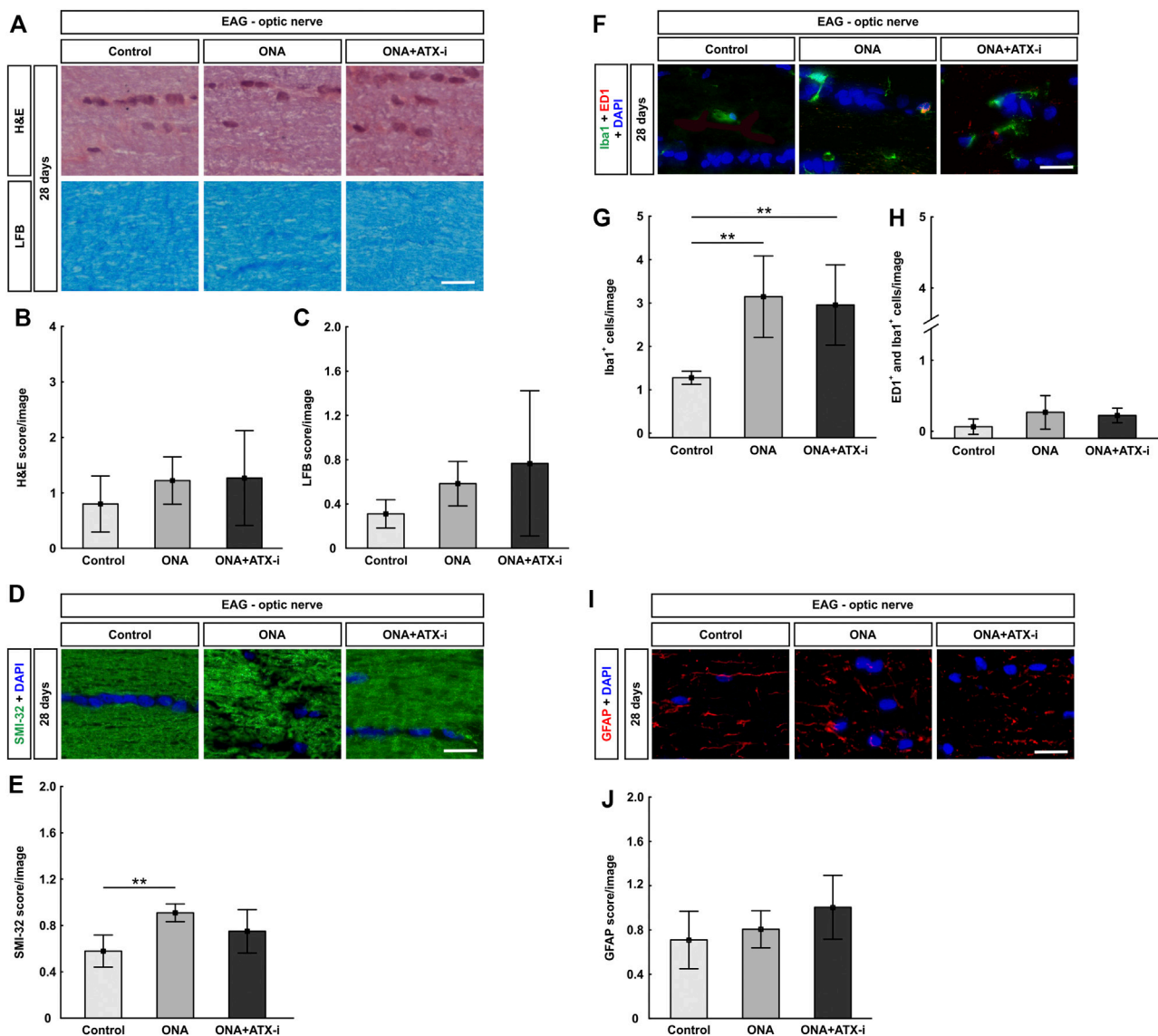
FIGURE 5 | Mild protection of EAG optic nerves. **(A)** Optic nerves were stained with H&E and LFB. **(B)** The H&E score revealed no signs of inflammation within all groups. **(C)** Also, no disruption of myelin could be observed via the LFB score in all groups. **(D)** The neurofilament was labelled with an antibody against SMI-32 (green) and DAPI stained cell nuclei (blue). **(E)** A disruption of neurofilaments could be detected in ONA optic nerves via SMI-32 score. No changed were noted in ONA + ATX-i animals compared to controls. **(F)** The total number of microglia was labelled with an antibody against Iba1 (green) and activated microglia were additionally stained with ED1 (red). DAPI counterstained cell nuclei (blue). **(G)** Significantly more Iba1$^+$ microglia were noted in ONA and in ONA + ATX-i optic nerves. **(H)** However, no alterations in regard to active microglia were noted within all groups. **(I)** Astrocytes were stained against anti-GFAP (red), while DAPI labelled cell nuclei (blue). **(J)** The GFAP score in ONA as well as ONA + ATX-i optic nerves was not altered in comparison to control ones. Values are mean ± SD. 5-6 nerves/group. Scale bars: 20 µm **$p < 0.01$.

localization with GFAP could be noted in the ONA group (**Figure 4F**).

Only Slight Optic Nerve Neurofilament Protection

The optic nerve H&E score showed no signs of inflammation in the ONA (1.22 ± 0.43; $p = 0.536$) as well as in ONA + ATX-i group (1.27 ± 0.86; $p = 0.470$) compared to controls (0.80 ± 0.51; **Figures 4A,B**). LFB scores, representing myelination, revealed no alterations between ONA animals (0.58 ± 0.20; $p = 0.531$) and control ones (0.31 ± 0.13). Furthermore, no differences were

noted in ONA + ATX-i optic nerves (0.77 ± 0.66; $p = 0.196$; **Figures 5A,C**).

SMI-32 labeling showed a significant higher score in the ONA group (0.91 ± 0.08) compared to controls (0.58 ± 0.14; $p = 0.003$). This indicates a disruption of neurofilaments. However, no alterations were noted in ONA + ATX-i optic nerves (0.75 ± 0.19; $p = 0.158$; **Figures 5D,E**), suggesting a protective effect by ATX-i.

A significant increase of Iba1$^+$ microglia was noted in the ONA (3.14 ± 0.94 cells/image; $p = 0.004$) as well as in the ONA + ATX-i group (2.96 ± 0.92 cells/image; $p = 0.009$) compared to

FIGURE 6 | Moderate effect on I/R retinas. **(A)** After 7 days, recordings of a-wave amplitudes exhibited significant differences between the control and both ischemic groups. **(B)** 14 days after ischemia induction, a-wave amplitudes of the ischemic group were significant lower when compared to control eyes. Nevertheless, the amplitude reduction in the ATX-I group was less prominent. **(C)** The I/R and the I/R + ATX-i group revealed significantly lower b-wave amplitudes than the control group 7 days after I/R. **(D)** 14 days after ischemia, a strong decline of the b-wave amplitudes was detected in both ischemic groups. **(E)** Staining with H&E was performed 7 as well as 14 days after ischemia induction to visualize the morphology of the retinal layers. **(F)** At 7 days, the GCL thickness was significantly thinner in I/R retinas compared to control ones. The thickness of the GCL was significantly reduced in the I/R and the I/R + ATX-i group compared to controls at 14 days. However, a broader GCL thickness was revealed in I/R + ATX-i retinas when compared to the I/R group. Values are mean ± SD. **(A,B)**: 5–6 eyes/group; **(C,D)**: 6–7 eyes/group; **(E)**: 5–6 retinas/group; **(F)**: 6–7 retinas/group. Abbreviations: GCL = ganglion cell layer; IPL = inner plexiform layer; INL = inner nuclear layer; OPL = outer plexiform layer; ONL = outer nuclear layer; OS = outer segment. Scale bar: 20 µm $*p < 0.05$; $**p < 0.01$; $***p < 0.001$; $\#p < 0.05$; $\#\#p < 0.01$.

controls (1.28 ± 0.15 cells/image; **Figures 4F,G**). However, alterations in ED1^{+} and Iba1^{+} active microglia numbers were detected neither in the ONA (0.27 ± 0.24 cells/image; $p = 0.148$) nor in the ONA + ATX-i optic nerves (0.22 ± 0.10 cells/image; $p = 0.292$) compared to controls (0.06 ± 0.11 cells/image; **Figures 5F,H**).

The GFAP, labelling astrocytes, score in the optic nerves revealed no differences in ONA animals (0.81 ± 0.17; $p = 0.802$) compared to controls (0.71 ± 0.26). Also, no changes were detectable in the ONA + ATX-i group (1.00 ± 0.29; $p = 0.163$; **Figures 5I,J**).

3.3.2 Effects of Compound 13 (ATX-I) in the I/R Model
Mild Protection of Retinal Function and Thickness After ATX-I Treatment
7 days after ischemia induction, a significant decrease in the a-wave amplitude was noted in the I/R and the I/R + ATX-i group in comparison to the control group at all measured light intensities ($p < 0.050$; **Figure 6A**). After 14 days, a significant reduction of the a-wave amplitude was detected in ischemic eyes in comparison to control ones at all light intensities ($p < 0.050$). The a-wave amplitude of the I/R + ATX-i group was comparable to the control ones at all light intensities ($p > 0.050$). When compared to the I/R group, a significant

increase in the a-wave amplitude was measurable in the I/R + ATX-i group at 0.1 cd s/m^{2} ($p = 0.027$; **Figure 6B**).

A significantly lower b-wave amplitude was revealed in all I/R and I/R + ATX-i eyes at all investigated light intensities 7 days after ischemia ($p < 0.001$; **Figure 6C**). At 14 days, the b-wave amplitude was significantly declined in both I/R and I/R + ATX-i eyes compared to control ones at all measured light intensities ($p < 0.001$; **Figure 6D**).

In relation to the control retinas (6.28 ± 1.57 µm), a significant reduction of the thickness of the GCL was measured after 7 days in the I/R (4.03 ± 0.84 µm; $p = 0.034$), but not in the I/R + ATX-i group (4.34 ± 1.63 µm; $p = 0.100$; **Figures 6E,F**). Regarding the 14 days point in time, the GCL was significantly thinner in the I/R (2.76 ± 0.16 µm; $p < 0.001$) and in I/R + ATX-i retinas (3.54 ± 0.34 µm; $p < 0.001$) compared to control ones (5.28 ± 0.43 µm). However, a significant broader thickness of the GCL was evaluated in the I/R + ATX-i group against the I/R group ($p = 0.003$; **Figures 6E,F**).

Mild Protection of Retinal Ganglion Cells
In comparison to the control group (48.29 ± 3.94 cells/mm), a significant RGC loss was observed 7 days post ischemia in the I/R group (10.95 ± 2.48 cells/mm; $p < 0.001$) and in the I/R + ATX-i

FIGURE 7 | Protection of retinal ganglion cells. **(A)** Retinal cross-sections stained with anti-Brn-3a (green) to label retinal ganglion cells at 7 and 14 days post I/R. Cell nuclei were visualized with DAPI (blue). **(B)** At both points in time, a significant lower number of RGCs was detectable in the I/R group and the IR + ATX-i group. However, significantly more RGCs were counted in the I/R + ATX-i group in comparison to the I/R group. **(C)** Western Blot analysis of retinal samples revealed a significantly less β-III-tubulin in both ischemic groups, the I/R and IR/+ATX-i group, at both points in time when compared to the control group. **(D)** Immunostaining of apoptotic cells with cleaved caspase 3 (red) after 7 and 14 days. Cell nuclei were labelled with DAPI (blue). **(E)** The number of cleaved caspase 3$^+$ cells was significantly higher in I/R and I/R + ATX-i retinas compared to controls at 7 and 14 days. Values are mean ± SD. 7 days: 5–6 retinas/group; 14 days: 6–7 retinas/group. Abbreviations: GCL = ganglion cell layer; IPL = inner plexiform layer; INL = inner nuclear layer. Scale bars = 20 μm *$p < 0.05$; **$p < 0.01$; ***$p < 0.001$; $^{\#}p < 0.05$; $^{\#\#}p < 0.01$.

group (17.61 ± 1.63 cells/mm; $p < 0.001$). However, significantly more Brn-3a$^+$ cells were noted in I/R + ATX-i retinas compared to I/R ones ($p = 0.008$), pointing towards a protective effect of ATX-i (**Figures 7A,B**). The protective effect on RGCs was retained 14 days after ischemia. Here a significant RGC loss was detected in the I/R group (5.81 ± 2.85 cells/mm; control: 56.32 ± 11.74 cells/mm; $p < 0.001$) and in the I/R + ATX-i group (21.62 ± 8.84 cells/mm; $p < 0.001$). However, a significant difference was noted between the I/R and the I/R + ATX-i group ($p = 0.017$), with a higher number of Brn-3a$^+$ RGCs in ATX-i treated eyes (**Figures 7A,B**).

Western Blot analysis revealed a significant decrease in β-III tubulin protein levels in the I/R (0.18 ± 0.17) and the I/R + ATX-i (0.28 ± 0.30) group compared to control retinas (1.39 ± 0.52; both: $p < 0.001$; **Figure 7C**) at 7 days. 14 days after I/R, the β-III-tubulin levels of both I/R groups (I/R: 0.06 ± 0.03 and I/R +

ATX-i: 0.13 ± 0.08) were also significantly decreased compared to control ones (0.60 ± 0.08; both: $p < 0.001$; **Figure 7C**).

The number of cleaved caspase 3$^+$ apoptotic RGCs was significantly increased in I/R (5.97 ± 1.93 cells/mm; $p = 0.012$) and I/R + ATX-i retinas (6.21 ± 1.62 cells/mm; $p = 0.014$) compared to controls (2.62 ± 1.59 cells/mm) at 7 days (**Figures 7D,E**). Also 14 days after I/R, significantly more cleaved caspase 3$^+$ cells were observed in I/R (5.38 ± 0.83 cells/mm; $p = 0.001$) and I/R + ATX-i animals (5.02 ± 1.52 cells/mm; $p = 0.002$) when compared to control ones (2.58 ± 0.72 cells/mm; **Figures 7D,E**).

Fewer Microglia Cells and Less Macroglia Response After ATX-I Treatment

The I/R (38.44 ± 7.75 cells/mm; $p < 0.001$) and I/R + ATX-i group (29.04 ± 5.19 cells/mm; $p < 0.001$) displayed significantly more
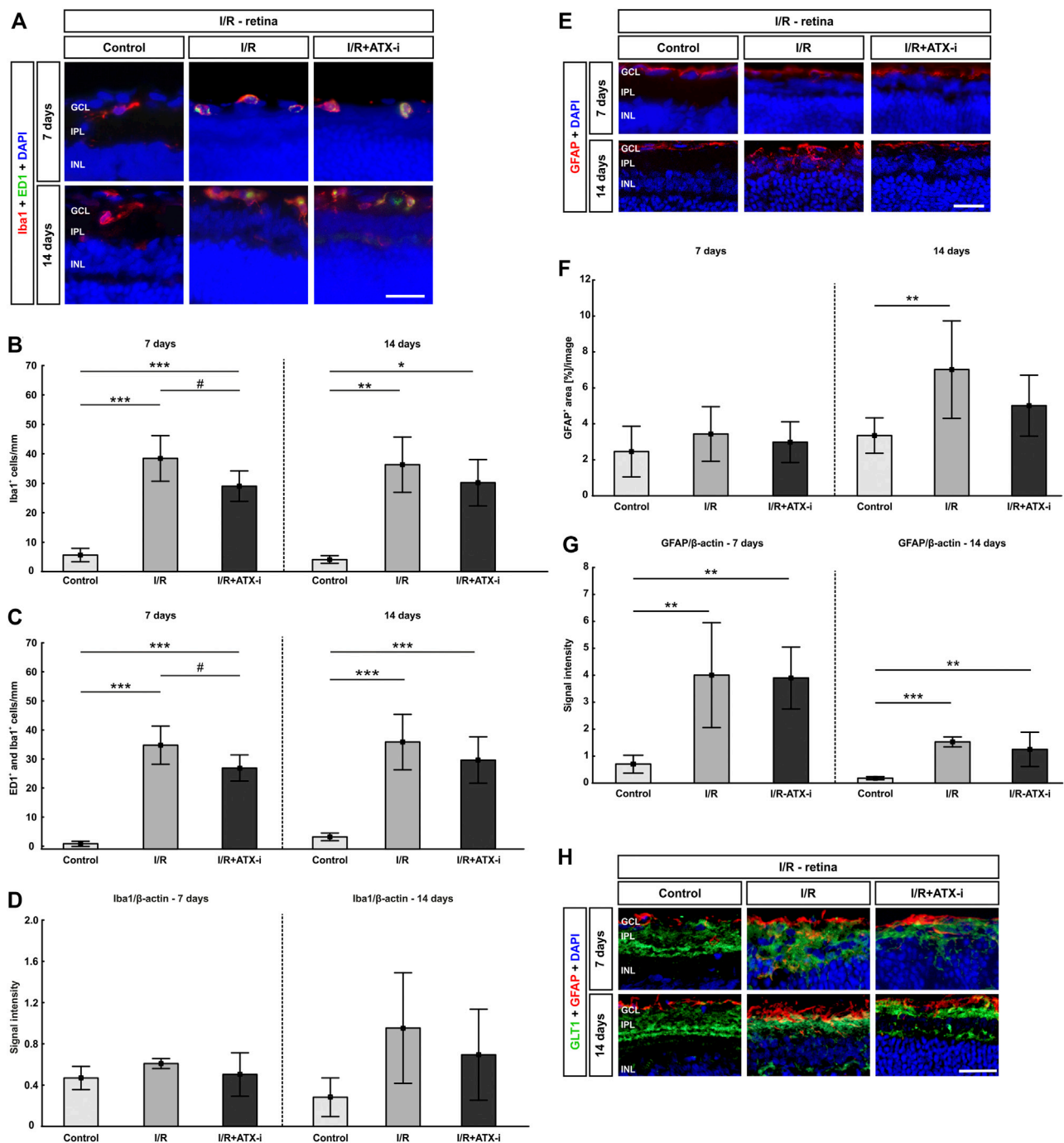
FIGURE 8 | Less retinal microglia after treatment. **(A)** Double immunostaining of microglia with Iba1 (red) and ED1 (green; active ones) after 7 and 14 days. Cell nuclei were marked with DAPI (blue). **(B)** Compared to control retinas, the number of Iba1^{+} microglia was significantly increased in the I/R group and in the I/R + ATX-i group at both points in time. However, 7 days after ischemia induction, significantly fewer Iba1^{+} cells were noted in the I/R + ATX-i in comparison to the I/R group. **(C)** Accordingly, significantly more ED1^{+} and Iba1^{+} co-labeled microglia were detected in the I/R and I/R + ATX-i group 7 as well as 14 days after I/R. Significantly fewer activated microglia were counted in the I/R + ATX-i group when compared to I/R retinas at 7 days. **(D)** After 7 days, no differences were seen in Iba1 protein level in retinal samples of both I/R groups via Western Blot. A trend to higher Iba1 protein levels was noted 14 days after ischemia induction in the I/R group, but not in the I/R + ATX-i group in comparison to control retinas. **(E)** Retinal sections were stained with GFAP (red) to detect astrocytes, while DAPI (blue) counterstained cell nuclei. **(F)** 7 days after ischemia, no changes could be observed in the I/R and I/R + ATX-i group concerning the GFAP[+] area in comparison to the control group. In contrast, 14 days after ischemia, the GFAP[+] area was significantly increased in the I/R group, while no changes were detected in the I/R + ATX-i group. **(G)** GFAP analysis via Western Blot showed a significant increase in GFAP signal intensity in both I/R groups after 7 and 14 days. **(H)** Retinas were co-labelled with antibodies against GFAP (red) and GLT1 (green). DAPI visualized cell nuclei (blue). In control retinas, GLT1 staining was mostly observed in the inner plexiform layer. A stronger expression of GLT1 and more co-localization with GFAP seemed to appear in the I/R groups, especially at 7 days. In I/R + ATX-i retinas, a co-localization with GFAP was not that prominent anymore. Values are mean ± SD. 7 days: 5–6 retinas/group; 14 days: 6–7 retinas/group. Abbreviations: GCL = ganglion cell layer; IPL = inner plexiform layer; INL = inner nuclear layer. Scale bars = 20 μm *$p < 0.05$; **$p < 0.01$; ***$p < 0.001$; #$p < 0.05$.
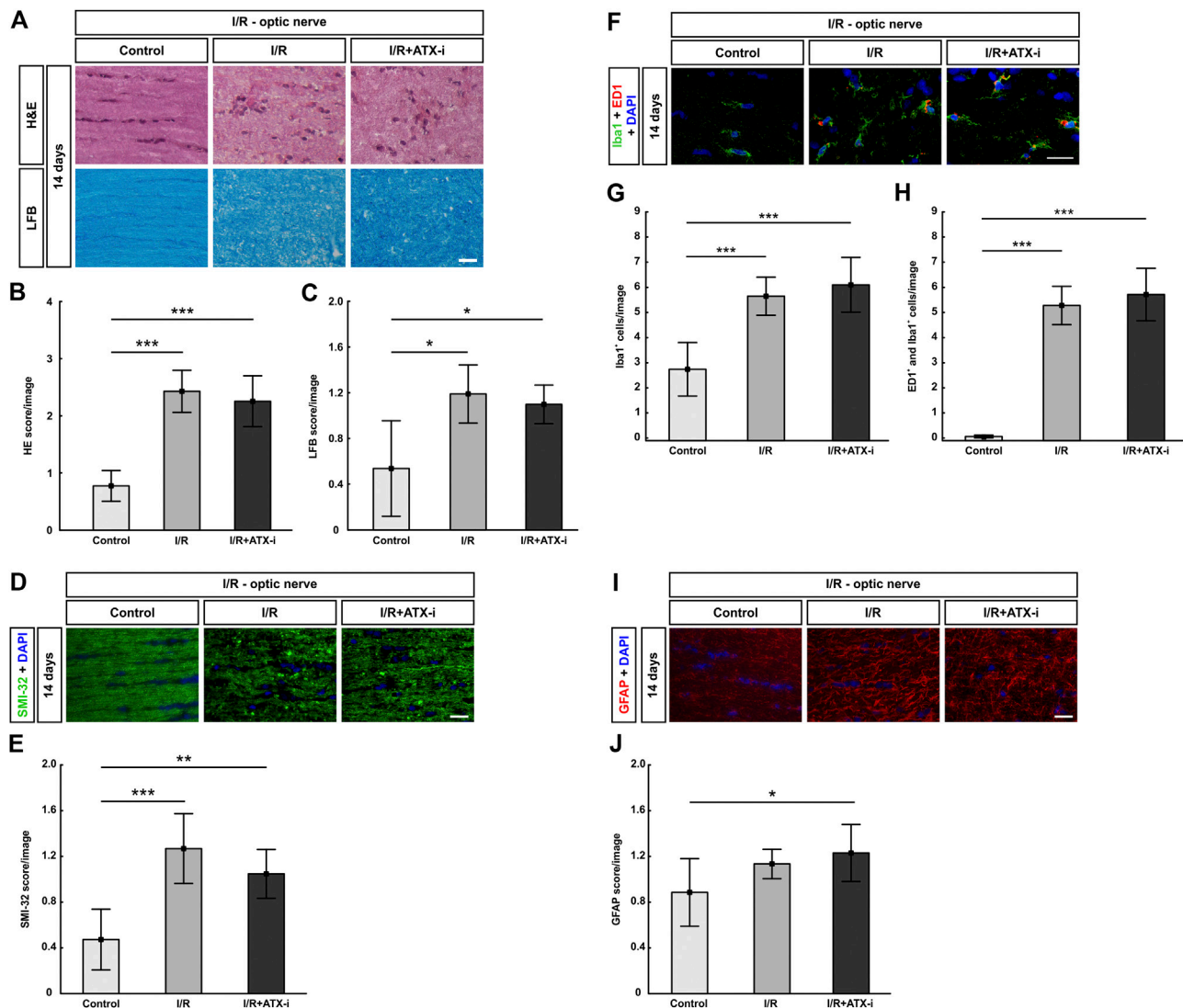
FIGURE 9 | No improvement of I/R optic nerves. **(A)** 14 days after I/R induction, staining with H&E was performed to visualize the optic nerve morphology and possible cell infiltration, while LFB was used for detection of demyelination signs. **(B)** Significantly more inflammatory cells (higher H&E score) were observed in the optic nerves of the I/R and the I/R + ATX-i group. **(C)** A significant loss of myelin (higher LFB score) was noticed in I/R and I/R + ATX-i optic nerves compared to control ones. **(D)** The longitudinal optic nerve sections were labelled with SMI-32 (green) and DAPI (blue; cell nuclei) to detect possible neurofilament changes. **(E)** A significant structural distortion was revealed of the optic nerves of the I/R and I/R + ATX-i group. **(F)** Double immunostaining of microglia with Iba1 (green) and ED1 (red) 14 days post I/R, cell nuclei were marked with DAPI (blue). **(G)** In comparison to controls, the number of Iba1$^+$ microglia was significantly increased in the I/R and in the I/R + ATX-i group. **(H)** In accordance, significant more ED1$^+$ and Iba1$^+$ co-labeled cells were detected in the optic nerves of both ischemic groups, with and without ATX-i treatment. **(I)** Anti-GFAP (red) was used to determine possible alterations in astrocyte expression, while DAPI (blue) counterstained cell nuclei. **(J)** Scoring of the GFAP-labelled tissue showed a significant higher score in the I/R + ATX-i group in comparison to control optic nerves. Values are mean ± SD. 5–6 nerves/group. Scale bars = 20 µm *$p <$ 0.05; **$p <$ 0.01; ***$p <$ 0.001.

Iba1$^+$ microglia 7 days after ischemia (control: 5.65 ± 2.29 cells/mm). However, the number of Iba1$^+$ cells was significantly lower in I/R + ATX-i retinas compared to I/R ones ($p =$ 0.045; **Figures 8A,B**). After 14 days, induction of ischemia led to a significant increase of Iba1$^+$ microglia cells in the I/R (45.5 ± 11.78 cells/mm; $p =$ 0.003) and I/R + ATX-i group (41.17 ± 9.33 cells/mm; $p =$ 0.013), when compared to the control retinas (26.28 ± 3.33 cells/mm; **Figures 8A,B**).

A significant increase in ED1$^+$ and Iba1$^+$ co-labeled cells was seen in the I/R (34.74 ± 6.57 cells/mm; $p <$ 0.001) as well as the I/R + ATX-i group (26.91 ± 4.48 cells/mm; $p <$ 0.001) in comparison to controls (0.81 ± 0.91 cells/mm) 7 days after ischemia induction. However, a significant decrease in the number of activated microglia was observed in the I/R + ATX-i group when compared to the I/R group ($p =$ 0.045; **Figures 8A,C**). At 14 days, significantly more activated microglia were counted in the I/R (34.20 ± 9.12 cells/mm; $p <$ 0.001) and the I/R + ATX-i

group (28.27 ± 7.63 cells/mm; $p < 0.001$) in contrast to control retinas (2.99 ± 1.26 cells/mm; **Figures 8A,C**).

In regard to Iba1 proteins levels, there were no differences between the control group (0.47 ± 0.11) and ischemic retinas (0.61 ± 0.05; $p = 0.292$) as well as I/R + ATX-i treated eyes (0.50 ± 0.21; $p = 0.921$; **Figure 8D**) at 7 days after ischemia via Western Blot analysis. 14 days after I/R, there was a trend to elevated Iba1 protein levels in the I/R group (0.95 ± 0.54; $p = 0.064$) was noted, but not in the I/R + ATX-i group (0.69 ± 0.44; $p = 0.309$) when compared to control retinas (0.28 ± 0.19; **Figure 8D**).

7 days after I/R, the GFAP$^+$ area in ischemic retinas was slightly increased (3.44 ± 1.52 area [%]/section; $p = 0.456$), whereas the area in the I/R + ATX-i group (2.98 ± 1.13 area [%]/section) was similar to the control group (2.46 ± 1.41 area [%]/section; $p = 0.823$; **Figures 8E,F**). After 14 days, the GFAP$^+$ area was significantly increased in ischemic eyes (7.02 ± 2.71 area [%]/section; $p = 0.010$), while no differences were revealed in the I/R + ATX-i group (5.01 ± 1.70 area [%]/section; $p = 0.251$) compared to the control group (3.35 ± 0.98 area [%]/section; **Figures 8E,F**).

At 7 days, the GFAP protein level, detected via Western Blot, was significantly upregulated in the I/R (4.00 ± 1.95; $p = 0.005$) and in the I/R + ATX-i group (3.90 ± 1.14; $p = 0.006$) compared to controls (0.71 ± 0.33; **Figure 8G**). Concerning the GFAP protein level at 14 days, it was significantly upregulated in the I/R group (1.60 ± 0.19; $p < 0.001$). In accordance with the immunohistological data, the protein level in the I/R + ATX-i group (1.31 ± 0.66) appeared to be lower than in the I/R group ($p = 0.470$), while still significantly increased in comparison to controls (0.19 ± 0.06; $p = 0.002$; **Figure 8G**).

In addition, retinas were co-labeled with anti-GFAP and anti-GLT1 7 and 14 days after I/R. In control retinas, GLT1 staining was predominantly observed in the inner plexiform layer at both points in time. A stronger expression of GLT1 and more co-localization with GFAP seemed to appear in the I/R groups especially at 7 days. In I/R + ATX-i retinas, a co-localization with GFAP was not that prominent anymore (**Figure 8H**).

Only Light Protection of Optic Nerve Neurofilaments With ATX-I
14 days after I/R, both the I/R (2.43 ± 0.37; $p < 0.001$) and the I/R + ATX-I (2.25 ± 0.44; $p < 0.001$) group displayed a significantly higher H&E score in the optic nerves compared to the control group (0.77 ± 0.27; **Figures 9A,B**).

Regarding the LFB score, the I/R (1.19 ± 0.25; $p = 0.011$) as well as the I/R + ATX-i group (1.09 ± 0.17, $p = 0.016$) showed a higher score and bright areas in the optic nerves indicating significant demyelination compared to control nerves (0.54 ± 0.42; **Figures 9A,C**).

Aligned neurofilament fibers were found in the control group, while a significant structural distortion was detected by SMI-32 scoring in the optic nerves of the I/R (1.27 ± 0.31; $p < 0.001$) and the I/R + ATX-i group (I/R + ATX-i: 1.05 ± 0.21; control: 0.47 ± 0.27, $p = 0.002$; **Figures 9D,E**). The I/R + ATX-i optic nerves, however, appeared to be slightly less damaged at the 14-days time point (**Figures 9D,E**).

Regarding microglia, the number of Iba1$^+$ cells was significantly upregulated in the I/R (5.65 ± 0.75 cells/image; $p < 0.001$) and I/R + ATX-i (6.10 ± 1.09 cells/image; $p < 0.001$) group in comparison to control optic nerves (2.74 ± 1.06 cells/image; **Figures 9F,G**). Likewise, the number of activated microglia (ED1$^+$ and Iba1$^+$) was significantly increased in I/R (5.28 ± 0.76 cells/image; $p < 0.001$) and I/R + ATX-i optic nerves (5.71 ± 1.04 cells/image; $p < 0.001$) in comparison to controls (0.06 ± 0.06 cells/image; **Figures 9F,H**).

GFAP scoring, for a possible astrogliosis, revealed a significant difference between the control (0.89 ± 0.30) and the I/R + ATX-i group (1.23 ± 0.25) at 14 days ($p = 0.039$). A slight trend to a higher score in the I/R group (1.13 ± 0.13; $p = 0.200$) compared to controls was also noted (**Figures 9I,J**).

4 DISCUSSION

4.1 Medicinal Chemistry
Our initial attempt to find new proprietary ATX-inhibitors was based on the seed compound PF-8380 (**1**) and relied on modifications of the molecule which are in essence: 1) the ZBG, 2) the core region, and 3) the structural element that fits into the lipophilic pocket (**Figure 1A**). Finally, the benzotriazole moiety was found to be one of the preferred ZBGs because it addressed key issues identified in **1**, such as formation of reactive metabolites while ensuring good potency and properties. The core could be replaced by a number of bicyclic or spirocyclic building blocks that resulted in retention of the *in vitro* potency and improvement of chemical stability over **1**. In combination with the previous modifications, introduction of a trifluoromethoxybenzyl moiety as the lipophilic pocket binder resulting in compound **13** provided the lead compound with the most balanced overall profile with regard to potency (IC$_{50}$ against ATX: 6 nM), lipophilicity (LogD), permeability, solubility, and low microsomal clearance *in vitro*. While for a number of compounds such as **14**, **7**, and **15** the low microsomal clearance *in vitro* did not translate into sufficient exposure in rat after oral dosing for unclear reasons, **13** provided an acceptable PK profile with good oral bioavailability and sufficient half live to allow for subsequent acute and chronic *in vivo* PD studies. In addition, screening of compound **13** in a panel of approximately 70 assays covering a variety of enzymes, receptors, and transporters revealed a low risk for off target effects (**Supplementary Table S2**).

4.2 Evaluation of PK/PD of Compound 13
Sustained ATX inhibition was demonstrated after oral dosing of **13** in an acute PK/PD study in rats. *In vivo*, LPA levels of total LPA or the different LPA species analyzed were lowered in a dose-dependent fashion and ATX activity was also inhibited *ex vivo* when plasma ATX activity was monitored with incubation of the sample (**Figure 2**). Besides the single dose PK, we evaluated food admix as an alternative route of drug administration which would substantially minimize the stress during chronic drug treatments to the animals compared to gavage or injections.

Based on the PK/PD relationship observed in the acute experiment, administration via food admix of **13** at a dose of 20 mg/kg results in an estimated average ATX inhibition of > 75% during the 2-weeks study at steady state. Therefore, food admix was chosen as the preferred route of administration of **13** for the *in vivo* studies.

4.3 *In vivo* Studies

Glaucomatous neuropathy is one of the most common causes of blindness worldwide (Weinreb et al., 2014; Egs, 2017). However, until now, the knowledge about underlying pathomechanisms remains sparse. Besides an elevated IOP, other mechanisms, such as ischemic processes and immunological alterations contribute to disease development (Grus et al., 2008; Joachim et al., 2012a; Schmid et al., 2014; Palmhof et al., 2019). Nonetheless, to date, IOP lowering is the only treatment option (Egs, 2017). Current medical or surgical approaches cannot reverse damage, but only slow down disease progression. Hence, novel, alternative therapies are needed that might eventually stop disease progression.

Based on the compelling link of an overactive ocular ATX-LPA axis with POAG, we sought to investigate if ATX inhibition using the novel ATX-inhibitor (ATX-i (**13**)) might protect RGCs beyond IOP control in two different glaucoma models, namely the EAG and the I/R model. In EAG animals, glaucomatous damage occurs after immunization with ocular antigens independently of IOP (Laspas et al., 2011; Noristani et al., 2016). In the current study, we observed a mild preservation of RGCs in ATX-i (**13**)-treated animals compared to ONA immunized rats (**Figures 3C,D**). RGCs are the neurons that transmit visual stimuli from the retina to the brain (Mead and Tomarev, 2016) and therefore, protection of these cells will preserve vision. Neither ONA immunization nor treatment with ATX-i (**13**) affected the IOP (**Supplementary Figure S1**). As previously shown, IOP stayed within the normal range in the EAG model (Laspas et al., 2011; Joachim et al., 2013). Other studies demonstrated that topically or intracamerally administrated ATX-inhibitors acutely decreased the IOP in healthy rabbits as well as in mice with elevated pressure due to laser peripheral iridotomy (Iyer et al., 2012; Nagano et al., 2019). In contrast, ATX-i (**13**), which was administered via the oral route, did not lower IOP in both models. This suggests that, as shown in mice (Nagano et al., 2019), IOP might have to be experimentally increased, in order to demonstrate IOP lowering by ATX inhibition in rodent models.

We noted an increase in serum and aqueous humor IgG levels in ONA immunized animals, while the IgG levels were lower in rats treated with the ATX-i (**13**) (**Figures 3A,B**). In prior studies, IgG deposits have been observed in POAG patients (Gramlich et al., 2013; Von Thun Und Hohenstein-Blaul et al., 2017) as well as in EAG retinas, optic nerves, and aqueous humor (Laspas et al., 2011; Joachim et al., 2013). ATX-i (**13**) lowered elevated IgG levels preferably in the aqueous humor and therefore contributes to a diminished immune response in the eye. In addition, as a consequence of increased IgG levels, significantly more microglia and activated microglia cells were observed in ONA animals

(**Figures 4A–C**). The reduced level of inflammation was also reflected in lower numbers of total and activated microglia in the ATX-i (**13**)-treated group. Microglia seem to play an important role in glaucoma in general (Karlstetter et al., 2015) which is in line with an activation of microglia observed in the EAG model previously (Joachim et al., 2012a; Noristani et al., 2016; Reinehr et al., 2019b). Microglia are responsive to LPA via LPA receptors, which regulate cell morphology, migration, and growth factor production (Schilling et al., 2004; Fujita et al., 2008; Muessel et al., 2013). In a septic mouse model, the blockade of LPA1 receptor signaling diminished microglia activation, transformation, and proliferation (Kwon et al., 2018). Furthermore, the LPA1 receptor was also shown to contribute to demyelination in spinal cord injury through microglia activation (Santos-Nogueira et al., 2015).

Besides microglia, we also investigated the macroglia response. Treatment with ATX-i (**13**) led to a decreased GFAP$^+$ area in contrast to ONA animals (**Figures 4D–F**), which is in line with the observed LPA-mediated proliferation of astrocytes *in vitro* (Shano et al., 2008). In LPA-primed astrocytes, several factors where secreted, which were responsible for neuronal differentiation, axon growth, as well as epidermal growth factor signaling (Tabuchi et al., 2000; Spohr et al., 2011). This suggests that inhibition of ATX lowers the observed GFAP response in the EAG model due to decreased LPA levels.

In a previous study, ONA led to nerve fiber and neurofilament degeneration 28 days after immunization (Noristani et al., 2016). In this study, however, we only detected an early sign of optic nerve degeneration such as disruption of the neurofilament, which could be prevented by ATX-i (**13**) treatment (**Figures 5D,E**). Interestingly, a higher number of microglia cells were observed in ONA and ONA + ATX-i optic nerves in contrast to controls. However, only few activated microglia were detected in all groups. In summary, ATX-i (**13**) did not lead to notable effects on microglia with the relative mild phenotype observed in this study (**Figures 5F–H**).

In contrast to the EAG model, I/R leads to a severe and early retinal damage with RGC loss occurring already 2 h after ischemia induction. Cone bipolar cells as well as cone photoreceptors decline 6 and 12 h after ischemia (Palmhof et al., 2019). In the study presented here, we analyzed the effect of ATX-i (**13**) at days 7 and 14 after I/R. Analyses via ERG revealed no significant protective effects of ATX-i (**13**) at day 7 on the I/R-induced loss of retinal function. Interestingly, at day 14, the a-wave amplitude, reflecting the photoreceptor response, was preserved in animals treated with ATX-i (**13**) (**Figures 6A–D**).

I/R injury affects the whole retina, resulting in a retinal thinning (Joachim et al., 2017; Palmhof et al., 2019). In this study, ATX-i (**13**) did not preserve GCL thickness at day 7 but to some extent at day 14 (**Figures 6E,F**). To investigate the retinal cell types, immunohistology and Western Blot analyses were performed. Similar to the EAG model, ATX-i (**13**) could also mildly protect RGCs (**Figures 7A–C**), although I/R in general leads to more severe retinal damage (Joachim et al., 2017). No effect of ATX-i (**13**) was noted in the number of cleaved caspase 3$^+$ apoptotic cells. At both points in time, more apoptotic cells in

the GCL were noted in I/R and I/R + ATX-i retinas (**Figures 7D,E**). Previously, more cleaved caspase 3$^+$ cells were observed already 2 h after I/R induction (Wagner et al., 2020). The severe damage following the ischemia induction could explain the lack of treatment effects on apoptotic cell numbers.

Ischemia injury has been shown to involve activation of microglia cells (Zhang et al., 2005; Cho et al., 2011; Schmid et al., 2014; Wagner et al., 2020), which play an important role as phagocytic cells to remove cell debris (Xu et al., 2016). In line with this, the total number as well as the number of activated microglia was elevated after I/R at both points in time. ATX-i (**13**) was able to reduce the retinal microglia number at 7, but not at 14 days, suggesting increased ATX-i (**13**) activity soon after I/R (**Figures 8A–D**). It is possible that the damage of the retina developed further independent of ATX-mediated LPA formation after day 7, which resulted in higher microglia counts, even in the treatment group at day 14.

LPA-dependent microglia activation was shown to contribute to secondary damage after spinal cord injury involving activation of LPA1 receptors. In this model, LPA levels increased in the spinal cord parenchyma during the first 14 days (Santos-Nogueira et al., 2015). Similarly, LPA1 receptor-mediated microglia activation was noted in a mouse model for transient middle cerebral artery occlusion (Gaire et al., 2019). It seems that elevated LPA levels can contribute to severe neuronal tissue damage by increased activation of microglia over time.

In contrast to the EAG model, a significant increase of GFAP$^+$ area was notable in I/R retinas after 14 days (**Figures 8E–H**). ATX-i (**13**) and the resulting LPA lowering seemed to ameliorate this long-lasting proliferation of astrocytes after ischemia.

Similar to the EAG model, inhibition of ATX had no effect on the neurodegeneration of the optic nerves 7 and 14 days after I/R (**Figure 9**). Since ATX-i and consequently LPA lowering did not seem to be sufficient for rescuing the optic nerve structures it is suggested that major factors other than elevated LPA levels and activated microglia contribute to the damaging effects.

5 CONCLUSION

We describe the generation of a set of novel spirocyclic and bicyclic ATX-inhibitors. The lead compound (**13**, ATX-i) of this new series with improved properties was suitable for investigation in two glaucoma *in vivo* models after oral administration in both an acute and chronic setting. Dose-dependent LPA lowering in rat was confirmed after acute administration. In the EAG and the I/R model, ATX inhibition led to some RGC protection and less gliosis, especially in the retina. Reduced microglia numbers and activation upon ATX-i (**13**) treatment suggests that neuroprotective effects are the result of LPA lowering and of reduced LPA receptor activity. Since ATX-i (**13**) was not able to fully protect cells from severe ischemic retinal and optic nerve damage, it is suggested that major factors other than elevated LPA levels and activated microglia contribute to the damaging

effects in both models. In summary, compound ATX-i (**13**) proved to be suitable to identify a crucial role for an overactive ATX-LPA axis in glaucomatous retinal damage. In addition to the demonstrated ATX-i mediated IOP lowering, retinal ATX-i might further contribute to reduce disease progression.

DATA AVAILABILITY STATEMENT

The raw data supporting the conclusions of this article will be made available by the authors, without undue reservation.

ETHICS STATEMENT

The animal study was reviewed and approved by Cantonal Veterinary Office, Baselstadt (Switzerland) and animal care committee of North Rhine-Westphalia (Landesamt für Natur, Umwelt und Verbraucherschutz Nordrhein-Westfalen, Germany; file no. 84-02.04.2013.A291 and 84-02.04.2016.A141).

AUTHOR CONTRIBUTIONS

DH and SR performed experiments, analyzed data and wrote the manuscript. PM and JH designed compounds, contributed to the manuscript and analyzed data. MP, PS, PD, NW, TB, GS, BG, MS, JB, MGR, SM, RG, and NS designed and/or performed experiments and analyzed data. CU and SCJ designed the study and revised the manuscript. All authors read and approved the final manuscript.

FUNDING

ACKNOWLEDGMENTS

SUPPLEMENTARY MATERIAL

The Supplementary Material for this article can be found online at: https://www.frontiersin.org/articles/10.3389/fphar.2021.699535/full#supplementary-material

REFERENCES

Abu El-Asrar, A. M., Mohammad, G., Nawaz, M. I., Siddiquei, M. M., Kangave, D., and Opdenakker, G. (2013). Expression of Lysophosphatidic Acid, Autotaxin and Acylglycerol Kinase as Biomarkers in Diabetic Retinopathy. *Acta Diabetol.* 50, 363–371. doi:10.1007/s00592-012-0422-1

Adachi, M., Takahashi, K., Nishikawa, M., Miki, H., and Uyama, M. (1996). High Intraocular Pressure-Induced Ischemia and Reperfusion Injury in the Optic Nerve and Retina in Rats. *Graefes Arch. Clin. Exp. Ophthalmol.* 234, 445–451. doi:10.1007/BF02539411

Casola, C., Reinehr, S., Kuehn, S., Stute, G., Spiess, B. M., Dick, H. B., et al. (2016). Specific Inner Retinal Layer Cell Damage in an Autoimmune Glaucoma Model Is Induced by GDNF with or without HSP27. *Invest. Ophthalmol. Vis. Sci.* 57, 3626–3639. doi:10.1167/iovs.15-18999R2

Cho, K. J., Kim, J. H., Park, H. Y., and Park, C. K. (2011). Glial Cell Response and iNOS Expression in the Optic Nerve Head and Retina of the Rat Following Acute High IOP Ischemia-Reperfusion. *Brain Res.* 1403, 67–77. doi:10.1016/j.brainres.2011.06.005

Egs (2017). European Glaucoma Society Terminology and Guidelines for Glaucoma, 4th Edition - Chapter 2: Classification and terminologySupported by the EGS Foundation: Part 1: Foreword; Introduction; Glossary; Chapter 2 Classification and Terminology. *Br. J. Ophthalmol.* 101, 73–127. doi:10.1136/bjophthalmol-2016-EGSguideline.002

Ferry, G., Moulharat, N., Pradère, J. P., Desos, P., Try, A., Genton, A., et al. (2008). S32826, a Nanomolar Inhibitor of Autotaxin: Discovery, Synthesis and Applications as a Pharmacological Tool. *J. Pharmacol. Exp. Ther.* 327, 809–819. doi:10.1124/jpet.108.141911

Fujita, R., Ma, Y., and Ueda, H. (2008). Lysophosphatidic Acid-Induced Membrane Ruffling and Brain-Derived Neurotrophic Factor Gene Expression Are Mediated by ATP Release in Primary Microglia. *J. Neurochem.* 107, 152–160. doi:10.1111/j.1471-4159.2008.05599.x

Gaire, B. P., Sapkota, A., Song, M. R., and Choi, J. W. (2019). Lysophosphatidic Acid Receptor 1 (LPA1) Plays Critical Roles in Microglial Activation and Brain Damage after Transient Focal Cerebral Ischemia. *J. Neuroinflammation* 16, 170. doi:10.1186/s12974-019-1555-8

Gierse, J., Thorarensen, A., Beltey, K., Bradshaw-Pierce, E., Cortes-Burgos, L., Hall, T., et al. (2010). A Novel Autotaxin Inhibitor Reduces Lysophosphatidic Acid Levels in Plasma and the Site of Inflammation. *J. Pharmacol. Exp. Ther.* 334, 310–317. doi:10.1124/jpet.110.165845

Giganti, A., Rodriguez, M., Fould, B., Moulharat, N., Cogé, F., Chomarat, P., et al. (2008). Murine and Human Autotaxin Alpha, Beta, and Gamma Isoforms: Gene Organization, Tissue Distribution, and Biochemical Characterization. *J. Biol. Chem.* 283, 7776–7789. doi:10.1074/jbc.M708705200

Gramlich, O. W., Beck, S., Von Thun Und Hohenstein-Blaul, N., Boehm, N., Ziegler, A., Vetter, J. M., et al. (2013). Enhanced Insight into the Autoimmune Component of Glaucoma: IgG Autoantibody Accumulation and Pro-inflammatory Conditions in Human Glaucomatous Retina. *PLoS One* 8, e57557. doi:10.1371/journal.pone.0057557

Grus, F. H., Joachim, S. C., Wuenschig, D., Rieck, J., and Pfeiffer, N. (2008). Autoimmunity and Glaucoma. *J. Glaucoma* 17, 79–84. doi:10.1097/IJG.0b013e318156a592

Hernandez, M. R., Agapova, O. A., Yang, P., Salvador-Silva, M., Ricard, C. S., and Aoi, S. (2002). Differential Gene Expression in Astrocytes from Human normal and Glaucomatous Optic Nerve Head Analyzed by cDNA Microarray. *Glia* 38, 45–64. doi:10.1002/glia.10051

Ho, L. T. Y., Osterwald, A., Ruf, I., Hunziker, D., Mattei, P., Challa, P., et al. (2020). Role of the Autotaxin-Lysophosphatidic Acid axis in Glaucoma, Aqueous Humor Drainage and Fibrogenic Activity. *Biochim. Biophys. Acta Mol. Basis Dis.* 1866, 165560. doi:10.1016/j.bbadis.2019.165560

Honjo, M., Igarashi, N., Kurano, M., Yatomi, Y., Igarashi, K., Kano, K., et al. (2018). Autotaxin-Lysophosphatidic Acid Pathway in Intraocular Pressure Regulation and Glaucoma Subtypes. *Invest. Ophthalmol. Vis. Sci.* 59, 693–701. doi:10.1167/iovs.17-23218

Horstmann, L., Kuehn, S., Pedreiturria, X., Haak, K., Pfarrer, C., Dick, H. B., et al. (2016). Microglia Response in Retina and Optic Nerve in Chronic Experimental Autoimmune Encephalomyelitis. *J. Neuroimmunol* 298, 32–41. doi:10.1016/j.jneuroim.2016.06.008

Igarashi, N., Honjo, M., Asaoka, R., Kurano, M., Yatomi, Y., Igarashi, K., et al. (2021). Aqueous Autotaxin and TGF-Bs Are Promising Diagnostic Biomarkers for Distinguishing Open-Angle Glaucoma Subtypes. *Sci. Rep.* 11, 1408. doi:10.1038/s41598-021-81048-3

Iyer, P., Lalane, R., 3rd, Morris, C., Challa, P., Vann, R., and Rao, P. V. (2012). Autotaxin-lysophosphatidic Acid axis Is a Novel Molecular Target for Lowering Intraocular Pressure. *PLoS One* 7, e42627. doi:10.1371/journal.pone.0042627

Joachim, S. C., Gramlich, O. W., Laspas, P., Schmid, H., Beck, S., Von Pein, H. D., et al. (2012a). Retinal Ganglion Cell Loss Is Accompanied by Antibody Depositions and Increased Levels of Microglia after Immunization with Retinal Antigens. *PLoS One* 7, e40616. doi:10.1371/journal.pone.0040616

Joachim, S. C., Jehle, T., Boehm, N., Gramlich, O. W., Lagreze, W. A., Pfeiffer, N., et al. (2012b). Effect of Ischemia Duration on Autoantibody Response in Rats Undergoing Retinal Ischemia-Reperfusion. *Ophthalmic Res.* 48, 67–74. doi:10.1159/000335965

Joachim, S. C., Reinehr, S., Kuehn, S., Laspas, P., Gramlich, O. W., Kuehn, M., et al. (2013). Immune Response against Ocular Tissues after Immunization with Optic Nerve Antigens in a Model of Autoimmune Glaucoma. *Mol. Vis.* 19, 1804–1814.

Joachim, S. C., Renner, M., Reinhard, J., Theiss, C., May, C., Lohmann, S., et al. (2017). Protective Effects on the Retina after Ranibizumab Treatment in an Ischemia Model. *PLoS One* 12, e0182407. doi:10.1371/journal.pone.0182407

Karlstetter, M., Scholz, R., Rutar, M., Wong, W. T., Provis, J. M., and Langmann, T. (2015). Retinal Microglia: Just Bystander or Target for Therapy. *Prog. Retin. Eye Res.* 45, 30–57. doi:10.1016/j.preteyeres.2014.11.004

Kuttruff, C. A., Ferrara, M., Bretschneider, T., Hoerer, S., Handschuh, S., Nosse, B., et al. (2017). Discovery of BI-2545: A Novel Autotaxin Inhibitor that Significantly Reduces LPA Levels *In Vivo*. *ACS Med. Chem. Lett.* 8, 1252–1257. doi:10.1021/acsmedchemlett.7b00312

Kwon, J. H., Gaire, B. P., Park, S. J., Shin, D. Y., and Choi, J. W. (2018). Identifying Lysophosphatidic Acid Receptor Subtype 1 (LPA1) as a Novel Factor to Modulate Microglial Activation and Their TNF-α Production by Activating ERK1/2. *Biochim. Biophys. Acta Mol. Cel Biol Lipids* 1863, 1237–1245. doi:10.1016/j.bbalip.2018.07.015

Laspas, P., Gramlich, O. W., Müller, H. D., Cuny, C. S., Gottschling, P. F., Pfeiffer, N., et al. (2011). Autoreactive Antibodies and Loss of Retinal Ganglion Cells in Rats Induced by Immunization with Ocular Antigens. *Invest. Ophthalmol. Vis. Sci.* 52, 8835–8848. doi:10.1167/iovs.10-6889

Liu, N., Kan, Q. C., Zhang, X. J., Xv, Y. M., Zhang, S., Zhang, G. X., et al. (2014). Upregulation of Immunomodulatory Molecules by Matrine Treatment in Experimental Autoimmune Encephalomyelitis. *Exp. Mol. Pathol.* 97, 470–476. doi:10.1016/j.yexmp.2014.10.004

Maher, T. M., Van Der Aar, E. M., Van De Steen, O., Allamassey, L., Desrivot, J., Dupont, S., et al. (2018). Safety, Tolerability, Pharmacokinetics, and Pharmacodynamics of GLPG1690, a Novel Autotaxin Inhibitor, to Treat Idiopathic Pulmonary Fibrosis (FLORA): a Phase 2a Randomised Placebo-Controlled Trial. *Lancet Respir. Med.* 6, 627–635. doi:10.1016/S2213-2600(18)30181-4

Matralis, A. N., Afantitis, A., and Aidinis, V. (2019). Development and Therapeutic Potential of Autotaxin Small Molecule Inhibitors: From Bench to Advanced Clinical Trials. *Med. Res. Rev.* 39, 976–1013. doi:10.1002/med.21551

Mead, B., and Tomarev, S. (2016). Evaluating Retinal Ganglion Cell Loss and Dysfunction. *Exp. Eye Res.* 151, 96–106. doi:10.1016/j.exer.2016.08.006

Mettu, P. S., Deng, P. F., Misra, U. K., Gawdi, G., Epstein, D. L., and Rao, P. V. (2004). Role of Lysophospholipid Growth Factors in the Modulation of Aqueous Humor Outflow Facility. *Invest. Ophthalmol. Vis. Sci.* 45, 2263–2271. doi:10.1167/iovs.03-0960

Muessel, M. J., Harry, G. J., Armstrong, D. L., and Storey, N. M. (2013). SDF-1α and LPA Modulate Microglia Potassium Channels through Rho Gtpases to Regulate Cell Morphology. *Glia* 61, 1620–1628. doi:10.1002/glia.22543

Nagano, N., Honjo, M., Kawaguchi, M., Nishimasu, H., Nureki, O., Kano, K., et al. (2019). Development of a Novel Intraocular-Pressure-Lowering Therapy Targeting ATX. *Biol. Pharm. Bull.* 42, 1926–1935. doi:10.1248/bpb.b19-00567

Nakamura, N., Yamagishi, R., Honjo, M., Igarashi, N., Shimizu, S., and Aihara, M. (2021). Effects of Topical TGF-B1, TGF-B2, ATX, and LPA on IOP Elevation and Regulation of the Conventional Aqueous Humor Outflow Pathway. *Mol. Vis.* 27, 61–77.

Narita, M., Goji, J., Nakamura, H., and Sano, K. (1994). Molecular Cloning, Expression, and Localization of a Brain-specific Phosphodiesterase I/nucleotide Pyrophosphatase (PD-I Alpha) from Rat Brain. *J. Biol. Chem.* 269, 28235–28242. doi:10.1016/s0021-9258(18)46919-0

Noristani, R., Kuehn, S., Stute, G., Reinehr, S., Stellbogen, M., Dick, H. B., et al. (2016). Retinal and Optic Nerve Damage Is Associated with Early Glial Responses in an Experimental Autoimmune Glaucoma Model. *J. Mol. Neurosci.* 58, 470–482. doi:10.1007/s12031-015-0707-2

Palmhof, M., Frank, V., Rappard, P., Kortenhorn, E., Demuth, J., Biert, N., et al. (2019). From Ganglion Cell to Photoreceptor Layer: Timeline of Deterioration in a Rat Ischemia/Reperfusion Model. *Front Cel Neurosci* 13, 174. doi:10.3389/fncel.2019.00174

Palmhof, M., Lohmann, S., Schulte, D., Stute, G., Wagner, N., Dick, H. B., et al. (2018). Fewer Functional Deficits and Reduced Cell Death after Ranibizumab Treatment in a Retinal Ischemia Model. *Int. J. Mol. Sci.* 19, 1636. doi:10.3390/ijms19061636

Pattabiraman, P. P., Maddala, R., and Rao, P. V. (2014). Regulation of Plasticity and Fibrogenic Activity of Trabecular Meshwork Cells by Rho GTPase Signaling. *J. Cel Physiol* 229, 927–942. doi:10.1002/jcp.24524

Pease, M. E., Hammond, J. C., and Quigley, H. A. (2006). Manometric Calibration and Comparison of TonoLab and TonoPen Tonometers in Rats with Experimental Glaucoma and in normal Mice. *J. Glaucoma* 15, 512–519. doi:10.1097/01.ijg.0000212276.57853.19

Reinehr, S., Gomes, S. C., Gassel, C. J., Asaad, M. A., Stute, G., Schargus, M., et al. (2019a). Intravitreal Therapy against the Complement Factor C5 Prevents Retinal Degeneration in an Experimental Autoimmune Glaucoma Model. *Front. Pharmacol.* 10, 1381. doi:10.3389/fphar.2019.01381

Reinehr, S., Reinhard, J., Gandej, M., Gottschalk, I., Stute, G., Faissner, A., et al. (2018). S100B Immunization Triggers NFκB and Complement Activation in an Autoimmune Glaucoma Model. *Sci. Rep.* 8, 9821. doi:10.1038/s41598-018-28183-6

Reinehr, S., Reinhard, J., Gandej, M., Kuehn, S., Noristani, R., Faissner, A., et al. (2016). Simultaneous Complement Response via Lectin Pathway in Retina and Optic Nerve in an Experimental Autoimmune Glaucoma Model. *Front. Cel Neurosci* 10, 140. doi:10.3389/fncel.2016.00140

Reinehr, S., Reinhard, J., Wiemann, S., Hesse, K., Voss, C., Gandej, M., et al. (2019b). Transfer of the Experimental Autoimmune Glaucoma Model from Rats to Mice-New Options to Study Glaucoma Disease. *Int. J. Mol. Sci.* 20, 2563. doi:10.3390/ijms20102563

Renner, M., Stute, G., Alzureiqi, M., Reinhard, J., Wiemann, S., Schmid, H., et al. (2017). Optic Nerve Degeneration after Retinal Ischemia/Reperfusion in a Rodent Model. *Front. Cel Neurosci* 11, 254. doi:10.3389/fncel.2017.00254

Rodrı́guez Sarmiento, R. M., Wirz, B., and Iding, H. (2003). Chemoenzymatic Preparation of Non-racemic N-Boc-Pyrrolidine-3,4-Dicarboxylic Acid 3-ethyl Esters and Their 4-hydroxymethyl Derivatives. *Tetrahedron: Asymmetry* 14, 1547–1551. doi:10.1016/S0957-4166(03)00284-2

Santos-Nogueira, E., López-Serrano, C., Hernández, J., Lago, N., Astudillo, A. M., Balsinde, J., et al. (2015). Activation of Lysophosphatidic Acid Receptor Type 1 Contributes to Pathophysiology of Spinal Cord Injury. *J. Neurosci.* 35, 10224–10235. doi:10.1523/JNEUROSCI.4703-14.2015

Schilling, T., Stock, C., Schwab, A., and Eder, C. (2004). Functional Importance of Ca2+-Activated K+ Channels for Lysophosphatidic Acid-Induced Microglial Migration. *Eur. J. Neurosci.* 19, 1469–1474. doi:10.1111/j.1460-9568.2004.03265.x

Schlamp, C. L., Li, Y., Dietz, J. A., Janssen, K. T., and Nickells, R. W. (2006). Progressive Ganglion Cell Loss and Optic Nerve Degeneration in DBA/2J Mice Is Variable and Asymmetric. *BMC Neurosci.* 7, 66. doi:10.1186/1471-2202-7-66

Schmid, H., Renner, M., Dick, H. B., and Joachim, S. C. (2014). Loss of Inner Retinal Neurons after Retinal Ischemia in Rats. *Invest. Ophthalmol. Vis.* 55, 2777–2787. doi:10.1167/iovs.13-13372

Shano, S., Moriyama, R., Chun, J., and Fukushima, N. (2008). Lysophosphatidic Acid Stimulates Astrocyte Proliferation through LPA1. *Neurochem. Int.* 52, 216–220. doi:10.1016/j.neuint.2007.07.004

Shindler, K. S., Guan, Y., Ventura, E., Bennett, J., and Rostami, A. (2006). Retinal Ganglion Cell Loss Induced by Acute Optic Neuritis in a Relapsing Model of Multiple Sclerosis. *Mult. Scler.* 12, 526–532. doi:10.1177/1352458506070629

Spohr, T. C. L. S. E., Dezonne, R. S., Rehen, S. K., and Gomes, F. C. A. (2011). Astrocytes Treated by Lysophosphatidic Acid Induce Axonal Outgrowth of Cortical Progenitors through Extracellular Matrix Protein and Epidermal Growth Factor Signaling Pathway. *J. Neurochem.* 119, 113–123. doi:10.1111/j.1471-4159.2011.07421.x

Tabuchi, S., Kume, K., Aihara, M., and Shimizu, T. (2000). Expression of Lysophosphatidic Acid Receptor in Rat Astrocytes: Mitogenic Effect and Expression of Neurotrophic Genes. *Neurochem. Res.* 25, 573–582. doi:10.1023/a:1007542532395

Tsai, T., Kuehn, S., Tsiampalis, N., Vu, M. K., Kakkassery, V., Stute, G., et al. (2018). Anti-inflammatory Cytokine and Angiogenic Factors Levels in Vitreous Samples of Diabetic Retinopathy Patients. *PLoS One* 13, e0194603. doi:10.1371/journal.pone.0194603

Velmeshev, D., Schirmer, L., Jung, D., Haeussler, M., Perez, Y., Mayer, S., et al. (2019). Single-cell Genomics Identifies Cell Type-specific Molecular Changes in Autism. *Science* 364, 685–689. doi:10.1126/science.aav8130

Von Thun Und Hohenstein-Blaul, N., Kunst, S., Pfeiffer, N., and Grus, F. H. (2017). Biomarkers for Glaucoma: from the Lab to the Clinic. *Eye (Lond)* 31, 225–231. doi:10.1038/eye.2016.300

Wagner, N., Reinehr, S., Palmhof, M., Schuschel, D., Tsai, T., Sommer, E., et al. (2020). Microglia Activation in Retinal Ischemia Triggers Cytokine and Toll-like Receptor Response. *J. Mol. Neurosci.* 71, 527–544. doi:10.1007/s12031-020-01674-w

Wang, J., Hamm, R. J., and Povlishock, J. T. (2011). Traumatic Axonal Injury in the Optic Nerve: Evidence for Axonal Swelling, Disconnection, Dieback, and Reorganization. *J. Neurotrauma* 28, 1185–1198. doi:10.1089/neu.2011.1756

Weinreb, R. N., Aung, T., and Medeiros, F. A. (2014). The Pathophysiology and Treatment of Glaucoma: a Review. *JAMA* 311, 1901–1911. doi:10.1001/jama.2014.3192

Wilmes, A. T., Reinehr, S., Kühn, S., Pedreiturria, X., Petrikowski, L., Faissner, S., et al. (2018). Laquinimod Protects the Optic Nerve and Retina in an Experimental Autoimmune Encephalomyelitis Model. *J. Neuroinflammation* 15, 183. doi:10.1186/s12974-018-1208-3

Wu, Y. Y., Zheng, B. R., Chen, W. Z., Guo, M. S., Huang, Y. H., and Zhang, Y. (2020). Expression and Role of Autophagy Related Protein P62 and LC3 in the Retina in a Rat Model of Acute Ocular Hypertension. *Int. J. Ophthalmol.* 13, 21–28. doi:10.18240/ijo.2020.01.04

Xu, L., He, D., and Bai, Y. (2016). Microglia-Mediated Inflammation and Neurodegenerative Disease. *Mol. Neurobiol.* 53, 6709–6715. doi:10.1007/s12035-015-9593-4

Yang, C., Lafleur, J., Mwaikambo, B. R., Zhu, T., Gagnon, C., Chemtob, S., et al. (2009). The Role of Lysophosphatidic Acid Receptor (LPA1) in the Oxygen-Induced Retinal Ganglion Cell Degeneration. *Invest. Ophthalmol. Vis. Sci.* 50, 1290–1298. doi:10.1167/iovs.08-1920

Zhang, C., Lam, T. T., and Tso, M. O. (2005). Heterogeneous Populations of Microglia/macrophages in the Retina and Their Activation after Retinal Ischemia and Reperfusion Injury. *Exp. Eye Res.* 81, 700–709. doi:10.1016/j.exer.2005.04.008

Alteration of EIF2 Signaling, Glycolysis, and Dopamine Secretion in Form-Deprived Myopia in Response to 1% Atropine Treatment: Evidence From Interactive iTRAQ-MS and SWATH-MS Proteomics Using a Guinea Pig Model

Ying Zhu[1†], Jing Fang Bian[2†], Da Qian Lu[2†], Chi Ho To[2,3,4], Carly Siu-Yin Lam[2,3,4], King Kit Li[2], Feng Juan Yu[2], Bo Teng Gong[5], Qiong Wang[1], Xiao Wen Ji[1], Hong Mei Zhang[1], Hong Nian[1], Thomas Chuen Lam[2,3,4,6]* and Rui Hua Wei[1]*

[1]Tianjin Key Laboratory of Retinal Functions and Diseases, Tianjin Branch of National Clinical Research Center for Ocular Disease, Eye Institute and School of Optometry, Tianjin Medical University Eye Hospital, Tianjin, China, [2]Centre for Myopia Research, School of Optometry, The Hong Kong Polytechnic University, Hong Kong SAR, China, [3]Centre for Eye and Vision Research (CEVR), Hong Kong SAR, China, [4]Research Centre for SHARP Vision (RCSV), The Hong Kong Polytechnic University, Hong Kong SAR, China, [5]Department of Ophthalmology, Tianjin Medical University General Hospital, Tianjin, China, [6]Shenzhen Research Institute, The Hong Kong Polytechnic University, Shenzhen, China

Purpose: Atropine, a non-selective muscarinic antagonist, effectively slows down myopia progression in human adolescents and several animal models. However, the underlying molecular mechanism is unclear. The current study investigated retinal protein changes of form-deprived myopic (FDM) guinea pigs in response to topical administration of 1% atropine gel (10 g/L).

Methods: At the first stage, the differentially expressed proteins were screened using fractionated isobaric tags for a relative and absolute quantification (iTRAQ) approach, coupled with nano-liquid chromatography-tandem mass spectrometry (nano-LC-MS/MS) ($n = 24$, 48 eyes) using a sample pooling technique. At the second stage, retinal tissues from another cohort with the same treatment ($n = 12$, 24 eyes) with significant ocular changes were subjected to label-free sequential window acquisition of all theoretical mass spectra (SWATH-MS) proteomics for orthogonal protein target confirmation. The localization of Alpha-synuclein was verified using immunohistochemistry and confocal imaging.

Results: A total of 1,695 proteins (8,875 peptides) were identified with 479 regulated proteins (FC ≥ 1.5 or ≤0.67) found from FDM eyes and atropine-treated eyes receiving 4-weeks drug treatment using iTRAQ-MS proteomics. Combining the iTRAQ-MS and SWATH-MS datasets, a total of 29 confident proteins at 1% FDR were consistently quantified and matched, comprising 12 up-regulated and 17 down-regulated proteins which differed between FDM eyes and atropine treated eyes (iTRAQ: FC ≥ 1.5 or ≤0.67,

SWATH: FC ≥ 1.4 or ≤0.71, *p*-value of ≤0.05). Bioinformatics analysis using IPA and STRING databases of these commonly regulated proteins revealed the involvement of the three commonly significant pathways: EIF2 signaling; glycolysis; and dopamine secretion. Additionally, the most significantly regulated proteins were closely connected to Alpha-synuclein (SNCA). Using immunostaining (*n* = 3), SNCA was further confirmed in the inner margin of the inner nuclear layer (INL) and spread throughout the inner plexiform layer (IPL) of the retina of guinea pigs.

Conclusion: The molecular evidence using next-generation proteomics (NGP) revealed that retinal EIF2 signaling, glycolysis, and dopamine secretion through SNCA are implicated in atropine treatment of myopia in the FDM-induced guinea pig model.

Keywords: Retina, iTRAQ-MS, SWATH-MS, FDM, Guinea pigs, Atropine
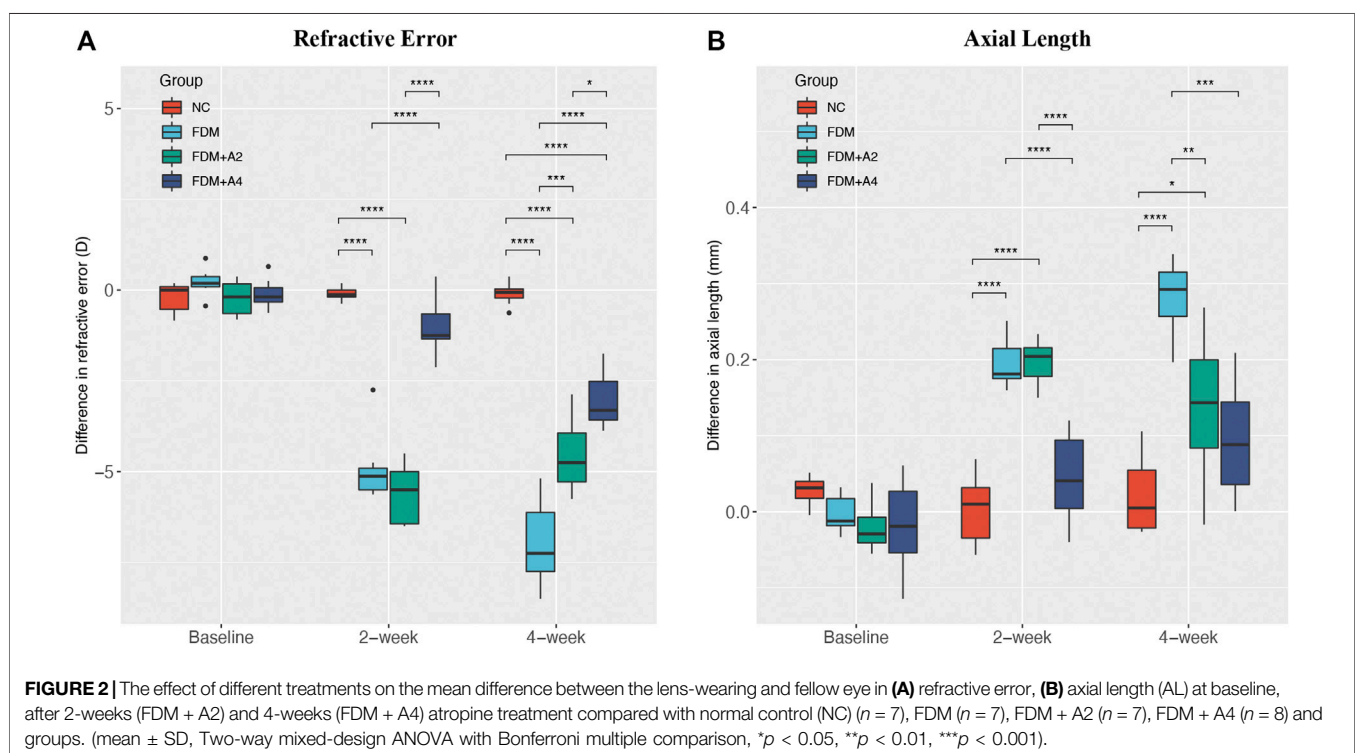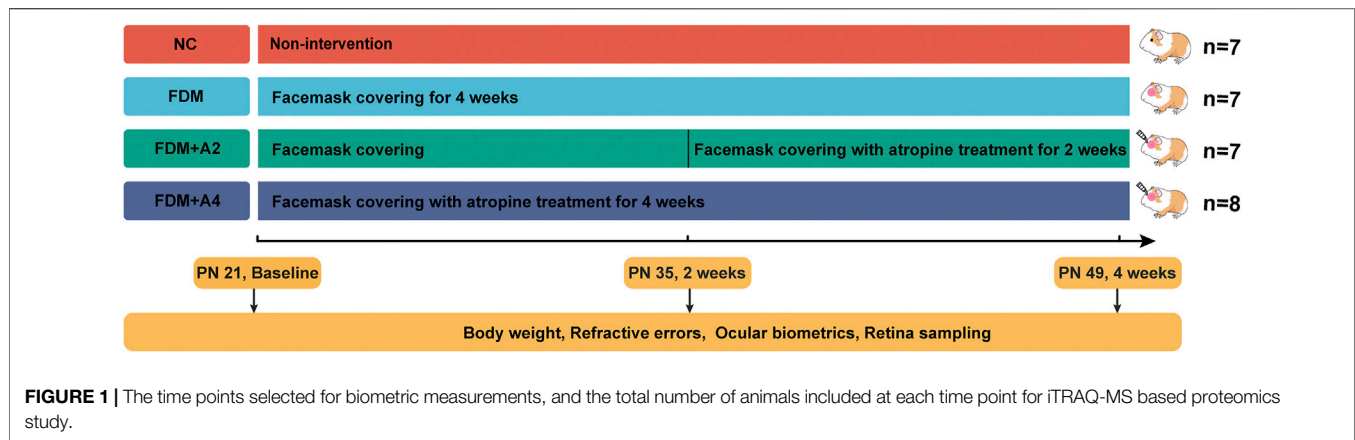
INTRODUCTION

Myopia (near-sightedness) has emerged as a worldwide public health issue (Morgan et al., 2012). High myopia (≤ 6.00 diopters) is associated with an increased risk of cataracts, glaucoma, and retinal detachment (Wong et al., 2014; Verkicharla et al., 2015; Saw et al., 2019). These high myopia-associated ocular complications may cause blindness or permanent visual loss. Although the exact molecular mechanism underlying myopia remains unclear, there are several routes of intervention for the prevention or delay of myopia progression, including the application of low dosage (0.01,0.5, and 1%) atropine (Chua et al., 2006; Chia et al., 2016; Yam et al., 2019), orthokeratology (Cho and Cheung, 2012; Hiraoka et al., 2018), and defocus lenses (Tse et al., 2005; Tse et al., 2007; Tse and To, 2011; McFadden et al., 2014; Lam et al., 2019).

Atropine is a non-selective muscarinic antagonist, which can assist in diagnosing refractive errors in young children (Wildsoet et al., 2019). The inhibitory effect of atropine on myopia progression has been found in different animal models, including the tree shrew (Wan et al., 2018), monkey (Raviola and Wiesel, 1985; Kiorpes et al., 1987; Tigges et al., 1999), and chick (Gallego et al., 2012), as well as in young children (Chia et al., 2012; Huang et al., 2016; Yam et al., 2019). However, its underlying molecular mechanism is still unclear. Animal studies have supported the theory that biochemical signal cascades are initialized from the retina in response to defocused visual stimuli to regulate eye growth through tissue remodeling at the sclera (Morgan, 2003; Wallman and Winawer, 2004; Troilo et al., 2019). Retinal neurotransmitters have been suggested to regulate eye growth based on animal studies. The retinal dopamine (DA) level was decreased in form-deprived myopia (FDM) animal models, including in chicks (Stone et al., 1989), rhesus monkeys (Iuvone et al., 1989), guinea pigs (Mao et al., 2011), and tree shrews (McBrien et al., 2001). A reduced retinal DA level was also found in Lens-induced myopia (LIM) chicks (Guo et al., 1995). Critical inhibitory neurotransmitters, antagonists of γ-aminobutyric acid (GABA) receptor, inhibited eye growth in the FDM model of chicks (Stone et al., 2003), while increased expression of GABA was found in the retinas of LIM guinea pigs (Zhao et al., 2017). In contrast, the release of retinal DA was increased in FDM chicks

after atropine treatment (Schwahn et al., 2000), and the retinal levels of GABA transporter 1 were also significantly decreased after atropine treatment (Barathi et al., 2014).

Proteomic approaches have become powerful tools to screen thousands of protein candidates simultaneously, which enables the detection of global regulation of protein expression (Pandey and Mann, 2000). Data-dependent acquisition (DDA) is a popular strategy in shotgun proteomics for target screening. Isobaric tags for relative and absolute quantification (iTRAQ) has remained a well-established multiplexing DDA approach for biomarker discovery in quantitative proteomics. However, limitations of DDA include suboptimal quantification and reproducibility (Liu et al., 2004; Michalski et al., 2011), under-sampling, and a bias towards high abundance proteins or peptides (Kiyonami et al., 2011). To overcome the limitations in DDA, data-independent acquisition (DIA) has rapidly gained attention as an alternative label-free strategy. In DIA, data reproducibility between technical replicates is increased, and low abundance precursors are better represented (Geromanos et al., 2009). DIA is successfully applied in the TripleTOF system (SCIEX), also termed SWATH (Gillet et al., 2012). The SWATH-MS based proteomics approach has become an increasingly popular proteomics platform (Gillet et al., 2012) for both clinical and basic research studies (Anjo et al., 2017), with broad applications in biomarker discovery and understanding of biological mechanisms (Simpson et al., 2009; Brown, 2014; Selevsek et al., 2015; Ortea et al., 2016; Anjo et al., 2017). It was also used to study retinal protein regulation during normal ocular growth (Shan et al., 2018a) and LIM (Bian et al., 2021) guinea pigs by our group. Moreover, it can be applied for the orthogonal verification of targets screened from the genomic data in cancer disease (Zhang et al., 2016).

To date, only one study has attempted the investigation of retinal protein changes after atropine treatment in LIM mouse model using an iTRAQ-MS based proteomics approach (Barathi et al., 2014). Two other mRNA expression studies investigated atropine-treated human scleral fibroblasts (Hsiao et al., 2019) and corneal epithelial cells (Chang et al., 2019). Hence, the knowledge of the retinal protein changes after atropine treated myopia was very minimal. The main objective of the present work was to characterize the whole retinal proteome and investigate

FIGURE 1 | The time points selected for biometric measurements, and the total number of animals included at each time point for iTRAQ-MS based proteomics study.

FIGURE 2 | The effect of different treatments on the mean difference between the lens-wearing and fellow eye in **(A)** refractive error, **(B)** axial length (AL) at baseline, after 2-weeks (FDM + A2) and 4-weeks (FDM + A4) atropine treatment compared with normal control (NC) ($n = 7$), FDM ($n = 7$), FDM + A2 ($n = 7$), FDM + A4 ($n = 8$) and groups. (mean ± SD, Two-way mixed-design ANOVA with Bonferroni multiple comparison, *$p < 0.05$, **$p < 0.01$, ***$p < 0.001$).

differentially expressed proteins, which could reveal the key molecular changes in FDM guinea pigs in response to atropine treatment. It also investigated the feasibility of using combined iTRAQ-MS and SWATH-MS protocols for other retinal diseases.

RESULTS

Refractive Errors and Ocular Dimensions Changes

During the 4-weeks study period, guinea pigs were randomly divided into four individual groups: the normal control group (NC, $n = 7$), the monocularly form-deprived myopia group (FDM, $n = 7$), the FDM with 2-weeks atropine-treatment

group (FDM + A2, $n = 7$), and the FDM with 4-weeks atropine-treatment group (FDM + A4, n = 8) (**Figure 1**). In general, there were no significant differences between the two eyes at baseline with respect to refractive error and other ocular parameters among the four groups. After 2-weeks FDM treatment, relative myopic changes were found in the FDM group (-4.902 ± 0.997 D, mean ± SD), FDM + A2 group (-5.625 ± 0.845 D, mean ± SD), and FDM + A4 group (−1.031 ± 0.773 D, mean ± SD) compared to control eyes, as expected. The mean refractive error changes (treated eyes minus control eyes) also showed significant differences among the normal control, FDM, FDM + A2, and FDM + A4 groups (two-way mixed-design ANOVA, all of $p < 0.001$, **Supplementary Table S1**, **Figure 2A**). In addition, less
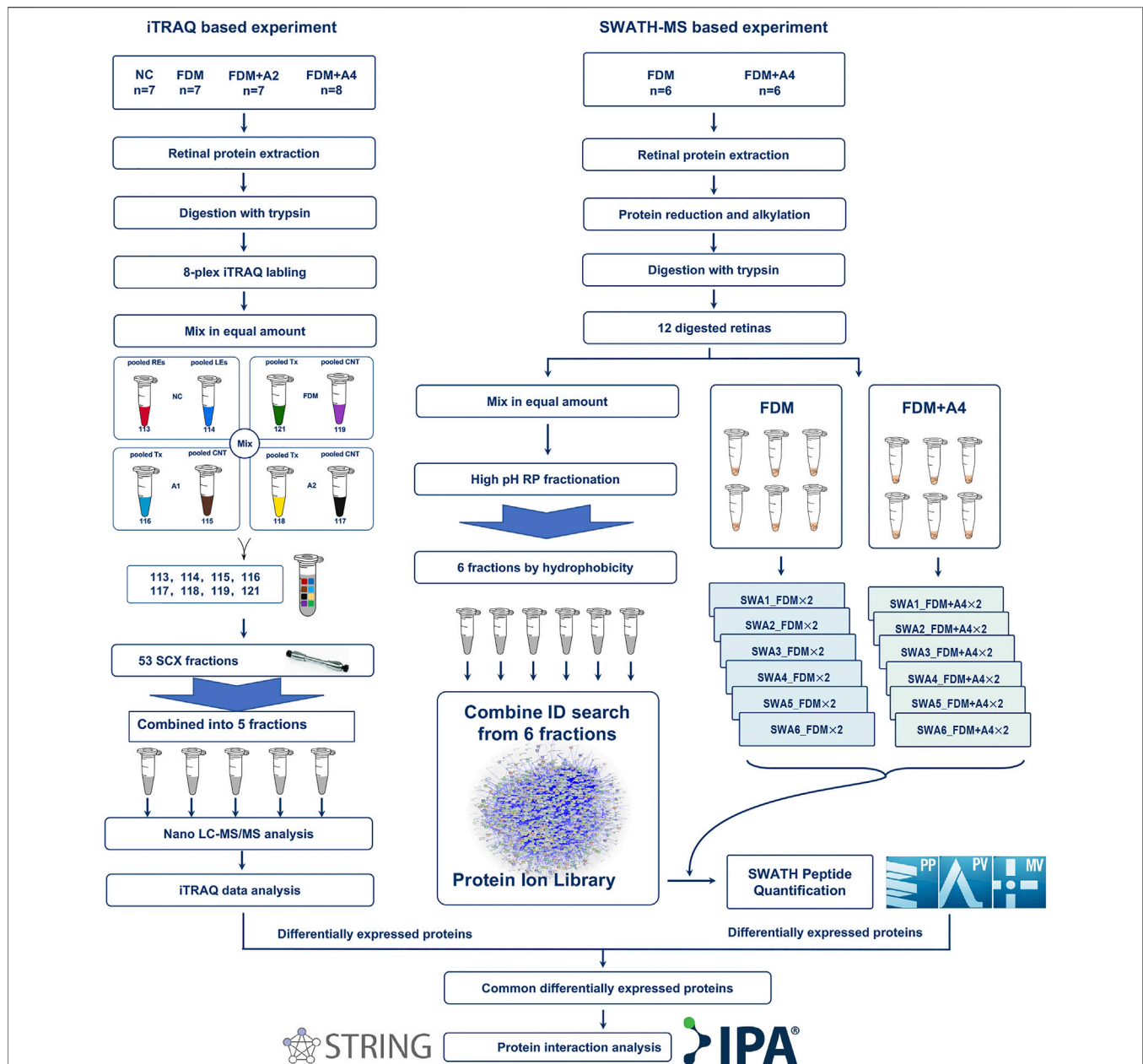
FIGURE 3 | Schematic workflow of quantitative proteomics using iTRAQ-MS and SWTAH-MS proteomics to study effects on protein regulation of atropine treatment on myopic (FDM) eyes. Overall, six individual retinal samples from each time point were equally pooled to form representative retinal lysates of specific groups using an iTRAQ based proteomic approach. Another new batch of six individual retinas was selected in the validated experiment using a SWATH based proteomic approach. The 2 μg digested protein from each sample was used as two technical replicates under SWATH-MS. Protein identification and quantification were performed using ProteinPilot, PeakView, and MarkerView software, followed by online bioinformatics analysis.

myopia was found in the FDM + A4 group compared to the FDM group (FDM + A4 *vs* FDM: −1.031 ± 0.773 D *vs.* −4.902 ± 0.997 D, mean ± SD, p = 3.03e-09, **Figure 2A**). Compared to contralateral control eyes, A-scan also confirmed the corresponding elongation of the vitreous chamber depth (VCD) ($p < 0.001$) and axial length (AL) in the treated eyes ($p < 0.001$, **Figure 2B**) in the FDM, FDM + A2, and FDM + A4 groups. Notably, the means of VCD (FDM + A4 *vs* FDM: 0.014 ±

0.017 mm *vs* 0.081 ± 0.017 mm, mean ± SD, p = 1.37e-06) and AL difference (FDM + A4 *vs* FDM: 0.044 ± 0.056 mm *vs* 0.196 ± 0.033 mm, mean ± SD, p = 2.77e-06, **Figure 2B**) in the FDM + A4 group were significantly smaller than the changes in the FDM group, which was consistent with the finding for refractive error.

The 4-weeks treatment also resulted in similar changes of ocular parameters towards myopia in FDM, FDM + A2, and FDM + A4 groups to the 2-weeks treatment. Significantly less

FIGURE 4 | A total of 1,695 identified proteins (1,545 gene names) were annotated using the PANTHER™ Classification System according to their molecular function **(A)** and biological process **(B)**.
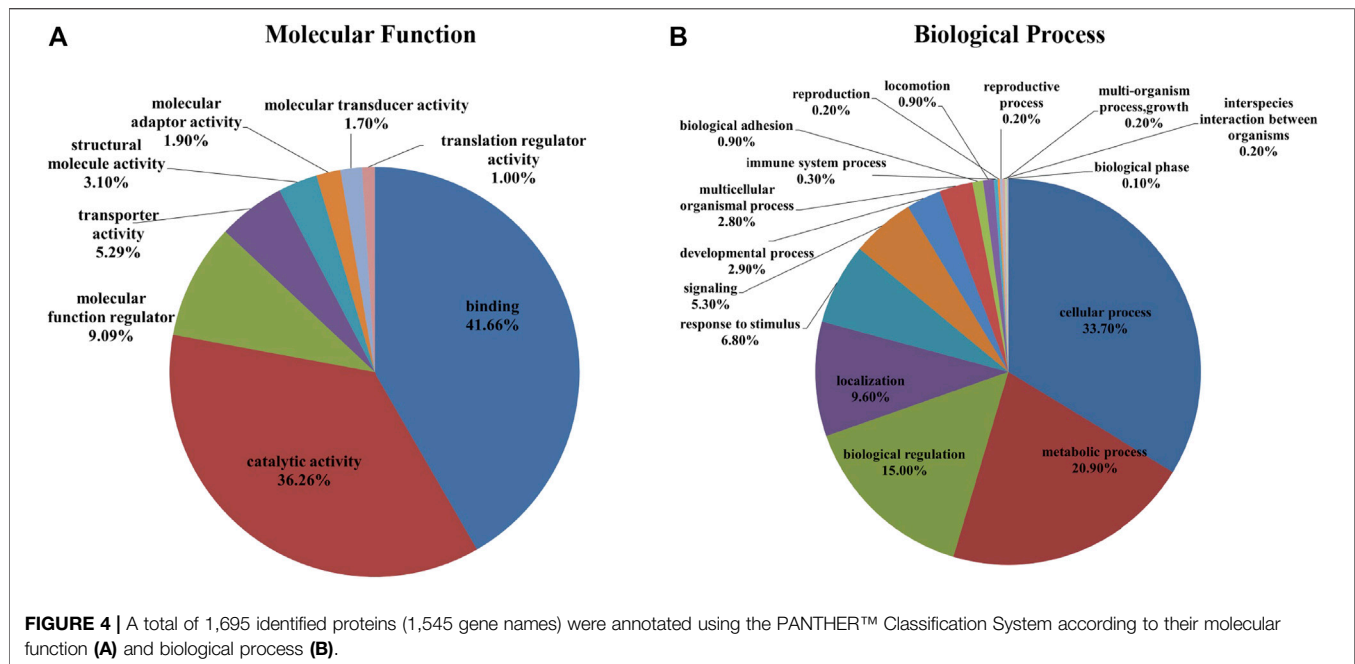
myopia was found in the FDM + A4 group compared to the FDM group (FDM + A4 vs FDM: −3.047 ± 0.737 D vs. −6.955 ± 1.194 D, mean ± SD, p < 0.001). Correspondingly, significantly smaller changes of axial length (FDM + A4 vs FDM: 0.094 ± 0.075 mm vs 0.282 ± 0.049 mm, p < 0.001, **Figure 2B**) were also observed in the FDM + A4 group compared to the FDM group. In addition, compared to the FDM + A2 group, a smaller elongation of AL (−0.043 mm) and enlargement of the VCD (−0.009 mm) were observed in the FDM + A4 group, although the differences did not reach statistical significance (p > 0.05, **Figure 2B**). However, less myopia was observed in the FDM + A4 group, compared with the FDM + A2 group (FDM + A4 vs FDM + A2: -3.047 ± 0.737 D vs. -4.545 ± 1.053 D, mean ± SD, p = 0.019, **Figure 2A**).

Protein Identification and Gene Ontology Function Classification Analysis Using the iTRAQ-MS Approach

In the iTRAQ-MS approach, retinal lysates of age-matched animals from each group (NC, FDM, FDM + A2, and FDM + A4) were labelled with different iTRAQ reagents and pooled together for MS analysis (Left panel in **Figure 3**). The protein identification using this approach, resulted in the identification of 1,695 proteins (8,875 peptides) at 1% global false discovery rate (FDR) by the DDA approach. Of these, 1,545 proteins (~90%) could be successfully converted to relevant guinea pigs' gene names using the Uniprot database (https://www.uniprot.org/) followed by Gene Ontology (GO) classification and analysis using the PANTHER™ database (http://www.pantherdb.org/). Among all the mapped gene IDs, the top three molecular functions of retinal proteins were "binding" (GO: 0005488) (43.70%), "catalytic activity" (GO: 0003824) (37.50%), and

"molecular function regulator" (GO: 0098772) (5.80%) (**Figure 4A**), whilst for biological processes, "cellular process" (GO: 0009987) (35.40%), "metabolic process" (GO: 0008152) (21.70%), and "biological regulation" (GO: 0065007) (14.10%) were identified as the major three groups in the retinal proteome (**Figure 4B**).

Protein Quantitation Using the iTRAQ-MS Approach

For quantitative analysis, a cut-off ratio of ≥1.5 or ≤0.67-fold change was considered differential expression. Two main comparisons were performed to explore the temporal atropine effect on FDM eyes, including the FDM + A2 group (FDM eyes with 2 weeks atropine treatment) vs FDM group (FDM eyes) and FDM + A4 group (FDM eyes with 4 weeks atropine treatment) vs FDM group (FDM eyes), respectively. Four-hundred and sixty-six differentially expressed proteins were initially found in the FDM + A2 group compared to the FDM group. To avoid the potential confounding factor of intrinsic protein difference (intra-ocular difference) between the right and left eyes, the same differentially expressed proteins, found between the two eyes in the normal control group (NC) were excluded. Also, as some key molecular signals are expected to be expressed in opposite directions between the myopic and atropine treated eyes, as reported by an earlier study using the LIM mouse (Barathi et al., 2014), several proteins with the same expression direction in FDM + A2 vs FDM group and FDM vs FDM_C group (contralateral control eyes in FDM group) were excluded, allowing the targeted protein list to be more specific to atropine treatments. Finally, 310 differentially expressed proteins (306 gene names) were considered as positive findings in the FDM + A2 vs FDM group (**Supplementary**

FIGURE 5 | A total of 5,961 identified proteins (5,830 gene names) were annotated with the PANTHER™ Classification System (www.pantherdb.org) according to their molecular function **(A)** and biological process **(B)**.
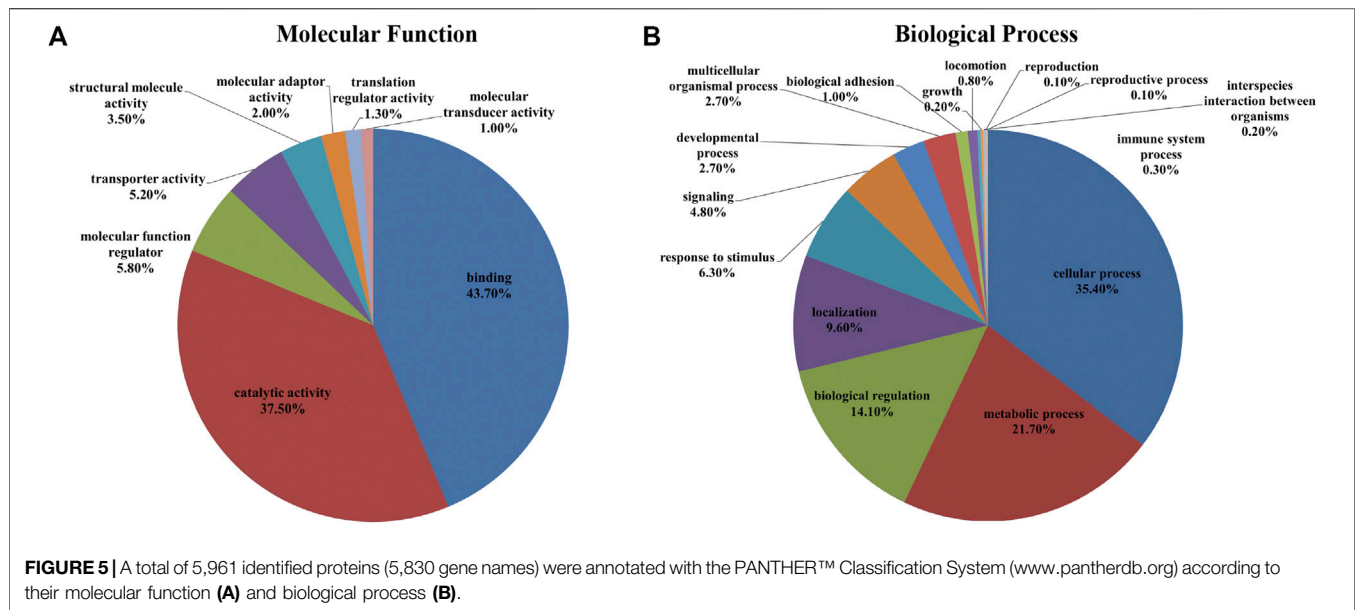
Table S2). Similarly, 668 differentially expressed proteins were initially found following comparison of the FDM + A4 group to the FDM group, using the same cut-off ratio. After applying the same filtering criteria as in the FDM + A2 group, 479 differentially expressed proteins (469 gene names) were considered as more specifically regulated proteins in the FDM + A4 vs FDM group (**Supplementary Table S3**).

Protein Identification and Gene Ontology Function Classification Analysis Using Sequential Window Acquisition of all Theoretical Mass Spectra Approach for Confirmation

To further confirm only highly confident candidates altered in response to atropine treated in FDM guinea pig, another new batch of retinas in the FDM group (n = 6) and FDM + A4 group (n = 6) were collected for further validation using SWATH-MS analysis (Right panel in **Figure 3**). Six animals (12 retinas) from the FDM + A4 and FDM groups were included in the statistical analysis with individual MS injection. Similar ocular biometrics were found in this new batch of animals (**Supplementary Table S4**) as in the iTRAQ experiment. To build a comprehensive ion library for extracting SWATH-MS files, pooled peptides from all 12 guinea pigs (FDM + A4 group and FDM group, n = 6 per group) were divided into six fractions using the High pH Reversed-Phase peptide fractionation technique. After combining the search of six separate IDA injections, a total of 5,961 proteins (51,871 peptides) were identified in this comprehensive ion library. All the raw MS files in iTRAQ-MS and SWATH-MS were subsequently published in Data in Brief (Zhu et al., 2020) and saved in the PeptideAtlas public repository (Desiere et al., 2006) with the accession number of PASS01507 for open access (http://www.peptideatlas.org/).

The identified proteins were loaded in the Uniprot database, which resulted in 5,830 proteins being converted to guinea pig

FIGURE 6 | Volcano plot of 774 differentially expressed retinal proteins in 4-weeks atropine treated eyes (FDM + A4 group) compared to 4-weeks FDM eyes (FDM group) using a SWATH-MS based proteomics approach. Criteria for significant differential expression were as log2 ratio (FDM + A4/FDM) ≥ 0.43 or ≤ -0.43 (~1.40FC), p-value ≤ 0.05, welch T-test.
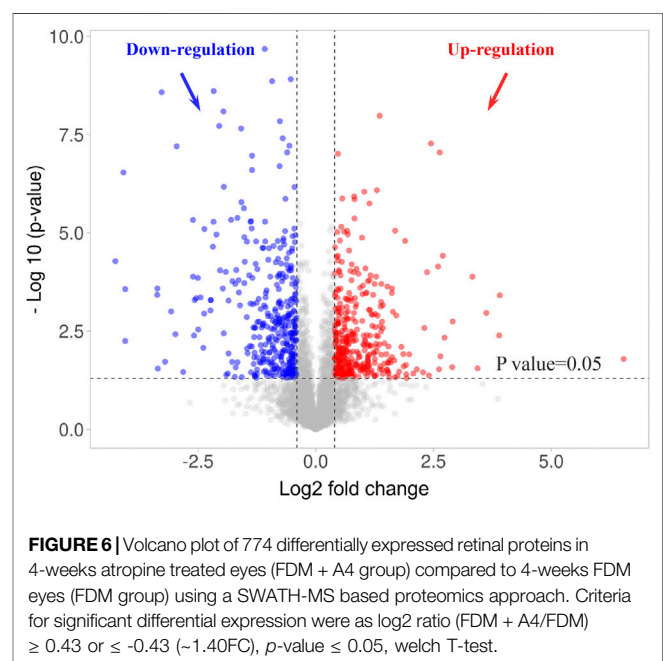
gene names. To better understand the fundamental protein functions of the comprehensive retinal proteome, GO function classification was performed again using the PANTHER ™ classification system. According to the GO analysis, the top three molecular functions of retinal proteins were binding (GO: 0005488) (41.66%), catalytic activity (GO: 0003824) (36.26%), and molecular function regulator (GO: 0098772) (9.09%) (**Figure 5A**), while the major biological processes included cellular process (GO: 0009987) (33.70%), metabolic process (GO: 0008152) (20.90%), and biological regulation (GO: 0065007) (15.00%) (**Figure 5B**).

TABLE 1 | Twenty-nine commonly regulated proteins with the same directional expression change found in the FDM + A4 group compared to the FDM group by both the iTRAQ-MS and SWATH-MS approach meeting criteria for differential expression (iTRAQ: FC ≥ 1.5 or ≤0.67, SWATH: n = 6, FC ≥ 1.4 or ≤0.71, p-value of ≤0.05, welch T-test). Red represents up-regulated proteins and blue down-regulated proteins.

NO.	Uniprot entry names	Gene name	Protein name	iTRAQ-MS		SWATH-MS	
				FDM + A2/FDM	FDM + A4/FDM	FDM + A4/FDM	p value
1	A0A286Y0L7	PKM	Pyruvate kinase	0.75	0.30	0.46	0.002
2	H0VPZ2_CAVPO	SNCA	Alpha-synuclein	0.95	0.39	0.21	0.001
3	H0UTZ2_CAVPO	MACROH2A1	Core histone macro-H2A	1.00	0.42	0.62	<0.001
4	H0WBS4_CAVPO	NUCKS1	Nuclear casein kinase and cyclin dependent kinase substrate 1	0.85	0.45	0.05	<0.001
5	H0W6L0_CAVPO	CDS2	Phosphatidate cytidylyltransferase	0.81	0.48	0.68	<0.001
6	H0W636_CAVPO	RPL13	60S ribosomal protein L13	1.67	0.49	0.53	0.021
7	H0UTH3_CAVPO	NECAP1	NECAP endocytosis associated 1	0.75	0.50	0.70	<0.001
8	A0A286XMP4_CAVPO	HNRNPD	Heterogeneous nuclear ribonucleoprotein D	0.67	0.55	0.51	0.011
9	A0A286XH94_CAVPO	GTF2I	General transcription factor Iii	0.82	0.56	0.18	<0.001
10	H0W051_CAVPO	SNCG	Gamma-synuclein	0.70	0.56	0.49	0.002
11	H0W577_CAVPO	BSG	Basigin	1.79	0.58	0.14	0.035
12	H0VRE0_CAVPO	SEC14L2	SEC14 like lipid binding 2	0.69	0.61	0.63	0.004
13	A0A286Y4P1_CAVPO	SEL1L	SEL1L adaptor subunit of ERAD E3 ubiquitin ligase	0.82	0.62	0.39	0.035
14	A0A286XH98_CAVPO	LOC100717315	Glutathione transferase	1.08	0.65	0.66	0.006
15	A0A286XWY9_CAVPO	XPNPEP1	X-prolyl aminopeptidase 1	1.13	0.66	0.71	0.002
16	A0A286XY99_CAVPO	LOC100734633	MFS domain-containing protein	0.83	0.67	0.71	<0.001
17	H0UZK2_CAVPO	SNAP25	Synaptosomal-associated protein	1.18	0.67	0.23	<0.001
18	H0UYD8_CAVPO	AP3M2	AP-3 complex subunit mu-2	0.88	1.54	1.41	0.004
19	H0UWL2_CAVPO	GSTZ1	Glutathione S-transferase zeta 1	8.24	1.58	1.55	<0.001
20	A0A286X9V5_CAVPO	ABHD11	Abhydrolase domain containing 11	0.79	2.00	1.46	0.050
21	H0W551_CAVPO	RPS19	40S ribosomal protein S19	1.06	2.01	1.39	0.002
22	A0A286XAQ3_CAVPO	TOMM22	Mitochondrial import receptor subunit TOM22 homolog	1.74	2.09	1.37	0.026
23	A0A286XTA4_CAVPO	MYEF2	Myelin expression factor 2	2.05	2.25	1.38	<0.001
24	H0VZ48_CAVPO	SERBP1	SERPINE1 mRNA binding protein 1	0.55	2.49	1.37	0.001
25	H0V3E4_CAVPO	POLR2C	RNA polymerase II subunit C	1.66	2.70	12.34	0.001
26	H0V5J3_CAVPO	PIP4K2B	PIPK domain-containing protein	3.13	3.37	1.39	<0.001
27	A0A286Y4G4_CAVPO	KRT3	Keratin 3	1.33	4.97	1.95	0.030
28	H0VFF0_CAVPO	RPS7	40S ribosomal protein S7	1.80	5.15	1.67	<0.001
29	A0A286Y0B2_CAVPO	RAB10	RAB10, member RAS oncogene family	5.97	5.81	1.56	0.001

T: treatment eyes; *C:* control eyes; *FDM:* form-deprived myopia group; *FDM + A2:* form-deprived myopia with 2-weeks atropine treatment group; *FDM + A4:* form-deprived myopia with 4-weeks atropine-treatment group.

Protein Quantitation Using Sequential Window Acquisition of all Theoretical Mass Spectra Approach

Considering the high repeatability of SWATH-MS based proteomics with a lower coefficient of variation (CV) in quantification (Collins et al., 2017) and a similar guinea pig retinal proteome study using SWATH-MS (Shan et al., 2018a), a slightly lower cut-off value was selected for this study (FDM + A4 *vs* FDM: ≥1.4 or ≤0.71 p-value of ≤0.05, welch T-test). After quantitative analysis, 774 proteins (714 gene names) were significantly changed when atropine treated eyes were compared to FDM eyes (**Supplementary Table S5**). VolcaNoseR (Goedhart and Luijsterburg, 2020) was used to generate a volcano plot, which showed the differentially expressed proteins (**Figure 6**). The fold change (FDM + A4 *vs* FDM) was converted to a log2 fold change in the x-axis, and the p-value was converted to log10 p-value in the y-axis. The details of differentially expressed proteins were shown in **Supplementary Table S5**. To better understand these significantly regulated proteins, we performed GO function classification using the PANTHER system again. Among all the mapped gene ID, the top three molecular

functions of retinal proteins were catalytic activity (GO: 0003824) (35.40%), binding (GO: 0005488) (41.70%), and molecular function regulator (GO:0098772) (9.20%) whereas cellular process (GO: 0009987) (34.70%), metabolic process (GO: 0008152) (22.00%), and biological regulation (GO:0065007) (14.10%) were the top three biological processes (**Supplementary Figure S1**).

Comparison of Commonly Regulated Proteins in the FDM + A4 and FDM Groups Using Both Approaches

Changes in protein expression in response to atropine treatment (FDM + A4 group *vs* FDM group), were observed in 50 proteins found by both the iTRAQ-MS and SWATH-MS approaches. Of these, proteins with expression regulation in the same direction by both methods were of particular interest, as they may be considered to represent the retinal response to atropine treatment during myopia progression with high confidence. As a result, 29 similarly differentially expressed proteins (12 up-regulation and 17 down-regulation) were considered highly confident targets for further analysis (**Table 1**).

TABLE 2 | Sixteen significant pathways with associated proteins were predicted by IPA from 29 differentially expressed proteins using iTRAQ and SWATH analysis. Criteria for significant pathways were as -lg (*p*-value) ≥ 1.3 (*p*-value <0.05), Fischer's exact test.

No	Ingenuity Canonical Pathways	-lg (*p*-value)	Associated gene(s) identified
1	EIF2 Signaling	2.66	RPL13, RPS19, RPS7
2	Huntington's Disease Signaling	2.38	POLR2C, SNAP25, SNCA
3	Synaptogenesis Signaling Pathway	2.25	SNAP25, SNCA, SNCG
4	Tyrosine Degradation I	2.24	GSTZ1
5	Sumoylation Pathway	2.19	SERBP1, SNCA
6	Regulation of eIF4 and p70S6K Signaling	1.74	RPS19, RPS7
7	Parkinson's Signaling	1.73	SNCA
8	Coronavirus Pathogenesis Pathway	1.63	RPS19, RPS7
9	mTOR Signaling	1.60	RPS19, RPS7
10	CDP-diacylglycerol Biosynthesis I	1.60	CDS2
11	Phosphatidylglycerol Biosynthesis II	1.56	CDS2
12	Glutathione Redox Reactions I	1.54	GSTZ1
13	D-myo-inositol (1,4,5)-Trisphosphate Biosynthesis	1.52	PIP4K2B
14	Glycolysis I	1.52	PKM
15	Glutathione-mediated Detoxification	1.42	GSTZ1
16	Nucleotide Excision Repair Pathway	1.40	POLR2C

FIGURE 7 | Protein-protein interaction analysis using IPA. Red represents up-regulated genes, and green down-regulated genes. The un-colored genes indicate additional linked proteins of this network that were not detected by the proteomics analysis. The solid lines represent a robust correlation with partner proteins, and dashed lines represent statistically significant, but less frequent correlations. The protein-protein interactions are indicated by arrows. The different shape nodes indicate different protein functions: enzymes (diamond); nuclear receptors (rectangle); transcription regulators (oval); cytokines (square); transporter (trapezoid); and others (circle).
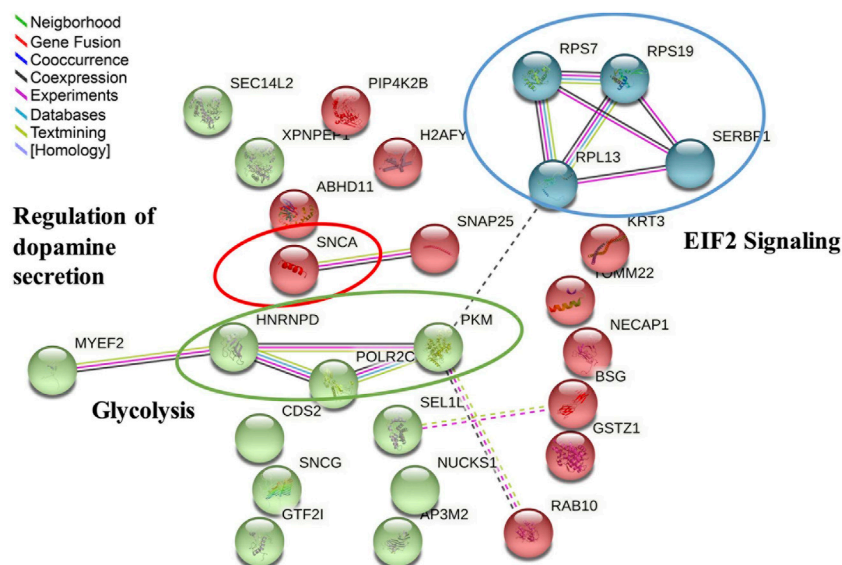
FIGURE 8 | Protein–protein interaction analysis of 29 significantly regulated proteins in response to atropine treatment found by the STRING database after kmeans clustering, including 27 matched nodes (gene names) and 14 edges (predicted functional associations). Key molecular functions are circled and named in the network analysis. The three main interaction clusters are colored in red, green, and blue after use of the K-Means clustering algorithm.

Pathways and Protein Interaction Analysis of 29 Commonly Regulated Proteins

To identify pathways for biological insights into control of ocular growth mechanisms using atropine, the common 29 proteins were uploaded to The Ingenuity Pathway Analysis (IPA) for pathway analysis. The p-value was calculated with Fischer's exact test, which reflected the likelihood that the association between a set of genes in our dataset and the canonical pathway was significant. Significant pathways were defined as p-values of less than 0.05. A total of 16 significant pathways were predicted by pathways analysis (**Table 2**). Among the significant pathways, the most significant was "EIF2 Signaling".

IPA was further used to analyze the protein-protein interactions associated with atropine treatment. The regulated proteins were highlighted in different colors (**Figure 7**). In addition, the most significant protein-protein interactions are also shown. These proteins formed a circle cluster, in which the majority of proteins were connected to Alpha-synuclein (SNCA), suggesting that SNCA may be the core candidate having a close interaction with other regulated proteins.

In addition, the same 29 commonly regulated proteins were also uploaded to the STRING online database to study protein and protein interactions. A total of 27 nodes (gene names) and 14 edges (predicted functional associations) were observed (**Figure 8**). Among enriched biological processes, the top three processes were regulation of acyl-CoA biosynthetic process (GO:0050812) (0.67% FDR), neurotransmitter uptake (GO:0001504) (1.49% FDR), and regulation of dopamine secretion (GO:0014059) (2.74%FDR). Of these, SNCA was found to be associated with all the top three processes. After the application of the kmeans clustering algorithm, the results showed three main interaction clusters, including EIF2 signaling, regulation of dopamine

secretion, and glycolysis clusters (**Figure 8**). Combining IPA and STRING analysis, SNCA was the most critical regulated protein, involved in multiple pathways and biological processes. The comparison between all the pathways enriched by IPA and interactions predicted by STRING also showed that EIF2 signaling, and glycolysis were the common significant pathways.

Alpha-Synuclein Immunoreactivity Pattern in the Retina

The SNCA expression pattern was then analyzed using immunohistochemistry in the retina of normal guinea pigs (n = 3). A similar localization of SNCA was found in all three animals. As shown in **Figures 9A–D**, high levels of SNCA (stained in green) were found in the inner margin of the inner nuclear layer (INL), and processing spreading throughout the inner plexiform layer (IPL) in the retina. Tyrosine hydroxylase (TH) is a marker for dopaminergic neurons in the central nervous system (Kastner et al., 1993). To further address the intracellular distribution of SNCA and dopamine (DA) in the guinea pig retina, double immunostainings with antibodies to α-synuclein and TH were performed. Colocalization of SNCA (green) and TH (red) was observed in some dopaminergic amacrine cells (white arrows) (**Figures 9A–D**). The negative control of staining is shown in **Figures 9E–H**.

DISCUSSION

Refractive Error and Ocular Dimensions Changes

After 2-weeks and 4-weeks FDM, relative myopic shifting of refractive errors, elongation of axial length, and vitreous chamber

FIGURE 9 | A representative immunoreactivity pattern of α-synuclein (SNCA) and Tyrosine hydroxylase (TH) in the retina of normal guinea pigs. SNCA immune-staining using green, and TH staining using red in panels of **(A–D)**. The panels of **(E–H)** represented the negative controls of staining, slide was not incubated with primary antibodies during staining. The following abbreviations were used: outer nuclear layer (ONL), ganglion cell layer (GCL), inner nuclear layer (INL), outer plexiform layer (OPL), inner plexiform layer (IPL), and outer segments (OS). Each bar equals 100 μm.

depths observed in the treated eyes were consistent with published parameters of FDM guinea pigs (Lu et al., 2006; Zhi et al., 2021). However, a larger myopic shift (−11.00 ± 0.75 D) in terms of refractive error was found in a previous study in 4-weeks FDM guinea pigs (Wu et al., 2014). This difference in outcomes may be due to the older animals included in the current study. After 2-weeks atropine treatment, less myopia was found in the FDM + A2 group (PN35 to PN49), compared to the FDM group. After a 4-weeks cumulative treatment (PN21 to PN49), notably less myopic shift was observed in the FDM + A4 group than the FDM + A2 group (2-weeks treatment), which indicated a more effective myopia retardation was achieved with a longer period of treatment. For the FDM + A4 group, relative myopic shifting of refractive errors was still observed from PN35 (2-weeks) to PN49 (4-weeks), which implied that longer FDM inducement triggered relatively higher myopia, which was consistent with published parameters from previous FDM studies (Lu et al., 2006). Comparison of the ocular parameters in the FDM + A2 and FDM + A4 groups revealed that the relative hyperopia (less myopia), and a reduced elongation of AL and VCD were found in the FDM + A4 group, which indicated that the myopia control effect of atropine was more effective with extended treatment tie in a doss dependent manner. Studies conducted on children have shown that different concentrations of atropine (low dose, 0.01%; moderate dose, >0.01% to <0.5%; and high dose, 0.5–1.0%) resulted in a slowing down of myopia from 40 to 60% (Gong et al., 2017; Zhao et al., 2020). The current study showed 1% atropine had a slowing down effect on eye growth at PN49 (2-weeks treatment)

of 35% in refraction (FDM + A2 vs FDM: - 4.55 D vs.—6.96 D) and 50% in AL (FDM + A2 vs FDM: 0.14 mm vs 0.28 mm). A considerably greater myopia control effect of 56% reduction in refraction (FDM + A4 vs FDM: -3.05 D vs. −6.95 D) and 67% in AL (FDM + A4 vs FDM: 0.09 mm vs 0.28 mm) was observed at PN49 (4-weeks treatment), which was similar to the findings reported with FDM guinea pigs using 1% atropine through peribulbar injection after 2-weeks treatment (Zhou X et al., 2020) and in children using a moderate dosage of atropine (0.05–0.5%) (Yam et al., 2019; Zhao et al., 2020).

Protein Identification and Gene Ontology Analysis

For protein identification, an approximately 3-fold more total retinal proteins were observed using SWATH-MS compared to iTRAQ-MS based proteomics. However, it is worth noting that the two approaches resulted in similar GO function classification profiles, especially for the top three functions and processes, representing proteins with high abundance. Using a similar SWATH-MS based MS platform, increases of 46 and 52% in terms of protein IDs and peptide IDs, respectively, were found in the current study, compared to a recent guinea pig retinal study published by our team without use of fractionation techniques (Bian et al., 2021). The results of the current study support the importance of generating a comprehensive spectral library or combining multiple high quality IDA files for a data-independent proteomic approach in biomarker discovery (Palmowski et al., 2019) Comparison with two recent studies of emmetropization

(Shan et al., 2018a) and LIM (Bian et al., 2021) in the retina of guinea pigs using the same SWATH approach, revealed very similar GO classification profiles. The GO function classification of retinal proteins, especially the major molecular functions and biological processes observed in our datasets, were consistent with those of previous studies in chicks (Lam et al., 2006), mice (Skeie and Mahajan, 2013), and humans (Velez et al., 2018). The results demonstrate that the overall retinal proteome and GO function classification was consistent and robust across species, regardless of optical or drug treatment.

Protein Quantitation Using iTRAQ Based Proteomics

The iTRAQ technique is widely employed in proteomic workflows requiring relative quantification for biomarker discovery (Aggarwal et al., 2006). In our iTRAQ based proteomics approach, six retinal lysates from individual animals were randomly pooled under each condition and isobaric labelled for quantitative analysis using a multiplexing approach. A similar pool design was also used in previous proteomics studies in myopic chicks vitreous (Yu et al., 2017) and the LIM mouse retina (Barathi et al., 2014). Using this effective screening design, the individual biological sample variations were reduced to individual protein abundance which was averaged within the same treated group. Also, the pooling approach greatly reduced the experimental running time and costs. In addition, more reliable quantification can be achieved across multiple conditions with reduced materials requirements. More differentially expressed proteins were found in the "FDM + A4 vs FDM group" compared to the "FDM + A2 vs FDM group", in line with the hypothesis that more significant changes could occur with a longer treatment period. Despite there being very limited reports of atropine treatment effects on the retina using high throughput omics approaches, the current study using an iTRAQ based proteomic approach found three commonly (Atp1a3, MYEF2, and Hsp90aa1) regulated proteins (FDM + A4 vs FDM group) that were also reported in a previous LIM mouse retinal study after a similar 4-weeks atropine treatment (Barathi et al., 2014). Different animal species (mouse vs guinea pig), two different paradigms of myopia models (LIM vs FDM), and different criteria for detecting differentially regulated proteins may partially account for the discrepancies between the two studies.

For two commonly upregulated proteins, Sodium/potassium-transporting ATPase subunit alpha (Atp1a3) is a catalytic component of the active enzyme, catalysing the hydrolysis of ATP coupled with the exchange of sodium and potassium ions across the plasma membrane. A previous study found a high expression of Atp1a3 in rat and mouse retinas (Wetzel et al., 1999). A recent whole-exome sequencing study reported that high expression of an ATP1A3 mutation led to cone-rod dystrophy through limiting mitochondrial reserve capacity (Zhou GH et al., 2020). Although abnormal mitochondrial function has been reported during myopia progression, ATP1A3 had not been previously implicated. Therefore, it may be speculated that up-regulation of ATP1A3 (FDM + A4 vs FDM) may retard myopia by maintaining normal mitochondrial function after atropine treatment. Further research is needed to characterize the relationship between ATP1A3 protein expression and myopia. Increased expression of Myelin Expression Factor 2 (MYEF2) was also noted after atropine treatment. MYEF2 is the transcriptional repressor of the myelin basic protein gene (MBP). Interestingly, in FDM chicks, 38% less myelinated axons were found in the retinal nerve fiber layer after 7-days FDM inducement compared to untreated eyes by means of immunohistochemical labelling against myelin basic protein (Swiatczak et al., 2019). Hence, it can be speculated that the increased expression of MYEF2 after atropine treatment could inhibit the expression of MBP, leading to a similar result to that seen in FDM chicks. Furthermore, MYEF2 is sensitive to FDM, but not to the atropine treatment. Further studies are needed to determine if MYEF2 is sensitive to LIM. The downregulated protein, Heat Shock Protein 90 Alpha Family Class A Member 1(Hsp90aa1) is a subtype of Heat shock protein 90 (HSP90) and acts as a molecular chaperone that catalyses protein folding and maintains "quality control" for a large number of "client" proteins. Although its relationship to myopia is not readily apparent from these functions, a prior study suggested that HSP90 could upregulate the expression of Hypoxia Inducible Factor 1 Subunit Alpha (HIF1α) in senescent ARPE-19 cells and subsequently promote the induction of distinct inflammatory factors (Chen et al., 2021). A previous myopia study also reported upregulation of HIF-1α in the myopic sclera of both mice and guinea pigs (Wu H et al., 2018). Collectively, despite the lack of direct evidence, reports suggest that increased levels of HIFα may contribute to myopia development. The downregulation of Hsp90aa1 after atropine treatment may reduce HIF1α, thereby slowing down myopia progression.

Protein Quantitation Using Sequential Window Acquisition of all Theoretical Mass Spectra Based Proteomics

To minimize potential false-positive findings due to the pooling strategy used in the iTRAQ screening approach, a new batch of retinal protein lysates from the FDM and FDM + A4 groups were selected for SWATH-MS based proteomics (n = 6) as more significant retarding effects in terms of biometric changes as well as more protein changes were observed with this technique than with the iTRAQ approach. Based on the filtering criteria (FC ≥ 1.4 or ≤0.71, p-value of ≤0.05, welch T-test), approximately 770 differentially expressed proteins were detected in FDM + A4 compared to FDM groups. This approach for identifying differentially expressed retinal proteins in the guinea pig FDM model has not been published previously. Only one iTRAQ-based proteomic study using the LIM mouse after 1% atropine treatment (Barathi et al., 2014), and two mRNA expression studies after 100 μM atropine-treated human scleral fibroblasts (Hsiao et al., 2019) and very low dose atropine (0.003%) treatment on corneal epithelial cells (Chang et al., 2019), respectively, have been reported. Specifically, fifteen altered proteins were identified in both studies using the SWATH approach and the previously reported LIM mouse study using

iTRAQ-based proteomics. Interestingly, despite the differences in ocular tissues and omics techniques, three (PTPRK, PSMC4, and CIT) commonly regulated proteins were also noted in the transcriptomic study using corneal epithelial cells when compared to those observed in the current study. However, the study of human scleral fibroblast did not show the details of 389 differentially expressed genes with at least a 2.0-fold change. Therefore, no comparison could be performed.

Pathway and Protein Interaction Analysis of 29 Commonly Regulated Proteins in iTRAQ and Sequential Window Acquisition of all Theoretical Mass Spectra Based Proteomics

By combining iTRAQ-MS and SWATH-MS proteomic approaches, 29 highly confident proteins (at 1% FDR with quantification of at least 2 peptides per protein) were found consistently regulated in response to atropine treatment in the same expression direction. Novel bioinformatics tools were employed for providing molecular insights at systems level. According to the IPA analysis results (**Table 2**), eukaryotic initiation factor 2 (EIF2) signaling was found to be the most significant pathway, which was supported by clustering by STRING (**Figure 6**). In previous myopia studies, decreased eukaryotic translation initiation factor 1A was found in the 4-days LIM guinea pig retina (Wu Y et al., 2018). In addition, reduced eukaryotic translation initiation factor 3 subunit 2 beta was identified 7-weeks FDM guinea pig sclera (Zhou et al., 2010). A recent retinal gene-expression study also revealed an association of EIF2 pathway activation with baseline refraction and susceptibility to FDM across eight different strains of mice (Tkatchenko et al., 2019). They reported that negative refractive errors were associated with activation of the EIF2 signaling pathway, and increased susceptibility to FDM was associated with the suppression of EIF2 signaling. Of the three associated down-regulated proteins involved in the EIF2 pathway identified by the current study (**Table 2**), **60S ribosomal protein L13 (RPL13)** is a large ribonucleoprotein complex responsible for synthesizing proteins in the cell. It has not been previously reported in myopia studies. One study has reported that the DNA methylation changes of RPL13 were associated with the onset of Alzheimer's disease (AD) (De Jager et al., 2014). In contrast, **40S ribosomal protein S19 (RPS19)** and **40S ribosomal protein S7 (RPS7)** were found up-regulated after atropine treatment in our dataset. They belong to the RPS family, which are components of the ribosome and plays a vital role in controlling translation and cellular homeostasis (Kondrashov et al., 2011). A previous study reported that eIF2A stimulated the initiator methionyl-tRNAi (Met-tRNAMeti) by binding to 40S ribosomal subunits in mouse (Golovko et al., 2016). Therefore, there may be a similar mechanism in guinea pigs. The up-regulation of RPS19 and RPS7 may indicate the activation of the EIF2 pathway after atropine treatment, which then decreases susceptibility to FDM.

Previous studies have confirmed the vital role of another pathway revealed by the STRING analysis (**Figure 6**):

glycolysis in the myopic mouse retina (Barathi et al., 2014) and myopic/recovery tree shrew sclera (Frost and Norton, 2012). The roles of three down-regulated proteins observed in atropine control of myopia are also involved in glycolysis. **Pyruvate kinase (PKM)** plays a vital role in glycolysis, as it can catalyze the transfer of a phosphoryl group from phosphoenolpyruvate to ADP, generating ATP and pyruvate. In a cancer study, the increased regulation of PKM2 suggested enhanced glycolysis for tumor cells *in vivo* (Christofk et al., 2008). In addition, an increased level of PKM2 was also reported in chick retina study which compared LIM to LIH (Yu et al., 2020). The current study also found a decreased level of PKM in atropine-treated FDM guinea pigs, confirming the vital role of PKM in both LIM and FDM animal models. Hence, as a cancer study revealed down-regulation PKM, this may indicate that atropine could diminish glycolysis during myopia progression. Another associated protein, **Heterogeneous nuclear ribonucleoprotein D (HNRNPD)** was also found to be significantly decreased after atropine treatment. Heterogeneous nuclear ribonucleoproteins (hnRNPs) represent a large family of RNA-binding proteins. (Zhang et al., 2018). No previous report has implicated HNRNPD in myopia development. A cancer study reported depletion of hnRNPA1 and hnRNPA2 resulted in a concomitant decrease of PKM2 mRNA in Hela and 293 cells (David et al., 2010). Therefore, decreased HNRNPD observed in the current study may also lead to the downregulation of PKM in retinal cells. Retinal glycolysis pathways were recently found to be implicated in the LIM chick myopia model (Yu et al., 2020). Therefore, the effect of atropine on retinal glycolysis should be further explored. Among other isolated candidate proteins, **Basigin (BSG)** is an interesting target worth mentioning. It is a transmembrane protein explicitly expressed by photoreceptors and essential for normal retinal maturation and development. *BSG* mutation has been implicated in early-onset high myopia and predisposed typical myopic phenotypes in human and mutant mice through a trio-based exonic screening study (Jin et al., 2017). Additionally, two previous studies showed that deficiency of this gene led to defective function and photoreceptor degeneration in the retina of mouse (Philp et al., 2003) and mice (Chen et al., 2004). Although the deficiency is different from protein expression changes, BSG was also involved in the binding of rod-derived cone viability factor to the glucose transporter GLUT1, which increases glucose influx into cone photoreceptors. The increased glucose promotes cone survival by stimulation of aerobic glycolysis (Aït-Ali et al., 2015). This evidence implies that the retina may be a target tissue in response to atropine treatment through regulating *BSG* expression. Overall, down-regulation of *PKM, HNRNPD,* and *BSG* may indicate reduced glycolysis in the retina after atropine treatment, which indirectly inhibits accelerated ocular elongation.

Another key molecule found responsive to atropine treatment is Dopamine (DA), which is a neurotransmitter in the retina produced in amacrine cells. DA has long been suggested as a stop signal in myopia research. The retinal DA level was decreased in FDM animal models, including in chicks (Stone et al., 1989), rhesus monkeys (Iuvone et al., 1989), guinea pigs (Mao et al.,

2011), and tree shrew (McBrien et al., 2001). A reduced retinal DA level was also found in LIM chicks (Guo et al., 1995). Furthermore, an increasing DA level was reported to prevent FDM in guinea pigs (Mao et al., 2010; Dong et al., 2011), mice (Yan et al., 2015), rabbits (Gao et al., 2006), and monkeys (Iuvone et al., 1991). In addition, a previous study suggested that an intravitreal injection of atropine increased dopamine release and the concentration of its metabolite DOPAC in the chick retina (Schwahn et al., 2000). Recent research also suggested that the metabolism of dopamine was changed by the action of the dysregulated genes after 100 μM atropine-treated human scleral fibroblasts (Hsiao et al., 2019). The findings of these studies confirm the potential association between DA and atropine found in our study. Overall, previous studies had revealed dopamine alteration was involved in myopia development and the common anti-myopic effects of atropine treatment in different species and tissues.

Among the commonly regulated proteins, Alpha-synuclein (SNCA) was identified as the most interesting and novel protein involved in atropine treatment. This protein is involved in multiple pathways and connected with other regulated proteins in the study (**Figure 5**). SNCA has been reported as a neuronal protein that plays several roles in synaptic activity, such as regulating synaptic vesicle trafficking and subsequent neurotransmitter release. However, SNCA has not been previously implicated in myopia development using conventional molecular approaches. It was considered as a possible biomarker for Parkinson's disease in human cerebrospinal fluid, plasma, or serum (Hong et al., 2010). It has previously been demonstrated that over-expression of SNCA could directly lead to apoptosis of dopamine neurons and then reduce the striatal DA level in rat primary culture, immortalized mesencephalon-derived cells (Zhou et al., 2000) and transgenic mice (Tofaris et al., 2006). A knockout mice study revealed that SNCA is an essential presynaptic, activity-dependent negative regulator of DA neurotransmission (Abeliovich et al., 2000). Remarkably, the over-expression level of SNCA (up-regulation, 1.92-fold) was comparable to the FDM control group based on iTRAQ-MS based proteomics data. In contrast, a reduced level of SNCA (down-regulation, 0.21-fold, $p < 0.001$) was found after atropine treatment using both approaches. Therefore, our results suggest the involvement of dopamine signaling in the anti-myopic effects of atropine in guinea pig eyes. However, further study is needed to investigate the SNCA effect on inhibiting the apoptosis of dopamine neurons or prompting their secretion.

Based on the immunohistochemistry (IHC) of SNCA and tyrosine hydroxylase (TH), similar patterns of distribution of SNCA in the INL and IPL were reported in the retinas of macaque (Martínez-Navarrete et al., 2007) and humans (Surguchov et al., 2001; Martínez-Navarrete et al., 2007). In addition, the same study (Martínez-Navarrete et al., 2007) also found colocalization of SNCA and glycine in amacrine cells of rat and rabbit retinas. In addition, studies have revealed localization of TH in amacrine cells in the retinas of rabbits (Brecha et al., 1984), rats (Debertin et al., 2015), and humans (Crooks and Kolb, 1992)., DA is released mainly in a paracrine manner by a population of

tyrosine hydroxylase expressing (TH+) amacrine cells (AC) of the mammalian retina (Debertin et al., 2015). Taken together, our results allow us to postulate an interaction of SNCA and DA secretion through TH in amacrine cells, which deserves further study.

Of the newly discovered proteins to be differentially expressed in response to atropine treatment, a decrease (down-regulation, 0.82-FC) of Mitochondrial import receptor subunit TOM22 homolog (TOMM22) was observed in the myopic retina, and the increased expression change (up-regulation, 1.4-FC, $p < 0.05$) was found after atropine treatment. *TOMM2* was associated with mitochondrial dysfunction. It is a central receptor component of the translocase of the outer membrane of mitochondria (TOM complex) and is responsible for the recognition and translocation of cytosolically synthesized mitochondrial preproteins. *TOMM22* has not been previously implicated in myopia development. However, a recent paper showed that yeast mitochondrial accumulation of amyloid β (Aβ) peptides requires *TOMM22* as the main Aβ receptor (Hu et al., 2018). Although abnormal mitochondrial function has been reported during myopia progression, amyloid β (Aβ) peptides and TOMM22 have not been previously implicated (Wojciechowski, 2011). One recent RNA seq study also reported increased mitochondrial metabolism was found in chicks 24 h after 7-days FDM chicks, which explained why dark-adapted (low temporal luminance modulation) retinae require ~ 20% more metabolic activity than the same light-adapted retina (Vocale et al., 2021). Therefore, our finding also highlighted the importance of characterizing the relationship between mitochondrial cascades and the anti-myopic effects of atropine.

The main limitation of this study was the use of sample pooling for the iTRAQ-MS proteomic approach, potentially increasing the risk for false-positive findings (e.g., by outlier effects). However, this risk was mitigated via SWTAH-MS proteomic analysis with individual biological samples ($n = 6$), which required differentially expressed proteins to be identified in consistent directional regulation of both proteomic analyses with significance in SWATH-MS proteomic analysis. The study also yielded technical comparisons of iTRAQ-MS and SWATH-MS based proteomics. Eight samples can be analyzed in one experiment using iTRAQ (Ross et al., 2004). After labeling, eight labels were combined and injected into MS together and analyzed simultaneously in DDA, which reduced the run-to-run variation and analysis time. Similar behavior of peptides, including retention time, the efficiency of ion, and response to electron spray ionization (ESI), has been observed (Xie et al., 2011). However, the limitations of DDA are bias of under-sampling low abundance precursor ions (Stahl et al., 1996), the potential difference in labeling efficiencies, and digestion effects (Elliott et al., 2009), which may contribute to fewer proteins being identified using iTRAQ. As SWATH-MS is a specific variant of the DIA method (Ludwig et al., 2018). All the peptides are fragmented in MS/MS, regardless of peptide intensity (Chapman et al., 2014). As a result, compared with DDA, data reproducibility between technical replicates is increased, and low abundance precursors are better represented (Geromanos et al., 2009). Hence, the total number

of proteins identified was three times higher using compared iTRAQ-MS based proteomics.

For SWATH-MS proteomics, fewer procedures are required without the need for the labeling of peptides. In addition, there is no limitation of the total sample number. Once the peptides are prepared, they are injected into LC-MS for analysis, and each sample runs individually. Therefore, a large number of biological samples can be analyzed by this more straightforward approach (Wasinger et al., 2013).

One of the most interesting, regulated proteins, the localization of SNCA was confirmed in the current study. Further validation experiments are needed to confirm the protein changes of SNCA, PKM, and BSG related to the atropine treatment in FDM guinea pigs. Based on our integrated label and label-free proteomics analysis, more targeted and specific pathways were identified for the first time in the FDM guinea pig retina in response to atropine treatment. Our established protocols confirmed the feasibility of applying high throughput proteomics for investigating novel mechanisms in the therapeutic treatment of myopia. Similar studies should be performed in the FDM or LIM guinea pig retina using a low dosage of atropine (0.01,0.05, and 0.1%) in the future to determine if common regulatory mechanisms could be repeated in different myopia paradigms and different dosages being used in human myopia control (Chia et al., 2012; Yam et al., 2019). In addition to analyzing retinal tissue, this combined iTRAQ-MS and SWTAH-MS proteomics approach can also be used to investigate potential protein signals in other ocular structures from the vitreous to the sclera for much more complete identification and quantitation of biomarkers and pathways at the posterior eyes in response to atropine treatment during myopia progression.

MATERIALS AND METHODS

Animals

Pigmented Guinea pigs (*Cavia porcellus,* the English short-hair stock, Danyang Changyi Experimental Animal Center Co., Ltd., China) were raised with their mother till postnatal day 18 (PN 18). All treatment and care of animals complied with the ARVO Statement, and the protocol for handling animals was in accordance with NIH Guidelines. The experimental period started from postnatal 3 weeks (PN 21) to 7 weeks (PN 49). The FDM model was established based on a published protocol (Lu et al., 2006). Guinea pigs were raised in standard cages (65 × 45 × 20 cm) at 25°C with sufficient food, water, and fresh vegetables daily. With lights on 8:00 AM, the 12 h:12 h light/dark cycle was controlled by straight fluorescent lamps, and the central ambient luminance over the cages was maintained around 300 lux. Animals were randomly assigned to four groups, including normal control group (NC, $n = 7$), monocular form-deprivation myopia group (FDM, $n = 7$), FDM with 2-weeks atropine-treatment group (FDM + A2, $n = 7$), and FDM with 4-weeks atropine-treatment group (FDM + A4, $n = 8$). For the NC animals, both eyes were exposed naturally without any lens attachment; For the FDM group, either the right or left eye was randomly covered by a white latex facemask, leaving the

contralateral eye, nose, mouth, and ears freely exposed from PN 21 to PN 49 (4 weeks FDM). In the atropine treatment groups, 10 g L^{-1} atropine gel (Xingqi Pharmaceutical Co. Ltd., China) was topically administered to the FDM eyes from PN35 to PN49 (FDM + A2 group, 2 weeks drug treatment) and from PN21 to PN49 (FDM + A4 group, 4 weeks drug treatment), respectively. Body weight and ocular biometrics were recorded at PN21, PN35, and PN49. For iTRAQ-MS based proteomics study, retinas from all twenty-nine guinea pigs were collected at PN49 (**Figure 8**). For SWATH-MS based proteomics study, retinas of another cohort of twelve guinea pigs (FDM group: $n = 6$, FDM + A4 group: $n = 6$) were also harvested at PN49 after 4 weeks treatment.

Ocular Biometric Measurements

The steak retinoscopy (66 vision. Tech, China) and A-scan ultrasonography (KN 1800, Kangning Medical electronic equipment development company, China) were used to measure refractive error and ocular dimensions, respectively. 0.5% Compound Tropicamide (Xingqi Pharmaceutical Co. Ltd., China) was used to paralyze the ciliary muscle and dilate the pupil. The refractive error was recorded as the average of 3 repeated measurements of spherical equivalent (SE), which is calibrated by the sum of spherical value and half of the cylindrical value. 0.4% Qxybuprocaine Hydrochloride (Santen Pharmaceutical Co. Ltd., Japan) was used for corneal anesthesia to reduce the discomfort of animals from the ultrasonic probe. The axial length (AL), anterior chamber depth (ACD), lens thickness (LT), vitreous chamber depth (VCD) was obtained by A-scan, which were averaged from 10 repeated measurements. All the measurements were performed by the same optometrist. The facemask was re-attached immediately after measurements.

Retinal Harvest and Protein Extraction

Guinea pigs were sacrificed at PN49 by cervical dislocation. The anterior segment, crystalline lens, and vitreous from the eye cup were removed, the retina was carefully peeled off from the posterior hemisphere without retinal pigment epithelium within 5 min as previously reported (Anjo et al., 2017). Two kinds of lysis buffer were included in this study to extract protein from retinal tissue. For the iTRAQ approach, 200 μl of Nitroextra (9 M Urea, SDS, Tritone X, and Protease inhibitors) was added into each frozen tissue. Samples were pooled and blended with sonication for 5 min. For the SWATH approach, collected retinal tissues were homogenized using liquid nitrogen-cooled Precellys® Evolution homogenizer (Bertin Technologies) with 200 μl of customized SDS lysis buffer (5%SDS, 50 mM TEAB, pH7.55) at 5,800 rpm for 120 s at 4°C. The recovered retinal lysates were then centrifuged at 21,380 × g for 30 min at 4°C, followed by collecting and storing the supernatant in a new tube at −80°C until further analysis. The total protein concentration was measured by Pierce™ Rapid Gold BCA protein assay (Thermo Fisher Scientific, United States) according to the manufacturer's protocol.

Protein Digestion and iTRAQ Labeling

Protein was cleaned up by pre-cooled acetone (320110, Sigma) and incubating at −20°C overnight. Then the protein pellet was

washed with pre-cooled acetone and dried in a biosafety cabinet. Proteins were resuspended in 8 M urea and reduced with 20 mM dithiothreitol (DTT) at 60°C for 1 h, then alkylated with 40 mM iodoacetamide at room temperature for 30 min protected from light. Samples were diluted to 2 M urea and digested with trypsin in a 1:100 (w: w) ratio at 37°C overnight. Approximately 100 µg aliquots of pooled desalted peptides from each experimental condition were chemically labeled with iTRAQ 8-plex reagent (4466096, SCIEX) in 100 mM TEAB. Labels were arranged as follows: 113: right eyes of NC; 114: left eyes of NC; 115: fellow control eyes of FDM + A2; 116: treated eyes of FDM + A2; 117: fellow control eyes of FDM + A4; 118: treated eyes of FDM + A4, 119: fellow control eyes of FDM; 121: treated eyes of FDM (Left panel in **Figure 3**). After the labeling reaction at room temperature for 2 h, all the labeled samples were cleaned up by C18 desalting. Differentially labeled peptide samples were resuspended in buffer A (10 mM KH2PO4, 20% acetonitrile (ACN), pH2.7). SCX chromatography was performed with a Poly SULFOETHY A™ (200 × 4.6 mm, 200 A) column using step gradients (0–10 min: 0%B, 29 min: 15%B, 44 min: 45%B, 46–53 min: 100%B) of Buffer A and B (10 mM KH2PO3, 20% ACN, 0.6 M KCl, pH2.7) and a flow rate of 1 min/ml. Fifty-three fractions in total were collected. Samples were further combined into five fractions based on the number of proteins identified in each 10 min fraction. Each fraction was desalted with ZipTip (Cat. ZTC18S960, Millipore) and dried in a spin vacuum for further LC-MS/MS analysis.

LC-MS/MS Analysis for iTRAQ

The dried peptide was dissolved in 0.1% formic acid (FA). About 3 µg peptides were analyzed by Eksigent ekspert™ nanoLC 425 system coupled to a TripleTOF 6,600 System (SCIEX, MA, United States). The peptides were trapped (ChromXP nanoLC Trap column 350 µm × 0.5 mm, ChromXP C18 3 µm) and eluted at a flow rate of 300 nL/min into a reverse phase C18 column using a linear gradient of ACN (3–36%) in 0.1% FA with a total run time of 120 min. The tandem mass spectra were recorded in positive-ion and "high-sensitivity" mode with a resolution of ~35,000 full-width half-maximum. Advanced DDA was used for MS/MS collection on the Triple TOF 6600 to obtain MS/MS spectra for the 20 most abundant and multiply charged ($z = 2, 3$, or 4) following each survey MS1 scan, allowing typically for 250 msec acquisition time per each MS/MS. After 2 repetitive occurrences, the dynamic exclusion was set for 30 s.

Protein Digestion in Sequential Window Acquisition of all Theoretical Mass Spectra Analysis

Proteins were digested as described recently for the mouse retina (Sze et al., 2021). In brief, a total of 50 µg proteins were reduced with DTT for 10 min, then alkylated with IAA at room temperature for 10 min with protection from light. The alkylation reaction was quenched by adding 0.2% phosphoric acid. Samples were added to the S-Trap protein binding buffer, and proteins were trapped by a filter in the S-Trap Micro Spin Column (Protifi, United States) (HaileMariam et al., 2018). After

trypsin (Promega, United States) digestion, the peptides were resuspended with 0.1% FA for LC-MS/MS analysis (calibrated at 0.5 µg/µl) using Pierce Quantitative Colorimetric Peptide Assay (Thermo Fisher Scientific, United States).

Both DDA and SWATH-MS analyses were performed by the TripleTOF 6,600 system (SCIEX, MA, United States) connected to an Eksigent ekspert™ nanoLC415 system similar to our previous protocols (Shan et al., 2018b; Cheung et al., 2020; Bian et al., 2021). For either IDA or SWATH acquisitions, 2 µg peptide was loaded to a trap column (100 µm × 2 cm, C18) for 15 min. Then, it was separated on a nano-LC column (100 µm × 30 cm, C18, 5 µm). An isolation of 100 Variable windows was selected in a looped mode over the full mass range of 100–1800 m/z scan in SWATH acquisition.

Ion Library Generation for Sequential Window Acquisition of all Theoretical Analysis

Peptides from 12 guinea pigs (FDM and FDM + A4 groups, $n = 6$ per group) were pooled together and then divided into six fractions using Pierce™ High pH Reversed-Phase peptide fractionation kit (84868, Thermo Scientific, United States). Six separate IDA injections were combined to generate an ion library (.group file) for SWATH analysis. It was searched against the guinea pig Uniprot database in ProteinPilot™ (v5.0, SCIEX, MA, United States) software utilizing the Paragon algorithms with the following parameters, identification as sample type, iodoacetamide as Cys alkylation, trypsin digestion, thorough search effort, and with FDR analysis activated. The resulting group file was used as the ion library file for all SWATH files processing and quantification.

Sequential Window Acquisition of all Theoretical Mass Spectra Acquisitions and Processing

Two micrograms (2 µg) of all 24 biological samples (both eyes of FDM group and FDM + A4 group) with two technical replicates each were injected for SWATH-MS quantification. The generated raw data (.wiff) were processed with PeakView (V2.2, SCIEX, MA, United States) to extract relevant transitions of each identified peptide/protein using the generated combined ion library. Fifteen peptides with high signal/noise ratios were selected for retention time calibration. The resulting data were exported to MarkerView (V1.3.1, SCIEX, MA, United States) for normalization using the MLR method (Lambert et al., 2013), followed by statistical analysis.

Bioinformatics Analysis and Pathway Analysis for Differentially Expressed Proteins

The Universal Protein Resource online database (UniProt, http://www.uniprot.org/, 9-March-2020) was used to convert protein names to gene names. Functional analysis of Gene Ontology (GO) annotations of identified retinal proteins was performed

using the PANTHER gene classification analysis software (PANTHER™ version 15.0, http://pantherdb.org/, 9-March-2020) (Mi et al., 2019). The STRING v11.0 (https://string-db.org/,13- July -2021) database was used to analyze the protein interaction of commonly regulated proteins by two approaches (Szklarczyk et al., 2019). The Ingenuity Pathway Analysis (IPA, Ingenuity Systems, Mountain View, CA, United States, 6—July—2021) was used for pathway analysis (Guerra, 2008).

Immunohistochemistry and Confocal Imaging

Guinea pigs were sacrificed by cervical dissection. After removing muscle and anterior segments of the eye, eyecup was fixed using 4% paraformaldehyde (P0099, Beyotime, China) for 0.5 h, followed by impregnating using 10% sucrose in PBS for 2 h, 20% sucrose for 2 h, and then 30% sucrose for 15 h, and finally embedding into Optimal Cutting Temperature (OCT) compound to freeze immediately with liquid nitrogen. The embedded tissue was sectioned into 10 μm thickness for immunofluorescence analysis. Retina slides were blocked with QuickBlock™ solution (P0260, Beyotime, China) for 1 h, then the primary antibodies (Mice anti-SNCA, 1:500, AHB0261, Invitrogen, United States; Rabbit anti TH, 1:1,000, AB152, Sigma-Aldrich, United States) were diluted with a blocking solution (P0262, Beyotime, China) and used to incubate retinas for 16 h at 4°C. After incubating and rinsing, secondary antibodies conjugated to Goat anti-Rabbit-Cy3 (1:1,000, A0516, Beyotime, China) and Goat anti-Mice-Alexa Fluor 488 (1:1,000, ab150113, Abcam, United States) were applied for 2 h at room temperature. Zeiss LSM800 (Carl Zeiss, Germany) and a confocal microscope was used to take micrographs at 10 × 20 fold.

Statistical Analysis

The biometric parameters in the normal control group, FDM group, FDM + A2 group, and FDM + A4 group were analyzed using Two-way mixed design ANOVA with Bonferroni multiple comparisons as previously reported (Kang et al., 2018) using the R program (v4.0.5, Shake and Throw) (Mair et al., 2015). The inter-group differences were defined as significant at $p < 0.05$ and highly significant at $p < 0.01$. ProteinPilot™ (v5.0, SCIEX, MA, United States) was used for iTRAQ analysis. The error tolerance for precursor mass was 15.0 ppm and fragment ion 0.2 Da. To identify the proteins with the most robust differential expression using iTRAQ based proteomics, the criteria of differentially expressed proteins had to fulfill the following criteria: 1) Proteins had an expression fold change (FDM + A2 vs FDM or FDM + A4 vs FDM) ≥1.5 or ≤0.67; 2) Proteins had a 1% FDR with at least 1 peptide with 95% confidence identified. Considering the high repeatability of SWATH-MS based proteomics (Collins et al., 2017), filtering criteria in SWATH-MS [proteins with fold change (FDM + A4 vs FDM) ≥1.4 or ≤0.71, p-value of ≤0.05, welch T-test) to determine significant regulation was lower than the cut-off threshold of

the iTRAQ-MS approach, the cut-off threshold was the same as described in our previous published paper of guinea pig retina using the same approach (Shan et al., 2018a).

CONCLUSIONS

In summary, the guinea pig model for FDM was successfully established with documentation of biometric parameter changes under our experimental conditions. In addition, the inhibitory effect of 1% atropine on FDM progression was also observed at two treatment time points. This study built the first FDM guinea pig retina proteome covering myopia development and atropine treatment with the largest high quality retinal proteome with 5,961 proteins (51,871 peptides) reported to date. Using iTRAQ-MS based proteomics for multiplex screening, hundreds of differential protein expressions were identified and quantified. Combining our established SWATH-MS protocol for orthogonal validation, 29 commonly regulated proteins were highlighted as promising targets in response to effective atropine treatment for the first time. In addition, the potential biological pathways involved in the anti-myopic effects of atropine were screened through index proteins, including EIF2 signaling, glycolysis, and regulation of dopamine. The localization of a key retinal protein (SNCA), which could play an important role involve in anti-myopic treatment of atropine, was further confirmed. In addition, other differentially expressed proteins explored in this study may have pivotal roles in the development of FDM and may be responsive to the atropine myopia control treatment. However, whether low dose Atropine (0.1%) treatment shares similar molecular pathways warrants further investigation. In conclusion, the present work has demonstrated the feasibility of using a combined iTRAQ-MS and SWATH-MS proteomic approach for exploring ocular drug treatment effects in a high-throughput manner.

DATA AVILAIBILITY STATEMENT

The raw data presented in this study are available on PeptideAtlas public repository (Zhao et al., 2020) with the accession number of PASS01507 for open access (http://www.peptideatlas.org/).

ETHICS STATEMENT

The animal study was reviewed and approved by Tianjin Medical University (# TJYY2020111028, the effect of atropine in form deprivation myopia).

AUTHOR CONTRIBUTIONS

Conceptualization, TL, RW, and CT; protein methodology, JB, Y-Zh and KL; animal model, BG, DL, QW and XJ; IHC validation, Y-Zh.; investigation, TL, JB, KL and FY; resources,

RW and TL; writing-original draft preparation, TL, JB, Y-Zh, and DL; writing-review and editing, TL and RW; supervision, TL, CT, CS-YL, RW and HN; project administration, TL and RW; funding acquisition, TL, RW, and HZ. All authors have read and agreed to the published version of the manuscript.

SUPPLEMENTARY MATERIAL

The Supplementary Material for this article can be found online at: https://www.frontiersin.org/articles/10.3389/fphar.2022.814814/full#supplementary-material

REFERENCES

Abeliovich, A., Schmitz, Y., Fariñas, I., Choi-Lundberg, D., Ho, W. H., Castillo, P. E., et al. (2000). Mice Lacking Alpha-Synuclein Display Functional Deficits in the Nigrostriatal Dopamine System. *Neuron* 25 (1), 239–252. doi:10.1016/s0896-6273(00)80886-7

Aggarwal, K., Choe, L. H., and Lee, K. H. (2006). Shotgun Proteomics Using the iTRAQ Isobaric Tags. *Brief. Funct. Genomic Proteomic* 5 (2), 112–120. doi:10.1093/bfgp/ell018

Aït-Ali, N., Fridlich, R., Millet-Puel, G., Clérin, E., Delalande, F., Jaillard, C., et al. (2015). Rod-Derived Cone Viability Factor Promotes Cone Survival by Stimulating Aerobic Glycolysis. *Cell* 161 (4), 817–832. doi:10.1016/j.cell.2015.03.023

Anjo, S. I., Santa, C., and Manadas, B. (2017). SWATH-MS as a Tool for Biomarker Discovery: From Basic Research to Clinical Applications. *Proteomics* 17 (3-4). doi:10.1002/pmic.201600278

Barathi, V. A., Chaurasia, S. S., Poidinger, M., Koh, S. K., Tian, D., Ho, C., et al. (2014). Involvement of GABA Transporters in Atropine-Treated Myopic Retina as Revealed by iTRAQ Quantitative Proteomics. *J. Proteome Res.* 13 (11), 4647–4658. doi:10.1021/pr500558y

Bian, J., Sze, Y.-H., Tse, D. Y.-Y., To, C.-H., McFadden, S. A., Lam, C. S.-Y., et al. (2021). SWATH Based Quantitative Proteomics Reveals Significant Lipid Metabolism in Early Myopic Guinea Pig Retina. *Int. J. Mol. Sci.* 22 (9), 4721. doi:10.3390/ijms22094721

Brecha, N. C., Oyster, C. W., and Takahashi, E. S. (1984). Identification and Characterization of Tyrosine Hydroxylase Immunoreactive Amacrine Cells. *Invest. Ophthalmol. Vis. Sci.* 25 (1), 66–70.

Brown, L. M. (2014). Quantitative Shotgun Proteomics with Data-independent Acquisition and Traveling Wave Ion Mobility Spectrometry: a Versatile Tool in the Life Sciences. *Adv. Exp. Med. Biol.* 806, 79–91. doi:10.1007/978-3-319-06068-2_4

Chang, W. A., Hsiao, Y. T., Lin, H. C., Jian, S. F., Chen, Y. J., and Kuo, P. L. (2019). Deduction of Novel Genes Potentially Involved in the Effects of Very Low Dose Atropine (0.003%) Treatment on Corneal Epithelial Cells Using Next-Generation Sequencing and Bioinformatics Approaches. *Medicina (Kaunas)* 55 (9), 589. doi:10.3390/medicina55090589

Chapman, J. D., Goodlett, D. R., and Masselon, C. D. (2014). Multiplexed and Data-independent Tandem Mass Spectrometry for Global Proteome Profiling. *Mass. Spectrom. Rev.* 33 (6), 452–470. doi:10.1002/mas.21400

Chen, S., Kadomatsu, K., Kondo, M., Toyama, Y., Toshimori, K., Ueno, S., et al. (2004). Effects of Flanking Genes on the Phenotypes of Mice Deficient in basigin/CD147. *Biochem. Biophys. Res. Commun.* 324 (1), 147–153. doi:10.1016/j.bbrc.2004.08.232

Chen, D. D., Peng, X., Wang, Y., Jiang, M., Xue, M., Shang, G., et al. (2021). HSP90 Acts as a Senomorphic Target in Senescent Retinal Pigmental Epithelial Cells. *Aging (Albany NY)* 13, 21547–21570. doi:10.18632/aging.203496

Cheung, J. K., Li, K. K., Zhou, L., To, C. H., and Lam, T. C. (2020). Data on Protein Changes of Chick Vitreous during normal Eye Growth Using Data-independent Acquisition (SWATH-MS). *Data Brief* 30, 105576. doi:10.1016/j.dib.2020.105576

Chia, A., Chua, W. H., Cheung, Y. B., Wong, W. L., Lingham, A., Fong, A., et al. (2012). Atropine for the Treatment of Childhood Myopia: Safety and Efficacy of 0.5%, 0.1%, and 0.01% Doses (Atropine for the Treatment of Myopia 2). *Ophthalmology* 119 (2), 347–354. doi:10.1016/j.ophtha.2011.07.031

Chia, A., Lu, Q. S., and Tan, D. (2016). Five-Year Clinical Trial on Atropine for the Treatment of Myopia 2: Myopia Control with Atropine 0.01% Eyedrops. *Ophthalmology* 123 (2), 391–399. doi:10.1016/j.ophtha.2015.07.004

Cho, P., and Cheung, S. W. (2012). Retardation of Myopia in Orthokeratology (ROMIO) Study: a 2-year Randomized Clinical Trial. *Invest. Ophthalmol. Vis. Sci.* 53 (11), 7077–7085. doi:10.1167/iovs.12-10565

Christofk, H. R., Vander Heiden, M. G., Harris, M. H., Ramanathan, A., Gerszten, R. E., Wei, R., et al. (2008). The M2 Splice Isoform of Pyruvate Kinase Is Important for Cancer Metabolism and Tumour Growth. *Nature* 452 (7184), 230–233. doi:10.1038/nature06734

Chua, W. H., Balakrishnan, V., Chan, Y. H., Tong, L., Ling, Y., Quah, B. L., et al. (2006). Atropine for the Treatment of Childhood Myopia. *Ophthalmology* 113 (12), 2285–2291. doi:10.1016/j.ophtha.2006.05.062

Collins, B. C., Hunter, C. L., Liu, Y., Schilling, B., Rosenberger, G., Bader, S. L., et al. (2017). Multi-laboratory Assessment of Reproducibility, Qualitative and Quantitative Performance of SWATH-Mass Spectrometry. *Nat. Commun.* 8 (1), 291. doi:10.1038/s41467-017-00249-5

Crooks, J., and Kolb, H. (1992). Localization of GABA, glycine, Glutamate and Tyrosine Hydroxylase in the Human Retina. *J. Comp. Neurol.* 315 (3), 287–302. doi:10.1002/cne.903150305

David, C. J., Chen, M., Assanah, M., Canoll, P., and Manley, J. L. (2010). HnRNP Proteins Controlled by C-Myc Deregulate Pyruvate Kinase mRNA Splicing in Cancer. *Nature* 463 (7279), 364–368. doi:10.1038/nature08697

De Jager, P. L., Srivastava, G., Lunnon, K., Burgess, J., Schalkwyk, L. C., Yu, L., et al. (2014). Alzheimer's Disease: Early Alterations in Brain DNA Methylation at ANK1, BIN1, RHBDF2 and Other Loci. *Nat. Neurosci.* 17 (9), 1156–1163. doi:10.1038/nn.3786

Debertin, G., Kántor, O., Kovács-Öller, T., Balogh, L., Szabó-Meleg, E., Orbán, J., et al. (2015). Tyrosine Hydroxylase Positive Perisomatic Rings Are Formed Around Various Amacrine Cell Types in the Mammalian Retina. *J. Neurochem.* 134 (3), 416–428. doi:10.1111/jnc.13144

Desiere, F., Deutsch, E. W., King, N. L., Nesvizhskii, A. I., Mallick, P., Eng, J., et al. (2006). The PeptideAtlas Project. *Nucleic Acids Res.* 34 (Database issue), D655–D658. doi:10.1093/nar/gkj040

Dong, F., Zhi, Z., Pan, M., Xie, R., Qin, X., Lu, R., et al. (2011). Inhibition of Experimental Myopia by a Dopamine Agonist: Different Effectiveness between Form Deprivation and Hyperopic Defocus in guinea Pigs. *Mol. Vis.* 17, 2824–2834.

Elliott, M. H., Smith, D. S., Parker, C. E., and Borchers, C. (2009). Current Trends in Quantitative Proteomics. *J. Mass. Spectrom.* 44 (12), 1637–1660. doi:10.1002/jms.1692

Frost, M. R., and Norton, T. T. (2012). Alterations in Protein Expression in Tree Shrew Sclera during Development of Lens-Induced Myopia and Recovery. *Invest. Ophthalmol. Vis. Sci.* 53 (1), 322–336. doi:10.1167/iovs.11-8354

Gallego, P., Martínez-García, C., Pérez-Merino, P., Ibares-Frías, L., Mayo-Iscar, A., and Merayo-Lloves, J. (2012). Scleral Changes Induced by Atropine in Chicks as an Experimental Model of Myopia. *Ophthalmic Physiol. Opt.* 32 (6), 478–484. doi:10.1111/j.1475-1313.2012.00940.x

Gao, Q., Liu, Q., Ma, P., Zhong, X., Wu, J., and Ge, J. (2006). Effects of Direct Intravitreal Dopamine Injections on the Development of Lid-Suture Induced Myopia in Rabbits. *Graefes Arch. Clin. Exp. Ophthalmol.* 244 (10), 1329–1335. doi:10.1007/s00417-006-0254-1

Geromanos, S. J., Vissers, J. P., Silva, J. C., Dorschel, C. A., Li, G. Z., Gorenstein, M. V., et al. (2009). The Detection, Correlation, and Comparison of Peptide Precursor and Product Ions from Data Independent LC-MS with Data Dependant LC-MS/MS. *Proteomics* 9 (6), 1683–1695. doi:10.1002/pmic.200800562

Gillet, L. C., Navarro, P., Tate, S., Röst, H., Selevsek, N., Reiter, L., et al. (2012). Targeted Data Extraction of the MS/MS Spectra Generated by Data-independent Acquisition: a New Concept for Consistent and Accurate Proteome Analysis. *Mol. Cel Proteomics* 11 (6), O111.016717. doi:10.1074/mcp.O111.016717

Goedhart, J., and Luijsterburg, M. S. (2020). VolcaNoseR Is a Web App for Creating, Exploring, Labeling and Sharing Volcano Plots. *Sci. Rep.* 10 (1), 20560. doi:10.1038/s41598-020-76603-3

Golovko, A., Kojukhov, A., Guan, B. J., Morpurgo, B., Merrick, W. C., Mazumder, B., et al. (2016). The eIF2A Knockout Mouse. *Cell Cycle* 15 (22), 3115–3120. doi:10.1080/15384101.2016.1237324

Gong, Q., Janowski, M., Luo, M., Wei, H., Chen, B., Yang, G., et al. (2017). Efficacy and Adverse Effects of Atropine in Childhood Myopia: A Meta-Analysis. *JAMA Ophthalmol.* 135 (6), 624–630. doi:10.1001/jamaophthalmol.2017.1091

Guerra, C. (2008). Ingenuity Pathways Analysis: Software for Discovering and Modelling Pathways and Networks in Your Systems Data. *Comp. Biochem. Physiol. A Mol. Integr. Physiol.* 150 (3), S50–S. doi:10.1016/j.cbpa.2008.04.619

Guo, S. S., Sivak, J. G., Callender, M. G., and Diehl-Jones, B. (1995). Retinal Dopamine and Lens-Induced Refractive Errors in Chicks. *Curr. Eye Res.* 14 (5), 385–389. doi:10.3109/02713689508999936

HaileMariam, M., Eguez, R. V., Singh, H., Bekele, S., Ameni, G., Pieper, R., et al. (2018). S-trap, an Ultrafast Sample-Preparation Approach for Shotgun Proteomics. *J. Proteome Res.* 17 (9), 2917–2924. doi:10.1021/acs.jproteome.8b00505

Hiraoka, T., Sekine, Y., Okamoto, F., Mihashi, T., and Oshika, T. (2018). Safety and Efficacy Following 10-years of Overnight Orthokeratology for Myopia Control. *Ophthalmic Physiol. Opt.* 38 (3), 281–289. doi:10.1111/opo.12460

Hong, Z., Shi, M., Chung, K. A., Quinn, J. F., Peskind, E. R., Galasko, D., et al. (2010). DJ-1 and Alpha-Synuclein in Human Cerebrospinal Fluid as Biomarkers of Parkinson's Disease. *Brain* 133 (Pt 3), 713–726. doi:10.1093/brain/awq008

Hsiao, Y. T., Chang, W. A., Kuo, M. T., Lo, J., Lin, H. C., Yen, M. C., et al. (2019). Systematic Analysis of Transcriptomic Profile of the Effects of Low Dose Atropine Treatment on Scleral Fibroblasts Using Next-Generation Sequencing and Bioinformatics. *Int. J. Med. Sci.* 16 (12), 1652–1667. doi:10.7150/ijms.38571

Hu, W., Wang, Z., and Zheng, H. (2018). Mitochondrial Accumulation of Amyloid β (Aβ) Peptides Requires TOMM22 as a Main Aβ Receptor in Yeast. *J. Biol. Chem.* 293 (33), 12681–12689. doi:10.1074/jbc.RA118.002713

Huang, J., Wen, D., Wang, Q., McAlinden, C., Flitcroft, I., Chen, H., et al. (2016). Efficacy Comparison of 16 Interventions for Myopia Control in Children: A Network Meta-Analysis. *Ophthalmology* 123 (4), 697–708. doi:10.1016/j.ophtha.2015.11.010

Iuvone, P. M., Tigges, M., Fernandes, A., and Tigges, J. (1989). Dopamine Synthesis and Metabolism in Rhesus Monkey Retina: Development, Aging, and the Effects of Monocular Visual Deprivation. *Vis. Neurosci.* 2 (5), 465–471. doi:10.1017/s0952523800012360

Iuvone, P. M., Tigges, M., Stone, R. A., Lambert, S., and Laties, A. M. (1991). Effects of Apomorphine, a Dopamine Receptor Agonist, on Ocular Refraction and Axial Elongation in a Primate Model of Myopia. *Invest. Ophthalmol. Vis. Sci.* 32 (5), 1674–1677.

Jin, Z. B., Wu, J., Huang, X. F., Feng, C. Y., Cai, X. B., Mao, J. Y., et al. (2017). Trio-based Exome Sequencing Arrests De Novo Mutations in Early-Onset High Myopia. *Proc. Natl. Acad. Sci. U S A.* 114 (16), 4219–4224. doi:10.1073/pnas.1615970114

Kang, B. S., Wang, L. K., Zheng, Y. P., Guggenheim, J. A., Stell, W. K., and Kee, C. S. (2018). High Myopia Induced by Form Deprivation Is Associated with Altered Corneal Biomechanical Properties in Chicks. *Plos One* 13 (11), e0207189. doi:10.1371/journal.pone.0207189

Kastner, A., Hirsch, E. C., Agid, Y., and Javoy-Agid, F. (1993). Tyrosine Hydroxylase Protein and Messenger RNA in the Dopaminergic Nigral Neurons of Patients with Parkinson's Disease. *Brain Res.* 606 (2), 341–345. doi:10.1016/0006-8993(93)91005-d

Kiorpes, L., Boothe, R. G., Hendrickson, A. E., Movshon, J. A., Eggers, H. M., and Gizzi, M. S. (1987). Effects of Early Unilateral Blur on the Macaque's Visual System. I. Behavioral Observations. *J. Neurosci.* 7 (5), 1318–1326. doi:10.1523/jneurosci.07-05-01318.1987

Kiyonami, R., Schoen, A., Prakash, A., Peterman, S., Zabrouskov, V., Picotti, P., et al. (2011). Increased Selectivity, Analytical Precision, and Throughput in Targeted Proteomics. *Mol. Cel Proteomics* 10 (2), M110.002931. doi:10.1074/mcp.M110.002931

Kondrashov, N., Pusic, A., Stumpf, C. R., Shimizu, K., Hsieh, A. C., Ishijima, J., et al. (2011). Ribosome-mediated Specificity in Hox mRNA Translation and Vertebrate Tissue Patterning. *Cell* 145 (3), 383–397. doi:10.1016/j.cell.2011.03.028

Lam, T. C., Li, K. K., Lo, S. C., Guggenheim, J. A., and To, C. H. (2006). A Chick Retinal Proteome Database and Differential Retinal Protein Expressions during Early Ocular Development. *J. Proteome Res.* 5 (4), 771–784. doi:10.1021/pr050280n

Lam, C. S. Y., Tang, W. C., Tse, D. Y.-y., Lee, R. P. K., Chun, R. K. M., Hasegawa, K., et al. (2019). Defocus Incorporated Multiple Segments (DIMS) Spectacle Lenses Slow Myopia Progression: a 2-year Randomised Clinical Trial. *Br. J. Ophthalmol.* 104, 363–368. doi:10.1136/bjophthalmol-2018-313739

Lambert, J. P., Ivosev, G., Couzens, A. L., Larsen, B., Taipale, M., Lin, Z. Y., et al. (2013). Mapping Differential Interactomes by Affinity Purification Coupled with Data-independent Mass Spectrometry Acquisition. *Nat. Methods* 10 (12), 1239–1245. doi:10.1038/nmeth.2702

Liu, H., Sadygov, R. G., and Yates, J. R. (2004). A Model for Random Sampling and Estimation of Relative Protein Abundance in Shotgun Proteomics. *Anal. Chem.* 76 (14), 4193–4201. doi:10.1021/ac0498563

Lu, F., Zhou, X., Zhao, H., Wang, R., Jia, D., Jiang, L., et al. (2006). Axial Myopia Induced by a Monocularly-Deprived Facemask in guinea Pigs: A Non-invasive and Effective Model. *Exp. Eye Res.* 82 (4), 628–636. doi:10.1016/j.exer.2005.09.001

Ludwig, C., Gillet, L., Rosenberger, G., Amon, S., Collins, B. C., and Aebersold, R. (2018). Data-independent Acquisition-Based SWATH-MS for Quantitative Proteomics: a Tutorial. *Mol. Syst. Biol.* 14 (8), e8126. doi:10.15252/msb.20178126

Mair, P., Hofmann, E., Gruber, K., Hatzinger, R., Zeileis, A., and Hornik, K. (2015). Motivation, Values, and Work Design as Drivers of Participation in the R Open Source Project for Statistical Computing. *Proc. Natl. Acad. Sci. U S A.* 112 (48), 14788–14792. doi:10.1073/pnas.1506047112

Mao, J., Liu, S., Qin, W., Li, F., Wu, X., and Tan, Q. (2010). Levodopa Inhibits the Development of Form-Deprivation Myopia in guinea Pigs. *Optom. Vis. Sci.* 87 (1), 53–60. doi:10.1097/OPX.0b013e3181c12b3d

Mao, J., Liu, S., Qin, W., Xiang, Q., and Wu, X. (2011). Exogenous Levodopa Increases the Neuro Retinal Dopamine of guinea Pig Myopic Eyes *In Vitro*. *Eye Sci.* 26 (4), 211–216. doi:10.3969/j.issn.1000-4432.2011.04.006

Martínez-Navarrete, G. C., Martín-Nieto, J., Esteve-Rudd, J., Angulo, A., and Cuenca, N. (2007). Alpha Synuclein Gene Expression Profile in the Retina of Vertebrates. *Mol. Vis.* 13 (98-100), 949–961.

McBrien, N. A., Cottriall, C. L., and Annies, R. (2001). Retinal Acetylcholine Content in normal and Myopic Eyes: a Role in Ocular Growth Control? *Vis. Neurosci.* 18 (4), 571–580. doi:10.1017/s0952523801184075

McFadden, S. A., Tse, D. Y., Bowrey, H. E., Leotta, A. J., Lam, C. S., Wildsoet, C. F., et al. (2014). Integration of Defocus by Dual Power Fresnel Lenses Inhibits

Myopia in the Mammalian Eye. *Invest. Ophthalmol. Vis. Sci.* 55 (2), 908–917. doi:10.1167/iovs.13-11724

Mi, H., Muruganujan, A., Huang, X., Ebert, D., Mills, C., Guo, X., et al. (2019). Protocol Update for Large-Scale Genome and Gene Function Analysis with the PANTHER Classification System (v.14.0). *Nat. Protoc.* 14 (3), 703–721. doi:10.1038/s41596-019-0128-8

Michalski, A., Cox, J., and Mann, M. (2011). More Than 100,000 Detectable Peptide Species Elute in Single Shotgun Proteomics Runs but the Majority Is Inaccessible to Data-dependent LC-MS/MS. *J. Proteome Res.* 10 (4), 1785–1793. doi:10.1021/pr101060v

Morgan, I. G., Ohno-Matsui, K., and Saw, S. M. (2012). Myopia. *Lancet* 379 (9827), 1739–1748. doi:10.1016/S0140-6736(12)60272-4

Morgan, I. G. (2003). The Biological Basis of Myopic Refractive Error. *Clin. Exp. Optom.* 86 (5), 276–288. doi:10.1111/j.1444-0938.2003.tb03123.x

Ortea, I., Rodríguez-Ariza, A., Chicano-Gálvez, E., Arenas Vacas, M. S., and Jurado Gámez, B. (2016). Discovery of Potential Protein Biomarkers of Lung Adenocarcinoma in Bronchoalveolar Lavage Fluid by SWATH MS Data-independent Acquisition and Targeted Data Extraction. *J. Proteomics* 138, 106–114. doi:10.1016/j.jprot.2016.02.010

Palmowski, P., Watson, R., Europe-Finner, G. N., Karolczak-Bayatti, M., Porter, A., Treumann, A., et al. (2019). The Generation of a Comprehensive Spectral Library for the Analysis of the Guinea Pig Proteome by SWATH-MS. *Proteomics* 19 (15), e1900156. doi:10.1002/pmic.201900156

Pandey, A., and Mann, M. (2000). Proteomics to Study Genes and Genomes. *Nature* 405 (6788), 837–846. doi:10.1038/35015709

Philp, N. J., Ochrietor, J. D., Rudoy, C., Muramatsu, T., and Linser, P. J. (2003). Loss of MCT1, MCT3, and MCT4 Expression in the Retinal Pigment Epithelium and Neural Retina of the 5A11/basigin-Null Mouse. *Invest. Ophthalmol. Vis. Sci.* 44 (3), 1305–1311. doi:10.1167/iovs.02-0552

Raviola, E., and Wiesel, T. N. (1985). An Animal Model of Myopia. *N. Engl. J. Med.* 312 (25), 1609–1615. doi:10.1056/NEJM198506203122505

Ross, P. L., Huang, Y. N., Marchese, J. N., Williamson, B., Parker, K., Hattan, S., et al. (2004). Multiplexed Protein Quantitation in *Saccharomyces cerevisiae* Using Amine-Reactive Isobaric Tagging Reagents. *Mol. Cel Proteomics* 3 (12), 1154–1169. doi:10.1074/mcp.M400129-MCP200

Saw, S. M., Matsumura, S., and Hoang, Q. V. (2019). Prevention and Management of Myopia and Myopic Pathology. *Invest. Ophthalmol. Vis. Sci.* 60 (2), 488–499. doi:10.1167/iovs.18-25221

Schwahn, H. N., Kaymak, H., and Schaeffel, F. (2000). Effects of Atropine on Refractive Development, Dopamine Release, and Slow Retinal Potentials in the Chick. *Vis. Neurosci.* 17 (2), 165–176. doi:10.1017/s0952523800171184

Selevsek, N., Chang, C. Y., Gillet, L. C., Navarro, P., Bernhardt, O. M., Reiter, L., et al. (2015). Reproducible and Consistent Quantification of the *Saccharomyces cerevisiae* Proteome by SWATH-Mass Spectrometry. *Mol. Cel Proteomics* 14 (3), 739–749. doi:10.1074/mcp.M113.035550

Shan, S. W., Tse, D. Y.-y., Zuo, B., To, C. H., Liu, Q., McFadden, S. A., et al. (2018a). Integrated SWATH-Based and Targeted-Based Proteomics Provide Insights into the Retinal Emmetropization Process in guinea pig. *J. Proteomics* 181, 1–15. doi:10.1016/j.jprot.2018.03.023

Shan, S. W., Tse, D. Y., Zuo, B., To, C. H., Liu, Q., McFadden, S. A., et al. (2018b). Data on Differentially Expressed Proteins in Retinal Emmetropization Process in guinea Pig Using Integrated SWATH-Based and Targeted-Based Proteomics. *Data Brief* 21, 1750–1755. doi:10.1016/j.dib.2018.08.119

Simpson, K. L., Whetton, A. D., and Dive, C. (2009). Quantitative Mass Spectrometry-Based Techniques for Clinical Use: Biomarker Identification and Quantification. *J. Chromatogr. B Analyt. Technol. Biomed. Life Sci.* 877 (13), 1240–1249. doi:10.1016/j.jchromb.2008.11.023

Skeie, J. M., and Mahajan, V. B. (2013). Proteomic Interactions in the Mouse Vitreous-Retina Complex. *PLoS One* 8 (11), e82140. doi:10.1371/journal.pone.0082140

Stahl, D. C., Swiderek, K. M., Davis, M. T., and Lee, T. D. (1996). Data-controlled Automation of Liquid Chromatography/tandem Mass Spectrometry Analysis of Peptide Mixtures. *J. Am. Soc. Mass. Spectrom.* 7 (6), 532–540. doi:10.1016/1044-0305(96)00057-8

Stone, R. A., Lin, T., Laties, A. M., and Iuvone, P. M. (1989). Retinal Dopamine and Form-Deprivation Myopia. *Proc. Natl. Acad. Sci. U S A.* 86 (2), 704–706. doi:10.1073/pnas.86.2.704

Stone, R. A., Liu, J., Sugimoto, R., Capehart, C., Zhu, X., and Pendrak, K. (2003). GABA, Experimental Myopia, and Ocular Growth in Chick. *Invest. Ophthalmol. Vis. Sci.* 44 (9), 3933–3946. doi:10.1167/iovs.02-0774

Surguchov, A., McMahan, B., Masliah, E., and Surgucheva, I. (2001). Synucleins in Ocular Tissues. *J. Neurosci. Res.* 65 (1), 68–77. doi:10.1002/jnr.1129

Swiatczak, B., Feldkaemper, M., Schraermeyer, U., and Schaeffel, F. (2019). Demyelination and Shrinkage of Axons in the Retinal Nerve Fiber Layer in Chickens Developing Deprivation Myopia. *Exp. Eye Res.* 188, 107783. doi:10.1016/j.exer.2019.107783

Sze, Y. H., Zhao, Q., Cheung, J. K. W., Li, K. K., Tse, D. Y. Y., To, C. H., et al. (2021). High-pH Reversed-phase Fractionated Neural Retina Proteome of normal Growing C57BL/6 Mouse. *Sci. Data* 8 (1), 27. doi:10.1038/s41597-021-00813-1

Szklarczyk, D., Gable, A. L., Lyon, D., Junge, A., Wyder, S., Huerta-Cepas, J., et al. (2019). STRING V11: Protein-Protein Association Networks with Increased Coverage, Supporting Functional Discovery in Genome-wide Experimental Datasets. *Nucleic Acids Res.* 47 (D1), D607–D13. doi:10.1093/nar/gky1131

Tigges, M., Iuvone, P. M., Fernandes, A., Sugrue, M. F., Mallorga, P. J., Laties, A. M., et al. (1999). Effects of Muscarinic Cholinergic Receptor Antagonists on Postnatal Eye Growth of Rhesus Monkeys. *Optom. Vis. Sci.* 76 (6), 397–407. doi:10.1097/00006324-199906000-00020

Tkatchenko, T. V., Shah, R. L., Nagasaki, T., and Tkatchenko, A. V. (2019). Analysis of Genetic Networks Regulating Refractive Eye Development in Collaborative Cross Progenitor Strain Mice Reveals New Genes and Pathways Underlying Human Myopia. *BMC Med. Genomics* 12 (1), 113. doi:10.1186/s12920-019-0560-1

Tofaris, G. K., Garcia Reitböck, P., Humby, T., Lambourne, S. L., O'Connell, M., Ghetti, B., et al. (2006). Pathological Changes in Dopaminergic Nerve Cells of the Substantia Nigra and Olfactory Bulb in Mice Transgenic for Truncated Human Alpha-Synuclein(1-120): Implications for Lewy Body Disorders. *J. Neurosci.* 26 (15), 3942–3950. doi:10.1523/JNEUROSCI.4965-05.2006

Troilo, D., Smith, E. L., Nickla, D. L., Ashby, R., Tkatchenko, A. V., Ostrin, L. A., et al. (2019). IMI - Report on Experimental Models of Emmetropization and Myopia. *Invest. Ophthalmol. Vis. Sci.* 60 (3), M31–M88. doi:10.1167/iovs.18-25967

Tse, D. Y., and To, C.-h. (2011). Graded Competing Regional Myopic and Hyperopic Defocus Produce Summated Emmetropization Set Points in Chick. *Invest. Ophthalmol. Vis. Sci.* 52 (11), 8056–8062. doi:10.1167/iovs.10-5207

Tse, D. Y., Chan, J. W., and To, C. H. (2005). Competing Defocus Introduced by Concentric Bifocal Lenses Results in Summated Emmetropization Response in Chicks. *Invest. Ophth Vis. Sci.* 46, 1974.

Tse, D. Y., Lam, C. S., Guggenheim, J. A., Lam, C., Li, K. K., Liu, Q., et al. (2007). Simultaneous Defocus Integration during Refractive Development. *Invest. Ophthalmol. Vis. Sci.* 48 (12), 5352–5359. doi:10.1167/iovs.07-0383

Velez, G., Machlab, D. A., Tang, P. H., Sun, Y., Tsang, S. H., Bassuk, A. G., et al. (2018). Proteomic Analysis of the Human Retina Reveals Region-specific Susceptibilities to Metabolic- and Oxidative Stress-Related Diseases. *PLoS One* 13 (2), e0193250. doi:10.1371/journal.pone.0193250

Verkicharla, P. K., Ohno-Matsui, K., and Saw, S. M. (2015). Current and Predicted Demographics of High Myopia and an Update of its Associated Pathological Changes. *Ophthalmic Physiol. Opt.* 35 (5), 465–475. doi:10.1111/opo.12238

Vocale, L. G., Crewther, S., Riddell, N., Hall, N. E., Murphy, M., and Crewther, D. (2021). RNA-seq and GSEA Identifies Suppression of Ligand-Gated Chloride Efflux Channels as the Major Gene Pathway Contributing to Form Deprivation Myopia. *Sci. Rep.* 11 (1), 5280. doi:10.1038/s41598-021-84338-y

Wallman, J., and Winawer, J. (2004). Homeostasis of Eye Growth and the Question of Myopia. *Neuron* 43 (4), 447–468. doi:10.1016/j.neuron.2004.08.008

Wan, L., Wei, C. C., Chen, C. S., Chang, C. Y., Lin, C. J., Chen, J. J., et al. (2018). The Synergistic Effects of Orthokeratology and Atropine in Slowing the Progression of Myopia. *J. Clin. Med.* 7 (9), 259. doi:10.3390/jcm7090259

Wasinger, V. C., Zeng, M., and Yau, Y. (2013). Current Status and Advances in Quantitative Proteomic Mass Spectrometry. *Int. J. Proteomics* 2013, 180605. doi:10.1155/2013/180605

Wetzel, R. K., Arystarkhova, E., and Sweadner, K. J. (1999). Cellular and Subcellular Specification of Na,K-ATPase Alpha and Beta Isoforms in the Postnatal Development of Mouse Retina. *J. Neurosci.* 19 (22), 9878–9889. doi:10.1523/jneurosci.19-22-09878.1999

Wildsoet, C. F., Chia, A., Cho, P., Guggenheim, J. A., Polling, J. R., Read, S., et al. (2019). IMI - Interventions Myopia Institute: Interventions for Controlling Myopia Onset and Progression Report. *Invest. Ophthalmol. Vis. Sci.* 60 (3), M106–M31. doi:10.1167/iovs.18-25958

Wojciechowski, R. (2011). Nature and Nurture: the Complex Genetics of Myopia and Refractive Error. *Clin. Genet.* 79 (4), 301–320. doi:10.1111/j.1399-0004.2010.01592.x

Wong, T. Y., Ferreira, A., Hughes, R., Carter, G., and Mitchell, P. (2014). Epidemiology and Disease burden of Pathologic Myopia and Myopic Choroidal Neovascularization: an Evidence-Based Systematic Review. *Am. J. Ophthalmol.* 157 (1), 9. doi:10.1016/j.ajo.2013.08.010

Wu, Y., Liu, Q., To, C., Li, K.-K., Chun, R., Yu, J., et al. (2014). Differential Retinal Protein Expressions during Form Deprivation Myopia in Albino Guinea Pigs. *CP* 11 (1), 37–47. doi:10.2174/1570164610666140109002531

Wu H, H., Chen, W., Zhao, F., Zhou, Q., Reinach, P. S., Deng, L., et al. (2018). Scleral Hypoxia Is a Target for Myopia Control. *Proc. Natl. Acad. Sci. U S A.* 115 (30), E7091–E100. doi:10.1073/pnas.1721443115

Wu Y, Y., Lam, C. S., Tse, D. Y., To, C. H., Liu, Q., McFadden, S. A., et al. (2018). Early Quantitative Profiling of Differential Retinal Protein Expression in Lens-Induced Myopia in guinea Pig Using Fluorescence Difference Two-Dimensional Gel Electrophoresis. *Mol. Med. Rep.* 17 (4), 5571–5580. doi:10.3892/mmr.2018.8584

Xie, F., Liu, T., Qian, W. J., Petyuk, V. A., and Smith, R. D. (2011). Liquid Chromatography-Mass Spectrometry-Based Quantitative Proteomics. *J. Biol. Chem.* 286 (29), 25443–25449. doi:10.1074/jbc.R110.199703

Yam, J. C., Jiang, Y., Tang, S. M., Law, A. K. P., Chan, J. J., Wong, E., et al. (2019). Low-Concentration Atropine for Myopia Progression (LAMP) Study: A Randomized, Double-Blinded, Placebo-Controlled Trial of 0.05%, 0.025%, and 0.01% Atropine Eye Drops in Myopia Control. *Ophthalmology* 126 (1), 113–124. doi:10.1016/j.ophtha.2018.05.029

Yan, T., Xiong, W., Huang, F., Zheng, F., Ying, H., Chen, J. F., et al. (2015). Daily Injection but Not Continuous Infusion of Apomorphine Inhibits Form-Deprivation Myopia in Mice. *Invest. Ophthalmol. Vis. Sci.* 56 (4), 2475–2485. doi:10.1167/iovs.13-12361

Yu, F. J., Lam, T. C., Liu, L. Q., Chun, R. K., Cheung, J. K., Li, K. K., et al. (2017). Isotope-coded Protein Label Based Quantitative Proteomic Analysis Reveals Significant Up-Regulation of Apolipoprotein A1 and Ovotransferrin in the Myopic Chick Vitreous. *Sci. Rep.* 7 (1), 12649. doi:10.1038/s41598-017-12650-7

Yu, F. J., Lam, T. C., Sze, A. Y., Li, K. K., Chun, R. K., Shan, S. W., et al. (2020). Alteration of Retinal Metabolism and Oxidative Stress May Implicate Myopic Eye Growth: Evidence from Discovery and Targeted Proteomics in an Animal Model. *J. Proteomics* 221, 103684. doi:10.1016/j.jprot.2020.103684

Zhang, H., Liu, T., Zhang, Z., Payne, S. H., Zhang, B., McDermott, J. E., et al. (2016). Integrated Proteogenomic Characterization of Human High-Grade Serous Ovarian Cancer. *Cell* 166 (3), 755–765. doi:10.1016/j.cell.2016.05.069

Zhang, P., Ji, D., Hu, X., Ni, H., Ma, W., Zhang, X., et al. (2018). Oncogenic Heterogeneous Nuclear Ribonucleoprotein D-like Promotes the Growth of Human colon Cancer SW620 Cells via its Regulation of Cell-Cycle. *Acta Biochim. Biophys. Sin (Shanghai)* 50 (9), 880–887. doi:10.1093/abbs/gmy085

Zhao, W., Bi, A. L., Xu, C. L., Ye, X., Chen, M. Q., Wang, X. T., et al. (2017). GABA and GABA Receptors Alterations in the Primary Visual Cortex of Concave Lens-Induced Myopic Model. *Brain Res. Bull.* 130, 173–179. doi:10.1016/j.brainresbull.2017.01.017

Zhao, C., Cai, C., Ding, Q., and Dai, H. (2020). Efficacy and Safety of Atropine to Control Myopia Progression: a Systematic Review and Meta-Analysis. *BMC Ophthalmol.* 20 (1), 478. doi:10.1186/s12886-020-01746-w

Zhi, Z., Xiang, J., Fu, Q., Pei, X., Zhou, D., Cao, Y., et al. (2021). The Role of Retinal Connexins Cx36 and Horizontal Cell Coupling in Emmetropization in Guinea Pigs. *Invest. Ophthalmol. Vis. Sci.* 62 (9), 27. doi:10.1167/iovs.62.9.27

Zhou, W., Hurlbert, M. S., Schaack, J., Prasad, K. N., and Freed, C. R. (2000). Overexpression of Human Alpha-Synuclein Causes Dopamine Neuron Death in Rat Primary Culture and Immortalized Mesencephalon-Derived Cells. *Brain Res.* 866, 33–43. doi:10.1016/s0006-8993(00)02215-0

Zhou, X., Ye, J., Willcox, M. D., Xie, R., Jiang, L., Lu, R., et al. (2010). Changes in Protein Profiles of guinea Pig Sclera during Development of Form Deprivation Myopia and Recovery. *Mol. Vis.* 16 (232-33), 2163–2174.

Zhou GH, G. H., Ma, Y., Li, M. L., Zhou, X. Y., Mou, H., and Jin, Z. B. (2020). ATP1A3 Mutation as a Candidate Cause of Autosomal Dominant Cone-Rod Dystrophy. *Hum. Genet.* 139 (11), 1391–1401. doi:10.1007/s00439-020-02182-y

Zhou X, X., Zhang, S., Zhang, G., Chen, Y., Lei, Y., Xiang, J., et al. (2020). Increased Choroidal Blood Perfusion Can Inhibit Form Deprivation Myopia in Guinea Pigs. *Invest. Ophthalmol. Vis. Sci.* 61 (13), 25. doi:10.1167/iovs.61.13.25

Zhu, Y., Bian, J., Lu, D., Wang, Q., Gong, B., Li, K. K., et al. (2020). Combined Retinal Proteome Datasets in Response to Atropine Treatment Using iTRAQ and SWATH-MS Based Proteomics Approaches in guinea Pig Myopia Model. *Data Brief* 33, 106526. doi:10.1016/j.dib.2020.106526

Dihydroartemisinin Inhibits Laser-Induced Choroidal Neovascularization in a Mouse Model of Neovascular AMD

Xun Li [1,2,3†], Sheng Gao [1,3†], Yun Zhang [1,3], Mei Xin [4], Cheng Zuo [5], Naihong Yan [1,2], Qingjie Xia [6] and Meixia Zhang [1,3]*

[1]Department of Ophthalmology, West China Hospital, Sichuan University, Chengdu, China, [2]Research Laboratory of Ophthalmology and Vision Science, West China Hospital, Sichuan University, Chengdu, China, [3]Research Laboratory of Macular Disease, West China Hospital, Sichuan University, Chengdu, China, [4]Department of Ophthalmology, Chengdu First People's Hospital, Chengdu, China, [5]Department of Ophthalmology, The Third People's Hospital of Chengdu, Chengdu, China, [6]Laboratory of Neurological Disease, Translational Neuroscience Center, West China Hospital, Sichuan University, Chengdu, China

Purpose: Choroidal neovascularization (CNV) is the main pathogenic process and a leading cause of severe vision loss in neovascular age-related macular degeneration (AMD). We investigated the antiangiogenic efficacy of dihydroartemisinin (DHA) in an experimental laser-induced CNV mouse model.

Methods: After fluorescein angiography confirmed that CNV was induced by laser photocoagulation in C57BL/6J mice, DHA or vehicle was given by intragastric administration once a day. On day 6 and day 12, fluorescein angiography, optic coherence tomography, and flat-mounting analysis were performed to grade CNV leakage, measure CNV thickness and evaluate CNV areas, respectively. Immunofluorescence staining and Western blot analysis were performed to evaluate the expression of NF-κB, VEGF, and VEGFR2. To confirm the safety of intragastric DHA application, changes in retinal morphology and neural cell apoptosis were tested by histopathological examination and TUNEL assay, and retinal function was determined by electroretinogram (ERG).

Results: Intragastric administration of DHA significantly suppressed CNV leakage and CNV formation in both thickness and area. Immunofluorescence showed that DHA suppressed VEGFR2 and NF-κB p65 expression in laser-induced lesions. Compared to the normal group, the protein expression of VEGF, VGFER2, NF-κB p65, and NF-κB1 p50 increased significantly in the vehicle group after laser photocoagulation, while it was profoundly inhibited by DHA treatment. In addition, histopathological examination, TUNEL analysis, and ERG test showed no obvious evidence of retinal toxicity caused by DHA.

Conclusion: Systemic administration of DHA can effectively inhibit laser-induced CNV formation in mice, which might be due to the suppression of the classic NF-κB signaling pathway and downregulation of VEGFR2 and VEGF expression. The current results suggest that DHA could be a natural potential alternative therapeutic strategy for neovascular AMD.

Keywords: dihydroartemisinin (DHA), neovascular age-related macular degeneration (nAMD), choroidal neovascularization, NF-κB signaling pathway, antiangiogenic efficacy

INTRODUCTION

Age-related macular degeneration (AMD) has been the most common cause of permanent visual damage and public health problems due to the aging population in the developed world (Chakravarthy and Peto, 2020; Apte, 2021). Choroidal neovascularization (CNV) is the main pathogenic process and a leading cause of severe vision loss in neovascular AMD (Jaffe et al., 2019; Zhao et al., 2019). Since the increased expression of vascular endothelial growth factor (VEGF) is crucial during pathogenic angiogenesis, anti-VEGF therapies have been successfully used to treat neovascular AMD (Wong et al., 2016). However, these treatments have several limitations, such as the requirement of repeat intravitreal injections, the development of tolerance, and the heavy burden on patients caused by the high costs. Currently, there are no satisfactory noninvasive treatments for neovascular AMD (Mehta et al., 2018). Thus, there is an urgency to seek cost-effective, less invasive, and more durable alternative therapies for CNV in AMD patients.

Dihydroartemisinin (DHA), an artificial semisynthetic derivative of artemisinin and the main metabolite of artemisinin in the body, has characteristics of high activity and low toxicity. In addition to its excellent antimalarial effect, the antiangiogenic efficacy of DHA has been shown in several cancer studies, including myeloma, leukemia, ovarian cancer, Lewis lung cancer and pancreatic cancer (Efferth, 2017). *In vitro*, DHA inhibits the growth, proliferation, migration and tube formation of endothelial cells by downregulating VEGF, all of which are closely linked with angiogenesis (Guo et al., 2014). Moreover, DHA regulates VEGFR2 promoter activity through the p65 binding motif and decreases the binding activity of p65 and the VEGFR2 promoter, suggesting that inhibition of the NF-κB pathway plays a major role in mediating the antiangiogenic effects of DHA (Dong et al., 2014). As a prototypical proinflammatory signaling pathway, recent studies have shown that NF-κB regulates many angiogenic factors in the development of cancers (Karin, 2006). Moreover, NF-κB was detected in the retinal pigment epithelium of human eyes with advanced stages of AMD (Feng et al., 2017). The inhibition of NF-κB by genetic deletion or pharmacological inhibition of IKK2 significantly reduces laser-induced CNV, suggesting a key role of NF-κB in CNV formation (Gaddipati et al., 2015; Ghosh et al., 2017). However, whether DHA attenuates choroidal neovascularization *in vivo* remains unknown.

In this study, we investigated the effect of DHA on laser-induced CNV in a mouse model to explore its potential application as a new therapy for neovascular AMD and preliminarily explored the underlying mechanism.

MATERIALS AND METHODS

Animals and Anesthesia

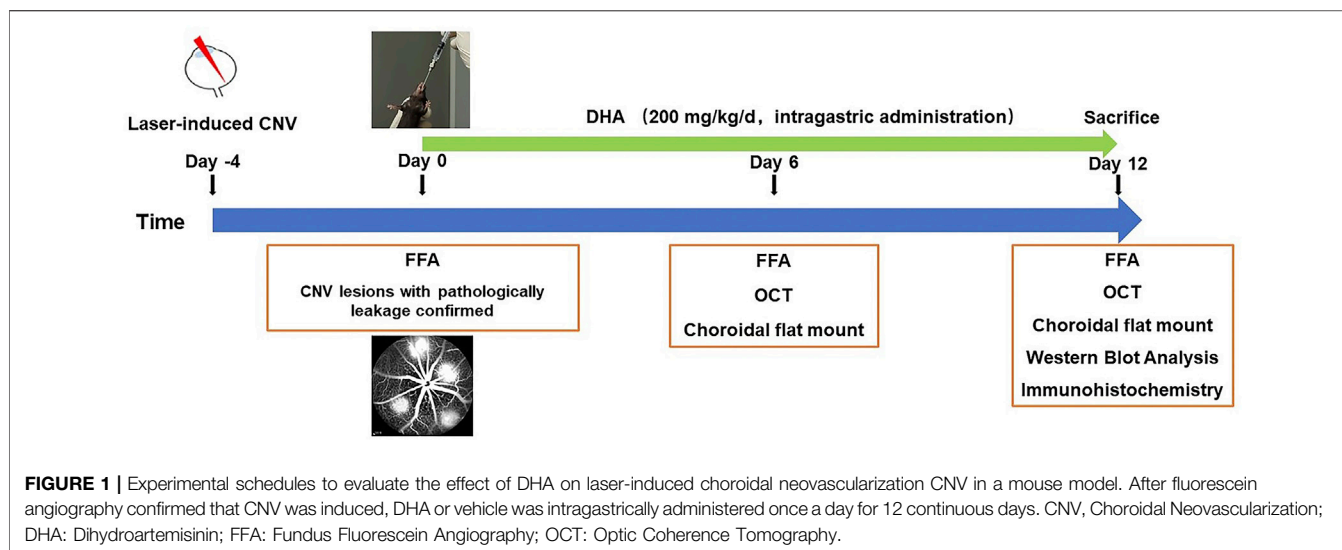Male C57BL/6J mice (DOSSY EXPERIMENTAL ANIMALS CO. LTD., Chengdu, China) aged 6–8 weeks old and weighing 18–20 g were used to minimize variability in the study. Animals were housed in metal breeding cages with free access to food and water in a room with a 12-h/12-h light/dark cycle. The humidity and temperature were maintained at 60% and 24–26°C, respectively. All animal procedures were approved by the Animal Care and Use Committee of Sichuan University and adhered to the Association for Research in Vision and Ophthalmology (ARVO) Statement for the Use of Animals in Ophthalmic and Vision Research. During all procedures, the mice were anesthetized with an intraperitoneal injection of 2% pentobarbital sodium (45 mg/kg body weight), and pupils were dilated with topical 5% tropicamide (Santen Pharmaceutical Co., LTD., Osaka, Japan). At different time points after laser-induced photocoagulation, the mice were euthanized by cervical dislocation.

Establishment of Mouse Choroidal Neovascularization Model

After dilating pupils, mice were placed on a platform under a slit lamp, and the corneas were anesthetized with oxybuprocaine hydrochloride eye drops (Santen Pharmaceutical Co., LTD., Osaka, Japan). 532 nm argon laser-induced photocoagulation was used to disrupt Bruch's membrane bilaterally in each mouse. Four spots of laser photocoagulation in the posterior pole of the retina were created with a power of 150–200 mW, duration of 100 m s, and 50 μm spot size using a slit lamp delivery system with a handheld coverslip as a contact lens. The laser spots are located approximately two to three optic disc diameters away from the optic nerve head, avoiding the main vessels. The appearance of a white bubble, which indicates a break of Bruch's membrane, is an important factor to obtain CNV, and only burns causing bubble formation were included in subsequent experiments. Spots with hemorrhage or failing to develop a bubble were excluded from the analysis.

Administration of DHA and Control Vehicle

DHA was supplied by the Center for Translational Neuroscience, West China Hospital, Sichuan University, and it was dissolved in 10% dimethyl sulfoxide (DMSO). Animals were randomly divided into three groups: control (vehicle only), DHA, and ranibizumab. Four days after laser photocoagulation, the DHA group received intragastric administration of DHA at a dose of 200 mg/kg/d for 12 consecutive days, and the control group mice received the same volume of vehicle (**Figure 1**). The ranibizumab group mice received an intravitreal injection of 2 μL (20 μg) ranibizumab as a positive control. Mice were anesthetized and pupils were dilated with topical 5% tropicamide. A shelving puncture of the sclera was made 1 mm behind the limbus with a 32-gauge needle, then a 33-gauge needle (Hamilton Bonaduz AG, Bonaduz, Switzerland) was inserted with a 45° injection angle into the vitreous. The direction and location of the needle was monitored through the microscope. The overall health of each mouse was

FIGURE 1 | Experimental schedules to evaluate the effect of DHA on laser-induced choroidal neovascularization CNV in a mouse model. After fluorescein angiography confirmed that CNV was induced, DHA or vehicle was intragastrically administered once a day for 12 continuous days. CNV, Choroidal Neovascularization; DHA: Dihydroartemisinin; FFA: Fundus Fluorescein Angiography; OCT: Optic Coherence Tomography.

evaluated by assessing its weight, general appearance, and alertness. All mice remained alert and responsive, and there were no adverse effects during the study period.

Fundus Fluorescein Angiography

Fundus fluorescein angiography (FFA) was performed on anesthetized mice using a Spectralis HRA + OCT ophthalmic diagnostic apparatus (Heidelberg, Germany) at the time points. Early-phase and late-phase FFA images were recorded at 1 to 2 min and after 5 min, respectively, after intraperitoneal injection of 0.2 ml 2% fluorescein sodium solution (Baiyunshan Mingxing Pharmaceutical Co., Ltd., Guangzhou, China). Images were evaluated by two masked retinal specialists who were not involved in laser photocoagulation or angiography. Then, lesions were graded according to a previously published grading system: 0, "no leakage," faint hyperfluorescence or mottled fluorescence; 1, "questionable leakage," hyperfluorescence lesion without a progressive increase in size or intensity; 2, "leaky," hyperfluorescence increasing in intensity but not in size; and 3, "pathologically significant leakage," hyperfluorescence increasing both in size and intensity (Ozone et al., 2016). Four days after laser photocoagulation, we performed FFA analysis and chose lesions with pathologically significant leakage for further observation because only these lesions had the clinical meaning of CNV. Then, the DHA was administered, as shown in **Figure 1**. Late-phase images were chosen for analysis of fluorescence leakage and leakage areas, which corresponded with the clearance time of fluorescence from the vasculature and to avoid interference with the observation of hyperfluorescence from CNV.

Spectral Domain-Optic Coherence Tomography (SD-OCT)

SD-OCT was performed using a Heidelberg Spectralis HRA + OCT (Heidelberg, Germany). The cornea was covered with hyaluronan gel (Freda, China) before the examination. For each CNV lesion, SD-OCT high-resolution multilinear horizontal scanning images were taken to calculate the thickness of the CNV lesion, which was defined as a spindle-shaped hyperreflective area at the subretinal space. Only the scan that passed through the center of the lesion was chosen to evaluate the CNV central thickness (CCT) (Zhao et al., 2018).

Flat-Mount Staining and CNV Size Measurement

Mice were euthanized, and eyes were enucleated and fixed in 4% paraformaldehyde solution for approximately 30 min. After washing in PBS, the anterior of the eye was cut off, and the whole retinas were removed carefully from the eyecups. To flatten the eyecups, four radial incisions in the remaining RPE-choroid-sclera complexes were made from the edge to the optic nerve head with the RPE facing up. Then, the complexes were washed in tris-buffered saline (0.5% BSA, 0.2% Tween-20, and 0.1% Triton X-100), incubated with isolectin B4 (1:200, Sigma–Aldrich, St Louis, MO, United States) overnight at 4°C, and mounted onto glass slides. The images were captured with a fluorescence microscope (Carl Zeiss, Germany), and the CNV lesion area was measured using ImageJ software after normalizing for different background fluorescence (NIH, Bethesda, MD, United States).

Immunohistochemistry

The eyecups were embedded in an optimal cutting temperature compound (Tissue Tek; Miles Laboratories, Elkhart, IN, United States) and snap-frozen. 10-μm thick cryostat sections were cut at-20°C, air dried, and incubated in blocking solution (5% normal donkey serum, 1% BSA, and 0.03% Triton X-100 in 1× PBS) for 1 hour at room temperature. The sections were stained with monoclonal antibodies against NF-κB p65 (CST, 8,242, Beverly, MA, United States) or with polyclonal antibodies against VEGFR2 (CST, 2,478, Beverly, MA, United States) at 4 °C overnight and then incubated with corresponding secondary antibodies conjugated to Alexa Fluor 488 (Invitrogen,

United States) for 1 h at room temperature in the dark, while the nuclei were stained with 4′6-diamidino-2-phenylindole (DAPI; Sigma Aldrich). A fluorescence microscope (Carl Zeiss, Germany) was used to take pictures.

Western Blot Analysis of NF-κB Signaling, VEGF, and VEGFR2

To determine whether DHA treatment affected the NF-κB signaling pathway, RPE-choroid complexes were microsurgically isolated and transformed immediately into 200 μL RIPA buffer (Beyotime Institute of Biotechnology, Haimen, China) supplemented with 1% protease inhibitor cocktail (Beyotime) at 4 °C. After electric homogenization, lysates were placed on ice for 60 min and centrifuged at 12,000 rpm for 20 min at 4°C. Samples were collected and preserved at-80°C. Protein concentrations were measured by the BCA Protein Assay Kit (Beyotime) with bovine serum albumin as the standard. Each sample containing 20 μg of total protein was separated by sodium dodecyl sulfate–polyacrylamide gel electrophoresis (SDS–PAGE) and then transferred to a polyvinylidene fluoride (PVDF) membrane (Millipore, Billerica, MA, United States). After blocking with 5% skim milk for 2 h at room temperature, the membranes were incubated with primary antibodies against NF-κB p65 (CST, 8,242, Beverly, MA, United States), VEGF (Abcam, 46,154, Cambridge, MA), VEGFR2 (CST, 2,478), NF-κB1 p105/p50 (CST, 13,586), NF-κB2 p100/p52 (CST, 37,359), Rel B (CST, 10,544) and β-actin (Beyotime, AA128) at 4 °C overnight. NF-κB1 p105/p50 Rabbit mAb was able to recognize endogenous levels of both the p105 precursor and p50 active form of NF-κB protein, as the same with NF-κB2 p100/p52 Rabbit mAb. The active forms of p50 and p52 were analyzed in this study to reflect the intracellular impact of DHA. The membranes were then incubated with goat anti-rabbit IgG (HRP)-conjugated or goat anti-mouse IgG (HRP)-conjugated antibodies for 2 h at room temperature.

Electroretinogram (ERG), Histopathologic Analysis, and TUNEL Assay

Mice received intragastric administration of either DHA or vehicle once a day for three consecutive weeks. The overall health of the mice was evaluated by assessing their weight, breathing, alertness, and general appearance. The dark-adapted ERG (Diagnosys LLC) was recorded after DHA treatment. Mice were dark-adapted overnight and anesthetized with pentobarbital sodium, and pupils were dilated with topical 5% tropicamide. Full-field ERG was performed after inserting a ground electrode near the tail and a reference electrode on the back subcutaneously. A golden-ring electrode was gently positioned on the cornea. All procedures were performed under dim red light. Responses to brief flashes were analyzed primarily by measuring the amplitudes of the a- and b-waves. The amplitude of the a-wave was measured from the baseline to the maximum a-wave peak, and the b-wave was measured from the nadir of the a-wave to the apex of the b-wave peak. Then, the eyes were enucleated and fixed in 4% paraformaldehyde solution,

conventionally dehydrated, embedded in paraffin wax and cut into 5.0 μm slices. As retinal thickness varies throughout the retina, all sections were parallel to the sagittal plane and through the optic nerve heads, and the regions were quantified at a constant distance from the optic nerve head. Sections were stained with hematoxylin-eosin (HE), observed, and photographed using a light microscope. Frozen sections of the eyeball were labeled by TdT-dUTP terminal nick-end labeling (TUNEL) with an apoptosis detection kit (Promega, United States) according to the manufacturer's instructions. Nonspecific signals were detected by the omission of the enzyme reaction. The mouse retina at 24 h after ischemia (IOP raised to 110 mmHg for 1 h) and reperfusion was selected as a positive control group (RIR).

Statistical Analysis

The data are expressed as the mean ± SEM where applicable. Statistical evaluation was conducted by one-way ANOVA followed by Tukey's multiple comparisons test depending on the normality of the data. A value of $p < .05$ was considered statistically significant. Analysis was performed using the statistical software SPSS 26.0 (SPSS, Inc. Chicago, IL, United States).

RESULTS

Antiangiogenic Effect of DHA on CNV

FFA was performed to evaluate the *in vivo* effect of DHA on CNV leakage. It was confirmed that angiographic leakage of CNV was less severe in the DHA group and ranibizumab group. The proportion of CNV formation with fluorescence leakage in each group is shown in **Table 1**. Pathologically significant leakage (grade 3 lesions) was observed in 26% of CNV lesions in the DHA group and 17% of CNV lesions in the ranibizumab group on day 6, both of which were less than that in the vehicle group (68%). This trend lasted until day 12. The average grade score was significantly lower in DHA (1.96 ± 0.77) or ranibizumab (1.74 ± 0.86) treated eyes compared with vehicle-treated eyes (2.58 ± 0.69) on day 6. And the similar situation was observed on day 12.

Inhibitory Effect of DHA on Laser-Induced CNV

The effect of DHA on the CNV lesion area was examined by FFA and choroidal flat-mount images, suggesting that the CNV area was significantly reduced after DHA treatment. Because of the advantage of FFA for continuously observing CNV lesions *in vivo*, the reduced leakage area of the same CNV was calculated (**Figure 2**). The mean reduction areas in the DHA group (5,895.84 ± 666.16 pixels, $p < .05$) and ranibizumab group (6,075.35 ± 576.87 pixels, $p < .05$) were larger than that in the vehicle group (3,202.80 ± 516.82 pixels) on day 6 (**Figure 2C**). After 12 days of administration, the mean reduction in the CNV leakage area was 6,901.25 ± 630.76 pixels in the DHA group and 7,657.69 ± 444.20 pixels in the ranibizumab group, both of which

TABLE 1 | CNV leakage grading.

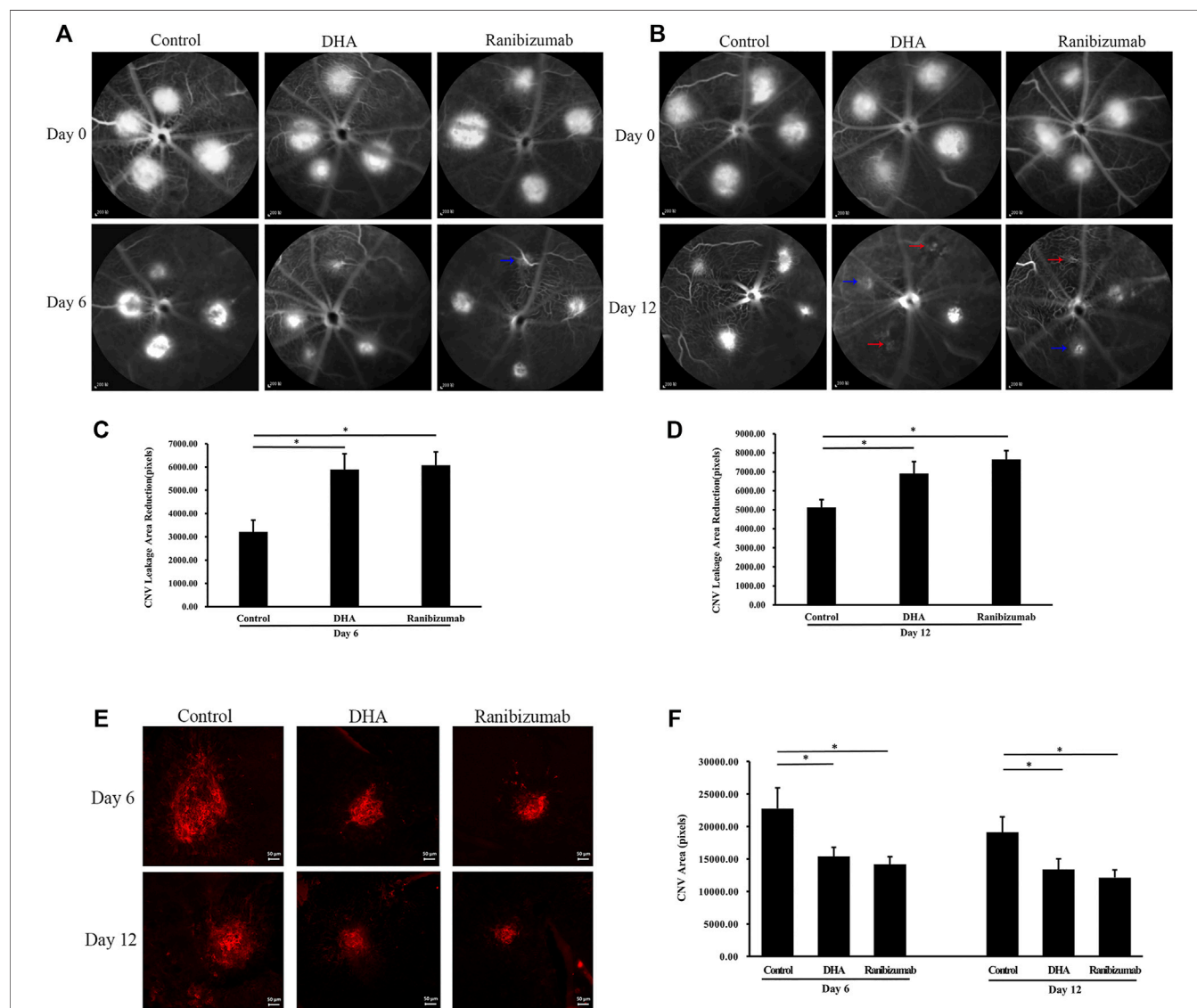|	Vehicle	DHA	Ranibizumab	Vehicle	DHA	Ranibizumab
	Day 6			Day 12		
Number of CNV (grade 3) (Percentage)	13/19 (68%)	6/23 (26%)	4/23 (17%)	13/25 (52%)	5/24 (20.8%)	2/23 (9%)
Average Leakage Grade score	2.58 ± 0.69	1.96 ± 0.77*	1.74 ± 0.86*	2.32 ± 0.80	1.67 ± 0.82#	1.17 ± 0.78#

*p< 0.05 vs vehicle on day 6.
#p< 0.05 vs vehicle on day 12 (one-way ANOVA, followed by Tukey's test).

FIGURE 2 | The effect of DHA on the CNV lesion area was shown by FFA and choroidal flat-mount staining. The CNV lesions were graded according to the intensity of the leaking fluorescence. Grade 1 was indicated by red arrows. Grade 2 was indicated by blue arrows. **(A,B)** Representative late-phase fluorescein angiograms on day 6 and day 12. Scale bar, 200 μm. **(C,D)** The reduction in the same CNV leakage area of the DHA group or ranibizumab group was significantly larger than that of the vehicle group on day 6 and day 12. **(E)** Representative choroidal flat-mount images of laser-induced vascular lesions (stained with isolectin B4) on day 6 and day 12. Scale bar, 50 μm. **(F)** The CNV area decreased significantly after DHA or ranibizumab treatment compared to that in the vehicle group. Data were analyzed by one-way ANOVA followed by Tukey's multiple comparisons test. *$p < .05$. CNV: Choroidal Neovascularization; DHA, Dihydroartemisinin; FFA, Fundus Fluorescein Angiography.
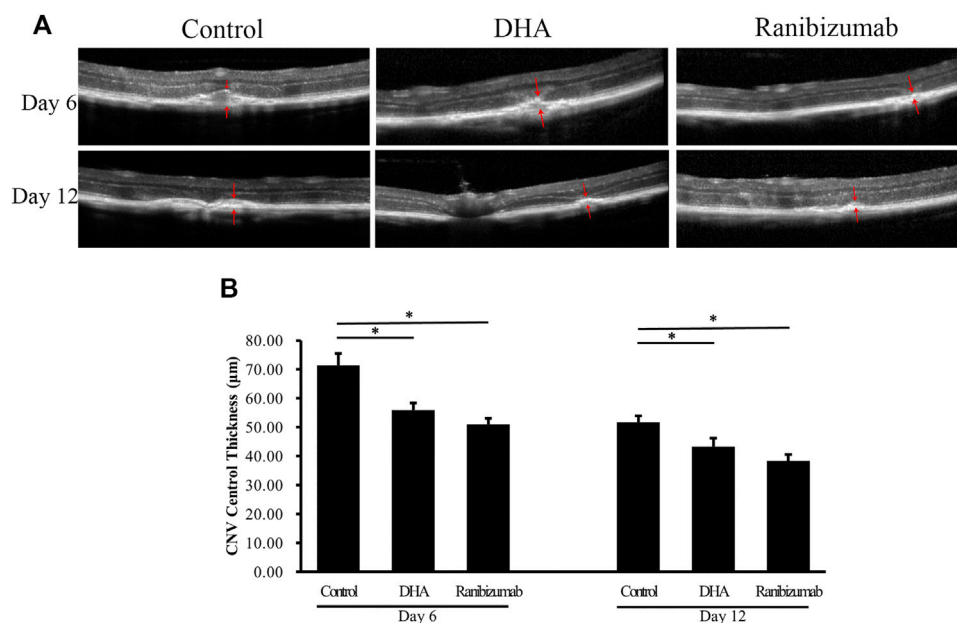
FIGURE 3 | The effect of DHA on CNV central thickness (CCT) examined by SD-OCT images. The CCT of the spindle-shaped CNV lesion is outlined by the red arrows. **(A)** Representative SD-OCT images of CNV in mice administered vehicle, DHA, or ranibizumab. Scale bar, 50 µm. **(B)** Compared to that in the vehicle group, the CCT decreased significantly with DHA or ranibizumab treatment. Data were analyzed by one-way ANOVA followed by Tukey's multiple comparisons test. *$p < .05$. CNV: Choroidal Neovascularization; DHA: Dihydroartemisinin.

were significantly larger than that in the vehicle group (5,127.05 ± 407.49 pixels, $p < .05$) (**Figure 2D**).

To demonstrate the effect of DHA on the CNV area, the results of choroidal flat mounts also showed a distinct reduction in the CNV lesion area after DHA treatment (**Figures 2E,F**). On day 6, the CNV area decreased significantly in the DHA group (15,395.26 ± 1,372.16 pixels, $p < 0.05$) and the ranibizumab group (14,190.14 ± 1,160.56 pixels, $p < .05$) compared to the vehicle group (22,758 ± 3,216.07 pixels). The trend among these groups was similar on day 12.

The effect of DHA on CNV central thickness (CCT) was examined by SD-OCT analysis, showing that CCT decreased significantly after DHA treatment (**Figure 3**). The mean CCT in the DHA group was 55.96 ± 2.35 µm on day 6 and 43.30 ± 2.95 µm on day 12, and both were reduced markedly compared to the vehicle group on day 6 (71.42 ± 4.02 µm, $p < .05$) and day 12 (51.77 ± 2.14 µm, $p < .05$). In addition, CCT in eyes treated with ranibizumab was significantly lower than that in the vehicle group ($p < .05$), while there was no difference between the DHA group and the ranibizumab group ($p > .05$).

Immunohistochemistry

Immunostaining showed that intragastric administration of DHA reduced VEGFR2 and NF-κB p65 expression at the site of CNV formation (**Figure 4**). Whether in the vehicle group or the DHA group, VEGFR2 had a little positive staining in retinal capillary endothelial cells, and there was no significant difference. However, for CNV formation spots, the positive staining area of VEGFR2 in the DHA group was smaller than that in the vehicle-treated group (white arrow). Similarly, the positive

staining of NF-κB p65 in CNV lesions in the DHA group was reduced compared to that in the vehicle group (yellow arrow).

Inhibition of NF-κB Activation *in vivo* by Treatment With DHA

To define the signaling pathway involved in the treatment of DHA, we focused on NF-κB as an upstream transcription factor of inflammatory mediators and analyzed the protein expression levels of NF-κB family members, such as NF-κB p65, NF-κB1 p105/p50, NF-κB2 p100/p52, and Rel B, as well as VEGF and VEGFR2 in homogenized RPE-choroid complex tissue. **Figure 5** shows that the expression of NF-κB p65, NF-κB1/p50, Rel B, VEGF, and VEGFR2 was markedly increased in the vehicle-treated group compared to the normal control ($p < .05$). These effects were partially reversed by treatment with DHA. After DHA intervention, the protein levels of NF-κB p65, NF-κB1 p50, VEGF, and VEGFR2 were reduced significantly ($p < .05$), while the expression of Rel B did not decrease compared to the vehicle group ($p > .05$). However, the three groups did not differ significantly in terms of NF-κB2 p52 expression level ($p > .05$). Therefore, DHA inhibited the expression of NF-κB p65, NF-κB1 p50, VEGF, and VEGFR2 in eyes with laser-induced CNV.

Toxicity of DHA on the Mouse Retina

To confirm the safety of intragastric DHA application, retinal cell death in mice was assessed by TUNEL assay after 3 weeks of administration of DHA or vehicle (**Figure 6A**). Compared to the normal group, there were almost no or very few TUNEL
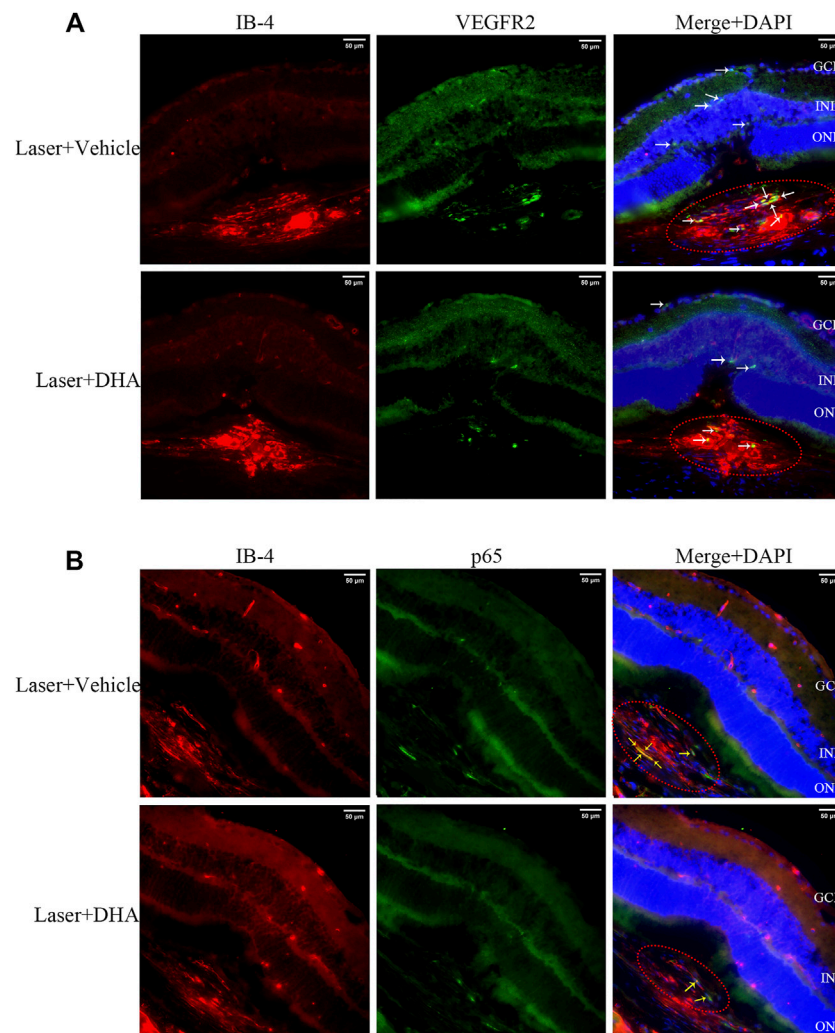
FIGURE 4 | VEGFR2 and NF-κB p65 expression at the site of choroidal neovascularization (CNV) lesions analyzed by immunostaining images. The CNV lesion was indicated by the red ellipse. **(A)** The sections were fluorescently labeled with VEGFR2 antibody (green) and isolectin B4 (red). VEGFR2 had a little positive staining in retinal capillary endothelial cells in both the vehicle and dihydroartemisinin (DHA) groups. However, in CNV formation spots, the positive staining area of VEGFR2 in the DHA group was smaller than that in the vehicle group (white arrow). **(B)** The sections were fluorescently labeled with NF-κB p65 antibody (green) and isolectin B4 (red). The positive staining area of NF-κB p65 in the DHA group was significantly reduced compared to that in the vehicle group, which was mainly seen in CNV areas (yellow arrow). GCL, Ganglion Cell Layer; INL, Inner Nuclear Layer; ONL, Outer Nuclear Layer. Scale bar, 50 μm.

+ cells in the mice administered vehicle or DHA, and the retinal cell apoptosis was unchanged among these three groups. Retinas with ischemia-reperfusion injury (RIR) were selected as a positive control, showing a significant rise in the number of TUNEL + cells in the retina (**Figure 6A**). All the mice remained alert and responsive during the study periods, and no adverse effects were observed based on body weight (**Figure 6B**). Similar to the normal mice, the layers of the neural retina in the vehicle or DHA group were closed organized, and the cells were neatly arranged, as shown by HE staining of ocular sections. There were no obvious differences both in histologic morphology (**Figure 6C**) and retinal thickness (**Figure 6D**) among the three groups. In addition, the ERG amplitudes versus flash intensity for dark-adapted a-wave and b-wave were recorded

and indicated that there was no significant difference among these three groups. These results suggested that intragastric administration of DHA causes no obvious intraocular toxicity within the dosage range used in this study.

DISCUSSION

The present study investigated the efficacy of DHA on experimental laser-induced CNV in mice and showed that intragastric administration of DHA markedly suppressed laser-induced CNV. The activation of NF-κB signaling was related to inflammatory and angiogenesis reactions, which have a key role in the development of CNV, and these changes were notably reduced following DHA administration. These data suggested
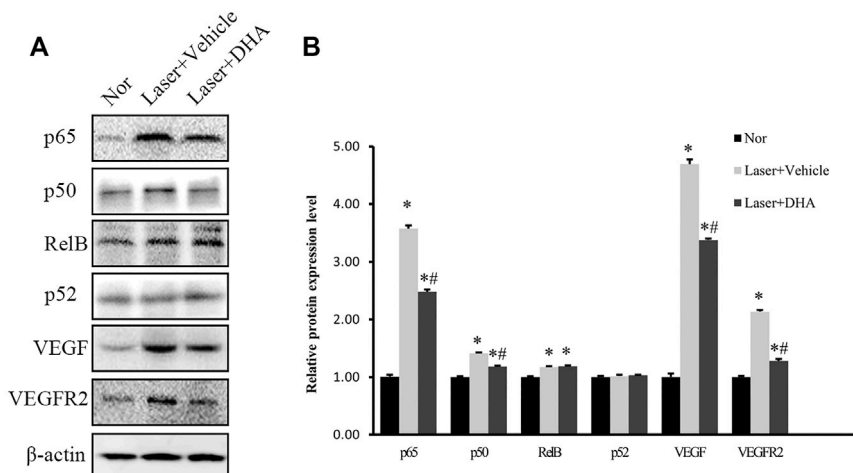
FIGURE 5 | The impact of DHA on the protein expression levels of the NF-κB family, VEGF, and VEGFR2 in the RPE-choroid complex of a laser-induced CNV mouse model. Mice were intragastrically administered vehicle or DHA once a day for 12 days. **(A)** The typical Western blot results showed changes in NF-κB family, VEGF, and VEGFR2 protein expression. **(B)** The quantitative analysis results demonstrated that the expression levels of NF-κB p65, NF-κB1 p50, Rel B, VEGF, and VEGFR2 were markedly increased in the vehicle group compared to the normal control group. DHA significantly inhibited the expression of NF-κB p65, NF-κB1 p50, VEGF, and VEGFR2. $n = 3$ experiments; $^*p < .05$ vs Nor; $^\#p < .05$ vs Laser + Vehicle; one-way ANOVA followed by Tukey's test. CNV: Choroidal Neovascularization; DHA: Dihydroartemisinin.
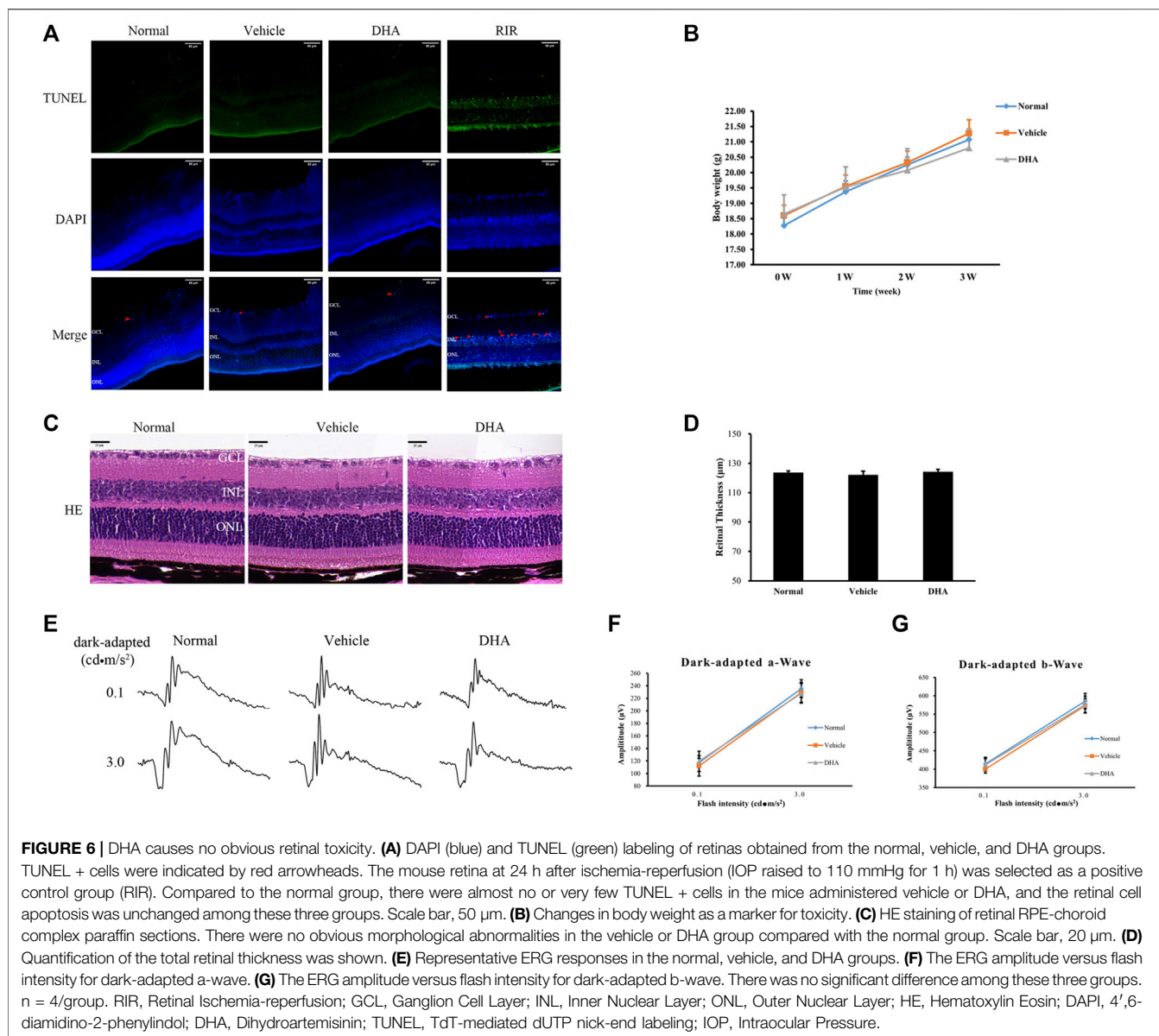
that DHA might have inhibitory effects on CNV by suppressing NF-κB signaling *in vivo* (**Figure 7**).

DHA, derived from the Chinese herbal medicine artemisinin, is known as a traditional antimalarial drug and shows anti-inflammatory and antiangiogenic properties (D'Alessandro et al., 2007). The anti-inflammatory effects of DHA have been studied broadly. In a lipopolysaccharide-induced acute kidney injury mouse model, treatment with DHA improved renal function by inhibiting NF-κB-mediated inflammation, ameliorating tubular cell apoptosis, and suppressing oxidative stress (Huang et al., 2019). In endothelial cells, DHA not only reduced prostaglandin (PG) E2 levels but also blunted the upregulation of the inflammatory cytokines interleukin (IL)-6 and IL-1β induced by PGE2, suggesting the potential of DHA for the treatment of inflammatory vascular diseases (Yin et al., 2018). In addition, artemisinin and its derivatives have been reported to be highly effective against a wide variety of tumors (Efferth, 2017). The anticancer activity of DHA partially depends on its antiangiogenic effect, since targeting angiogenesis has become a major strategy for tumor therapy (Dai et al., 2021). Several previous studies demonstrated that DHA can inhibit angiogenesis by reducing the expression of HIFα, VEGF, and VEGF receptors (Huang et al., 2010; Dong et al., 2014; Cheong et al., 2020), which are therapeutic targets of CNV. In a rat model of corneal neovascularization, both 20 mg/L and 10 mg/L DHA could significantly reduce the proportion of NV area to the whole cornea by topical administration (Zhong et al., 2011). Considering the importance of inflammation and angiogenesis in CNV formation, we investigated the role of DHA in a mouse model of laser-induced CNV.

Although the pathogenesis underlying CNV has not been fully elucidated, increasing experimental and clinical studies have revealed that inflammation and NF-κB signaling are critical

factors that promote CNV formation. The NF-κB pathway has long been considered one of the potent prototypical proinflammatory signaling pathways, and its role in several aspects of human health has been established (Gambhir et al., 2015). In both colorectal and lung carcinoma, NF-κB plays a key role in pathological angiogenesis, and strategies to inhibit NF-κB are effective in decreasing tumors (Debusk et al., 2008; Sakamoto et al., 2009; Panahi et al., 2016). Izumi-Nagai et al. showed that carotenoids inhibited the activation of NF-κB signaling, including IκB-α degradation and p65 nuclear translocation, leading to the significant suppression of CNV (Izumi-Nagai et al., 2007; Izumi-Nagai et al., 2008). Additionally, the VEGF/VEGFR2 signaling axis drives tumor vascularization by activating proangiogenic signaling in endothelial cells (ECs), which is commonly targeted by antiangiogenic therapies. VEGFR2 has been identified as a downstream target gene regulated by NF-κB signaling that directly binds the VEGFR2 upstream promoter and activates its transcription (Rönicke et al., 1996; Dong et al., 2014). In the present study, we observed that DHA notably suppressed CNV leakage and decreased CNV areas. The protein levels of VEGF, VGFER2, NF-κB p65, and NF-κB1 p50 increased significantly in the eyes of experimental laser-induced CNV, and these changes were profoundly inhibited following DHA administration. These results demonstrated that DHA may inhibit CNV formation by regulating the NF-κB/VEGFR2 signaling axis *in vivo*.

Considering the limitations of anti-VEGF in patients with neovascular AMD, DHA has its own advantages. As one of the most common causes of blindness, neovascular AMD has been a global health problem in the elderly population. Currently, intravitreal anti-VEGF drugs, including ranibizumab, bevacizumab, aflibercept, and brolucizumab, have revolutionized the treatment of neovascular AMD (Mettu et al., 2020). However, many patients suffer from an

FIGURE 6 | DHA causes no obvious retinal toxicity. **(A)** DAPI (blue) and TUNEL (green) labeling of retinas obtained from the normal, vehicle, and DHA groups. TUNEL + cells were indicated by red arrowheads. The mouse retina at 24 h after ischemia-reperfusion (IOP raised to 110 mmHg for 1 h) was selected as a positive control group (RIR). Compared to the normal group, there were almost no or very few TUNEL + cells in the mice administered vehicle or DHA, and the retinal cell apoptosis was unchanged among these three groups. Scale bar, 50 μm. **(B)** Changes in body weight as a marker for toxicity. **(C)** HE staining of retinal RPE-choroid complex paraffin sections. There were no obvious morphological abnormalities in the vehicle or DHA group compared with the normal group. Scale bar, 20 μm. **(D)** Quantification of the total retinal thickness was shown. **(E)** Representative ERG responses in the normal, vehicle, and DHA groups. **(F)** The ERG amplitude versus flash intensity for dark-adapted a-wave. **(G)** The ERG amplitude versus flash intensity for dark-adapted b-wave. There was no significant difference among these three groups. n = 4/group. RIR, Retinal Ischemia-reperfusion; GCL, Ganglion Cell Layer; INL, Inner Nuclear Layer; ONL, Outer Nuclear Layer; HE, Hematoxylin Eosin; DAPI, 4′,6-diamidino-2-phenylindol; DHA, Dihydroartemisinin; TUNEL, TdT-mediated dUTP nick-end labeling; IOP, Intraocular Pressure.

incomplete response to anti-VEGF therapy, and intravitreal injection causes potential complications, such as vitreous hemorrhage, infection, and retinal detachment. Repeated injections lead to a higher chance of drug resistance and poor patient compliance (Wei et al., 2018). Compared to anti-VEGF therapy, DHA may avoid these disadvantages. First, DHA, used for treating malaria clinically for many years, has been proven to be safe and has fewer side effects *in vivo* (Gutman et al., 2017). DHA within the dosage range in this study caused no obvious abnormalities in detailed retinal morphology and apoptosis of retinal cells, which was analyzed by HE staining and TUNEL assay. Second, DHA can be administered via the oral route, which is more acceptable to patients and prevents the adverse effects caused by intravitreal injection (Okada et al., 2020). Third, as a cost-effective drug, DHA has potential application prospects for the treatment of CNV to reduce the economic burden in patients

with neovascular AMD. These advantages give DHA potent applications for the treatment of CNV.

To better evaluate the clinical significance of DHA, only lesions with clinical meaning of CNV were chosen for experiments in this study, which were confirmed by FFA 4 days after laser photocoagulation (**Figure 1**). Previous studies have shown that experimental CNV can be clearly identified by FFA on day 4 after laser photocoagulation in all cases by leakage and as fibrovascular and tubular structures in histological HE-stained sections (Hoerster et al., 2012). Then, the CNV-inhibiting effect of DHA was compared with intravitreal injections of ranibizumab. Whether in CNV areas or thicknesses, there was no significant difference between the DHA group and ranibizumab group ($p > .05$). These results showed broad clinical application prospects of DHA in the treatment of CNV. However, some questions remained to be addressed in
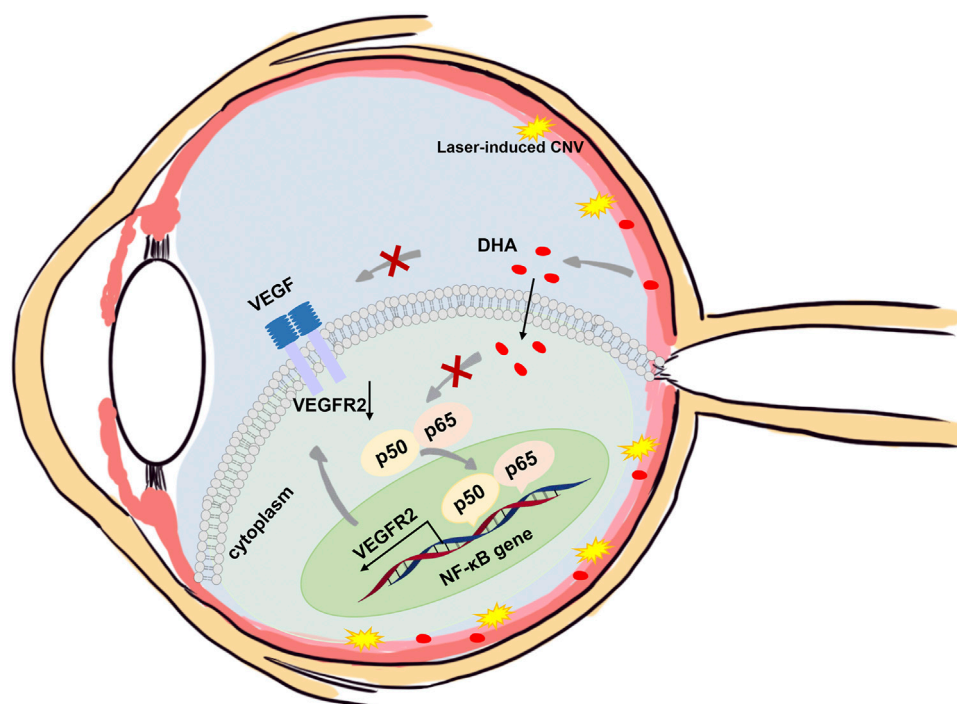
FIGURE 7 | Schematic illustration of the mechanisms of the anti-CNV effects of DHA. In addition to the downregulation of VEGF expression, DHA inhibits VEGFR2 expression and angiogenesis through suppression of the NF-κB pathway.

our study. As for the laser-induced CNV mouse model, diminished tubular structures observed by fluorescence and confocal microscopy of perfused flat-mounts showed spontaneous regression of CNV after 2 weeks. This tendency to spontaneous RPE recovery and CNV regression constitutes a major limitation of this model for interventional studies. Furthermore, the potential mechanism by which DHA inhibits CNV may not be limited to the NF-κB/VEGFR2 signaling axis and needs to be elucidated in more detail in future experiments.

In summary, the present study has demonstrated for the first time that systemic administration of DHA attenuates vascular leakage and the formation of CNV through a laser-induced CNV mouse model, which has been used for most neovascular AMD study experiments. This effect might be due to the suppression of the classic NF-κB signaling pathway and downregulation of VEGFR2 and VEGF expression. Our data indicate that DHA could be a natural potential alternative therapeutic strategy for neovascular AMD.

DATA AVAILABILITY STATEMENT

The raw data supporting the conclusion of this article will be made available by the authors, without undue reservation.

ETHICS STATEMENT

The animal study was reviewed and approved by the Animal Ethics Committee, West China Hospital.

AUTHOR CONTRIBUTIONS

XL and SG performed the experiments, analyzed the data, and wrote the manuscript. MZ and XL designed the study. YZ, MX, and CZ performed experiments and analyzed the data. MZ, QX, and NY designed the study and critically read the manuscript. MZ contributed to the critical revision of the manuscript for important intellectual content and approved the final version of the manuscript. All authors have read and approved the final manuscript.

FUNDING

REFERENCES

Apte, R. S. (2021). Age-Related Macular Degeneration. *N. Engl. J. Med.* 385, 539–547. doi:10.1056/NEJMcp2102061

Chakravarthy, U., and Peto, T. (2020). Current Perspective on Age-Related Macular Degeneration. *JAMA J. Am. Med. Assoc.* 324 (8), 794–795. doi:10.1001/jama.2020.5576

Cheong, D. H. J., Tan, D. W. S., Wong, F. W. S., and Tran, T. (2020). Anti-malarial Drug, Artemisinin and its Derivatives for the Treatment of Respiratory Diseases. *Pharmacol. Res.* 158, 104901. doi:10.1016/j.phrs.2020.104901

D'Alessandro, S., Gelati, M., Basilico, N., Parati, E. A., Haynes, R. K., and Taramelli, D. J. T. (2007). Differential Effects on Angiogenesis of Two Antimalarial Compounds, Dihydroartemisinin and Artemisone: Implications for Embryotoxicity. *Toxicology* 241, 66–74. doi:10.1016/j.tox.2007.08.084

Dai, X., Zhang, X., Chen, W., Chen, Y., Zhang, Q., Mo, S., et al. (2021). Dihydroartemisinin: A Potential Natural Anticancer Drug. *Int. J. Biol. Sci.* 17, 603–622. doi:10.7150/ijbs.50364

Debusk, L. M., Massion, P. P., and Lin, P. C. (2008). I B Kinase- Regulates Endothelial Cell Motility and Tumor Angiogenesis. *Cancer Res.* 68, 10223–10228. doi:10.1158/0008-5472.can-08-1833

Dong, F., Zhou, X., Li, C., Yan, S., Deng, X., Cao, Z., et al. (2014). Dihydroartemisinin Targets VEGFR2 via the NF-Kb Pathway in Endothelial Cells to Inhibit Angiogenesis. *Cancer Biol. Ther.* 15, 1479–1488. doi:10.4161/15384047.2014.955728

Efferth, T. (2017). From Ancient Herb to Versatile, Modern Drug: Artemisia Annua and Artemisinin for Cancer Therapy. *Semin. Cancer Biol.* 46, 65–83. doi:10.1016/j.semcancer.2017.02.009

Feng, L., Ju, M., Lee, K. V., Mackey, A., Evangelista, M., Iwata, D., et al. (2017). A Proinflammatory Function of Toll-Like Receptor 2 in the Retinal Pigment Epithelium as a Novel Target for Reducing Choroidal Neovascularization in Age-Related Macular Degeneration. *Am. J. Pathol.* 87 (10), 2208–2221. doi:10.1016/j.ajpath.2017.06.015

Gaddipati, S., Lu, Q., Kasetti, R. B., Miller, M. C., Lu, Q., Trent, J. O., et al. (2015). IKK2 Inhibition Using TPCA-1-Loaded PLGA Microparticles Attenuates Laser-Induced Choroidal Neovascularization and Macrophage Recruitment. *Plos One* 10, e0121185. doi:10.1371/journal.pone.0121185

Gambhir, S., Vyas, D., Hollis, M., Aekka, A., and Vyas, A. (20152015). Nuclear Factor Kappa B Role in Inflammation Associated Gastrointestinal Malignancies. *World J. Gastroenterol.* 21 (11), 3174–3183. doi:10.3748/wjg.v21.i11.3174

Ghosh, S., Shang, P., Yazdankhah, M., Bhutto, I., Hose, S., Montezuma, S. R., et al. (2017). Activating the AKT2-Nuclear Factor-Kb-Lipocalin-2 axis Elicits an Inflammatory Response in Age-Related Macular Degeneration. *J. Pathol.* 241, 583–588. doi:10.1002/path.4870

Guo, L., Dong, F., Hou, Y., Cai, W., Zhou, X., Huang, A. L., et al. (2014). Dihydroartemisinin Inhibits Vascular Endothelial Growth Factor-Induced Endothelial Cell Migration by a P38 Mitogen-Activated Protein Kinase-Independent Pathway. *Exp. Ther. Med.* 8, 1707–1712. doi:10.3892/etm.2014.1997

Gutman, J., Kovacs, S., Dorsey, G., Stergachis, A., and Ter Kuile, F. O. (2017). Safety, Tolerability, and Efficacy of Repeated Doses of Dihydroartemisinin-Piperaquine for Prevention and Treatment of Malaria: A Systematic Review and Meta-Analysis. *Lancet Infect. Dis.* 17 (16), 184–193. doi:10.1016/S1473-3099(16)30378-4

Hoerster, R., Muether, P. S., Vierkotten, S., Schröder, S., Kirchhof, B., and Fauser, S. (2012). *In-Vivo* and *Ex-Vivo* Characterization of Laser-Induced Choroidal Neovascularization Variability in Mice. *Graefes Arch. Clin. Exp. Ophthalmol.* 250, 1579–1586. doi:10.1007/s00417-012-1990-z

Huang, X. J., Ma, Z. Q., Zhang, W. P., Lu, Y. B., and Wei, E. Q. (2010). Dihydroartemisinin Exerts Cytotoxic Effects and Inhibits Hypoxia Inducible Factor-1alpha Activation in C6 Glioma Cells. *J. Pharm. Pharmacol.* 59, 849–856. doi:10.1211/jpp.59.6.0011

Huang, X. T., Liu, W., Zhou, Y., Hao, C. X., Zhou, Y., Zhang, C. Y., et al. (2019). Dihydroartemisinin Attenuates Lipopolysaccharide-Induced Acute Lung Injury in Mice by Suppressing NF-κB Signaling in an Nrf2-Dependent Manner. *Int. J. Mol. Med.* 44, 2213–2222. doi:10.3892/ijmm.2019.4387

Izumi-Nagai, K., Nagai, N., Ohgami, K., Satofuka, S., Ozawa, Y., Tsubota, K., et al. (2008). Inhibition of Choroidal Neovascularization with an Anti-Inflammatory Carotenoid Astaxanthin. *Invest. Ophthalmol. Vis. Sci.* 49, 1679–1685. doi:10.1167/iovs.07-1426

Izumi-Nagai, K., Nagai, N., Ohgami, K., Satofuka, S., Ozawa, Y., Tsubota, K., et al. (2007). Macular Pigment Lutein Is Antiinflammatory in Preventing Choroidal Neovascularization. *Arterioscler Thromb. Vasc. Biol.* 27, 2555–2562. doi:10.1161/ATVBAHA.107.151431

Jaffe, G. J., Ying, G. S., Toth, C. A., Daniel, E., Grunwald, J. E., Martin, D. F., et al. (2019). Macular Morphology and Visual Acuity in Year Five of the Comparison of Age-Related Macular Degeneration Treatments Trials. *Ophthalmology* 126, 252–260. doi:10.1016/j.ophtha.2018.08.035

Karin, M. (2006). Nuclear Factor-kappaB in Cancer Development and Progression. *Nature* 441, 431–436. doi:10.1038/nature04870

Mehta, H., Tufail, A., Daien, V., Lee, A. Y., Nguyen, V., Ozturk, M., et al. (2018). Real-World Outcomes in Patients with Neovascular Age-Related Macular Degeneration Treated with Intravitreal Vascular Endothelial Growth Factor Inhibitors. *Prog. Retin. Eye Res.* 65, 127–146. doi:10.1016/j.preteyeres.2017.12.002

Mettu, P. S., Allingham, M. J., and Cousins, S. W. (2020). Incomplete Response to Anti-VEGF Therapy in Neovascular AMD: Exploring Disease Mechanisms and Therapeutic Opportunities. *Prog. Retin. Eye Res.* 82, 100906. doi:10.1016/j.preteyeres.2020.100906

Okada, M., Mitchell, P., Finger, R. P., Eldem, B., and Loewenstein, A. (2020). Non-Adherence or Non-Persistence to Intravitreal Injection Therapy for Neovascular Age-Related Macular Degeneration: A Mixed-Methods Systematic Review. *Ophthalmology* 128 (2), 234–247. doi:10.1016/j.ophtha.2020.07.060

Ozone, D., Mizutani, T., Nozaki, M., Ohbayashi, M., Hasegawa, N., Kato, A., et al. (2016). Tissue Plasminogen Activator as an Antiangiogenic Agent in Experimental Laser-Induced Choroidal Neovascularization in Mice. *Invest. Ophthalmol. Vis. Sci.* 57, 5348–5354. doi:10.1167/iovs.16-19617

Panahi, Y., Darvishi, B., Ghanei, M., Jowzi, N., Beiraghdar, F., Varnamkhasti, B. S. J. C., et al. (2016). Molecular Mechanisms of Curcumins Suppressing Effects on Tumorigenesis, Angiogenesis and Metastasis, Focusing on NF-Kb Pathway. *Cytokine Growth Factor. Rev.* 28, 21–29. doi:10.1016/j.cytogfr.2015.12.004

Rönicke, V., Risau, W., and Breier, G. (1996). Characterization of the Endothelium-specific Murine Vascular Endothelial Growth Factor Receptor-2 (Flk-1) Promoter. *Circ. Res.* 79, 277–285. doi:10.1161/01.res.79.2.277

Sakamoto, K., Maeda, S., Hikiba, Y., Nakagawa, H., Hayakawa, Y., Shibata, W., et al. (2009). Constitutive NF-kappaB Activation in Colorectal Carcinoma Plays a Key Role in Angiogenesis, Promoting Tumor Growth. *Clin. Cancer Res.* 15, 2248–2258. doi:10.1158/1078-0432.CCR-08-1383

Wei, X., Zhang, T., Yao, Y., Zeng, S., Li, M., Xiang, H., et al. (2018). Efficacy of Lenvatinib, a Multitargeted Tyrosine Kinase Inhibitor, on Laser-Induced CNV Mouse Model of Neovascular AMD. *Exp. Eye Res.* 168, 2–11. doi:10.1016/j.exer.2017.12.009

Wong, C. W., Yanagi, Y., Lee, W. K., Ogura, Y., Yeo, I., Wong, T. Y., et al. (2016). Age-related Macular Degeneration and Polypoidal Choroidal Vasculopathy in Asians. *Prog. Retin. Eye Res.* 53, 107–139. doi:10.1016/j.preteyeres.2016.04.002

Yin, J., Xia, W., Zhang, Y., Ding, G., Chen, L., Yang, G., et al. (2018). Role of Dihydroartemisinin in Regulating Prostaglandin E 2 Synthesis cascade and Inflammation in Endothelial Cells. *Heart Vessels* 33 (11), 1411–1422. doi:10.1007/s00380-018-1190-9

Zhao, M., Mantel, I., Gelize, E., Li, X., Xie, X., Arboleda, A., et al. (2019). Mineralocorticoid Receptor Antagonism Limits Experimental Choroidal Neovascularization and Structural Changes Associated with Neovascular Age-Related Macular Degeneration. *Nat. Commun.* 10, 369. doi:10.1038/s41467-018-08125-6

Zhao, M., Xie, W., Tsai, S. H., Hein, T. W., Rocke, B. A., Kuo, L., et al. (2018). Intravitreal Stanniocalcin-1 Enhances New Blood Vessel Growth in a Rat Model of Laser-Induced Choroidal Neovascularization. *Invest. Ophthalmol. Vis. Sci.* 59, 1125–1133. doi:10.1167/iovs.17-23083

Zhong, Y. Y., Zhang, H. F., Zhong, J. X., Bai, L., and Lu, X. H. (2011). Topical Dihydroartemisinin Inhibits Suture-Induced Neovascularization in Rat

Corneas through ERK1/2 and P38 Pathways. *Int. J. Ophthalmol.* 4, 150–155. doi:10.3980/j.issn.2222-3959.2011.02.08

Publisher's Note: All claims expressed in this article are solely those of the authors and do not necessarily represent those of their affiliated organizations, or those of the publisher, the editors and the reviewers. Any product that may be evaluated in this article, or claim that may be made by its manufacturer, is not guaranteed or endorsed by the publisher.

Check for updates

Diabetic Corneal Neuropathy: Pathogenic Mechanisms and Therapeutic Strategies

Ting Zhou, Allie Lee, Amy Cheuk Yin Lo * and Jeremy Sze Wai John Kwok

Department of Ophthalmology, Li Ka Shing Faculty of Medicine, The University of Hong Kong, Pokfulam, Hong Kong SAR, China

Diabetes mellitus (DM) is a major global public health problem that can cause complications such as diabetic retinopathy, diabetic neuropathy, and diabetic nephropathy. Besides the reporting of reduction in corneal nerve density and decrease in corneal sensitivity in diabetic patients, there may be a subsequent result in delayed corneal wound healing and increased corneal infections. Despite being a potential cause of blindness, these corneal nerve changes have not gained enough attention. It has been proposed that corneal nerve changes may be an indicator for diabetic neuropathy, which can provide a window for early diagnosis and treatment. In this review, the authors aimed to give an overview of the relationship between corneal nerves and diabetic neuropathy as well as the underlying pathophysiological mechanisms of corneal nerve fiber changes caused by DM for improved prediction and prevention of diabetic neuropathy. In addition, the authors summarized current and novel therapeutic methods for delayed corneal wound healing, nerve protection and regeneration in the diabetic cornea.

Keywords: corneal nerve damage, corneal confocal microscopy, diabetic complications, dry eye, nerve regeneration, ocular disease, ocular surface

INTRODUCTION

Diabetes mellitus (DM) is a chronic metabolic disorder characterized by abnormally increased blood glucose level, which over time leads to severe systemic damage such as diabetic foot ulcers, nephropathy and neuropathy. According to World Health Organization (WHO), about 422 million people worldwide suffer from DM, and 1.6 million deaths are directly attributed to DM each year (WHO, 2021). Over the past few decades, the number of cases and prevalence of DM have been increasing steadily. Thus, the huge public health challenge and economic burden that many countries are about to face emphasize the importance of effective treatment and prevention for various complications associated with DM.

Abbreviations: AGEs, advanced glycation end products; ARI, aldose reductase inhibitor; BDNF, brain-derived neurotrophic factor; CCM, corneal confocal microscopy; CNTF, ciliary neurotrophic factor; DHA, docosahexaenoic acid; DM, diabetes mellitus; DN, diabetic neuropathy; DR, diabetic retinopathy; FFA, free fatty acid; GDNF, glial cell line-derived neurotrophic factor; GLP-1, glucagon-like peptide 1; IGF-1, insulin-like growth factor-1; LDL-C, low-density lipoprotein cholesterol; NADPH, nicotinamide adenine dinucleotide phosphate; NGF, nerve growth factor; NPD1, neuroprotectin D1; NT-3, neurotrophin-3; OGF, opioid growth factor; PKC, protein kinase C; PPAR, proliferator-activated receptor; rhNGF, recombinant human nerve growth factor; ROS, reactive oxygen species; SP, Substance P; STZ, streptozotocin; TID, type 1 diabetes; T2D, type 2 diabetes; VEGF, vascular endothelial growth factor; VIP, vasoactive intestinal peptide; WHO, World Health Organization.

The complications of DM include cardiovascular disease, nephropathy, retinopathy and neuropathy (Markoulli et al., 2018). Among them, diabetic retinopathy has been well-recognized. Besides, it was reported that more than half of the patients were presented with alternation of anterior segment (such as cornea, conjunctiva, lacrimal gland and lens) during DM progression (Vieira-Potter et al., 2016; Barsegian et al., 2018); but these symptoms are sometimes overlooked. Indeed, DM patients have shown a progressive loss in corneal nerve fiber and a decrease in corneal sensitivity (Dogru et al., 2001; Pritchard et al., 2015), which subsequently led to delayed nerve regeneration and wound healing after injury, dry eye, persistent epithelial defects, and neurotrophic ulcers (Kaiserman et al., 2005; Pritchard et al., 2011). These complications may cause severe vision loss or even blindness, reminding us that it is vital to understand the effects of DM on corneal nerves (Bikbova et al., 2018; Han et al., 2018).

In this review, the authors outlined the association between DM and corneal nerves and summarized the current knowledge regarding the underlying pathophysiologic mechanisms of corneal nerve fiber changes caused by DM. Also, the authors explored current and the most recent therapeutic approaches for nerve protection and regeneration in the diabetic cornea.

DIABETIC CORNEAL NEUROPATHY

Clinical Perspectives of Corneal Neuropathy in Diabetes Mellitus

The cornea is one of the most important parts of optical system. Its transparent and avascular physiological characteristics ensure clear vision (Al-Aqaba et al., 2019). The cornea is innervated by the trigeminal nerve; it indeed is the most densely innervated structure in the entire human body. The cornea is also one of the most sensitive body parts to pain as the number of free epithelial nerve endings are 300–600 times that of the skin. Cornea contains a large number of small nerve fibers like myelinated A-δ fibers and unmyelinated C fibers. The physiological function of A-δ fibers is cold sensation and nociception, while C fibers are mainly responsible for warm, cold, thermal perception (Körei et al., 2016). These sensory nerves also control reflex function and tear secretion. In addition, the corneal nerves play a crucial neurotrophic role through releasing neurotrophic factors to maintain integral and healthy structure and function of the ocular surface, and are the major determinant in maintaining ocular surface homeostasis, corneal sensitivity, epithelial health, and wound healing (Byun et al., 2015; Labetoulle et al., 2019).

It was reported that neuropathy of the cornea occurred in the early stage of DM (Zhao et al., 2019). The clinical symptoms in diabetic patients with corneal neuropathy are photophobia, eye irritation or pain (Bikbova et al., 2018). Some patients have no symptoms, but subclinical changes in the cornea may exist (Rehany et al., 2000; Scheler et al., 2012). Chronic hyperglycemia in diabetic patients can cause damage to the trigeminal nerve, leading to a reduction or loss of corneal nerves, most of which are damages to A-δ and C nerve fibers. Damage or loss of corneal innervation can in turn lead to reduced

corneal nerve fiber density, attenuated corneal sensitivity, dry eyes, delayed wound healing, subsequently developing into corneal ulcers, perforations, and even blindness (Shaheen et al., 2014).

In vivo corneal confocal microscopy (CCM) is an essential method to investigate the fine structure of corneal nerves in detail. It provides real-time visualization of corneal nerve fibers in a non-invasive way, allowing long-term longitudinal studies in both patients and animal models (Leckelt et al., 2016). The acquired corneal images can be analyzed by appropriate software for the identification of quantitative indicators (Schaldemose et al., 2020). Using CCM, several published studies reported corneal nerve fiber changes in diabetic patients. Whether it is type 1 diabetes (TID) or type 2 diabetes (T2D), the nerve fiber length, nerve fiber density and nerve branch density in these patients were significantly reduced (Chen et al., 2018; Li et al., 2019; Lewis et al., 2020). Lagali et al. revealed that as type 2 diabetes continued, the sub-basal nerve plexus showed a progressive degeneration (Lagali et al., 2017). They found a reduction of the main nerve branches, an apparent loss of the secondary nerve fiber branches as well as a loss of the connection with the primary nerve. In addition, one study examined the correlation between corneal nerve parameters and glucose variability. It explored whether short-term measures of blood glucose control were related to structural and functional alternations of corneal nerve in TID patients and found that significant loss of corneal nerve length in the inferior whorl occurred in patients with increased glucose variability and time above range (Issar et al., 2020). Moreover, the decrease in corneal keratocyte density was associated with damage in the sub-basal nerve plexus in diabetic patients (Kalteniece et al., 2018a). Other studies found that the density of the sub-basal nerve plexus in diabetic patients was attenuated while the density of Langerhans cells was increased (Qu et al., 2018; Ferdousi et al., 2019). These changes (lower corneal keratocyte density and higher Langerhans cells density) were related to delayed corneal epithelial healing (Qu et al., 2018). These data can help clinicians to better understand when and how diabetic corneal neuropathy develops and monitor cornea alternation and its progression.

Many clinical studies also explored the association between diabetic corneal nerve damage and complications of DM with CCM. Several studies demonstrated that changes in corneal nerve fibers were related to the development of diabetic retinopathy (DR). One study reported that in T2D patients, corneal nerve damage preceded the development of DR (Bitirgen et al., 2014). In TID patients with a four-year development of DM with/without DR, it was found that their corneal nerve fiber length was one of the predictors for worsening of DR (Srinivasan et al., 2018). The authors also reported that neuronal degeneration of both cornea and retina may occur in early stage of DR, so examination of corneal nerve was necessary especially when clinical signs of DR was absent (Srinivasan et al., 2017; Srinivasan et al., 2018). Meanwhile, reduction of corneal nerve fiber density, corneal nerve fiber length and nerve fractal dimension occurred in T2D patients with diabetic nephropathy. These corneal alternations were related to the
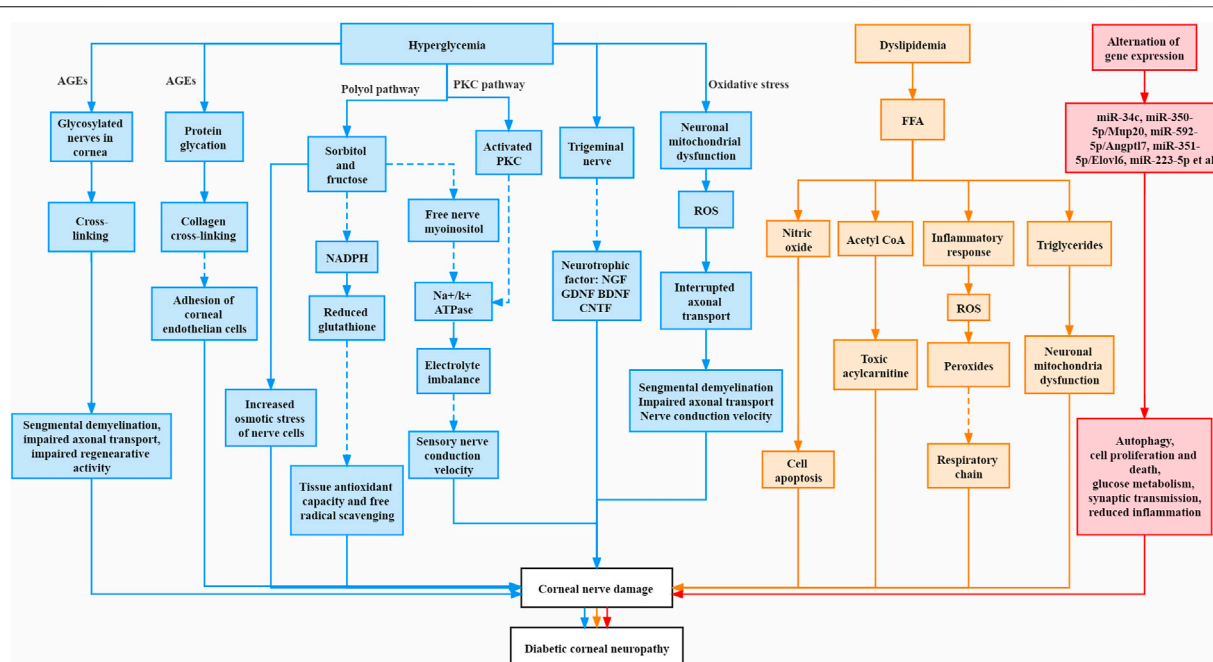
FIGURE 1 | Pathogenesis of corneal neuropathy in diabetes mellitus. The Solid line represents increase and promotion, and the dashed line represents decrease and inhibition.

decline of kidney function (Tummanapalli et al., 2020a). There were more clinical studies that focused on the damage of corneal nerve in diabetic neuropathy (DN). Edwards et al. demonstrated that the length and density of corneal nerve fibers in diabetic patients with mild DN were significantly reduced (compared to the control group and diabetic patients without DN) (Edwards et al., 2012). Similarly, other studies have reached consistent conclusions. They stated that the parameters of corneal nerve fibers could predict the development of DN and are a potential clinical biomarker for evaluating DN (Deák et al., 2019). Compared with controls, the corneal parameters of T1D and T2D patients, such as nerve fiber density, branch density, and nerve fiber length, were significantly reduced, and these indicators progressively worsened when the severity of DN increased (Kalteniece et al., 2020). The corneal nerve fibers in the inferior whorl region of diabetic patients were shown to be more sensitive to the damage than those in the central cornea, suggesting that the reduction of corneal nerve fibers is more significant in the inferior region (Kalteniece et al., 2018b; Ferdousi et al., 2020). Moreover, corneal nerve fiber damage was more severe in patients with painful neuropathy when compared with painless neuropathy (Kalteniece et al., 2018b). The results obtained from all these studies indicated an important association of corneal nerve with DM while corneal nerve fibers may be a reproducible biomarker for detection and assessment of early nerve damage in diabetes.

Of note, current diagnosis tests for DN patients without obvious symptoms include filament test, quantitative sensory test, nerve conduction test, muscle response test (electromyography), and autonomic test. All of these are tests

designed for assessing large nerve fiber function (Selvarajah et al., 2019). However, impairment of small nerve fibers (type C and A-δ nerve fiber) is considered the earliest alteration in the course of DN, which progresses to large nerve fiber (Körei et al., 2016). Since the gold standard test for small fiber neuropathy is skin biopsy with intraepidermal nerve fiber density analysis, this invasive procedure makes it hard to implement in routine clinical practice (Basantsova et al., 2019). By the time when DN is detected with the aforementioned tests for large nerve fibers, it is very often well established already; but the neuropathic process can no longer be reversed. In conclusion, the detection of corneal nerve fiber with CCM may provide an open window for diagnosis of DN. It may potentially be a biomarker for the progression, or even treatment efficacy of DN. This emphasizes the importance of understanding the pathogenic mechanisms of corneal neuropathy in diabetes.

Pathogenesis

Many pathological changes were involved in diabetic corneal neuropathy, which interplayed and complemented each other, leading to abnormalities in cornea, including severe damage to corneal nerves (Roszkowska et al., 2021). The mechanism is summarized in **Figure 1**.

Hyperglycemia

Advanced Glycation End Products

Advanced glycation end products (AGEs) are reactive metabolites produced by the glycation of proteins or lipids that are exposed to sugar molecules and form non-enzymatic covalent bonds with each other (Babizhayev et al., 2015). The structural and functional

proteins of peripheral nerves were reported to be glycosylated and they underwent cross-linking over time in diabetic patients and diabetic animal models. This resulted in an elevation of AGE level and in turn led to segmental demyelination, impaired axon transport and impaired regenerative activity (Sugimoto et al., 2008). In addition, AGEs may cause cross-linking of collagen fibris (Sady et al., 1995). Kaji et al. reported that glycosylated laminin and fibronectin reduced cell adhesion of corneal endothelial cells, thus leading to abnormalities of the diabetic cornea (Kaji et al., 2001). Moreover, AGEs were shown to change the structure and function of corneal epithelium, stroma and basement membrane (Bejarano and Taylor, 2019).

The Polyol Pathway

The polyol pathway is also known as the sorbitol-aldose reductase pathway. Chronic hyperglycemia leads to excessive glucose in nerve cells, resulting in saturation of the normal glycolytic pathway. Excess glucose is then shunted to the polyol pathway; it is first converted to sorbitol and then fructose by intracellular enzymes reductase and sorbitol dehydrogenase, respectively (Stavniichuk et al., 2012). These two sugar molecules (sorbitol and fructose) tend to accumulate within nerve cells because nerve cell membrane is impermeable to them, thus increasing the osmotic stress of nerve cells (Oates, 2008). At the same time, during the reduction process, aldose reductase consumes the cofactor nicotinamide adenine dinucleotide phosphate (NADPH) and leads to a decrease of reduced glutathione production, tissue antioxidant capacity and free radical scavenging, thereby causing tissue damage (Lyu et al., 2019). In addition, excessive amounts of sorbitol and fructose results in the decrease of free nerve myoinositol, which is sugar alcohol required for normal nerve conduction velocity (Greene et al., 1992). A decrease in its level can lead to a reduction in membrane sodium potassium adenosine triphosphatase (Na^+/K^+ ATPase) activity, resulting in electrolyte imbalance, reducing nerve conduction velocity, and destroying the structure of nerve fibers (Zhu et al., 2019).

Protein Kinase C Activation Pathway

Protein kinase C (PKC) is also an important pathogenic mechanism. In DM, increased intracellular glucose level plays a role in the synthesis of PKC activator diacylglycerol. The activation of PKC inhibits Na^+/K^+ ATPase activity, thereby affecting nerve conduction and nerve regeneration (Geraldes and King, 2010). A study found that the use of the PKC inhibitor ruboxistaurin mesylate improved microvascular blood flow and nerve conduction, thereby alleviating the symptoms of DN and improving the life quality of diabetic patients (Casellini et al., 2007).

Neurotrophic Factors

Results of several *in vitro* studies indicated that there is a mutual trophic support between the corneal nerve plexus and the corneal epithelium. The corneal nerve plexus secretes neuropeptides to maintain epithelial homeostasis and enhance wound healing. The corneal epithelium releases neurotrophic factors, such as nerve growth factor (NGF) and glial cell line-derived neurotrophic

factor (GDNF), which can accelerate epithelial wound healing and stimulate neurite survival (Bikbova et al., 2016; Barsegian et al., 2018). Brain-derived neurotrophic factor (BDNF) is found in both corneal epithelial cells and corneal neurons (Byun et al., 2015). Therefore, the corneal nerve is closely related to the corneal epithelium. Neuropeptides released by sensory nerves could support epithelial cells and dendritic cells in the cornea to maintain its homeostasis. Chronic hyperglycemia may affect the neuropeptide secretion from the corneal nerves, thereby affecting the proliferation of cells in cornea (Markoulli et al., 2017; Zhang J. et al., 2020). In the denervated cornea of rats, the rate of mitosis of corneal epithelial cells was changed (Ferrari et al., 2011). Gao et al. discovered that the number of dendritic cells, the main source of ciliary neurotrophic factor (CNTF), in the diabetic cornea was reduced. They demonstrated that the neural communication of dendritic cells was affected, resulting in impaired innervation and regeneration of sensory nerves (Gao et al., 2016). Zhou et al. found that in diabetic mice, a reduction of ciliary neurotrophic factor (CNTF) caused impaired corneal epithelial wounds, while CNTF supplementation could improve this pathology (Zhou et al., 2015). These articles demonstrated that diabetes could affect the corneal nerves through the secretion of neurotrophic factors, and at the same time affect the function of the corneal epithelium.

Oxidative Stress

Oxidative stress refers to the phenomenon that cells and tissues contain excessively high levels of reactive oxygen species (ROS), and the biological system has limited ability to reduce these active products to non-toxic substances (Pizzino et al., 2017). During hyperglycemia, there is an excessive influx of glucose into the mitochondria accelerating the oxidative metabolism of glucose in the mitochondria and the production of superoxide ions, thereby promoting the production of ROS (Babizhayev et al., 2015). Mitochondrial fission has been reported to occur in the neurites in response to hyperglycemia, generating oxidative stress and activating caspase 3. This was an indication of hyperglycemia-induced neurite damage (Vincent et al., 2010). In T2D patients, the length and density of corneal nerve fiber were decreased together with expanded beads in corneal nerve fiber. The bead is a novel parameter for a composite of accumulated mitochondria, glycogen particles and vesicles, which might be a predictor of slow sensory nerve conduction velocity in DM (Ishibashi et al., 2016). Mitochondrial abnormalities might be initiated by interrupted axonal transport, causing mitochondria to aggregate or cluster. As swollen mitochondria were difficult to be transported compared to smaller mitochondria, this eventually led to axonal demyelination and conduction dysfunction (Hamid et al., 2014). Mitochondrial damage is also related to the reduction of neurotrophic factors such as NGF and neurotrophin-3 (NT-3) (Zherebitskaya et al., 2009). One study found that increased 8-hydroxydeoxyguanosine (a marker of oxidative stress) was detected in the cornea of diabetic rats when compared with the control group (Kim et al., 2011a). This indicated a potential role of oxidative stress in the apoptosis of diabetic corneal cells.

Neuro-Immune Interactions

Neuro-immune interactions may also play a role in diabetic corneal neuropathy. In diabetic mouse models, high concentrations of Langerhans cells and dendritic cells, the main antigen-presenting cells, were found in the cornea and they aggregated around corneal nerve fibers (Leppin et al., 2014). When compared with the control group, the number of dendritic cells and Langerhans cells of diabetic patients elevated significantly, which negatively correlated with the length and density of corneal nerve fibers (Tavakoli et al., 2011). Another clinical study reported that early immune activation and corneal nerve degeneration occurred in adolescents with T1D (Ferdousi et al., 2019). In addition, it was reported that DNase I could promote corneal nerve regeneration and corneal sensitivity through decreasing the neutrophils extracellular traps caused by neutrophil aggregation (Zhang J. et al., 2020). However, this view is controversial (Ljubimov, 2017), and no concrete conclusion has been reached yet. It is not clear whether the infiltration of immune cells in the cornea precedes the induction of hyperglycemia.

Lipids

In addition to the effects of long-term hyperglycemia, dyslipidemia may also be a key factor in neuropathy, especially in T2D. Firstly, dyslipidemia can lead to an excessive increase in the level of free fatty acid (FFA), which can cause an elevation in nitric oxide, thereby leading to cell apoptosis (Stickings and Cunningham, 2002). Secondly, FFA enters the mitochondria and is catabolized by ß-oxidation to generate acetyl CoA. Excessive accumulation of acetyl CoA after dyslipidemia facilitates its conversion into toxic acylcarnitine substances, leading to nerve injury. Also, ß-oxidation activates inflammatory cells to release cytokines and induces the production of ROS, resulting in the production of peroxides. The oxidation of low-density lipoprotein inversely induces the generation of ROS, inhibits the electron transfer in the respiratory chain and aggravates nerve injury, which in turn forms a vicious circle (Roselló-Busquets et al., 2019; Rumora et al., 2019). Also, it is reported that decreased corneal nerve fiber length has an inverse correlation with low-density lipoprotein cholesterol (LDL-C) in T1D patients (Ferdousi et al., 2021). Moreover, when excessive FFA exhausts the oxidizing capacity of tissues, they are markedly deposited in non-fat tissues in the form of triglycerides, causing damage to these tissues. This phenomenon is called lipotoxicity. It is worth noting that the ability of neuronal mitochondria to metabolize and consume fatty acids is very limited (Schönfeld and Reiser, 2013). High levels of active oxygen can easily induce fatty acid peroxidation. If neuronal cells cannot clear up these peroxidized fatty acids in time, pathological changes will occur in the neurons, leading to neuropathy (Sultana et al., 2013).

Alternation of Gene Expression

Recently, several studies focused on the difference of gene expression between normal and diabetic trigeminal ganglion tissues. It was reported that in the trigeminal nerve tissue of T1D mice, abnormal expression of miR-34c could decrease sensory neuron growth of trigeminal nerve and the repair of corneal nerve endings by regulating the autophagy-related proteins Atg4B and LC3-II, thereby causing corneal neuropathy (Hu et al., 2019). Another study showed that some miRNA-mRNA pairs, such as miR-350-5p/Mup20, miR-592-5p/Angptl7 and miR-351-5p/Elovl6, are related to diabetic corneal neuropathy. And they reported that dysregulated genes could affect cell proliferation and death, glucose metabolism, and synaptic transmission (Zhang et al., 2020a). Recently, they further identified the miR-223-5p/*Hpgds* axis after screening by RNA sequencing. They reported that *Hpgds* is the direct target gene of miR-223-5p, and downregulation of miR-223-5p could promote corneal nerve regeneration by ameliorating inflammation (Zhang et al., 2021).

These studies provided new investigations on the pathogenesis of corneal neuropathy in DM and suggested that these alternations may be targets for gene therapy on diabetic corneal neuropathy.

TREATMENT

Strict glycemic control is a vital prerequisite for the treatment in diabetic complications. So far, treatment of diabetic corneal diseases is still symptomatic. Here, we summarized and discussed current and innovative treatments for diabetes-related corneal pathologies. The advantages and limitations of various treatments are summarized in **Table 1**.

Glycemic Control

Since chronic hyperglycemia can cause nerve damage through a variety of pathological mechanisms, strict glycemic control is believed to be an essential means to treat diabetes and reduce the progression of its related complications (Ponirakis et al., 2021a). Many drugs have been used to control blood glucose; they include oral drugs such as metformin, glucagon-like peptide-1 (GLP-1) receptor agonist or sodium–glucose cotransporter type 2 inhibitor, as well as injection drugs such as insulin.

Through analyzing the data of 1172 T1D patients, a prospective study of European Diabetes identified that the incidence of neuropathy was associated with potential risk factors like the duration of diabetes, total cholesterol and LDL-C and triglycerides, body mass index, hypertension and smoking (Tesfaye et al., 2005). Studies demonstrated that in TID and T2D patients, DN might be prevented or delayed by the improvement in glycemic control (Ishibashi and Tavakoli, 2018; Mahelková et al., 2018). A clinical trial found that after application of insulin eye drops in 14 diabetic patients, the rate of corneal epithelial regeneration and the healing rate of epithelial defects increased (Bastion and Ling, 2013). In two animal studies, the authors reported that insulin eye drops could prevent corneal sub-basal nerve or sub-epithelial nerve loss in streptozotocin (STZ)-induced diabetic mice (T1D) (Chen et al., 2013; Yorek et al., 2014). In addition, Song et al. found that early insulin treatment was beneficial to normalise the circadian rhythm of the cornea in mice with T1D (Song et al., 2016). Moreover, in T1D rats, metformin treatment showed a protective

TABLE 1 | Clinical and experimental therapeutic strategies for anterior segment disorders associated with diabetes.

Treatment strategy	Therapeutic agents/procedures	Clinical or experimental	Advantages	Limitations	References
Glycemic control	Insulin, Exenatide and pioglitazone	Clinical and experimental (rat, mouse)	Prevent nerve loss, Increase epithelial wound healing	Controversial effects in T2D, Increase IGF-1, exacerbate retinopathy	Smith et al. (1999); Chen et al. (2013); Yorek et al. (2014); Song et al. (2016); Khan et al. (2020); Ponirakis et al. (2020); Ponirakis et al. (2021b)
	Pancreatic islet cell transplantation	Clinical and experimental (rabbit)	Improve glycemic stability Reduce DN occurrence	Life-long immunosuppressive agents, Surgical complications, Not cost-effective	Wallner et al. (2016); Foster et al. (2018); Senior et al. (2018); Vantyghem et al. (2019)
Pharmacological intervention	Lipid-lowering drugs: statins	Clinical and experimental (rat)	Anti-inflammation, Reduce DN progression	Controversial effects	Bhalla et al. (2015); Miao Wang et al. (2021)
	Lipid-lowering drugs: fibrates	Clinical and experimental (rat, mouse)	Increase corneal nerve density, Improve corneal sensitivity	Side effects in T2D patients	Matlock et al. (2020)
	Supplements of fatty acids and its metabolites: menhaden oil, resolvin D1, DHA	Clinical and experimental (rabbit, rat, mouse)	Reverse corneal nerve loss, Promote neurite outgrowth, Resist oxidative stress	Very high dosage for clinical translation, Cotreatment with enalapril, a-lipoic acid, salsalate showed better effects	Lee et al. (2015); Serhan et al. (2015); Coppey et al. (2020); Lewis et al. (2021)
	ARI: Ranirestat, CT-112, ONO-2235	Clinical and experimental (rat)	Promote epithelial regeneration, Improve corneal sensitivity	Controversial effects in clinical trials	Fujishima and Tsubota (2002); Nakahara et al. (2005); Takamura et al. (2013)
	Trophic factor supplements: NGF	Clinical and experimental (rabbit, mouse)	Promote corneal nerve regeneration, Recover corneal sensitivity, Promote epithelial wound healing	Limited sources, High cost, Severe side effects	Bonini et al. (2000); Apfel (2002)
	Trophic factor supplements: SP	Experimental (rabbit, rat, mouse)	Promote epithelial wound healing	Only have effects when co-treatment with IGF-1	Abdelkader et al. (2011); Rocha-Neto et al. (2019); Tummanapalli et al. (2019)
	Trophic factor supplements: C-peptide	Experimental (rat, mouse)	Increase sub-basal nerve density	Short biological half-life, Unclear mechanism, Difficult clinical translation	Jolivalt et al. (2015)
	Trophic factor supplements: GLP-1	Experimental (mouse)	Increase neurite outgrowth	Few studies on cornea	Himeno et al. (2011)
	Trophic factor supplements: VIP	Experimental (mouse)	Promote nerve regeneration, Promote epithelial wound healing	Few studies	Zhang et al. (2020b)
	Trophic factor supplements: ARA290	Clinical	Increase corneal nerve density	Few studies	Brines et al. (2015)
	Antioxidants or anti-inflammatory drugs: Naltrexone	Experimental (rat, mouse)	Promote corneal epithelial regeneration	Difficult ocular delivery system	Sassani et al. (2016)
	Vitamin B12	Clinical	Reduce DN occurrence and progression	Few studies on cornea	Fogagnolo et al. (2020)
	Vitamin D	Clinical and experimental (rat, in vitro)	Related to DN and corneal nerve, Up-regulate NGF	Few studies on cornea	Lv et al. (2015); Almurdhi et al. (2017); Alam et al. (2021)
Bariatric surgery	Anti-inflammatory procedure	Clinical	Improve corneal nerve fiber length, corneal nerve fiber density and nerve branch density	Surgical complications, Not cost-effective	Iqbal et al. (2021); Adam et al. (2021)
Gene therapy	Targets: c-met, MMP-10 Method: adenovirus, adeno-associated virus	Experimental (human diabetic organ-cultured cornea)	Improve corneal wound healing rate	Adeno-associated virus has low transgene expression than adenovirus	Saghizadeh et al. (2014); Kramerov et al. (2016)
	Targets: miR-34c, miR-181a Method: Subconjunctival injection	Experimental (mouse, human diabetic organ-cultured cornea)	Promote corneal nerve regeneration	Multiple targets, Unpredictable side effects	Hu et al. (2019); Hu et al. (2020)

TABLE 1 | (Continued) Clinical and experimental therapeutic strategies for anterior segment disorders associated with diabetes.

Treatment strategy	Therapeutic agents/procedures	Clinical or experimental	Advantages	Limitations	References
	Targets: HMGB1; *fl2*; miRNAs like miR-205 and miR-146a; drug delivery; CaMKKβ and PGC-1α Method: nanoparticles	Experimental (rabbit, rat, mouse)	Increase corneal epithelial regeneration	No clinical studies	Saleh et al. (2020); Hou et al. (2021); Jessi Wang et al. (2021); Lavker et al. (2021); Tsai et al. (2021)

function in hyperglycemia-induced ocular deteriorations like corneal epithelial defects and damaged Bowman's membrane through ameliorating oxygenated free radicals in the endothelial cells by inhibiting protein kinase C, reducing mitochondrial respiratory chain pathways (Nahar et al., 2021). These data indicated that insulin might be used for the treatment of diabetic corneal defects. However, in T2D, the role of glycemic control in complications is controversial. One clinical trial found that in T2D subjects, treatment with exenatide plus pioglitazone or basic bolus insulin therapy for more than 12 months could significantly improve corneal nerve morphology, which was manifested by increased corneal nerve length and branch density, indicating the promotion of corneal nerve regeneration (Ponirakis et al., 2020). Nonetheless, another clinical trial demonstrated that treatment with exenatide combined with pioglitazone or insulin had a limited effect on nerve regeneration in T2D subjects with high insulin resistance (Ponirakis et al., 2021b). However, it should be noted that in non-diabetic cornea of rats, topical insulin had no effect on wound healing (Zagon et al., 2007). Also, insulin treatment may up-regulate insulin-like growth factor-1 (IGF-1), activate vascular endothelial growth factor production, increase the susceptibility to T2D and DR, and exacerbate retinopathy (Smith et al., 1999; Khan et al., 2020). Therefore, before insulin is considered as the treatment for diabetic corneal disorder, it is necessary to monitor the changes in retina.

Restoring insulin secretion is another means to treat diabetes and its complications. Pancreatic transplantation may be an effective way to restore normal glycemic (Tavakoli and Liong, 2012). A recent study demonstrated that in T1D patients, improvement in corneal nerve fiber regeneration was found after simultaneous transplantation of pancreas and kidney (Azmi et al., 2019). Nevertheless, suitable organs are limited, and surgery also brings huge risks and unpredictable postoperative complications. Hence, an alternative method, pancreatic islet cell transplantation has been considered to restore endogenous insulin production. Islet cell transplantation is a procedure to infuse purified islet cells from a deceased donor into the recipient's liver. Therefore, it requires the use of immunosuppressive agents for life-long treatment (Senior et al., 2018). Overall, studies indicated that pancreatic islet cell transplantation may improve glycemic stability and may reduce the occurrence of diabetic complications (retinopathy and neuropathy) (Foster et al., 2018; Vantyghem et al., 2019). However, pancreatic islet cell transplantation can cause surgical complications such as infection, and the lifetime effectiveness is uncertain. An economic evaluation compared the cost of islet cell transplantation to insulin treatment and found that islet cell transplantation was not cost-effective (Wallner et al., 2016).

It was reported that worsening of DR occurred when diabetic patients changed from poor glycemic control to tight glycemic control (Bain et al., 2019), which emphasized the importance of monitoring blood glucose level. Recently, greater glucose variability was shown to be related to poor ocular nerve function, which was mentioned in *Clinical perspectives of corneal neuropathy in diabetes mellitus Section* (Issar et al., 2020). Therefore, more studies about treatments with less glucose variability in the prevention of neuropathy are needed.

Pharmacological Intervention
Lipid-Lowering Drugs
Lipids include fatty acids, glycerolipids, sphingolipids and sterols (Fahy et al., 2005). In *Lipids Section*, we have concluded that dyslipidemia plays an essential role in DN. Moreover, a recent study revealed that T2D patients with metabolic syndrome manifested poorer peripheral nerve structure and function when compared with T2D patients alone (Issar et al., 2021), which again stressed the importance of lowering the level of harmful lipids.

Statins are the most used lipid-lowering drugs. According to published reports, statin treatment can improve neuropathic indicators by anti-inflammation in vincristine sulphate-induced DN in rats (Bhalla et al., 2015). A clinical trial revealed that simvastatin/ezetimibe and rosuvastatin could significantly reduce lipid peroxidation in patients with DN (Villegas-Rivera et al., 2015). However, other studies did not find significant association between statins and DN (Miao Wang et al., 2021). Fibrates are also used to lower triglyceride and increase high-density lipoprotein. Moreover, peroxisome proliferator-activated receptor (PPAR) played vital roles in modulating inflammation and metabolism. A drug in one of the fibrate classes, fenofibrate, is a PPARα agonist used to treat abnormal blood lipid levels. Knockout of PPARα in T1D mice and rats aggravated the reduction in corneal nerve fiber density and lowering in corneal sensitivity, which could be prevented by fenofibrate (Matlock et al., 2020).

Nevertheless, in T2D patients with/without DN, low levels of LDL-C could decrease nerve conduction velocity and amplitude and increase nerve lesions, despite being an effective treatment for dyslipidemia in T2D patients (Jende et al., 2019). A case report revealed that when PCSK9 inhibitor-alirocumab (Praluent) was used to treat patients with pre-diabetes and dyslipidemia, their level of LDL-C was reduced (Franco et al., 2019). The effects of

triglyceride-lowering drugs on diabetic corneal neuropathy are largely unclear, and more well-designed experiments are warranted.

Supplements of Fatty Acids and Its Metabolites

Menhaden oil is a source of omega-3 fatty acids and is enriched in docosahexaenoic acid (DHA). It can be used as a dietary supplement for human (Shevalye et al., 2015). In both T1D and T2D rat models, the number of their corneal nerves was significantly reduced, indicating that the nerve fibers were excessively damaged. After treatment with a diet rich in menhaden oil, loss of corneal nerve was reversed, indicating that omega-3 fatty acids are a beneficial treatment (Coppey et al., 2020; Lewis et al., 2021). Another study found that in a T2D mouse model, the use of menhaden oil or resolvin D1 can reverse the attenuation in corneal innervation and motor and sensory nerve conduction velocity. In addition, through *in vitro* experiments, the author found that resolvin D1 stimulated neurite outgrowth in the dorsal root ganglion (Shevalye et al., 2015). Resolvin D1 is the metabolite of DHA and has anti-inflammatory and neuroprotective effects (Lee et al., 2015). DHA is involved in neuroprotection, synaptic function, and brain and retina development. DHA is the precursor of neuroprotectin D1 (NPD1), which could resist oxidative stress induced by cell injury (Serhan et al., 2015). One study reported that in injured rabbit cornea, treatment with NPD1 could attenuate inflammatory response, increase corneal sensitivity and stimulate neurite outgrowth (Cortina et al., 2013). In fact, corneas treated with DHA and pigment epithelium-derived factors exhibited increased NPD1 synthesis (Cortina et al., 2013).

Moreover, one article compared the effects of menhaden oil, resolvin D1 and salsalate on DN (Yorek et al., 2016). The authors found that in T1D mice, monotherapy could improve both motor and sensory nerve conduction velocities and increase the density of nerves in corneal epithelium, with no difference among the three drugs. Salsalate, a prodrug of salicylate, is used to treat pain and inflammation associated with rheumatic diseases in humans. Salsalate could reduce circulating triglycerides (Davidson et al., 2018), block vascular insulin resistance mediated by free fatty acid and reduce inflammation (Yorek et al., 2016) by reducing NF-κB and increasing nitric oxide to prevent ischemic nerve damage (McCarty, 2010). The authors found that the combined use of menhaden oil and salsalate could increase the level of plasma resolvin D1 when compared with that observed in monotherapy (Yorek et al., 2016). The authors put forward the hypothesis that under the same curative effect, the effective concentration of menhaden oil could be reduced to reach the highest standard of human dietary dose in order to increase its clinical feasibility.

Meanwhile, the combined use of enalapril, *a*-lipoic acid and menhaden oil in T2D rats could help the recovery of corneal sub-basal nerve fiber length and corneal sensitivity (Davidson et al., 2017). Alpha-lipoic acid is a free radical scavenger that can alleviate oxidative stress. Previous studies have shown that alpha-lipoic acid administration led to clinically significant improvement and prevention of neurological damage progression (Ziegler et al., 2011). Additionally, when combined with aldose reductase inhibitors, it could further enhance the

improvement effect (Yorek et al., 2014). Enalapril is an angiotensin converting enzyme inhibitor that is widely used to treat hypertension and diabetic nephropathy. The authors hypothesized that the mechanism of this combination therapy might be a reduction of oxidative stress and inflammation and an increase omega-3 polyunsaturated fatty acids.

Therefore, the aforementioned fatty acids and its metabolites provide other options for potential new treatments for diseases involving corneal nerve injury.

Aldose Reductase Inhibitors

Aldose reductase is the rate-limiting enzyme in the polyol pathway, whose activation by hyperglycemia can cause corneal nerve injury. It is also a key promoter of inflammation and cytotoxic conditions. Therefore, in theory, aldose reductase inhibitor (ARI) can reduce corneal nerve injury and promote corneal epithelial regeneration *via* attenuating the activation of polyol pathway (Markoulli et al., 2018). Takamura et al. found that rats fed with galactose have corneal abnormalities like those in diabetic animals. Treatment with ARI (ranirestat) has been found to facilitate corneal wound healing in rats by reducing the expression of matrix metalloproteinase (MMP)-10 (Takamura et al., 2013).

However, the therapeutic effect of another ARI (CT-112) is controversial. One study reported that the topical application of CT-112 to 39 diabetic patients could reverse the abnormal morphology of corneal epithelial cells and reduce corneal sensitivity (Hosotani et al., 1995). Interestingly, a randomized double-masked clinical trial using CT-112 found that after 4 and 8 weeks of treatment, the healing of corneal epithelial wounds was accelerated, but no changes in corneal sensitivity were found (Nakahara et al., 2005).

Another double-masked clinical trial (Fujishima and Tsubota, 2002) found an effective improvement of corneal epithelial injury and recovery of corneal sensitivity with treatment of oral ARI (ONO-2235).

Hence, different ARIs may have different effects in diabetic patients, and more studies need to be conducted to determine the efficacy of individual drug. The effectiveness of combinational administration should be tested as well.

Trophic Factor Supplements
Insulin-like Growth Factor-1

IGF-1 is a peptide with multiple functions in central and peripheral nervous system. In both human and animal models of TID and T2D, the level of serum IGF-1 was significantly reduced (Aghanoori et al., 2019). The density of corneal sub-basal nerves in type 2 diabetic mice was reported to be reduced, and retrobulbar injections of IGF-I could increase nerve density and prevent corneal damage (Ueno et al., 2014). Using STZ-induced diabetic rats, one study revealed that IGF-1 enhanced mitochondrial function and drove axon growth through AMP-activated protein kinase, which prevented the death of distal fibers in DN (Aghanoori et al., 2019).

Nerve Growth Factor

NGF is a protein involved in the growth, differentiation, and survival of neurons. NGF, NT-3, NT-4, BDNF and GDNF are

present in the cornea (You et al., 2000). Many studies have reported the association between NGF and ocular surface health. One study demonstrated (Lambiase et al., 2000) that NGF could facilitate the proliferation of corneal epithelial cells and accelerate epithelial wound healing in rabbits. During corneal wound healing, a variety of cytokines such as interleukin 1, were released to regulate the synthesis of NGF (Wilson et al., 1996). In mice with moderate to severe neurotrophic keratitis, topical NGF eye drops enhanced corneal epithelial healing, and improved corneal sensitivity and visual function (Bonini et al., 2000). Besides, damaged nerve repair and nutritional function abnormalities occurred in mice with vascular endothelial growth factor (VEGF)-B deficiency, which could be recovered with the administration of VEGF-B (Guaiquil et al., 2014). Indeed, SA treatment upregulated the expression of VEGF in cornea nerve after injury, thereby enhancing the repair ability of corneal nerve (Di et al., 2017). In another study, it was reported that exogenous VEGF-B could activate the PI-3K/Akt-GSK3β-mTOR signaling pathway. As a result, regeneration of diabetic corneal nerve fiber was promoted, with improved corneal sensitivity and a higher level of corneal pigment epithelial-derived factor (Li et al., 2017).

These findings indicated that neurotrophins were involved in the regulation of physiological and pathological processes on the ocular surface. It is therefore believed that NGF may become a potential therapeutic agent for ocular disorders. Numerous studies have investigated the use of recombinant human nerve growth factor (rhNGF). Yet, the role of rhNGF remained to be discussed. Several phase II or III clinical trials showed conflicting results on its early efficacy due to limited dosage testing (high dosage may cause severe side effects) and investigations in different populations (Apfel, 2002). Increasing the dose and at the same time reducing the adverse effects have become an urgent problem to be solved. One study reported that their laboratory could produce large amounts of rhNGF, whose pharmacological effects performed well without apparent side effects (Colangelo et al., 2005). This certainly provided supportive evidence for further clinical trials.

Neuropeptides

Neuropeptides co-exist with neurotransmitters in nerve cells, acting as both transmitters and trophic factors.

Substance P (SP) is a neuropeptide that acts as a neurotransmitter and neuromodulator and is mainly released by sensory nerve fibers. SP is present in the normal cornea in physiologically relevant concentrations (Nishida et al., 1996). The concentration of substance P in tears is thought to reflect the level of neuropeptides in ocular tissues (Suvas 2017). Compared with diabetic patients without DN, the SP concentration in tears of T1D patients with DN is significantly lower, and it was related to corneal nerve fiber density (Tummanapalli et al., 2019). Yet, there was no difference in substance P concentration in T2D patients with DN (Tummanapalli et al., 2020b). An article found that in T1D rats, reduction in hyporesponsiveness of C nerve fiber was found, which was related to the significantly decreased levels of substance P and calcitonin gene-related peptide (Rocha-Neto et al., 2019). One study revealed that in T1D mice, exogenous

SP could accelerate skin wound healing, possibly because SP treatment induced an acute inflammatory response, which promoted cell proliferation and activated M2 macrophages (Leal et al., 2015). Thus, exogenous SP may be an effective treatment for neuropathy in diabetes. However, SP administration in rabbits had no significant effect on the healing of corneal epithelial wounds. But studies have found that topical co-treatment of SP and IGF-1 could facilitate the proliferation and migration of corneal epithelial cells in diabetic corneal neuropathy (Abdelkader et al., 2011).

C-peptide is a neuropeptide. During insulin biosynthesis, proinsulin is cleaved into insulin and C-peptide (Steiner et al., 1967). Due to the short biological half-life of C-peptide, Peg-C-peptide (a long-acting form of C-peptide) has been developed to increase patient compliance and facilitate translation into clinical applications. Jolivalt et al. found that T1D mice treated with C-peptide or Peg-C-peptide showed a significant increase in the corneal sub-basal nerve, but its specific mechanism was still unclear (Jolivalt et al., 2015).

Studies revealed that the synthesis of SP was regulated by NGF and exogenous NGF treatment in diabetic rats could restore nerve SP levels (Lindsay and Harmar, 1989). Meanwhile, C peptide could promote both NGF and SP levels (Kamiya et al., 2006). These results suggested that factors may interact with each other, whether the combination treatment can produce a synergistic effect deserves more research.

Another neuropeptide, GLP-1, has a role in inhibiting glucagon secretion and stimulating insulin secretion. It has been reported that GLP-1 receptor agonists had neuroprotective effects. In T1D mice, exendin-4 (a GLP-1 receptor agonist) could increase sensory and motor nerve conduction velocity and intraepidermal nerve fiber density as well as significantly promote neurite outgrowth from dorsal root ganglions (Himeno et al., 2011). However, in T2D mice, although exendin-4 improved motor nerve conduction velocity, it had no effect on sensory nerves (Kan et al., 2012). There is still a lack of research on the effect of GFP-1 on diabetic corneal nerves.

Vasoactive intestinal peptide (VIP) is an immunosuppressive neuropeptide that belongs to the glucagon superfamily. Recently, Zhang et al. found that the exogenous use of neuropeptides such as calcitonin gene-related peptide, SP and VIP could partially restore damaged corneal epithelial wounds and inhibit the overexpression of pro-inflammatory factors in T1D mice corneas. In addition, the authors further discovered that VIP up-regulated the expression of NGF, CNTF, anti-inflammatory cytokines and improved corneal epithelial wound healing and nerve regeneration through VIP/VIP type 1 receptor/Sonic Hedgehog pathway (Zhang et al., 2020b).

ARA 290 is a non-hematopoietic peptide designed based on the structure of erythropoietin. In one phase II clinical trial, treatment with ARA 290 in T2D patients markedly increased the mean corneal nerve fiber density when compared with the placebo group (Brines et al., 2015).

These studies showed that neurotrophic factors interact with neuropeptides. When the cornea is injured, their expression and function may form a positive feedback loop: NGF from the healed corneal epithelial cells and CNTF from the dendritic cells can

induce regeneration of sensory nerve, which in turn cause the release of more neuropeptides to nourish and maintain the proliferation and migration of corneal epithelial cells and dendritic cells. DM disrupts this interaction, leading to corneal injury. Based on the published data, we hypothesized that combination treatment with both neurotrophic factors and neuropeptides might be a promising approach for diabetic corneal damage.

Antioxidants or Anti-inflammatory Drugs
Naltrexone
The endogenous opioid system affects the proliferation of many cells like neurons and glial cells. Opioid growth factor (OGF) has been detected in bovine and rabbit corneal epithelium and was found to have an inhibitory effect on the proliferation and growth of corneal epithelial cells (McLaughlin et al., 2010).

Naltrexone is a long-acting and potent opioid antagonist that can block the interaction of OGF and its receptor OGFr. In both *in vitro* and *in vivo* studies, treatment with naltrexone could significantly facilitate DNA synthesis, cell division, cell migration, corneal epithelial wound healing, and corneal epithelium proliferation and growth (Sassani et al., 2016). Interestingly, the combined topical use of naltrexone and insulin has no additive or synergistic effect on corneal epithelial regeneration in T1D rats (Klocek et al., 2009).

Although a lot of evidence demonstrated the effectiveness of naltrexone aqueous solution, there are very few reports on its ocular delivery system and therefore more research is needed for its use in clinical treatment of diabetic corneal damage.

Other Antioxidants
Antioxidants such as *ß*-carotene (Abdul-Hamid and Moustafa, 2014) and carnosine (Shevalye et al., 2015) have also been shown to have effects on diabetic corneal repair and can be used to combat the consequences of AGEs on the ocular surface. One recent study found that an antioxidant mitoquinone reduced the oxidative stress produced by mitochondria in nerves (Fink et al., 2020). Adding mitoquinone to the diet of diabetic rats accelerated nerve conduction velocity, increased corneal and intraepidermal nerve fiber density and restored corneal sensitivity.

Other drugs have also been investigated. 1,5-isoquinolinediol, an inhibitor of poly(ADP-ribose) polymerase, partially reversed the epithelial innervation loss, corneal sensitivity reduction and epithelial wound healing delay (Byun et al., 2015). Meanwhile, administration of KIOM-79 (a mixture of 80% ethanol extracts of parched Puerariae radix, gingered Magnoliae cortex, Glycyrrhizae radix and Euphorbiae radix) protected keratocyte from cell death, lessened oxidative stress in corneas *via* suppression of the AGEs/NF-κB signal pathway (Kim et al., 2011b).

Other Drugs
Vitamin B
One recent study reported that topical vitamin B12 and citicoline treatment could ameliorate the morphology and function of corneal nerves in diabetic patients, indicating a neuroprotective effect (Fogagnolo et al., 2020). Despite these promising results, more clinical trials need to be conducted to provide more evidence for the use of vitamin B in patients with diabetic corneal neuropathy.

Vitamin D
In recent years, several studies have focused on the relationship between vitamin D and DN. A clinical study involving nearly 10,000 subjects demonstrated that 50% of T2D patients had low serum vitamin D levels (Herrmann et al., 2015). Furthermore, a systematic review (involving 1,484 T2D patients) reported a marked association between vitamin D deficiency and the development of DN (Lv et al., 2015). Other studies revealed that the vitamin D level of painful DN patients was significantly lower than that of painless DN patients (Alam et al., 2021), and the corneal nerve fiber density decreased more significantly in patients with low vitamin D level (Almurdhi et al., 2017). The possible mechanism behind vitamin D's effects is unclear. But previous animal studies have found that treating diabetic rats with a vitamin D analog promoted NGF production in their sciatic nerves (Riaz et al., 1999). Similarly, it has been found that Tacalcitol, an active vitamin D3, could up-regulate NGF level in human epidermal keratinocytes (Fukuoka et al., 2001). The involvement of growth factors is indicated, and further investigations are essential.

Bariatric Surgery
Interestingly, two recent studies found an association between obesity and corneal nerve fibers. One study showed that in patients with severe obesity, early corneal nerve fiber and keratocyte density were attenuated (Iqbal et al., 2021). After bariatric surgery, corneal nerve regeneration was observed. Another study showed that in obese T2D patients, corneal nerve fiber length, corneal nerve fiber density and nerve branch density were significantly improved after bariatric surgery (Adam et al., 2021). These protection function may be related to an improvement in inflammation (Adam et al., 2021; Iqbal et al., 2021).

Gene Therapy
Gene therapy has obvious potential in the treatment of corneal diseases because the cornea carries many advantages suitable for genetic research. One advantage is that the cornea has immune privilege, which means that it can tolerate antigens without evoking inflammatory immune responses. Another advantage is that the cornea can be cultured *in vitro* and maintained for several weeks, making it possible to optimize gene transfer to improve the effectiveness and safety of gene therapy. Nonetheless, due to the lack of information on the genetic causes of corneal diseases and the goals of gene therapy, clinical transformation is still slow. It has been reported that epigenetics may play a role in diabetic complications including corneal changes (Kowluru et al., 2015). DM may cause specific changes in gene expression levels and patterns, which may be corrected by gene therapy.

Viral gene therapy is an effective delivery tool for delivering specific genes to the cornea (Ljubimov and Saghizadeh, 2015). Nevertheless, traditional viruses may induce inflammation, immune responses, and uncontrolled virus integration. New

recombinant adenovirus, adeno-associated virus and lentivirus are main types of viral vectors commonly used in cornea transfection, which will not evoke serious immune response and can transfect non-dividing cells. Studies have shown that both adenovirus and adeno-associated virus can deliver target genes into the human cornea successfully. However, compared with adeno-associated virus transduction, the transgene expression level with adenovirus transduction was much higher, which made it a good choice as a gene therapy vehicle (Liu et al., 2008).

In studies of gene therapy, the authors mentioned that in diabetic cornea, c-met is down-regulated and protease is up-regulated (Saghizadeh et al., 2014; Kramerov et al., 2016). Therefore, adenovirus gene therapy implemented with upregulation of c-met by gene overexpression as well as silencing of MMP-10 and cathepsin F by short hairpin RNA technology could improve the wound healing rate of diabetic cornea and restore the expression of some stem cell markers in the limbus. Combination therapy using these three adenoviruses had the best effect, and the EGFR-Akt and p38 pathways were found to be involved.

In addition, there are other gene therapy targets such as microRNAs to effectively normalize the pathologies in the diabetic cornea. Studies have found that miR-146a inhibitor (antagomir) promoted the wound healing of the cultured diabetic cornea by activating EGFR, and restored some stem cell expression markers (Winkler et al., 2014). Inspired by miRNA research, a study found that inhibition of miR-34c expression in T1D mice increased the expression of autophagy-related protein Atg4B in the trigeminal ganglion, and markedly promoted the growth of trigeminal sensory neurons and the regeneration of corneal nerve fibers (Hu et al., 2019). Interestingly, another study obtained the same experimental effect. It reported that subconjunctival injection of miR-181a antagomir in diabetic mice resulted in corneal nerve fiber regeneration and trigeminal sensory neuron growth through ATG5-mediated autophagy activation and BCL-2 mediated apoptosis inhibition (Hu et al., 2020). Although research related to microRNAs has made some progress, it should be noted that when compared with other targeted therapies that only affect specific genes or pathways, most miRNAs act on multiple targets and can simultaneously regulate many different genes in multiple pathways. This property may generate unpredictable side effects. Therefore, miRNAs treatment should be used cautiously and the delivery route and its biodistribution need to be repeatedly verified.

Nanotechnology also has potential applications in gene delivery. Viral vector has better transduction efficiency than nanocarriers like nanoparticles. Yet, many advantages, such as ease of synthesis and operation, low production cost, accommodation in large-size vectors, less inflammatory response, no risk for genomic insertion and mutation, made nanotechnology an attractive target (Han et al., 2012). Numerous studies on nanotechnology for corneal injury have emerged. It has been reported that dipotassium glycyrrhizinate-micelle formulation encapsulating active agents (Hou et al., 2021), nanoparticle-encapsulated Fidgetin-like 2 siRNA (Jessi Wang et al., 2021), and high-density lipoprotein nanoparticles with a gold nanoparticle core (Lavker et al., 2021) showed promising results in accelerating corneal re-epithelialization and anti-inflammation. In addition, poly (lactic-co-glycolic acid) nanoparticles could be a drug release system of Lingzhi to reduce oxidative damage in corneal epithelium cells (Tsai et al., 2021). In conclusion, nanotechnology is a potential therapeutic approach for gene transfer and drug delivery in diabetic corneal neuropathy.

In addition, using plasmid with PGC-1α promoter, using gene silencing and nanotechnology to knockdown CaMKKβ, the authors revealed that muscarinic toxin 7 augmented elevated mitochondrial function, neurite outgrowth in dorsal root ganglia neurons, and increased corneal nerve density through Ca^{2+}/Calmodulin-Dependent Protein kinase β (Saleh et al., 2020).

Overall, gene therapy may be a promising way to restore abnormalities of diabetic corneal but there is an urgent need for further studies in its clinical use.

SUMMARY

Diabetic corneal defects could be a biomarker for evaluating DN. Since studies (see *Clinical Perspectives of Corneal Neuropathy in Diabetes Mellitus Section*) showed that in diabetic patients, corneal defects commenced and showed a progressive degeneration as DM continued. Moreover, there was also reported a greater loss of corneal nerve fiber in DN patients when compared with diabetic subjects without DN. In addition, parameters of corneal nerve fibers worsened with increasing severity of DN. Therefore, it is essential to recognize and treat diabetic corneal neuropathy timely.

Firstly, since the complications of diabetes are caused by chronic hyperglycemia through a variety of pathological mechanisms, strict glycemic control is an important way to treat and reduce the progression of diabetic complications. Secondly, there have been many lipid-related clinical trials. Although the effects of triglyceride-lowering drugs such as statins and fibrates on diabetic corneal nerves are largely unknown, the fatty acids and their metabolites such as menhaden oil, resolvein D1, or their combined administration with free radical scavengers have provided alternative options for potential new therapies in diseases involving corneal nerve damage. Therefore, more elaborate and well-planned experimental and clinical studies are needed. Moreover, various ARI drugs have been shown to have different efficacy in diabetic patients, indicating the need for more clinical trials to determine what medication plan would yield better therapeutic effects. Growth factors such as IGF-1 and NGF have shown initial promising results in animal experiments. However, the reported serious side effects caused by high doses need to be addressed, since low doses have not achieved great efficacy in clinical trials. There were also many animal studies on neuropeptides such as SP and C-peptide, which reported that the combined therapy of neurotrophic factors and neuropeptides might be a promising therapeutic agent for ocular disorders. Meanwhile, vitamin B, vitamin D and naltrexone initially showed promising results. Yet, more clinical

trials should be conducted to identify an effective ocular delivery system and provide evidence of their effects on diabetic corneal neuropathy. In addition, some progress has been made in microRNAs research. Due to the possibility of unpredictable side effects, miRNAs therapy should be used with caution, and their delivery methods and biodistribution need to be verified. Also, nanotechnology has become a promising therapeutic method for gene transfer and drug delivery. In general, gene therapy may be a potential method to restore diabetic corneal abnormalities, but again further clinical trials are needed.

CONCLUSION

Diabetes mellitus has adverse effects on corneal nerve fibers, corneal sensitivity and corneal epithelial regeneration. Corneal nerve damage in diabetic patients usually precedes neuropathy in other tissues and is associated with the severity of DN, making it a potential early indicator of DN. Corneal confocal microscopy is an examination method that quantitatively evaluates the morphology of the corneal nerve, facilitating the use of corneal nerve plexus as an early biomarker to access DN. It is

essential to increase the awareness of damage on diabetic ocular surface and take actions to timely detect diabetic corneal neuropathy and monitor its subclinical progress.

At the current stage, the prevention of corneal nerve damage and the promotion of corneal nerve regeneration have achieved positive preliminary results, but most of the published work involved animal models and some preliminary clinical studies. Further investigations on the mechanism of diabetic corneal neuropathy, potential biomarkers, and pathogen-oriented therapy need to be conducted.

AUTHOR CONTRIBUTIONS

FUNDING

REFERENCES

Abdelkader, H., Patel, D. V., McGhee, C. Nj., and Alany, R. G. (2011). New Therapeutic Approaches in the Treatment of Diabetic Keratopathy: a Review. *Clin. Exp. Ophthalmol.* 39 (3), 259–270. doi:10.1111/j.1442-9071.2010.02435.x

Abdul-Hamid, M., and Moustafa, N. (2014). Amelioration of Alloxan-Induced Diabetic Keratopathy by Beta-Carotene. *Exp. Toxicol. Pathol.* 66 (1), 49–59. doi:10.1016/j.etp.2013.08.003

Adam, S., Azmi, S., Ho, J. H., Liu, Y., Ferdousi, M., Siahmansur, T., et al. (2021). Improvements in Diabetic Neuropathy and Nephropathy after Bariatric Surgery: a Prospective Cohort Study. *Obes. Surg.* 31 (2), 554–563. doi:10.1007/s11695-020-05052-8

Aghanoori, M. R., Smith, D. R., Shariati-Ievari, S., Ajisebutu, A., Nguyen, A., Desmond, F., et al. (2019). Insulin-like Growth Factor-1 Activates AMPK to Augment Mitochondrial Function and Correct Neuronal Metabolism in Sensory Neurons in Type 1 Diabetes. *Mol. Metab.* 20, 149–165. doi:10.1016/j.molmet.2018.11.008

Al-Aqaba, M. A., Dhillon, V. K., Mohammed, I., Said, D. G., and Dua, H. S. (2019). Corneal Nerves in Health and Disease. *Prog. Retin. Eye Res.* 73, 100762. doi:10.1016/j.preteyeres.2019.05.003

Alam, U., Petropoulos, I. N., Ponirakis, G., Ferdousi, M., Asghar, O., Jeziorska, M., et al. (2021). Vitamin D Deficiency Is Associated with Painful Diabetic Neuropathy. *Diabetes Metab. Res. Rev.* 37 (1), e3361. doi:10.1002/dmrr.3361

Almurdhi, M. M., Reeves, N. D., Bowling, F. L., Boulton, A. J., Jeziorska, M., and Malik, R. A. (2017). Distal Lower Limb Strength Is Reduced in Subjects with Impaired Glucose Tolerance and Is Related to Elevated Intramuscular Fat Level and Vitamin D Deficiency. *Diabet Med.* 34 (3), 356–363. doi:10.1111/dme.13163

Apfel, S. C. (2002). Nerve Growth Factor for the Treatment of Diabetic Neuropathy: what Went Wrong, what Went Right, and what Does the Future Hold. *Int. Rev. Neurobiol.* 50, 393–413. doi:10.1016/s0074-7742(02)50083-0

Azmi, S., Jeziorska, M., Ferdousi, M., Petropoulos, I. N., Ponirakis, G., Marshall, A., et al. (2019). Early Nerve Fibre Regeneration in Individuals with Type 1 Diabetes after Simultaneous Pancreas and Kidney Transplantation. *Diabetologia* 62 (8), 1478–1487. doi:10.1007/s00125-019-4897-y

Babizhayev, M. A., Strokov, I. A., Nosikov, V. V., Savel'yeva, E. L., Sitnikov, V. F., Yegorov, Y. E., et al. (2015). The Role of Oxidative Stress in Diabetic Neuropathy: Generation of Free Radical Species in the Glycation Reaction and Gene Polymorphisms Encoding Antioxidant Enzymes to Genetic Susceptibility to Diabetic Neuropathy in Population of Type I Diabetic Patients. *Cell Biochem Biophys* 71 (3), 1425–1443. doi:10.1007/s12013-014-0365-y

Bain, S. C., Klufas, M. A., Ho, A., and Matthews, D. R. (2019). Worsening of Diabetic Retinopathy with Rapid Improvement in Systemic Glucose Control: A Review. *Diabetes Obes. Metab.* 21 (3), 454–466. doi:10.1111/dom.13538

Barsegian, A., Lee, J., Salifu, M. O., and McFarlane, S. I. (2018). Corneal Neuropathy: An Underrated Manifestation of Diabetes Mellitus. *J. Clin. Endocrinol. Diabetes* 2 (1), 111

Basantsova, N. Y., Starshinova, A. A., Dori, A., Zinchenko, Y. S., Yablonskiy, P. K., and Shoenfeld, Y. (2019). Small-fiber Neuropathy Definition, Diagnosis, and Treatment. *Neurol. Sci.* 40 (7), 1343–1350. doi:10.1007/s10072-019-03871-x

Bastion, M. L., and Ling, K. P. (2013). Topical Insulin for Healing of Diabetic Epithelial Defects?: A Retrospective Review of Corneal Debridement during Vitreoretinal Surgery in Malaysian Patients. *Med. J. Malaysia* 68 (3), 208–216.

Bejarano, E., and Taylor, A. (2019). Too Sweet: Problems of Protein Glycation in the Eye. *Exp. Eye Res.* 178, 255–262. doi:10.1016/j.exer.2018.08.017

Bhalla, S., Singh, N., and Jaggi, A. S. (2015). Dose-related Neuropathic and Anti-neuropathic Effects of Simvastatin in Vincristine-Induced Neuropathic Pain in Rats. *Food Chem. Toxicol.* 80, 32–40. doi:10.1016/j.fct.2015.02.016

Bikbova, G., Oshitari, T., Baba, T., Bikbov, M., and Yamamoto, S. (2018). Diabetic Corneal Neuropathy: Clinical Perspectives. *Clin. Ophthalmol.* 12, 981–987. doi:10.2147/OPTH.S145266

Bikbova, G., Oshitari, T., Baba, T., and Yamamoto, S. (2016). Neuronal Changes in the Diabetic Cornea: Perspectives for Neuroprotection. *Biomed. Res. Int.* 2016, 5140823. doi:10.1155/2016/5140823

Bitirgen, G., Ozkagnici, A., Malik, R. A., and Kerimoglu, H. (2014). Corneal Nerve Fibre Damage Precedes Diabetic Retinopathy in Patients with Type 2 Diabetes Mellitus. *Diabet Med.* 31 (4), 431–438. doi:10.1111/dme.12324

Bonini, S., Lambiase, A., Rama, P., Caprioglio, G., and Aloe, L. (2000). Topical Treatment with Nerve Growth Factor for Neurotrophic Keratitis. *Ophthalmology* 107 (7), 1347–1351. doi:10.1016/s0161-6420(00)00163-9

Brines, M., Dunne, A. N., van Velzen, M., Proto, P. L., Ostenson, C. G., Kirk, R. I., et al. (2015). ARA 290, a Nonerythropoietic Peptide Engineered from Erythropoietin, Improves Metabolic Control and Neuropathic Symptoms in Patients with Type 2 Diabetes. *Mol. Med.* 20 (1), 658–666. doi:10.2119/molmed. 2014.00215

Byun, Y. S., Kang, B., Yoo, Y. S., and Joo, C. K. (2015). Poly(ADP-Ribose) Polymerase Inhibition Improves Corneal Epithelial Innervation and Wound Healing in Diabetic Rats. *Invest. Ophthalmol. Vis. Sci.* 56 (3), 1948–1955. doi:10. 1167/iovs.14-16259

Casellini, C. M., Barlow, P. M., Rice, A. L., Casey, M., Simmons, K., Pittenger, G., et al. (2007). A 6-month, Randomized, Double-Masked, Placebo-Controlled Study Evaluating the Effects of the Protein Kinase C-Beta Inhibitor Ruboxistaurin on Skin Microvascular Blood Flow and Other Measures of Diabetic Peripheral Neuropathy. *Diabetes care* 30 (4), 896–902. doi:10.2337/dc06-1699

Chen, D. K., Frizzi, K. E., Guernsey, L. S., Ladt, K., Mizisin, A. P., and Calcutt, N. A. (2013). Repeated Monitoring of Corneal Nerves by Confocal Microscopy as an index of Peripheral Neuropathy in Type-1 Diabetic Rodents and the Effects of Topical Insulin. *J. Peripher. Nerv Syst.* 18 (4), 306–315. doi:10.1111/jns5.12044

Chen, X., Graham, J., Petropoulos, I. N., Ponirakis, G., Asghar, O., Alam, U., et al. (2018). Corneal Nerve Fractal Dimension: A Novel Corneal Nerve Metric for the Diagnosis of Diabetic Sensorimotor Polyneuropathy. *Invest. Ophthalmol. Vis. Sci.* 59 (2), 1113–1118. doi:10.1167/iovs.17-23342

Colangelo, A. M., Finotti, N., Ceriani, M., Alberghina, L., Martegani, E., Aloe, L., et al. (2005). Recombinant Human Nerve Growth Factor with a Marked Activity *In Vitro* and *In Vivo. Proc. Natl. Acad. Sci. U S A.* 102 (51), 18658–18663. doi:10.1073/pnas.0508734102

Coppey, L., Davidson, E., Shevalye, H., Obrosov, A., Torres, M., and Yorek, M. A. (2020). Progressive Loss of Corneal Nerve Fibers and Sensitivity in Rats Modeling Obesity and Type 2 Diabetes Is Reversible with Omega-3 Fatty Acid Intervention: Supporting Cornea Analyses as a Marker for Peripheral Neuropathy and Treatment. *Diabetes Metab. Syndr. Obes.* 13, 1367–1384. doi:10.2147/DMSO.S247571

Cortina, M. S., He, J., Russ, T., Bazan, N. G., and Bazan, H. E. (2013). Neuroprotectin D1 Restores Corneal Nerve Integrity and Function after Damage from Experimental Surgery. *Invest. Ophthalmol. Vis. Sci.* 54 (6), 4109–4116. doi:10.1167/iovs.13-12075

Davidson, E. P., Coppey, L. J., Shevalye, H., Obrosov, A., Kardon, R. H., and Yorek, M. A. (2017). Impaired Corneal Sensation and Nerve Loss in a Type 2 Rat Model of Chronic Diabetes Is Reversible with Combination Therapy of Menhaden Oil, α-Lipoic Acid, and Enalapril. *Cornea* 36 (6), 725–731. doi:10.1097/ICO.0000000000001182

Davidson, E. P., Coppey, L. J., Shevalye, H., Obrosov, A., and Yorek, M. A. (2018). Effect of Dietary Content of Menhaden Oil with or without Salsalate on Neuropathic Endpoints in High-Fat-Fed/Low-Dose Streptozotocin-Treated Sprague Dawley Rats. *J. Diabetes Res.* 2018, 2967127. doi:10.1155/2018/2967127

Deák, E. A., Szalai, E., Tóth, N., Malik, R. A., Berta, A., Csutak, A., et al. (2019). Longitudinal Changes in Corneal Cell and Nerve Fiber Morphology in Young Patients with Type 1 Diabetes with and without Diabetic Retinopathy: A 2-Year Follow-up Study. *Investig. Ophthalmol. Vis. Sci.* 60 (2), 830–837. doi:10.1167/iovs.18-24516

Di, G., Zhao, X., Qi, X., Zhang, S., Feng, L., Shi, W., et al. (2017). VEGF-B Promotes Recovery of Corneal Innervations and Trophic Functions in Diabetic Mice. *Sci. Rep.* 7, 40582. doi:10.1038/srep40582

Dogru, M., Katakami, C., and Inoue, M. (2001). Tear Function and Ocular Surface Changes in Noninsulin-dependent Diabetes Mellitus. *Ophthalmology* 108 (3), 586–592. doi:10.1016/s0161-6420(00)00599-6

Edwards, K., Pritchard, N., Vagenas, D., Russell, A., Malik, R. A., and Efron, N. (2012). Utility of Corneal Confocal Microscopy for Assessing Mild Diabetic Neuropathy: Baseline Findings of the LANDMark Study. *Clin. Exp. Optom.* 95 (3), 348–354. doi:10.1111/j.1444-0938.2012.00740.x

Fahy, E., Subramaniam, S., Brown, H. A., Glass, C. K., Merrill, A. H., Jr, Murphy, R. C., et al. (2005). A Comprehensive Classification System for Lipids. *J. Lipid Res.* 46 (5), 839–861. doi:10.1194/jlr.E400004-JLR200

Ferdousi, M., Kalteniece, A., Azmi, S., Petropoulos, I. N., Ponirakis, G., Alam, U., et al. (2021). Diagnosis of Neuropathy and Risk Factors for Corneal Nerve Loss in Type 1 and Type 2 Diabetes: A Corneal Confocal Microscopy Study. *Diabetes care* 44 (1), 150–156. doi:10.2337/dc20-1482

Ferdousi, M., Kalteniece, A., Petropoulos, I., Azmi, S., Dhage, S., Marshall, A., et al. (2020). Diabetic Neuropathy Is Characterized by Progressive Corneal Nerve Fiber Loss in the Central and Inferior Whorl Regions. *Invest. Ophthalmol. Vis. Sci.* 61 (3), 48. doi:10.1167/iovs.61.3.48

Ferdousi, M., Romanchuk, K., Mah, J. K., Virtanen, H., Millar, C., Malik, R. A., et al. (2019). Early Corneal Nerve Fibre Damage and Increased Langerhans Cell Density in Children with Type 1 Diabetes Mellitus. *Sci. Rep.* 9 (1), 8758. doi:10. 1038/s41598-019-45116-z

Ferrari, G., Chauhan, S. K., Ueno, H., Nallasamy, N., Gandolfi, S., Borges, L., et al. (2011). A Novel Mouse Model for Neurotrophic Keratopathy: Trigeminal Nerve Stereotactic Electrolysis through the Brain. *Invest. Ophthalmol. Vis. Sci.* 52 (5), 2532–2539. doi:10.1167/iovs.10-5688

Fink, B., Coppey, L., Davidson, E., Shevalye, H., Obrosov, A., Chheda, P. R., et al. (2020). Effect of Mitoquinone (Mito-Q) on Neuropathic Endpoints in an Obese and Type 2 Diabetic Rat Model. *Free Radic. Res.* 54 (5), 311–318. doi:10.1080/10715762.2020.1754409

Fogagnolo, P., Melardi, E., Tranchina, L., and Rossetti, L. (2020). Topical Citicoline and Vitamin B12 versus Placebo in the Treatment of Diabetes-Related Corneal Nerve Damage: a Randomized Double-Blind Controlled Trial. *BMC Ophthalmol.* 20 (1), 315. doi:10.1186/s12886-020-01584-w

Foster, E. D., Bridges, N. D., Feurer, I. D., Eggerman, T. L., Hunsicker, L. G., and Alejandro, R. (2018). Improved Health-Related Quality of Life in a Phase 3 Islet Transplantation Trial in Type 1 Diabetes Complicated by Severe Hypoglycemia. *Diabetes care* 41 (5), 1001–1008. doi:10.2337/dc17-1779

Franco, D. C., Neupane, N., Riaz, M., Mohammadzadeh, S., and Sachmechi, I. (2019). Chronic Inflammatory Demyelinating Polyradiculoneuropathy Association with Low Cholesterol Levels: A Case Report in a Patient Taking PCSK9 Inhibitor. *J. Neurol. Res.* 9 (4-5), 72–74. doi:10.14740/jnr552

Fujishima, H., and Tsubota, K. (2002). Improvement of Corneal Fluorescein Staining in post Cataract Surgery of Diabetic Patients by an Oral Aldose Reductase Inhibitor, ONO-2235. *Br. J. Ophthalmol.* 86 (8), 860–863. doi:10. 1136/bjo.86.8.860

Fukuoka, M., Sakurai, K., Ohta, T., Kiyoki, M., and Katayama, I. (2001). Tacalcitol, an Active Vitamin D3, Induces Nerve Growth Factor Production in Human Epidermal Keratinocytes. *Skin Pharmacol. Appl. Skin Physiol.* 14 (4), 226–233. doi:10.1159/000056351

Gao, N., Yan, C., Lee, P., Sun, H., and Yu, F. S. (2016). Dendritic Cell Dysfunction and Diabetic Sensory Neuropathy in the Cornea. *J. Clin. Invest.* 126 (5), 1998–2011. doi:10.1172/JCI85097

Geraldes, P., and King, G. L. (2010). Activation of Protein Kinase C Isoforms and its Impact on Diabetic Complications. *Circ. Res.* 106 (8), 1319–1331. doi:10.1161/CIRCRESAHA.110.217117

Greene, D. A., Sima, A. A., Stevens, M. J., Feldman, E. L., and Lattimer, S. A. (1992). Complications: Neuropathy, Pathogenetic Considerations. *Diabetes Care* 15 (12), 1902–1925. doi:10.2337/diacare.15.12.1902

Guaiquil, V. H., Pan, Z., Karagianni, N., Fukuoka, S., Alegre, G., and Rosenblatt, M. I. (2014). VEGF-B Selectively Regenerates Injured Peripheral Neurons and Restores Sensory and Trophic Functions. *Proc. Natl. Acad. Sci. U S A.* 111 (48), 17272–17277. doi:10.1073/pnas.1407227111

Hamid, H. S., Mervak, C. M., Münch, A. E., Robell, N. J., Hayes, J. M., Porzio, M. T., et al. (2014). Hyperglycemia- and Neuropathy-Induced Changes in Mitochondria within Sensory Nerves. *Ann. Clin. Transl Neurol.* 1 (10), 799–812. doi:10.1002/acn3.119

Han, S. B., Yang, H. K., and Hyon, J. Y. (2018). Influence of Diabetes Mellitus on Anterior Segment of the Eye. *Clin. Interv. Aging* 14, 53–63. doi:10.2147/CIA. S190713

Han, Z., Conley, S. M., Makkia, R., Guo, J., Cooper, M. J., and Naash, M. I. (2012). Comparative Analysis of DNA Nanoparticles and AAVs for Ocular Gene Delivery. *PloS one* 7 (12), e52189. doi:10.1371/journal.pone.0052189

Herrmann, M., Sullivan, D. R., Veillard, A. S., McCorquodale, T., Straub, I. R., Scott, R., et al.FIELD Study Investigators (2015). Serum 25-hydroxyvitamin D: a Predictor of Macrovascular and Microvascular Complications in Patients with Type 2 Diabetes. *Diabetes care* 38 (3), 521–528. doi:10.2337/dc14-0180

Himeno, T., Kamiya, H., Naruse, K., Harada, N., Ozaki, N., Seino, Y., et al. (2011). Beneficial Effects of Exendin-4 on Experimental Polyneuropathy in Diabetic Mice. *Diabetes* 60 (9), 2397–2406. doi:10.2337/db10-1462

Hosotani, H., Ohashi, Y., Yamada, M., and Tsubota, K. (1995). Reversal of Abnormal Corneal Epithelial Cell Morphologic Characteristics and Reduced Corneal Sensitivity in Diabetic Patients by Aldose Reductase Inhibitor, CT-112. *Am. J. Ophthalmol.* 119 (3), 288–294. doi:10.1016/s0002-9394(14)71169-9

Hou, Y., Xin, M., Li, Q., and Wu, X. (2021). Glycyrrhizin Micelle as a Genistein Nanocarrier: Synergistically Promoting Corneal Epithelial Wound Healing through Blockage of the HMGB1 Signaling Pathway in Diabetic Mice. *Exp. Eye Res.* 204, 108454. doi:10.1016/j.exer.2021.108454

Hu, J., Hu, X., and Kan, T. (2019). MiR-34c Participates in Diabetic Corneal Neuropathy via Regulation of Autophagy. *Invest. Ophthalmol. Vis. Sci.* 60 (1), 16–25. doi:10.1167/iovs.18-24968

Hu, J., Huang, Y., Lin, Y., and Lin, J. (2020). Protective Effect Inhibiting the Expression of miR-181a on the Diabetic Corneal Nerve in a Mouse Model. *Exp. Eye Res.* 192, 107925. doi:10.1016/j.exer.2020.107925

Iqbal, Z., Kalteniece, A., Ferdousi, M., Adam, S., D'Onofrio, L., Ho, J. H., et al. (2021). Corneal Keratocyte Density and Corneal Nerves Are Reduced in Patients with Severe Obesity and Improve after Bariatric Surgery. *Invest. Ophthalmol. Vis. Sci.* 62 (1), 20. doi:10.1167/iovs.62.1.20

Ishibashi, F., Kojima, R., Taniguchi, M., Kosaka, A., Uetake, H., and Tavakoli, M. (2016). The Expanded Bead Size of Corneal C-Nerve Fibers Visualized by Corneal Confocal Microscopy Is Associated with Slow Conduction Velocity of the Peripheral Nerves in Patients with Type 2 Diabetes Mellitus. *J. Diabetes Res.* 2016, 3653459. doi:10.1155/2016/3653459

Ishibashi, F., and Tavakoli, M. (2018). Impact of Normoglycemia in Reducing Microvascular Complications in Patients with Type 2 Diabetes: A Follow-Up Study. *Front. Endocrinol. (Lausanne)* 9, 52. doi:10.3389/fendo.2018.00052

Issar, T., Tummanapalli, S. S., Borire, A. A., Kwai, N. C. G., Poynten, A. M., Arnold, R., et al. (2021). Impact of the Metabolic Syndrome on Peripheral Nerve Structure and Function in Type 2 Diabetes. *Eur. J. Neurol.* 28 (6), 2074–2082. doi:10.1111/ene.14805

Issar, T., Tummanapalli, S. S., Kwai, N. C. G., Chiang, J. C. B., Arnold, R., Poynten, A. M., et al. (2020). Associations between Acute Glucose Control and Peripheral Nerve Structure and Function in Type 1 Diabetes. *Diabet Med.* 37 (9), 1553–1560. doi:10.1111/dme.14306

Jende, J. M. E., Groener, J. B., Rother, C., Kender, Z., Hahn, A., Hilgenfeld, T., et al. (2019). Association of Serum Cholesterol Levels with Peripheral Nerve Damage in Patients with Type 2 Diabetes. *JAMA Netw. Open* 2 (5), e194798. doi:10.1001/jamanetworkopen.2019.4798

Jolivalt, C. G., Rodriguez, M., Wahren, J., and Calcutt, N. A. (2015). Efficacy of a Long-Acting C-Peptide Analogue against Peripheral Neuropathy in Streptozotocin-Diabetic Mice. *Diabetes Obes. Metab.* 17 (8), 781–788. doi:10.1111/dom.12477

Kaiserman, I., Kaiserman, N., Nakar, S., and Vinker, S. (2005). Dry Eye in Diabetic Patients. *Am. J. Ophthalmol.* 139 (3), 498–503. doi:10.1016/j.ajo.2004.10.022

Kaji, Y., Amano, S., Usui, T., Suzuki, K., Tanaka, S., Oshika, T., et al. (2001). Advanced Glycation End Products in Descemet's Membrane and Their Effect on Corneal Endothelial Cell. *Curr. Eye Res.* 23 (6), 469–477. doi:10.1076/ceyr.23.6.469.6968

Kalteniece, A., Ferdousi, M., Azmi, S., Marshall, A., Soran, H., and Malik, R. A. (2018a). Keratocyte Density Is Reduced and Related to Corneal Nerve Damage in Diabetic Neuropathy. *Invest. Ophthalmol. Vis. Sci.* 59 (8), 3584–3590. doi:10.1167/iovs.18-23889

Kalteniece, A., Ferdousi, M., Azmi, S., Mubita, W. M., Marshall, A., Lauria, G., et al. (2020). Corneal Confocal Microscopy Detects Small Nerve Fibre Damage in Patients with Painful Diabetic Neuropathy. *Sci. Rep.* 10 (1), 3371. doi:10.1038/s41598-020-60422-7

Kalteniece, A., Ferdousi, M., Petropoulos, I., Azmi, S., Adam, S., Fadavi, H., et al. (2018b). Greater Corneal Nerve Loss at the Inferior Whorl Is Related to the Presence of Diabetic Neuropathy and Painful Diabetic Neuropathy. *Sci. Rep.* 8 (1), 3283. doi:10.1038/s41598-018-21643-z

Kamiya, H., Zhang, W., Ekberg, K., Wahren, J., and Sima, A. A. (2006). C-peptide Reverses Nociceptive Neuropathy in Type 1 Diabetes. *Diabetes* 55 (12), 3581–3587. doi:10.2337/db06-0396

Kan, M., Guo, G., Singh, B., Singh, V., and Zochodne, D. W. (2012). Glucagon-like Peptide 1, Insulin, Sensory Neurons, and Diabetic Neuropathy. *J. Neuropathol. Exp. Neurol.* 71 (6), 494–510. doi:10.1097/NEN.0b013e3182580673

Khan, N., Paterson, A. D., Roshandel, D., Raza, A., Ajmal, M., Waheed, N. K., et al. (2020). Association of IGF1 and VEGFA Polymorphisms with Diabetic Retinopathy in Pakistani Population. *Acta Diabetol.* 57 (2), 237–245. doi:10.1007/s00592-019-01407-5

Kim, J., Kim, C. S., Kim, H., Jeong, I. H., Sohn, E., and Kim, J. S. (2011b). Protection against Advanced Glycation End Products and Oxidative Stress during the Development of Diabetic Keratopathy by KIOM-79. *J. Pharm. Pharmacol.* 63 (4), 524–530. doi:10.1111/j.2042-7158.2010.01206.x

Kim, J., Kim, C. S., Sohn, E., Jeong, I. H., Kim, H., and Kim, J. S. (2011a). Involvement of Advanced Glycation End Products, Oxidative Stress and Nuclear Factor-kappaB in the Development of Diabetic Keratopathy. *Graefes Arch. Clin. Exp. Ophthalmol.* 249 (4), 529–536. doi:10.1007/s00417-010-1573-9

Klocek, M. S., Sassani, J. W., McLaughlin, P. J., and Zagon, I. S. (2009). Naltrexone and Insulin Are Independently Effective but Not Additive in Accelerating Corneal Epithelial Healing in Type I Diabetic Rats. *Exp. Eye Res.* 89 (5), 686–692. doi:10.1016/j.exer.2009.06.010

Körei, A. E., Istenes, I., Papanas, N., and Kempler, P. (2016). Small-Fiber Neuropathy: A Diabetic Microvascular Complication of Special Clinical, Diagnostic, and Prognostic Importance. *Angiology* 67 (1), 49–57. doi:10.1177/0003319715583595

Kowluru, R. A., Kowluru, A., Mishra, M., and Kumar, B. (2015). Oxidative Stress and Epigenetic Modifications in the Pathogenesis of Diabetic Retinopathy. *Prog. Retin. Eye Res.* 48, 40–61. doi:10.1016/j.preteyeres.2015.05.001

Kramerov, A. A., Saghizadeh, M., and Ljubimov, A. V. (2016). Adenoviral Gene Therapy for Diabetic Keratopathy: Effects on Wound Healing and Stem Cell Marker Expression in Human Organ-Cultured Corneas and Limbal Epithelial Cells. *J. Vis. Exp.* (110), e54058. doi:10.3791/54058

Labetoulle, M., Baudouin, C., Calonge, M., Merayo-Lloves, J., Boboridis, K. G., Akova, Y. A., et al. (2019). Role of Corneal Nerves in Ocular Surface Homeostasis and Disease. *Acta Ophthalmol.* 97 (2), 137–145. doi:10.1111/aos.13844

Lagali, N. S., Allgeier, S., Guimarães, P., Badian, R. A., Ruggeri, A., Köhler, B., et al. (2017). Reduced Corneal Nerve Fiber Density in Type 2 Diabetes by Wide-Area Mosaic Analysis. *Invest. Ophthalmol. Vis. Sci.* 58 (14), 6318–6327. doi:10.1167/iovs.17-22257

Lambiase, A., Manni, L., Bonini, S., Rama, P., Micera, A., and Aloe, L. (2000). Nerve Growth Factor Promotes Corneal Healing: Structural, Biochemical, and Molecular Analyses of Rat and Human Corneas. *Invest. Ophthalmol. Vis. Sci.* 41 (5), 1063–1069.

Lavker, R. M., Kaplan, N., McMahon, K. M., Calvert, A. E., Henrich, S. E., Onay, U. V., et al. (2021). Synthetic High-Density Lipoprotein Nanoparticles: Good Things in Small Packages. *Ocul. Surf.* 21, 19–26. doi:10.1016/j.jtos.2021.03.001

Leal, E. C., Carvalho, E., Tellechea, A., Kafanas, A., Tecilazich, F., Kearney, C., et al. (2015). Substance P Promotes Wound Healing in Diabetes by Modulating Inflammation and Macrophage Phenotype. *Am. J. Pathol.* 185 (6), 1638–1648. doi:10.1016/j.ajpath.2015.02.011

Leckelt, J., Guimarães, P., Kott, A., Ruggeri, A., Stachs, O., and Baltrusch, S. (2016). Early Detection of Diabetic Neuropathy by Investigating CNFL and IENFD in Thy1-YFP Mice. *J. Endocrinol.* 231 (2), 147–157. doi:10.1530/JOE-16-0284

Lee, J. E., Sun, Y., Gjorstrup, P., and Pearlman, E. (2015). Inhibition of Corneal Inflammation by the Resolvin E1. *Invest. Ophthalmol. Vis. Sci.* 56 (4), 2728–2736. doi:10.1167/iovs.14-15982

Leppin, K., Behrendt, A. K., Reichard, M., Stachs, O., Guthoff, R. F., Baltrusch, S., et al. (2014). Diabetes Mellitus Leads to Accumulation of Dendritic Cells and Nerve Fiber Damage of the Subbasal Nerve Plexus in the Cornea. *Invest. Ophthalmol. Vis. Sci.* 55 (6), 3603–3615. doi:10.1167/iovs.14-14307

Lewis, E. J. H., Lovblom, L. E., Cisbani, G., Chen, D. K., Bazinet, R. P., Wolever, T. M. S., et al. (2021). Baseline omega-3 Level Is Associated with Nerve Regeneration Following 12-months of omega-3 Nutrition Therapy in Patients with Type 1 Diabetes. *J. Diabetes Complications* 35 (3), 107798. doi:10.1016/j.jdiacomp.2020.107798

Lewis, E. J. H., Lovblom, L. E., Ferdousi, M., Halpern, E. M., Jeziorska, M., Pacaud, D., et al. (2020). Rapid Corneal Nerve Fiber Loss: A Marker of Diabetic Neuropathy Onset and Progression. *Diabetes care* 43 (8), 1829–1835. doi:10.2337/dc19-0951

Li, D., Chen, Y. G., Zhang, C. J., Tian, J., and Li, X. (2017). Safflower Extract and Aceglutamide Injection Promoting Recovery of Peripheral Innervations via Vascular Endothelial Growth Factor-B Signaling in Diabetic Mice. *Chin. Med. J. (Engl)* 130 (23), 2829–2835. doi:10.4103/0366-6999.219143

Li, Q., Zhong, Y., Zhang, T., Zhang, R., Zhang, Q., Zheng, H., et al. (2019). Quantitative Analysis of Corneal Nerve Fibers in Type 2 Diabetics with and without Diabetic Peripheral Neuropathy: Comparison of Manual and Automated Assessments. *Diabetes Res. Clin. Pract.* 151, 33–38. doi:10.1016/j.diabres.2019.03.039

Lindsay, R. M., and Harmar, A. J. (1989). Nerve Growth Factor Regulates Expression of Neuropeptide Genes in Adult Sensory Neurons. *Nature* 337 (6205), 362–364. doi:10.1038/337362a0

Liu, J., Saghizadeh, M., Tuli, S. S., Kramerov, A. A., Lewin, A. S., Bloom, D. C., et al. (2008). Different Tropism of Adenoviruses and Adeno-Associated Viruses to Corneal Cells: Implications for Corneal Gene Therapy. *Mol. Vis.* 14, 2087–2096.

Ljubimov, A. V. (2017). Diabetic Complications in the Cornea. *Vis. Res* 139, 138–152. doi:10.1016/j.visres.2017.03.002

Ljubimov, A. V., and Saghizadeh, M. (2015). Progress in Corneal Wound Healing. *Prog. Retin. Eye Res.* 49, 17–45. doi:10.1016/j.preteyeres.2015.07.002

Lv, W. S., Zhao, W. J., Gong, S. L., Fang, D. D., Wang, B., Fu, Z. J., et al. (2015). Serum 25-hydroxyvitamin D Levels and Peripheral Neuropathy in Patients with Type 2 Diabetes: a Systematic Review and Meta-Analysis. *J. Endocrinol. Invest.* 38 (5), 513–518. doi:10.1007/s40618-014-0210-6

Lyu, Y., Zeng, X., Li, F., and Zhao, S. (2019). The Effect of the Duration of Diabetes on Dry Eye and Corneal Nerves. *Cont Lens Anterior Eye* 42 (4), 380–385. doi:10.1016/j.clae.2019.02.011

Mahelková, G., Burdová, M. C., Malá, Š., Hoskovcová, L., Dotřelová, D., and Štechová, K. (2018). Higher Total Insulin Dose Has Positive Effect on Corneal Nerve Fibers in DM1 Patients. *Invest. Ophthalmol. Vis. Sci.* 59 (10), 3800–3807. doi:10.1167/iovs.18-24265

Markoulli, M., Flanagan, J., Tummanapalli, S. S., Wu, J., and Willcox, M. (2018). The Impact of Diabetes on Corneal Nerve Morphology and Ocular Surface Integrity. *Ocul. Surf.* 16 (1), 45–57. doi:10.1016/j.jtos.2017.10.006

Markoulli, M., You, J., Kim, J., Duong, C. L., Tolentino, J. B., Karras, J., et al. (2017). Corneal Nerve Morphology and Tear Film Substance P in Diabetes. *Optom. Vis. Sci.* 94 (7), 726–731. doi:10.1097/OPX.0000000000001096

Matlock, H. G., Qiu, F., Malechka, V., Zhou, K., Cheng, R., Benyajati, S., et al. (2020). Pathogenic Role of PPARα Downregulation in Corneal Nerve Degeneration and Impaired Corneal Sensitivity in Diabetes. *Diabetes* 69 (6), 1279–1291. doi:10.2337/db19-0898

McCarty, M. F. (2010). Salsalate May Have Broad Utility in the Prevention and Treatment of Vascular Disorders and the Metabolic Syndrome. *Med. Hypotheses* 75 (3), 276–281. doi:10.1016/j.mehy.2009.12.027

McLaughlin, P. J., Sassani, J. W., Klocek, M. S., and Zagon, I. S. (2010). Diabetic Keratopathy and Treatment by Modulation of the Opioid Growth Factor (OGF)-OGF Receptor (OGFr) axis with Naltrexone: a Review. *Brain Res. Bull.* 81 (2-3), 236–247. doi:10.1016/j.brainresbull.2009.08.008

Nahar, N., Mohamed, S., Mustapha, N. M., Lau, S., Ishak, N. I. M., and Umran, N. S. (2021). Metformin Attenuated Histopathological Ocular Deteriorations in a Streptozotocin-Induced Hyperglycemic Rat Model. *Naunyn Schmiedebergs Arch. Pharmacol.* 394 (3), 457–467. doi:10.1007/s00210-020-01989-w

Nakahara, M., Miyata, K., Otani, S., Miyai, T., Nejima, R., Yamagami, S., et al. (2005). A Randomised, Placebo Controlled Clinical Trial of the Aldose Reductase Inhibitor CT-112 as Management of Corneal Epithelial Disorders in Diabetic Patients. *Br. J. Ophthalmol.* 89 (3), 266–268. doi:10.1136/bjo.2004.049841

Nishida, T., Nakamura, M., Ofuji, K., Reid, T. W., Mannis, M. J., and Murphy, C. J. (1996). Synergistic Effects of Substance P with Insulin-like Growth Factor-1 on Epithelial Migration of the Cornea. *J. Cel Physiol* 169 (1), 159–166. doi:10.1002/(SICI)1097-4652(199610)169:1<159:AID-JCP16>3.0.CO;2-8

Oates, P. J. (2008). Aldose Reductase, Still a Compelling Target for Diabetic Neuropathy. *Curr. Drug Targets* 9 (1), 14–36. doi:10.2174/138945008783431781

Pizzino, G., Irrera, N., Cucinotta, M., Pallio, G., Mannino, F., Arcoraci, V., et al. (2017). Oxidative Stress: Harms and Benefits for Human Health. *Oxidative Med. Cell. longevity* 2017, 1–13. doi:10.1155/2017/8416763

Ponirakis, G., Abdul-Ghani, M. A., Jayyousi, A., Almuhannadi, H., Petropoulos, I. N., Khan, A., et al. (2020). Effect of Treatment with Exenatide and Pioglitazone or Basal-Bolus Insulin on Diabetic Neuropathy: a Substudy of the Qatar Study. *BMJ Open Diabetes Res. Care* 8 (1), e001420. doi:10.1136/bmjdrc-2020-001420

Ponirakis, G., Abdul-Ghani, M. A., Jayyousi, A., Zirie, M. A., Qazi, M., Almuhannadi, H., et al. (2021a). Painful Diabetic Neuropathy Is Associated with Increased Nerve Regeneration in Patients with Type 2 Diabetes Undergoing Intensive Glycemic Control. *J. Diabetes Investig.* 12 (9), 1642–1650. doi:10.1111/jdi.13544

Ponirakis, G., Abdul-Ghani, M. A., Jayyousi, A., Zirie, M. A., Al-Mohannadi, S., Almuhannadi, H., et al. (2021b). Insulin Resistance Limits Corneal Nerve Regeneration in Patients with Type 2 Diabetes Undergoing Intensive Glycemic Control. *J. Diabetes Investig.* 12, 2002–2009. doi:10.1111/jdi.13582

Pritchard, N., Edwards, K., Russell, A. W., Perkins, B. A., Malik, R. A., and Efron, N. (2015). Corneal Confocal Microscopy Predicts 4-year Incident Peripheral Neuropathy in Type 1 Diabetes. *Diabetes care* 38 (4), 671–675. doi:10.2337/dc14-2114

Pritchard, N., Edwards, K., Shahidi, A. M., Sampson, G. P., Russell, A. W., Malik, R. A., et al. (2011). Corneal Markers of Diabetic Neuropathy. *Ocul. Surf.* 9 (1), 17–28. doi:10.1016/s1542-0124(11)70006-4

Qu, J. H., Li, L., Tian, L., Zhang, X. Y., Thomas, R., and Sun, X. G. (2018). Epithelial Changes with Corneal Punctate Epitheliopathy in Type 2 Diabetes Mellitus and Their Correlation with Time to Healing. *BMC Ophthalmol.* 18 (1), 1. doi:10.1186/s12886-017-0645-6

Rehany, U., Ishii, Y., Lahav, M., and Rumelt, S. (2000). Ultrastructural Changes in Corneas of Diabetic Patients: an Electron-Microscopy Study. *Cornea* 19 (4), 534–538. doi:10.1097/00003226-200007000-00026

Riaz, S., Malcangio, M., Miller, M., and Tomlinson, D. R. (1999). A Vitamin D(3) Derivative (CB1093) Induces Nerve Growth Factor and Prevents Neurotrophic Deficits in Streptozotocin-Diabetic Rats. *Diabetologia* 42 (11), 1308–1313. doi:10.1007/s001250051443

Rocha-Neto, L. M., Gamarra-Suárez, J. R., Freitas, F. F., Muzilli, A., Jr, Abdalla, H. B., Macedo, C. G., et al. (2019). Early Phase of Type 1 Diabetes Decreases the Responsiveness of C-Fiber Nociceptors in the Temporomandibular Joint of Rats. *Neuroscience* 416, 229–238. doi:10.1016/j.neuroscience.2019.08.011

Roselló-Busquets, C., de la Oliva, N., Martínez-Mármol, R., Hernaiz-Llorens, M., Pascual, M., Muhaisen, A., et al. (2019). Cholesterol Depletion Regulates Axonal Growth and Enhances Central and Peripheral Nerve Regeneration. *Front. Cel. Neurosci.* 13, 40. doi:10.3389/fncel.2019.00040

Roszkowska, A. M., Licitra, C., Tumminello, G., Postorino, E. I., Colonna, M. R., and Aragona, P. (2021). Corneal Nerves in Diabetes-The Role of the *In Vivo* Corneal Confocal Microscopy of the Subbasal Nerve Plexus in the Assessment of Peripheral Small Fiber Neuropathy. *Surv. Ophthalmol.* 66 (3), 493–513. doi:10.1016/j.survophthal.2020.09.003

Rumora, A. E., LoGrasso, G., Hayes, J. M., Mendelson, F. E., Tabbey, M. A., Haidar, J. A., et al. (2019). The Divergent Roles of Dietary Saturated and Monounsaturated Fatty Acids on Nerve Function in Murine Models of Obesity. *J. Neurosci.* 39 (19), 3770–3781. doi:10.1523/JNEUROSCI.3173-18.2019

Sady, C., Khosrof, S., and Nagaraj, R. (1995). Advanced Maillard Reaction and Crosslinking of Corneal Collagen in Diabetes. *Biochem. Biophys. Res. Commun.* 214 (3), 793–797. doi:10.1006/bbrc.1995.2356

Saghizadeh, M., Dib, C. M., Brunken, W. J., and Ljubimov, A. V. (2014). Normalization of Wound Healing and Stem Cell Marker Patterns in Organ-Cultured Human Diabetic Corneas by Gene Therapy of Limbal Cells. *Exp. Eye Res.* 129, 66–73. doi:10.1016/j.exer.2014.10.022

Saleh, A., Sabbir, M. G., Aghanoori, M. R., Smith, D. R., Roy Chowdhury, S. K., Tessler, L., et al. (2020). Muscarinic Toxin 7 Signals via Ca2+/Calmodulin-dependent Protein Kinase Kinase β to Augment Mitochondrial Function and Prevent Neurodegeneration. *Mol. Neurobiol.* 57 (6), 2521–2538. doi:10.1007/s12035-020-01900-x

Sassani, J. W., Mc Laughlin, P. J., and Zagon, I. S. (2016). The Yin and Yang of the Opioid Growth Regulatory System: Focus on Diabetes-The Lorenz E. Zimmerman Tribute Lecture. *J. Diabetes Res.* 2016, 9703729. doi:10.1155/2016/9703729

Schaldemose, E. L., Hammer, R. E., Ferdousi, M., Malik, R. A., Nyengaard, J. R., and Karlsson, P. (2020). An Unbiased Stereological Method for Corneal Confocal Microscopy in Patients with Diabetic Polyneuropathy. *Sci. Rep.* 10 (1), 12550. doi:10.1038/s41598-020-69314-2

Scheler, A., Spoerl, E., and Boehm, A. G. (2012). Effect of Diabetes Mellitus on Corneal Biomechanics and Measurement of Intraocular Pressure. *Acta Ophthalmol.* 90 (6), e447–51. doi:10.1111/j.1755-3768.2012.02437.x

Schönfeld, P., and Reiser, G. (2013). Why Does Brain Metabolism Not Favor Burning of Fatty Acids to Provide Energy? - Reflections on Disadvantages of the Use of Free Fatty Acids as Fuel for Brain. *J. Cereb. Blood Flow Metab.* 33 (10), 1493–1499. doi:10.1038/jcbfm.2013.128

Selvarajah, D., Kar, D., Khunti, K., Davies, M. J., Scott, A. R., Walker, J., et al. (2019). Diabetic Peripheral Neuropathy: Advances in Diagnosis and Strategies for Screening and Early Intervention. *Lancet Diabetes Endocrinol.* 7 (12), 938–948. doi:10.1016/S2213-8587(19)30081-6

Senior, P. A., Senior, P. A., AlMehthel, M., Miller, A., and Paty, B. W. (2018). Diabetes and Transplantation. *Can. J. Diabetes* 42 Suppl 1 (Suppl. 1), S145–S149. doi:10.1016/j.jcjd.2017.10.017

Serhan, C. N., Dalli, J., Colas, R. A., Winkler, J. W., and Chiang, N. (2015). Protectins and Maresins: New Pro-resolving Families of Mediators in Acute Inflammation and Resolution Bioactive Metabolome. *Biochim. Biophys. Acta* 1851 (4), 397–413. doi:10.1016/j.bbalip.2014.08.006

Shaheen, B. S., Bakir, M., and Jain, S. (2014). Corneal Nerves in Health and Disease. *Surv. Ophthalmol.* 59 (3), 263–285. doi:10.1016/j.survophthal.2013. 09.002

Shevalye, H., Yorek, M. S., Coppey, L. J., Holmes, A., Harper, M. M., Kardon, R. H., et al. (2015). Effect of Enriching the Diet with Menhaden Oil or Daily Treatment with Resolvin D1 on Neuropathy in a Mouse Model of Type 2 Diabetes. *J. Neurophysiol.* 114 (1), 199–208. doi:10.1152/jn.00224.2015

Smith, L. E., Shen, W., Perruzzi, C., Soker, S., Kinose, F., Xu, X., et al. (1999). Regulation of Vascular Endothelial Growth Factor-dependent Retinal Neovascularization by Insulin-like Growth Factor-1 Receptor. *Nat. Med.* 5 (12), 1390–1395. doi:10.1038/70963

Song, F., Xue, Y., Dong, D., Liu, J., Fu, T., Xiao, C., et al. (2016). Insulin Restores an Altered Corneal Epithelium Circadian Rhythm in Mice with Streptozotocin-Induced Type 1 Diabetes. *Sci. Rep.* 6, 32871. doi:10.1038/srep32871

Srinivasan, S., Dehghani, C., Pritchard, N., Edwards, K., Russell, A. W., Malik, R. A., et al. (2017). Corneal and Retinal Neuronal Degeneration in Early Stages of Diabetic Retinopathy. *Invest. Ophthalmol. Vis. Sci.* 58 (14), 6365–6373. doi:10. 1167/iovs.17-22736

Srinivasan, S., Dehghani, C., Pritchard, N., Edwards, K., Russell, A. W., Malik, R. A., et al. (2018). Ophthalmic and Clinical Factors that Predict Four-Year Development and Worsening of Diabetic Retinopathy in Type 1 Diabetes. *J. Diabetes Complications* 32 (1), 67–74. doi:10.1016/j.jdiacomp.2017. 09.002

Stavniichuk, R., Shevalye, H., Hirooka, H., Nadler, J. L., and Obrosova, I. G. (2012). Interplay of Sorbitol Pathway of Glucose Metabolism, 12/15-lipoxygenase, and Mitogen-Activated Protein Kinases in the Pathogenesis of Diabetic Peripheral Neuropathy. *Biochem. Pharmacol.* 83 (7), 932–940. doi:10.1016/j.bcp.2012. 01.015

Steiner, D. F., Cunningham, D., Spigelman, L., and Aten, B. (1967). Insulin Biosynthesis: Evidence for a Precursor. *Science* 157 (3789), 697–700. doi:10. 1126/science.157.3789.697

Stickings, P., and Cunningham, J. M. (2002). Interleukin-1beta-induced Nitric Oxide Production and Inhibition of Insulin Secretion in Rat Islets of Langerhans Is Dependent upon the Nitric Oxide Synthase Cofactor Tetrahidrobiopterin. *Cytokine* 18 (2), 81–85. doi:10.1006/cyto.2002.0881

Sugimoto, K., Yasujima, M., and Yagihashi, S. (2008). Role of Advanced Glycation End Products in Diabetic Neuropathy. *Curr. Pharm. Des.* 14 (10), 953–961. doi:10.2174/138161208784139774

Sultana, R., Perluigi, M., and Butterfield, D. A. (2013). Lipid Peroxidation Triggers Neurodegeneration: a Redox Proteomics View into the Alzheimer Disease Brain. *Free Radic. Biol. Med.* 62, 157–169. doi:10.1016/j.freeradbiomed.2012. 09.027

Suvas, S. (2017). Role of Substance P Neuropeptide in Inflammation, Wound Healing, and Tissue Homeostasis. *J. Immunol.* 199 (5), 1543–1552. doi:10.4049/ jimmunol.1601751

Takamura, Y., Matsumoto, T., Tomomatsu, T., Matsumura, T., Takihara, Y., and Inatani, M. (2013). Aldose Reductase Inhibitor Counteracts the Enhanced Expression of Matrix Metalloproteinase-10 and Improves Corneal Wound Healing in Galactose-Fed Rats. *Mol. Vis.* 19, 2477–2486.

Tavakoli, A., and Liong, S. (2012). Pancreatic Transplant in Diabetes. *Adv. Exp. Med. Biol.* 771, 420–437. doi:10.1007/978-1-4614-5441-0_30

Tavakoli, M., Boulton, A. J., Efron, N., and Malik, R. A. (2011). Increased Langerhan Cell Density and Corneal Nerve Damage in Diabetic Patients: Role of Immune Mechanisms in Human Diabetic Neuropathy. *Cont Lens Anterior Eye* 34 (1), 7–11. doi:10.1016/j.clae.2010.08.007

Tesfaye, S., Chaturvedi, N., Eaton, S. E., Ward, J. D., Manes, C., Ionescu-Tirgoviste, C., et al. EURODIAB Prospective Complications Study Group (2005). Vascular Risk Factors and Diabetic Neuropathy. *N. Engl. J. Med.* 352 (4), 341–350. doi:10. 1056/NEJMoa032782

Tsai, I. L., Tsai, C. Y., Kuo, L. L., Woung, L. C., Ku, R. Y., and Cheng, Y. H. (2021). PLGA Nanoparticles Containing Lingzhi Extracts rescue Corneal Epithelial Cells from Oxidative Damage. *Exp. Eye Res.* 206, 108539. doi:10.1016/j.exer. 2021.108539

Tummanapalli, S. S., Issar, T., Kwai, N., Pisarcikova, J., Poynten, A. M., Krishnan, A. V., et al. (2020b). A Comparative Study on the Diagnostic Utility of Corneal Confocal Microscopy and Tear Neuromediator Levels in Diabetic Peripheral Neuropathy. *Curr. Eye Res.* 45 (8), 921–930. doi:10.1080/02713683.2019. 1705984

Tummanapalli, S. S., Issar, T., Yan, A., Kwai, N., Poynten, A. M., Krishnan, A. V., et al. (2020a). Corneal Nerve Fiber Loss in Diabetes with Chronic Kidney Disease. *Ocul. Surf.* 18 (1), 178–185. doi:10.1016/j.jtos.2019.11.010

Tummanapalli, S. S., Willcox, M. D. P., Issar, T., Yan, A., Pisarcikova, J., Kwai, N., et al. (2019). Tear Film Substance P: A Potential Biomarker for Diabetic Peripheral Neuropathy. *Ocul. Surf.* 17 (4), 690–698. doi:10.1016/j.jtos.2019. 08.010

Ueno, H., Hattori, T., Kumagai, Y., Suzuki, N., Ueno, S., and Takagi, H. (2014). Alterations in the Corneal Nerve and Stem/progenitor Cells in Diabetes: Preventive Effects of Insulin-like Growth Factor-1 Treatment. *Int. J. Endocrinol.* 2014, 312401. doi:10.1155/2014/312401

Vantyghem, M.-C., Chetboun, M., Gmyr, V., Jannin, A., Espiard, S., Le Mapihan, K., et al. (2019). & Members of the Spanish Back Pain Research Network Task Force for the Improvement of Inter-disciplinary Management of Spinal MetastasisTen-Year Outcome of Islet Alone or Islet after Kidney Transplantation in Type 1 Diabetes: A Prospective Parallel-Arm Cohort Study. *Diabetes care* 42 (11), 2042–2049. doi:10.2337/dc19-0401

Vieira-Potter, V. J., Karamichos, D., and Lee, D. J. (2016). Ocular Complications of Diabetes and Therapeutic Approaches. *Biomed. Res. Int.* 2016, 3801570. doi:10. 1155/2016/3801570

Villegas-Rivera, G., Román-Pintos, L. M., Cardona-Muñoz, E. G., Arias-Carvajal, O., Rodríguez-Carrizalez, A. D., Troyo-Sanromán, R., et al. (2015). Effects of Ezetimibe/Simvastatin and Rosuvastatin on Oxidative Stress in Diabetic Neuropathy: A Randomized, Double-Blind, Placebo-Controlled Clinical Trial. *Oxid Med. Cel Longev* 2015, 756294. doi:10.1155/2015/756294

Vincent, A. M., Edwards, J. L., McLean, L. L., Hong, Y., Cerri, F., Lopez, I., et al. (2010). Mitochondrial Biogenesis and Fission in Axons in Cell Culture and Animal Models of Diabetic Neuropathy. *Acta Neuropathol.* 120 (4), 477–489. doi:10.1007/s00401-010-0697-7

Wallner, K., Shapiro, A. M., Senior, P. A., and McCabe, C. (2016). Cost Effectiveness and Value of Information Analyses of Islet Cell Transplantation in the Management of 'unstable' Type 1 Diabetes Mellitus. *BMC Endocr. Disord.* 16, 17. doi:10.1186/s12902-016-0097-7

Wang, J., Dey, A., Kramer, A. H., Miao, Y., Liu, J., Baker, L., et al. (2021). A Novel Therapeutic Approach to Corneal Alkaline Burn Model by Targeting Fidgetin-like 2, a Microtubule Regulator. *Trans. Vis. Sci. Tech.* 10 (1), 17. doi:10.1167/ tvst.10.1.17

Wang, M., Li, M., and Xie, Y. (2021). The Association between Statins Exposure and Peripheral Neuropathy Risk: A Meta-Analysis. *J. Clin. Pharm. Ther.* 46 (4), 1046–1054. doi:10.1111/jcpt.13393

Wilson, S. E., He, Y. G., Weng, J., Li, Q., McDowall, A. W., Vital, M., et al. (1996). Epithelial Injury Induces Keratocyte Apoptosis: Hypothesized Role for the Interleukin-1 System in the Modulation of Corneal Tissue Organization and Wound Healing. *Exp. Eye Res.* 62 (4), 325–327. doi:10. 1006/exer.1996.0038

Winkler, M. A., Dib, C., Ljubimov, A. V., and Saghizadeh, M. (2014). Targeting miR-146a to Treat Delayed Wound Healing in Human Diabetic Organ-Cultured Corneas. *PloS one* 9 (12), e114692. doi:10.1371/journal.pone. 0114692

World Health Organization (2021). Effect of Fidarestat Andα-Lipoic Acid on Diabetes-Induced Epineurial Arteriole Vascular Dysfunction. Available at: https://www.who.int/health-topics/diabetes (Accessed Oct 15, 2021).

Yorek, M. S., Coppey, L. J., Shevalye, H., Obrosov, A., Kardon, R. H., and Yorek, M. A. (2016). Effect of Treatment with Salsalate, Menhaden Oil, Combination of Salsalate and Menhaden Oil, or Resolvin D1 of C57Bl/6J Type 1 Diabetic Mouse on Neuropathic Endpoints. *J. Nutr. Metab.* 2016, 5905891. doi:10.1155/2016/ 5905891

Yorek, M. S., Obrosov, A., Shevalye, H., Lupachyk, S., Harper, M. M., Kardon, R. H., et al. (2014). Effect of Glycemic Control on Corneal Nerves and Peripheral Neuropathy in Streptozotocin-Induced Diabetic C57Bl/6J Mice. *J. Peripher. Nerv Syst.* 19 (3), 205–217. doi:10.1111/jns.12086

You, L., Kruse, F. E., and Völcker, H. E. (2000). Neurotrophic Factors in the Human Cornea. *Invest. Ophthalmol. Vis. Sci.* 41 (3), 692–702.

Zagon, I. S., Klocek, M. S., Sassani, J. W., and McLaughlin, P. J. (2007). Use of Topical Insulin to Normalize Corneal Epithelial Healing in Diabetes Mellitus. *Arch. Ophthalmol.* 125 (8), 1082–1088. doi:10.1001/archopht. 125.8.1082

Zhang, J., Dai, Y., Wei, C., Zhao, X., Zhou, Q., and Xie, L. (2020). DNase I Improves Corneal Epithelial and Nerve Regeneration in Diabetic Mice. *J. Cel Mol Med* 24 (8), 4547–4556. doi:10.1111/jcmm.15112

Zhang, Y., Dou, S., Qi, X., Zhang, Z., Qiao, Y., Wang, Y., et al. (2021). Transcriptional Network Analysis Reveals the Role of miR-223-5p during Diabetic Corneal Epithelial Regeneration. *Front. Mol. Biosci.* 8, 737472. doi:10.3389/fmolb.2021.737472

Zhang, Y., Gao, N., Wu, L., Lee, P. S. Y., Me, R., Dai, C., et al. (2020b). Role of VIP and Sonic Hedgehog Signaling Pathways in Mediating Epithelial Wound Healing, Sensory Nerve Regeneration, and Their Defects in Diabetic Corneas. *Diabetes* 69 (7), 1549–1561. doi:10.2337/db19-0870

Zhang, Y., Jiang, H., Dou, S., Zhang, B., Qi, X., Li, J., et al. (2020a). Comprehensive Analysis of Differentially Expressed microRNAs and mRNAs Involved in Diabetic Corneal Neuropathy. *Life Sci.* 261, 118456. doi:10.1016/j.lfs.2020. 118456

Zhao, H., He, Y., Ren, Y. R., and Chen, B. H. (2019). Corneal Alteration and Pathogenesis in Diabetes Mellitus. *Int. J. Ophthalmol.* 12 (12), 1939–1950. doi:10.18240/ijo.2019.12.17

Zherebitskaya, E., Akude, E., Smith, D. R., and Fernyhough, P. (2009). Development of Selective Axonopathy in Adult Sensory Neurons Isolated

from Diabetic Rats: Role of Glucose-Induced Oxidative Stress. *Diabetes* 58 (6), 1356–1364. doi:10.2337/db09-0034

Zhou, Q., Chen, P., Di, G., Zhang, Y., Wang, Y., Qi, X., et al. (2015). Ciliary Neurotrophic Factor Promotes the Activation of Corneal Epithelial Stem/ progenitor Cells and Accelerates Corneal Epithelial Wound Healing. *Stem Cells* 33 (5), 1566–1576. doi:10.1002/stem.1942

Zhu, L., Titone, R., and Robertson, D. M. (2019). The Impact of Hyperglycemia on the Corneal Epithelium: Molecular Mechanisms and Insight. *Ocul. Surf.* 17 (4), 644–654. doi:10.1016/j.jtos.2019.06.007

Ziegler, D., Low, P. A., Litchy, W. J., Boulton, A. J., Vinik, A. I., Freeman, R., et al. (2011). Efficacy and Safety of Antioxidant Treatment with α-lipoic Acid over 4 Years in Diabetic Polyneuropathy: the NATHAN 1 Trial. *Diabetes care* 34 (9), 2054–2060. doi:10.2337/dc11-0503

Long-Term Biocompatibility of a Highly Viscously Thiol-Modified Cross-Linked Hyaluronate as a Novel Vitreous Body Substitute

Jose Hurst [1†], Annekatrin Rickmann [2†], Nele Heider [1], Christine Hohenadl [3], Charlotte Reither [3], Andreas Schatz [1], Sven Schnichels [1*†], Kai Januschowski [1,4†] and Martin S. Spitzer [1,5†]

[1]Centre of Ophthalmology, University Eye Hospital Tübingen, Tübingen, Germany, [2]Eye Clinic Sulzbach, Knappschafts Hospital Sulzbach/Saar, Sulzbach, Germany, [3]Croma Pharma GmbH, Leobendorf, Austria, [4]Mount St. Peter Eye Clinic Trier, Trier, Germany, [5]Department of Ophthalmology, University Medical Center Hamburg-Eppendorf (UKE), Hamburg, Germany

Purpose: In surgical ophthalmology, the treatment of complicated retinal and vitreous diseases is one of the central challenges. For this purpose, the vitreous body is removed as part of the standard therapy and replaced by a temporary tamponade to stabilize the position of the retina. Since the tamponading properties of previous materials such as silicone oils, gases, or semi-fluorinated alkanes are a combination of their surface tension and their buoyancy vector, they cannot completely fill the vitreous cavity. The aim of this work was to test *in vivo* a novel vitreous body substitute (ViBos strong) based on cross-linked hyaluronic acid for its compatibility.

Methods: A pars plana vitrectomy with posterior vitreous detachment was performed in the right eye of 18 pigmented rabbits, with subsequent injection of ViBos strong. Follow-up examination included slit-lamp examination, funduscopy, intraocular pressure measurements (IOP), optical coherence tomography (OCT), and electroretinogram (ERG) measurements. The rabbits were sacrificed at three different time points (1, 3, and 6 months; each 6 animals) and examined macroscopically and prepared for histological examination (HE staining) and immunohistochemistry (Brn3a and glial fibrillary acidic protein (GFAP)).

Results: ViBos strong demonstrated good intraoperative handling and remained stable for at least 1 month and degraded slowly over 6 months. IOP was within clinical acceptable values at all follow-up examinations. Retinal function was well preserved after instillation of the hydrogel and comparable to the untreated eye after 6 months in OCT, ERG, and histological examinations. An increase in the GFAP expression was found in the surgery eyes, with a peak in the 3-month group. The Brn3a expression was not significantly affected by vitrectomy with ViBos strong.

Conclusion: Highly viscously thiol-modified cross-linked hyaluronate showed a good biocompatibility in rabbit eyes over 6 months after vitrectomy, making it a promising potential as a vitreous substitute.

Keywords: vitreoretinal surgery, hyaluronic acid, thiol-modified, crosslinked, vitreous substitute, artificial vitreous

INTRODUCTION

In the treatment of pathologies affecting the posterior pole, the vitreous body needs to be removed by vitrectomy following stabilization of the retina with an endotamponade, like silicone oils or gases. Current clinically used endotamponades are effective, especially in promoting retinal reattachment, but are disadvantageous due to their hydrophobic nature, refractive index, and density compared to the human vitreous, resulting in immediate blurred vision after surgery and complications such as raised intraocular pressure (IOP), prolonged inflammation, emulsification, or cataract formation (Kim et al., 2008; Duan et al., 2011; Lin et al., 2021; Schulz et al., 2021). The basic reason for the limitation of endotamponades is their hydrophobic character in a hydrophilic environment of the vitreous cavity and acting *via* the two physical functions "buoyancy vector" and "surface/interfacial tension." The tamponade vector can only act in one direction, so complete filling of the vitreous cavity is not possible (Schnichels et al., 2017; Szurman, 2017). Furthermore, while gas endotamponades diffuse out over time, silicone oils are nonbiodegradable and must be surgically removed (Duan et al., 2011; Lin et al., 2021).

Therefore, there is great demand to develop an ideal vitreous endotamponade that mimics the physiological properties of a natural vitreous body to improve therapeutic efficacy and safety. Recent tamponade strategies aim at hydrophilic, polymeric hydrogel-based systems due to their favorable physical and mechanical properties such as high water content, high optical transparency, suitable refractive indices, viscosity, swelling pressure, adjustable rheological properties, and adaptable biocompatibility (Schulz et al., 2020; Lin et al., 2021; Schulz et al., 2021; Wang et al., 2021). The tamponade effect of a hydrogel is exerted by the viscosity and swelling pressure, the latter *via* the high water-binding property; therefore, it seems logical to develop hydrogels based on hyaluronic acid, as this is one of the main components of the natural vitreous body (Nakagawa et al., 1997; Schramm et al., 2012). To further enhance the mechanical stability, chemical cross-linking was investigated as a possible solution (Roy et al., 2012; Spitzer et al., 2012; Schnichels et al., 2017). However, to avoid the risk of potential toxic effects of unreacted cross-linkers, thiolated hyaluronic acid forming disulfide bridges by air oxidation without the need of additional chemical cross-linkers was previously introduced as a promising potential novel vitreous body substitute (Schnichels et al., 2017; Januschowski et al., 2019). These hydrogels showed superior efficacy over silicone oil in a rabbit model of retinal detachment (Schnichels et al., 2017).

Further long-term *in vivo* studies are needed to exclude side effects on surrounding tissue, particular to the retina. Therefore, the aim of the study was to evaluate the long-term biostability and histocompatibility of a highly viscously thiol-modified cross-linked hyaluronate (TCHA) in a rabbit model after vitrectomy.

MATERIALS AND METHODS

Preparation of TCHA Hydrogels

The test substance is a biodegradable, clear, viscous hydrogel, free of visible particles, homogenized and prepared as injectable gel implant, which had been steam sterilized. The steam processing does not affect the physicochemical properties of the hydrogel. Formulations were prepared in physiological phosphate buffer (320 mOsmol/kg, pH 7.4) and contained 2.2% (ViBos strong) HA. Cross-linking was achieved by induced disulfide bridge formation in substituted thiol groups. The rheological analysis and the determination of the refractive index were performed as described in Schnichels et al. (2017).

Animals and Experimental Setup

All animal procedures and methods were performed in accordance with the Statement for the Use of Animals in Ophthalmic and Vision Research of the Association for Research in Vision and Ophthalmology (ARVO), complied with institutional guidelines and EU and German law, and were conducted under research permission AK1/14, granted by the *Regierungspräsidium* Tübingen, Germany.

All experiments were performed on chinchilla bastard rabbits (ChBB:CH; Charles River Laboratories, Sulzfeld, Germany), after an acclimatization period of at least 5 weeks. Housing and husbandry conditions were compliant with EU guidelines 2010/63/EU. The animals were housed in a pathogen-free facility, one rabbit per cage (Tecniplast, Tecniplast Deutschland GmbH, Hohenpeißenberg, Germany), with straw bedding, allowed free water and food access, and kept in 12-h light/dark cycles, 18°C, and air humidity of 55 ± 10%.

The 18 animals were divided into three subgroups (defined as follow-up 1, 3, or 6 months) of six rabbits each. At the end of the follow-up period, the animals were sacrificed and processed for histology and immunohistology.

The preoperative examinations of the 2-month-old pigmented rabbits included ERG (electroretinography), OCT (optical coherence tomography), and slit-lamp and fundus examination of both eyes and measurement of IOP. Postoperative follow-up examinations are defined in **Table 1**. ERGs, OCT examination, and surgeries were performed under general anesthesia using intramuscular injections of ketamine 10% (0.25 mg/kg) (Ketanest; Parke Davis, Berlin, Germany) and medetomidine hydrochloride (35 mg/kg) (Sedator; Eurovet, Bladel, Netherlands). Slit-lamp and fundus examination examinations were performed under sedation with 25 mg/kg medetomidine. In addition, local anesthesia with Oxybuprocaine drops (Novesine 0.4%; Novartis, Nürnberg, Germany) was applied throughout all the examinations, IOP measurement, and surgeries. Postoperatively, all animals received 5 mg/kg carprofen to reduce any possible pain.

Slit-Lamp and Fundus Examination

Each rabbit was pre- and postoperatively at all follow-up examinations carefully examined on both eyes, specifically to signs of inflammation, fibrin, and small blood clots or signs of incipient cataract with a Kowa SL-15 portable slit lamp.

Measuring the Intraocular Pressure

IOP of both eyes was measured pre- and postoperatively at all follow-up examinations using a Schiötz tonometer (Winters Tonometer, Germany). The rabbits were placed in the lateral

TABLE 1 | Examination schedule.

Examination schedule					
	Preoperative examination	Day 1+3+7 post-OP	1 month post-OP	3 months post-OP	6 months post-OP
Weight	X	x	x	x	x
Slit lamp	X	x	x	x	x
IOP OS/OD	X	x	x	x	x
Funduscopy	X	x	x	x	x
ERG	X		x	x	x
OCT	x		x	x	x

position, and the Schiötz tonometer was launched smoothly perpendicular to the rabbit eye for three times.

Optical Coherence Tomography

The retina was examined at baseline and at 1, 3, and at 6 months using a high-resolution OCT (SPECTRALIS®, Heidelberg Engineering, Heidelberg, Germany). The OCT scanner acquired images with an optical resolution of 7 μm axially and 30 μm laterally and a digital resolution of 3.9 μm axially and 11 μm laterally. The maximum scan depth was 1.9 mm in tissue. The image size was 1,536 × 496 pixels. During each examination, the optic nerve head and visual streak were examined. Thereafter, retinal thickness was determined temporally from the visual streak (volume scan with 25 scans).

Electroretinography

ERG measurements were performed with an Espion (Diagnosys LLC, Cambridge, UK). After the baseline examination, we scheduled the follow-up examinations after 1, 3, and 6 months postoperatively. 45 min before ERG measurement, one drop of tropicamide 0.5% (Mydriatikum Stulln, Stulln, Germany) was applied for pupil dilation in both eyes. The dark adaptation time period was 30 min. To record the ERG, two contact lens electrodes and three needle electrodes (subcutaneous, one in the right upper lid, one in the left upper lid, and one in the neck) were mounted. To avoid exposure keratopathy, METHOCEL (2% methylcellulose; OmniVision GmbH, Puchheim, Germany) was applied regularly to the cornea. Measurements were performed only when acceptable impedance levels of less than $10 \, k\Omega$ at $25 \, Hz$ (using the machine's built-in algorithm) were reached. The used dark-adapted and light-adapted ERG protocols, as well as oscillatory potentials, were performed as described in Schnichels et al. (2017).

Surgery

Pars plana vitrectomy (ppV) was performed under a standard ophthalmic operating microscope (Carl Zeiss Meditec, Inc., Oberkochen, Germany) by one experienced surgeon. In each case, the right eye was operated, and the left eye served as the control. A standard 20/23-gauge vitrectomy system was used (PentaSys 2, Fritz Ruck Ophthalmologische Systeme GmbH, Eschweiler, Germany). Initially, a sclerotomy was placed in the infratemporal quadrant and an infusion line was connected and

sutured with 7–0 vicryl (Johnson & Johnson Intl, New Brunswick, NJ, USA). Two further sclerotomies were similarly placed through the pars plana in the two superior quadrants and a light and vitrector inserted into the vitreous. Then, a subtotal vitrectomy without specific posterior vitreous detachment was performed. After vitrectomy with fluid-air exchange, the port was removed and the entire vitreous cavity was filled with ViBos strong using a curved 20-G Weber cannula until egress was witnessed from the second sclerotomy. At the end, the sclerotomies and the conjunctival wounds were closed using 7.0 vicryl absorbable sutures (Ethicon, Norderstedt, Germany). No leaks were witnessed. The operated eye received ointment bid Gentamicin sulfate 5 mg with dexamethasone 0.3 mg (Dexamytrex®, Bausch + Lomb, Berlin, Germany) for 1 week to control postoperative inflammation and prevent postoperative infection.

Histology and Immunohistochemistry

At the end of the examination period, both eyes were removed and were incubated for 5 days in 4.5% formaldehyde. Subsequently, the eyes were first cut in two halves for macroscopical examination and the lens was removed. Afterward, the eye cups were processed for histology and immunohistochemistry with anti-GFAP (glial fibrillary acidic protein) and anti-Brn3a (brain-specific homeobox/POU domain protein 3A) antibodies (Quina et al., 2005). Three representative Brn3a sections (×200) of each case with attached retina were used for the determination of the number of the retinal ganglion cells. The amount of GFAP staining was graded by three independent, blinded examiners (N.S., J.H., S.S.), and an average score for each section was created. The staining was graded as mild (Schulz et al., 2021), moderate (Lin et al., 2021), strong (Kim et al., 2008), or very strong (Duan et al., 2011).

RESULTS

Slit-Lamp Examination/Fundoscopy

Rabbits are very prone to noninfectious inflammation after intraocular surgery. Thus, it was not surprising that 13 out of 18 rabbits showed a mild to moderate fibrinous reaction in the anterior chamber on the first postoperative day. A mild amount of fibrin was present in six out of 18 rabbits up to 1 month after surgery. However, after 3 months no fibrin could be detected in
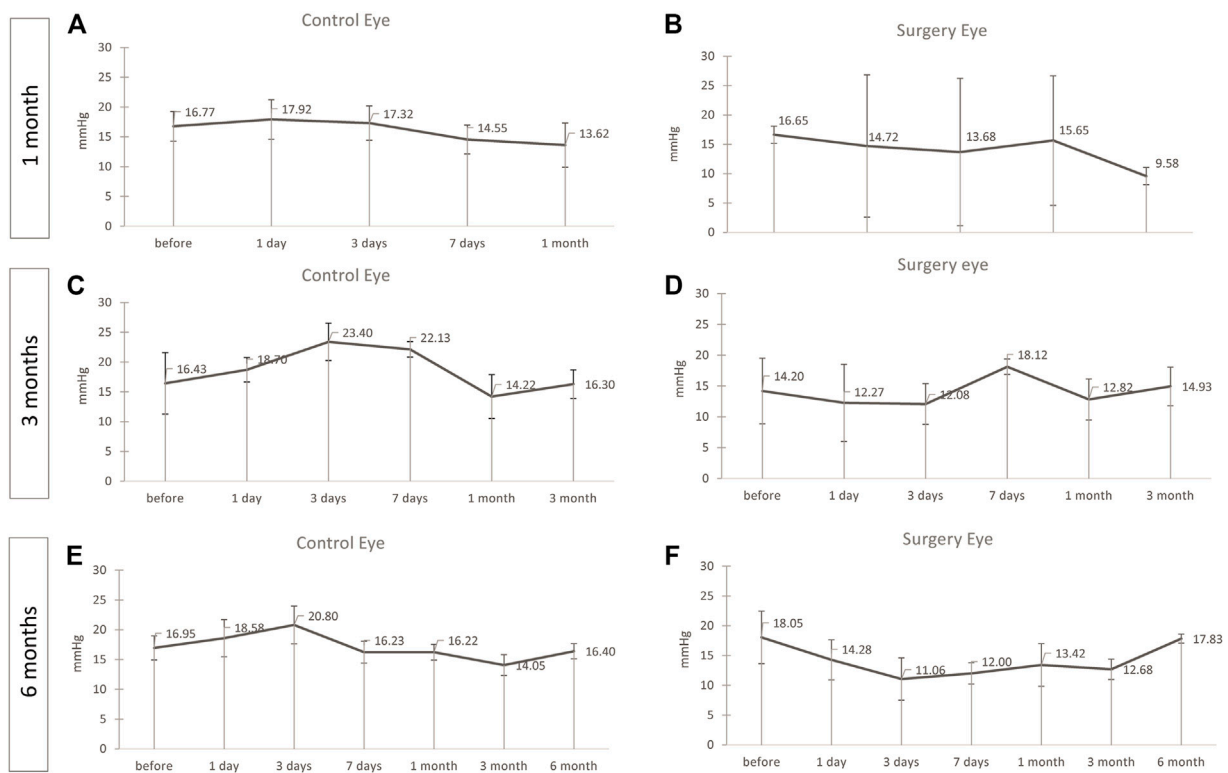
FIGURE 1 | No significant changes in the intraocular pressure (IOP) was noticed. IOP during the follow-up of the operated and contralateral eye after 1 **(A,B)**, 3 **(C,D)**, and 6 **(E,F)** months after surgery. The IOP was well within clinically tolerable levels in all groups, but slightly lower in the operated eye than in the contralateral control eye in the 1-month group [**(A,B)**, $p = .22$] and the M3 group [**(C,D)**, $p = .028$]. A similar, but not significant, trend was seen in the M6 group [**(E,F)**, $p = .058$]. Points and error bars indicate mean and standard deviation.

any of the animals. There were no signs of infections in any of the rabbits. The cornea stayed clear in all rabbits throughout the entire study.

The formation of cataracts could be observed in five out of 18 animals (28%). Two of these cases were observed in the 1-month group (M1), three in the 3-month group (M3), and none in the 6-month group (M6). All cases with a developed cataract were due to an iatrogenic touch of the posterior lens capsule during the surgery. Thus, all cataracts which developed were most likely iatrogenic due to the surgical procedure and not related to ViBos strong. Also, the type of cataract that developed (posterior capsular cataracts commencing from the area of iatrogenic lens touch) is in agreement with the assumption that the lens opacification was due to technical surgical complication, but not to the hydrogel. Moreover, in the group with the longest follow-up in which no surgical complications occurred, the lenses of all animals stayed clear throughout the entire study.

Four out of the 18 rabbits developed retinal detachments (three in M1 with a follow-up of 1 month; one in M3 with a follow-up of 3 months; none in M6 with a follow-up of 6 months). These cases were more likely to be considered iatrogenic complications. The cases with retinal detachment and flat ERG were excluded from further OCT and ERG analysis. Fundoscopy in all other cases without pronounced

cataracts or retinal detachment was unremarkable; especially, no inflammatory reactions at the posterior segment were noticed. During follow-up, the degradation of the hydrogel in the vitreous cavity could not be reliably quantified funduscopically due to the examination conditions and the clear optical properties of the hydrogel.

Evaluation of Intraocular Pressure

After instillation of ViBos, the IOP never reached worrisome high or low levels at any time point after surgery. Although the IOP in the M1 group after 1 month of surgery was slightly lower on average than the contralateral control eye, the IOP was still well within clinically tolerable levels (mean IOP over the entire period: control eye: 16.03 ± 1.8; surgery eye: 14.05 ± 2.7; $p = .22$, **Figures 1A,B**). The same was detected in the M3 group with a 3-month follow-up (control eye: 18.95 ± 3.8; surgery eye: $14.04 \pm 0.2.5$; $p = .028$, **Figures 1C,D**). A similar, but not significant, trend was seen in the M6 group (control eye: 16.74 ± 2.4; surgery eye: 13.26 ± 2.3; $p = .058$, **Figures 1E,F**).

Retinal OCT Evaluation

In order to visualize the retinal attachment and the fundus of the eye, OCT examinations were performed in each rabbit pre- and postoperatively. The integrity, attachment, and thickness of the retina were examined during the follow-up of 6 months, and at no
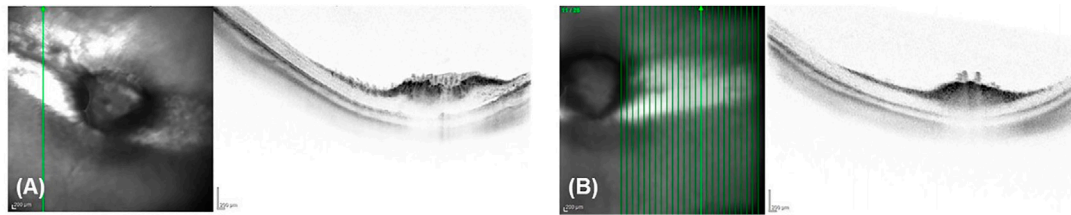
FIGURE 2 | Retinal thickness was not affected. Representative OCT 6 months after surgery showing no difference of integrity, attachment, and thickness of the retina between a treated **(A)** and a control eye **(B)**.
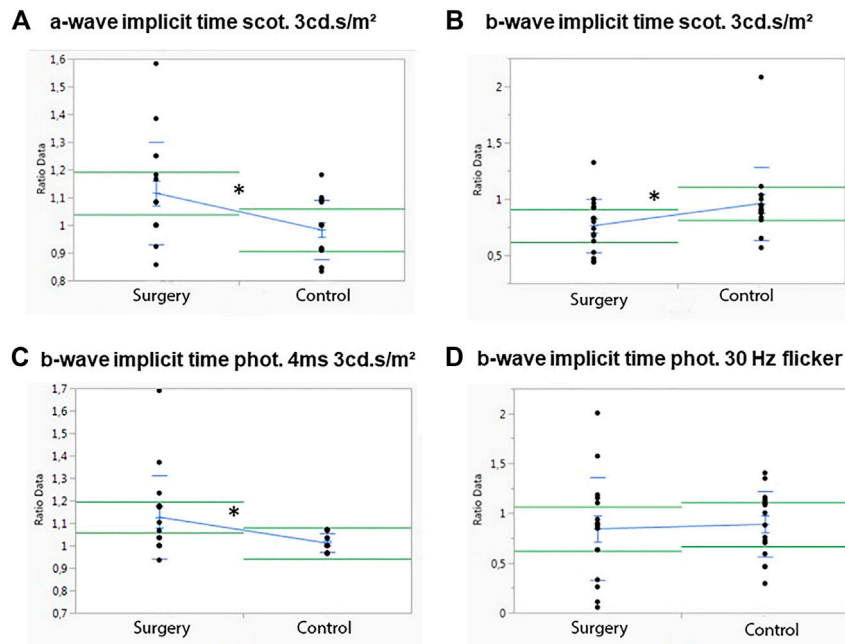

FIGURE 3 | Influence of ViBos strong on the physiological activity of the retina after 1 month. **(A)** A significant higher a-wave implicit time (scotopic standard flash at 3 cd s/m^2) for the operated compared to the control eyes was measured (p = .02). **(B)** Significant differences were detected for the b-wave implicit time (scotopic standard flash at 3 cd s/m^2) of the control eyes (p = .031). **(C)** Significant differences were recorded for the b-wave implicit time (photopic 4 ms at 3 cd s/m^2) (p = .028). **(D)** No significant changes for the b-wave implicit time (30 Hz flicker at 3 cd s/m^2) were noted (p = .769).

time point any difference between treated and control eyes could be observed (**Figure 2**).

Scotopic and Photopic ERG

Baselines of all ERG measurement of each group were analyzed for differences between the operated and the control eye. There was no statistically significant difference between the right and left eyee at baseline, and ERG measurements were normally distributed (data not shown).

In M1, no significant differences between the operated and the control eye were observed for the scotopic a-wave amplitude, but the operated eyes showed a significant higher implicit time than the control eyes (p = .02) (**Figure 3A**). The scotopic b-wave amplitude revealed no differences, but the control eyes had a significant higher b-wave implicit time than the operated eyes (p = .031) (**Figure 3B**).

No differences were measured in the photopic (photopic 4 ms at 3 cd s/m^2) a-wave amplitude or in the a-wave implicit time after 1 month (data not shown). The same was true for the photopic b-wave amplitude, but a significant increase in the photopic single flash b-wave time (p = .028) was observed (**Figure 3C**). Apart from that, no differences in the control eye were noted for the b-wave implicit time with a 30-Hz flicker at 3 cd s/m^2, p = .769) (**Figure 3D**).

In M3 which was followed for 3 months, significant differences between the operated and the control eye were observed only for the scotopic b-wave implicit time (p = .045) (**Figure 4D**). A trend in the scotopic a-wave amplitude, where the control eyes showed a higher a-wave implicit time (p = .05), was noted (**Figure 4B**). Otherwise, no differences in the control eyes were observed in this group (**Figures 4A,C,E**). There were also no significant differences in photopic a- or b-wave amplitudes or for the implicit time (data not shown).
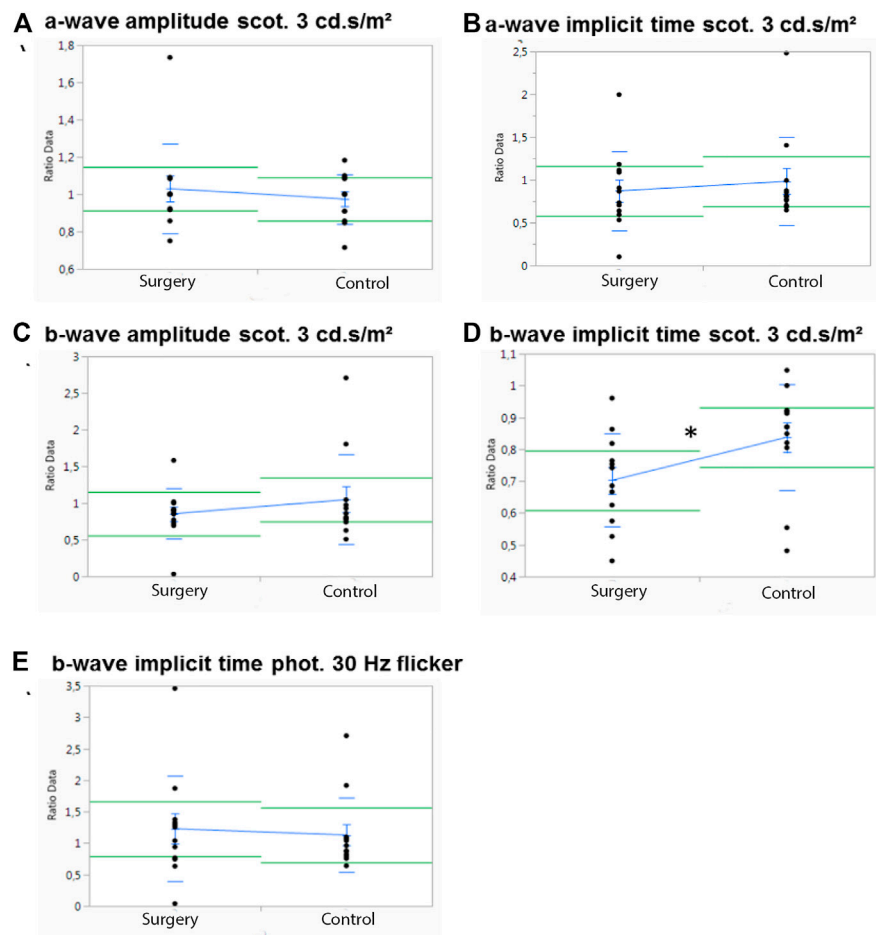
FIGURE 4 | Influence of ViBos strong on the physiological activity of the retina after 3 months. **(A,B)** No significant differences were noted for a-wave amplitudes and a-wave implicit time at 3 cd s/m^2 (p = .58 and p = .05, respectively). **(C,D)** There was no effect on the scotopic b-wave amplitudes, but a significant higher b-wave implicit time (p = .045) was observed in the control group (scotopic standard flash at 3 cd s/m^2). **(E)** No significant differences were noted for the b-wave implicit time (30 Hz flicker at 3 cd s/m^2) (p = .742).

In M6, no significant differences of the ERG measurements between the operated (gel-filled) and the control eye were observed at any time point (data not shown).

Macroscopic Examination

Macroscopic examination 1 month after implantation of the substitute into the vitreous cavity of the operated eyes showed a complete filling with the tamponade and a partly filled eye after 3 months (**Figures 5B,D**). The partner eye was always examined as a comparison for possible macroscopically visible changes (**Figures 5A,C and E**). After 6 months, no gel could be detected by macroscopic examination (**Figure 5F**). Remarkably, the lens stayed clear throughout the entire follow-up period—except in the cases of iatrogenic lens touch during surgery.

Histological Examination

Hematoxylin/eosin (HE) staining was used to examine the retinal structure for its physiological make-up or abnormalities of the

structure. In all the eyes examined, only one animal in the 3-month group was found to have high-grade changes in the cell assemblies and a loss of structure of the retinal structure due to retinal detachment. In the remaining seventeen rabbits of the study, no abnormalities of the retinal structure could be detected. In summary, normally structured retinas without any signs of intraretinal or intravitreal inflammation were observable after histological (HE), periodic acid–Schiff (PAS), and immunohistochemistry stainings (**Figure 6** and data not shown).

GFAP and Brn3a Protein Expression (Immunohistochemistry)

The expression of *glial fibrillary acidic protein* (GFAP) is an indicator for glial activation and retinal fibrosis. Although the GFAP expression was significantly upregulated in all operated eyes throughout the entire study (1 month: 2.92 vs. 1.2; p = .08, 3 months: 3.32 vs. 1.38; p = .0043 and 6 months: 2.40 vs. 1.71; p = .026), the total amount of GFAP expression decreased over time.
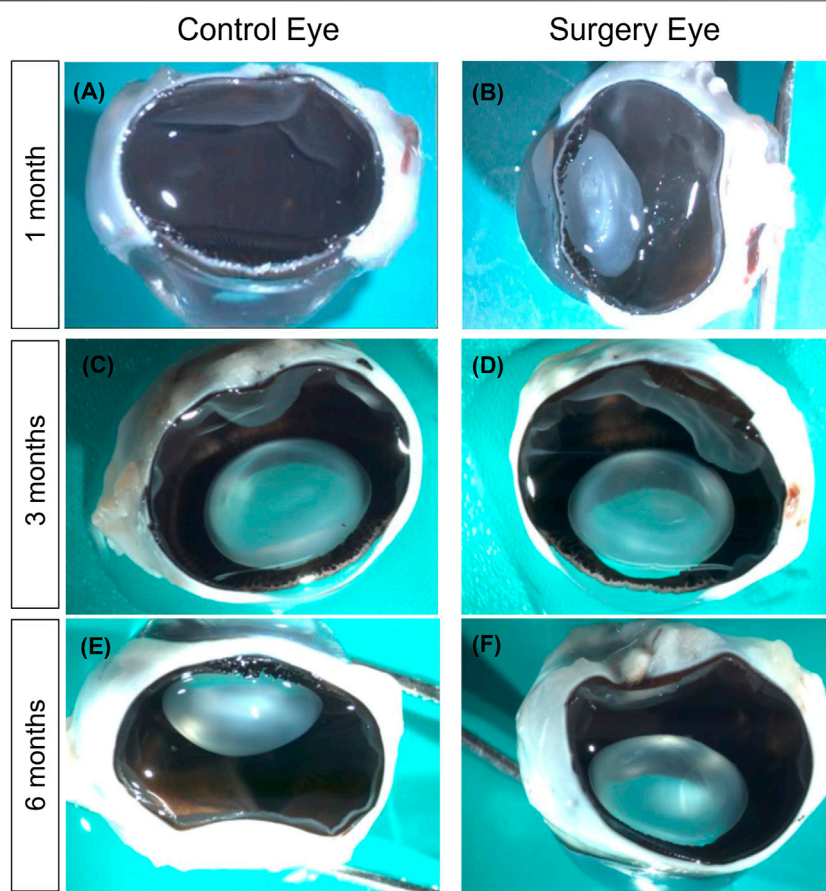
FIGURE 5 | Macroscopic examination of the eyes. **(A,B)** Macroscopic examination after 1 month. The retina of the surgery eye (right) remained completely attached, and the lens was clear apart from a moderate posterior capsular opacification that was due to lens touch during surgery. The vitreous cavity was nearly completely filled with the vitreous substitute. Notably, formaldehyde fixation for histology liquefied the vitreous substitute **(B)**. Macroscopic examination after 3 months **(C,D)**. No differences between treated **(D)** and untreated eyes **(C)** could be observed. However, most of the vitreous substitute had dissolved **(D)**. **(E,F)** Macroscopic examination after 6 months. No differences between treated **(F)** and untreated eyes **(E)**. No vitreous substitute was present at this time point anymore. Magnification ×200.
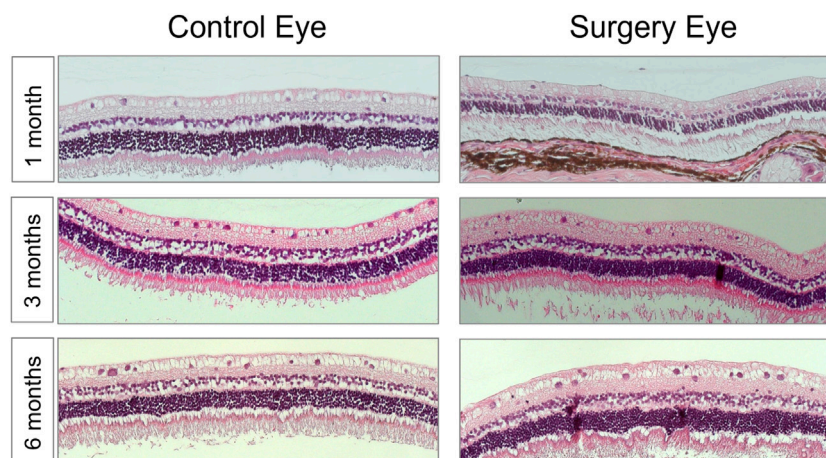
FIGURE 6 | The morphology of the retina was not affected by the vitreous replacement. Representative images of HE-stained retina over the entire time course. 1 month postoperatively; 3 months postoperatively; 6 months postoperatively. No signs of structural damage or toxicity to the retina were detectable. Magnification ×200.
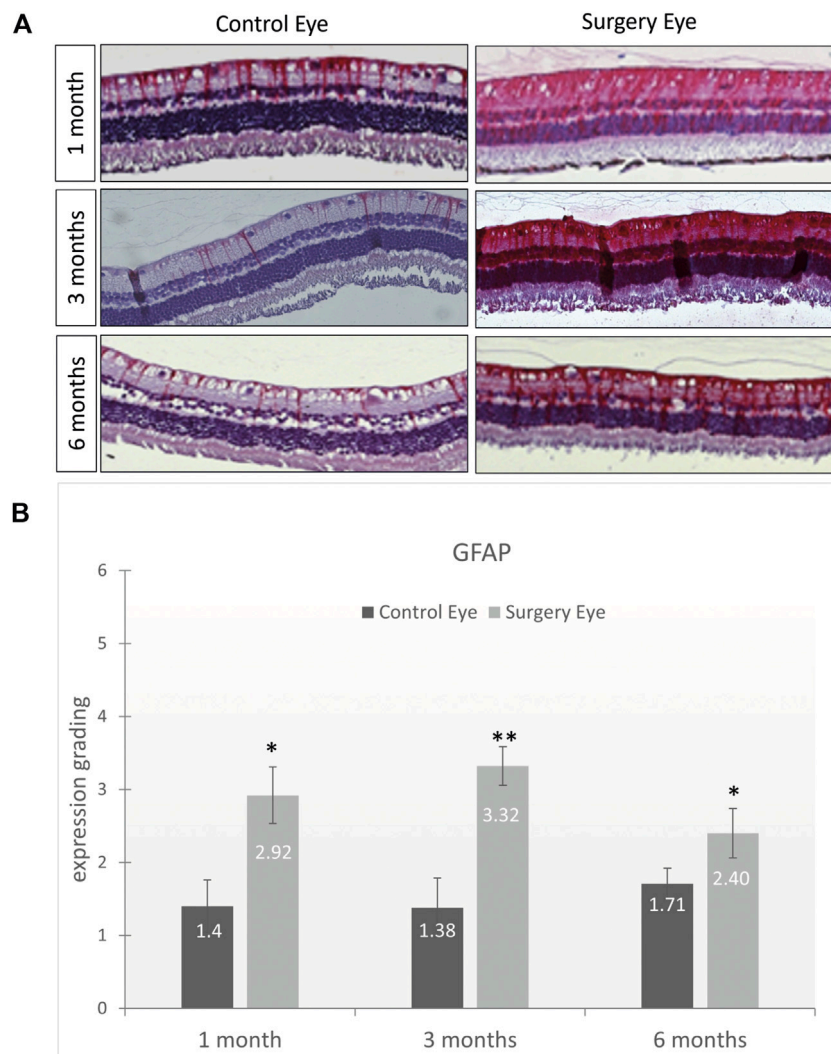
FIGURE 7 | Low activation of macroglial cells by ViBos strong. **(A)** Representative pictures of GFAP staining. **(B)** The GFAP staining was graded as mild (Schulz et al., 2021), moderate (Lin et al., 2021), strong (Kim et al., 2008), or very strong (Duan et al., 2011). Although the GFAP expression was significantly upregulated in all operated eyes throughout the entire study, the total amount of GFAP expression decreased over time. After 1 month, the control eyes got a grading of 1.4 and the surgery eyes 2.92 (p = .028; n = 3 pairs). The expression of GFAP after 3 months was graded with 1.38 in the control eyes and 3.32 in the surgery eyes (p = .0043; n = 5 pairs). A slight decrease was observed after 6 months with a grading of 1.71 on the control eyes and 2.3 in the surgery eyes (p = .026; n = 6 pairs). Bars and error bars indicate mean and standard deviation. Significances are indicated as * with respect to control eyes, using the following significance level: *p < .05; **p < .01.

The level of upregulation, although statistically significant, is most likely clinically irrelevant as vitrectomy itself causes a significant glial activation and GFAP upregulation. Since the partner eyes that were used for comparison did not receive surgery, the moderate GFAP upregulation in the ViBos strong-filled eyes underlines the good biocompatibility of ViBos strong (**Figure 7**).

The Brn3a serves as a marker for RGCs. The expression of Brn3a was not significantly affected by vitrectomy with ViBos strong. Thus, the number of RGCs was not diminished after ViBos strong injection (**Figure 8**). The stable number of Brn3a-positive cells in the ganglion cell layer (GCL) through the whole observation time indicates excellent biocompatibility of ViBos strong and its degradation products even after 6 months. The mean percentage of RGCs in

the GCL in the operated eyes of the 1-month group was 43.27% (SD 9.61), and that of the nonoperated partner eyes 52.09% (SD: 6.84). In the operated eyes of the 3-month study, the RGC ratio was 61.51% (SD 3.82) vs. 60.65% (SD: 6.14) of the nonoperated partner eyes. In the 6-month group, the average percentage of RGZ in the operated eyes was 59.43% (SD: 3.62) and 61.02% (SD: 1.65) in the non-operated partner eyes. No significant differences were found between the groups.

DISCUSSION

Here we presented the result of a long-term *in vivo* study (1, 3, and 6 months) of a highly viscous hydrophilic hydrogel based on
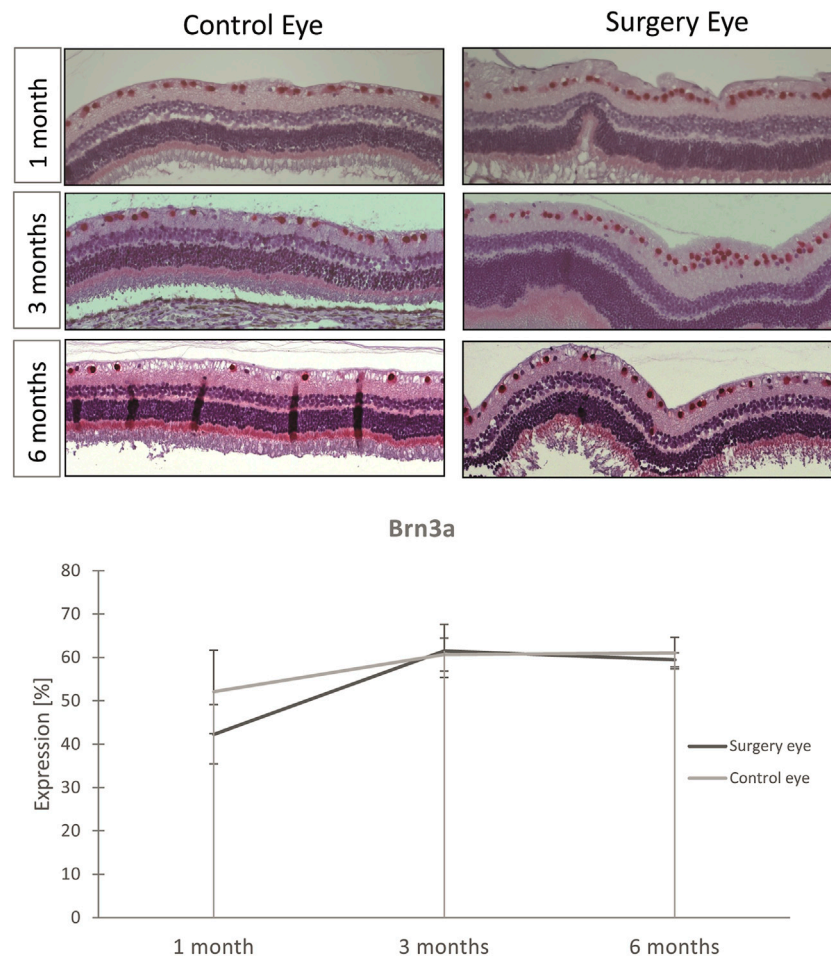
FIGURE 8 | Influence of ViBos strong on retinal ganglion cells. **(A)** Representative pictures of the Brn3a staining. **(B)** Quantitative representation of the relative Brn3a expression. After 1 month, the average percentage of RGC in the ganglion cell layer was 43.27% in the operated eyes and 52.09% in the nonoperated fellow eyes ($p = .243$; $n = 3$ pairs). In the operated eyes of the study over 3 months, it was 61.51% compared to the controls with 60.65% ($n = 5$ pairs). In the 6-month group, the average percentage of RGC in the operated eyes was 59.43% and that of the non-operated fellow eyes 61.02% (n = 6 pairs). Points and error bars indicate mean and standard deviation.

thiolated cross-linked hyaluronate (ViBos strong). Good biocompatibility without toxicity or evidence of anatomic or functional changes in a rabbit model was demonstrated in the whole period of 6 months. It could thus be confirmed that ViBos strong is well injectable, transparent, biocompatible, stable over time, and biodegradable (Schnichels et al., 2017).

Despite many years of research, very few polymeric hydrogels can be applied practically in the vitreous cavity yet, due to either a short intravitreal half-life or inflammatory or even toxic effects at the retina and in the vitreous cavity (Nakagawa et al., 1997; Suri and Banerjee, 2006; Wang et al., 2021). Although it seemed obvious to develop VBS based on native hyaluronate (HA), previous studies could only show a very short half-life of less than 14 days (Nakagawa et al., 1997) of non-cross-linked HA in the vitreous cavity and an increase in IOP due to intensive swelling of the hydrogel (Pruett et al., 1979).

To prevent rapid biodegradation, chemically modified and UV cross-linked HA was developed and demonstrated a good biocompatibility, an excellent refractive index of 1.338, and a

residence time of the hydrogel in the vitreous cavity of at least 6 weeks to several months, without inflammatory or toxic reaction and no lens opacification (Schramm et al., 2012; Spitzer et al., 2012; Barth et al., 2016; Barth et al., 2019; Gong et al., 2020). However, drawbacks of chemically cross-linked hydrogels are the potential toxicity of the monomers and/or cross-linkers remaining in the eye, and the need for precise control over the injection time (Naahidi et al., 2017; Schulz et al., 2021). Therefore, a stable thiol-modified hydrogel built by natural formation of disulfide bridges by air oxidation without additional chemical cross-linkers (Schnichels et al., 2017) was used for this study. Physicochemical characterization of the naturally cross-linked gel revealed a refractive index similar to the human vitreous, and the transparent, hydrophilic material was shown to be highly elastic but still easily injectable and comparable shear moduli to other vitreous substitutes (Swindle et al., 2008; Santhanam et al., 2016; Schnichels et al., 2017).

Stability and persistence of a vitreous substitute within the vitreous cavity over a longer time period is of great importance,

especially in the treatment of complicated retinal detachments where an effective compression of retinal tears according to the orientation of the holes is mandatory. The potential of ViBos strong has already been demonstrated in a retinal detachment model in rabbits by Schnichels et al. in which both the good biocompatibility and the superior efficacy for reattachment of the retina compared to silicone oil could be shown over 1 month (Schnichels et al., 2017). The ViBos is intended to adhere to all locations of the retina due to its swelling properties. This should prevent the occurrence of re-detachment and PVR contralateral to the buoyancy vector, as we see with hydrophobic tamponades and their residual intravitreal fluid. However, this was not explicitly investigated in this study.

Our study with long-term results follows up on these findings and shows that an injection of ViBos strong through a 20-gauge needle was uneventful and showed complete filling of the vitreous cavity with gradual degradation after 3 months. Overall complications were minor with expected fibrin reaction of the anterior chamber after the surgery, and iatrogenic cataract and retinal detachment at the beginning of the experiments, which is in concordance with other studies (Schnichels et al., 2017; Gong et al., 2020). The defined stability of the hydrogel did not lead to a clinically relevant increase of the IOP at any time but had a tendency to a lower IOP. Especially in the first 24 h after vitreoretinal surgery, which are the most critical (Wong et al., 2011) as most of the hydrogel swelling occurs at that time, the IOP was within safe parameters (Januschowski et al., 2019). While the hydrogel degraded slowly over 6 months, there was no evidence of impairment of retinal function from potential degradation products in the OCT and histological examinations. In accordance, retinal function was well preserved after the instillation of the hydrogel. Some minor impairments of the ERGs 1 or 3 months postoperatively were most likely due to the surgical procedure and not due to the filling with ViBos strong. This assumption is strongly supported by the normal ERG findings 6 months after surgery. Moreover, it was most remarkable that after 6 months of follow-up the ERG of the eyes that underwent surgery was not significantly different from the ERG of the contralateral control eye, given the fact that vitrectomy on its own can cause some decrease of retinal function. A similar observation with normalization of ERG function after vitreoretinal surgery was also shown in another model (Liu et al., 2019). Whether the hydrogel itself also has an influence on ERG accuracy has not been conclusively clarified to

date. However, this seems very unlikely as the hydrogels unlike the hydrophobic silicone oil mainly consist of water. The water content of thy hydrogels is very similar to that of the natural vitreous.

In conclusion, the tested hydrogel had a very good tolerance without toxic properties on the retina. The good optical properties of the hyaluronic acid-based hydrogel, which almost correspond to the physiological vitreous body, could also enable good visual properties of the patients postoperatively. Therefore, the proven biocompatibility of ViBos strong over 6 months is significant for the application in the clinical field and might be a promising agent for further studies of retinal tamponades.

DATA AVAILABILITY STATEMENT

The raw data supporting the conclusion of this article will be made available by the authors, without undue reservation.

ETHICS STATEMENT

The animal study was reviewed and approved by the Regierungspräsidium Tübingen, Germany.

AUTHOR CONTRIBUTIONS

JH, SS, KJ, and MS contributed to the conception and design of the study; NH and MS performed the experiments; NH and JH performed the statistical analysis; JH and AR wrote the first draft of the manuscript; SS, NH, CH, CR, AS, KJ, and MS wrote sections of the manuscript. All authors contributed to the manuscript revision and read and approved the submitted version.

FUNDING

REFERENCES

Barth, H., Crafoord, S., Andréasson, S., and Ghosh, F. (2016). A Cross-Linked Hyaluronic Acid Hydrogel (Healaflow(®)) as a Novel Vitreous Substitute. *Graefes Arch. Clin. Exp. Ophthalmol.* 254, 697–703. doi:10.1007/s00417-015-3256-z

Barth, H., Crafoord, S., Arnér, K., and Ghosh, F. (2019). Inflammatory Responses after Vitrectomy with Vitreous Substitutes in a Rabbit Model. *Graefes Arch. Clin. Exp. Ophthalmol.* 257, 769–783. doi:10.1007/s00417-019-04242-0

Duan, A., She, H., and Qi, Y. (2011). Complications after Heavy Silicone Oil Tamponade in Complicated Retinal Detachment. *Retina* 31, 547–552. doi:10.1097/IAE.0b013e3181eef2fd

Gong, Y., Chen, K., Wu, Y., Guo, X. H., and Zhang, T. (2020). Effect on Rabbits' Intraocular Structure by Cross-Linked Hyaluronic Formations as Vitreous Substitute. *Int. J. Ophthalmol.* 13, 1531–1537. doi:10.18240/ijo.2020.10.04

Januschowski, K., Schnichels, S., Hurst, J., Hohenadl, C., Reither, C., Rickmann, A., et al. (2019). *Ex Vivo* biophysical Characterization of a Hydrogel-Based Artificial Vitreous Substitute. *PLoS One* 14, e0209217. doi:10.1371/journal.pone.0209217

Kim, S. S., Smiddy, W. E., Feuer, W. J., and Shi, W. (2008). Outcomes of Sulfur Hexafluoride (SF6) versus Perfluoropropane (C3F8) Gas Tamponade for Macular Hole Surgery. *Retina* 28, 1408–1415. doi:10.1097/IAE.0b013e3181885009

Lin, Q., Lim, J. Y. C., Xue, K., Su, X., and Loh, X. J. (2021). Polymeric Hydrogels as a Vitreous Replacement Strategy in the Eye. *Biomaterials* 268, 120547. doi:10.1016/j.biomaterials.2020.120547

Liu, Z., Liow, S. S., Lai, S. L., Alli-Shaik, A., Holder, G. E., Parikh, B. H., et al. (2019). Retinal-detachment Repair and Vitreous-Like-Body Reformation via a Thermogelling Polymer Endotamponade. *Nat. Biomed. Eng.* 3, 598–610. doi:10.1038/s41551-019-0382-7

Naahidi, S., Jafari, M., Logan, M., Wang, Y., Yuan, Y., Bae, H., et al. (2017). Biocompatibility of Hydrogel-Based Scaffolds for Tissue Engineering Applications. *Biotechnol. Adv.* 35, 530–544. doi:10.1016/j.biotechadv.2017.05.006

Nakagawa, M., Tanaka, M., and Miyata, T. (1997). Evaluation of Collagen Gel and Hyaluronic Acid as Vitreous Substitutes. *Ophthalmic Res.* 29, 409–420. doi:10.1159/000268042

Pruett, R. C., Schepens, C. L., and Swann, D. A. (1979). Hyaluronic Acid Vitreous Substitute. A Six-Year Clinical Evaluation. *Arch. Ophthalmol.* 97, 2325–2330. doi:10.1001/archopht.1979.01020020541006

Quina, L. A., Pak, W., Lanier, J., Banwait, P., Gratwick, K., Liu, Y., et al. (2005). Brn3a-expressing Retinal Ganglion Cells Project Specifically to Thalamocortical and Collicular Visual Pathways. *J. Neurosci.* 25, 11595–11604. doi:10.1523/JNEUROSCI.2837-05.2005

Roy, S., Thi, H. D., Feusier, M., and Mermoud, A. (2012). Crosslinked Sodium Hyaluronate Implant in Deep Sclerectomy for the Surgical Treatment of Glaucoma. *Eur. J. Ophthalmol.* 22, 70–76. doi:10.5301/ejo.5000054

Santhanam, S., Liang, J., Struckhoff, J., Hamilton, P. D., and Ravi, N. (2016). Biomimetic Hydrogel with Tunable Mechanical Properties for Vitreous Substitutes. *Acta Biomater.* 43, 327–337. doi:10.1016/j.actbio.2016.07.051

Schnichels, S., Schneider, N., Hohenadl, C., Hurst, J., Schatz, A., Januschowski, K., et al. (2017). Efficacy of Two Different Thiol-Modified Crosslinked Hyaluronate Formulations as Vitreous Replacement Compared to Silicone Oil in a Model of Retinal Detachment. *PLoS One* 12, e0172895. doi:10.1371/journal.pone.0172895

Schramm, C., Spitzer, M. S., Henke-Fahle, S., Steinmetz, G., Januschowski, K., Heiduschka, P., et al. (2012). The Cross-Linked Biopolymer Hyaluronic Acid as an Artificial Vitreous Substitute. *Invest. Ophthalmol. Vis. Sci.* 53, 613–621. doi:10.1167/iovs.11-7322

Schulz, A., Januschowski, K., and Szurman, P. (2021). Novel Vitreous Substitutes: the Next Frontier in Vitreoretinal Surgery. *Curr. Opin. Ophthalmol.* 32, 288–293. doi:10.1097/ICU.0000000000000745

Schulz, A., Rickmann, A., Wahl, S., Germann, A., Stanzel, B. V., Januschowski, K., et al. (2020). Alginate- and Hyaluronic Acid-Based Hydrogels as Vitreous Substitutes: An *In Vitro* Evaluation. *Transl Vis. Sci. Technol.* 9, 34. doi:10.1167/tvst.9.13.34

Spitzer, M. S., Sat, M., Schramm, C., Schnichels, S., Schultheiss, M., Yoeruek, E., et al. (2012). Biocompatibility and Antifibrotic Effect of UV-Cross-Linked Hyaluronate as a Release-System for Tranilast after Trabeculectomy in a Rabbit Model-Aa Pilot Study. *Curr. Eye Res.* 37, 463–470. doi:10.3109/02713683.2012.658593

Suri, S., and Banerjee, R. (2006). *In Vitro* evaluation of *In Situ* Gels as Short Term Vitreous Substitutes. *J. Biomed. Mater. Res. A.* 79, 650–664. doi:10.1002/jbm.a.30917

Swindle, K. E., Hamilton, P. D., and Ravi, N. (2008). *In Situ* formation of Hydrogels as Vitreous Substitutes: Viscoelastic Comparison to Porcine Vitreous. *J. Biomed. Mater. Res. A.* 87, 656–665. doi:10.1002/jbm.a.31769

Szurman, P. (2017). Glaskörperersatz in der Ablatiochirurgie - warum wir eine ganz neue Tamponadestrategie brauchen!. *Klin Monatsbl Augenheilkd* 234, 1094–1102. doi:10.1055/s-0043-114422

Wang, T., Ran, R., Ma, Y., and Zhang, M. (2021). Polymeric Hydrogel as a Vitreous Substitute: Current Research, Challenges, and Future Directions. *Biomed. Mater.* 16, 16. doi:10.1088/1748-605X/ac058e

Wong, R., Gupta, B., Williamson, T. H., and Laidlaw, D. A. (2011). Day 1 Postoperative Intraocular Pressure Spike in Vitreoretinal Surgery (VDOP1). *Acta Ophthalmol.* 89, 365–368. doi:10.1111/j.1755-3768.2009.01703.x

New Pharmacological Approaches for the Treatment of Neurotrophic Keratitis

Su Yin Koay and Daniel F. P. Larkin*

Cornea and External Diseases Service, Moorfields Eye Hospital, London, United Kingdom

Neurotrophic keratitis (NK) is a rare degenerative condition that is caused by damage to the trigeminal nerve, with partial or complete loss of corneal sensory innervation. The loss of innervation leads to impaired healing of corneal epithelium, which subsequently results in punctate epithelial erosions, persistent epithelial defects, corneal ulcers and corneal perforation. Management of NK is often supportive and aims to promote epithelial healing and prevent progression of disease. Multiple novel pharmacological approaches have been proposed to address the underlying pathophysiology of NK, which are discussed in this paper.

Keywords: neurotrophic keratitis, persistent epithelial defect, nerve growth factor, corneal ulcer, neurotization

INTRODUCTION

Neurotrophic keratitis (NK) is caused by damage to the trigeminal nerve, with partial or complete loss of corneal innervation and sensation. This leads to impairment in the sensory and trophic function of the corneal nerves, as well as reduction of both protective reflexes and trophic neuromodulators, with consequent breakdown of the corneal epithelium (Dua et al., 2018; Versura et al., 2018). It is a rare degenerative condition with an estimated prevalence of 1.6–4.2 cases per 10,000 persons (Mastropasqua et al., 2017). NK can occur as a result of congenital abnormalities, ocular pathology (most commonly herpetic infections), neurological conditions or surgery, and systemic conditions such as diabetes mellitus (Bonini et al., 2003). It may also occur due to direct damage to corneal nerve endings following chronic usage of certain eye drops such as timolol. (**Table 1**).

NK is classified into three stages according to the Mackie classification (Bonini et al., 2003). In *Stage 1*, epithelial changes are seen. Clinical findings include epithelial hyperplasia and irregularity, punctate keratopathy, dellen, decreased tear break-up times, stromal scarring and superficial vascularization (**Figure 1A**). Persistent epithelial defects (PEDs) are the hallmark of *Stage 2*, these are usually oval in shape with a characteristic rolled and smooth edge (**Figure 1B**). Stromal edema, Descemet's membrane folds or anterior chamber inflammatory cells may also be seen. In *Stage 3*, a corneal ulcer with stromal involvement is present (**Figure 1C**). This may progress to corneal melting and subsequent perforation.

The management of NK is challenging, and vision loss often occurs despite treatment to support epithelialization. Visual prognosis depends on the underlying etiology and the degree of corneal hypoanesthesia. This has led to the development of new medical treatments to treat this condition, which is the focus of this article. Surgical management is also briefly reviewed as this is often necessary when managing NK.

ASSESSMENT OF NK

Corneal sensitivity can be measured qualitatively by touching all four quadrants of the cornea with a twisted cotton swab. Quantitative testing can be performed with the Cochet-Bonnet esthesiometer

TABLE 1 | Classified causes of neurotrophic keratopathy.

Inherited and Congenital
Familial dysautonomia (Riley Day)
Familial corneal anesthesia
Hereditary and sensory autonomic neuropathy types IV and V
Mobius syndrome
Goldenhar syndrome
Ocular
Herpes simplex keratitis
Herpes zoster keratitis
Corneal surgery (keratoplasty, refractive surgery)
Contact lens wear
Chemical or physical burns
Chronic ocular surface inflammation
Corneal dystrophies (granular, lattice)
Drug toxicity (timolol, diclofenac)
Orbital neoplasia
Neurological
Traumatic/surgical resection of trigeminal nerve
Surgical ablation for trigeminal neuralgia
Compressive/infiltrative lesion, e.g. acoustic neuroma, aneurysm
Stroke
Systemic
Diabetes mellitus
Leprosy
Vitamin A deficiency

(**Figure 2**), which records the patient's response or blink to a length of a protruding nylon filament (between 0 and 60 mm). The filament is used to touch the cornea, following which pressure is applied to induce a bend in the filament. The filament length is gradually reduced until the patient is able to report the filament touching the cornea. A normally innervated cornea usually detects touch at a filament length of 40 mm. A shorter filament length corresponds with poorer corneal sensation.

Slit lamp examination with dilated fundoscopy may give clues to the etiology of the NK. In addition, it is also important to perform a full cranial nerve examination in all patients as the involvement of the other cranial nerves may allow localization of a neurological lesion. For example, involvement of the facial (VII) or vestibulocochlear (VIII) nerve may indicate a potential acoustic neuroma. *In vivo* confocal microscopy (IVCM) is not particularly helpful for diagnosis, but may have a role in longitudinal evaluation of patients in clinical trials of new treatments or neurotization surgery. Guillon-Rolf et al. demonstrated a statistically significant reduction in sub-basal nerve plexus nerve fiber density, fiber length and branch density with IVCM in patients with congenital corneal anesthesia (**Figure 3**). (Guillon-Rolf et al., 2020)

MANAGEMENT OF NK

The aim of management in NK is to prevent progression of disease (Lambiase et al., 1999). In Stage 1, management focuses on preventing breakdown of corneal epithelium. In addition, any eyelid position abnormalities (e.g., lagophthalmos) and potentially toxic topical medications should be identified and addressed.

The aims in stages 2 and 3 are to promote epithelial healing, and to prevent the development of infective keratitis or corneal melt (Semeraro et al., 2014a). Regular monitoring is essential as patients are often unaware of any worsening of symptoms.

Conventional Medical Treatment

Ocular lubricants are used in all stages of NK, and promote epithelialization by reducing biomechanical shear forces and diluting pro-inflammatory mediators in the tear film (Dua et al., 2018). Frequent use of non-preserved ocular lubricants is encouraged in all stages of NK and include hypromellose, carbomer gels, hydroxypropylguar, hyaluronate and hyaluronate combinations (carboxymethylcellulose, polysaccharide, soybean with phospholipids, xanthan gum, trehalose).

When an epithelial defect is present, prophylactic topical antibiotics help to reduce the risk of infective keratitis.

Matrix metalloproteinases inhibitors such as oral tetracyclines, oral erythromycin and topical azithromycin restrict neutrophil collagenase and epithelial gelatinase gene expression, suppress alpha-1 antitrypsin degradation and scavenge reactive oxygen species (Dua et al., 2018). This can reduce the risk of corneal melt in patients with stage 3 NK (Trinh et al., 2021).

Blood Product Derivatives

Autologous serum eye drops were first reported to be beneficial for Sjögren's syndrome-related dry eye disease in 1984 (Fox et al., 1984). Serum eye drops contain growth factors (epidermal growth factor (EGF) and transforming growth factor (TGF)), vitamins (A, C), glucose, natural antimicrobials (surface IgA, defensins, lysozyme), and proteins involved in wound healing (fibronectin) (Rauz and Saw, 2010). These biological properties help to facilitate epithelialization by inducing cellular migration and adhesion (Matsumoto et al., 2004). Whilst there is a lack of randomized controlled trial data, serum eye drops have been reported to promote substantial improvement of PEDs unresponsive to conventional treatment within 7–28 days. (Tsubota et al., 1999; Lekhanont et al., 2013; Semeraro et al., 2014b; Azari and Rapuano, 2015; Shtein et al., 2020).

Matsumoto et al.(Matsumoto et al., 2004) used 20% autologous serum in 14 eyes with NK and achieved complete epithelial healing in 17.1 ± 8.0 days. Mean pretreatment corneal sensitivity was 11.8 ± 11.6 mm, which increased to 30.0 ± 22.9 mm after treatment with autologous serum. In addition, autologous serum eye drops have been shown to improve corneal nerve morphology with increased number, length, width, and density of subepithelial corneal nerves detected with IVCM post treatment (Rao et al., 2010; Aggarwal et al., 2015; Abedi and Hamrah, 2018).

Human umbilical cord serum has been shown to contain higher concentrations of EGF, NGF and TGF-β compared to peripheral blood serum (Yoon et al., 2006; Yoon et al., 2007). Vajpayee et al. (Vajpayee et al., 2003) reported that umbilical cord serum has been reported to lead to a faster median percentage decrease in the size of PEDs at 7, 14 and 21 days ($p < 0.05$) compared to peripheral blood serum. Yoon et al. (Yoon et al., 2007) treated 28 NK eyes with 20% umbilical serum reported complete epithelial defect healing in all eyes, with a mean healing
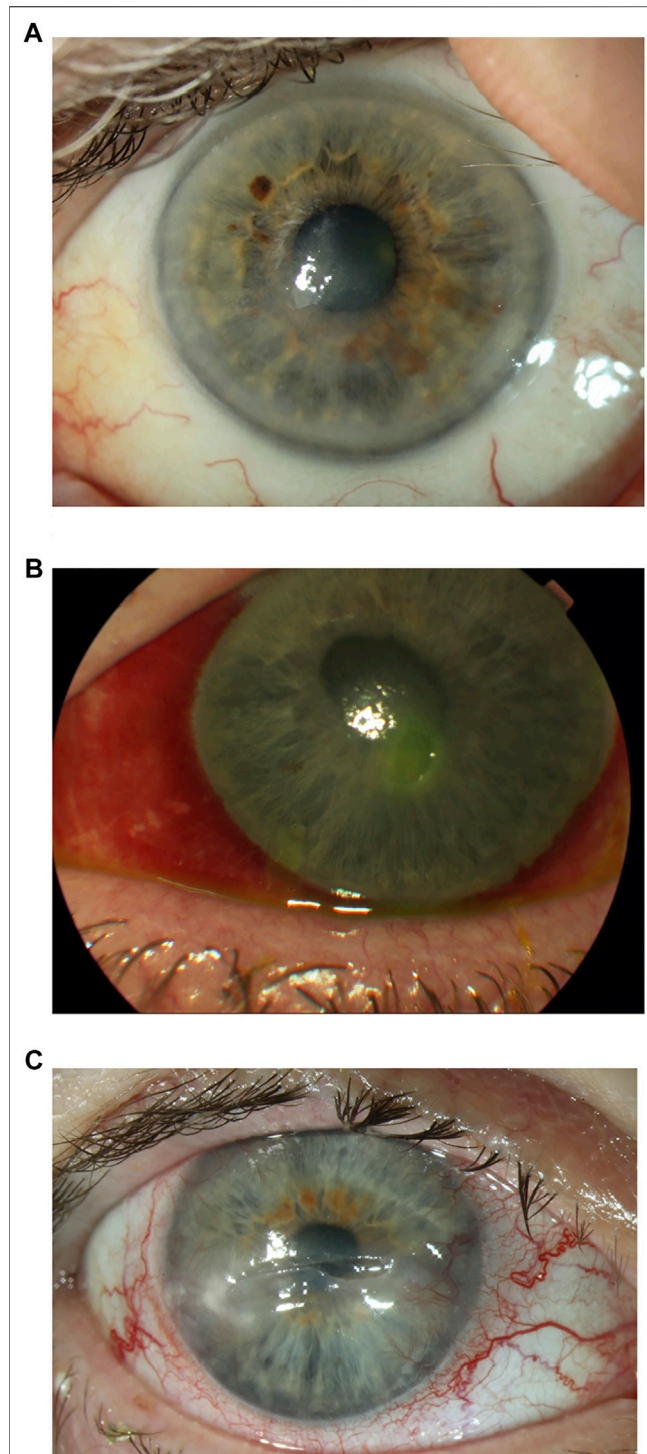
FIGURE 1 | Clinical appearance of neurotrophic keratitis (NK) stages 1, 2 and 3. **Figure 1A**. Stage 1 NK: Superficial opacity and punctate corneal epitheliopathy. **Figure 1B**. Stage 2 NK: Persistent epithelial defect. **Figure 1C**. Stage 3 NK: Ulceration with thinning to mid-stroma.

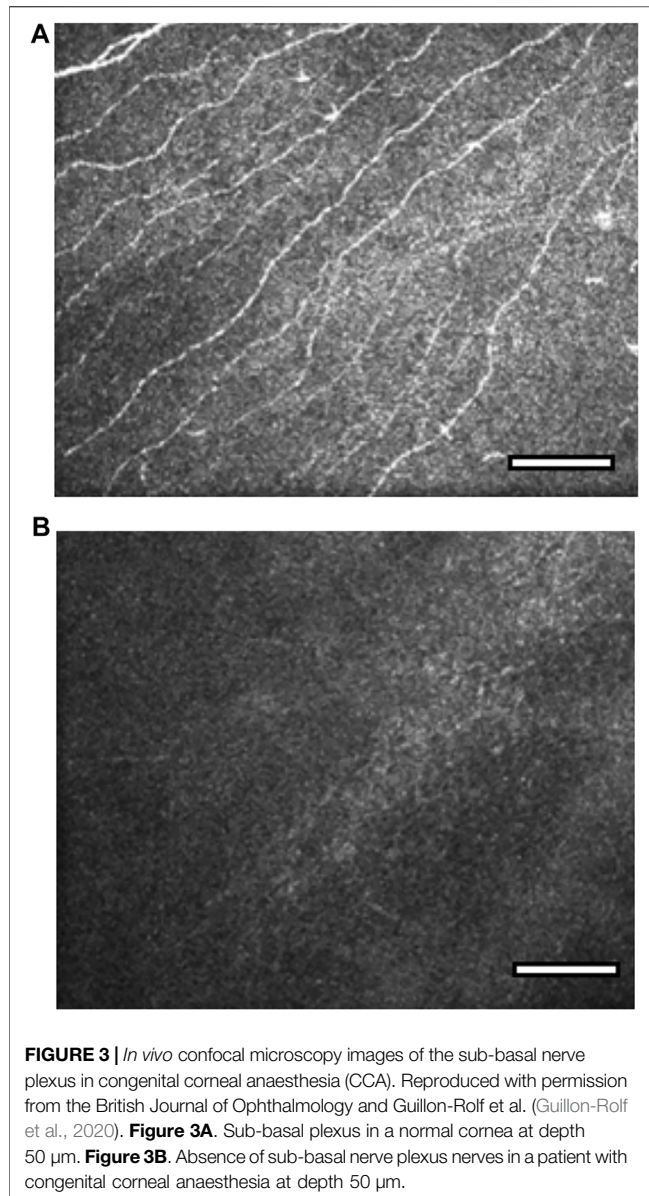
FIGURE 2 | Cochet-Bonnet esthesiometer.

tortuosity (Giannaccare et al., 2017). Nevertheless, the small volumes obtained and the cost of preparation limits its widespread use (Dua et al., 2018).

Platelet rich plasma (PRP) and plasma rich in growth factors (PRGF) have been reported to be effective for promoting resolution of persistent epithelial defects which are unresponsive to conventional treatments (You et al., 2020). It contains a number of growth factors such as platelet-derived growth factor (PDGF), EGF, fibroblast growth factor (FGF), TGF, nerve growth factor (NGF), and insulin-like growth factor (IGF). (Mussano et al., 2016). In a cell culture inflammatory model where ocular surface fibroblasts treated with pro-inflammatory interleukin 1-beta (IL-1β) and tumor necrosis factor alpha (TNFα), PRGF appeared to exert more potent regenerative and anti-inflammatory effects compared to autologous serum (Anitua et al., 2016).

Wróbel-Dudzińska et al. treated 25 eyes with stages 2/3 NK with PRP, and reported complete healing of ulceration in 80% ($n = 20$), and considerable improvement in ulcer size in 16% ($n = 4$) (Wróbel-Dudzińska et al., 2018). Kim et al. reported that mean epithelial healing time of PEDs after infective keratitis was 10.09 ± 2.49 days (range 2–30 days) with PRP, compared to 17.83 ± 3.07 days (range 5–38 days) with autologous serum (Kim et al., 2012). An ongoing randomized non-masked trial (NCT03653650) aims to compare PRP + bandage contact lens; lubricants + bandage contact lens and lubricant ointment + eye patching in PEDs.

Matrix Regenerating Agents

ReGeneraTing Agents (RGTAs) are biodegradable glucose-based polymers which are chemically bioengineered to form analogs of the extracellular matrix component. RGTAs mimic the action of heparan sulfates bound to extracellular matrix proteins, allowing them to form a bioskeleton scaffold that induces cell adhesion whilst providing proteolytic protection for the components involved in tissue healing (e.g., collagen, fibronectin, elastin) (Arvola et al., 2016) Their large molecular structure makes it

time of 4.4 ± 4.0 weeks. Umbilical serum has also been shown to improve corneal nerve morphology (assessed with IVCM), with an increase of total nerve number and a decrease of nerve

FIGURE 3 | *In vivo* confocal microscopy images of the sub-basal nerve plexus in congenital corneal anaesthesia (CCA). Reproduced with permission from the British Journal of Ophthalmology and Guillon-Rolf et al. (Guillon-Rolf et al., 2020). **Figure 3A**. Sub-basal plexus in a normal cornea at depth 50 μm. **Figure 3B**. Absence of sub-basal nerve plexus nerves in a patient with congenital corneal anaesthesia at depth 50 μm.

unlikely to penetrate through the cornea. RGTA is usually instilled every 2-3 days, more frequent instillation is not recommended as it may negatively impact the healing process (Barritault et al., 2017).

Cacicol (Laboratoires Théa, Clermont-Ferrand, France) belongs to the RGTA family and is the first ophthalmic matrix therapy product. Results appear to be promising for the treatment of corneal ulcers resistant to conventional treatments. Aifa et al. administered RGTA for severe corneal neurotrophic ulcers, and achieved complete healing in eight of 11 eyes (73%) after a mean of 8.7 weeks (range 1–22 weeks) (Aifa et al., 2012). Mean ulcer area decreased from 11.12 to 6.37% ($p = 0.048$) in the first week, and to 1.56% ($p = 0.005$) at 1 month (Aifa et al., 2012). Guerra et al. reported corneal healing (defined as a decrease of the corneal ulcer area) in all 25 eyes with NK within an average of 4.1 ± 2.3 weeks. (Guerra et al., 2017). Cochener et al. administered

RGTA to 20 patients (20 eyes) with stage 2/3 NK unresponsive to conventional treatment in a prospective observational study (Cochener et al., 2019). Total corneal healing was observed in 13 eyes (65%) within 1–3 months, with relapses reported in four eyes (20%) several months after cessation of treatment. A randomized multicenter double masked study (NCT01242839) which reported to have completed in June 2014 compared the healing rate of chronic corneal ulcers with the use of calcicol versus placebo drops, but results have not been published. The manufacturer ceased the production of calcicol in December 2019 for commercial reasons.

Recombinant Human Nerve Growth Factor (rhNGF)

NGF is a neurotrophin that stimulates corneal re-innervation and healing after injury, induces epithelial cell proliferation and differentiation, maintains corneal epithelial stem cells, and can promote tear production (Deeks and Lamb, 2020). Cenegermin is a rhNGF produced in *Escherichia coli* which was developed following encouraging results of murine NGF in the treatment of NK (Lambiase et al., 1998; Bonini et al., 2000).

The REPARO study (Bonini et al., 2018) was a phase II European multicenter, randomized, double-masked, vehicle-controlled trial that assessed the safety and efficacy of rhNGF in stage 2/3 NK. 156 patients were randomized 1:1:1 to rhNGF 10 μg/ml, 20 μg/ml, or vehicle; drops were administered 6 times a day for 8 weeks. At week 4, 19.6% of vehicle-treated patients achieved corneal healing versus 54.9% receiving rhNGF 10 μg/ml (+35.3%; $p < 0.001$) and 58.0% receiving rhNGF 20 μg/ml (+38.4%, $p < 0.001$). At week 8, 43.1% of vehicle-treated patients achieved less than 0.5 mm lesion staining versus 74.5% receiving rhNGF 10 μg/ml (+31.4%; $p = 0.001$) and 74.0% receiving rhNGF 20 μg/ml (+30.9%; $p = 0.002$).

Median time to corneal healing was 56, 29 and 28 days in the vehicle, rhNGF 10 μg/ml and rhNGF 20 μg/ml groups. More than 96% of patients who healed after rhNGF treatment did not get a recurrence of the PED or corneal ulcer during the follow up period of 48–56 weeks. Treatment was well tolerated, with mild ocular side effects (conjunctival hyperaemia, photophobia and ocular pain) that did not require discontinuation of treatment. The authors hypothesized that these side effects may represent improvement of corneal sensitivity due to the therapeutic actions of rhNGF.

NGF0214 (Pflugfelder et al., 2020) was a further randomized, double-masked, vehicle-controlled trial of rhNGF performed in the United States. 48 patients with stage 2/3 NK were randomized 1:1 to rhNGF (cenegermin) 20 μg/ml or vehicle eye drops. After 8 weeks, 16 of 23 rhNGF-treated patients (69.6%) achieved less than 0.5 mm of lesion staining compared to seven of 24 vehicle-treated patients (29.2%) (+40.4%, $p = 0.006$). There were no statistically significant improvements in corneal sensitivity, but reflex tearing (a possible indication of corneal sensitivity and nerve function) exhibited trends favoring rhNGF treatment.

Neither the REPARO or NGF0214 study showed statistically significant improvements in visual acuity measures. It is however important to remember that in NK, visual acuity does not necessarily correlate with NK severity or healing status.

Following these two studies, cenegermin 0.002% ophthalmic solution (Oxervate; Dompé Farmaceutici SpA, Milan, Italy) received approval from the European Commission (EC) and the United States Food and Drug Administration. At the time of writing, it is commercially available in Europe, the United States, Switzerland, Israel, Canada and Australia. Despite EC approval, cenergermin is not available in the United Kingdom, following a decision on grounds of cost-effectiveness by the UK's National Institute for Health and Care Excellence (NICE NC for H and CE, 2018).

Mastropasqua et al. evaluated the structural changes that occur as a result of rhNGF treatment in 18 patients with NK with IVCM (Mastropasqua et al., 2020). There was a significant increase in the mean sub-basal nerve density, diameter and number of nerve branches at weeks four and eight in comparison to baseline, with a nerve regeneration rate of $1079.1 \pm 835\,\mu m/mm^2$ at 4 weeks and $661.9 \pm 835\,\mu m/mm^2$ at 8 weeks. Despite documented regeneration of sub-basal nerve plexus following 8 weeks of treatment, the nerve fiber density, number of nerve branches and corneal nerve diameter were still statistically significantly less in the NK group compared to healthy controls. NCT04627571 (ongoing) is investigating the structural effects of rhNGF on the sub-basal corneal nerve density at 1 year in stage 2/3 NK.

Udonitrectag (also known as MT8 or REC 0559) is a low molecular weight, synthetic peptido-mimetic of NGF. MT8 binds the tropomyosin kinase A (TrkA) receptor, mimicking the anti-apoptotic and corneal trophic activity of NGF. It has been shown to improve healing of corneal epithelium and stroma in rabbit wound healing models. Its use in stage 2/3 NK is being investigated in a phase II multicenter, double masked, randomized trial (NCT04276558).

Insulin

Insulin is a peptide that is closely related to insulin-like growth factor (IGF) and has been implicated in wound repair. Shanley et al. (Shanley et al., 2004) showed that exposure of corneal epithelium to insulin facilitated closure of *in vitro* small wounds through enhanced cell migration. The effect of topical insulin on corneal wound healing has been well reported in rodent models, and improves corneal re-epithelialization in diabetic rats (Zagon et al., 2007). The mechanisms are not clearly understood, but is thought to be due to restoration of corneal nerves and/or improved epithelial cell migration. (Wang et al., 2017). It is notable that insulin has been demonstrated to have a biological effect on corneal epithelialization, and diabetes mellitus is a recognized cause of neurotrophic keratitis.

Wang et al. (Wang et al., 2017) used topical insulin in six eyes with non-healing neurotrophic ulcers, and achieved complete corneal re-epithelialization in 7–25 days following initiation of treatment. Topical insulin was prepared by mixing regular insulin in artificial tears with a polyethylene glycol and propylene glycol base at a concentration of 1 unit per mL, and was prescribed 2–3 times daily.

In a prospective non-randomized study (Diaz-Valle et al., 2020), 21 eyes with PEDs were treated with topical insulin 1 unit

per ml. 17 eyes (81%) had complete epithelial healing, mean time to reepithelization was 34.8 ± 29.9 days (median 23; range 7–114). Four eyes (19%) still had an epithelial defect but the mean PED size reduced by 91.5%.

A double masked, randomized trial (Fai et al., 2017) compared three concentrations of topical insulin (0.5 units, 1 unit and 2 units per drop) to placebo for the treatment of post-vitrectomy epithelial defects in 32 diabetic eyes. Topical insulin 0.5 units was superior to other concentrations and achieved a 100% healing rate within 72 h, compared with 62.5% for placebo, 75% for topical insulin 1 unit/drop, and 62.5% for insulin 2 units/drop. The authors postulate that the lack of benefit in using higher concentrations may be a result of greater toxicity and a decreased migration of epithelial cells during the healing process due to higher viscosity.

Topical insulin is well tolerated and does not cause ocular side effects when used in concentrations up to 100 units/ml (Bartlett et al., 1994). It is not absorbed systemically, and as such blood glucose levels and serum immunoreactive insulin levels are unchanged (Bartlett et al., 1994). Supported by evidence in the above reports, topical insulin is becoming more widely used in NK, and is manufactured locally rather than being produced commercially. An insulin concentration of 1 units/ml (Humulin S in Systane lubricant eye drops) has been used successfully in a number of patients in Moorfields Eye Hospital (S Ahmad, personal communication, 5 March 2022).

Substance P and Insulin-Like Growth Factor 1 (IGF-1)

IGF-1 has been shown to be an important modulator of corneal wound healing, and acts synergistically with substance P to promote corneal epithelium wound healing (Nishida et al., 1996). The peptide SSSR, corresponding to a four-amino acid sequence in the C domain of IGF-1, is the minimal essential sequence for the synergistic stimulation with substance P of corneal epithelial migration (Yamada et al., 2006). The combination of the substance P-derived peptide (FGLM-amide) and SSSR likely targets corneal epithelial cells directly, bypassing nerve fibres and triggering epithelial migration through activation of intracellular signal transduction systems (Yamada et al., 2008).

Nakamura et al.(Yamada et al., 2008) treated 26 eyes with NK associated PEDs with a topical combination of substance P-derived peptide (FGLM-amide) and IGF-1-derived peptide (SSSR). Complete closure of epithelial defects was achieved in 19 of the 26 eyes (73%) within 4 weeks of treatment initiation. Of note, three of the seven non-responders had limbal stem cell deficiency, which may explain the lack of efficacy of the treatment given the role of limbal stem cells in epithelial healing.

Nishida et al.(Nishida et al., 2007) also used FGLM-amide and IGF-1 drops to treat nine eyes with PEDs from NK, and achieved complete epithelial healing in 89% at 28 days.

FGLM-amide and IGF-1 drops are not commercially available at present.

Thymosin Beta 4 (Tβ4)

Tβ4 is a naturally-occurring 43-amino acid peptide that has been shown to promote corneal wound re-epithelialization, diminish inflammation, and inhibit apoptosis (Katzman and Jeng, 2014). Dunn et al. (Dunn et al., 2010) showed that Tβ4 drops promote healing in nine patients with chronic neurotrophic PEDs. Six patients with geographic defects showed rapid epithelial corneal healing, where four had complete healing and two had defects <0.1 mm. However the three patients with punctate epithelial defects did not show demonstrable changes in their clinical findings. Tβ4 eye drops were well tolerated by the patients, who all reported subjective improvement in ocular redness and foreign body sensation during the course of treatment (Dunn et al., 2010). Tβ4 drops are developed by RegeneRx Biopharmaceuticals, Inc. (Maryland, United States) but are only in use for clinical trials at present (NCT03937882).

Connexin43 (Cx43) Antisense Oligodeoxynucleotides (AsODN)

Transiently blocking the expression of the gap junction protein Cx43 using AsODNs or blocking hemichannels has been demonstrated to limit inflammation, edema and lesion spread and to provide improved healing in acute wound models (Grupcheva et al., 2012; Ormonde et al., 2012). Ormonde et al. (Ormonde et al., 2012) used Cx43-AsODN delivered in cold, thermoreversible Poloxamer407 gel (under an amniotic membrane graft or bandage contact lens) to treat PEDs from ocular burns. Ocular inflammation improved within 1-2 days, and all five eyes had complete and stable reepithelialization. To date there have been no studies reporting its use in NK, and Cx43 is not commercially available.

Non-specific Ocular Surface Support

Therapeutic bandage contact lenses (BCLs) can be helpful in the treatment of NK, as they protect the advancing epithelial cells from being sloughed-off by the blinking eyelids, as well as by providing anesthetic relief (Katzman and Jeng, 2014). In a non-randomized comparative study, the healing time of NK related corneal ulcers was 10.80 ± 4.44 days with a soft silicone hydrogel BCL versus 46.70 ± 13.88 days in the control group ($p < 0.05$) (Sun et al., 2014). Scleral contact lenses allow a reservoir of fluid to be created between the contact lens and the ocular surface, which can also be helpful in NK (Grey et al., 2012). However there is a risk of infective keratitis with contact lens wear, even when prophylactic topical antibiotics are used (Saini et al., 2013; Zhu et al., 2019).

Punctal occlusion with silicone punctal plugs or surgical permanent occlusion is also often used to support the tear film in NK eyes (Sacchetti and Lambiase, 2014).

Surgical Management

Tarsorrhaphy is a useful adjunct to promote healing of the ocular surface in stage 2/3 NK. This can either be temporary or permanent. Lateral tarsorrhaphies are usually permanent whilst central ones are typically temporary on account of the effect on vision in that eye. In some cases Botulinum toxin can be used instead of resorting to surgery, and has been shown to be effective for inducing temporary ptosis to protect the cornea (Kirkness et al., 1988). This has the advantage over central tarsorrhaphy of avoiding any surgical damage to the lid margin, instillation of eye drops is easy for patients and the ptosis reverses over 4–6 weeks.

Amniotic membrane (AM) transplantation is a form of ocular surface reconstruction which has been shown to be effective in the management of NK (Chen et al., 2000; Khokhar et al., 2005). AM contains growth factors such as NGF, keratinocyte growth factor, and hepatocyte growth factor, which have all been shown to promote corneal epithelial wound healing (Mead et al., 2020). It can either be performed in a single or multilayer (for deep ulcers with stromal tissue loss), with either in-lay or over-lay techniques used. In the in-lay technique, the AM is applied as a permanent basement membrane substitute and is sutured with the epithelial side facing outwards, allowing recipient epithelial cells to migrate onto the AM. An AM in-lay will be permanently incorporated and remodeled into the host cornea (Seitz et al., 2006). In the over-lay technique, the AM acts as a 'patch' or biological 'bandage' and is sutured with the epithelial side facing inwards, and will detach from the corneal surface after 1-2 weeks. (Meller et al., 2011). The sandwich technique is a combination of both the in-lay and over-lay techniques.

Corneal neurotization (CN) has is a potentially curative surgical procedure for NK (Terzis et al., 2009). Two main surgical approaches have been described. Direct CN (DCN) involves the transposition of the contralateral or ipsilateral supraorbital/supratrochlear nerves to the anesthetic cornea, whilst indirect CN (ICN) involves interposition of a nerve graft (typically the sural nerve) between the supraorbital and/or supratrochlear nerves and the affected cornea (Fogagnolo et al., 2020). A prospective comparative series comparing DCN and ICN showed that there was no difference between the groups: NK was healed in all patients after a mean period of 3.9 months, mean corneal sensitivity improved from 3.07 to 22.11 mm ($p < 0.001$), and a corneal sub-basal nerve plexus was detectable in all eyes (Fogagnolo et al., 2020). Catapano et al. (Catapano et al., 2019) reported on 19 eyes which had ICN, with a significant improvement in mean central corneal sensitivity from 0.8 ± 2.5 mm to 49.7 ± 15.5 mm at final follow-up ($p < 0.001$). The number of episodes of corneal epithelial defects after MICN was significantly reduced compared with the year leading up to the procedure (21 vs. 89%; $p < 0.0001$).

CONCLUSION

NK is a challenging disease to treat, and patients often lose vision. The aim of therapy is to treat any underlying causative factors and to promote epithelial healing, whilst preventing progression of disease. The emergence of rhNGF and NGF

mimetics hold exciting and promising possibilities, and may be useful in cases of NK that are refractory to conventional non-specific treatment.

ETHICS STATEMENT

Written informed consent was obtained from the individuals for the publication of any potentially identifiable images or data included in this article.

REFERENCES

Abedi, F., and Hamrah, P. (2018). Corneal Subbasal Nerve Recovery in an Acute Case of Ultraviolet Keratitis Treated with Autologous Serum Eye Drops. *J. Ophthalmol.* 2018, 4905487. doi:10.1155/2018/4905487

Aggarwal, S., Kheirkhah, A., Cavalcanti, B. M., Cruzat, A., Colon, C., Brown, E., et al. (2015). Autologous Serum Tears for Treatment of Photoallodynia in Patients with Corneal Neuropathy: Efficacy and Evaluation with *In Vivo* Confocal Microscopy. *Ocul. Surf.* 13 (3), 250–262. doi:10.1016/j.jtos.2015.01.005

Aifa, A., Gueudry, J., Portmann, A., Delcampe, A., and Muraine, M. (2012). Topical Treatment with a New Matrix Therapy Agent (RGTA) for the Treatment of Corneal Neurotrophic Ulcers. *Invest. Ophthalmol. Vis. Sci.* 53 (13), 8181–8185. doi:10.1167/iovs.12-10476

Anitua, E., Muruzabal, F., de la Fuente, M., Riestra, A., Merayo-Lloves, J., and Orive, G. (2016). PRGF Exerts More Potent Proliferative and Anti-inflammatory Effects Than Autologous Serum on a Cell Culture Inflammatory Model. *Exp. Eye Res.* 151, 115–121. doi:10.1016/j.exer.2016.08.012

Arvola, R. P., Robciuc, A., and Holopainen, J. M. (2016). Matrix Regeneration Therapy: A Case Series of Corneal Neurotrophic Ulcers. *Cornea* 35 (4), 451–455. doi:10.1097/ICO.0000000000000759

Azari, A. A., and Rapuano, C. J. (2015). Autologous Serum Eye Drops for the Treatment of Ocular Surface Disease. *Eye Contact Lens Sci. Clin. Pract.* 41 (3), 133–140. doi:10.1097/icl.0000000000000104

Barritault, D., Gilbert-Sirieix, M., Rice, K. L., Siñeriz, F., Papy-Garcia, D., Baudouin, C., et al. (2017). RGTA® or ReGeneraTing Agents Mimic Heparan Sulfate in Regenerative Medicine: from Concept to Curing Patients. *Glycoconj J.* 34 (3), 325–338. doi:10.1007/s10719-016-9744-5

Bartlett, J. D., Turner-Henson, A., Atchison, J. A., Woolley, T. W., and Pillion, D. J. (1994). Insulin Administration to the Eyes of Normoglycemic Human Volunteers. *J. Ocul. Pharmacol.* 10 (4), 683–690. doi:10.1089/jop.1994.10.683

Bonini, S., Lambiase, A., Rama, P., Caprioglio, G., and Aloe, L. (2000). Topical Treatment with Nerve Growth Factor for Neurotrophic Keratitis. *Ophthalmology* 107 (7), 1347–1351. ; discussion 1351-1352. doi:10.1016/s0161-6420(00)00163-9

Bonini, S., Lambiase, A., Rama, P., Sinigaglia, F., Allegretti, M., Chao, W., et al. (2018). Phase II Randomized, Double-Masked, Vehicle-Controlled Trial of Recombinant Human Nerve Growth Factor for Neurotrophic Keratitis. *Ophthalmology* 125 (9), 1332–1343. doi:10.1016/j.ophtha.2018.02.022

Bonini, S., Rama, P., Olzi, D., and Lambiase, A. (2003). Neurotrophic Keratitis. *Eye (Lond)* 17 (8), 989–995. doi:10.1038/sj.eye.6700616

Catapano, J., Fung, S. S. M., Halliday, W., Jobst, C., Cheyne, D., Ho, E. S., et al. (2019). Treatment of Neurotrophic Keratopathy with Minimally Invasive Corneal Neurotisation: Long-Term Clinical Outcomes and Evidence of Corneal Reinnervation. *Br. J. Ophthalmol.* 103 (12), 1724–1731. doi:10.1136/bjophthalmol-2018-313042

Chen, H. J., Pires, R. T., and Tseng, S. C. (2000). Amniotic Membrane Transplantation for Severe Neurotrophic Corneal Ulcers. *Br. J. Ophthalmol.* 84 (8), 826–833. doi:10.1136/bjo.84.8.826

AUTHOR CONTRIBUTIONS

S-YK and DL both equally contributed to the writing and approved the manuscript.

FUNDING

Cochener, B., Zagnoli, C., Hugny-Larroque, C., and Derrien, S. (2019). Healing of Resistant Corneal Neurotrophic Ulcers Using a Matrix Regenerating Agent. *J. Fr Ophtalmol* 42 (2), 159–165. doi:10.1016/j.jfo.2018.05.009

Deeks, E. D., and Lamb, Y. N. (2020). Cenegermin: A Review in Neurotrophic Keratitis. *Drugs* 80 (5), 489–494. doi:10.1007/s40265-020-01289-w

Diaz-Valle, D., Burgos-Blasco, B., Gegundez-Fernandez, J. A., Garcia-Caride, S., Puebla-Garcia, V., Peña-Urbina, P., et al. (2020). Topical Insulin for Refractory Persistent Corneal Epithelial Defects. *Eur. J. Ophthalmol.* 31(5):2280-2286. doi:10.1177/1120672120958307

Dua, H. S., Said, D. G., Messmer, E. M., Rolando, M., Benitez-del-Castillo, J. M., Hossain, P. N., et al. (2018). Neurotrophic Keratopathy. *Prog. Retin. Eye Res.* 66, 107–131. doi:10.1016/j.preteyeres.2018.04.003

Dunn, S. P., Heidemann, D. G., Chow, C. Y., Crockford, D., Turjman, N., Angel, J., et al. (2010). Treatment of Chronic Nonhealing Neurotrophic Corneal Epithelial Defects with Thymosin Beta4. *Ann. N. Y Acad. Sci.* 1194, 199–206. doi:10.1111/j.1749-6632.2010.05471.x

Fai, S., Ahem, A., Mustapha, M., Mohd Noh, U. K., and Bastion, M. C. (2017). Randomized Controlled Trial of Topical Insulin for Healing Corneal Epithelial Defects Induced during Vitreoretinal Surgery in Diabetics. *Asia Pac. J. Ophthalmol. (Phila)* 6 (5), 418–424. doi:10.22608/APO.201780

Fogagnolo, P., Giannaccare, G., Bolognesi, F., Digiuni, M., Tranchina, L., Rossetti, L., et al. (2020). Direct versus Indirect Corneal Neurotization for the Treatment of Neurotrophic Keratopathy: A Multicenter Prospective Comparative Study. *Am. J. Ophthalmol.* 220, 203–214. doi:10.1016/j.ajo.2020.07.003

Fox, R. I., Chan, R., Michelson, J. B., Belmont, J. B., and Michelson, P. E. (1984). Beneficial Effect of Artificial Tears Made with Autologous Serum in Patients with Keratoconjunctivitis Sicca. *Arthritis Rheum.* 27 (4), 459–461. doi:10.1002/art.1780270415

Giannaccare, G., Buzzi, M., Fresina, M., Velati, C., and Versura, P. (2017). Efficacy of 2-Month Treatment with Cord Blood Serum Eye Drops in Ocular Surface Disease: An *In Vivo* Confocal Microscopy Study. *Cornea* 36 (8), 915–921. doi:10.1097/ICO.0000000000001257

Grey, F., Carley, F., Biswas, S., and Tromans, C. (2012). Scleral Contact Lens Management of Bilateral Exposure and Neurotrophic Keratopathy. *Cont Lens Anterior Eye* 35 (6), 288–291. doi:10.1016/j.clae.2012.07.009

Grupcheva, C. N., Laux, W. T., Rupenthal, I. D., McGhee, J., McGhee, C. N., and Green, C. R. (2012). Improved Corneal Wound Healing through Modulation of Gap Junction Communication Using Connexin43-specific Antisense Oligodeoxynucleotides. *Invest. Ophthalmol. Vis. Sci.* 53 (3), 1130–1138. doi:10.1167/iovs.11-8711

Guerra, M., Marques, S., Gil, J. Q., Campos, J., Ramos, P., Rosa, A. M., et al. (2017). Neurotrophic Keratopathy: Therapeutic Approach Using a Novel Matrix Regenerating Agent. *J. Ocul. Pharmacol. Ther.* 33 (9), 662–669. doi:10.1089/jop.2017.0010

Guillon-Rolf, R., Hau, S., and Larkin, D. F. P. (2020). Clinical and Confocal Imaging Findings in Congenital Corneal Anaesthesia. *Br. J. Ophthalmol.* 105 (11), 1491–1496. bjophthalmol-2020-316672. doi:10.1136/bjophthalmol-2020-316672

Katzman, L. R., and Jeng, B. H. (2014). Management Strategies for Persistent Epithelial Defects of the Cornea. *Saudi J. Ophthalmol.* 28 (3), 168–172. doi:10.1016/j.sjopt.2014.06.011

Khokhar, S., Natung, T., Sony, P., Sharma, N., Agarwal, N., and Vajpayee, R. B. (2005). Amniotic Membrane Transplantation in Refractory Neurotrophic

Corneal Ulcers: a Randomized, Controlled Clinical Trial. *Cornea* 24 (6), 654–660. doi:10.1097/01.ico.0000153102.19776.80

Kim, K. M., Shin, Y. T., and Kim, H. K. (2012). Effect of Autologous Platelet-Rich Plasma on Persistent Corneal Epithelial Defect after Infectious Keratitis. *Jpn. J. Ophthalmol.* 56 (6), 544–550. doi:10.1007/s10384-012-0175-y

Kirkness, C. M., Adams, G. G., Dilly, P. N., and Lee, J. P. (1988). Botulinum Toxin A-Induced Protective Ptosis in Corneal Disease. *Ophthalmology* 95 (4), 473–480. doi:10.1016/s0161-6420(88)33163-5

Lambiase, A., Rama, P., Aloe, L., and Bonini, S. (1999). Management of Neurotrophic Keratopathy. *Curr. Opin. Ophthalmol.* 10 (4), 270–276. doi:10.1097/00055735-199908000-00009

Lambiase, A., Rama, P., Bonini, S., Caprioglio, G., and Aloe, L. (1998). Topical Treatment with Nerve Growth Factor for Corneal Neurotrophic Ulcers. *N. Engl. J. Med.* 338 (17), 1174–1180. doi:10.1056/NEJM199804233381702

Lekhanont, K., Jongkhajornpong, P., Choubtum, L., and Chuckpaiwong, V. (2013). Topical 100% Serum Eye Drops for Treating Corneal Epithelial Defect after Ocular Surgery. *Biomed. Res. Int.* 2013, 521315–521317. doi:10.1155/2013/521315

Mastropasqua, L., Lanzini, M., Dua, H. S., D' Uffizi, A., Di Nicola, M., Calienno, R., et al. (2020). In Vivo Evaluation of Corneal Nerves and Epithelial Healing after Treatment with Recombinant Nerve Growth Factor for Neurotrophic Keratopathy. *Am. J. Ophthalmol.* 217, 278–286. doi:10.1016/j.ajo.2020.04.036

Mastropasqua, L., Massaro-Giordano, G., Nubile, M., and Sacchetti, M. (2017). Understanding the Pathogenesis of Neurotrophic Keratitis: The Role of Corneal Nerves. *J. Cel Physiol* 232 (4), 717–724. doi:10.1002/jcp.25623

Matsumoto, Y., Dogru, M., Goto, E., Ohashi, Y., Kojima, T., Ishida, R., et al. (2004). Autologous Serum Application in the Treatment of Neurotrophic Keratopathy. *Ophthalmology* 111 (6), 1115–1120. doi:10.1016/j.ophtha.2003.10.019

Mead, O. G., Tighe, S., and Tseng, S. C. G. (2020). Amniotic Membrane Transplantation for Managing Dry Eye and Neurotrophic Keratitis. *Taiwan J. Ophthalmol.* 10 (1), 13–21. doi:10.4103/tjo.tjo_5_20

Meller, D., Pauklin, M., Thomasen, H., Westekemper, H., and Steuhl, K. P. (2011). Amniotic Membrane Transplantation in the Human Eye. *Dtsch Arztebl Int.* 108 (14), 243–248. doi:10.3238/arztebl.2011.0243

Mussano, F., Genova, T., Munaron, L., Petrillo, S., Erovigni, F., and Carossa, S. (2016). Cytokine, Chemokine, and Growth Factor Profile of Platelet-Rich Plasma. *Platelets* 27 (5), 467–471. doi:10.3109/09537104.2016.1143922

NICE NC for H and CE. *Final Appraisal Determination – Cenegermin for Treating Neurotrophic Keratitis [Internet].* 2018. Available from: https://www.nice.org.uk/guidance/ta532/documents/final-appraisal-determination-document. [Accessed 2021 Feb 25].

Nishida, T., Chikama, T., Morishige, N., Yanai, R., Yamada, N., and Saito, J. (2007). Persistent Epithelial Defects Due to Neurotrophic Keratopathy Treated with a Substance P-Derived Peptide and Insulin-like Growth Factor 1. *Jpn. J. Ophthalmol.* 51 (6), 442–447. doi:10.1007/s10384-007-0480-z

Nishida, T., Nakamura, M., Ofuji, K., Reid, T. W., Mannis, M. J., and Murphy, C. J. (1996). Synergistic Effects of Substance P with Insulin-like Growth Factor-1 on Epithelial Migration of the Cornea. *J. Cel Physiol* 169 (1), 159–166. doi:10.1002/(SICI)1097-4652(199610)169:1<159::AID-JCP16>3.0.CO;2-8

Ormonde, S., Chou, C. Y., Goold, L., Petsoglou, C., Al-Taie, R., Sherwin, T., et al. (2012). Regulation of Connexin43 gap junction Protein Triggers Vascular Recovery and Healing in Human Ocular Persistent Epithelial Defect Wounds. *J. Membr. Biol.* 245 (7), 381–388. doi:10.1007/s00232-012-9460-4

Pflugfelder, S. C., Massaro-Giordano, M., Perez, V. L., Hamrah, P., Deng, S. X., Espandar, L., et al. (2020). Topical Recombinant Human Nerve Growth Factor (Cenegermin) for Neurotrophic Keratopathy: A Multicenter Randomized Vehicle-Controlled Pivotal Trial. *Ophthalmology* 127 (1), 14–26. doi:10.1016/j.ophtha.2019.08.020

Rao, K., Leveque, C., and Pflugfelder, S. C. (2010). Corneal Nerve Regeneration in Neurotrophic Keratopathy Following Autologous Plasma Therapy. *Br. J. Ophthalmol.* 94 (5), 584–591. doi:10.1136/bjo.2009.164780

Rauz, S., and Saw, V. P. (2010). Serum Eye Drops, Amniotic Membrane and Limbal Epithelial Stem Cells-Ttools in the Treatment of Ocular Surface Disease. *Cell Tissue Bank* 11 (1), 13–27. doi:10.1007/s10561-009-9128-1

Sacchetti, M., and Lambiase, A. (2014). Diagnosis and Management of Neurotrophic Keratitis. *Clin. Ophthalmol.* 8, 571–579. doi:10.2147/OPTH.S45921

Saini, A., Rapuano, C. J., Laibson, P. R., Cohen, E. J., and Hammersmith, K. M. (2013). Episodes of Microbial Keratitis with Therapeutic Silicone Hydrogel Bandage Soft Contact Lenses. *Eye Contact Lens* 39 (5), 324–328. doi:10.1097/ICL.0b013e31829fadde

Seitz, B., Resch, M. D., Schlötzer-Schrehardt, U., Hofmann-Rummelt, C., Sauer, R., and Kruse, F. E. (2006). Histopathology and Ultrastructure of Human Corneas after Amniotic Membrane Transplantation. *Arch. Ophthalmol.* 124 (10), 1487–1490. doi:10.1001/archopht.124.10.1487

Semeraro, F., Forbice, E., Braga, O., Bova, A., Di Salvatore, A., and Azzolini, C. (2014). Evaluation of the Efficacy of 50% Autologous Serum Eye Drops in Different Ocular Surface Pathologies. *Biomed. Res. Int.* 2014, 1–11.

Semeraro, F., Forbice, E., Romano, V., Angi, M., Romano, M. R., Filippelli, M. E., et al. (2014). Neurotrophic Keratitis. *Ophthalmologica* 231 (4), 191–197. doi:10.1159/000354380

Shanley, L. J., McCaig, C. D., Forrester, J. V., and Zhao, M. (2004). Insulin, Not Leptin, Promotes *In Vitro* Cell Migration to Heal Monolayer Wounds in Human Corneal Epithelium. *Invest. Ophthalmol. Vis. Sci.* 45 (4), 1088–1094. doi:10.1167/iovs.03-1064

Shtein, R. M., Shen, J. F., Kuo, A. N., Hammersmith, K. M., Li, J. Y., and Weikert, M. P. (2020). Autologous Serum-Based Eye Drops for Treatment of Ocular Surface Disease: A Report by the American Academy of Ophthalmology. *Ophthalmology* 127 (1), 128–133. doi:10.1016/j.ophtha.2019.08.018

Sun, Y. Z., Guo, L., and Zhang, F. S. (2014). Curative Effect Assessment of Bandage Contact Lens in Neurogenic Keratitis. *Int. J. Ophthalmol.* 7 (6), 980–983. doi:10.3980/j.issn.2222-3959.2014.06.12

Terzis, J. K., Dryer, M. M., and Bodner, B. I. (2009). Corneal Neurotization: a Novel Solution to Neurotrophic Keratopathy. *Plast. Reconstr. Surg.* 123 (1), 112–120. doi:10.1097/PRS.0b013e3181904d3a

Trinh, T., Santaella, G., Mimouni, M., Mednick, Z., Cohen, E., Sorkin, N., et al. (2021). Assessment of Response to Multimodal Management of Neurotrophic Corneal Disease. *Ocul. Surf.* 19, 330–335. doi:10.1016/j.jtos.2020.11.003

Tsubota, K., Goto, E., Shimmura, S., and Shimazaki, J. (1999). Treatment of Persistent Corneal Epithelial Defect by Autologous Serum Application. *Ophthalmology* 106 (10), 1984–1989. –9. doi:10.1016/S0161-6420(99)90412-8

Vajpayee, R. B., Mukerji, N., Tandon, R., Sharma, N., Pandey, R. M., Biswas, N. R., et al. (2003). Evaluation of Umbilical Cord Serum Therapy for Persistent Corneal Epithelial Defects. *Br. J. Ophthalmol.* 87 (11), 1312–1316. doi:10.1136/bjo.87.11.1312

Versura, P., Giannaccare, G., Pellegrini, M., Sebastiani, S., and Campos, E. C. (2018). Neurotrophic Keratitis: Current Challenges and Future Prospects. *Eye Brain* 10, 37–45. doi:10.2147/EB.S117261

Wang, A. L., Weinlander, E., Metcalf, B. M., Barney, N. P., Gamm, D. M., Nehls, S. M., et al. (2017). Use of Topical Insulin to Treat Refractory Neurotrophic Corneal Ulcers. *Cornea* 36 (11), 1426–1428. doi:10.1097/ICO.0000000000001297

Wróbel-Dudzińska, D., Alio, J., Rodriguez, A., Suchodoła-Ratajewicz, E., Kosior-Jarecka, E., Rymgayłło-Jankowska, B., et al. (2018). Clinical Efficacy of Platelet-Rich Plasma in the Treatment of Neurotrophic Corneal Ulcer. *J. Ophthalmol.* 2018, 3538764.

Yamada, N., Matsuda, R., Morishige, N., Yanai, R., Chikama, T. I., Nishida, T., et al. (2008). Open Clinical Study of Eye-Drops Containing Tetrapeptides Derived from Substance P and Insulin-like Growth Factor-1 for Treatment of Persistent Corneal Epithelial Defects Associated with Neurotrophic Keratopathy. *Br. J. Ophthalmol.* 92 (7), 896–900. doi:10.1136/bjo.2007.130013

Yamada, N., Yanai, R., Kawamoto, K., Nagano, T., Nakamura, M., Inui, M., et al. (2006). Promotion of Corneal Epithelial Wound Healing by a Tetrapeptide (SSSR) Derived from IGF-1. *Invest. Ophthalmol. Vis. Sci.* 47 (8), 3286–3292. doi:10.1167/iovs.05-1205

Yoon, K. C., Im, S. K., Park, Y. G., Jung, Y. D., Yang, S. Y., and Choi, J. (2006). Application of Umbilical Cord Serum Eyedrops for the Treatment of Dry Eye Syndrome. *Cornea* 25 (3), 268–272. doi:10.1097/01.ico.0000183484.85636.b6

Yoon, K. C., You, I. C., Im, S. K., Jeong, T. S., Park, Y. G., and Choi, J. (2007). Application of Umbilical Cord Serum Eyedrops for the Treatment of Neurotrophic Keratitis. *Ophthalmology* 114 (9), 1637–1642. doi:10.1016/j.ophtha.2006.12.014

You, J., Hodge, C., Hoque, M., Petsoglou, C., and Sutton, G. (2020). Human Platelets and Derived Products in Treating Ocular Surface Diseases - A

Systematic Review. *Clin. Ophthalmol.* 14, 3195–3210. doi:10.2147/OPTH. S265701

Zagon, I. S., Klocek, M. S., Sassani, J. W., and McLaughlin, P. J. (2007). Use of Topical Insulin to Normalize Corneal Epithelial Healing in Diabetes Mellitus. *Arch. Ophthalmol.* 125 (8), 1082–1088. doi:10.1001/archopht.125.8.1082

Zhu, B., Liu, Y., Lin, L., Huang, X., Zhang, Y., Zheng, J., et al. (2019). Characteristics of Infectious Keratitis in Bandage Contact Lens Wear Patients. *Eye Contact Lens* 45 (6), 356–359. doi:10.1097/ICL.0000000000000593

Conflict of Interest: The authors declare that the research was conducted in the absence of any commercial or financial relationships that could be construed as a potential conflict of interest.

Publisher's Note: All claims expressed in this article are solely those of the authors and do not necessarily represent those of their affiliated organizations, or those of the publisher, the editors and the reviewers. Any product that may be evaluated in this article, or claim that may be made by its manufacturer, is not guaranteed or endorsed by the publisher.

Check for
updates

Stimulation of C-Kit+ Retinal Progenitor Cells by Stem Cell Factor Confers Protection Against Retinal Degeneration

Xi Chen[1]*[†], Shanshan Li[1][†], Xiaoli Liu[2], Jingjie Zhao[3], Lanting Wu[1], Ran You[1] and Yanling Wang[1]*

[1]Department of Ophthalmology, Beijing Friendship Hospital, Capital Medical University, Beijing, China, [2]Department of Pediatric Newborn Medicine, Brigham and Women's Hospital and Harvard Medical School, Boston, MA, United States, [3]Department of Traditional Chinese Medicine, Beijing Friendship Hospital, Capital Medical University, Beijing, China

C-kit/CD117, expressed in a series of tissue-specific progenitor cells, plays an important role in tissue regeneration and tissue homeostasis. We previously demonstrated that organoid-derived c-kit+ retinal progenitor cells can facilitate the restoration of degenerated retina. Meanwhile, we have identified a population of endogenous c-kit+ cells in retinas of adult mouse. However, the exact role of these cells in retinal degeneration remains unclear. Here, we demonstrated that stimulation of endogenous c-kit+ cells by stem cell factor (SCF) conferred protection against retinal degeneration. Retinal degeneration was induced by intravitreal injection of N-methyl-D-aspartate (NMDA). NMDA challenge increased the total number of c-kit+ cells in the retinal ganglion cell layer (GCL), while deregulated the protein level of SCF, which was mainly expressed in Müller cells. Both flash electroretinogram (fERG) and light/dark transition tests showed that intravitreal injection of SCF effectively improved the visual function of NMDA-treated mice. Mechanistically, SCF administration not only prevented the loss of retinal ganglion cells (RGCs), but also maintained the function of RGCs as quantified by fERG. Further, we performed transcriptome sequencing analysis of the retinal cells isolated from SCF-treated mice and the parallel control. Gene Ontology analysis showed that SCF-induced transcriptome changes were closely correlated with eye development-related pathways. Crystallins and several protective factors such as *Pitx3* were significantly upregulated by SCF treatment. Our results revealed the role of SCF stimulated c-kit+ cells in the protection of RGCs in NMDA-treated mice, *via* inhibiting the loss of RGCs. Administration of SCF can act as a potent strategy for treating retinal degeneration-related diseases.

Keywords: retinal degeneration, c-kit, stem cell factor, retinal ganglion cell, crystallins

INTRODUCTION

The death of neurons is the leading cause of blindness in retinal degeneration (Pascolini and Mariotti, 2012; Wong et al., 2014). For example, in patients with glaucoma, retinal ganglion cells (RGCs), the neurons in the mammalian retina, undergo progressive degeneration, which leads to an irreversible vision loss (Cuenca et al., 2014). Rescue of retinal neurons has been considered as an effective strategy for the retina regeneration therapy (Jin et al., 2019; Singh et al., 2020). Stem/progenitor cell

transplantation can be differentiated into retinal neurons, while the preparation of transplantable cells is inevitably complicated (Schwartz et al., 2015; Schwartz et al., 2016; Mandai et al., 2017). Reprogramming Müller cells can also regenerate retinal neurons *via* virus-mediated genome editing, while it can yet be applied due to safety issues (Jorstad et al., 2017; Yao et al., 2018; Hoang et al., 2020; Jorstad et al., 2020; Zhou et al., 2020). Neuroprotective factors, such as brain-derived neurotrophic factor (BDNF), can promote cell survival and prevent retinal neuron death, with some drawbacks such as short half-lives of these factors and the inability to cross the blood-retina barrier. Therefore, to develop a simple, safe and effective strategy to facilitate the repair of injured retina remains a key challenge.

In the previous study, we have demonstrated that c-kit[+] retinal progenitor cells (RPCs) would be a promising cell source for repairing the injured retina. By enriching c-kit[+] RPCs from human embryonic stem cell-derived retinal organoids, we found that subretinal transplantation of c-kit[+] RPCs into retinal degeneration models could significantly improve vision and delaying retinal degeneration (Zou et al., 2019). Moreover, we have previously identified a population of c-kit^{+} cells in retinas of both postnatal and adult mouse, especially containing regenerative potential during adulthood (Zhou et al., 2015; Chen et al., 2016; Chen et al., 2017). However, the exact role of these c-kit^{+} cells in the retina remains unclear.

Here, we reported that activation of endogenous c-kit^{+} cells can protect against retinal degeneration. In pathological conditions, such as N-methyl-D-aspartate (NMDA) challenge, the total number of c-kit^{+} cells in the retina was increased, while the expression level of SCF was downregulated. Supplementation of exogenous SCF can effectively facilitate the preservation of the retinal function, by inhibiting the loss of RGCs. Transcriptome analysis showed that several eye development-related factors, such as Crystallins, were significantly upregulated by SCF treatment. In summary, our study demonstrated the protective role of SCF/c-kit signaling on the retinal injury, and indicated exogenous SCF as a potent candidate for the treatment of retinal degeneration-related diseases.

MATERIALS AND METHODS

Mice

C57BL/6J mice were provided by the Institutional Animal Care of Beijing Friendship Hospital Affiliated to Capital Medical University. Four-week-old mice (males and females) were randomly assigned to groups, and maintained under a standard 12-h light/dark cycle at 24.5°C. All experimental procedures were approved by the Office of Research Ethics Committee at Beijing Friendship Hospital Affiliated to Capital Medical University (ethics approval number: 18-2020).

Intravitreal Injections

Animals were anaesthetized with 1.5–2% isoflurane. Intravitreal injection of NMDA (100 mM in PBS, 2 μl per eye; Cat# M3262, Sigma-Aldrich, United States) was performed using a sharp 32-guage needle (micro-syringe equipped of Hamilton Storage,

United States). Two days post NMDA challenge, intravitreal injection of recombinant SCF (50 ng/μl in PBS, 2 μl per eye; Cat# 455-MC, Novus Biologicals, United States) and SU 5416 (c-kit inhibitor, ic-kit, 50 ng/μl in PBS, 2 μl per eye; Cat# 3037, Tocris Bioscience, United Kingdom) were performed. Mice injected with an equal volume of PBS (2 μl per eye) were served as control.

Tissue Preparation and Immunofluorescence

Immunohistochemistry was performed as described previously (Chen et al., 2016; Chen et al., 2017). Briefly, mouse eyeballs were prefixed in prefixation buffer (5% acetic acid, 0.4% paraformaldehyde, 0.315% saline, and 37.5% ethanol), then incubated in 4% paraformaldehyde overnight at 4°C, followed by embedded in paraffin. Eyecups were sectioned at 5 μm on a microtome (Leica, Germany). Slides were then deparaffinized, rehydrated, and boiled in 10 mM citrate buffer, followed by incubation in 5% donkey serum for 30 min at room temperature. Slides were then incubated with indicated primary antibodies at 4°C overnight, rinsed with PBS, and then incubated in species-matched fluorophore-conjugated secondary antibodies for 1 h at 37°C. Nuclei were counterstained with 4',6-diamidino-2-phenylindole (DAPI). Images were obtained using confocal microscopy of Fluo View FV1000 (Olympus, Japan). To perform the immuno-positive cell quantification, immuno-positive cells were counted in sections of the whole retina from the nasal side to the temporal side across the optic disk, and at lease six sections per mouse were analyzed. The numbers of immuno-positive cells obtained of each section from one mouse were averaged, following the protocol described previously (De la Huerta et al., 2012; Li et al., 2016; Zou et al., 2019).

The primary antibodies used were as follows: anti-c-kit at 10 μg/ml (Cat# AF1356, R&D Systems, United States), anti-glutamine synthetase (GS) at 1:200 (Cat# ab73593, ab64613; Abcam, United Kingdom), anti-SCF at 1:200 (Cat# ab64677; Abcam), anti-Connexin 43 (Cx43) at 1:100 (Cat# ab78055; Abcam), anti-Iba1 at 1:200 (Cat# ab178847; Abcam), anti-NeuN at 1:200 (Cat# ab209898; Abcam), and anti-Calretinin at 1:400 (Cat# MAB1568; Millipore). The secondary antibodies used were as follows: donkey anti-goat IgG Alexa Fluor 488 at 1:500 (Cat# ab150129; Abcam), donkey anti-rabbit Alexa Fluor 555 at 1:500 (Cat# ab150074; Abcam), donkey anti-mouse Alexa Fluor 555 at 1:500 (Cat# ab150106; Abcam), donkey anti-mouse Alexa Fluor 647 at 1:500 (Cat# ab150107; Abcam), donkey anti-rabbit IgG Alexa Fluor 488 at 1:500 (Cat# ab150073; Abcam), goat anti-chicken IgG Alexa Fluor 555 at 1:500 (Cat# ab150170; Abcam).

Analysis of Microglia

The method was performed as described previously (Zou et al., 2019). Briefly, five 40× field views were captured from three 15 μm-thick retinal sections per eye using the Olympus confocal imaging system with 1-μm z-steps. By using a grid system, the number of grid-crossing points per individual microglia cell was

counted ($n > 3$ eyes per group). The number of Iba1^{+} cells was counted in five eyes per group.

Electroretinogram Recording

Corneal scotopic flash electroretinogram (fERG) of mice was performed at corresponding time point after intravitreal injection of NMDA (at lease five mice in each time point) as described previously (Chen et al., 2016). Briefly, after adaption darkness overnight, mice were anesthetized with 1.5–2% isoflurane. The animal body temperature was maintained at 37°C by using a heating pad. The pupils of mice were dilated with tropicamide and phenylephrine eye drops (Santen Pharmaceutical, Japan). The recording electrodes of gold loops were placed on the cornea. The reference electrodes and grounding electrodes of gold needles were inserted subcutaneously into angulus oculi and tail respectively. We obtained flash recordings at the light intensities of −2.5, −0.5, −0.02, 0.5 and 2.5 log (cd^*s/m^2) using Reti-scan system (Roland Consult, Germany). Waves measured at 2.5 log10 (cd^*s/m^2) were presented. The fERG procedures were performed under the environment of dim red light. The amplitudes of a-wave and b-wave were analyzed among groups.

Scotopic threshold responses (STRs) were elicited using a −4.5 log10 (cd^*s/m^2) stimulus using Reti-scan system (Roland Consult) as described previously (Holcombe et al., 2008). Thirty flashes with an interstimulus interval of 2s were averaged. Amplitudes of the positive STR (pSTR) and negative STR (nSTR) were measured for about 140 and 220 ms after the stimulus flash, respectively.

For photopic negative response (PhNR) analysis, flash strength was 10 log10 (cd^*s/m^2), and 50 responses were averaged for each eye as described previously (Jnawali et al., 2020). The PhNR was measured from baseline to the trough immediately following the b-wave.

Light/Dark Transition Test

Light/dark transition test was performed as described previously (Chen et al., 2016). The light/dark box consists of one light chamber (45 × 30 × 40 cm) and one dark chamber (15 × 30 × 40 cm), and these two compartments were connected with a door (10 × 10 cm). Mice were maintained in dark environment overnight, and adapted in the dark chamber for 2 min. The door was then opened, and mice were allowed to freely move into the light chamber for 5 min with 300 lux of tungsten filament bulb over the center of the compartment. All of the mice were tested naïve (only one test per mouse). Four paws completely through the door were defined as entering the light chamber. The time of exploratory behavior in the light compartment was analyzed.

Western Blotting

Eye samples were prepared after mice with euthanized. Retinas were then isolated and homogenized in an ice-cold mixture of RIPA buffer (Beyotime, China) containing protease inhibitor cocktail (Beyotime). Extracts were separated using 12% sodium dodecyl sulfate poly-acrylamide gels and transferred onto polyvinylidene fluoride membranes. Membranes were incubated in TBST (12.5 mM Tris–HCl, pH 7.6, 75 mM NaCl,

0.1% Tween 20) containing 5% fat-free milk for 1 h at room temperature, then transferred into solution containing primary antibodies at 4°C overnight, and probed with indicated secondary antibodies in TBST for 2 h at room temperature. Membranes were exposed on an Odyssey infrared imaging system with the Odyssey Application software V1.2.15 (LI-COR Biosciences, United States). All blots were analyzed by ImageJ (National Institutes of Health, United States). The relative levels of SCF were determined by normalizing against β-actin. The primary antibodies used were as follows: anti-SCF at 1:1000 (Cat# ab64677; Abcam), anti-β-actin at 1:1000 (Cat# ab179467; Abcam). The secondary antibody used was peroxidase-conjugated goat anti-rabbit IgG at 1:2000 (Beyotime).

Flow Cytometry

Flow cytometry was used to identify c-kit^{+} cells and was performed as described previously (Chen et al., 2016; Chen et al., 2017). Briefly, the retinas were dissociated in PBS containing collagenase I (10 mg/ml) and collagenase II (25 mg/ml, Worthington Biochemical, United States). The dissociated cells were filtered through a 40-μm filter (BD Biosciences, United States) and then blocked with CD32/16 for 15 min at room temperature. Then, the cell suspensions were incubated with c-kit antibody conjugated with APC fluorescence (1:50; Cat# 17-1172-83; eBioscience, Thermo Fisher Scientific, United States) or isotype control (1:50; Cat# 17-4031-82; eBioscience) for 30 min at 4°C. After each procedure, cells were rinsed with staining buffer (eBioscience). Cells were counted using a FACSCalibur Flow Cytometer and at least 10,000 events were collected for each sample and analyzed using FlowJo software (FlowJo, United States).

Cell Culture

Thec-kit^{+} cells were sorted from retinal cells of postnatal day 1 pups after cultured for one passage by fluorescence-activated cell sorting, then were cultured in medium containing DMEM/F12 medium (Lonza Biologics, United States) supplemented with 10% fetal bovine serum (Thermo Fisher Scientific, United States), 20 ng/ml murine basic fibroblast growth factor (PeproTech, United States), 20 ng/ml murine epidermal growth factor (PeproTech), insulin/transferrin/sodium selenite (1:500; Lonza Biologics), and 10 ng/ml leukemia inhibitor factor (EMD Millipore, United States) as described (Chen et al., 2016). BV2 mouse microglia cells were cultured in high-glucose DMEM supplemented with 10% FBS. For in vitro co-culture assay, BV2 microglia cells and c-kit^{+} cells were cultured separately at a density of 1×10^5 cells/well for 6 h, and then treated with 1 μg/ml LPS or 50 ng/ml SCF respectively for 24 h. The LPS-treated BV2 cells were seeded on 24-well cell culture inserts, and co-cultured with SCF-treated C-Kit^{+} cells seeded in the lower chamber (EMD Millipore) at a density of 10^3–10^5 per well for 24 and 48 h. Monocultures of microglia with or without LPS treatment were served as controls. All of the cultures were maintained under consistent and equivalent conditions. The experiments were performed in triplicate, and each result represents the mean of three independent experiments.

Gene Functional Annotation Analysis

For transcriptome analysis, total retinal cells were incubated in RNAiso Plus (Takara, Japan) at a concentration of 2×10^6 cells/ml and stored at $-80°C$. All samples were transported to the Genomics Institute on dry ice for the transcriptome study. The mRNA sample was enriched using oligo (dT) magnetic beads and fragmented into short fragments using fragmentation buffer. The corresponding cDNA libraries were produced and qualified using an Agilent 2100 Bioanalyzer and an ABI StepOnePlus Real-Time PCR System. Primary raw reads produced by HiSeq 4000 (Illumina, United States) were qualified and filtered to obtain clean reads. A heatmap analysis of gene expression levels were created based on the averaged fragments per kilobase of exon per million fragments mapped (FPKM) values of genes. Genes with fold change ≥2 and adjusted p values ≤0.001 were considered as the differentially expressed genes (DEGs). Annotation analysis of Gene Ontology (GO) was performed to determine the on-going biological process. RNA-seq data were deposited in the Gene Expression Omnibus (GSE192458).

RNA Isolation and Real-time Quantitative Polymerase Chain Reaction (PCR)

Total RNA was purified using TRIzol reagent (Invitrogen, United States) followed by chloroform extraction. After reverse transcription performed using the PrimeScriptTM RT reagent kit with gDNA Eraser (Takara, Japan), real-time qPCR reactions were performed using a CFX96 Real-time qPCR System (Bio-Rad, United States) using SYBR® Premix Ex TaqTM II (Takara) to measure the expression of various genes. The level of *GAPDH* mRNA expression was used to normalize differences in the levels among different transcripts. The primers used are listed in **Supplementary Table S1**.

Statistical Analysis

All statistical differences were performed on SPSS 23.0 by one-way ANOVA test among comparisons groups. Data are presented as mean ± standard deviation (SD). Differences were considered as significant at $p < 0.05$.

RESULTS

Increased Number of C-Kit⁺ Cells in NMDA-Treated Mice

C-kit, also known as CD117, is a type III receptor tyrosine kinase expressed in various types of stem cells, such as hematopoietic stem cells (Edling and Hallberg, 2007; Lennartsson and Ronnstrand, 2012). C-kit⁺ RPCs transplantation has been demonstrated as a potential strategy to improve vision and delay retinal degeneration. We have previously identified a population of c-kit⁺ RPCs in the retinas of both postnatal and adult mice (Chen et al., 2016; Chen et al., 2017). Further, in c-kit-Cre LacZ mice, the expression of β-galactosidase was restricted to RGCs and amacrine cells in the retina, suggesting these c-kit⁺ cells may differentiate into retinal neurons (Harada et al., 2011). However, the biological significance of these endogenous c-kit⁺ RPCs in the degenerative retina remains unclear. To elucidate this issue, we examined the distribution and abundance of c-kit⁺ cells in retina of the retinal degeneration mice model generated by NMDA injection. Consistent with previous reports, administration of NMDA led to a loss of RGCs and a decrease in the thickness of the inner plexiform layer (IPL), both of which are typical symptoms of retinal degeneration (**Figures 1A–C**).

We next examined the distribution and abundance of c-kit⁺ cells in retina of these retinal degeneration mice by immunohistochemistry. The morphology and distribution of c-kit⁺ cells were not markedly affected by NMDA treatment (**Figures 1A–C**). However, an increase in the number of c-kit⁺ cells in both retinal ganglion cell layer (GCL) and inner nuclear layer (INL) were observed in retinas after 1 week post NMDA challenge, compared with that in the wild-type (WT) retinas, and the effect was sustained for at least 2 weeks ($p < 0.05$; **Figures 1D,E**). These data confirmed that c-kit⁺ cells indeed existed in both GCL and INL in the retina.

The tissue was dissociated into single cell suspensions, and the presence of c-kit⁺ cells was established by flow cytometry (**Supplementary Figure S1**). Consistent with the results by immunofluorescence staining, the percentages of c-kit⁺ cells in the entire retina were notably higher after NMDA treatment ($p < 0.001$), especially 1 week post NMDA challenge. The increased number of c-kit⁺ cells in the retina of NMDA-treated mice suggested that these cells might be involved in retinal degeneration process.

The Expression of SCF Was Downregulated After NMDA Treatment

C-kit can be activated by its ligand stem cell factor (SCF), a growth factor that exists as a soluble or membrane-bound form (Cardoso et al., 2017). The functional SCF/c-kit signaling is critical for the survival and development of stem cells in hematopoiesis, pigmentation and reproduction (Lennartsson et al., 2005). We thus examined the expression of SCF in mouse retinas. In the retina of WT mice, SCF-expressing cells were mainly localized in INL as well as inner limiting membrane, adjacent to c-kit⁺ cells (**Figure 2A**). These SCF-positive cells can also express glutamine synthetase (GS), a marker of Müller cells, suggesting that in the INL, Müller cells act as an endogenous source of SCF. Also, the gap junction protein Connexin 43 (Cx43) was distributed between c-kit⁺ cells and SCF-expressing Müller cells (**Supplementary Figure S2**).

As NMDA challenge influenced the abundance of c-kit⁺ cells, we then examined the expression of SCF in retinas with NDMA stimulation. Comparing to WT mice, the expression of SCF in retinas was downregulated after NMDA exposure, obtained by immunofluorescence and Western blot analysis (**Figures 2B–D**), and also confirmed by real-time qPCR (**Supplementary Figure S3**). Together with the previous observation showing the increased number of c-kit⁺ cells (**Figures 1D,E**), these data indicated that the insufficient activation of SCF/c-kit signaling may be involved in the progression of NMDA-induced retinal degeneration.
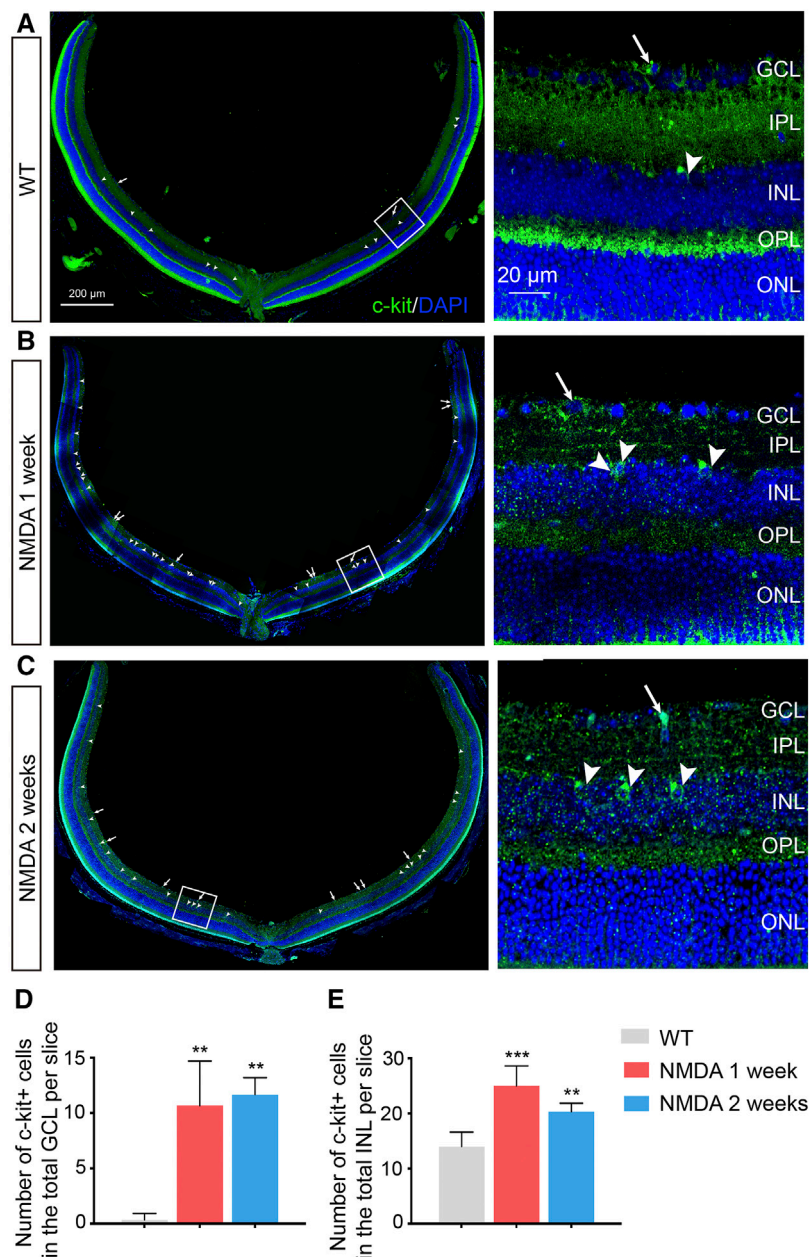
FIGURE 1 | Increased Number of C-kit$^+$ Cells in NMDA-treated Mice. **(A–C)** Representative images of c-kit$^+$ cell staining (green) in retinas of indicated mice with NMDA exposure. Area in the white boxes **(A–C)** was shown at higher magnification and displayed to the right. White arrow, the c-kit$^+$ cell body in the retinal ganglion cell layer (GCL); white arrowhead, the c-kit$^+$ cell body in the inner nuclear layer (INL). DAPI, 4′, 6-Diamino-2-Phenylendole; ONL, outer nuclear layer. Scale bars represented 200 μm of left panel, 20 μm of right panel. **(D,E)** The total number of c-kit$^+$ cells in the GCL **(D)** and INL **(E)** were then quantitated and plotted as the mean ± SD per slice. $n \geq 3$ for each time point, *$p < 0.05$ vs WT, **$p < 0.01$, ***$p < 0.001$.

Exogenous SCF Treatment Improved Visual Function of NMDA-Treated Mice

In view of the decreased SCF expression and increased number of c-kit$^+$ cells in the NMDA-induced degenerative retinas, we wondered whether exogenous SCF supplementation can compromise the retinal degeneration and improve the vision function. To do so, recombinant SCF (50 ng/μl) was intravitreally administrated at 2 days post NMDA injection, while control group received same amount of PBS or c-kit inhibitor (ic-kit, 50 ng/μl) at the same timepoint after NMDA damage, respectively (**Figure 3A**).

To detect the retinal function of indicated mice, we performed flash electroretinogram (fERG) and the light/dark transition tests at 1- and 2-week post SCF administration (**Figure 3**). Mice
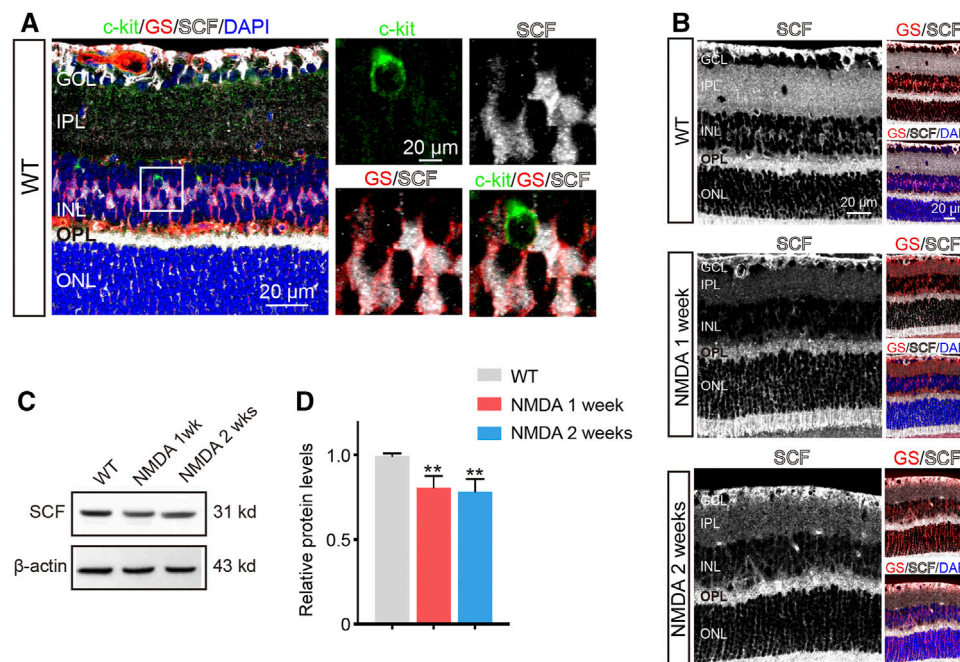
FIGURE 2 | The Expression of SCF was Downregulated after NMDA Treatment. **(A)** c-kit-positive cells (green), glutamine synthetase (GS)-positive cells (red) and SCF-positive cells (white) located in the inner nuclear layer (INL). The white box in left panel was shown at higher magnification in right panels. **(B)** Immunofluorescence staining of SCF (white) and GS (red) in the retinas of WT and NMDA-treated mice. Scale bars represented 20 μm. **(C,D)** The expression of SCF were analyzed by Western blotting analysis **(C)** and quantitated by ImageJ and plotted as the mean expression ± SD ($n = 3$ eyes/group, $**p < 0.01$ vs WT) **(D)**. The level of SCF was corrected for β-actin loading control and normalized to the levels of control cells.

receiving SCF showed markedly increased amplitudes of both the a-wave (**Figures 3B,C**) and b-wave (**Figures 3B,D**) at 0.5 log10 (cd*s/m^2; the data for the other light intensity not shown), compared with PBS and ic-kit groups. Moreover, in the light/dark transition test (**Figure 3E**), mice receiving SCF injection for 1 and 2 weeks showed a behavioral aversion to light, and spent less time in the light chamber (**Figure 3F**), indicating that exogenous SCF improved retinal function of NMDA-treated mice.

Microglia are considered as the major source of pro-inflammatory factors that contribute to retinal degeneration. Here we found that the activation of microglia has also been downregulated by SCF supplementation (**Figure 4**). Based on the results of Iba1 staining, reactive microglia were mainly distributed in the GCL, IPL and outer plexiform layer (OPL) in NMDA-treated retina (**Figure 4A**). However, in SCF-treated group, the number of activated microglia were significantly decreased, compared with control groups ($p < 0.05$; **Figure 4B**). The morphology change is another key feature for microglia activation, we thus quantified the microglia morphology using a grid cross-counting system as reported previously (Luckoff et al., 2016; Luckoff et al., 2017; Bian et al., 2020). By counting the grid-crossed points of Iba1$^+$ cells, we found that SCF treatment markedly compromise the activation of the microglia. Moreover, the histogram data demonstrated that the microglia in the SCF-treated group mainly showed

ramified shapes, while most microglia in the control group adopt an amoeboid morphology (**Figure 4C**). Also, it was demonstrated that SCF stimulated c-kit$^+$ cells inhibited proliferation and pro-inflammatory factors expression of microglia *in vitro* (**Supplementary Figure S4**). Taken together, these data demonstrated that exogenous SCF treatment can inhibit the hyperactivation of microglia in the NMDA-treated retina, and thus improve the visual function.

SCF Supplementation Compensated for the Loss of RGCs in NMDA-Treated Mice

The loss of RGCs, which can trigger the activation of microglia, is the leading cause of visual impairment in NMDA-induced retinal degeneration (Niwa et al., 2016). Since SCF supplementation can improve the NMDA-induce retinal degeneration, we then examined the protective role of SCF on RGCs. Both morphologic and functional assessments for RGCs were performed. As shown in **Figures 5A,B** and **Supplementary Figure S5**, the number of RGCs (indicated as Calretinin$^+$ cells and NeuN$^+$ cells) was markedly decreased after NMDA exposure. In line with previously observation (**Figure 3**), SCF treatment indeed attenuated the loss of RGCs. Further, we found that the administration of SCF increased the proportion of c-kit$^+$ cells in GCL (**Supplementary Figure**
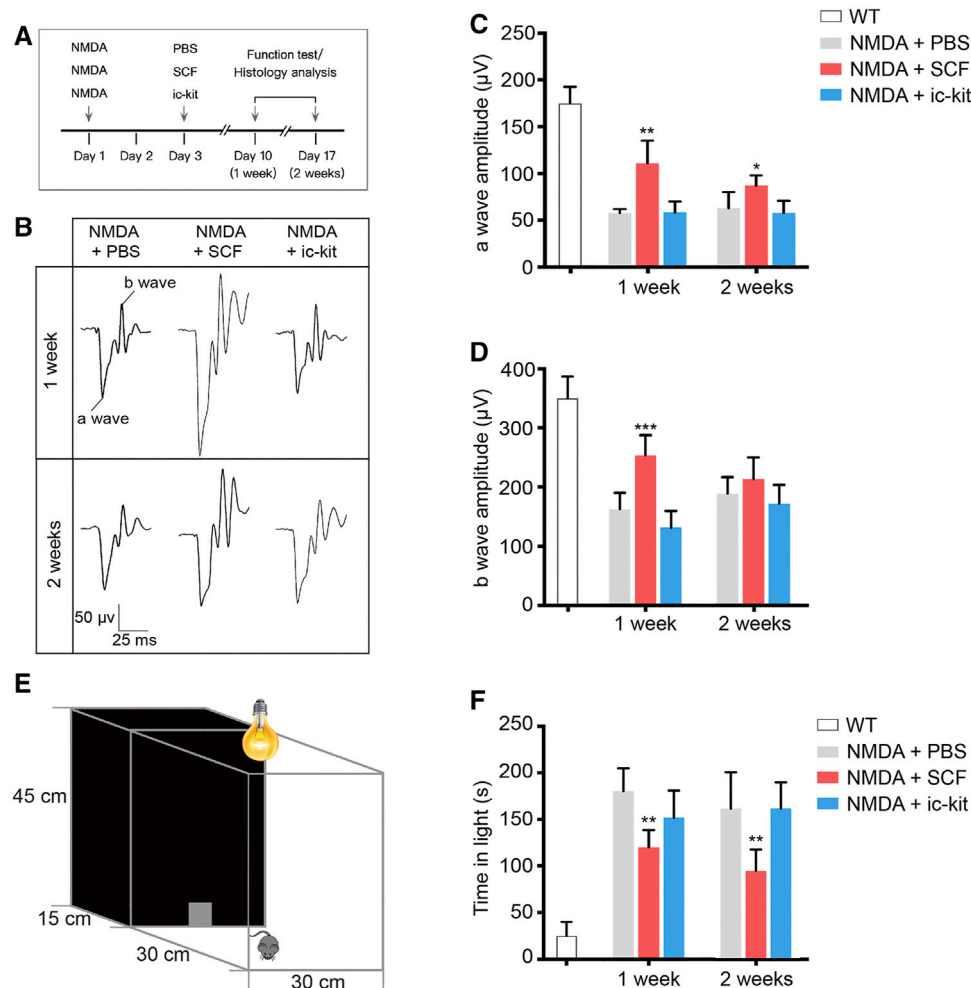
FIGURE 3 | Exogenous SCF Treatment Improved Visual Function of NMDA-treated Mice. **(A)** Scheme of time points for intravitreal injections, function test and histology analysis. **(B)** Representative waves of three groups of mice measured through flash electroretinogram (fERG) tests at 2.5 log(cd*s/m²). **(C,D)** Statistical analysis of the amplitudes of fERG a-wave **(C)** and b-wave **(D)** in the indicated groups. **(E)** Diagram showing the setup of the light/dark transition test. **(F)** Time spent in the light compartment was recorded. Data were shown as the mean ± SD ($n \geq 5$ for each time point). $^{*}p < 0.05$, $^{**}p < 0.01$, $^{***}p < 0.001$, compared with NMDA + PBS controls.

S6). The majority of the increased RGCs also expressed c-kit (**Figure 5C**), indicating that after SCF treatment, c-kit^{+} cells may compensate for the loss of RGCs in NMDA mice.

We next examined the function of RGCs using specialized fERG. By comparing the ERG amplitudes recorded obtained from indicated groups, we found a significant increase in the pSTR of SCF-treated mice at 1- and 2-week post treatment ($p < 0.05$; **Figures 6A–C**). Compared to the control eyes, the PhNR amplitudes in the SCF-injected eyes were consistently increased, and stayed negative for at least 2 weeks ($p < 0.05$; **Figures 6D,E**). Taken together, these data demonstrated that exogenous SCF supplementation protected RGCs from NMDA-induced cell death, therefore delayed the progression of the retinal degeneration.

RNA-Seq Reveals the Involvement of Key Genes for SCF Treatment

We next investigated the mechanism underlying the protective role of SCF/c-kit signaling on retinal degeneration. To do so, we employed a parallel transcriptome analysis by RNA sequencing. Retinal cells from SCF-treated mice after 1 week were isolated as described previously (Chen et al., 2017). A total of 359 genes were found to be differentially expressed in retinas from NMDA-treated mice with 1-week SCF treatment, compared with the cells derived from time-matched control retinas (NMDA plus PBS). The 359 differentially expressed genes (DEGs) included 287 upregulated genes and 72 downregulated genes (**Figure 7A**).
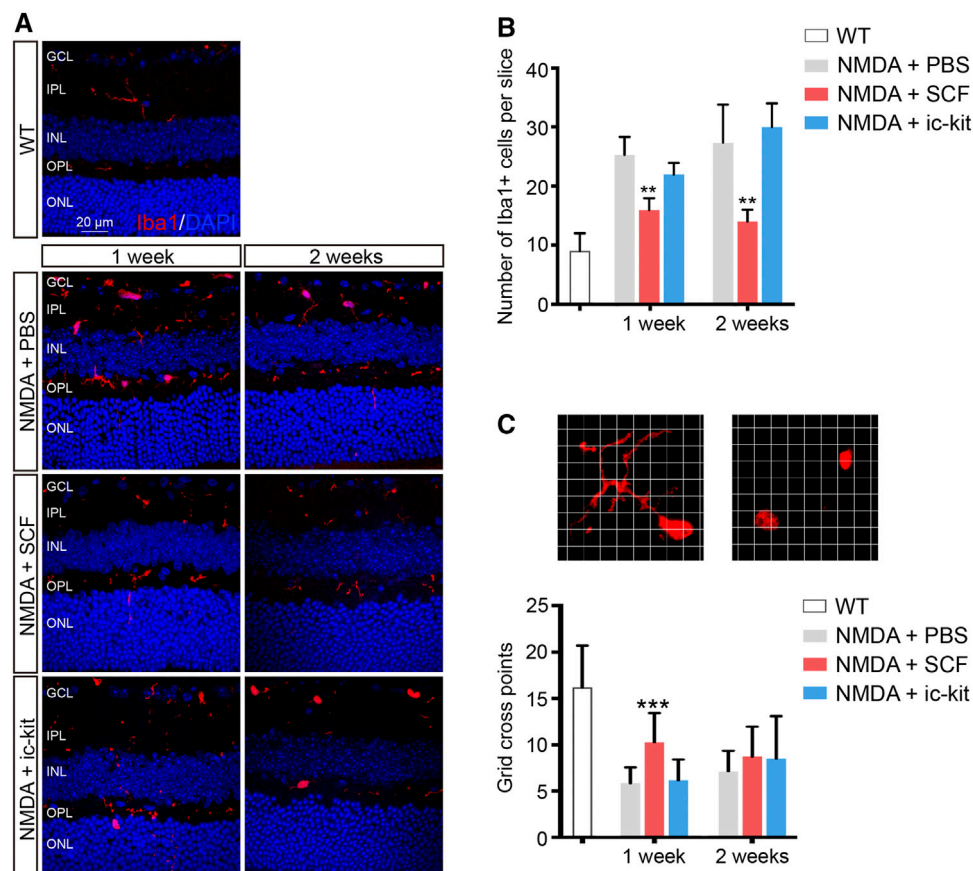
FIGURE 4 | Activation of Microglia was Suppressed by SCF Supplementation. **(A)** Immunofluorescence detection of the morphology and distribution proportion of Iba1^{+} cells (red) in indicated mice. Scale bars represented 20 μm. **(B)** Number of Iba1^{+} cells were quantitated in each group ($n \geq 5$ for each time point). **(C)** Representative images of ramified (left panel) or ameboid-like (right panel) Iba1^{+} microglia in grid crossing of each grid with a side length of 3 μm. Statistical analysis of the grid-crossing points per microglia ($n \geq 21$ per group). The data were shown as mean ± SD. **$p < 0.01$, ***$p < 0.001$, compared with NMDA + PBS controls.

We then utilized the GO classification to analyzed the enriched pathways that were induced by SCF treatment. Accordingly, 359 DEGs identified in the present study were categorized into 14 functional groups ($p < 0.00001$). In the molecular function and biological process of GO classification categories, 1 and 13 functional groups were identified, respectively (**Supplementary Table S2**). SCF-treated retinas showed an enrichment in eye development-related pathways, including lens development, camera-type eye development, *etc.* (**Figure 7B**), suggesting SCF stimulated c-kit^{+} cells might contribute to RGC survival and retinal structure reconstruction.
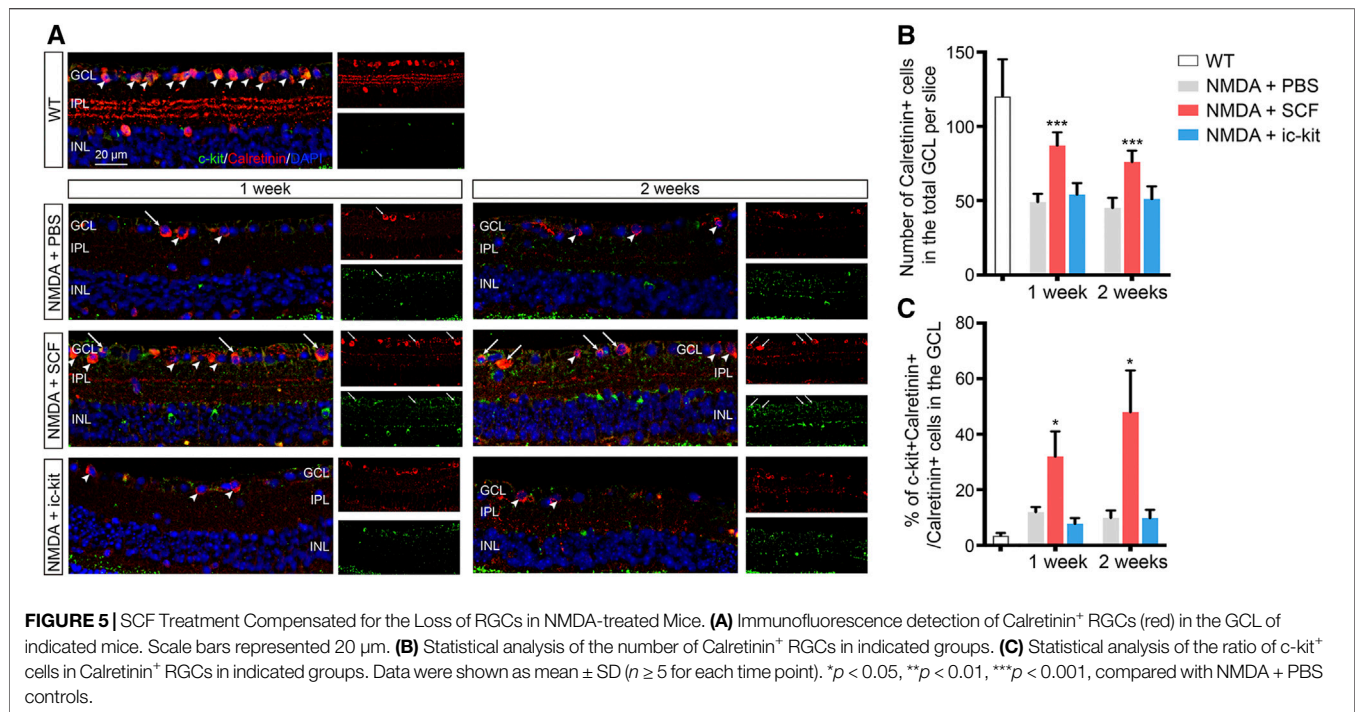
To further analyze the DEGs, we found that the expression of multiple members from α, β and γ Crystallins family (*Cryaa, Cryab, Cryba1, Cryba2, Crygb, etc.*) were significantly up-regulated after SCF stimulation (**Figures 7C,D**). In addition, a series of factors that promote neuron survival were also significantly up-regulated with SCF exposure. The top10 up-regulated DEGs included *Pitx3, Foxe3, Gja3, Gja8, Wnt7a, Wnt7b, Rspo1, etc.* (**Figure 7E**). We confirmed these transcriptomic analysis results using qRT-PCR (**Figures 7F,G**). Taken together, these RNA-seq data revealed a change in the

molecular signature of the retina, and suggested that the protective effect of SCF/c-kit pathway on NDMA-induced retinal degeneration may be mediated by both Crystallins and a series of protective factors.

DISCUSSION

Degenerative retinal disease is one of the leading causes of vision loss, while there are currently a limited number of effective treatments available (Ahmad et al., 2020). Here we found that stimulation of the endogenous c-kit^{+} cells by SCF compromised the NMDA-induced experimental retinal injury. Mechanistically, this effect, associated with the protection of RGCs, was possibly mediated *via* the upregulation of Crystallins and neuron-protective genes such as Pitx3, Foxe3 and Gja3. These finding suggested that applying SCF to stimulate endogenous c-kit^{+} cells would be an effective strategy for retina therapy.

Despite the controversy regarding the role of c-kit[+] cardiac stem cells in the heart, various tissue-specific progenitor cells do express c-kit, and can facilitate the tissue regeneration in response to SCF stimulation. Activation of SCF/c-kit signaling in the

FIGURE 5 | SCF Treatment Compensated for the Loss of RGCs in NMDA-treated Mice. **(A)** Immunofluorescence detection of Calretinin⁺ RGCs (red) in the GCL of indicated mice. Scale bars represented 20 μm. **(B)** Statistical analysis of the number of Calretinin⁺ RGCs in indicated groups. **(C)** Statistical analysis of the ratio of c-kit⁺ cells in Calretinin⁺ RGCs in indicated groups. Data were shown as mean ± SD ($n \geq 5$ for each time point). *$p < 0.05$, **$p < 0.01$, ***$p < 0.001$, compared with NMDA + PBS controls.

progenitor cell niche stimulates several pathways mediating proliferation, survival, and migration (Stankov et al., 2014). We have previously identified a population of c-kit⁺ RPCs in retinas of postnatal mice. Both photoreceptors in the outer nuclear layer, and retinal neurons and Müller cells in the INL are the progeny of c-kit⁺ cells in vivo (Chen et al., 2017). Further, we have demonstrated that subretinal transplantation of c-kit⁺ cells, either isolated from newborn mice retinas or human embryonic stem cell-derived retinal organoids, can improve the visual function in retinal degeneration mice (Chen et al., 2016; Zou et al., 2019). Both of these findings suggest the protective role of c-kit⁺ cells in the degenerative retinal diseases. Intriguingly, we also found that c-kit expression persisted at low levels in retinas of adult mice, up to 57 weeks of age (Chen et al., 2017). However, whether SCF/c-kit signaling in the retina of adult mice can also facilitate the restoration of the retinal function remains unclear. In the present study, we found that in degenerative retinas, the proportion of c-kit⁺ cells increased, while the expression of c-kit ligand SCF decreased. After supplementing SCF exogenously, the NMDA-induced RGC loss was alleviated, and reductions in visual function after NMDA treatment were ameliorated, suggesting that the SCF/c-kit signaling contributes to the tissue homeostasis in the mice retinas. When the proliferating cells labeled by proliferating cell nuclear antigen (PCNA), we did not spot proliferating cells in GCL (c-kit⁺ cells or other RGCs). Very few of c-kit⁺ cells in INL were marked by PCNA, indicating low level of proliferating c-kit⁺ cells in INL. Above all, we speculated that SCF treatment might attenuate the loss of RGC, instead of c-kit⁺ cells proliferating and differentiating into new RGC. In the future research, tracing the changes of RGC through lineage tracing animal models may help us to better identify the origin of RGC.

Müller cells can interact with neurons, and are responsible for the maintenance of the homeostasis of the retina. In the present study, we found that the endogenous SCF was mainly derived from Müller cells. Intriguingly, we found that Cx43 was distributed between c-kit⁺ cells and SCF-expressing Müller cells, suggesting physical connection between these cells may exist. In the retina, Cx43 is expressed within the perivascular endfeet of astrocytes, Müller cells, retinal pigment epithelium and some neurons, and has been functionally associated with vascular regulation (Gonzalez-Casanova et al., 2021). The regulatory role of Cx43 in the endogenous SCF/c-kit signaling pathway has not been fully explored. Further investigation is needed to demonstrate the mechanisms and functional significances underlying these interactions.

Neuro-protective strategies could be promising to promote cell survival and prevent retinal neuron death (Pardue and Allen, 2018). Neuroprotective factors, including BDNF, ciliary neurotrophic factor, etc., have considerable potential to act as a powerful neuroprotective agent (Du et al., 2020; Dulz et al., 2020). However, significant challenges remain due to short half-lives of these factors and the inability to easily cross the blood brain or blood retina barrier (Pardue and Allen, 2018). Local delivery to the eye might avoid some of these limitations, while still causing increasing risk of infection and tissue injury. Here, we reported a long-lasting neuroprotective effect of SCF in the retinal degeneration mice. After a single administration of SCF, the protective effect sustained for at least 2 weeks, according to the reduction of RGC loss, the protection of RGC function and the restoration of visual function detected by light/dark transition test and fERG. The long-lasting effect of SCF has also been reported in the central nervous system (Qiu et al., 2020). In the traumatic brain injury (TBI) model, exogenous supplementation of SCF
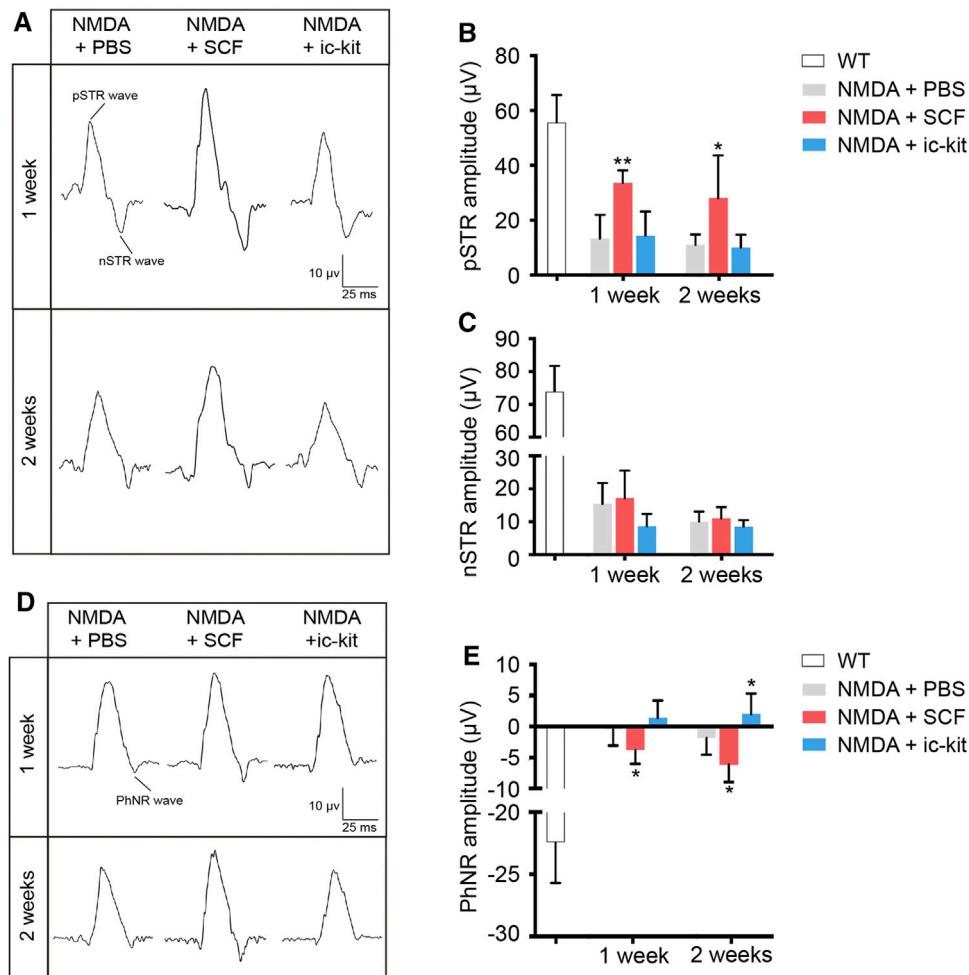
FIGURE 6 | SCF Treatment Maintained the Function of RGCs in NMDA-treated Mice. **(A)** Specialized fERG tests for detecting the function of RGCs were performed at designed timepoints. Representative waves of positive scotopic threshold responses (pSTR) and negative STR (nSTR) in these groups. **(B,C)** Amplitudes of pSTR **(B)** and nSTR **(C)** were compared among groups. **(D)** Representative waves of photopic negative response (PhNR). **(E)** Statistical analysis of PhNR amplitudes among groups. Data were shown as mean ± SD ($n = 5$ for each time point). *$p < 0.05$, **$p < 0.01$, compared with the control group (NMDA + PBS).

significantly showed superior efficacy in improving long-term functional outcome, enhancing neural plasticity, rebalancing neural structure networks disturbed by severe TBI, and promoting remyelination, as long as lasting for 21 weeks after treatment (Qiu et al., 2020). In addition, SCF has been covalently immobilized on polymeric substrate materials, such as hyaluronic acid/gelatin double network hydrogel, for the sustained release (Zhang et al., 2018). We will investigate the protective effect of these modifications of SCF in our further study.

During our study, Li et al. overexpressed SCF in photoreceptors by AAV8 virus, in attempts to treating photoreceptor degeneration (Li et al., 2020b). In support of our findings, this study indicated the role of SCF in preventing retinal degeneration. However, we and three independent groups all suggested that in the retina, the expression of c-kit is restricted to RGCs and amacrine cells, but not photoreceptors (Morii et al., 1994; Koso et al., 2007; Harada et al., 2011). Here our data

reported the pro-survival role of SCF/c-kit signaling in NMDA-induced cytotoxicity in RGCs.

The fERG is a valuable tool for assessing the function of retinal cells and circuits *in vivo*. For very weak flashes from darkness, receptoral potential of opposite polarity to the b-wave dominates the ERG. This negative-going response has been called the scotopic threshold response (STR). The STR is thought to reflect activity of the proximal retinal, i.e. RGC and amacrine cell (Holcombe et al., 2008; Saszik et al., 2002). In mice, the STR comprises positive and negative elements (pSTR and nSTR). In our study, we found a significant increase in the pSTR of SCF-treated mice at 1- and 2-week post treatment (**Figures 6A–C**). Selective pSTR attenuation occurs following optic nerve crush or transection, suggesting this component is primarily of RGC origin (Bui and Fortune, 2004; Liu et al., 2014). Therefore, the differential effect of SCF treatment upon individual STR responses may reflect differential perturbation of RGC and amacrine cell function, which verified the therapeutic effects of
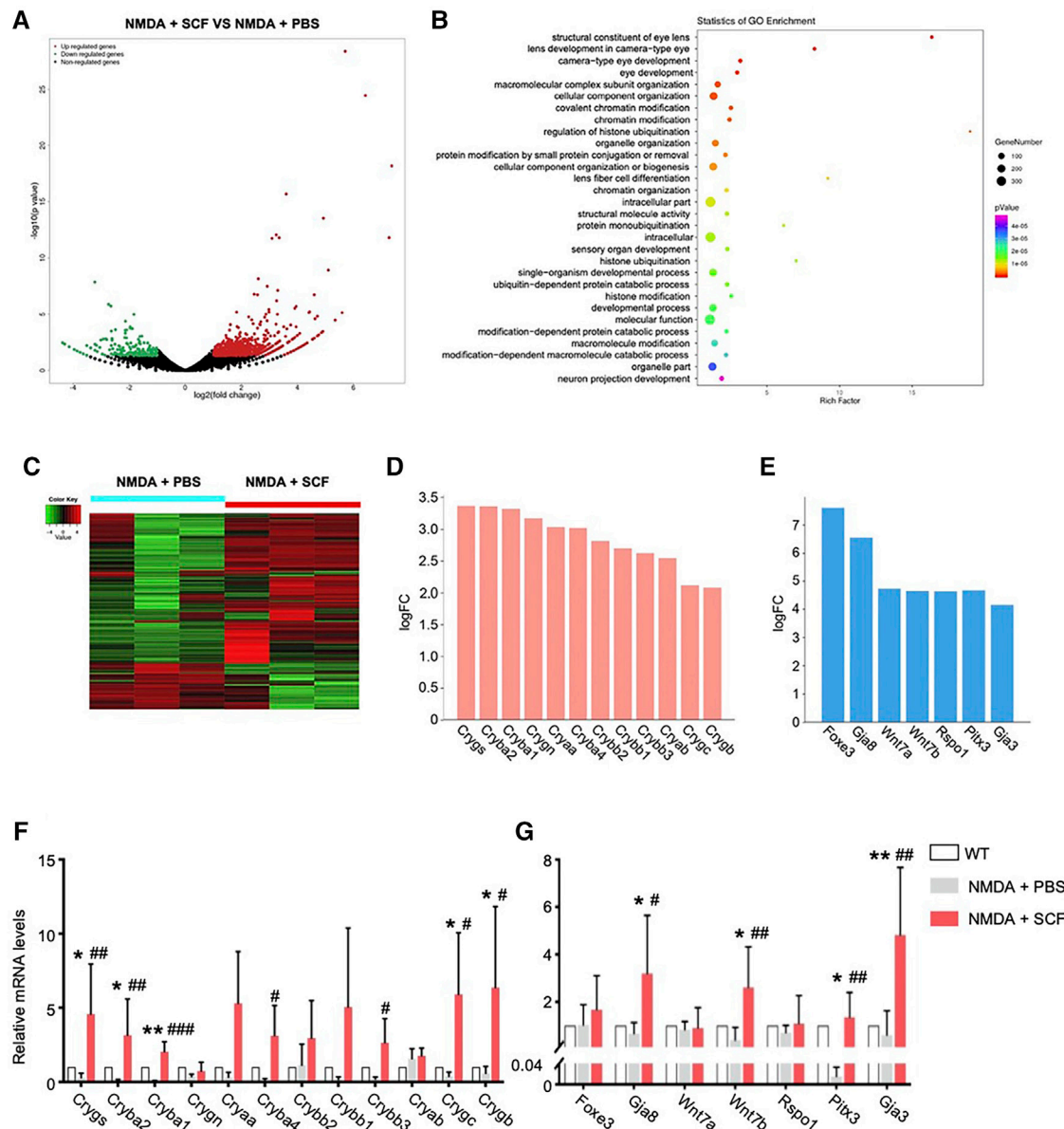
FIGURE 7 | RNA-seq Revealed the Involvement of Key Genes for SCF Treatment. **(A)** Volcano plot of differentially expressed genes (DEGs) in SCF group compared with controls after 1 week treatment. **(B)** Gene Ontology (GO) analysis showing the enriched gene functions of SCF group versus control group. **(C)** Heatmap analysis showing DEGs in indicated groups. The relative abundance of each genus was indicated by a gradient of color from green (low abundance) to red (high abundance). **(D)** Crystallins family members were significantly up-regulated in SCF treated retinas. **(E)** Among top10 DEGs in SCF exposed mice, several neuro-protective factors were up-regulated, including Wnt7 related genes, *Foxe3/Pitx3*, and gap junction protein coding genes *Gja8/Gja3*. **(F)** Real-time qPCR analysis showing relative mRNA expression for the Crystallins family members among WT, NMDA +PBS and NMDA + SCF treated mice after 1 week. **(G)** Real-time qPCR analysis confirming the expression for the genes highly expressed in RNA-seq analysis. Data were shown as mean ± SD (n = 5 for each time point). *p < 0.05, **p < 0.01, compared with WT mice, #p < 0.05, ##p < 0.01, ###p < 0.001, compared with the NMDA + PBS group.

SCF on RGCs. The photopic negative response (PhNR), a later negative going response evident in light adapted conditions, has been related to RGC activity in rodents. Besides, the decreased amplitude of PhNR is positively correlated with the loss of RGCs (Li et al., 2005; Chrysostomou and Crowston, 2013). Our study showed the PhNR amplitudes in the SCF-injected eyes were consistently increased (**Figures 6D,E**). Taken together, these

data demonstrated that exogenous SCF supplementation protected RGCs from NMDA-induced cell death, therefore delayed the progression of the retinal degeneration.

NMDA has been described as the glutamate analog that shows the greatest potency in increasing calcium influx and inducing neurotoxicity. Previous results have shown that NMDA neurotoxicity induces significant changes in the full field ERG

response, a thinning on the inner retinal layers, and RGC death. Electroretinogram results showed a significant decrease of both a-wave and b-wave amplitude in NMDA injuried mice (Zheng et al., 2015; Xiao et al., 2021). The RGCs are the final retinal elements in the direct pathway from the eye to the brain. The information gathered by photoreceptors is projected next onto bipolar cells, which, in turn, send projects to RGCs. With NMDA injury, the function of the RGCs is significantly hindered, which results in the transmission of light signal is blocked, and the overall function of the retina is reduced. Therefore, with SCF treatment attenuating the loss of RGCs, the amplitude of STR and PhNR of SCF treated NMDA mice was higher than NMDA mice without SCF treatment. As the function of RGCs was rescued, the functions of bipolar cells and photoreceptors were also protected to a certain extent. Therefore, the amplitudes of a-wave and b-wave in the SCF+NMDA group were higher than those in the NMDA injury group (**Figure 3**).

Microglia monitor and maintain the physiological homeostasis of their microenvironment. Previous studies have reported that SCF inhibits microglial proliferation *in vitro* when microglia are stimulated by CSF-1 (Zhang and Fedoroff, 1998). In our experiments, we showed that microglia was significantly activated after NMDA administration. With SCF treatment, the number of activated microglia were significantly decreased (**Figures 4A,B**). Microglia can acquire many morphological phenotypes. The "resting" microglia have a ramified shape and the "activated" microglia an ameboid shape. In the central nervous system, SCF-treated microglia showed a neuroprotective phenotype expressing anti-inflammatory cytokines, growth factors, and M2 markers as compared to the phenotype shown by granulocyte macrophage-colony stimulating factor-derived microglia expressing inflammatory cytokines and M1 markers (Terashima et al., 2018). Thus, we quantified the microglia morphology using a grid cross-counting system as reported previously (Luckoff et al., 2016; Luckoff et al., 2017; Bian et al., 2020). By counting the grid-crossed points of Iba1^{+} cells, we found that the microglia in the SCF-treated group mainly showed ramified shapes, while most microglia in the control group adopt an amoeboid morphology (**Figure 4C**). Taken together, these data demonstrated that exogenous SCF treatment can inhibit the hyperactivation of microglia in the NMDA-treated retina, and thus improve the visual function. Also, we found that c-kit was mainly expressed in neurons of GCL and INL, not in microglia in the retina (**Figure 1**). Therefore, we speculate that SCF could not directly act on retinal microglia, but reduce the activation of microglia by reducing neuron death and improving retinal microenvironment.

To further analyze the RNA-seq data, we found that the expression of multiple members from α, β and γ Crystallins family (*Cryaa*, *Cryab*, *Cryba1*, *Cryba2*, *Crygb*, *etc.*) were significantly up-regulated after SCF stimulation (**Figure 7D**), and also confirmed by real-time qPCR (**Figure 7F**). Both αA- and αB-crystallin has been reported to protect retinal neurons from cell death. Knockout of either αA- or αB-crystallin results in increased apoptosis and necroptosis of photoreceptors (Wang T. et al., 2021). Also, αB-Crystallin alleviates endotoxin-induced retinal inflammation and inhibits microglial activation and autophagy to protect injured retina (Wang F. et al., 2021). Our previous research also demonstrated that the Crystallins members plays an important role in promoting the survival of RGCs (A et al.,

2019), indicating that the upregulation of Crystallins may be a critical downstream pathway in SCF-mediated retinal protection.

In addition, a series of factors that promote neuron survival were also significantly up-regulated with SCF exposure, including *Pitx3* and *Gja3* (**Figures 7E,G**), which are involved in neuronal degeneration, cell survival and immune modulation, and represent important candidate gene sets that regulate the retinal homeostasis (Anand et al., 2018; Akula et al., 2019; Li et al., 2020a). Also, it has been reported that these neuroprotective genes (including Gja3, Pitx3, Wnt7a, Foxe3, as well as Cryaa) are the top downregulated genes in the retinas of streptozotocin (STZ)-induced diabetic rats (Liu et al., 2016), suggesting this gene expressing profile may be characterized as a critical signature that play an important role in the maintenance of the retinal function. It has been documented that Wnt pathway is involved in processes of neurogenesis, dendritic development and axon guidance during development, and can inhibit neuronal damage by up-regulating anti-apoptotic proteins such as Survivin (Shi et al., 2020; Kassumeh et al., 2021). *In vitro*, exogenous administration of Wnt3a can bind to the frizzled receptor and LRP5/6 on the surface of RGCs, and promote the survival and axon regeneration of RGCs by down-regulating Ripk1 and Ripk3, *etc.* (Udeh et al., 2019). With NMDA-induced RGCs injury, Wnt pathway was significantly suppressed, suggesting that Wnt-related pathway may be critical for the survival of RGCs (Boesl et al., 2020). In the present study, we found the upon SCF stimulation, *Wnt7b* was significantly up-regulated, suggesting that this pathway may be critical for the protective effect of c-kit^{+} cells on RGCs (**Figure 7G**). Additional investigations, however, are needed to support this speculation, and both the origin and the targets in retina of Wnt7 should be addressed.

CONCLUSION

In summary, our study demonstrates that in the NMDA-induced retinal degeneration mice model, endogenous c-kit^{+} cells can be stimulated by the treatment of SCF. The activation of c-kit^{+} cells confer protection against retinal degeneration, *via* inhibiting the loss of RGCs. Administration of SCF can act as a potent strategy for treating retinal degeneration-related diseases.

DATA AVAILABILITY STATEMENT

The datasets presented in this study can be found in online repositories. The names of the repository/repositories and accession number(s) can be found below: GSE192458.

ETHICS STATEMENT

The animal study was reviewed and approved by The study protocol was approved by the Office of Research Ethics Committee at Beijing Friendship Hospital Affiliated to Capital Medical University (ethics approval number: 18-2020).

AUTHOR CONTRIBUTIONS

FUNDING

ACKNOWLEDGMENTS

SUPPLEMENTARY MATERIAL

The Supplementary Material for this article can be found online at: https://www.frontiersin.org/articles/10.3389/fphar.2022.796380/full#supplementary-material

REFERENCES

Ahmad, I., Teotia, P., Erickson, H., and Xia, X. (2020). Recapitulating Developmental Mechanisms for Retinal Regeneration. *Prog. Retin. Eye Res.* 76, 100824. doi:10.1016/j.preteyeres.2019.100824

Akula, M., Park, J. W., and West-Mays, J. A. (2019). Relationship between Neural Crest Cell Specification and Rare Ocular Diseases. *J. Neurosci. Res.* 97, 7–15. doi:10.1002/jnr.24245

Anand, D., Agrawal, S. A., Slavotinek, A., and Lachke, S. A. (2018). Mutation Update of Transcription Factor Genes FOXE3, HSF4, MAF, and PITX3 Causing Cataracts and Other Developmental Ocular Defects. *Hum. Mutat.* 39, 471–494. doi:10.1002/humu.23395

Bian, B., Zhao, C., He, X., Gong, Y., Ren, C., Ge, L., et al. (2020). Exosomes Derived from Neural Progenitor Cells Preserve Photoreceptors during Retinal Degeneration by Inactivating Microglia. *J. Extracell Vesicles* 9, 1748931. doi:10.1080/20013078.2020.1748931

Boesl, F., Drexler, K., Müller, B., Seitz, R., Weber, G. R., Priglinger, S. G., et al. (2020). Endogenous Wnt/β-Catenin Signaling in Müller Cells Protects Retinal Ganglion Cells from Excitotoxic Damage. *Mol. Vis.* 26, 135–149.

Bui, B. V., and Fortune, B. (2004). Ganglion Cell Contributions to the Rat Full-Field Electroretinogram. *J. Physiol.* 555, 153–173. doi:10.1113/jphysiol.2003.052738

Cardoso, H. J., Figueira, M. I., and Socorro, S. (2017). The Stem Cell Factor (SCF)/c-KIT Signalling in Testis and Prostate Cancer. *J. Cel Commun Signal* 11, 297–307. doi:10.1007/s12079-017-0399-1

Chen, X., Chen, Z., Li, Z., Zhao, C., Zeng, Y., Zou, T., et al. (2016). Grafted C-kit+/SSEA1- Eye-wall Progenitor Cells Delay Retinal Degeneration in Mice by Regulating Neural Plasticity and Forming New Graft-To-Host Synapses. *Stem Cel Res Ther* 7, 191. doi:10.1186/s13287-016-0451-8

Chen, X., Wang, S., Xu, H., Pereira, J. D., Hatzistergos, K. E., Saur, D., et al. (2017). Evidence for a Retinal Progenitor Cell in the Postnatal and Adult Mouse. *Stem Cel Res* 23, 20–32. doi:10.1016/j.scr.2017.06.010

Chrysostomou, V., and Crowston, J. G. (2013). The Photopic Negative Response of the Mouse Electroretinogram: Reduction by Acute Elevation of Intraocular Pressure. *Invest Ophthalmol Vis Sci.* 54, 4691–4697. doi:10.1167/iovs.13-12415

Cuenca, N., Fernández-Sánchez, L., Campello, L., Maneu, V., De la Villa, P., Lax, P., et al. (2014). Cellular Responses Following Retinal Injuries and Therapeutic Approaches for Neurodegenerative Diseases. *Prog. Retin. Eye Res.* 43, 17–75. doi:10.1016/j.preteyeres.2014.07.001

De la Huerta, I., Kim, I. J., Voinescu, P. E., and Sanes, J. R. (2012). Direction-selective Retinal Ganglion Cells Arise from Molecularly Specified Multipotential Progenitors. *Proc. Natl. Acad. Sci. U S A.* 109, 17663–17668. doi:10.1073/pnas.1215806109

Du, R., Wang, X., and He, S. (2020). BDNF Improves Axon Transportation and Rescues Visual Function in a Rodent Model of Acute Elevation of Intraocular Pressure. *Sci. China Life Sci.* 63, 1–10. doi:10.1007/s11427-019-1567-0

Dulz, S., Bassal, M., Flachsbarth, K., Riecken, K., Fehse, B., Schlichting, S., et al. (2020). Intravitreal Co-administration of GDNF and CNTF Confers Synergistic and Long-Lasting Protection against Injury-Induced Cell Death of Retinal Ganglion Cells in Mice. *Cells* 9, 2082. doi:10.3390/cells9092082

Edling, C. E., and Hallberg, B. (2007). c-Kit--a Hematopoietic Cell Essential Receptor Tyrosine Kinase. *Int. J. Biochem. Cel Biol* 39, 1995–1998. doi:10.1016/j.biocel.2006.12.005

Gonzalez-Casanova, J., Schmachtenberg, O., Martinez, A. D., Sanchez, H. A., Harcha, P. A., and Rojas-Gomez, D. (2021). An Update on Connexin Gap Junction and Hemichannels in Diabetic Retinopathy. *Int. J. Mol. Sci.* 22, 3194. doi:10.3390/ijms22063194

Harada, C., Guo, X., Namekata, K., Kimura, A., Nakamura, K., Tanaka, K., et al. (2011). Glia- and Neuron-specific Functions of TrkB Signalling during Retinal Degeneration and Regeneration. *Nat. Commun.* 2, 189. doi:10.1038/ncomms1190

Hoang, T., Wang, J., Boyd, P., Wang, F., Santiago, C., Jiang, L., et al. (2020). Gene Regulatory Networks Controlling Vertebrate Retinal Regeneration. *Science* 370, eabb8598. doi:10.1126/science.abb8598

Holcombe, D. J., Lengefeld, N., Gole, G. A., and Barnett, N. L. (2008). Selective Inner Retinal Dysfunction Precedes Ganglion Cell Loss in a Mouse Glaucoma Model. *Br. J. Ophthalmol.* 92, 683–688. doi:10.1136/bjo.2007.133223

Jin, Z. B., Gao, M. L., Deng, W. L., Wu, K. C., Sugita, S., Mandai, M., et al. (2019). Stemming Retinal Regeneration with Pluripotent Stem Cells. *Prog. Retin. Eye Res.* 69, 38–56. doi:10.1016/j.preteyeres.2018.11.003

Jnawali, A., Lin, X., Patel, N. B., Frishman, L. J., and Ostrin, L. A. (2020). Retinal Ganglion Cell Ablation in guinea Pigs. *Exp. Eye Res.* 202, 108339. doi:10.1016/j.exer.2020.108339

Jorstad, N. L., Wilken, M. S., Grimes, W. N., Wohl, S. G., VandenBosch, L. S., Yoshimatsu, T., et al. (2017). Stimulation of Functional Neuronal Regeneration from Müller Glia in Adult Mice. *Nature* 548, 103–107. doi:10.1038/nature23283

Jorstad, N. L., Wilken, M. S., Todd, L., Finkbeiner, C., Nakamura, P., Radulovich, N., et al. (2020). STAT Signaling Modifies Ascl1 Chromatin Binding and Limits Neural Regeneration from Muller Glia in Adult Mouse Retina. *Cell Rep* 30, 2195–e5. doi:10.1016/j.celrep.2020.01.075

Kassumeh, S., Weber, G. R., Nobl, M., Priglinger, S. G., and Ohlmann, A. (2021). The Neuroprotective Role of Wnt Signaling in the Retina. *Neural Regen. Res.* 16, 1524–1528. doi:10.4103/1673-5374.303010

Koso, H., Satoh, S., and Watanabe, S. (2007). c-Kit marks Late Retinal Progenitor Cells and Regulates Their Differentiation in Developing Mouse Retina. *Dev. Biol.* 301, 141–154. doi:10.1016/j.ydbio.2006.09.027

Lennartsson, J., Jelacic, T., Linnekin, D., and Shivakrupa, R. (2005). Normal and Oncogenic Forms of the Receptor Tyrosine Kinase Kit. *Stem Cells* 23, 16–43. doi:10.1634/stemcells.2004-0117

Lennartsson, J., and Rönnstrand, L. (2012). Stem Cell Factor Receptor/c-Kit: from Basic Science to Clinical Implications. *Physiol. Rev.* 92, 1619–1649. doi:10.1152/physrev.00046.2011

Li, H., Jiang, H., Rong, R., Jiang, J., Ji, D., Song, W., et al. (2020a). Identification of GJA3 p.S50P Mutation in a Chinese Family with Autosomal Dominant Congenital Cataract and its Underlying Pathogenesis. *DNA Cel Biol* 39, 1760–1766. doi:10.1089/dna.2020.5605

Li, H., Lian, L., Liu, B., Chen, Y., Yang, J., Jian, S., et al. (2020b). KIT Ligand Protects against Both Light-Induced and Genetic Photoreceptor Degeneration. *Elife* 9, e51698. doi:10.7554/eLife.51698

Li, Z., Zeng, Y., Chen, X., Li, Q., Wu, W., Xue, L., et al. (2016). Neural Stem Cells Transplanted to the Subretinal Space of Rd1 Mice Delay Retinal Degeneration by Suppressing Microglia Activation. *Cytotherapy* 18, 771–784. doi:10.1016/j.jcyt.2016.03.001

Li, B., Barnes, G. E., and Holt, W. F. (2005). The Decline of the Photopic Negative Response (PhNR) in the Rat After Optic Nerve Transection. *Doc Ophthalmol* 111, 23–31. doi:10.1007/s10633-005-2629-8

Liu, Y., McDowell, C. M., Zhang, Z., Tebow, H. E., Wordinger, R. J., and Clark, A. F. (2014). Monitoring Retinal Morphologic and Functional Changes in Mice Following Optic Nerve Crush. *Invest. Ophthalmol. Vis. Sci.* 55, 3766–3774. doi:10.1167/iovs.14-13895

Liu, Y. J., Lian, Z. Y., Liu, G., Zhou, H. Y., and Yang, H. J. (2016). RNA Sequencing Reveals Retinal Transcriptome Changes in STZ-Induced Diabetic Rats. *Mol. Med. Rep.* 13, 2101–2109. doi:10.3892/mmr.2016.4793

Lückoff, A., Caramoy, A., Scholz, R., Prinz, M., Kalinke, U., and Langmann, T. (2016). Interferon-beta Signaling in Retinal Mononuclear Phagocytes Attenuates Pathological Neovascularization. *EMBO Mol. Med.* 8, 670–678. doi:10.15252/emmm.201505994

Lückoff, A., Scholz, R., Sennlaub, F., Xu, H., and Langmann, T. (2017). Comprehensive Analysis of Mouse Retinal Mononuclear Phagocytes. *Nat. Protoc.* 12, 1136–1150. doi:10.1038/nprot.2017.032

A, L., Zou, T., He, J., Chen, X., Sun, D., Fan, X., et al. (2019). Rescue of Retinal Degeneration in Rd1 Mice by Intravitreally Injected Metformin. *Front. Mol. Neurosci.* 12, 102. doi:10.3389/fnmol.2019.00102

Mandai, M., Watanabe, A., Kurimoto, Y., Hirami, Y., Morinaga, C., Daimon, T., et al. (2017). Autologous Induced Stem-Cell-Derived Retinal Cells for Macular Degeneration. *N. Engl. J. Med.* 376, 1038–1046. doi:10.1056/NEJMoa1608368

Morii, E., Kosaka, J., Nomura, S., Fukuda, Y., and Kitamura, Y. (1994). Demonstration of Retinal Cells Expressing Messenger RNAs of the C-Kit Receptor and its Ligand. *Neurosci. Lett.* 166, 168–170. doi:10.1016/0304-3940(94)90477-4

Niwa, M., Aoki, H., Hirata, A., Tomita, H., Green, P. G., and Hara, A. (2016). Retinal Cell Degeneration in Animal Models. *Int. J. Mol. Sci.* 17, 110. doi:10.3390/ijms17010110

Pardue, M. T., and Allen, R. S. (2018). Neuroprotective Strategies for Retinal Disease. *Prog. Retin. Eye Res.* 65, 50–76. doi:10.1016/j.preteyeres.2018.02.002

Pascolini, D., and Mariotti, S. P. (2012). Global Estimates of Visual Impairment: 2010. *Br. J. Ophthalmol.* 96, 614–618. doi:10.1136/bjophthalmol-2011-300539

Qiu, X., Ping, S., Kyle, M., Chin, L., and Zhao, L. R. (2020). Long-term Beneficial Effects of Hematopoietic Growth Factors on Brain Repair in the Chronic Phase of Severe Traumatic Brain Injury. *Exp. Neurol.* 330, 113335. doi:10.1016/j.expneurol.2020.113335

Saszik, S. M., Robson, J. G., and Frishman, L. J. (2002). The Scotopic Threshold Response of the Dark-Adapted Electroretinogram of the Mouse. *J. Physiol.* 543, 899–916. doi:10.1113/jphysiol.2002.019703

Schwartz, S. D., Regillo, C. D., Lam, B. L., Eliott, D., Rosenfeld, P. J., Gregori, N. Z., et al. (2015). Human Embryonic Stem Cell-Derived Retinal Pigment Epithelium in Patients with Age-Related Macular Degeneration and Stargardt's Macular Dystrophy: Follow-Up of Two Open-Label Phase 1/2 Studies. *Lancet* 385, 509–516. doi:10.1016/S0140-6736(14)61376-3

Schwartz, S. D., Tan, G., Hosseini, H., and Nagiel, A. (2016). Subretinal Transplantation of Embryonic Stem Cell-Derived Retinal Pigment Epithelium for the Treatment of Macular Degeneration: An Assessment at 4 Years. *Invest. Ophthalmol. Vis. Sci.* 57, ORSFc1–9. doi:10.1167/iovs.15-18681

Shi, W., Tang, Y., Zhi, Y., Li, Z., Yu, S., Jiang, J., et al. (2020). Akt Inhibition-dependent Downregulation of the Wnt/β-Catenin Signaling Pathway Contributes to Antimony-Induced Neurotoxicity. *Sci. Total Environ.* 737, 140252. doi:10.1016/j.scitotenv.2020.140252

Singh, M. S., Park, S. S., Albini, T. A., Canto-Soler, M. V., Klassen, H., MacLaren, R. E., et al. (2020). Retinal Stem Cell Transplantation: Balancing Safety and Potential. *Prog. Retin. Eye Res.* 75, 100779. doi:10.1016/j.preteyeres.2019.100779

Stankov, K., Popovic, S., and Mikov, M. (2014). C-KIT Signaling in Cancer Treatment. *Curr. Pharm. Des.* 20, 2849–2880. doi:10.2174/13816128113199990593

Terashima, T., Nakae, Y., Katagi, M., Okano, J., Suzuki, Y., and Kojima, H. (2018). Stem Cell Factor Induces Polarization of Microglia to the Neuroprotective Phenotype In Vitro. *Heliyon* 4, e00837. doi:10.1016/j.heliyon.2018.e00837

Udeh, A., Dvoriantchikova, G., Carmy, T., Ivanov, D., and Hackam, A. S. (2019). Wnt Signaling Induces Neurite Outgrowth in Mouse Retinal Ganglion Cells. *Exp. Eye Res.* 182, 39–43. doi:10.1016/j.exer.2019.03.004

Wang, F., Jiang, Z., Lou, B., Duan, F., Qiu, S., Cheng, Z., et al. (2021a). αB-Crystallin Alleviates Endotoxin-Induced Retinal Inflammation and Inhibits Microglial Activation and Autophagy. *Front. Immunol.* 12, 641999. doi:10.3389/fimmu.2021.641999

Wang, T., Yao, J., Jia, L., Fort, P. E., and Zacks, D. N. (2021b). Loss of alphaA or alphaB-Crystallin Accelerates Photoreceptor Cell Death in a Mouse Model of P23H Autosomal Dominant Retinitis Pigmentosa. *Int. J. Mol. Sci.* 23, 70. doi:10.3390/ijms23010070

Wong, W. L., Su, X., Li, X., Cheung, C. M., Klein, R., Cheng, C. Y., et al. (2014). Global Prevalence of Age-Related Macular Degeneration and Disease burden Projection for 2020 and 2040: a Systematic Review and Meta-Analysis. *Lancet Glob. Health* 2, e106–16. doi:10.1016/S2214-109X(13)70145-1

Xiao, L., Hou, C., Cheng, L., Zheng, S., Zhao, L., and Yan, N. (2021). DZNep Protects against Retinal Ganglion Cell Death in an NMDA-Induced Mouse Model of Retinal Degeneration. *Exp. Eye Res.* 212, 108785. doi:10.1016/j.exer.2021.108785

Yao, K., Qiu, S., Wang, Y. V., Park, S. J. H., Mohns, E. J., Mehta, B., et al. (2018). Restoration of Vision after De Novo Genesis of Rod Photoreceptors in Mammalian Retinas. *Nature* 560, 484–488. doi:10.1038/s41586-018-0425-3

Zhang, S. C., and Fedoroff, S. (1998). Modulation of Microglia by Stem Cell Factor. *J. Neurosci. Res.* 53, 29–37. doi:10.1002/(SICI)1097-4547(19980701)53:1<29::AID-JNR4>3.0.CO;2-L

Zhang, Y., Pan, X., Shi, Z., Cai, H., Gao, Y., and Zhang, W. (2018). Sustained Release of Stem Cell Factor in a Double Network Hydrogel for *Ex Vivo* Culture of Cord Blood-Derived CD34+ Cells. *Cell Prolif* 51, e12407. doi:10.1111/cpr.12407

Zheng, S., Yang, H., Chen, Z., Zheng, C., Lei, C., and Lei, B. (2015). Activation of Liver X Receptor Protects Inner Retinal Damage Induced by N-Methyl-D-Aspartate. *Invest. Ophthalmol. Vis. Sci.* 56, 1168–1180. doi:10.1167/iovs.14-15612

Zhou, H., Su, J., Hu, X., Zhou, C., Li, H., Chen, Z., et al. (2020). Glia-to-Neuron Conversion by CRISPR-CasRx Alleviates Symptoms of Neurological Disease in Mice. *Cell* 181, 590–e16. doi:10.1016/j.cell.2020.03.024

Zhou, P. Y., Peng, G. H., Xu, H., and Yin, Z. Q. (2015). c-Kit⁺ Cells Isolated from Human Fetal Retinas Represent a New Population of Retinal Progenitor Cells. *J. Cel Sci* 128, 2169–2178. doi:10.1242/jcs.169086

Zou, T., Gao, L., Zeng, Y., Li, Q., Li, Y., Chen, S., et al. (2019). Organoid-derived C-Kit+/SSEA4- Human Retinal Progenitor Cells Promote a Protective Retinal Microenvironment during Transplantation in Rodents. *Nat. Commun.* 10, 1205. doi:10.1038/s41467-019-08961-0

Advantages of publishing in Frontiers

OPEN ACCESS
Articles are free to read
for greatest visibility
and readership

FAST PUBLICATION
Around 90 days
from submission
to decision

HIGH QUALITY PEER-REVIEW
Rigorous, collaborative,
and constructive
peer-review

TRANSPARENT PEER-REVIEW
Editors and reviewers
acknowledged by name
on published articles

Frontiers
Avenue du Tribunal-Fédéral 34
1005 Lausanne | Switzerland

Visit us: www.frontiersin.org
Contact us: frontiersin.org/about/contact

**REPRODUCIBILITY OF
RESEARCH**
Support open data
and methods to enhance
research reproducibility

DIGITAL PUBLISHING
Articles designed
for optimal readership
across devices

FOLLOW US
@frontiersin

IMPACT METRICS
Advanced article metrics
track visibility across
digital media

EXTENSIVE PROMOTION
Marketing
and promotion
of impactful research

LOOP RESEARCH NETWORK
Our network
increases your
article's readership